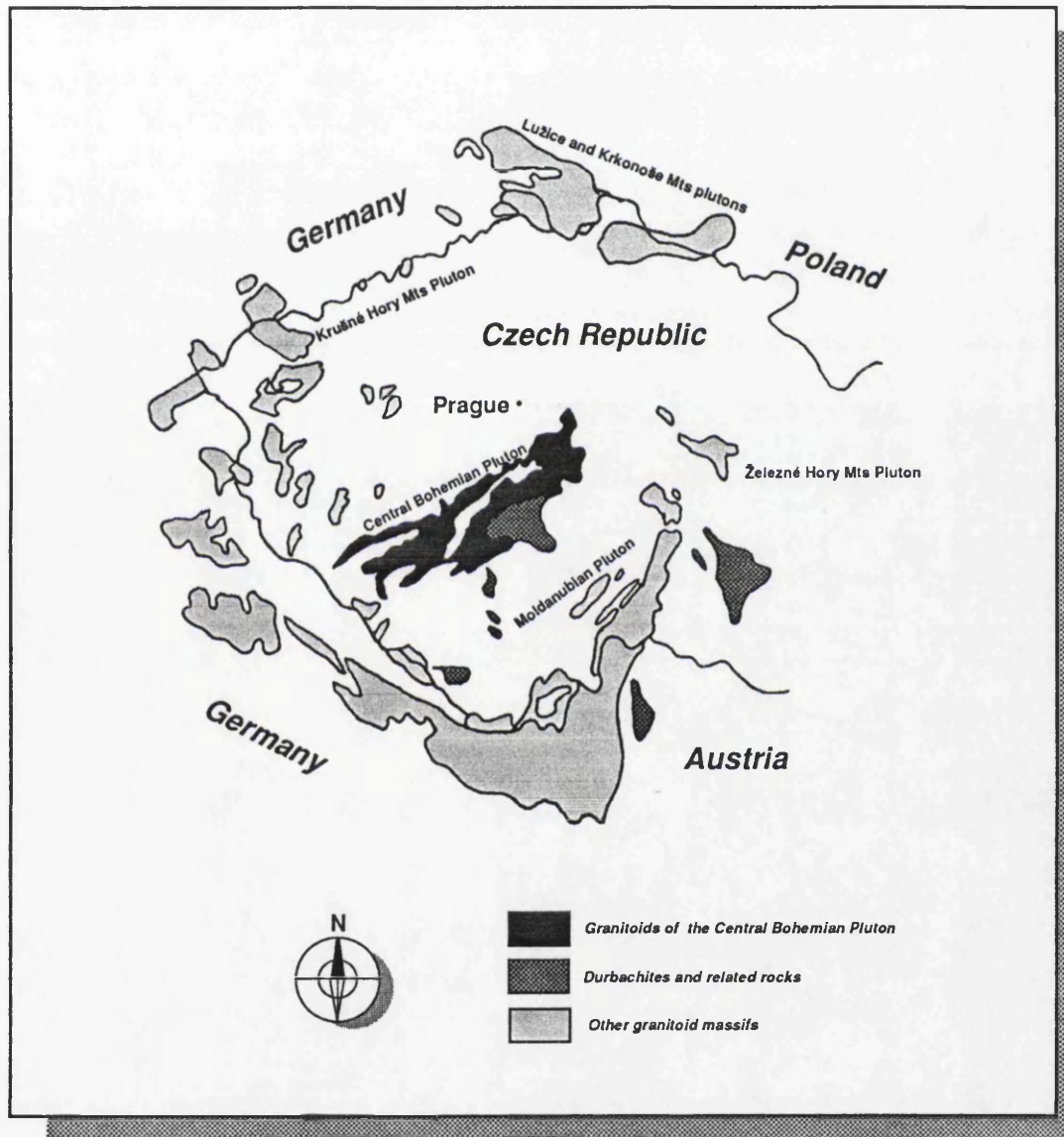


Geochemistry and petrogenesis of the Central Bohemian Pluton, Czech Republic

by

Vojtěch Janoušek



*A thesis submitted for the degree of Doctor of Philosophy
Department of Geology and Applied Geology,
University of Glasgow*

Glasgow, August 1994

ProQuest Number: 13834134

All rights reserved

INFORMATION TO ALL USERS

The quality of this reproduction is dependent upon the quality of the copy submitted.

In the unlikely event that the author did not send a complete manuscript and there are missing pages, these will be noted. Also, if material had to be removed, a note will indicate the deletion.



ProQuest 13834134

Published by ProQuest LLC (2019). Copyright of the Dissertation is held by the Author.

All rights reserved.

This work is protected against unauthorized copying under Title 17, United States Code
Microform Edition © ProQuest LLC.

ProQuest LLC.
789 East Eisenhower Parkway
P.O. Box 1346
Ann Arbor, MI 48106 – 1346



Thesis
9903
copy.1

The granitoids are corundum-normative indicating the nature of "S" granites. The $^{87}\text{Sr}/^{86}\text{Sr}$ ratios were not determined so far, but from the content of Sr we may suggest that it will be higher than 0.706.

Palivcová (1984)

Neither experimental nor geological studies confirm (operation of) magma mixing.

Vlašimský et al. (1992)

1. Declaration

I declare that all the material presented in this thesis represents a result of three year independent research carried out at Department Geology and Applied Geology, University of Glasgow and at the Isotope Geosciences Unit, Scottish Universities Research and Reactor Centre, East Kilbride under the supervision of Prof. Donald R. Bowes, Prof. Bernard E. Leake and Dr. Graeme Rogers. Any previously published or unpublished works used herein have been given the full acknowledgement.

Vojtěch Janoušek
22 August, 1994

2. Acknowledgements

This work has been undertaken in period 1991-1994 at the Department of Geology and Applied Geology, University of Glasgow thanks to generous financial support by the University of Glasgow Postgraduate Scholarship and the ORS scholarship.

I would like to acknowledge Professors Donald R. Bowes and Bernard E. Leake as well as Dr. Graeme Rogers for their guidance, expertise, time and encouragement. The advice and support of Drs Colin Braithwaite, Colin Farrow and Brian Bell is also very much appreciated.

In Prague Drs Emil Jelínek, František V. Holub, Arnošt Dudek and Stanislav Vrána, have offered generously both their advice and practical help. Drs Emil Jelínek, Milan Klečka and Věra Vaňková have supplied samples for the whole-rock geochemistry study.

I thank also others who have contributed to this work, particularly Pete Ainsworth, Bob Cumberland, Rob Ellam, Jim Gallagher, Vincent Gallagher, Bill Higgins, Jim Kavanagh, Anne Kelly, Martin McCartney, Robert MacDonald, Murdo MacLeod, Douglas Maclean, Roddy Morrison, Tracy Shimmield, Kate Sampson and Dugie Turner.

The postgraduate community at the department, especially Richard Cox, John Hughes, Jan Košler and Jeremy Preston are thanked for their help and companionship. I am also grateful to João Lopes, Martin Ďuriš, Jorge Atouguia, Hitoshi Osaka and the Glasgow University Research Club for keeping my spirits high.

Last, but not least, I thank my parents for their (life-long) patience and support.

3. Abstract

An integrated study of the petrography, mineral chemistry, whole-rock major, trace and Sr - Nd isotope geochemistry of selected intrusions of the Hercynian Central Bohemian Pluton (CBP) has revealed compositional and genetic diversity within this igneous complex. This composite pluton covers 3200 km² and has intruded in early Carboniferous times the boundary between two major units, the Teplá-Barrandian Unit and the Moldanubian (s.s.) Unit; parts of its roof are preserved as the so-called Metamorphic Islet Zone. At least five petrogenetic suites can be distinguished in the CBP: Sázava (gabbro, quartz diorite, tonalite, trondhjemitic and granodiorite) Blatná (quartz monzonite, granodiorite, granite), Čertovo břemeno (melasyenite and melagranite), Říčany (granite) and S-type anatectic granitoids.

The Sázava and Blatná suites contain hornblende and relatively Fe-rich biotite, unlike the Říčany and Čertovo břemeno suites with (secondary) actinolite and actinolitic hornblende and Mg-rich biotite. Based on the Al in hornblende geobarometry, the majority of the amphiboles studied (Sázava, Blatná, Kozárovice intrusions) have not crystallized deeper than 5 - 10 km. In contrast, brown cores of the amphiboles from Teletín quartz diorite may have originated at much greater depths, possibly up to 30 km.

The abundance of mafic microgranular enclaves, syn-plutonic dykes and the presence of specific microtextural phenomena in many of the studied intrusions (like mantled plagioclases, amphibole-biotite clots, quartz and K-feldspar xenocrysts, quenched textures) point to contemporaneous intrusion of acid and basic magmas and their interaction (magma mixing). Besides the classic petrographic methods, cathodoluminescence has been proven to be a valuable tool for studying these features, in particular resorption and overgrowth features in the feldspar crystals.

Each of the suites shows a distinctive range of the major, trace and Sr-Nd isotopic data. The total range of $(^{87}\text{Sr}/^{86}\text{Sr})_{330} = 0.7051 - 0.7129$ and $\epsilon_{\text{Nd}}^{330} = +0.2 - -8.9$ is comparable with granitoids of other parts of the Hercynian belt. Two-stage $T_{\text{DM}}^{\text{Nd}}$ model ages ranging from 1.05 Ga (Sázava suite) to 1.65 Ga (Čertovo břemeno and Říčany suites) are interpreted as reflecting a mixed source, rather than a major crust-formation event. In the CBP, there is a conspicuous trend towards isotopically more evolved compositions with time (in succession Sázava, Blatná, Říčany and Čertovo břemeno suites) that is interpreted as being due to enrichment of the mantle by an incompatible-element-enriched and, or high $^{87}\text{Sr}/^{86}\text{Sr}$ component, possibly associated with an earlier (late Proterozoic ?) subduction environment.

In the northern CBP, the Sázava suite may have originated by re-melting of adjacent metabasites of the Jílové Zone or the Metamorphic Islet Zone, by partial melting of a mantle source with an isotopic composition similar to Bulk Earth, or mixing of magmas derived from both sources. This is compatible with an abundance of mafic microgranular enclaves and a paucity of both surmicaceous enclaves and metasedimentary xenoliths. The basic rocks, associated with, and at least partly contemporaneous with, the Sázava suite have probably acted as a heat source as well as one of the major components of the Sázava magma. The geochemical modelling implies extensive fractional crystallization of mainly amphibole and plagioclase, with some biotite and orthite. The peraluminous Požárý intrusion, with low ΣREE and high positive Eu anomalies, may have been derived from the Sázava parent largely by fractional crystallization or by small degrees of melting of a metabasic

parent. Mixing tests performed on the Teletín quartz diorite are compatible with its origin by hybridization of the Sázava tonalite with a gabbroic melt.

Overall, the processes which produced the most mafic members of the Blatná and Čertovo břemeno suites appear to have been similar. These shoshonitic basic rocks, generated from an isotopically heterogeneous source, acted as parents, undergoing contamination by the crustal material, as well as a heat source facilitating its melting.

The variation within the Blatná suite can be modelled by mixing between a moderately enriched ($(^{87}\text{Sr}/^{86}\text{Sr})_{330} \sim 0.708$, $\epsilon_{\text{Nd}}^{330} \sim -3$) mantle component, close in composition to monzonitic rocks of the suite (Lučkovice monzonite), with either an isotopically evolved metasedimentary component (most likely of Moldanubian provenance) or with the most acidic magma of the Blatná intrusion. In the second case, about 60 - 70 % and 70 - 80 % of the most evolved Blatná granodiorite is needed to produce the least evolved members of the Kozárovce and Blatná suites, respectively. These could have further developed by fractional crystallization (or rather AFC) of amphibole > plagioclase + K-feldspar >> biotite (Kozárovce) or plagioclase > biotite > amphibole > orthite (Blatná).

The Čertovo břemeno suite, including the minettes, originated from strongly enriched ($(^{87}\text{Sr}/^{86}\text{Sr})_{330} \sim 0.7128$, $\epsilon_{\text{Nd}}^{330} \sim -7$) mantle-derived magmas. These may have evolved through closed-system fractionation, or have interacted with S-type leucogranitic magmas of similar isotopic composition that were derived from the Moldanubian Unit. For the Sedlčany intrusion, about 40 % of the basic magma could have mixed with leucogranitic magma, and further evolved by limited AFC of plagioclase – K-feldspar > biotite – amphibole assemblage.

The peraluminous Říčany suite is likely to have been produced by partial melting of peraluminous lithologies within the Moldanubian Unit although an origin by mixing between magmas resembling the Čertovo břemeno suite and metasediments of the Teplá-Barrandian Unit cannot be ruled out. Whole-rock compositional data show that it is a reversely-zoned body, and imply K-feldspar-dominated fractionation in a deep magma-chamber prior the high-level intrusion. The reverse zoning could have been achieved either by emplacement in a single batch from a stratified magma chamber, or in several batches following cauldron subsidence or stoping.

The geochemical data point to an overall progression with time from calc-alkaline magmas (Sázava suite) towards K-rich calc-alkaline (Blatná suite) and shoshonitic compositions (Čertovo břemeno and Říčany suites). This evolution is interpreted as a transition from a magmatic arc to a post-collision uplift setting. Alternatively, the volcanic-arc like signature of the Sázava and also the Blatná suites may have been inherited from their source rocks.

4. Table of contents

<i>1. Declaration</i>	<i>ii</i>
<i>2. Acknowledgements</i>	<i>ii</i>
<i>3. Abstract</i>	<i>iii</i>
<i>4. Table of contents</i>	<i>v</i>
<i>5. List of illustrations</i>	<i>viii</i>
<i>6. List of tables</i>	<i>xii</i>
I. Introduction	1
I.1. Geological setting	1
I.2. Main rock units and their distribution	2
I.3. Age	3
I.4. Objectives of thesis	4
II. Field relations and petrography	7
II.1. Sázava intrusion (including Teletín quartz diorite)	8
II.2. Požáry intrusion	15
II.3. Kozárovce intrusion (including Těchnice granodiorite)	19
II.4. Blaná intrusion (including Červená granodiorite)	28
II.5. Sedlčany intrusion	35
II.6. Říčany intrusion	41
II.7. Other intrusions	46
II.7.1. Čertovo břemeno intrusion	46
II.7.2. Tábor intrusion	47
II.7.3. Kozlovice intrusion	47
II.7.4. Maršovice intrusion	48
II.7.5. Kosova Hora intrusion	48
II.7.6. Klatovy intrusion	48
II.7.7. Marginal type intrusion	48
II.7.8. Nečín intrusion	48
II.7.9. Dehetník intrusion	49
II.7.10. Benešov intrusion	49
II.7.11. Leucogranitoids	49
II.8. Discussion and implications of the field relations and petrography	49
II.8.1. Terminology	49
II.8.2. Genetic constraints based on petrography and field relations	49
II.8.3. Relative age of the intrusions in the CBP	50
II.8.4. Order of crystallization	51
II.8.5. Cathodoluminescence	51

III. Mineral chemistry	53
III.1. Mineral chemistry of the individual intrusions	55
III.1.1. Sázava intrusion (including Teletín quartz diorite)	55
I. Sázava quartz diorite to tonalite	55
II. Teletín quartz diorite	56
III.1.2. Požáry intrusion	58
III.1.3. Kozárovice intrusion (including Kozárovice quartz monzonite)	59
I. Kozárovice granodiorite	59
II. Kozárovice quartz monzonite.....	60
III.1.4. Blatná intrusion	61
III.1.5. Sedlčany intrusion	61
III.1.6. Říčany intrusion	62
III.2. Comparison of the mineral chemistry of the particular minerals	63
III.2.1. Plagioclase	63
III.2.2. Biotite.....	63
III.2.3. Amphibole.....	64
III.3. Implications of the mineral chemistry	66
IV. Whole-rock geochemistry	68
IV.1. Major elements	68
IV.1.1. Major-element–based subdivision of the CBP	69
IV.1.2. Harker plots	70
IV.1.3. Major-element character of the studied suites.....	71
IV.2. Trace elements	74
IV.2.1. Bivariate plots with SiO ₂	74
IV.2.2. Inter- and intra-suites variation of the trace elements	74
Large Ion Lithophile elements (LILE).....	75
High Field Strength elements (HFSE)	75
Transition metals.....	77
Rare Earth Elements (REE)	77
IV.3. Petrogenetic constraints based on whole-rock geochemistry	79
IV.3.1. The Sázava suite	80
IV.3.2. The Blatná suite	84
IV.3.3. The Čertovo břemeno suite.....	88
IV.3.4. The Říčany suite.....	90
IV.4. Tectonic affiliations of the granitoids.....	93
IV.5. Implications of the whole-rock geochemistry	97
Sázava suite.....	97
Blatná suite.....	97
Čertovo břemeno suite.....	98
Říčany suite.....	98

V. Sr-Nd isotope geochemistry and petrogenetic implications	99
V.1. Theoretical background.....	99
V.1.1. Epsilon values and model ages	99
V.1.2. Mixing of two isotope systems	101
V.2. Sr-Nd isotope results	102
V.3. Discussion	103
V.3.1. Comparison with other Hercynian granitoids in Europe	103
I. Sr-Nd isotopic data	103
II. Neodymium model ages.....	104
V.3.2. Petrogenetic implications.....	105
I. Sázava suite	105
II. Blatná suite.....	106
III. Čertovo břemeno suite	107
IV. Říčany suite.....	110
V.3.3. Summary	111
V.4. Towards a petrogenetic model of the CBP	111
VI. Conclusions	116
VII. Appendix.....	120
Appendix I. List of samples, Central Bohemian Pluton	120
Appendix II. Techniques.....	126
2.1. Sampling and sample preparation.....	126
2.2. Electron microprobe, BSE and CL study.....	126
2.3. X-ray fluorescence	126
2.5. Ferrous iron determination.....	128
2.6. Loss on ignition	128
2.7. ICP-MS	128
2.8. Sr and Nd isotopes	130
2.8.1 Chemistry	130
2.8.2. Mass Spectrometry.....	131
2.9. Software	132
2.9.1. BTRAP.....	132
2.9.2. NORMAN.....	133
Appendix III. Major element data and normative values	134
Appendix IV. Trace element geochemistry concentrations [XRF]	148
Appendix V. REE and other trace element concentrations [ICP-MS].....	152
Appendix VI. Composition of feldspars	155
Appendix VII. Composition of biotites	179
Appendix VIII. Composition of amphiboles	192
Appendix IX. Geochronology in the CBP	207
VIII. References	209

5. List of illustrations

FIGURES:

Chapter I.

- I.1. Geological sketch of the Eastern Hercynides
- I.2. Basic gravity structures of the Bohemian Massif on the territory of the Czech Republic
- I.3. Geological sketch of country rock distribution
- I.4. Principal rock types in the Central Bohemian Pluton
- I.5. Petrochemical classification of the Central Bohemian Pluton (*Holub, 1992*)
- I.6. Standard plotting symbols

Chapter II.

- II.1. Map of the Sázava and Požáry intrusions, including the main bodies of the associated basic rocks and the adjacent rock units
- II.2. Map of the Kozárovec (including Těchnice) intrusion and adjacent rock units
- II.3. Map of the Blatná (including Červená) intrusion and adjacent rock units
- II.4. Map of the Sedlčany intrusion and adjacent rock units
- II.5. Map of the Říčany intrusion and adjacent rock units
- II.6. Disrupted syn-plutonic dykes, Teletín
- II.7. Syn-plutonic dykes from Cortes Island, British Columbia
- II.8. Double enclave, Shap granite, Cumbria, England
- II.9. Intrusion of syn-plutonic dykes and origin of the 'enclave trains'
- II.10. Net-veining of the Kozárovec quartz monzonite by the surrounding granodiorite; Kozárovec II
- II.11. The IUGS Q - A - P ternary plot for classification of magmatic rocks
- II.12. Sketches of analysed mantled plagioclases, Sázava intrusion (including Teletín quartz diorite)
- II.13. An content across mantled plagioclase, Teletín quartz diorite
- II.14. Sketches of analysed plagioclases, Požáry intrusion
- II.15. Sketches of the analysed plagioclases, Kozárovec intrusion
- II.16. Zoned pseudomorphs of hornblende and actinolite + biotite after pyroxene, Kozárovec granodiorite
- II.17. Variation in An and Or from margin to core of zoned plagioclase, Kozárovec granodiorite
- II.18. Variation in An across the zoned plagioclase, Kozárovec quartz monzonite
- II.19. Variation in An and Or across oscillatory zoned plagioclase, Blatná granodiorite
- II.20. Sketches of analysed plagioclases, Sedlčany granite
- II.21. Sketches of analysed feldspars, Říčany granite

Chapter III.

- III.1.1. Composition feldspars from the Sázava (quartz diorite to tonalite), Požáry (trondhjemite) and Teletín (quartz diorite) in the Or - Ab - An ternary
- III.1.2. Classification of Sázava and Požáry biotites in the $100 \text{ Fe}^*/(\text{Fe}^* + \text{Mg})$ versus Al^{IV} diagram

- III.1.3. Position in the IMA classification of amphiboles from the Sázava intrusion (including the Teletín quartz diorite)
- III.1.4. Al^{IV} versus ΣAl plot of amphiboles, Sázava intrusion
- III.1.5. Scan across a zoned amphibole, Teletín quartz diorite
- III.1.6. Composition of the Kozárovec feldspars in the Or - Ab - An ternary diagram
- III.1.7. Classification of the Kozárovec biotites in the $100 Fe^*/(Fe^*+Mg)$ versus Al^{IV} diagram
- III.1.8. Position of the Kozárovec amphiboles in the classification diagram of *Leake (1978)*
- III.1.9. Al^{IV} versus ΣAl plot of amphiboles, Kozárovec intrusion
- III.1.10. Composition of the Blatná feldspars in the Or - Ab - An ternary diagram
- III.1.11. Classification of the Blatná biotites in the $100 Fe^*/(Fe^*+Mg)$ versus Al^{IV} diagram
- III.1.12. Position of the Blatná amphiboles in the classification diagram of *Leake (1978)*
- III.1.13. Al^{IV} versus ΣAl plot of amphiboles, Blatná intrusion
- III.1.14. Composition of the Sedlčany feldspars in the Or - Ab - An ternary diagram
- III.1.15. Classification of the Sedlčany biotites in the $100 Fe^*/(Fe^*+Mg)$ versus Al^{IV} diagram
- III.1.16. Position of the Sedlčany amphiboles in the classification diagram of *Leake (1978)*
- III.1.17. Composition of the Říčany feldspars in the Or - Ab - An ternary diagram
- III.1.18. Classification of the Říčany biotites in the $100 Fe^*/(Fe^*+Mg)$ versus Al^{IV} diagram
- III.2.1. Summary of biotite classification, Central Bohemian Pluton
- III.2.2. Composition of biotites, Central Bohemian Pluton
- III.2.3. Summary of classification of analysed amphiboles, Central Bohemian Pluton
- III.2.4. Position of studied amphiboles in diagram of *Giret et al. (1980)*
- III.2.5. Chemical variation of calcic amphiboles, Central Bohemian Pluton
- III.2.6. 'Aluminium in hornblende' geobarometry, as applied to amphiboles from the Central Bohemian Pluton

Chapter IV.

- IV.1.1. AFM plot
- IV.1.2. Q'-ANOR classification diagram; after *Streckeisen and Le Maitre (1979)*
- IV.1.3. Harker plots for the Sázava suite
- IV.1.4. Harker plots for the Blatná suite
- IV.1.5. Harker plots for the Čertovo břemeno suite
- IV.1.6. Harker plots for the Říčany suite
- IV.1.7. Plot of Shand's index (A/CNK vs. A/NK)
- IV.1.8. ACF plot
- IV.1.9. Major element characteristics of granitoids from the CBP
- IV.1.10. $CaO - Na_2O - K_2O$ ternary diagram
- IV.1.11. P - Q ("nomenclature") diagram of *Debon and Le Fort (1983, 1988)*
- IV.1.12. The B - A ("characteristic minerals") plot of *Debon and Le Fort (1988)*
- IV.1.13. Plot of B versus $Mg/(Fe+Mg)$ of *Debon and Le Fort (1988)*
- IV.1.14. The Q - B - F diagram (quartz - dark minerals - feldspars)
- IV.1.15. Classification of aluminous associations using B as function of Q and $K/(Na+K)$
- IV.2.1. Bivariate plots of SiO_2 vs. trace elements for the Sázava suite

-
- IV.2.2. Bivariate plots of SiO₂ vs. trace elements for the Blatná suite
 - IV.2.3. Bivariate plots of SiO₂ vs. trace elements for the Čertovo břemeno suite
 - IV.2.4. Bivariate plots of SiO₂ vs. trace elements for the Říčany suite
 - IV.2.5. Trace element composition range of selected intrusions
 - IV.2.6. Rb versus Sr diagram for the rocks of the CBP
 - IV.2.7. K versus Rb diagram for the rocks of the CBP
 - IV.2.8. Diagrams showing the distribution of some of the HFSE and transition metals in individual suites of the Central Bohemian Pluton
 - IV.2.9. Variation in Zr content of melts and restites with degree of melting of a crustal source
 - IV.2.10. Rare Earth Elements patterns for the Sázava and Blatná suites
 - IV.2.11. Rare Earth Elements patterns for the Čertovo břemeno and Říčany suites
 - IV.2.12. Comparison of Rare Earth Element patterns for the Blatná, Čertovo břemeno and Říčany suites

 - IV.3.1. Plot of R₁ versus R₂ values of *De la Roche et al. (1980)* (after *Batchelor and Bowden, 1985*) (petrogenetic implications)
 - IV.3.2. Mixing test for the Teletín quartz diorite
 - IV.3.3. REE modelling for the Sázava suite
 - IV.3.4. Fractional crystallization modelling for the Blatná suite (Blatná s.s., Červená, Kozárove, Těchnice)
 - IV.3.5. Mixing tests for the Blatná suite
 - IV.3.6. REE modelling for the Blatná suite
 - IV.3.7. Fractional crystallization modelling for the Sedlčany granite
 - IV.3.8. Mixing test for the Čertovo břemeno and Říčany suites
 - IV.3.9. Fractional crystallization modelling for the Říčany granite
 - IV.3.10. Binary plots showing the inverse nature of the zoning in the Říčany granite
 - IV.3.11. Cartoon illustrating one of the possible scenarios for the origin of reversely-zoned plutons: the Lacome Complex, Québec
 - IV.3.12. Possible origin of the reverse zoning in the Říčany intrusion

 - IV.4.1. Tectonic discrimination of granitoids of the CBP (after *Maniar and Piccoli, 1989*)
 - IV.4.2. The tectonic discrimination of granitoids of the CBP (after *Maniar and Piccoli, 1989*)
 - IV.4.3. Plot of R₁ versus R₂ values of *De la Roche et al. (1980)*, after *Batchelor and Bowden (1985)* (geotectonic implications)
 - IV.4.4. Tectonic classification of granitoids of the CBP (after *Pearce et al., 1984*)
 - IV.4.5. Tectonic discrimination of potassic rocks of the CBP (*Müller et al., 1992*)
 - IV.4.6. Ocean Ridge Granite normalised spiderdiagrams for the Central Bohemian Pluton
 - IV.4.7. Ocean Ridge Granite normalised spiderdiagrams for the Central Bohemian Pluton
 - IV.4.8. A-type discrimination diagrams
 - IV.4.9. Rb - Hf - Ta triangular plot for tectonic environment discrimination (after *Harris et al., 1986*)
-

Chapter V.

- V.1. Derivation of the two-stage model Nd age
- V.2. Diagram illustrating why the Nd model ages of rocks from mixed sources do not correspond to crust-formation events
- V.3. $(^{87}\text{Sr}/^{86}\text{Sr})_{330}$ versus $\epsilon_{\text{Nd}}^{330}$ plot of the granitoids of the CBP and their country rocks
- V.4. Comparison of the $(^{87}\text{Sr}/^{86}\text{Sr})_i$ versus ϵ_{Nd}^i data for other Hercynian granitoids and lamprophyres with data for the granitoids of the CBP
- V.5. $1/\text{Sr}$ versus $(^{87}\text{Sr}/^{86}\text{Sr})_{330}$ plot of rocks of the CBP and their country rocks, together with the data for granitoids from the Moldanubian Pluton
- V.6. Compilation of two-stage depleted mantle Nd model ages for granitoids from the European Hercynides
- V.7. Schematic model for the origin of the Sázava suite
- V.8. Modelling of a simple binary mixing for the rocks of the Blatná suite

Chapter VII. (Appendices)

- VII.1. Location of samples, Central Bohemian Pluton
- VII.2. Comparison between Zr concentrations determined using the XRF and ICP-MS techniques
- VII.3. Typical session with the programme BTRAP: main menu, the model calculations and the isochron plot
- VII.4. Example of a session with the programme NORMAN: main menu, and two output screens for the calculations after *Debon and Le Fort (1989)*
- VII.5. Listing of one of the standard functions of the programme NORMAN (LAROCHE.EXE)
- VII.6. Example of an user-defined function of the programme NORMAN for calculating the Q'-ANOR parameters of *Streckeisen and Le Maitre, 1979* (PKC.DEF)

PHOTOGRAPHS (Chapter II.)

- II.1.1. - II.1.8. Sázava intrusion(1): field photographs
- II.1.9. - II.1.16. Sázava intrusion (2): microscopy
- II.1.17. - II.1.20. Sázava intrusion (3): cathodoluminescence
- II.1.21. Sázava intrusion (4): cathodoluminescence
- II.2.1. - II.2.3. Požáry intrusion: cathodoluminescence
- II.3.1. - II.3.7. Kozárovec intrusion (1): field photographs
- II.3.8. - II.3.15. Kozárovec intrusion (2): microscopy & Kozárovec quartz monzonite
- II.3.16. - II.3.19. Kozárovec intrusion (3): cathodoluminescence
- II.4.1. - II.4.7. Blatná intrusion (1): field photographs
- II.4.8. - II.4.15. Blatná intrusion (2): microscopy
- II.4.16. - II.4.23. Blatná intrusion (2): microscopy
- II.5.1. - II.5.8. Sedlčany intrusion (1): field photographs and photomicrographs
- II.5.9. - II.5.12. Sedlčany intrusion (2): orthite
- II.5.13. - II.5.16. Sedlčany intrusion (3): cathodoluminescence
- II.6.1. - II.6.4. Říčany intrusion (1): field and microphotographs
- II.6.5. - II.6.8. Říčany intrusion (2): cathodoluminescence
- II.7.1. - II.7.4. Čertovo břemeno intrusion: field photographs

6. List of tables

Chapter I.

- I.1. Main subdivision schemes, Central Bohemian Pluton

Chapter II.

- II.1. Modal data, Central Bohemian Pluton
II.2. Traverse across mantled plagioclase, Teletín quartz diorite (SaD-1)
II.3. Traverse across zoned plagioclase, Kozárovice granodiorite (Koz-2)
II.4. Traverse across zoned plagioclase, Kozárovice quartz monzonite (KozD-1)
II.5. Traverse across oscillatory zoned plagioclase, Blatná granodiorite, Hudčice (Bl-8)

Chapter III.

- III.1. Geothermobarometry for the Sázava intrusion (including the Teletín quartz diorite) - (lower P-T assemblage)
III.2. Geothermobarometry for the Teletín quartz diorite - (higher P-T assemblage)
III.3. Geothermobarometry for the Kozárovice intrusion
III.4. Geothermobarometry for the Blatná intrusion

Chapter IV.

- IV.1. HFSE content of particular rocks suites, CBP
IV.2. Zircon saturation calculations (*Watson and Harrison, 1983*)
IV.3. REE content of particular rock suites, CBP
IV.4. Trace element partition coefficients used for modelling
IV.5. Least-squares modelling; major elements, Sázava suite
IV.6. Least-squares modelling; major elements, Blatná suite
IV.7. Least-squares modelling; major elements, Sedlčany granite
IV.8. Theoretical compositions of two end-members of the Bohemian durbachite suite (*Holub, 1990*) compared to an analysis of the Říčany granite

Chapter V.

- V.1. Sr-Nd isotopic data, Central Bohemian Pluton and its country rocks

I. Introduction

I.1. Geological setting

The Bohemian Massif is, after the French Massif Central, the second largest outcrop of the Hercynian belt in Europe (90 000 km², *Matte et al.*, 1990). Within it, the boundary between two major units, the Teplá-Barrandian Unit in the NW and the Moldanubian (s.s.) Unit in the SE, has been intruded by granitoids of the Central Bohemian Pluton (CBP) that forms a composite NE - SW-trending body, stretching for almost 150 km from near Prague to Klatovy and covering about 3200 km² (*Kodým*, 1966) [Figs I.1., I.3.]. This Pluton is extremely variable in composition, with masses of gabbro, diorite, quartz monzonite, tonalite, trondhjemite, granodiorite and granite within it. In addition there are (melanocratic) syenites to melagranites, with many mafic types corresponding to rocks of the durbachite suite of classic occurrences in the Black Forest, Germany.

The contact of the Pluton with the dominantly metasedimentary Teplá-Barrandian Unit is sharp, with strong thermal metamorphism, whereas the contact with the also mainly metasedimentary Moldanubian Unit is bordered in many parts by a zone of intense migmatization of the adjacent paragneisses, and has been interpreted as representing a deeper level of intrusion (*Kodým*, 1966). The relation of both units to one another is not clear, but the NE - SW elongation of the CBP appears to follow an important tectonic zone, which is marked by a steep gravity gradient between generally positive Teplá-Barrandian and negative Moldanubian units (*Marek and Palivcová*, 1968; *Blížkovský et al.*, 1988). This Central Bohemian Suture (*Máška and Zoubek*, 1960; Central Bohemian Deep-Seated Weakened Zone: *Zeman*, 1978; Central Bohemian Shear Zone: *Rajlich*, 1990) [Fig. I.2.] consists of the NE - SW-trending Klatovy and Benešov deep-seated faults, which are offset by the NW - SE-trending Sázava and Jáchymov deep faults (*Blížkovský et al.*, 1988; cf. *Marek and Palivcová*, 1968). An alternative interpretation is that it represents a ramp region in a major shear zone complex that exerted a major control on the emplacement of the Central Bohemian Pluton (*Košler*, 1993). This emplacement model envisages intrusion of magma as large-scale sheets into mainly steep parts of a ductile extensional shear zone, in a manner similar to that described by *Hutton et al.* (1990).

The Teplá-Barrandian Unit consists mainly of Lower Brioverian weakly-metamorphosed sediments (greywacke, siltstone and shale) intercalated with dark shale and chert and locally also with abundant volcanic and volcanoclastic rocks (tholeiitic basalts and low-K calc-alkaline Na-rhyolites, dacites and andesites). The Lower Brioverian assemblage is overlain by Upper Brioverian flysch without volcanic rocks (*Chaloupský*, 1989). On these Precambrian rocks unconformably rest unmetamorphosed Palaeozoic pelitic and carbonate sediments of the Barrandian s.s. (Cambrian to mid-Devonian) (*Kukal*, 1994). The Givetian siliciclastic termination of the mainly carbonate Devonian sedimentation in the Barrandian s.s. has the characteristics of a flysch assemblage and its existence is indicative of tectonic instability immediately prior to the Hercynian orogenesis (*Kukal, loc.cit.*).

The Moldanubian Unit is a tectonic assemblage of medium- to high-grade metamorphic rocks, intruded by numerous granitoid masses and has been subdivided into a structurally lower Drosendorf Unit and overlying Gföhl Unit (*Franke*, 1989). The Drosendorf Unit consists of the (lower) Monotonous Group (or Unit) made up mainly of paragneisses with migmatites, and the (upper) Varied Group (or Variegated Unit) of paragneisses with intercalations of amphibolite, calc-silicate gneiss, quartzite, graphite schist and carbonate rock (*Chaloupský*, 1989). The Gföhl Unit which occurs on the flanks of a major NE-trending antiform, now mainly occupied by the CBP (*Franke*, 1989) consists of

anatectic gneiss, granulite, serpentinite and high-grade mafic rocks. Overall, the Moldanubian Unit is a tectonic assemblage made up of several crustal segments of contrasting age ranging from ~ 2 Ga to Lower Palaeozoic but the overall picture has yet to be established because of a complex polyphase deformational history (cf. *Vrána, 1994* and references therein).

In the roof of the Central Bohemian Pluton, there is an 80 km long belt in which remnants of the metamorphic mantle (so-called Metamorphic Islet Zone) are preserved. The metamorphic islets [M.I.; Fig. I.3.] represent roof pendants of the CBP. The principal rock types in them are Proterozoic to Palaeozoic (up to lower - ? mid Devonian in the Sedlčany-Krásná Hora Metamorphic Islet: *Chlupáč, 1988*) metasediments (pelites, psammites, calc-silicate rocks, marbles) and metavolcanic rocks, all of them affected by dynamothermal and parts also by thermal metamorphism. In the Mirovice and Sedlčany-Krásná Hora Metamorphic Islets there are tonalitic - granodioritic orthogneisses (Mírotice and Staré Sedlo complexes) that represent tectonothermally modified products of granitoid plutonism of mid - late Devonian age (*Košler, 1993; Košler et al., 1993*).

In addition to the Metamorphic Islet Zone, the roof pendants of the CBP include the Jílové Zone, a belt of deformed and metamorphosed Precambrian volcanic and volcanogenic rocks, that extends from Jílové for 60 km south-westwards [Fig. I.3.]. This zone consists of tholeiitic and high-alumina calc-alkaline basalts, andesites, trachyandesites, basaltic trachyandesites, dacites, rhyolites and boninites (*Waldhausrová, 1984; Fediuk, 1992 a,b*) intruded by tonalites, trondhjemites, diorites and gabbros. Two assemblages have been distinguished, the older being tholeiitic and of island-arc character whereas the younger is calc-alkaline in character and has affinities to an active continental margin setting (*Waldhausrová, loc.cit.*). The volcanic rocks of the Jílové Zone and Teplá-Barrandian Unit show many comparable features (*Svoboda, 1966*).

I.2. Main rock units and their distribution

There exists an extensive geological bibliography related to the Central Bohemian Pluton. Apart from numerous specific papers (referred to in the relevant chapters of this thesis), some of the publications review the CBP as a whole but most deal only with the petrology, although a small number deal with the geochemistry as well. They include *Orlov (1928, 1934, 1935, 1938)*, *Štěpánek (1930)*, *Kettner (1930)*, *Svoboda (1932)*, *Palivcová (1965)*, *Steinöcher (1969)*, *Vejnar (1973, 1974a)*, *Tauson et al. (1977)*, *Minařík et al. (1979)*, *Rajlich and Vlašimský (1983)*, *Bouška et al. (1984)*, *Palivcová (1984)*, *Machart (1989, 1992)*, *Palivcová et al. (1989a, 1989b)*, *Holub (1989a, 1992)* and *Vlašimský et al. (1992)*. References to other studies are also listed in these publications. Many internal features and relationships of intrusions to other rocks are recorded in these papers and the significance of these observations is reviewed in Chapter II. The geochemical data are integrated with petrography and their significance assessed in Chapters III-V. However much of the presently published geochemical data is for major elements: only a few sets of trace element data are given and no isotopic data are available on which petrogenetic modelling could be based.

Many petrographic types have been recognised in the CBP and these have been mainly named after major centres of quarrying (Kozárovce, Blatná, Sedlčany, Nečín, Požáry) or the nearest town or village (e.g. Benešov, Klatovy); a few have been named after a prominent topographic feature (Sázava - a river; Čertovo břemeno, the Devil's Burden - a hill) or position in the Pluton (Marginal). In all, the granitoids of the CBP have been divided into more than 20 major intrusions (e.g. *Kodym, 1966*).

[Fig. I.4.]. In addition, dozens of other names exist, either for minor intrusions or simply as a continuation of historical tradition.

Much of the northern part of the CBP is formed of the irregularly-shaped mass of the Sázava tonalite [Fig. I.4.], together with the smaller generally circular intrusions of the Říčany granite and the Požáry trondhjemite. The Říčany intrusion is cut by the Jevany leucogranite and the central part of the Sázava body is penetrated by the Mrač granite [see Figs II.1, II.5]. The southern contact of the Sázava intrusion is rimmed by the Maršovice granodiorite, whereas in the east it is in contact with so-called Benešov type [Chapter II].

In the central part, granodiorite is the dominant rock type and makes up most of the Kozárovec, Těchnice, Blatná and Nečín intrusions. The Kozárovec granodiorite [Fig. II.2.] encloses a minor body of the Zalužany quartz monzonite and the adjacent Mirovice Metamorphic Islet is cut by several stocks of the Lučkovice monzonite - monzogabbro.

In the south, the Blatná granodiorite [Fig. II.3.] is rimmed by the Červená granodiorite that sends numerous apophyses into the adjacent high-grade metasediments of the Moldanubian Unit. In the southwest, the so-called Klatovy apophysis is formed by SW - NE elongate intrusions of the Klatovy and Kozlovice granodiorites, as well as the Marginal type granite, the latter extending further northeastwards where it forms a narrow rim of the contact of the CBP against the Teplá-Barrandian Unit.

In the eastern part of the CBP are the ellipsoidal-shaped body of the Sedlčany granite, the oval-shaped (with eastwards-pointing Votice apophysis) Čertovo břemeno melagranite ('durbachite') and the roughly circular intrusion of the Tábor syenite. The central part of the Sedlčany intrusion is penetrated by a minor intrusion of the Kosova Hora granodiorite [Fig. II.4.], whereas the eastern contact of the Čertovo břemeno intrusion is rimmed by granodiorite that in literature was referred to as Dehetník type.

Apart from the above-mentioned major granitoid masses, there are also numerous minor bodies of basic rocks (mainly gabbros; black on Fig. I.4.) and leucogranites, which are too small to be shown on the maps.

Details concerning the petrography and field relations of the main intrusive masses are given in Chapter II. A summary of main subdivision schemes is given in Table I.1, while the subdivision of Holub (1992), based on major element geochemistry, is shown on Figure I.5.

1.3. Age

From the following geological evidence the age of the Central Bohemian Pluton is established to be Early Carboniferous.

(1) Granitoids of the CBP (the Sedlčany and Čertovo břemeno intrusions) caused contact metamorphism of the Sedlčany-Krásná Hora Metamorphic Islet in which there are present sediments as young as lower - ?mid Devonian (Afanasyev *et al.*, 1977; Chlupáč, 1988). The Čertovo břemeno intrusion cuts the foliation of the adjacent Staré Sedlo orthogneisses, whose protolith has been dated at 380 - 365 Ma (U-Pb, zircon; Košler *et al.*, 1993) and whose age of cooling after the ductile deformation (Rb - Sr biotite - whole-rock) is ca. 340 - 330 Ma (Košler, 1993), i.e. early Carboniferous (Visean; Harland *et al.*, 1990).

(2) The CBP is affected by a number of near-vertical planar, generally weak features, variably expressed by weak fracture cleavage, alteration, silicification or haematite growth (Gruntorád *et al.*,

1988). There are also NW-trending faults. The orientation of some of these planar features corresponds with weak cleavages associated with upright folds recognised in Western Bohemia and interpreted as representing the effects of "later" phases of deformation in the Hercynian orogenic belt (Bowes *et al.*, 1994; D.R. Bowes, *pers.com.*, 1994).

(3) Upper Carboniferous (Stephanian C) and Permian (Autunian) sediments (*Working Group for Regional Geological Classification of the Bohemian Massif*, 1994) of the Blanice Furrow onlap the north-eastern part of the CBP (Říčany granite) and their basal conglomerates contain boulders of this granite (Kodym, 1925; Kašpar, 1936; Steinocher, 1969; Afanasjev *et al.*, 1977).

Overviews of the geochronological information on the CBP itself have been given in Steinocher (1969), Bernard and Klomínský (1975), Afanasjev *et al.* (1977), Dubanský (1984), and Dudek *et al.* (1988). The earliest geochronological data were obtained by the K-Ar method (Šmejkal 1960, 1964; Pudilová 1968; Pudilová and Dubanský, 1969; Steinocher, 1969; Afanasjev *et al.*, 1977). Despite the low accuracy of the majority of these data, the K-Ar ages would date the cooling and uplift, not the emplacement of the CBP [for more detailed discussion, see Appendix IX.].

The Rb-Sr whole-rock method has so far been applied only to the Blatná granodiorite (van Bremen *et al.*, 1982; Bendl, 1988; Bendl and Vokurka, 1989) and the Říčany granite (Janoušek, 1991), producing only a single isochron, with the age of 331 ± 4 Ma (van Bremen *et al.*, 1982) that provides an lower limit of the crystallization age [Appendix IX.].

Despite the dearth of accurate geochronological information, it could be concluded that the majority of intrusions are Early Carboniferous (also e.g. Steinocher, 1969; Afanasjev *et al.*, 1977), with the available evidence pointing to magmatic activity at ~ 330 Ma.

1.4. Objectives of thesis

Although there is extensive bibliography concerned with granitoids of the CBP, there is still only limited geochemical data and practically no work integrating, in a coherent way, field petrography, microstructural study and geochemistry. Moreover, there is only a limited amount of Sr isotope data and no Nd isotope data for the CBP. Thus this thesis approaches the petrogenesis of the CBP on the basis of a large body of new major, trace, REE and isotopic data. However, meaningful use of such data is only possible on the basis of detailed information relating to the geological position and petrographic nature of the analysed material. Accordingly, the main objectives of this thesis include:

- (1) to critically evaluate field and petrographic information concerning the variability and relative age of different granitoid masses,
- (2) to demonstrate variations in petrography, mineral chemistry, whole-rock geochemistry and whole-rock Sr - Nd isotope geochemistry of the CBP using some of the larger intrusions covering much of the overall time-span and geochemical variability (Blatná, Červená, Kozárovce, Požáry, Říčany, Sázava, Sedlčany and Těchnice),
- (3) to establish criteria for distinguishing cognate groups of intrusions and separating these from others, and
- (4) to formulate a genetic model accounting for the observed variations.

Accordingly, the overall content of the forthcoming chapters is as follows.

II. Field relations and petrography

This chapter provides an overview of information on contacts, enclaves, dykes and other features seen in the field and of textural and mineralogical variation, particularly as shown by microscopic study, together with their implications on the relative age and subdivision of the CBP. The petrographic criteria influenced directly the choice of samples for the further geochemical (especially ICP-MS) and Sr - Nd isotope study. The detailed study of the field relations as well as petrography are considered to provide a firm foundation for interpretation of the geochemical data.

Apart from standard petrographic techniques, cathodoluminescence (CL) has also been employed, as it can reveal otherwise hidden zoning patterns of minerals, caused by either crystal growth or magma mixing. Additionally, it clearly shows the distribution of accessory minerals such as apatite and is beneficial in studying the effects of deformation and alteration processes (e.g. leaching of feldspars, growth of secondary clay minerals, and, in particular, of calcite) (*Marshall, 1988; Wenzel and Ramseyer, 1992*). Particular attention has been paid to the plagioclase zoning ('plagioclase stratigraphy'), disequilibrium phenomena (presence of xenocrysts and reaction textures) and alteration. To save much cross-referencing, the data on zoning patterns of plagioclase obtained using the electron microprobe are given here rather than in the next chapter.

III. Mineral chemistry

In this chapter a summary of variation in mineral chemistry of the rock forming minerals is given, followed by a grouping of the intrusions according to observed similarities.

IV. Whole-rock geochemistry

The fourth chapter focuses on the character of the major and trace element geochemistry as well as similarities and differences in composition of investigated granitoids. The aim is to group the studied intrusions into suites with similar geochemical signatures, and, consequently, to be in a position to study the variability, classification and geotectonic affiliations of these suites. This chapter deals with geochemical modelling of processes modifying the magma during ascent and emplacement, notably assimilation and fractional crystallization (AFC), based on the whole-rock geochemistry.

V. Sr-Nd isotope geochemistry and petrogenetic implications

The fifth chapter concentrates on the Sr and Nd isotope signatures of samples from the intrusions investigated and discusses intra- and inter-suite variability as well as genetic implications. The results are compared with data for other granitoids of the Hercynian belt in Europe. At the end of this chapter the results of the various lines of study are integrated to establish a genetic model for the individual intrusions, cognate geochemical suites, and the CBP overall.

VI. Conclusions

This chapter provides a summary of main conclusions.

VII. Appendix

In the Appendix are given a list of samples [Appendix I], followed by a description of analytical techniques [Appendix II], tables of the whole-rock geochemical data [Appendix III-V], mineral chemistry [Appendix VI-VIII] concluding with remarks on geochronology of the CBP [Appendix IX].

IX. References

As shown above, these main chapters are numbered by Roman numerals, whereas their sections are numbered by Arabic ones (as VL3.4.). There is corresponding labelling for tables [Tab. III.3.], photographs [Photo VL3.] and figures [Fig. VII.5.], which are presented at the end of each of the major chapters. If not stated otherwise, the symbols for particular rock types in various plots are the standard ones and can be found in Figure L.6. and again as fold out sheets in the end of Chapters III. and IV.

Table I.1: Main subdivision schemes, Central Bohemian Pluton
[see Figs 1.4. and 1.5.]

<i>Palivcová (1965)</i>		
I.	Dark, mostly porphyritic, frequently foliated "durbachitic", granodioritic, syenodioritic to syenitic types	Čertovo břemeno, Dehetník, Červená, Tábor
II.	Mainly fine-grained predominantly biotite-carrying granitoids, specified as "hybrid rocks"	Kozlovice, Maršovice, Kosova Hora, Benešov
III.	Medium-grained grey granitoids of the "normal type"	Blatná, Kozárovice, Těchnice, Sázava, Klatovy, Sedlčany
IV.	Light-coloured biotite granitoids, mostly coarse-grained and porphyritic	Požáry, Marginal, Říčany
V.	'Acid granites' (i.e. leucogranites)	
VI.	Basic rocks	
<i>Steinöcher (1969)</i>		
I.		Sázava, 'Vltava' (i.e. Kozárovice), gabbros and related mafic rocks, Požáry, Blatná, Nečín
II.	1	Benešov, Klatovy
	2	Říčany, Maršovice, Těchnice, leucogranites
	3	Kosova Hora, Marginal, Kozlovice
III.		Tábor, Čertovo břemeno, Sedlčany
		Červená, Dehetník
<i>Vejnar (1974a)</i>		
A	1	Benešov (melanocratic), Červená, Sedlčany
	2	Sázava (including Kozárovice and Těchnice)
	3	Blatná, Klatovy
B	1	Marginal, Říčany, Jevany, leucogranites
	2	Těchnice, Benešov (rest), Kosova Hora
	3	Požáry, Nečín
C		Čertovo břemeno, Tábor
D		basic rocks
<i>Afanasjev et al. (1977)</i>		
I.	Durbachites	Tábor, Čertovo břemeno, etc.
II.	Gabbros, tonalites and granodiorites	Sázava, Blatná, etc.
III.	Granodiorites-granites	Marginal, Říčany, Požáry etc.
IV.	Hybrid fine-grained granitoids	Kozlovice, Benešov, Mrač etc.
<i>Holub (1992)</i>		
I.	Sázava type and associated basic rocks	Sázava and associated basic rocks
II.	Main granodiorite types of the central and southern part of the CBP and associated monzonitic rocks	Kozárovice, Těchnice, Červená, Blatná, Klatovy, Marginal, Zalužany, Lučkovice
III.	Perpotassic lamproid plutonic rocks	Čertovo břemeno, Tábor
IV.	Ca-poor granitoids with an affinity to the lamproid rocks	Sedlčany, Říčany
V.	Ca-poor granitoids with strong metasedimentary contribution	Kozlovice, Maršovice, Kosova Hora
VI.	Ca-rich acid granitoids	Požáry, Nečín

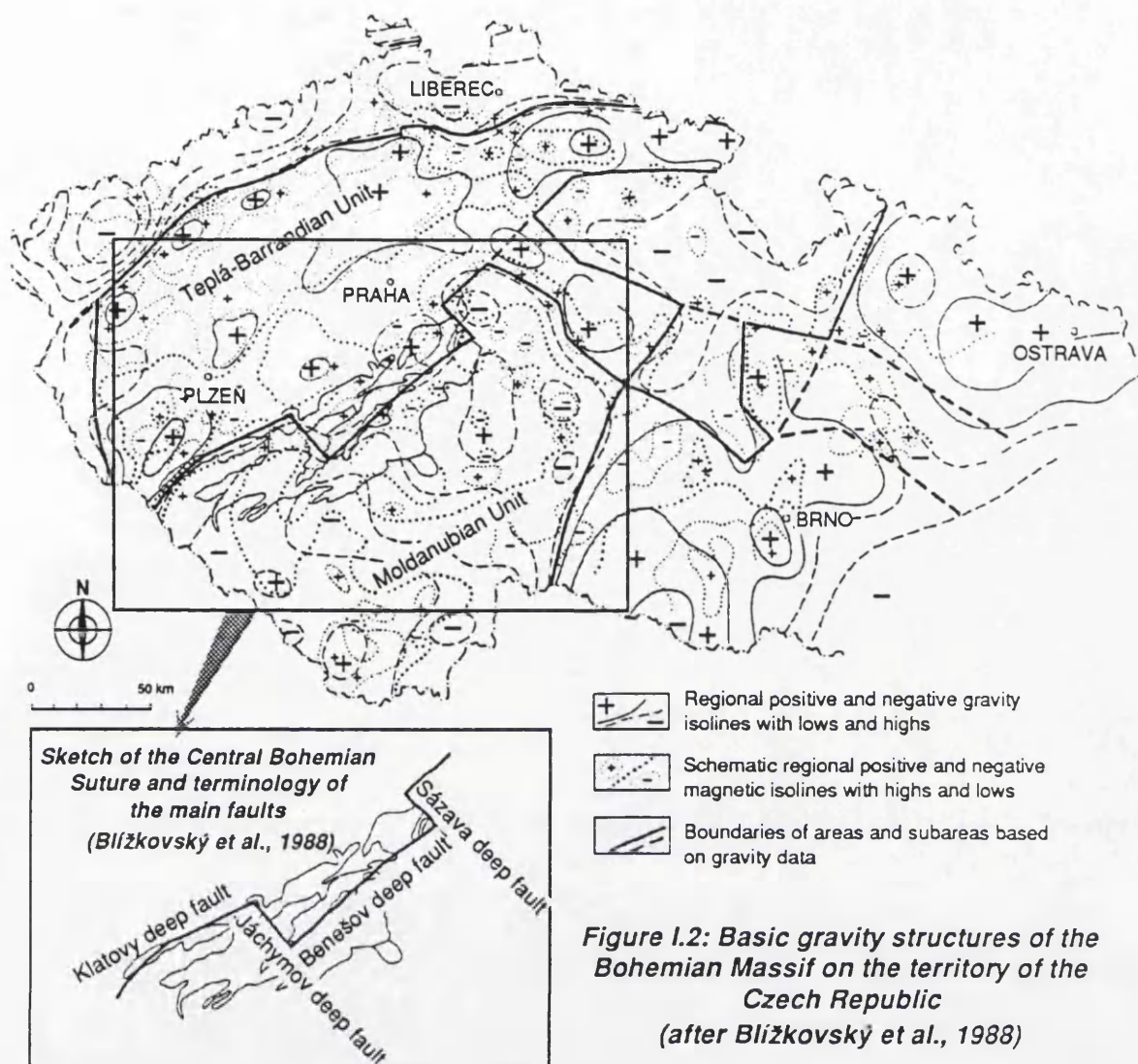


Figure I.3: Geological sketch of country rock distribution

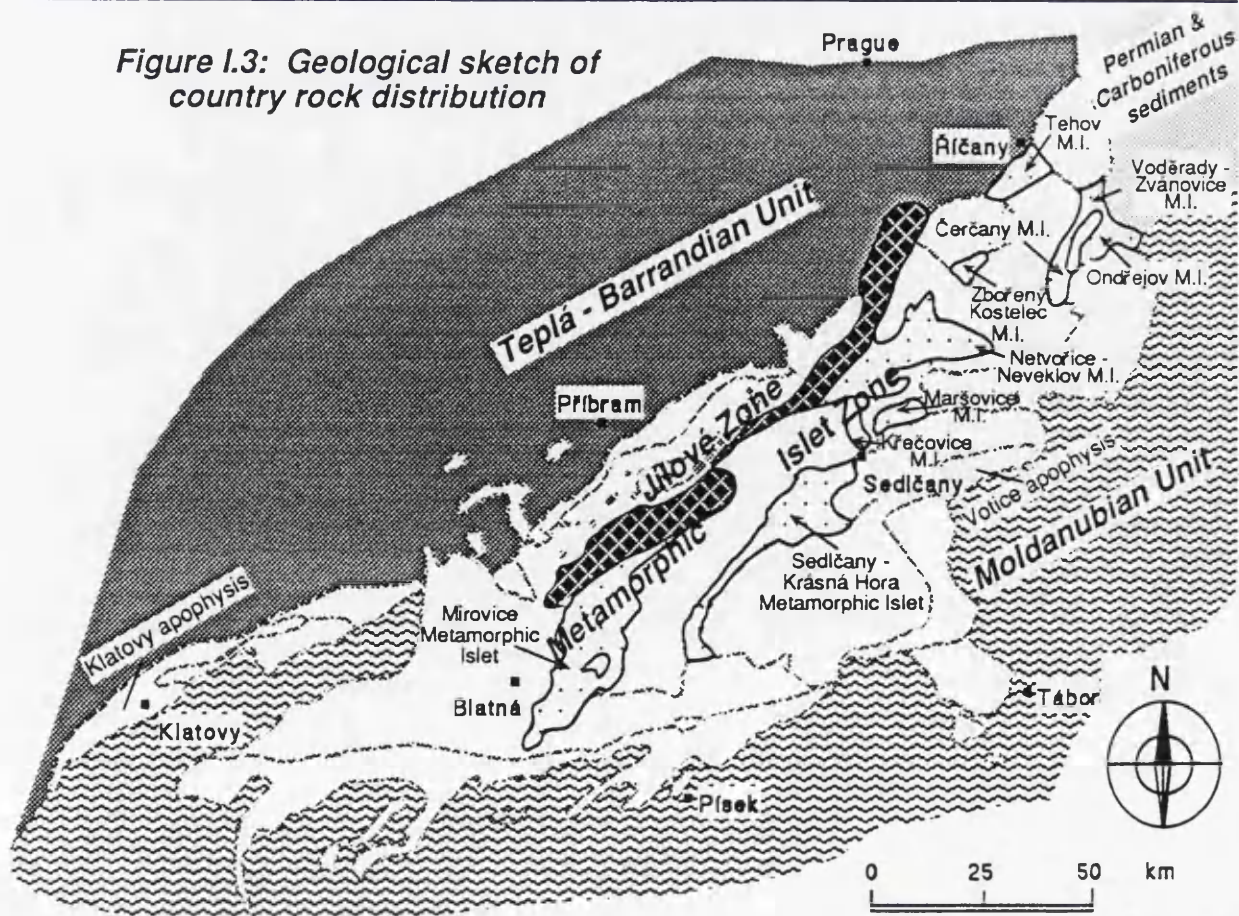


Figure I.4: Principal rock types in the Central Bohemian Pluton

Due to their small size, there are the additional rock types are shown by their initial letters as follows:

Jevany (J), Kosova Hora (K), Lučkovice (L),
Zalužany (Z), Mrač (M).

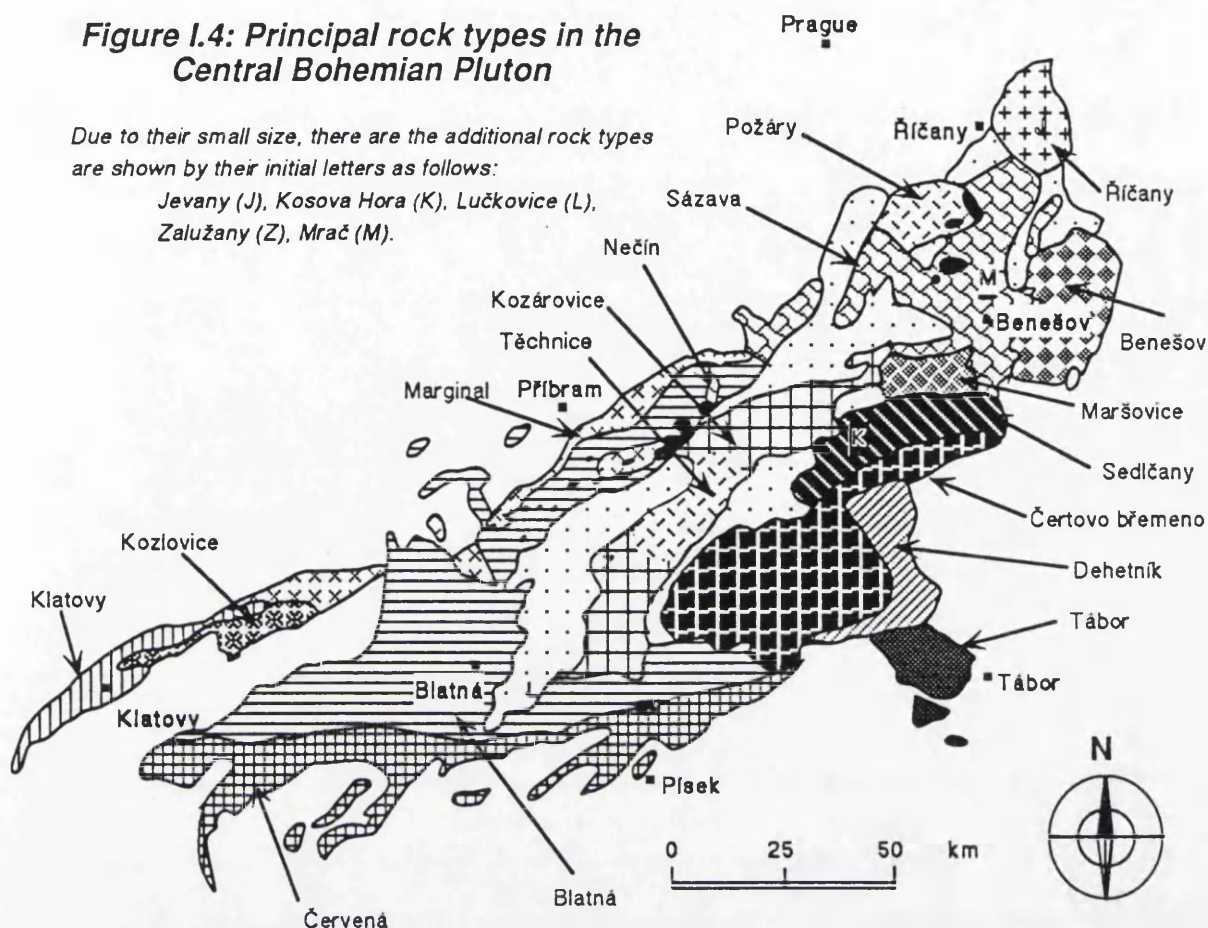

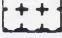

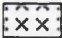


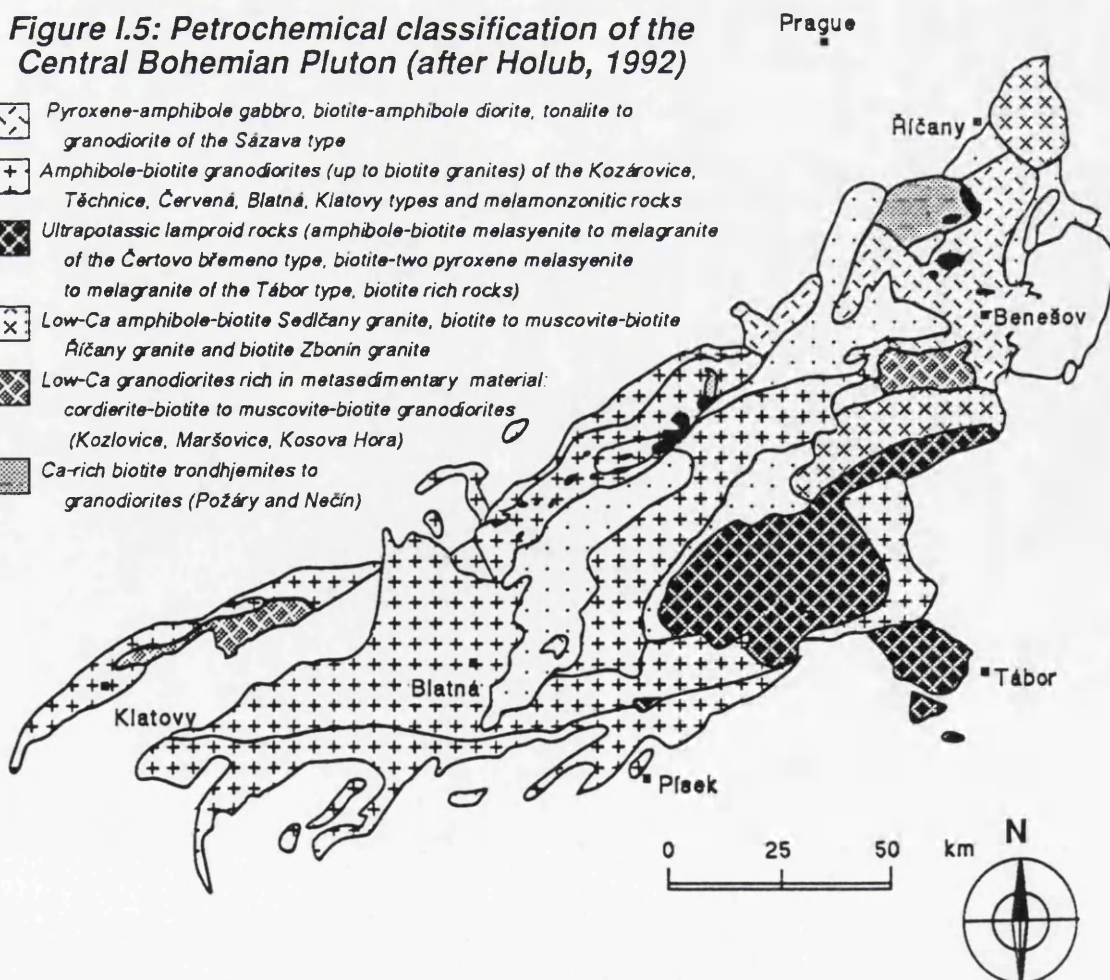


Figure I.5: Petrochemical classification of the Central Bohemian Pluton (after Holub, 1992)

-  Pyroxene-amphibole gabbro, biotite-amphibole diorite, tonalite to granodiorite of the Sázava type
-  Amphibole-biotite granodiorites (up to biotite granites) of the Kozárovce, Těchnice, Červená, Blatná, Klatovy types and melamonzonitic rocks
-  Ultrapotassic lamproid rocks (amphibole-biotite melasyenite to melagranite of the Čertovo břemeno type, biotite-two pyroxene melasyenite to melagranite of the Tábor type, biotite rich rocks)
-  Low-Ca amphibole-biotite Sedlčany granite, biotite to muscovite-biotite Říčany granite and biotite Zbonín granite
-  Low-Ca granodiorites rich in metasedimentary material: cordierite-biotite to muscovite-biotite granodiorites (Kozlovice, Maršovice, Kosova Hora)
-  Ca-rich biotite trondhjemites to granodiorites (Požáry and Nečín)



- Sázava suite:
 - ⊕ Sázava tonalite and quartz diorite
 - Basic rocks associated with Sázava intrusion
 - Teletín quartz diorite
 - Požáry trondhjemite and Nečín granodiorite
- Blatná suite:
 - ⊙ Mrač monzogranite
 - ◇ Kozárovice (s.s.) granodiorite
 - ⊕ Těchnice granodiorite (porphyritic Kozárovice)
 - ◇ Kozárovice quartz monzonite
 - ◇ Zalužany quartz monzonite
 - ◇ Lučkovice monzonite
 - Blatná (s.s.) granodiorite
 - Hudčice diorite
 - ▣ Červená granodiorite
 - ▣ Mafic microgranular enclave, Červená granodiorite
 - △ Klatovy granodiorite
 - ▽ Marginal monzogranite
- Čertovo břemeno suite:
 - Sedlčany monzogranite
 - Čertovo břemeno monzogranite to quartz syenite
 - ◆ Tábor quartz syenite
- Říčany suite:
 - + Říčany granite
 - × Jevany leucogranite
 - ◆ Mafic microgranular enclaves, Říčany intrusion

Figure I.6: Standard plotting symbols used throughout this thesis for particular intrusions (repeated at the end of Chapters III. and IV.)

II. Field relations and petrography

This chapter gives field and petrographic observations, both new and from the literature, relevant to the genetic interpretation of the granitoid masses being investigated. The approach is the same for the various intrusions, with the field data relating contact relationships (indicative of relative age) and internal characteristics, including the presence of atypical rock types and enclaves being preceded by a general outline of the nature of the particular intrusion and followed by petrographic data from microscopic study.

Following *Bates and Jackson (1987)*, rocks with average grain size < 1 mm are referred to as fine-grained, 1 - 5 mm as medium-grained and > 5 mm as coarse-grained. The nomenclature of enclaves follows that of *Didier and Barbarin (1991)*, with the term 'enclave' and 'megacryst' employed in a non-genetic sense, in contrast with 'xenolith' and 'xenocryst' that are used to refer to material that is foreign to the host magma. The observations are numbered (e.g. 3.VII.), with the number of the section (3 for the Kozárovec intrusion) and a Roman numeral for the particular observation. The names of localities are highlighted by expanded spacing (as K o z á r o v e c). For each intrusion, a geological map is provided [Figs II.1.-II.5.]. After the observations, major conclusions and interpretations are drawn with reference made to the number(s) of the relevant observation(s).

The microscopic descriptions given are mainly for the rock types used for isotope studies and petrogenetic modelling. In each description the first two paragraphs summarise the information on the modal data, classification, texture, mineral succession, alteration and deformation. The subsequent paragraphs deal with the main rock-forming minerals in detail in order of their decreasing abundance. Particular emphasis has been put on the intensity of the alteration processes, as this has directly affected the choice of the samples for the subsequent geochemical [Chapter IV.] and particularly the Sr - Nd isotope work [Chapter V.]. The next paragraph deals with the cathodoluminescence observations and concludes with brief characteristics of enclaves and related phenomena.

The modal composition of the samples has been obtained by point counting from standard thin-sections [Tab. II.1.], whose area, however, is much too small to be representative of rocks with phenocrysts as big as a few centimetres; for instance, the Ríčany granite would be classified as a quartz monzonite as the content of K-feldspar is clearly overestimated. Therefore, stained rock slabs or point counting directly on the outcrop (e.g. *Hutchison, 1974*) are commonly used for porphyritic rocks. As a viable alternative, the major-element or norm-based classifications (*Streckeisen and Le Maitre, 1979; Debon and Le Fort, 1988*) have been preferred in this work [Chapter IV.1.]. The modal analyses of the non- (or slightly) porphyritic granitoids were plotted directly into the IUGS classification ternary plot (*Streckeisen, 1976; Le Maitre, 1989*) [Fig. II.11.].

Zoning patterns in plagioclase have been studied in order to distinguish between different generations, to assess the likelihood of the presence of xenocrysts and to examine links between the chemical composition and features revealed by cathodoluminescence. For clarity, sketches of photomicrographs and CL pictures are given and analysed points marked. The numbering is in accordance with the complete analyses in Appendix VI. and each feldspar is labelled by its An content. The scans are numbered separately, however, and the appropriate analyses are presented in tables at the end of this chapter.

II.1. Sázava intrusion (including Teletín quartz diorite)

The Sázava intrusion forms much of the northern CBP [Fig. II.1.]. West of the main mass, and separated from it by a belt of metavolcanic rocks (Jílové Zone), is a smaller body, referred to as the Slapy apophysis. To the east of the main mass is a small mass of tonalite, similar to the Sázava intrusion, that penetrates metabasites of the Ondřejov Metamorphic Islet.

The prevailing rock types are amphibole - biotite to biotite - amphibole quartz diorite, tonalite and granodiorite, which enclose abundant mafic microgranular enclaves (MME) and less common xenoliths of metabasite (amphibolite). Surmicaceous enclaves are absent.

In its eastern part, the Sázava intrusion is cut by a stock of the Mrač biotite granite. There are numerous bodies of pyroxene - amphibole gabbro (including Pecerady and Velké Popovice), some with olivine (Tužinka) within the intrusion together with less frequent gabbrodiorite, (quartz) diorite (Teletín) and rare hornblende (e.g. Palivcová, 1984). In all there are about 80 of these basic bodies (Palivcová, 1978) and most occur in a 70 km long NE - SW-trending belt between Čerčany and Hudčice [Figs II.1., II.3.] that crosses the boundary of the Blatná and Marginal intrusions. The rocks of these basic bodies appear to be cogenetic, and therefore they will be dealt with together.

The main mass of the Sázava intrusion is adjacent to Proterozoic - Palaeozoic metasediments of the Metamorphic Islet Zone (Vodčrady-Zvánovice, Ondřejov, Čerčany, Netvořice-Neveklov, Zbořený Kostelec and Tehov Metamorphic Islets) as well as Proterozoic metavolcanic rocks of the Jílové Zone and low-grade metasediments of the Teplá-Barrandian Unit (W). The intrusion is also in contact with the Říčany (N), 'Benešov' (E), Sedlčany, Maršovice (S), Blatná (SW) and Požáry (NW) intrusions.

Field observations

- I. Tonalites with a strong planar fabric, that are similar to the Sázava type, penetrate metabasites (amphibolites) of the Ondřejov Metamorphic Islet, break them up and enclose them as abundant, mainly angular xenoliths (Na Mariánci). In the amphibolites there are a few elongate lenses of tonalite.
- II. In the Mrač quarry there are several alternating subhorizontal units of the Sázava and Mrač granitoids separated by horizontal shear zones (ca. 0.25 m in width). This assemblage is displaced by normal faults [Photo II.1.1.]. The dominantly tectonic character of the contact between both types was recorded by Čepěk and Koutek (1941).
- III. The contact between the Sázava and Benešov intrusions is complicated and obscured by zones of intense deformation and abundant aplite dykes (Vejnar et al., 1975).
- IV. A stock of tonalite and granodiorite whose petrography is similar to that of the Sázava intrusion but with a core of pyroxene - amphibole gabbro is cut by the Marginal type granite in uranium mines south of Příbram, 30 km SW of the main Sázava intrusion (Vlašimský, 1973 and references therein).
- V. Angular xenoliths of the Sázava tonalite with common MME are enclosed by the fine-grained biotite monzogranite of the Mrač mass [Photo II.1.2.]. Contacts of these xenoliths with their host are usually sharp, and rarely there are thin leucogranite reaction rims (up to 0.5 cm in width) developed.
- VI. The Požáry trondhjemite encloses numerous angular xenoliths of the Sázava tonalite (Prosečnice, Krhanice) [Photo II.1.3.] (details in 2 II.).
- VII. Xenoliths of the Sázava tonalite occur in the Marginal type granite (A. Dudek, pers.com., 1991).

VIII. Xenoliths of coarse-grained amphibole gabbro (up to 1 cm amphibole phenocrysts) were found in the Krhanice quarry.

IX. Xenoliths of metabasite (amphibolite) from the quarry Na Mariánci are either angular (close to the contact) or round, and macroscopically are difficult to distinguish from the MME that are common elsewhere in the intrusion (*cf. Vejnar et al., 1975*).

X. Biotite - amphibole MME are ubiquitous throughout the Sázava intrusion (e.g. Mrač, Teletín). With the exception of Teletín, they are usually round or lenticular, with sharp contacts. Neither reaction rims nor chilled margins were found. The MME may reach over 30 cm (Mrač) or even several metres (Teletín); but elsewhere they do not exceed 10 cm in diameter (Prosečnice) [Photos II.1.2.-II.1.4.]. In Teletín the enclaves are often elongate, with a strong alignment [Photo II.1.5.] which, in general, is parallel to the contact with the Jílové zone (SW - NE) (*Dudek and Fediuk, 1958*). Many of the MME, and especially the larger ones, are angular [Photo II.1.5.] and many are frozen in various stages being broken into smaller pieces [Photo II.1.6.]. There are also some bent enclaves present [Photo II.1.7.]. Enclaves with embayments of mafic granitoid rich in plagioclase megacrysts and double enclaves are relatively uncommon (*see Lang et al., 1978*). Linear 'trains' of elongate angular MME were recorded by *Dudek and Fediuk (1958)* [Fig. II.6.]. (*cf. also Dudek and Záruba, 1967; Lang et al., 1978; Palivcová, 1984; Palivcová et al., 1989a*). Zones with abundant MME, similar to those from Teletín, occur in the Slapy apophysis (*Palivcová, 1972*).

XI. Surticaceous enclaves have not been observed.

XII. The most common dykes cutting the Sázava intrusion are aplites and pegmatites (e.g. Teletín, Mrač), lamprophyres (mainly spessartites, less frequently minettes - Krhanice: *Pivec jr., 1992*) (*cf. Palivcová, 1972*) and gabbro- and diorite-porphyrries. Of these dyke rocks, the amphibole-bearing lamprophyres, microdiorites and microgabbros have not been recorded anywhere else in the CBP (*Holub, 1992*).

XIII. Secondary minerals, including actinolite, titanite and epidote, occur in the leucodiorites of the Slapy apophysis (*Palivcová and Hejl, 1976; Poubová and Jurek, 1976; Palivcová et al., 1977*).

XIV. In the eastern part of the Sázava intrusion, the degree of deformation increases towards the SE, i.e. towards the contact with the Benešov intrusion and some of the granitoids of both of these masses show a corresponding degree of cataclasis and an identical (quartz-dioritic) composition (*Vejnar et al., 1975*). The so-called Benešov type is, in fact, a heterogeneous complex of various rock types, including quartz diorites, granites and ultrapotassic rocks (*Vejnar et al., 1975; Holub, 1992*) and is usually strongly cataclastic in aspect.

XV. The basic rocks (gabbros, gabbrodiorites and diorites) from the northern CBP all have a considerable proportion of magmatic amphibole and macroscopically obvious quartz ocelli with amphibole coronas are common (*Hanuš and Palivcová, 1970, 1971 a,b; Palivcová, 1978*) (S of Přebíram, Pecerady). The ocellar varieties often occur close to contacts of the gabbroid bodies with the surrounding granitoids (*Palivcová, 1978*). In some of the basic bodies, the grain size decreases towards their margins (e.g. Pecerady) (*Palivcová, 1984*).

Interpretation of field observations

The contact of the Sázava intrusion with the metabasites of the Metamorphic Islet Zone is intrusive in character, with the granitoid mass invading the country-rock and breaking it up. There is no evidence to support the proposal by *Palivcová (1966)* of development as a result of in situ

metasomatism. Isolated lenses of tonalite that are occasionally enclosed in the metabasite represent either finger-shaped penetrations (in 3D) or boudins (I.I., I.IX.).

The Sázava mass is older than the Mrač (I.V.), Požárý (I.VI.) and Marginal (I.IV., I.VII.) intrusions but the age relationship with the Benešov mass (I.III.) is not clear. However, at least part of the so-called 'Benešov type' is formed by quartz diorites, whose petrography and deformation resembles those of the adjacent Sázava mass and, for this reason, the 'Benešov type' could, at least partly, be made of deformed Sázava granitoids. The geological situation of this part of the CBP, and the position of the 'Benešov type' in particular, requires further investigation (*cf. Holub, 1992*) (I.XIV.), but is not included in this study.

The coarse-grained gabbro enclaves present in Krhanice may be interpreted either as representing cumulates formed early in the crystallization history of the intrusion or xenoliths of independent basic bodies (I.VIII.). Xenoliths of metabasites of the Metamorphic Islet Zone are common in the eastern part of the intrusion (I.IX.) and these could represent a potential contaminant of the Sázava magma. In contrast, metasedimentary xenoliths have not been recorded from the Sázava intrusion and so assimilation of considerable quantities of metasedimentary material during ascent and emplacement is unlikely. Furthermore, the absence of the surmicaceous enclaves (I.XI.) and the abundance of MME (I.X.) point to a negligible metasedimentary but a high (meta-)basic igneous input in the Sázava magma genesis (*cf. Didier, 1987; Montel et al., 1991*).

The angular and broken MME from Teletín (I.X.) must have been essentially solid when introduced into the tonalitic magma, unlike the bent ones, which had to be at least partly in a plastic state (*also see Dudek and Fediuk, 1958*). The alignment of enclaves appears to be controlled by the magma flow (fluidal alignment). The conclusion of *Dudek and Fediuk (1958)*, *Lang et al. (1978)* and many others was that the enclaves represent earlier differentiates of the Sázava magma. The situation in the Teletín quarry, however, resembles magma-mixing zones, widespread in the calc-alkaline granitoids world-wide (*e.g. Castro et al., 1990 a,b; 1991 a,b*). To avoid confusion with other dioritic rocks in the Sázava body, the rock making up the enclaves and small bodies in the Teletín quarry, will be called 'Teletín quartz diorite'. Nevertheless, the intrusion of the basic rocks (gabbros?) in the western part of the Sázava intrusion was at least partly contemporaneous with the tonalites themselves (also I.XV.) and magma mixing was probably of great importance in this part of the Sázava body.

The MME 'trains' from Teletín [I.X., Fig. II.6.] resemble disrupted syn-plutonic dykes (*also Lang et al., 1978; Palivcová et al., 1989a; cf. Pitcher, 1991, 1993 and 4.XII.*) [Fig. II.7.] whose origin is considered to be linked to an early propagation of cracks in a solidifying magma that, in turn, was connected to an abrupt increase in magma viscosity at about 35 % (or possibly even 50 %) of the remaining melt - the so-called critical-melt fraction (CMF; *van der Molen and Paterson, 1979; Wickham, 1987*). From this point on, the magma behaviour changed from suspension-controlled to granular-controlled and the magma became a non-Newtonian (Bingham) body. The fracture and flow phenomena can, inevitably, coexist in granite plutons depending on rate of application of stress as well as local solid-melt segregation (*Pitcher, 1993*). The existence of these features, however, is based solely on the photograph of *Dudek and Fediuk (1958)* as the dyke has been destroyed by quarrying.

The Slapy apophysis of the Sázava intrusion has suffered considerable post-consolidation hydrothermal and tectonic disturbance (I.XIII.). Granitoids of the eastern part of the main intrusion show effects of a strong cataclasis (I.XIV.) and Mrač and Sázava types are seen to be in tectonic contact (I.II.). Accordingly it is clear that the strong cataclasis of the granitoids was not restricted to the area of the 'Benešov type' and it has taken place after intrusion of the Mrač granite.

The presence of the igneous amphibole and therefore of 'wet' gabbroids in parts of the CBP, together with compositional variability and other features, were interpreted by *Palivcová (1984)* as being indicative of affinity to an 'Andinotype batholithic association'. This conclusion is assessed in **Chapter IV.4**. The quartz ocelli, common in the basic bodies, appear to be xenocrystic in origin (*e.g. Vernon, 1990; Hibbard, 1991*) and provide (together with **1.X.**) evidence of them being contemporaneous with the surrounding granitoid masses (Sázava, Blatná and Marginal). The finer-grained marginal facies of the basic intrusions could be viewed as chilled margins, and therefore these bodies ought to be younger or of the same age as the surrounding granitoids (*Palivcová, 1984*) (**1.XV.**). Accordingly there must have been a number of stages of emplacement of the basic bodies.

Microscopy

(I) The Sázava biotite - amphibole to amphibole - biotite tonalite, granodiorite to quartz diorite (Sa-1 to Sa-13; **Appendix L**) contains about 40 - 75 % plagioclase, 2 - 35 % amphibole, 15 - 35 % quartz, ~ 10 % biotite and 0 - 12 % K-feldspar (*cf. Palivcová, 1972*). The common accessory minerals include titanite, apatite, zircon, orthite, epidote and an opaque ore mineral. The average grain size is 0.5 - 1.5 mm and the texture is hypidiomorphic.

Based on petrographic observations, minerals most likely crystallized in the following order: amphibole, plagioclase → biotite → K-feldspar, quartz. The Sázava intrusion was subjected to relatively severe hydrothermal alteration, especially in its western part, as shown by local abundance of calcite and epidote, as well as by the advanced argillitization of plagioclase and chloritization of biotite. There is also a good evidence of post-crystallization deformation in the form of broken and distorted plagioclases, as well as undulose extinction or even cataclasis of the quartz grains.

PLAGIOCLASE The plagioclase of andesine to bytownite composition is present as subhedral to almost euhedral prisms, on average 0.7 - 1.5 mm, but up to 3 mm across. The albite and pericline twin lamellae are common but the combined Carlsbad-albite twins are rare. The plagioclase crystals often show zoning, either oscillatory, or, more frequently, discontinuous normal (*i.e.* with calcic cores).

The argillitization is of varied intensity: the most altered samples come from the Mr ač quarry and the least altered are those from T e l e t í n. The alteration starts along the cleavage and in the more basic cores of the crystals. Apart from sericite and clay minerals, secondary epidote may also occur (saussuritization).

The plagioclase often exhibits undulose extinction or is broken down into sub-grains (Mr ač). Some of the crystals show bent twin lamellae, the other twin-lamellae wedging out in the centre of the crystals [**Photo II.1.9.**].

In places, the plagioclase encloses clusters of strongly resorbed relics of originally larger biotite flakes. There are scarce inclusions of small subhedral to euhedral crystals of amphibole, usually aligned parallel to the albite twin lamellae (010). Relatively small (0.2 - 0.3 mm) subhedral or anhedral plagioclases are often enclosed by large amphibole crystals [**Photo II.1.10.**]. However, larger plagioclase crystals seem to be of the same age or younger than the amphibole. Anhedral plagioclases enclosed by the biotite flakes are locally common and, generally speaking, the majority of biotite appears to be younger. The plagioclase is surrounded by interstitial quartz and K-feldspar.

Plagioclase shows mainly ochre - yellow luminescence, sometimes with slight greenish hue - especially near to the edges of the crystals. The more basic cores of the crystals, however, are bright yellow [**Photo II.1.17.**]. The oscillatory zoning can be quite complex, as in the sample from

Krhanice (Sa-10). Moreover, the CL study also confirms other evidence for late brittle deformation; plagioclase crystals are often brecciated [Photo II.1.17.]

A conspicuous feature of the Sázava plagioclase at some localities (Krhanice, Sa-10) is discontinuous zoning, i.e. the occurrence of 'mantled plagioclases' in sense of *Hibbard (1981)*. The normally-zoned rims of the mantled crystals have a uniform andesine composition (An 32 - 35) [Fig. II.12 a] as do the small unzoned (optically and in CL) plagioclases of the matrix (~ An 35). The cores, with brighter yellow luminescence, have a higher anorthite proportion (generally An 40 - 50, but rarely reaching An 76). In contrast, the plagioclase from Mráč and Teletín (Sa-3 and Sa-7) show little or no zoning, and their composition is uniform at about An 45 - 50 (andesine). The An content of these plagioclases coincides with that of the cores of mantled plagioclases from Krhanice.

AMPHIBOLE Anhedral - subhedral, poikilitic prisms of amphibole are on average 1.2 - 2 mm (up to 4.5 mm) long. Simple twins on (100) are much more common than the polysynthetic twins [Photos II.1.10.-II.1.11.].

The maximum extinction angle of amphibole ($Z^{\wedge}c$) is 20 - 25° ('common' hornblende). It is usually strongly pleochroic: X: light yellow-green, Y: dark green, Z: dark bluish-green. In contrast, the Teletín sample (Sa-7) has a pale amphibole with weaker pleochroism, and in the X direction it is almost colourless. Also its maximum extinction angle ($Z^{\wedge}c$) is somewhat lower: 12 - 15° (actinolite?).

Some of the amphiboles enclose calcite patches, which have originated, at least partly, by partial dissolution of hornblende but there is also a possibility that some of the calcium was brought in by hydrothermal solutions. The CL reveals common worm-like aggregates of calcite, following the leached zones along the cleavage of the host amphiboles [Photos II.1.17., II.1.21.]. Inclusions are apatite (common) and tiny, euhedral zircons (rare). The amphibole tends to form clots, together with biotite and titanite. Its crystals are strongly corroded and surrounded by quartz and plagioclase. Amphibole encloses a considerable amount of very small, subhedral plagioclase crystals as well as biotite, both of which are usually aligned parallel to its cleavage. On the other hand, in the Mráč quarry, tiny round amphibole crystals and biotite flakes, associated with acicular apatite, are enclosed by the plagioclase crystals.

QUARTZ Quartz occurs in the form of anhedral crystals, or rather accumulations of sub-grains, on average 0.5 - 2 mm (up to 4 mm) across. The quartz grains show strong undulose extinction, and are broken into numerous sub-grains (consertal texture) or are even cataclastic (Mráč). Sub-parallel 'bubble trains', which were explained as cracks, partially sealed by differential solution and deposition of silica (*Fairbairn, 1949, and the references therein*), are common. The quartz is, together with K-feldspar, the youngest mineral.

BIOTITE Biotite forms anhedral flakes on average 0.25 - 1 mm (up to 2.5 mm) across. It is strongly pleochroic: X: pale straw yellow, Y = Z: dark red-brown. The number of the pleochroic haloes varies, but it is generally small. Chloritization of biotite is minimal; it only occurs along the cleavage of a few biotite flakes and there titanite forms a common by-product. The number of apatite and especially of zircon inclusions is very limited. In contrast, euhedral inclusions mainly of primary titanite are common [Photo II.1.11.]. The biotite is associated with, and often enclosed by, amphibole, and also locally by plagioclase. It appears to be generally younger than plagioclase. Biotite is strongly resorbed by quartz.

K-FELDSPAR K-feldspar occurs in the form of subhedral to anhedral prismatic crystals, about 1 mm (up to 5 mm) across. Cross-hatched twinning is rare (only Sa-10 of Prosečnice) and the K-feldspar is only slightly perthitic. The proportion of K-feldspar is variable,

but it is usually small and even zero, as for instance in the sample from Teletín. The K-feldspar was affected by slight argillitization, preferentially along the cleavage. Commonly, it shows an undulose extinction and is broken into several sub-grains (Mráč). Plagioclase is enclosed and surrounded by the interstitial K-feldspar which must be younger. Myrmekite occurs commonly at the boundary with plagioclase. The K-feldspar encloses tiny (< 0.1 mm) euhedral flakes of biotite and rarely also some amphibole. It exhibits light blue luminescence, lacking any apparent variation.

CALCITE

Additional evidence of the post-magmatic hydrothermal alteration suffered by the Sázava intrusion is given by the abundance of calcite. The best tool for observing the calcite distribution proved to be CL, as calcite exhibits conspicuous bright orange-red luminescence [Photo II.1.17.]. It is mainly interstitial, either following the rims of plagioclase crystals or forming roughly triangular grains (up to 0.6 mm across) at their triple-junctions, only occasionally penetrating plagioclase along the cleavage. The calcite may be localised in the most altered parts of the plagioclase crystals, as well as in areas of pronounced cataclasis, but often it is distributed quite randomly. The calcite is most abundant in the sample from Teletín (Sa-7), which otherwise seemed to be the freshest sample collected. The textural evidence suggests that argillitization and crystallization of calcite were caused by two separate events, with the calcite formation being mainly later.

ACCESSORY MINERALS

Of the intrusions in the CBP, the Sázava mass and its associated basic rocks contain anomalously high epidote contents, with the mineral appearing to be of both primary and secondary origin (*Kodymová and Vejnar, 1974*). Although *Zen and Hammarstrom (1984)* considered that the primary epidote is common in granitoids that crystallized at moderately-high pressures (more than about 7 kbar) and under fairly oxidising conditions, its primary-magmatic origin has been questioned, for instance, by *Pitcher (1993)*. The opaque minerals are represented mainly by magnetite and pyrite.

II. The Teletín quartz diorite (SaD-1 to SaD-3) is composed of about 50 % plagioclase, 30 % hornblende, 10 % quartz and 10 % biotite. The plagioclase (~ 1 mm across) is typically subhedral, showing abundant albite twin lamellae. Some effects of deformation can be seen, such as bent twin-lamellae and brittle fractures. Sample SaD-2 particularly suffered a strong deformation, and is cut by cataclastic bands with quartz ribbons.

The optical microscopy and, in particular, the CL study have revealed a discontinuous zoning in the plagioclase with bright-yellow (CL) cores, that were partly resorbed and overgrown by ochre (CL) rims [Photos II.1.13.-16., II.1.18.-II.1.20.]. The most common type of zoning is discontinuous normal, with the rims being andesine (An 44 - 48), and the cores bytownite - anorthite (~ An 80 - 90) [Photos II.1.18.-19.; Fig. II.12 b-c]. Sometimes these cores are overgrown by an additional zone of less basic bytownite composition (An 70 - 77). This pattern was verified by a microprobe scan across one of the mantled plagioclases from Photo II.1.19. [Tab. II.2, Fig. II.13.]. The composition of the rim varies little between An 40 - 50 but abruptly increases initially to An 70 and after that remains constant at about An 90. The central peak splits into two due to the rim protrusion.

The second type of the zoning pattern of the Teletín plagioclases is that with an apparent calcic spike and patchily zoned core [Photo II.1.20., Fig. II.12 d]. The core, composed of patches of andesine (An 48) and more calcic plagioclase (An 61 and 87), is overgrown by a bytownite zone (An 78) and andesine (An 49) rim ('boxy-cellular' plagioclase; *Hibbard, 1991*).

Unzoned small plagioclases of the matrix correspond to andesine (An 47 - 48), i.e. similar in composition to the rims of both types of mantled plagioclases. Their composition also matches that of plagioclases from the Sázava mass.

Amphibole forms anhedral, interstitial crystals on average 1 - 1.5 mm (up to 3.5 mm) across. It occasionally shows simple or polysynthetic twinning on (100). The maximum extinction angle found was 20° and strong pleochroism is shown: X: pale olive green, Y: deep olive green, Z: dark bluish-green. Some of the crystals have relic cores of brown hornblende (*also Lang et al., 1978*) (see Chapter III. for discussion of the origin of these cores).

Quartz (~ 0.6 mm) is anhedral, interstitial, with strong undulose extinction. Anhedral biotite flakes, on average 0.8 - 1.2 mm (max. 1.6 mm) across, are strongly pleochroic: X: dull ochre, almost colourless; Y = Z rusty-brown. The biotite lacks pleochroic haloes, but is commonly rimmed by opaque ore minerals. Some flakes are enclosed by amphibole. Common accessory minerals include acicular apatite and isometric grains of an opaque ore mineral. Of interest is the presence of chrome spinelides in the both hybrid rocks and the Sázava tonalite in Teletín (*Lang et al., 1978*), which were not recorded from any other locality in the Sázava intrusion, apart from sub-microscopic inclusions in magnetite of the gabbros (*Rub et al., 1977*). The presence of chrome spinelides in the Teletín quartz diorite and its tonalite host provides evidence of material exchange between the two.

ENCLAVES

The additional samples studied comprise (1) Sam-7, a strongly resorbed ellipsoidal amphibole-biotite MME, 10 cm long, from Teletín and (2) Pom-5, a round amphibole-biotite MME from Prosečnice.

(1) The Teletín MME (Sam-7) shows a fabric indicative of pronounced effects of deformation (of both enclaves and matrix). Kinking of biotite is common, as is cracking and cataclasis of quartz grains. Plagioclases usually have bent primary and newly-formed secondary twin-lamellae, and some are broken. Amphibole is more abundant than biotite, the former occurring as tiny anhedral crystals, interstitial to plagioclases. Lobate biotite flakes are usually strongly deformed, and 'flow round' the plagioclase augen. Many plagioclases of the enclaves and particularly larger plagioclases of the host are mantled [Photo II.1.12.] and their cores often enclose tiny round hornblende grains. The resorption surfaces between cores and rims are very obvious, and sometimes are enhanced by thin calcite rims. Acicular apatite is a frequent accessory.

(2) The sample from Prosečnice (Pom-5) represents an enclave type widespread in the Sázava body. It is hornblende-rich; the subhedral hornblende crystals form monomineralic clots with lobate outlines. Some of the larger hornblendes contain dark rings of a fine-grained opaque mineral. Biotite is relatively rare; it encloses abundant zircon inclusions. Plagioclase occurs both as small euhedral laths, and as larger mantled prisms. Both K-feldspar and quartz are interstitial and poikilitic. Apatite, which is present as short-prismatic as well as acicular crystals, is not particularly abundant. One subhedral crystal of metamict orthite was found. Next to the enclave, the host tonalite contains either individual xenocrysts or their aggregates (microenclaves), including mantled plagioclases, which were probably derived from the broken parts of the MME.

INTERPRETATION

The discontinuously-zoned plagioclases from Teletín, containing often patchy-zoned cores, are 'mantled plagioclases' in sense of *Hibbard (1981)* for which two main explanations have been proposed.

- (a) The calcic cores were resorbed and later overgrown by an andesine rim, similar, for instance, to the textures interpreted by *Wiebe (1968)* on the basis of the model of origin of patchy zoning by *Vance (1965)*. The resorption of the calcic cores could be caused either by a sudden rise in temperature or a drop in pressure (rapid ascent), shifting both the solidus and liquids downwards (*Vance, 1965; Wiebe, 1968*). Interaction between superheated acid and chilled basic magmas or loss of volatiles, may also account for resorption of calcic plagioclase followed by precipitation of a more sodic one (*Vance, 1965*). The hypothesis of *Vance (loc. cit.)* would also explain presence of small round amphibole inclusions within the cores [Photo II.1.20.], as they may have crystallized from pockets of liquid trapped after the resorption event (*Vance, loc.cit.*).
- (b) The second explanation assumes a strong undercooling of the mafic magma, resulting in rapid (dendritic) crystal growth and origin of 'boxy-cellular' morphology (*Hibbard, 1981; Hibbard, 1991*). The likely reason for quenching is an interaction with relatively cooler acid magma - i.e. magma mixing (*Barbarin, 1990 b; Vernon, 1990, 1991; Hibbard, 1991*). The cellular calcic plagioclase may be greatly resorbed as a result of reaction with the acid melt (*Hibbard, 1991*).

It seems that the both models explain some of the observed features of the Teletín plagioclases: the first model appears to be applicable to many prevalently euhedral plagioclase cores, with occasional embayments of the sodic rim [Photos II.1.14.-II.1.16., II.1.18.-II.1.19]. These plagioclases have probably crystallized in depth, prior to the magma mixing event with the pressure release during their ascent leading to (limited) resorption. The second model accounts for the origin of the patchy zoned (boxy cellular) crystals [Photos II.1.13., II.1.20.] that have apparently crystallized during the quenching (magma mixing) stage. Subsequently, after interaction with the acid magma, they were partially resorbed and overgrown by more sodic mantles. At the same time small, unzoned plagioclases with composition matching that of the rims of the mantled ones nucleated.

In discussing genesis of calcic cores of discontinuously-zoned plagioclase, it is necessary to mention an alternative hypothesis of *Chappell et al. (1987)*. According to their model, the unzoned calcic cores originated during slow prograde ultrametamorphism (melting) of the granite source rocks, i.e. are restitic in origin, and were overgrown by later magmatic plagioclase. However, such a restitic origin is unlikely, as the cores commonly show oscillatory zoning, and hence are better explained by a melt-melt disequilibrium (*Bateman, 1993a*).

As both enclaves appear to be of hybrid origin, on the basis of the presence of mantled plagioclases with obvious resorption surfaces, the acicular (quenched; *Wyllie et al., 1962*) apatite, and the oikocrysts of quartz and K-feldspar, there must have been a time gap between the magma-mixing event and onset of their crystallization (*Vernon; 1990, 1991*; see also section on enclaves from the Kozárovec intrusion).

II.2. Požáry intrusion

The oval-shaped Požáry intrusion occurs in the northern part of the CBP [Fig. II.1.]. Its is composed of biotite trondhjemite and leucocratic quartz diorite, usually without amphibole. The number of enclaves is generally very limited but increases towards contacts with the Sázava intrusion, the Velké Popovice gabbro body (MME) and the Teplá-Barrandian Unit (metasedimentary xenoliths). Few dykes cut the Požáry intrusion which is surrounded mainly by low-grade metasediments of the Teplá-Barrandian Unit (N) and Proterozoic-Palaeozoic metasediments of the Metamorphic Islet Zone

(Tehov and Zbořený Kostelec Metamorphic Islets; NE and SW). In the S and W, it is in contact with the Sázava intrusion.

Field observations

I. The contact of the Požáry intrusion with the Proterozoic metasediments of the Teplá-Barrandian Unit is intrusive. There is pronounced thermal metamorphism and finger-like penetrations of the trondhjemite into the country rocks. The metasediments are displaced by numerous faults, parallel to the contact (*Vejnar et al., 1975*).

II. The trondhjemite encloses angular blocks (up to several meters across) of Sázava tonalite, and in places exhibits structures, indicative of a magma flow around essentially solid xenoliths [Photo II.1.3.]. (also Čepěk and Koutek, 1941; Hejtmán, 1941, and many others) (Prosečnice). In the Krhanice quarry, it not only encloses angular xenoliths of the Sázava tonalite but also is in a sharp contact with the latter, in places with a leucocratic chilled margin (~ 1 cm thick) [Photo II.1.4.]. In contrast, *Vejnar et al. (1975)* recorded a transition between the Sázava and Požáry intrusions at Čerčany.

III. Close to the contact with Proterozoic rocks of the Teplá-Barrandian Unit, the trondhjemite encloses xenoliths of biotite- and biotite - cordierite hornfels (*Vejnar et al., 1975*). However, no metasedimentary xenoliths were observed in the southwestern part of the body (Krhanice, Prosečnice).

IV. The amount of MME in the intrusion is typically very limited except adjacent to the Velké Popovice basic body (*Vejnar et al., 1975*) and contacts with the Sázava tonalite (Krhanice). In the latter case, the enclaves have wavy margins, and form swarms aligned roughly parallel to the contact [Photo II.1.4.]. In the zones with a higher concentration of MME, the proportion of amphibole increases while the K-feldspar disappears and the trondhjemite contains quartz ocelli and plagioclase with biotite coronas (*Vejnar et al., 1975*).

V. An enclave swarm of elongate MME, enclosed in the Požáry trondhjemite (close to the contact with Sázava) occurs in the Krhanice quarry [Photo II.1.8.]. A projection of the swarm is towards a gabbro dyke (2.VL); both have the same strike of ca. 040° but the outcrop is not continuous.

VI. The number of dykes cutting the intrusion is generally small (also e.g. Kettner, 1926; Kodym, 1966) and only aplite dykes and pegmatite schlieren (Prosečnice) are common (also Hejtmán, 1941) but there is one (15 m across) dyke of coarse-grained biotite - amphibole quartz gabbro that cuts the trondhjemite in Krhanice. The contact is sharp, intrusive, but without a chilled margin.

VII. In the western part, the trondhjemite shows typically well-developed and undisturbed jointing and no effects of deformation (Prosečnice). In contrast, the eastern part shows the effects of severe cataclasis, as is the case in the adjacent part of the Sázava intrusion (I.XIV.) (*Vejnar et al., 1975*).

Interpretation of field observations

The contact of the Požáry intrusion with metasedimentary rocks of the Teplá-Barrandian Unit is intrusive and the presence of a distinct thermal aureole suggests that the depth of intrusion was not great (2.I.)

The Požáry trondhjemite is younger than the Sázava tonalite (2.II.). The significance of the observation of *Vejnar et al. (1975)* (2.II.) is difficult to assess, as the exposure they saw is inaccessible - it was a water supply gallery. In the opinion of *Vejnar et al. (loc.cit.)*, the Požáry trondhjemite is

enriched by MME close to the contact with the Sázava intrusion, and by their assimilation becomes similar in appearance to the rock of the Sázava mass.

Metasedimentary xenoliths are common only close to the contact with the Teplá-Barrandian Unit, hence the contribution of the metasedimentary material is unlikely to be significant in the western part of the body (2.III.). This is in contrast to hypothesis of *Vejnar et al. (loc.cit.)*, who have explained the genesis of the Sázava and Požáry granitoids by assimilation of different rocks, namely MME for Sázava, and aluminium-rich metasedimentary xenoliths for Požáry. However close to the contact with the Teplá-Barrandian Unit, the metasedimentary input could have been important.

The MME that are abundant around the Velké Popovice gabbro body could represent either hybrids of the gabbro and Požáry trondhjemite or fragments of disrupted chilled margin of the gabbro intrusion (2.IV.). On the other hand, the MME at the contact with the Sázava type might represent either a refractory residuum after partial assimilation of the tonalite or, more likely, of its mafic microgranular enclaves. The trondhjemite, rich in quartz ocelli, could be interpreted as a hybrid, contaminated by an enclave-derived material (*Vejnar et al. 1975*) (2.IV.).

The enclave swarm (2.V.) appears to be a continuation of the gabbro dyke (2.VI.) and the simplest explanation would be that the dyke is syn-plutonic. However no relation between the two phenomena was observed in field. The time span between the injection of the gabbro dyke and (partial) solidification of the surrounding trondhjemite must have been limited as the dyke is coarse-grained and is not chilled against its host (2.VI.).

The finding of *Vejnar et al. (loc.cit.)* about the Sázava and Požáry intrusions sharing comparable deformation (1.XIV., 2.VII.) could be of considerable importance, as it implies that both masses (and also possibly the 'Benešov type' ?) suffered the same cataclasis and, therefore, either belong to the older intrusions of the CBP or the deformation was relatively late (2.VII.).

Microscopy

The Požáry biotite ± amphibole trondhjemite (Po-1 to Po-5) consists of 55 - 70 % plagioclase, 20 - 30 % quartz, 5 % K-feldspar, 4 - 8 % biotite, and sometimes a small amount of amphibole. The common accessory minerals include apatite, titanite and an opaque ore mineral. Calcite, muscovite and epidote occur as alteration products. The average grain size is 0.5 - 1.5 mm, with somewhat larger crystals of the K-feldspar (3 - 4 mm). The texture is usually hypidiomorphic; the texture of the Krhanice sample appears to be cumulative in origin.

The likely order of crystallization is: plagioclase → biotite → K-feldspar → quartz. Due to its very small modal abundance the paragenetic position of amphibole is not clear. The effect of strong hydrothermal alteration is shown by advanced argillitization of plagioclase and chloritization of biotite. Similarly, the presence of the secondary muscovite and epidote, as well as abundance of calcite and an opaque ore mineral, provide firm evidence of a late hydrothermal activity. The deformation is manifested in particular by breaking up of plagioclase grains, an undulose extinction and fracturing of the quartz and biotite grains.

PLAGIOCLASE

Plagioclase (mainly andesine) forms subhedral prismatic crystals, on average 0.5 - 1 mm across (up to 1.7 mm). Most show albite twin lamellae; pericline and the Carlsbad twins are much less common. The plagioclase crystals often show zoning, both oscillatory and discontinuous. The albite twin lamellae often wedge out and secondary twin lamellae might be developed pointing to a late deformation. Relatively high degrees of post-crystallization hydrothermal alteration are shown as the grains are very often full of sericite, and even large flakes of

secondary muscovite are quite common. Moreover, the alteration products locally comprise epidote and calcite, which preferentially replace the plagioclase crystals along the cleavage.

The plagioclase appears to be older than biotite, although there are some strongly resorbed biotite crystals enclosed in it. It is surrounded by anhedral or interstitial K-feldspar. At their contact, myrmekite is common. Quartz is interstitial and younger. The texture, with euhedral-subhedral plagioclase crystals some of which are broken and with other phases only filling gaps [Photo II.2.3.], may represent a disrupted cumulate. Especially sample Po-1 (from Krhanice), with a limited amount of mafic minerals and quartz as well as a high content of euhedral plagioclase, could represent an orthocumulate (Cox *et al.*, 1979; Bard, 1987; Philpotts, 1990).

The luminescence of the plagioclase is ochre yellow, but the cores of crystals are often much brighter [Photos II.2.1.-II.2.3.]. Alteration is shown by a brownish colour. Concentric zoning of the ochre and yellow luminescence is common, sometimes being repetitive (oscillatory zoning). The broken nature of many of the plagioclase grains and the effects of healing by the matrix K-feldspar are clearly shown [Photo II.2.3.], suggesting, that the deformation was late syn-crystallization, in a crystal mush (*cf.* McCarthy and Groves, 1979). The brownish colour in CL shown by the disrupted parts, and at the immediate K-feldspar - plagioclase contacts, is possibly due to subsolidus diffusion or leaching.

The composition of the plagioclase from this intrusion ranges between An 28 and An 52. Common are discontinuously-zoned crystals, with andesine rims (An 28 - 37; on average about An 32) and cores of basic andesine - labradorite composition (An 46 - 64) [Fig. II.14 a,b]. The small unzoned plagioclases of the matrix have a composition matching that of the rims of the zoned crystals. One zoned crystal, with an andesine core (~ An 35) and oligoclase rim (An 16) was seen.

As for the Sázava intrusion, there is also a link between the luminescence colour and the An content: the brighter yellow luminescence is shown by the more calcic plagioclases [Fig. II.14., Photos II.2.2., II.2.3.]. On the other hand, the middle zone of the crystals on Figure II.14 a, with its distinct luminescence (compared to the rim) has only 3 % more of An.

QUARTZ

Quartz occurs in the form of interstitial, anhedral crystals, on average 1 - 1.4 mm (up to 5 mm) across. It shows strong undulose extinction, fracturing or even sub-grain development. The quartz contains a great deal of hair-like subparallel cracks, which generally follow one direction, with some filled by secondary minerals such as calcite or sericite. The quartz is poikilitic to plagioclase, as well as to biotite and amphibole. It is the youngest mineral, as it is moulded on the K-feldspar.

K-FELDSPAR

The K-feldspar occurs as anhedral grains, on average 3 - 4 mm (up to 5 mm across), filling the space between plagioclase crystals. Some of the crystals possess pronounced cross-hatched twinning indicative of microcline, and some of them are perthitic. There is little evidence of either later alteration or deformation. It frequently encloses both biotite and plagioclase but has quartz moulded on to it.

The blue luminescence emitted by the K-feldspar often exhibits zoning, with the brighter blue zones usually corresponding to the areas of most pronounced alteration of the K-feldspar grains.

BIOTITE

Biotite occurs in the form of anhedral to subhedral flakes, usually 1.5 mm (up to 2.5 mm) across. It shows a strong pleochroism: X: straw yellow, Y = Z: dark (reddish)-brown. Pleochroic haloes are quite rare, and usually small and pale.

It has suffered a strong hydrothermal alteration, being usually replaced by an aggregate of chlorite and titanite. Although the chlorite is often associated with muscovite, white mica does not seem

to be only an alteration product: some relatively fresh biotite flakes host muscovite lamellae parallel to their cleavage. In sections cut roughly parallel to the base, many of the flakes reveal abundant cracks. In places, they are even broken into several sub-grains with slightly different extinction. Recrystallization at the edges of biotite flakes, especially at the contact with the K-feldspar, is relatively common.

Inclusions within the biotite flakes are predominantly elongate crystals (or needles) of apatite. In the Prosečnice quarry, there are abundant tiny euhedral dipyrarnidal crystals of zircon (0.03 - 0.09 mm); in contrast, zircon is rare in Krhanice. The biotite is likely to be generally younger than plagioclase, as it is interstitial to the plagioclase crystals but there are also present strongly resorbed biotite flakes enclosed by plagioclase. Both quartz and K-feldspar surround and resorb the biotite, which is, therefore, older. In the K-feldspar, there are many inclusions of biotite with well-preserved crystal shape.

AMPHIBOLE

Crystals of amphibole are on average 0.7 - 1 mm long and are generally anhedral. This mineral was found only in the sample from the Krhanice quarry, even there it is more of an accessory than an essential mineral. The amphibole is deep green, sometimes with a slight bluish hue. Scarce needles of pale green actinolite (an alteration product) occur at the edges of the amphibole crystals which are often associated with biotite but its relation to the majority of minerals is impossible to determine; there is only evidence for quartz being younger.

ACCESSORY

Compared with other intrusions in the CBP, the Požáry trondhjemite is poor in apatite and zircon; its main accessory minerals are opaque ores (magnetite - *Kodymová and Vejnar, 1974*). Fairly abundant (especially in Krhanice) are large anhedral grains of an opaque ore mineral, interstitial to the plagioclase grains.

MINERALS

CALCITE

Calcite is very abundant in form of roughly triangular crystals, interstitial to the plagioclase grains. In CL, two generations of calcite can be distinguished, both emitting bright red-orange luminescence, with rims of some of the grains being somewhat brighter than the cores [Photo II.2.1.].

II.3. Kozárove intrusion (including Těchnice granodiorite)

The Kozárove intrusion which forms a central part of the CBP is elongate and NE - SW trending [Fig. II.2.]. There is also small kidney-shaped mass of the Kozárove granodiorite penetrating the Mirovice orthogneisses further to the SW.

The predominant rock type is a biotite - amphibole to amphibole - biotite granodiorite, with a variable proportion of K-feldspar phenocrysts up to 2 cm in size. A porphyritic granodiorite (of so-called Těchnice type) occurs in the central part of the Kozárove intrusion and is rimmed at the NE and SW by essentially even-grained granodiorite (Kozárove s.s.). Various types of enclaves, including country-rock xenoliths, MME and surmicaceous enclaves are abundant.

A small roughly circular body of pyroxene - amphibole quartz monzonite (of so-called Zalužany type) crops out south of village of Kozárove. Additionally, a fine-grained biotite - amphibole quartz monzonite body was encountered at bottom of the quarry Kozárove II and there are small masses of coarse-grained pyroxene - biotite - amphibole melamonzonite, biotite - pyroxene - amphibole (mela-) monzogabbro and biotite - amphibole gabbro in southern part of the Mirovice Metamorphic Islet (Lučkovice); for details on their mineralogy and geochemistry, see *Ledvinková (1985)*, *Holub (1990)* and *Bowes and Košler (1993)*.

Adjacent to the Kozárove intrusion are Proterozoic metavolcanic rocks of the Jílové Zone, Proterozoic-Palaeozoic metasediments of the Metamorphic Islet Zone (Mirovice, Sedlčany-Krásná Hora, Maršovice and Netvořice-Neveklov Metamorphic Islets) including the Devonian orthogneisses (south of Mirovice and Sedlčany-Krásná Hora Metamorphic Islets: *Košler, 1993*) and the Blatná (S), Čertovo břemeno, Sedlčany and Maršovice (E) intrusions.

Field observations

- I. The contact between the Kozárove and Těchnice granodiorites is sharp with neither a chilled margin nor a reaction rim present (K a m ý k). Also at this locality a small sub-vertical apophysis of the even-grained granodiorite (with a few phenocrysts) (Kozárove s.s.) intrudes the porphyritic one (Těchnice) but has not been observed to cut the phenocrysts. Elsewhere a transitional boundary between the even-grained and porphyritic facies has been recorded (*Hejtmán, 1948; Kodým and Suk, 1960*). The Kozárove granodiorite is never completely phenocryst-free (see also *Hejtmán, 1948; Kodým and Suk, 1960*) and in the vicinity of the village of K o z á r o v i c e, the number and size of the K-feldspar phenocrysts increases towards the NE.
- II. The contact with the Blatná intrusion has been recorded as being sharp, but no further information concerning its character has been given (*Kodým and Suk, 1958*).
- III. No contacts with the Sázava, Čertovo břemeno and Sedlčany intrusions have been observed and the Kozárove granodiorite has been considered to be a part of the Sázava intrusion by some workers (*e.g. Vejnar, 1973, 1974a; Němec, 1974*).
- IV. At the contact with the granodiorite host, the quartz monzonite from K o z á r o v i c e II is cracked, net-veined and eventually broken into mafic microgranular enclaves either angular [Photo IL3.12.] or round, some resembling 'pillows' [Fig IL10.]. No chilled margins were observed but some of the contacts are diffuse.
- V. The occurrence of a single xenolith of granodiorite considered to be of the Těchnice type within the Blatná granodiorite was recorded by *Kodým (1955)*.
- VI. Xenoliths of banded hornfels and amphibolite are common in the southwestern part of the body (K o z á r o v i c e quarries). Ellipsoidal (feldspar - epidote) calc-silicate xenoliths with 1 - 2 cm thick amphibole-rich reaction rims are scarce (K o z á r o v i c e II) (*cf. Hejtmán, 1955*). The occurrence of a small angular xenolith of a coarse-grained amphibole diorite (gabbro?), with a thick finer-grained hornblende reaction rim was exceptional (K o z á r o v i c e I). The lithology of the metasedimentary xenoliths differs from the mainly argillaceous metasediments of the adjacent Mirovice Metamorphic Islet (*Hejtmán, 1955*). Metasedimentary xenoliths are most common in the northeastern part of the intrusion, where they are represented mainly by angular xenoliths of banded hornfels [Photo IL3.1.] but xenoliths of tremolite- and wollastonite-bearing calc-silicate rock and marble are also present (*cf. Zárubová, 1934; Zeithamová and Holub, 1989; Zeithamová, 1990*) (S o l o p y s k y, D e š t n o).
- VII. MME, which are usually round and several dm - over 1 m in size, are abundant. In K o z á r o v i c e II, they tend to be more angular and larger than elsewhere. They contain common megacrysts of plagioclase (up to 2 mm) and rare quartz ocelli and ovoids (up to 2 cm). The outlines of these enclaves are typically sharp, some of them showing narrow leucocratic haloes depleted in dark minerals. Occasionally, there are embayments of darker granodiorite rich in plagioclase megacrysts [Photo IL3.2.] penetrating the enclaves.
- VIII. There are many 'double enclaves' (*Pitcher, 1993*). Their contact with the granodiorite host is diffuse but the boundary between the two zones is generally sharp [Photo IL3.3.]. The inner part

consists of a typical MME in which plagioclase is absent or present as only a few megacrysts. In contrast, the outer part contains a much higher proportion of plagioclase.

IX. Surmicaceous enclaves are not common. They are mainly round and less than 2 cm in diameter. Some, which are greenish in colour, are composed of diopside, with a thin amphibole - biotite rim (*Hejtman, 1955*). Others are enclosed by MME (*Kozárovice I*).

X. Biotite - amphibole schlieren occur in places and are associated with the most resorbed metasedimentary xenoliths and MME (*Kozárovice III*).

XI. There are parallel-sided zones, in which the granodiorite encloses swarms of enclaves of various types, including MME and surmicaceous enclaves, together with xenoliths of calc-silicate rock, hornfels, gneiss and coarse-grained diorite [*Photo II.3.4.*] (*Solopysky, Deštno*). Many of the blocks show evidence of resorption with related magma contamination. These dyke-like zones trend roughly N - S (*Zeithamová and Holub, 1989; Zeithamová, 1990*). The zone observed at *Solopysky* has a sharp contact, is approximately 25 cm wide and could be followed for about 5 m.

XII. Locally there is a banding (or schlieren) present that consists of alternating light (macroscopically similar to the granodiorite) and darker bands. These bands are well-defined but there is no change in grain size [*Photos II.3.5.- II.3.6.*] (*Kozárovice III*).

XIII. Numerous dykes of aplite, pegmatite, gabbro-, diorite-, syenite- and granite-porphyrries, minettes, kersantites and spessartites cut the intrusion (*Němec, 1974; Žežulková, 1982a*). Two suites of dyke rocks could be distinguished in the southern CBP, older and younger than the Čertovo břemeno mass. The older group consists of gabbro-, granodiorite-, diorite-porphyrries, some of the granite porphyries and spessartites; the younger one comprises tourmaline leucogranites, alkali minettes, minettes, kersantites, syenite porphyries and the rest of the granite porphyries (*Žežulková, 1982a*).

XIV. There were observed two fine-grained (lamprophyre?) dykes, one of them being truncated by a fresh portion of the granodiorite [*Photo II.3.7.*], that macroscopically resembles the older one (somewhat coarser-grained) (*Kozárovice III*). The dyke appeared to be slightly sheared along the contact. Both dykes, exposed close to and sub-parallel to the banding (*3.XII*), had locally diffuse contacts and, as a rule, no chilled margins.

XV. In places, especially in the centre of the intrusion, the granodiorite is hydrothermally altered (e.g. around the Krásná Hora Sb deposit). This, together with the poor exposure, makes the collection of unaltered samples of the porphyritic facies (*Těchnice* type) difficult.

XVI. The Zalužany monzonite contains no enclaves. The only inhomogeneities are infrequent small round pilites (pseudomorphs of actinolite after olivine; *Bates and Jackson, 1987*), up to 0.5 cm across, and aplitic and pegmatitic schlieren (*see also Hejtman, 1948*).

XVII. The quartz monzonite from *Kozárovice II* is a dark, fine-grained rock with plagioclase megacrysts (up to 0.5 cm) and rare quartz ocelli. Occasionally, it encloses xenoliths of hornfels with no reaction rims but, next to the hornfels - quartz monzonite contact, the host becomes richer in plagioclase megacrysts.

Interpretation of field relations

In the *Kozárovice* intrusion, two facies can be distinguished: (1) a porphyritic facies in the centre of the body (*Těchnice*), and (2) an (essentially) even-grained facies (*Kozárovice s.s.*). The *Těchnice* granodiorite in *Kamýk* appears to represent the older of the two but was still in a plastic state when cut by the even-grained *Kozárovice (s.s.)* granodiorite (*3.I*). In the vicinity of the village of *Kozárovice*, the increase in the proportion of K-feldspar phenocrysts towards the NE (towards the

centre of the intrusion) may correspond to a transition to the porphyritic facies in accord with observations of *Hejtman (1948)* and *Kodym and Suk (1960)*, but the age difference between the facies is likely to be small (3.I.). There is evidence of emplacement in more than one magma pulse (3.XIV.).

There is no clear evidence about the relative age of the Kozárovec and Blatná intrusions, as the observation of *Kodym (1955)* has not been confirmed (3.II., 3.V.). Unlike Sázava, the part of the Kozárovec intrusion is porphyritic (Těchnice granodiorite) and it contains different enclaves (both MME and surmicaceous, also common metasedimentary ones) (3.III.; cf. 3.VI - 3.IX. with 1.X. - 1.XI.). The Sázava intrusion is cut by additional types of dyke rocks not present in the Kozárovec intrusion (*Holub, 1992*) (1.XII., 3.XIII.). Also the geochemistry of the Kozárovec mass differs from that of the Sázava mass (Chapters III.-V.; cf. *Holub, 1989a, 1992*) and, therefore, Kozárovec is indeed a separate intrusion.

Phenomena similar to those observed in the quartz monzonite from Kozárovec II (3.IV.) have been described from 'net-vein' complexes world-wide and such a net-veining is thought to point to contemporaneous intrusion of the basic and acid magmas (*Shelley, 1993, Pitcher, 1993*). After coming into contact with the acid magma, the basic magma cools down and solidifies rapidly, while the acid magma which is superheated, becomes fairly mobile and invades the basic one. As a result, the mafic solid is cracked and the fractures filled by a complex of felsic veins. Occasionally the basic magma may form pillow-like structures, or enclose globules of acid material (ocelli) and chilled margins are frequently observed (*Shelley, loc. cit.*). Although, in Kozárovec, no macroscopically obvious chilled margins have been seen, they might be observable only on the micro-scale, as is usually the case for fine-grained rocks (*Clarke, 1992*). The application of the interpretation of *Shelley (loc.cit.)* would argue for the hybrid character of the Kozárovec quartz monzonite (3.XVII.).

The source of the abundant metasedimentary xenoliths in the Kozárovec quarries is likely to be more distant than the Mirovice Metamorphic Islet, possibly analogous to the rocks of the Sedlčany-Krásná Hora Metamorphic Islet (3.VI.). However, the abundance of angular metasedimentary xenoliths implies a shallow depth of intrusion and only a short transport of the xenoliths (e.g. *Maury and Didier, 1991*); some metasedimentary xenoliths, especially of marble and calc-silicate rock (*Solopysky, Deštno*) might be linked to the rocks of the adjacent Sedlčany - Krásná Hora Metamorphic Islet (e.g. *Zeithamová, 1990*).

The abundance of large and sometimes angular MME in the quarry Kozárovec II (3.VII.) could be attributed to a continuation of the process of net-veining of the quartz monzonite stock as seen at the bottom of the quarry (3.IV.). The explanation of the double enclaves (3.VIII.) follows that of *Pitcher (1993)* [Fig. II.8.]: the outer parts are the result of the mixing of acid and basic magmas, whereas the inner parts represent retained blobs of the non-hybrid basic magma. A similar explanation is applicable also to the embayments of the darker megacryst-rich granitoid (3.VII.).

The surmicaceous enclaves are interpreted as a residuum after anatexis of the metamorphic precursor of the granitoid magma, or after melting of pelitic xenoliths captured by the magma during ascent (deep xenoliths) (*Didier, 1987; Montel et al., 1991*). They, therefore, may point to an important role for metasedimentary material in genesis of the particular magma (3.IX.).

All the above types of enclaves tend to cluster into parallel-sided zones, which are polygenic enclave swarms in sense of *Barbarin and Didier (1991)*. The genesis of these swarms has been explained by controlled concentration at the bottom or near the margins of magma chambers, followed by re-injection in form of dyke-like bodies. The possibility of cracking of the not fully solidified magma (Bingham body behaviour) is discussed in explanation of the MME from Teletín (1.X.).

The presence of biotite - amphibole schlieren (3.X.) is interpreted as pointing to the advanced stages of assimilation of the metasedimentary material and therefore to the importance of the metasedimentary input in magmatic evolution (process of assimilation and fractional crystallization - AFC: *De Paolo, 1981*; also 3.IX.). In contrast, the banding in quarry Kozárovec III (3.XII.) has originated late (as one of the MME is cross-cut by the bands) but the plastic deformation of bands suggests that the granodiorite had yet to completely solidify. This banding is strikingly similar to the 'ladder dykes' described by *Reid et al. (1993)* from the Sierra Nevada, and thus may also be cumulative in origin.

The Kozárovec intrusion is cut by dykes belonging to both suites distinguished by *Žežulková (1982a)* and hence it is likely to be older than the Čertovo břemeno mass as well as both suites (3.XIII.).

The presence of the lamprophyre dyke (3.XIV.), truncated by a fresh portion of the granodiorite, implies that the granodiorite must have been at least partly solidified prior to the injection of the dyke. On the other hand, the temperature contrast between both of the granodiorite pulses and dyke had to be small, as no chilled margins are developed either at the contacts of the dyke or between both pulses. The dykes from Kozárovec III had to be late syn-plutonic, as evidenced also by their diffuse contacts.

An alternative explanation of this phenomenon follows that of *Hill (1988)* who has accounted for the origin of 'enclave trains' (monogenic enclave swarms) in the granitoids as being the result of intrusion of syn-plutonic dykes [Fig. II.9.]. In this process the partly solidified magma chamber is cut by a propagating crack, which provides a conduit for the injection of the mafic magma. The dyke, after crossing the wall of the magma chamber, adds mafic liquid to the acid magma and triggers extensive mixing. Subsequently, the dyke is chilled and dismembered and the hybrid liquids, suspended crystals and enclaves are re-distributed parallel to the pluton walls. This model of *Hill (loc.cit.)* could be applicable to the truncated dyke, despite the fact that there is no 'enclave train' present next to it.

The quartz monzonite from Kozárovec II is likely to be hybrid in origin, as indicated by the presence of quartz ocelli, net-veining (3.IV, 3.XVII.), as well as microtextural evidence and the mineral chemistry [Chapter III.1.3.]. Therefore, the term 'Kozárovec quartz monzonite' will be used to avoid the confusion with the other monzonitic rocks occurring in the environs of villages of Zalužany and Lučkovice.

Microscopy

(I) The Kozárovec amphibole - biotite granodiorite (Koz-1 to Koz-13) consists of 30 - 45 % plagioclase, 10 - 30 % K-feldspar (its proportion is difficult to judge in the porphyritic varieties), 10 - 20 % quartz, a variable proportion of amphibole (up to 20 %) and 10 - 20 % biotite. Apatite, titanite, zircon and opaque minerals are common accessory minerals. The average grain size is 0.5 - 2 mm and the texture is hypidiomorphic.

On the basis of mutual relationships the likely order of crystallization is amphibole, biotite → plagioclase → K-feldspar, quartz. The effects of hydrothermal alteration are shown particularly by argillitization of plagioclases, as well as by chloritization of biotites, although this is relatively minor. Very rarely, some secondary calcite can be found. There is some limited evidence of brittle deformation: kinking of biotites, broken plagioclase and amphibole crystals, and undulose extinction and fractures in quartz grains.

PLAGIOCLASE

Plagioclase of andesine composition occurs mainly as subhedral prismatic crystals, 0.8 - 1.5 mm across, but a few crystals up to 4 mm are also present. Most show albite twin lamellae, a few show Carlsbad - albite type twinning and rarely pericline twins are seen. Oscillatory zoning is common [Photo II.3.8.].

Alteration is most pronounced within the crystal cores and along the cleavage planes, with the most altered crystals being those enclosed in K-feldspar. Calcite is not common (apart from Koz-1 and Koz-9). Where it does occur, it is present either as rare aggregates associated with altered cores of plagioclase or in form of interstitial triangular-shaped grains.

Some of the plagioclases are crossed by small cracks filled by quartz, some are broken and show anomalous twinning or bent twin lamellae, due to the post-crystallization deformation.

On the basis of the textural features, the plagioclase is interpreted as being younger than the amphibole and the majority of the biotite. However, the small euhedral laths of plagioclase may also be rarely seen being enclosed in amphibole crystals, suggesting that at least some amphibole crystallization occurred after plagioclase had started crystallizing. There is also evidence of overlap of crystallization intervals of biotite and plagioclase [Photo II.3.9.]. The plagioclase is surrounded by quartz as well as by K-feldspar. K-feldspar may be poikilitic to small plagioclase grains, either euhedral or round [Photo II.3.10.]. At the contact between plagioclase and K-feldspar, myrmekite is common.

Under CL, plagioclase exhibits an ochre - rose luminescence, sometimes with a slight bluish hue. The altered parts are brownish; this is the case especially for the cores of the crystals. The plagioclase frequently shows oscillatory zoning, with repetition of zones of brighter and duller luminescence [Photo II.3.16.].

The composition of plagioclases from the Kozárovec intrusion shows a complicated pattern [cf. Fig. II.15 a] The majority of the small optically unzoned plagioclases corresponds to andesine An₄₁₋₄₄, but they have sometimes cores of andesine - labradorite An₅₀₋₅₂ (Koz-4 from Kozárovec II) and could be overgrown by an oligoclase-andesine rim (An₂₈₋₃₃; Koz-4).

The nature of the compositional zoning of larger optically zoned plagioclases was studied by a scan across plagioclase with two resorption surfaces (Koz-2 from Kozárovec I, Photo II.3.16., Tab. II.3., Fig. II.17.). The rim is normally zoned, with the An content increasing from An₂₃ to An₃₈. There is no compositional difference at the first resorption surface, whereas the second is marked by a sharp increase in calcium (An₄₆; discontinuous zoning) and a marked Or peak (Or_{3.8}). The core exhibits inverse zoning, with the calcium content decreasing inwards (An₄₆ to An₃₈).

Also normally-zoned rims of other plagioclases are of oligoclase - andesine composition (~ An₂₅₋₂₉, sometimes up to An₃₈, rarely ~ An₁₆). The next zone is composed of andesine (An₃₉₋₄₇), and there are sometimes slightly less calcic cores present (An₃₇₋₃₈; e.g. Kozárovec II).

K-FELDSPAR

K-feldspar forms anhedral to subhedral prisms that are strongly perthitic [Photo II.3.18.] as well as poikilitic masses, especially in the even-grained facies (Kozárovec s.s.) [Photo II.3.10.]. Carlsbad twinning is relatively common and cross-hatched twinning is present in parts. The average crystal size is 2.5 - 3.5 mm, although in the porphyritic facies, it may attain few cm.

This mineral shows only little effect of alteration or deformation. The K-feldspar is likely to be the second youngest mineral: it encloses euhedral to subhedral crystals of amphibole, plagioclase and biotite [Photo II.3.10.]. There are reaction relationships between K-feldspar and both plagioclase and biotite, which result in recrystallization at the edges of the biotite. At the contact with plagioclases, thick rims of myrmekite are developed. As quartz is sometimes moulded on K-feldspar, the K-feldspar

ought to be older. However, at least a part of the crystallization interval is shared by both minerals, as indicated by occurrence of strings of round quartz grains enclosed near the edges of K-feldspar megacrysts in the porphyritic facies (Těchnice; Koz-12).

These K-feldspar megacrysts were described as porphyroblasts, replacing older plagioclase, by *Pivec (1970)*. Although the plagioclases enclosed by K-feldspar are often resorbed, there are several features pointing to a phenocrystic origin, the most important being the Carlsbad twinning, the (macroscopically) euhedral shape and the concentric zones of inclusions accreted on K-feldspar growth surfaces (heterogeneous nucleation) (*Vernon, 1986; Pitcher, 1993*). The resorption of plagioclase prior to the onset of crystallization of K-feldspar was documented, for instance, by *Hogan (1993)*. The CL of K-feldspar is bright light blue, lacking any variation [Photo IL.3.17.].

QUARTZ Quartz forms anhedral crystals, on average 0.7 - 1.2 mm across, usually showing strong undulose extinction. Individual quartz grains are often broken into several smaller sub-grains with zigzag margins. In places, it is even cataclastic. The fractures are subparallel, suggesting the possible effects of directed pressure.

Quartz appears to be the youngest mineral, but in relation to the K-feldspar, there is some ambiguity and there was probably an overlap of their crystallization intervals. The quartz moulds on plagioclases and biotites, and is clearly younger than them.

AMPHIBOLE Amphibole crystals are prismatic, euhedral or subhedral, and vary between 1.2 - 1.5 mm (up to 4 mm) in length. Twinning, both simple or repeated on (100) is common. The maximum extinction angle is 20 - 26° suggesting this amphibole is probably 'common hornblende'. It shows a strong pleochroism: X: olive brown-green, Y: dark green, Z: dark bluish-green. Rare examples of broken crystals the amphiboles can be found, indicating that the amphiboles were subject to the brittle deformation.

Some of the hornblendes preserve relict pyroxene cores (Koz-2 and Koz-6). Usually, the amphibole grains occur in clots, together with biotite (*Castro and Stephens, 1992*). Inclusions of tiny biotite flakes in the amphibole crystals are less common [Photo IL.3.11.]; this disequilibrium texture (*Castro, 1993*) will be dealt with in the section about enclaves. Although there are numerous inclusions of apatite crystals, zircon (up to 0.06 mm; surrounded by pleochroic haloes) is considerably rarer. Euhedral plagioclases enclosed by amphiboles are scarce. Amphibole forms chadacrysts in the K-feldspar [Photo IL.3.15.] and it appears to be, after pyroxene and some biotite, the oldest of the main rock-forming minerals.

BIOTITE Biotite occurs in the form of anhedral - subhedral flakes. Their average size is 0.7 - 1.2 mm (up to 2 mm). The biotite is strongly pleochroic: X: pale straw yellow, Y = Z: dark brown. Pleochroic haloes are quite rare and pale.

Biotite is usually fresh, with chloritization affecting only a few flakes along the cleavage. Secondary cleavage as well as bent cleavages can be seen. Sometimes the biotite is recrystallized at the edges. Several broken biotite flakes were also found in the K-feldspar matrix.

Euhedral crystals of apatite are abundant as inclusions in biotites. On the other hand, zircon crystals are rare and usually tiny in size. There is (mainly secondary?) titanite associated with biotite, especially if the former is chloritized. Biotite - amphibole clots are conspicuous in which, in most cases, biotite appears to be the younger constituent. Some of the biotite flakes enclose nearly euhedral amphibole crystals, but in other examples, biotite flakes enclosed by the amphiboles may be found [Photo IL.3.11.] forming a texture similar to that described by *Castro (1993)*. The crystallization

intervals of biotite, which normally looks to be older, and plagioclase, partially overlap [Photo IL.3.14.]. The biotite is obviously older than K-feldspar and quartz.

ACCESSORY MINERALS The common accessory minerals of the Kozárovec granodiorite are apatite, zircon, pyrite, titanite and orthite. *Kodymová and Vejnar (1974)* documented the occurrence of ilmenite, fluorite and monazite in the Těchnice granodiorite.

(II) In the Kozárovec quartz monzonite (KozD-1), tiny elongate (or even needle-like) euhedral - subhedral hornblende crystals [Photo IL.3.13.] are conspicuous. They typically enclose small lobate biotite inclusions. These textures are similar to those found in the granodiorite itself [Photo IL.3.11.]. The biotite inclusions appear to be remnants of individual flakes that were resorbed and incorporated into the growing hornblende crystals. This is a disequilibrium texture and does not represent a normal crystallization sequence in calc-alkaline rocks, in which amphibole is the earlier crystallized mineral. This reversion can be explained either by decrease in activity a_{SiO_2} or increase in $a_{\text{Al}_2\text{O}_3}$ of the melt (*Castro, 1993; Bateman, 1993b*). Such changes in composition of the granitic melt result in equilibrium crystallization of hornblende instead of biotite, being caused by a sudden basification of the magma due to influx of basic magma. In Kozárovec, the amphibole crystallization was followed by second generation of biotite. Somewhat larger hornblende crystals form clots, which are, apart from biotite inclusions, almost monomineralic and many of them are of roughly square outline, resembling pyroxene phenocrysts. The replacement of the early-magmatic pyroxene by biotite - amphibole (actinolite) aggregates is the preferred model of origin of the clots (*Castro and Stephens, 1992; Bateman, 1993b*), although *Chappell et al. (1987)* considered the pseudomorphed pyroxene to be restitic in origin.

Both quartz and K-feldspar form large poikilitic crystals [Photos IL.3.15., IL.3.17.-IL.3.19.], similar to the textures described by *Vernon (1990, 1991)* who explained the origin of similar oikocrysts as being due to their delayed crystallization following a magma-mixing event, caused by a difference of the (higher) quenching temperature and (lower) saturation temperature of the two. On this basis their presence implies a time gap between the magma mixing and the onset of their crystallization. The acicular (quenched; *Wyllie et al., 1962*) apatite is a common constituent of the Kozárovec quartz monzonite [Photos IL.3.13 -IL.3.15.], and mafic hybrids, world-wide, are often rich in apatite. The possible reason could be the sluggish diffusion of P in the melts that leads to selective loss of other more mobile components to the granitic melt and to relative concentration of phosphorus in the mafic phase (*Watson and Capobianco, 1981; Harrison and Watson, 1984; Vernon, 1990*).

Plagioclase occurs in two habits, as small optically unzoned laths (a) and as large rectangular discontinuously-zoned crystals (b). The latter usually encloses abundant apatite needles in its outer zone [Photo IL.3.14.].

(a) The smaller lath-shaped optically unzoned crystals show dull ochre luminescence, very often with bright yellow cores [Photo IL.3.17.] and have uniform oligoclase-andesine composition (An 27 - 39). The larger zoned ones have (andesine)-labradorite cores (An 47 and An 62) and oligoclase rims (An 28) and the discontinuous zoning is clearly seen using CL.

(b) The strongly altered cores of large rectangular plagioclases [Photos IL.3.18.-IL.3.19.] show an ochre or dull yellow luminescence, while the overgrowths display bright yellow spikes and dull ochre rims. This zoning is also revealed from probe studies [Tab. IL.4., Fig. IL.18.]; the average composition of the core is about An 40, and this is overgrown by a calcic spike (~ An 70) and then by a normally-zoned oligoclase - andesine rim (An 28 - 39). Additional analyses of the plagioclases with calcic spikes

show the same pattern: the andesine cores (An 37 - 47) are overgrown by labradorite spikes (An 62 - 67) and normally-zoned oligoclase-andesine rims (An 25 - 39). However some plagioclases with calcic cores and sodic rims also occur [Fig. II.15 b].

The large plagioclases with andesine cores (i.e. of composition similar to the cores of plagioclases of the granodiorite of the main part of the Kozárovec intrusion) could represent:

- (1) Xenocrysts, incorporated into the quartz monzonite magma from the granodiorite. In this case in the more basic magma the andesine cores would have been resorbed and overgrown by calcic (labradorite) spikes. At this stage lath-shaped plagioclase, having a matching labradorite composition, would also have started to nucleate. There may have been the only limited interaction between a minor amount of more acidic magma and the predominant basic magma before the major magma-mixing event, at which stage there would have been a larger volume of the acid magma. As a consequence, the oligoclase-andesine rims would have overgrown the previously-formed cores. At the same time, numerous unzoned, lath-shaped crystals would have formed and such a high nucleation rate would imply a high degree of undercooling. This magma-mixing event has also been recorded by some of the plagioclases of the granodiorite itself (Koz-4; Kozárovec II), causing slight reversals in the zoning and probably accounting for the presence of infrequent labradorite cores (see above).
- (2) Skeletal plagioclase phenocrysts (cellular morphology) of calcic plagioclase that grew during the thermal adjustment between the interacting mafic and acid magmas from the mafic melt (Hibbard, 1981). Subsequently, the calcic dendrite would have been infilled and overgrown by a more sodic plagioclase.

ENCLAVES

The studied sample was Kozm-1, an elongate MME (15 x 4 cm), without reaction rim from quarry Kozárovec I.

The sample Kozm-1 contains subhedral elongate hornblende crystals, which are more abundant than blade-shaped biotite flakes. This blade-shaped biotite is an unusual morphology which has been attributed to magma-mixing of a Mg and Fe-rich aluminosilicate system with one rich in potassium (Hibbard, 1991).

Some of the larger hornblende crystals have cores of relict pyroxene; in one case, subhedral clinopyroxene, about 1 mm across, was overgrown by a hornblende corona. Most of the hornblende is present as monomineralic clots with circular outlines. Some of the clots are scattered in the granodiorite host and probably were derived from the broken enclave rims. Small, lath-shaped crystals of plagioclase are common. Some of the plagioclases are, however, larger and these are usually mantled (i.e. discontinuously zoned).

For both the MME and Kozárovec quartz monzonite, the presence of mantled plagioclases, amphibole coronas around the relict pyroxene cores, square outlines of many of the biotite-amphibole clots, resorbed biotites in centres of amphiboles, blade-shaped biotites (of the second generation), small lath-shaped plagioclase crystals and acicular apatite (cf. Hibbard, 1981, 1991; Barbarin, 1990b; Vernon, 1990, 1991; Castro and Stephens, 1992; Bateman 1993b; Castro, 1993), together with field relations (see above) provide convincing evidence for operation of magma-mixing processes in the Kozárovec body at least in that part near the village of Kozárovec.

II.4. Blatná intrusion (including Červená granodiorite)

This U-shaped intrusion forms most of the southern and south-western part of the CBP [Fig. II.3.]. In literature, its southernmost part has been referred to as Červená granodiorite which, compared with Blatná s.s., is more mafic, has a higher proportion of amphibole, more abundant MME, a well-developed planar fabric and shows effects of a stronger deformation.

In the Blatná intrusion, the most common rock type is an amphibole - biotite to biotite granodiorite, the latter forming the central part of the intrusion (so-called biotite facies) (Řečice, Paštiky, Defurovy Lažany) with a transitional boundary between the two (also Dudek and Fediuk, 1953, 1960). The granodiorite is either even-grained (majority of the biotite facies; cf. Dudek and Fediuk, 1953) or contains a minor proportion of K-feldspar phenocrysts (up to 2 cm in size; Tužice, Velenov). The amphibole content increases both southwards (towards the Červená granodiorite) and northeastwards (Hudčice). MME and surmicaceous enclaves are generally common but less so in the biotite facies. Metasedimentary xenoliths are also less common in the biotite facies than in the main part of the intrusion but show a marked increase in number towards the Metamorphic Islet Zone and the Moldanubian Unit.

In the northern part, the Blatná body is intruded by a stock of Nečín granodiorite and encloses numerous basic bodies (mainly gabbroids).

The Blatná intrusion is adjacent to low-grade Proterozoic metasediments of the Teplá-Barrandian Unit (NW), high-grade paragneisses and migmatites of the Moldanubian Unit (W and S), and to metasediments and orthogneisses of the Mirovice Metamorphic Islet as well as Proterozoic metavolcanic rocks of the Jílové Zone. The intrusion is also in contact with the Marginal (NW), Sázava (N), Kozárovce and Čertovo břemeno (NE) intrusions.

Field observations

- I. The contact of the Červená granodiorite with the Moldanubian Unit is sharp, with a marginal zone of fine-grained contaminated granodiorite, up to 10 m wide, which shows a considerable increase in content of apatite (up to 10 %) and zircon (the main accessory mineral of the adjacent Moldanubian rocks) and a decrease in proportions of amphibole and pyroxene which are absent in the country rocks (Souček 1965, 1969, 1972, 1974). The intrusion caused thermal metamorphism and metasomatism of the Moldanubian rocks, which manifests itself by growth of porphyroblasts of plagioclase and K-feldspar (typically 1 - 2 mm), and more rarely, of cordierite, resulting in the so-called 'pearl gneisses' that pass gradually into Moldanubian migmatites (Souček, 1974) (Písek).
- II. The contact between Blatná (s.s.) and Červená parts of the intrusion is transitional (also Kodým, 1966, Žežulková, 1982) although Urban (1930) and Kodým and Suk (1958) record it as being either sharp or locally diffuse.
- III. Blocks (up to 80 m across) of the Blatná granodiorite, cut by minette dykes and enclosed by the Čertovo břemeno durbachite were described by Holub and Žežulková (1978 - Zvíkovské Podhradí). None of the dykes passed into the surrounding durbachite. There are also penetrations of the Čertovo břemeno intrusion into the Blatná mass (Holub and Žežulková, loc.cit.; Andrusov, 1932; Kodým et al., 1963). Kotek and Zikmund (1965) recorded xenoliths of Červená granodiorite in Čertovo břemeno durbachite, and vice versa while Zikmund (1974) described (1) the Čertovo břemeno and Blatná masses as passing gradually into each other, (2) injections of the Čertovo břemeno durbachite into Červená granodiorite and (3) angular xenoliths of the former in the latter.

- IV. The Blatná granodiorite encloses angular xenoliths of granite similar to the Marginal type (*Kodym and Suk, 1960*).
- V. A single xenolith considered to be similar to the Těchnice granodiorite in the Blatná mass was recorded by *Kodym (1955)*.
- VI. Angular and elongate country-rock xenoliths are typically of infrequent occurrence in the Blatná granodiorite (s.s.). These are mainly migmatitic and biotite paragneisses (*cf. Dudek and Fediuk 1953, 1960*). There are also carbonate xenoliths, with narrow dark fine-grained reaction rims (Řečice) but these are rare. There also some xenoliths of orthogneiss (Hudčice) (*Dudek and Fediuk, 1956*). In contrast to the rest of the body, xenoliths of metasediments are abundant in Hudčice (*also Vachtl, 1933*) where the products of widespread assimilation of the metasedimentary material are seen in various stages of digestion (*Vachtl, 1933; Dudek and Fediuk, 1956*). Large xenoliths are broken, net-veined, invaded and digested by the granodiorite, which, as a consequence, has been greatly contaminated [Photo II.4.1.]. Some of the xenoliths are surrounded by thin aplitic reaction rims.
- VII. In the Červená granodiorite, metasedimentary xenoliths are common, especially close to the contact with the Moldanubian Unit (*cf. Vejnar, 1955, Holub, 1989*). They are paragneisses, which differ from the adjacent Moldanubian pearl gneisses (4.I.) by their lack of muscovite, presence of amphibole, high apatite content and different An of plagioclases (*Souček, 1971*) (Písek). There are also xenoliths of amphibolite and scarce carbonate xenoliths that become more abundant further west (*Vejnar, 1954; Holub, 1989b*) (Horažďovice, Strakonice), where carbonates are a common constituent of the adjacent Moldanubian Unit (*Kodym and Suk, 1958*).
- VIII. In the Blatná granodiorite (s.s.), MME are fairly common but their number is less in the biotite facies (Defurovy Lážany, Řečice). They are mainly round in shape [Photo II.4.2.], on average 5 - 10 cm across, and often contain plagioclase megacrysts up to 2 mm in size (*also Dudek and Fediuk 1953, 1960*). In the more deformed portions of the granodiorite, the enclaves are ellipsoidal [Photos II.4.3., II.4.4.]. In the most deformed ones, some of the MME are represented as amphibole - biotite schlieren (Vahlovice, Vlčkovice, Tužice). In Hudčice, MME have not been identified unequivocally; they might be macroscopically difficult to distinguish from xenoliths of the granodiorite porphyry or Hudčice diorite (4.XII. and 4.XIII.). Ellipsoidal MME, abundant in the Červená granodiorite, are cognate with their host and were transported mainly in a solid state (*Souček, 1971*).
- IX. Surmicaceous enclaves are relatively common in the Blatná intrusion. They are usually round in shape, generally smaller than the MME (several cm) but some are larger (up to 30 x 20 cm; Defurovy Lážany).
- X. A parallel-sided zone of a strongly contaminated porphyritic granodiorite encloses abundant broken MME, surmicaceous enclaves and metasedimentary xenoliths as a polygenic enclave swarm in Tužice.
- XI. Dykes cutting the Blatná intrusion include aplopegmatites, microgranites, granite-, granodiorite-, syenite-, syenogabbro- and syenodiorite-porphyrries, lamprophyres (minettes and kersantites) (*Vejnar, 1954, Kodym and Suk, 1958, 1960; Dudek and Fediuk, 1953, 1960; Žežulková, 1982a*) with the aplopegmatite dykes being particularly common, especially in the biotite facies. They are, on average, 10 cm across (up to 50 cm), with sharp contacts against the granodiorite (Řečice, Defurovy Lážany). Several sub-vertical lamprophyre dykes intrude a severely deformed and altered zone in Vlčkovice and several sub-vertical minette dykes, the thickest 3 m in width, occur in Kozlí. One of them is strongly sheared, and the host granodiorite shows a weak planar fabric. The

two suites of the dyke rocks that have been distinguished in the southern CBP, one older and one younger than intrusion of Čertovo břemeno (see 3.XIII.) are both present in the Blatná mass (Žežulková, 1982a).

XII. A granodiorite porphyry dyke without chilled margin and broken into angular xenoliths that remain more-or-less in situ cuts granodiorite in the Hudčice quarry [Photo II.4.5.]. Close to one margin of the dyke is a small mass of diorite, rich in plagioclase megacrysts, quartz ocelli and round enclaves similar to the porphyry, with a sharp contact against a thin aplitic band (that may represent a chilled margin of the granodiorite) [Photos II.4.5.- II.4.6.]. Elsewhere the diorite passes gradationally into the Blatná granodiorite. In the quarry also occur angular blocks, similar to the diorite, that are also in sharp contact with an aplitic rim to the granodiorite [Photo II.4.7.].

XIII. E - W trending bodies of a strongly altered granodiorite with pink - red feldspars and secondary chlorite, epidote and clay minerals are seen at a number of localities in the environs of the town of Blatná. These bodies were studied in connection to the prospection for the uranium mineralization and the alteration effects diminish towards the surrounding fresh granodiorite (Dudek and Fediuk, 1953, 1960; Knotek and Lang, 1985).

XIV. In the Červená granodiorite, there is alignment of elongate MME that records a flow fabric; Superimposed on this is a generally parallel dimensional orientation of minerals in both the host granodiorite and the enclaves (Tužice, Vlčkovice) [Photo II.4.3.]. Locally, the superimposed fabric is less prominent than the strong alignment of the enclaves, especially in the Blatná granodiorite close to the Mirovice Metamorphic Islet (Vahlovice, Jindřichovice, Buzice) [Photo II.4.4.] (also Orlov, 1932; Kodým and Suk, 1958). In contrast, in the biotite facies, the granodiorite shows little or no dimensionally-oriented fabric but a regular and undisturbed jointing pattern (also e.g. Orlov, 1938).

Interpretation of field relations

The Červená granodiorite is a marginal facies of the Blatná intrusion (also Holub, 1992; Malecha et al., 1960; Kodým and Suk, 1960), richer in amphibole, having more abundant MME and showing a strong planar fabric. There is a transition between the two (4.II.).

The contact of the Červená granodiorite with the rocks of the Moldanubian Unit is intrusive in character (4.I.) and on this basis the hypothesis of its origin as the result of metasomatism (feldspathization) of the Moldanubian rocks (Röhlichová, 1964b) is rejected. At the contact, assimilation of the Moldanubian country-rock is widespread, which led Malecha et al. (1960) to propose that the Červená granodiorite was a variant of the Blatná granodiorite contaminated by assimilation of Moldanubian rocks.

The Blatná intrusion is probably older than Čertovo břemeno durbachite, despite ambiguous observations of Knotek and Zikmund (1965) and Zikmund (1974) (4.III.). It is younger than the Marginal type granite (4.IV.) but its relation to the Kozárovce intrusion is not clear, as the observation of Kodým (1955) has not been confirmed (4.V.).

The metasedimentary xenoliths are mainly pelitic, and the proportion of carbonate xenoliths increases towards the Moldanubian marble occurrences (4.VI., 4.VII.). At the contacts with the Moldanubian Unit and the Metamorphic Islet Zone, assimilation of the metasedimentary material has been widespread and its contribution to magma could have been considerable (AFC) (e.g. Písek, Hudčice) (4.I., 4.VI., 4.VII.).

Presence of both MME and surmicaceous enclaves, especially in the amphibole - biotite granodiorites (4.VIII., 4.IX.) implies a mixed crustal - mantle source (*Didier, 1987; Montel et al., 1991*). The mantle input could have been both in form of basic mantle-derived igneous rocks, or melts of immature sediments with a high proportion of young, mantle-derived component.

All the enclave types tend to form polygenic enclave swarms: the genesis of these swarms is discussed in the section on the Kozárovec intrusion (3.XL)

The association of the dyke rocks is similar for both Blatná and Červená types, and includes some of the older types, not present in the Čertovo břemeno intrusion and the latter, therefore, is interpreted as being younger (4.XI.).

The Hudčice dyke of the granodiorite porphyry (4.XII.) intruded an almost solidified granodiorite, which was, however, still mobile enough to break it into angular fragments but still sufficiently hot so that no chilled margin at the dyke - granodiorite contact developed. The granodiorite probably behaved plastically, as a Bingham body (cf. 1.X.). and the dyke of porphyry must be, therefore, late syn-plutonic (cf. *Pitcher 1991, 1993*) [Fig. II.7.]. The aplitic rim might represent a chilled margin but because it lacks gradation, it is more likely to be either a result of reaction of both magmas or a veinlet utilising the dyke - granodiorite boundary.

The transitional contact of the diorite batch from Hudčice (4.XII.) is likely to have developed due to material exchange with the granodiorite and the plagioclase megacrysts are probably xenocrysts: their number decreases away from the transitional boundary. This rock will be referred to as 'Hudčice diorite' and its origin is likely to be connected with the nearby dyke of the granodiorite porphyry, whose xenoliths it encloses. Apart from this case, there was no field evidence of magma mixing found in the Blatná intrusion.

In places in the central part (biotite facies), the Blatná granodiorite suffered strong hydrothermal alteration (4.XIII.), possibly in connection with a later (uranium ?) mineralization.

The degree of deformation of the granodiorite increases towards the Mirovice Metamorphic Islet in the east and the Moldanubian Unit in the south; essentially no deformation is expressed in the centre of the intrusion (4.XIV.). The strong elongation and alignment of the MME in Vahlovice appear to be controlled mainly by the magma-flow (cf. *Vernon et al., 1988*), although there is some macroscopic evidence of superimposed solid-state deformation. Also the host granodiorite has suffered a solid-state deformation, as documented mainly by microstructural evidence (see below). The granitoids emplaced strictly by magmatic flow could still rotate the foliations in the country rocks, develop magmatic foliations that increase in intensity towards external contacts and have flattened enclaves indicative of greater than 60 % shortening near these margins (*Paterson et al., 1989*). The superimposed solid-state deformation might have originated as consequence of either ballooning or regional deformation (contemporaneous or post-dating the emplacement). To resolve the issue, a detailed structural work needs to be undertaken in marginal parts of the Blatná intrusion, and, more importantly, in the country rocks, where both foliations and cleavage-porphyroblast relationships are to be examined (*Paterson et al., 1989*).

Microscopy

The Blatná and Červená (amphibole -) biotite granodiorites (Bl-1 to Bl-8, Cv-1 to Cv-3) consist of 20 - 35 % quartz, 25 - 45 % plagioclase, 5 - 30 % K-feldspar, 15 - 25 % biotite and up to 5 % amphibole. Among the accessory minerals, apatite prevails over zircon, titanite and opaque minerals; some orthite also occurs. The texture is hypidiomorphic.

The likely order of crystallization is amphibole → biotite, plagioclase → quartz, K-feldspar. The effects of late hydrothermal alteration are shown by considerable argillization of plagioclase and by limited chloritization of biotite. In places, secondary calcite and epidote also occur. There is firm evidence of post-crystallization deformation at some of localities (e.g. Vahlovice, Hudčice; to some extent also at Tužice, Defurovy Lažany and Paštiky) as, for instance, the kinking of biotites, undulose extinction and fracturing of quartz grains, the cataclasis of quartz and, more rarely, also of plagioclase.

PLAGIOCLASE Plagioclase of oligoclase - andesine composition forms subhedral prismatic crystals, on average 1 - 2 mm (up to 5 mm) across. The majority of them show albite twin lamellae, a few Carlsbad-albite and, infrequently, pericline type twinning. Oscillatory-zoned plagioclase crystals are quite common [Photo II.4.8.].

The degree of alteration of plagioclase varies considerably throughout the intrusion with argillitization of plagioclase being almost complete in the central part (e.g. Řečice); elsewhere the products of this process are shown only along cleavages and in crystal cores. At some of the localities (Vlčkovice, Velenovy, Hudčice) calcite occurs, probably as an alteration product, often associated with epidote. Calcite may form grains up to 0.3 mm across, and in Vlčkovice it fills thin veinlets.

Some of the plagioclase, especially in the southern part of the body, exhibits effects of relatively strong deformation such as the bending of crystals [Photo II.4.12.]. Plagioclase from Vahlovice and, to some extent, also from Hudčice, has suffered cataclasis with rims of the larger crystals showing the effects of crushing [Photo II.4.13.].

Plagioclase encloses small subhedral flakes of biotite, but the relation between these two minerals is generally more complicated. In places plagioclase surrounds biotite, but elsewhere biotite flakes mould on big, subhedral crystals of plagioclase or enclose tiny round plagioclase grains. The plagioclase is older than both quartz and K-feldspar, and myrmekite is common at the contact with K-feldspar [Photo II.4.9.]. Small round grains of plagioclase are frequent inclusions in the younger K-feldspar phenocrysts.

Plagioclase emits ochre - rose luminescence, sometimes with a bluish hue. Usually, it is zoned with somewhat more bluish cores. The altered zones are variously white (Tužice) or black (sericitization; Vahlovice).

In a sample from Velenovy (BI-3), the andesine cores (An 32 - 38) are overgrown by oligoclase rims (An 26 - 28). In two plagioclases from Vahlovice (BI-5), reverse zoning was observed: the normally zoned andesine rims (An 31 - 37) enclose cores of oligoclase (An 28 - 29). The small unzoned plagioclases show little variation throughout the intrusion (An 30 - 39) and are compositionally similar to the tiny plagioclases enclosed by K-feldspar (An 32 - 36).

The zoning of plagioclases from Hudčice (BI-8) is more complex, including discontinuous and oscillatory zoning. They are mantled plagioclases with cores up to An 49 and rims of An 33 - 37. A scan across an oscillatory zoned plagioclase from Hudčice [Tab. II.5., Fig II.19.] shows a calcic spike (maximum at An 55) in the plagioclase which otherwise has uniform andesine composition (An 32 to An 42). Such an abrupt change in the An content of the crystallizing plagioclase argues for a sudden basification of the magma, presumably by an influx of basic magma into the magma chamber. The obvious candidate is the syn-plutonic dyke of granodiorite porphyry, forming hybrid types in the quarry.

Generally speaking it is possible to agree with conclusions of *Knotek and Lang (1985)*, who have reported the composition of plagioclases from both Blatná and Červená granodiorites (S of town of Blatná) to be An 15 - 45 with maximum at about An 25 - 30.

QUARTZ Anhedral quartz grains are, on average, 1.5 - 2.5 mm across. Some of them (Vlčkovice, Vahlovice, Hudčice, and Paštiky) are more affected by the post-crystallization deformation than others. In the more deformed samples, apart from common, strong undulose extinction, bubble trains and subparallel crack systems are present. The quartz is often cataclastic, broken into many sub-grains [Photo II.4.14.]. Elsewhere the quartz is almost undeformed, and virtually without undulose extinction (the central part of the body, e.g. Řečice).

Quartz appears to be the youngest mineral, as it moulds on both biotite and plagioclase, and some of the K-feldspar. However, a few round quartz grains also occur within the K-feldspars.

K-FELDSPAR K-feldspar occurs in the form of subhedral to anhedral prismatic crystals, on the average 1 - 2 mm across (up to 6 mm). Towards the SW (Defurovy Lažany and Tužice quarries), it becomes increasingly perthitic. In the same direction, the amount of the K-feldspar with cross-hatched twinning (microcline) increases. Carlsbad twinning is not particularly common.

K-feldspar is much more resistant to the alteration than plagioclase. No effects of a later deformation could be seen.

Small crystals of plagioclase and biotite [Photo II.4.10.] are common inclusions in the K-feldspar phenocrysts, providing a firm evidence of K-feldspar being younger. The relation between quartz and K-feldspar, however, is not clear: the K-feldspar crystals usually retain crystal faces against the subhedral quartz but, in turn, there are also round quartz grains enclosed by the K-feldspar phenocrysts. Accordingly it is interpreted that at least a part of the crystallization interval of both minerals was shared.

The K-feldspar exhibits bright light blue luminescence. Some of the K-feldspar crystals are weakly zoned, usually with lighter cores. Veinlets of somewhat brighter bluish hue, cutting across the K-feldspar grains, are very common.

BIOTITE Biotite flakes are subhedral - anhedral, on average 0.7 - 1.2 mm (up to 2.5 mm) across. It is strongly pleochroic: X: straw yellow, Y = Z: dark rusty-brown. Pleochroic haloes are infrequent, and, apart from samples from Paštiky, Velenovy and Hudčice, are pale and very small.

Chloritization is limited, usually following the cleavage planes; only in the Řečice sample is the biotite extensively altered. In majority of the samples, the biotites coexisting with the more altered plagioclase show the greatest effects of alteration. In the samples from Tužice, Velenovy, Defurovy Lažany and Hudčice, kink bands occur [Photo II.4.15.].

Euhedral apatite crystals are common within the biotite but the proportion of euhedral zircon inclusions varies considerably. Biotite is associated with titanite, which, locally, is the product of alteration related to intense chloritization. In Vlčkovice, the titanite occurs in form of chains of crystals, roughly parallel to the cleavage of the biotite host. Some of the biotites are rimmed by an opaque ore mineral. Biotite is clearly older than K-feldspar and quartz. Its relation to plagioclase is not clear, however, and both minerals have probably shared similar crystallization interval. Amphibole, if present, is often associated with biotite, and probably is older. Rarely, biotite is enclosed in the amphibole crystals.

AMPHIBOLE

The amphibole prisms are, on average, 1 - 1.2 mm (up to 3.5 mm) long. They are subhedral to anhedral, with common polysynthetic twins on (100).

The maximum extinction angle ($Z^{\wedge}c$) is 18 - 24°, corresponding to common hornblende. It is strongly pleochroic: X: olive yellow-green, Y: dark green, Z: deep bluish-green.

Apatite and, more scarcely, zircon, surrounded by pale pleochroic haloes, form inclusions in the amphibole crystals. The amphibole seems to be, with the exception of tiny biotite flakes it sometimes encloses, the oldest rock-forming mineral. It is surrounded by both K-feldspar and quartz. Quite often, it is associated with biotite and euhedral titanite in clots, for instance in Vahlovice [Photo IL.4.11.].

ACCESSORY**MINERALS**

The main accessory minerals of the Blatná granodiorite (s.s.) are zircon, apatite, titanite and pyrite; less abundant are orthite and epidote. The association is very similar in the Červená granodiorite, but content tends to be higher (*Kodymová and Vejnár, 1974*). Of particular interest is the presence at Vlčkovice of orthite crystals, full of euhedral ore mineral inclusions [Photo IL.4.23.].

ENCLAVES ETC.

Several types of MME were studied: (1) a lobate amphibole - biotite enclave from Vahlovice (5 cm in diameter, diffuse margins; Blm-7); (2) an amphibole-biotite MME with feldspar megacrysts up to 0.5 cm long from Tužice (Blm-2), and (3) a lenticular biotite - amphibole enclave with feldspar megacrysts from Vlčkovice, (18 x 18 x 6 cm; CvE-1). Also studied were (4) a flattened surmicaceous enclave (30 x 20 cm) from Defurovy Lažany (Blm-10), (5) a Hudčice diorite (BID-1) and granodiorite porphyry also from Hudčice (Blm-13).

(1) The Vahlovice MME (Blm-7) is rich in subhedral biotite [Photo IL.4.19.] and the gaps are filled by anhedral quartz and plagioclase. There is a great abundance of short prismatic apatite and an equidimensional opaque ore mineral, sometimes with a square outline.

(2) The MME from Tužice (Blm-2) contains several plagioclase megacrysts up to 0.5 cm across. They are subhedral, usually without zoning, like the plagioclases of the matrix. Amphibole forms weakly pleochroic, almost colourless subhedral prisms, surrounding older plagioclases. Sometimes, it preserves cores of amphibole with stronger pleochroism or patches of relict pyroxene; apatite inclusions are common. Several clots were observed, up to 3 mm in size, formed mainly by a mosaic of the more pleochroic hornblende grains, surrounded by a biotite corona. Biotite occurs as subhedral - anhedral flakes of strong pleochroism; they lack inclusions, but are often surrounded by thin rims of opaque ores. K-feldspar forms oikocrysts, enclosing the earlier-formed minerals [Photo IL.4.17.]. Tiny round quartz grains are notably rare. Apatite of long-prismatic habit is very common. Twinned prisms of euhedral oscillatory zoned orthite, also occur along the enclave-granodiorite contact [Photo IL.4.18.].

(3) The enclave from the Červená granodiorite (CvE-1) is not a typical MME, as its average grain size (~ 0.5 mm with plagioclase megacrysts up to 0.5 cm) approaches that of the host granodiorite. The texture, however, is characteristic. Plagioclase megacrysts show albite twin lamellae and frequently convolute zoning. Mantled plagioclase megacrysts are much less common. In these, obvious resorption surfaces can be observed, marked by a ring of tiny acicular apatite and round biotite; the rim of plagioclase is much richer in apatite than the core. Biotite occurs as anhedral, lobate flakes with thin rims of opaque minerals and titanite. Both biotite and pale, weakly pleochroic, subhedral to anhedral hornblende are interstitial to larger plagioclases. Quartz, in the form of round grains, is rare. Accessory

minerals are abundant, including both prismatic and acicular apatite, round zircon and small euhedral titanite. The latter often surrounds the edges of biotite flakes, and appears to be mainly secondary in origin.

(4) The biotite of the surmicaceous enclave (**Blm-10**) occurs in the form of subhedral or anhedral flakes, strongly pleochroic, and virtually inclusion-free. About half of the flakes show numerous strictly parallel kink folds indicative of directed pressure. The space between the biotite grains is filled by small subhedral plagioclase, quartz and K-feldspar. Abundant, large euhedral - subhedral crystals of titanite are prominent. This titanite is often poikilitic, with chadacrysts of round quartz and plagioclase [**Photo II.4.16.**]. Such a texture has been attributed by *Hibbard (1991)* to the effects of magma mixing. Some of the titanites contain parallel polysynthetic lamellae, representing mechanical twinning glide planes at $(110)_Z$, that may be caused by shock (such as at nuclear test sites) or by oriented stress (*Deer et al., 1982; Ribbe, 1982*). Only one set of twin lamellae could be produced, from which the direction of the principal stress could be deduced. The sample is also rich in anhedral (resorbed?) or round apatite crystals.

(5, 6) The Hudčice diorite and granodiorite porphyry (**BID-1, Blm-13**) have glomeroporphyritic texture with plagioclase phenocrysts which are up to 5 mm in size, and show a complicated oscillatory and convolute zoning [**Photo II.4.20.**]. They have arcuate margins and contain frequently secondary twin lamellae, or are fractured. At least part of them, most likely the highly irregular fragments of plagioclase and K-feldspar crystals (**Blm-13**), appear to be xenocrystic in origin. Quartz ocelli (up to 2.5 mm across), surrounded by fine-grained hornblende rims, are unequivocally xenocrystic (*e.g. Vernon, 1990; Hibbard, 1991*; for explanation of their origin, see section on the Říčany granite) [**Photo II.4.21.**]. Round biotite flakes may attain up to 0.5 mm in size. The groundmass is made up of pale subhedral amphibole, less common biotite, anhedral quartz and plagioclase, and acicular apatite. The amphiboles tend to cluster into nearly monomineralic clots, as do the biotites. Frequently, biotites form spherulites with a grain of an opaque mineral (of squared outline) in the centre [**Photo II.4.22.**].

II.5. Sedlčany intrusion

This SW - NE elongate intrusion occurs in the eastern part of the CBP [**Fig. II.4.**]. The prevailing rock type is a porphyritic amphibole - biotite to biotite granite, with the latter present only in the central part of the body (biotite facies; *Kosova Hora*). Various types of enclaves, including MME, surmicaceous enclaves and metasedimentary xenoliths are abundant, especially in the western part.

In the centre of the Sedlčany intrusion there occurs a small body of fine-grained muscovite - biotite granodiorite (with cordierite) of the *Kosova Hora* type (not to be confused with the biotite facies of the Sedlčany intrusion that surrounds it), which contains numerous biotite schlieren, pointing to marked assimilation of metasedimentary material (*Kodym, 1966*).

The Sedlčany intrusion is adjacent to high-grade metamorphic rocks of the Moldanubian Unit, Proterozoic-Palaeozoic metasediments of the Metamorphic Islet Zone (Sedlčany-Krásná Hora and Maršovice Metamorphic Islets) and the Maršovice (N), Čertovo břemeno (S) and Kozárovce (W) intrusions.

Field relations

- I. Sedlčany granite causes a contact metamorphism of the adjacent Sedlčany-Krásná Hora Metamorphic Islet, in which sediments as young as mid-Devonian are present (*Afanasjev et al., 1977; Chlupáč, 1988*).
- II. The Sedlčany granite passes gradually into Čertovo břemeno durbachite (*Svoboda, 1932*).
- III. There is no evidence of relative age relations with either Kozárovce or Maršovce intrusions.
- IV. Metasedimentary xenoliths, mainly of biotite hornfels, paragneiss and calc-silicate rock [Photo IL.5.1.], are relatively infrequent in the eastern part of the body (Vrchotovy Janovice), but they become more abundant in the western (Kosova Hora) and especially in the southwestern (Vápenice) parts. Ellipsoidal, partially assimilated carbonate xenoliths, up to 15 cm across, with fine-grained green (diopside-bearing ?) reaction rims about 2 cm thick were found in Vrchotovy Janovice. Other carbonate xenoliths are zoned and partly resorbed [Photo IL.5.2.], with diopside-rich rims and centres of pink axinite (up to 0.5 cm crystals) in the Vápenice quarries (XRD determination: *Zeithamová, 1990*). Quartz-free Al-rich gneiss xenoliths with corundum and hercynite have also been recorded (*Zeithamová and Holub, 1989; Zeithamová, 1990*).
- V. Commonly enclosed by the Sedlčany granite are quartz xenoliths (or ovoids), often with thin amphibole coronas (e.g. Vápenice) [Photo IL.5.3]. Elongate aplitic xenoliths (up to 25 cm long) with partly arcuate margins also occur (Vrchotovy Janovice).
- VI. MME are abundant in the Sedlčany intrusion, especially in the western part (Vápenice). They are round or ellipsoidal in shape, with sharp contacts. A few are broken and net-veined by the host granite (Vrchotovy Janovice, Vápenice) [Photo IL.5.3.]. The enclaves in the southwestern part of the intrusion (Vápenice) are not only more abundant but also tend to be larger (up to 1 m) and more angular. They are of various types, ranging from equigranular fine-grained to plagioclase megacryst-rich (up to 0.5 cm) types. Occasionally they contain round K-feldspar megacrysts (up to 2 cm; Vápenice), quartz ocelli and xenoliths (\pm amphibole coronas) [Photo IL.5.4.], and angular xenoliths of hornfels (Vápenice). Biotite and amphibole tend to cluster into macroscopically obvious clots. In the Vápenice quarries there are MME with an inner zone, in which plagioclase megacrysts are absent or rare, and an outer zone rich in plagioclase megacrysts - double enclaves (similar to Photo IL.3.3.; cf. 3.VIII.).
- VII. A few MME are resorbed at the edges, and, in the most advanced stage, they could show effects of almost complete digestion by the magma, leaving residual amphibole - biotite schlieren (Vápenice). Amphibole - biotite schlieren, up to 50 cm in length, subhorizontally disposed, have also been observed in Bořená Hora.
- VIII. Surmicaceous enclaves are considerably rarer and smaller than the MME; they are mainly round and up to 15 cm in diameter. One of them, however, was angular and enclosed two quartz xenoliths (Vápenice).
- IX. Relatively common are pilitic pseudomorphs, with olive green cores and thin black (amphibole - biotite) rims, often enclosed by the MME (Vrchotovy Janovice) (*also Holub, 1990*).
- X. Dykes of aplite are common in Kosova Hora but not present in either Vápenice or Vrchotovy Janovice.
- XI. The Sedlčany and Čertovo břemeno intrusions show an uniform tectonic and fluidal fabric (*Beneš, 1970*). There is no field evidence of late deformation and the granite shows well-developed jointing.

Interpretation of field relations

The Sedlčany granite is a zoned body, with the central part made up of the biotite facies. Little is known from contact relationships about its relative age (5.II., 5.III.), but the emplacement must post-date mid-Devonian (5.I.). The structure shared by both the Sedlčany and the Čertovo břemeno intrusions suggests that they are of similar age (5.XI.). Nevertheless, the lack of deformation and scarcity of dykes cutting the Sedlčany intrusion (5.X.) imply a relatively young age amongst the granitoids of the CBP.

The abundance of metasedimentary xenoliths and the evidence for magmatic reaction (5.IV.) could point to the importance of the high-level assimilation (AFC) (Maury and Didier, 1991). The high percentage of the carbonate xenoliths, especially in Vápenice, may imply a source similar to the adjacent Sedlčany-Krásná Hora Metamorphic Islet, where the carbonates are common (also Zeithamová, 1990). In the Sedlčany granite, however, the proportion of the xenoliths derived from the Metamorphic Islet Zone and Moldanubian Unit is difficult to assess (Holub, 1989b). Moreover the rocks of the Metamorphic Islet Zone (Sedlčany-Krásná Hora Metamorphic Islet) were interpreted as being transitional with the rocks of the Moldanubian Unit in the Votice area (Suk, 1973, Chlupáč, 1988), which would mean that such a distinction is unnecessary and misleading. Suk (1973) considered this transition to be a result of Precambrian - Eocambrian Barrovian-type metamorphism that shows an increasing grade from the NW (Jílové Zone) to the SE (Moldanubian Unit). The Al-rich xenoliths from Vápenice are similar to those described by Holub (1980) from the Čertovo břemeno intrusion.

The aplitic xenoliths from Vrchotovy Janovice (5.V.) (felsic microgranular enclaves in terminology of Didier and Barbarin, 1991) could represent either disrupted syn-plutonic dykes, or fragments of a chilled margin of the intrusion.

MME are ubiquitous in the Sedlčany granite (5.VI.). Their source magma penetrated similar country rocks as the Sedlčany intrusion, as both contain matching metasedimentary xenoliths. The MME must have been introduced into the Sedlčany magma soon after they acquired their xenoliths (as they are angular) at relatively shallow depth (Maury and Didier, 1991). The presence of pilites (5.IX.), implies that the parental magma of the MME was probably olivine-bearing (also Holub, 1990). For explanation of the origin of the double enclaves, see 3.VIII. (Pitcher, 1993) [Fig. II.8.].

Presence of the surmicaceous enclaves (5.VIII.) points to an important contribution of the metasedimentary material to the origin of the magma (besides shallow-level AFC; 5.IV.) and, together with the abundance of the MME, to a mixed mantle - crustal source (Didier, 1987; Montel et al., 1991). On the other hand, the evidence of assimilation of the MME and the origin of the amphibole - biotite schlieren (5.VII.) reveals an additional contamination mechanism that was potentially operative in genesis of the Sedlčany granite. However, the origin of some of the schlieren is uncertain: apart from resorption of enclaves, they could have resulted from as different processes as gravitational segregation, double (heat - material) diffusion and shear-flow (Clarke, 1992).

Microscopy

The Sedlčany intrusion is a uniform porphyritic biotite to amphibole - biotite granite (Se-1 to Se-16). Its average composition is 20 - 40 % quartz, 20 - 35 % plagioclase, 15 - 40 % K-feldspar (Se-1 from Vrchotovy Janovice only 8 %), 15 - 25 % biotite, and up to 4 % amphibole. The most prominent accessory minerals are apatite, zircon, titanite, orthite and an opaque ore mineral. The average grain size the rock is 0.5 - 2 mm; the texture is hypidiomorphic.

The likely order of crystallization is: amphibole → biotite → plagioclase → quartz → K-feldspar. Usually only limited effects of alteration are evident, the most marked being the argillization of plagioclase; chloritization of biotite is rare. Evidence for post-crystallization deformation, especially in the Vrchotovy Janovice and Bořená Hora samples, is given by undulose extinction and fracturing of the quartz grains.

QUARTZ

Anhedral quartz crystals cluster into aggregates up to 5 mm in size. They usually show strong undulose extinction and enclose abundant bubble trains. The grains are often broken into number of sub-grains, and at some localities a cataclastic texture is seen (Vrchotovy Janovice and, to some extent, also Bořená Hora). The degree of deformation generally decreases westwards, with the Vápenice samples being the least affected.

The quartz is moulded on plagioclase and locally also on biotite and amphibole. Sometimes, small biotites are enclosed by quartz. The relation to the K-feldspar is unclear: quartz seems to be either older or of similar age.

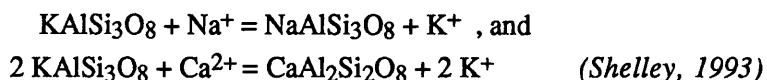
PLAGIOCLASE

Plagioclase of oligoclase-andesine composition forms subhedral, prismatic crystals, on average 1 - 1.7 mm across (up to 3 mm). Also present are some small, round or, more rarely, euhedral plagioclase crystals enclosed by the K-feldspar phenocrysts. Most of the plagioclases show albite twin lamellae; a few show Carlsbad-albite and pericline twinning. Oscillatory zoning is common [Photo II.5.5.].

The extent of alteration is quite variable. There are samples with plagioclase hardly showing any effect of alteration at all (Vrchotovy Janovice) as well as samples with a half of plagioclases altered to an aggregate of clay minerals, in places with muscovite and epidote (Vápenice). The small plagioclase crystals, enclosed by K-feldspar phenocrysts, have usually suffered the most intense alteration. In the most altered zones, a limited amount of calcite is present with CL studies showing it to be present in some of the Kosova Hora and rarely in the Vápenice samples. It exhibits the usual orange-red luminescence, and is enclosed by biotite, K-feldspar and plagioclase. In places it is associated with altered plagioclase but more often is distributed more-or-less randomly. There is no evidence of brittle deformation of the plagioclase grains.

The plagioclase encloses tiny biotite flakes, often oriented parallel to, or at angles of 45° and 90° to, albite twin lamellae. Some of the biotites are not resorbed at all, and are still euhedral. In places, however, several anhedral biotite inclusions have a common optical orientation, suggesting that they might be relics of larger biotite flakes. Typically thick myrmekite rims are developed at the plagioclase - K-feldspar boundary.

In CL alternating ochre yellow and yellow zones show up zoning in plagioclase much of which is a fine-scale oscillatory zoning [Photos II.5.13., II.5.16.]. In the Vrchotovy Janovice sample, the CL of plagioclase is grey, or greyish blue. Altered zones (with the occurrence of sericite and clay minerals) show dark brown, almost black, luminescence. The contacts with the K-feldspars are somewhat more bluish in colour, inclusive of zones of intense myrmekitization, [Photos II.5.14.-II.5.15.] probably due to leaching and diffusional exchange between the two. It appears likely that the generally accepted model of the myrmekite formation involving combined deuteric reactions



is applicable to the Sedlčany intrusion.

The composition of plagioclases from the Sedlčany granite does not vary greatly, ranging between oligoclase and andesine. The cores of oscillatory zoned plagioclases correspond to andesine (An 35 - 38) and their rims to oligoclase (An 24 - 29). However the complicated character of at least some of the oscillatory zoned plagioclases is illustrated by sample Se-6 [Photo II.5.13., Fig. II.20 a] in which a core of andesine (An 41 - 44) is overgrown by a slightly more sodic zone (An 36), a calcic spike (An 45) and rim of oligoclase (An 26). The composition of optically unzoned plagioclases, including those enclosed by the K-feldspar phenocrysts, ranges between An 33 - 42; rare are oligoclase rims (An 19; Se-7 of Vápenice II.). The plagioclases enclosed by K-feldspars are usually bordered by a thin rim of albite (An 1.7). The late plagioclase, filling the fractures in older oscillatory zoned plagioclases (Se-9, Vrchotovy Janovice), corresponds to oligoclase (An 19 and An 28).

For the Sedlčany granite, cathodoluminescence proved to be an unreliable indicator of the plagioclase composition as the bright yellow core [Photo II.5.13., Fig. II.20 a] has virtually the same An content as the surrounding much duller zones; likewise the distinct thin bright layer on [Photo II.5.14., Fig. II.20 b]. Clearly, in case of the Sedlčany granite, the factors determining the luminescence of plagioclase are not directly related to the An content.

K-FELDSPAR The K-feldspar is present as anhedral to subhedral prisms, on average 1.2 - 2 mm (up to 8 mm) across. It is strongly perthitic. Carlsbad twins are frequent, unlike cross-hatched twinning (indicative of microcline) but the proportion of microcline is higher in the eastern part of the body (Vrchotovy Janovice).

In a few samples (especially from Kosova Hora) thin calcite veinlets cross the K-feldspar phenocrysts but no other evidence of alteration or of deformation has been seen.

The K-feldspar frequently encloses tiny round or subhedral (typically strongly altered) plagioclase crystals overgrown by exsolved albite rims. Relics of anhedral amphibole inclusions are rarely found. Of interest are tiny quartz grains, forming concentric rings close to the outer edge of K-feldspar crystals (Kosova Hora and Bořená Hora). The K-feldspar generally seems to have crystallized along with the quartz.

The K-feldspar emits bright light blue luminescence; the crystals are zoned, with alternating stripes of brighter and duller CL. The rims of the K-feldspar phenocrysts are typically dull blue. In the sample from Vrchotovy Janovice (Se-1), there were found subparallel cracks, running across the K-feldspar crystals, followed by a slight alteration (leaching?). In places, the brecciation of K-feldspar is revealed by the CL study [Photo II.5.15.].

BIOTITE Biotite occurs in the form of anhedral to subhedral flakes, whose average size is 0.7 - 1.0 mm (up to 3 mm). Its pleochroism is strong: X: very pale straw yellow, Y = Z: ochre brown or light rusty-brown. Pleochroic haloes are common in biotites from Vápenice, unlike in some of the Vrchotovy Janovice samples, where the pleochroic haloes are considerably less abundant and less prominent.

There is little chloritization of biotite but where present, titanite and rare rutile are associated products. In the Vrchotovy Janovice and Bořená Hora samples, the biotite is locally slightly cataclastic and has bent cleavage. In contrast, no evidence of post-crystallization deformation was recognised in the Vápenice samples.

The biotite occurs mainly in clots, which are either monomineralic, or accompanied by hornblende. Biotite from Vápenice encloses a considerable proportion of euhedral apatite crystals, as well as tiny round or elongate zircon grains (< 0.25 mm across). In contrast, some of the biotites from Vrchotovy Janovice have few inclusions. In places, rims of an opaque ore mineral are

developed. The biotites are often enclosed by the younger plagioclases. Also quartz and K-feldspar resorb the older biotite. Although a few tiny biotite flakes are enclosed by amphibole, biotite seems be generally younger.

AMPHIBOLE

Subhedral amphibole crystals are present in all except the *Kosova Hora* samples. On average they are 0.5 - 0.7 mm (up to 4.5 mm) across and they frequently show polysynthetic twinning on (100). Almost colourless needles of actinolite are rare. The amphibole is only slightly pleochroic, almost colourless: X: very pale green, Y: very light olive green, Z: pale olive green. The maximum extinction angle ($Z^{\wedge}c$) was 17 - 20°. Apart from one broken amphibole prism (*Vrchotovy Janovice*), and an unusual development of the secondary cleavage at the same locality, it is unaffected by the later deformation.

The amphibole is associated with biotite, forming clots but also may enclose tiny biotite flakes. Amphiboles, about 1.2 mm in size, with biotite coronas, probably represent pseudomorphs after pyroxene [Photo IL5.6.] (*Castro and Stephens, 1992; Bateman, 1993b*). Some long hornblende crystals are full of oriented inclusions of biotite and abundant secondary titanite, both of them following the cleavage of the amphibole host (Se-3, *Vápenice*). In *Vápenice*, actinolite occurs either at the edges of amphiboles, or as aggregates of colourless needles. Inclusions of euhedral zircon and apatite are common. Both quartz and K-feldspar are moulded on and fill gaps around the amphibole.

ACCESSORY MINERALS

The *Sedlčany* granite is rich in apatite, zircon, pyrite, orthite and in places also in monazite (*Kodymová and Vejnar, 1974*). Large (up to 2 mm across) euhedral crystals of metamict orthite are particularly noticeable [Photos IL5.9 - IL5.12.]. Its proportion is quite variable (up to 4 grains per section) and is not present in the biotite facies (*Kosova Hora*). Very complicated zoning patterns are shown, with several resorption surfaces, zoning and strong alteration. The metamictization is connected with increase in volume and propagation of cracks, which were subsequently healed by crystallization of secondary oxides (*V. Bouška, pers. com.*). This process probably accounts for the origin of the worm-like textures of higher mean atomic number seen on the BSE photograph.

ENCLAVES

Two samples of MME from the *Sedlčany* intrusion are described: (1) Sem-1, a relatively leucocratic amphibole-biotite MME from *Vrchotovy Janovice*, ellipsoidal (20 cm in diameter), with megacrysts of feldspar up to 5 mm, and (2) Sem-6, from *Vápenice I*, an ellipsoidal amphibole-biotite MME (10 x 15 cm), with macroscopically obvious amphibole-biotite clots.

(1) The enclave Sem-1 is rich in felsic minerals, especially plagioclase. Plagioclase occurs as both small subhedral crystals, and megacrysts, which are often mantled [Photo IL5.7.]. The cores of the mantled plagioclases commonly show oscillatory zoning, whereas the rims are full of abundant tiny biotite flakes and acicular apatite, which are not seen in the cores. Similar relationships were observed in case of a large K-feldspar phenocryst, which was overgrown by a microcline-rich rim full of inclusions. Such a texture could indicate that the feldspar began crystallizing in the granite, and then was incorporated into the MME magma, where it acquired the rim. There are two different generations of biotite present: tiny, euhedral crystals (quenched ?), as well as larger blade-shaped ones, with flow alignment (post-mixing growth ?). Pale green subhedral amphibole crystals are only weakly pleochroic. They enclose inclusions of tiny biotite, apatite and an opaque mineral.

Biotite or amphibole - biotite clots are absent. Quartz grains are frequently large, some of them are round and inclusions-free (ocellar), whereas others are poikilitic, over 0.5 mm in size. The former may be xenocrystic, the latter possibly have originated after the quenching stage (*Vernon, 1990*; see also discussion of KozD-1 from Kozárove), as could have the infrequent K-feldspar oikocrysts.

(2) In sample Sem-6, biotite is more abundant than hornblende. It is subhedral to euhedral, small and with apparent flow alignment. Rarely, it forms monomineralic clots. Similarly, pale green subhedral crystals of hornblende tend to cluster into clots, up to 2.5 mm in size, with minor amounts of biotite, which is also a common inclusion in amphiboles. Both K-feldspar and quartz occur as poikilitic megacrysts [Photo II.5.8.], originating in the post-quenching stage. Both of them may be somewhat broken; in such zones, myrmekite is common. Unlike the K-feldspar, plagioclase is rare; it forms subhedral laths, often strongly altered. Abundant is acicular apatite [Photo II.5.8.].

The studied MME of the Sedlčany intrusion appear to be hybrid in origin. The evidence is, as in case of previous intrusions, based on presence of mantled plagioclase with rims full of inclusions of quenched apatite and biotite, quartz ocelli, K-feldspar and quartz oikocrysts and blade-shaped biotite (see the previous sections for interpretation of the above phenomena as well as for corresponding references).

II.6. Říčany intrusion

This igneous body of porphyritic biotite granite with a variable but minor proportion of muscovite is circular in shape, and occurs in the northernmost part of the CBP [Fig. II.5.]. The intrusion is zoned, with the outer zone rich in K-feldspar phenocrysts (so-called porphyritic facies; *Katzer, 1888*; *Kašpar, 1936*), whereas in the central part the phenocrysts (up to 3 cm) are scarce (*Žernovka*). A gradational relationship between the two facies has been recorded (*Orlov, 1933*; *Kašpar, loc.cit.*). Various types of enclaves, including MME, surmicaceous enclaves and metasedimentary xenoliths (the latter mainly close to the contact with the Teplá-Barrandian Unit) are abundant.

The central part of the Říčany granite has been intruded by several bodies of a fine-grained two-mica leucogranite (so-called Jevany type); the southern contact is rimmed by the Marginal aplite.

The intrusion is adjacent to low-grade Proterozoic metasediments of the Teplá-Barrandian Unit (W), upper Carboniferous and Permian sediments of the Blanice Furrow (E), metasediments of Metamorphic Islet Zone (Voděrády-Zvánovice and Tehov Metamorphic Islets, S) and the Sázava intrusion (S).

Field observations

I. The contact of the Říčany intrusion with the Proterozoic rocks of Teplá - Barrandian Unit is intrusive in character, with a narrow zone (ca. 0.5 km) of strong thermal metamorphism and disrupted country rock xenoliths within the granite (*Kodym, 1925*).

II. Sediments of the Blanice Furrow onlap the eastern part of the Říčany body (*Kodym, 1925*; *Kašpar, 1936*) and their basal conglomerates contain boulders of this granite (e.g. *Steinöcher, 1969*; *Afanasjev et al, 1977*). The age of the sediments deposited in the Blanice Furrow ranges between Late Carboniferous (Stephanian C) and Permian (Autunian) (*Working Group for Regional Geological Classification of the Bohemian Massif, 1994*).

- III. Metasedimentary xenoliths are common close to the contact with adjacent Teplá-Barrandian Unit (*Kodym, 1925*) but they are rare in the central part of the intrusion (*Žernovka*).
- IV. Biotite-bearing MME are abundant throughout the body. They are of various sizes and appearance: the more mafic ones are small, usually round, whereas the more leucocratic ones tend to be larger (up to several meters) and angular (*Žernovka*). Although many enclaves are partially resorbed by the host granite (seen as biotite schlieren), the contacts of intact enclaves are mainly sharp and lack reaction rims. Many of the round enclaves are surrounded by coronas rich in K-feldspar phenocrysts, up to several dm thick. (*Žernovka*; also *Katzer, 1888*; *Palivcová et al., 1992*). A common constituent of the lighter enclaves are quartz ocelli [Photo II.6.1.] (cf. *Palivcová et al., 1992*) and also a small proportion of round simply-twinned K-feldspar megacrysts, similar to the phenocrysts of the host granite [Photo II.6.1.]. Surmicaceous enclaves, round and often resorbed, are common (*Žernovka*).
- V. Sub-vertical parallel-sided zones, in which there are numerous MME, up to 5 m in width (*Cimbáľníková et al., 1977*) were observed in *Doubek* (*Palivcová et al., 1992*) and *Žernovka*. In the latter quarry, such a zone is full of MME enclosed in a matrix of a coarse-grained granite of pegmatoid appearance, rich in large K-feldspar megacrysts and rarely with some tourmaline.
- VI. Many dykes of inhomogeneous aplites cut the southwestern part of the intrusion (*Němec, 1978*). The contacts of the Říčany intrusion with the Teplá-Barrandian Unit is cut by numerous dykes of granite pegmatite with schorl and beryl, commonly associated with zones of a strong hydrothermal alteration (*Březí*).
- VII. Cassiterite-bearing tourmaline-quartz veins penetrate metasediments of the Tehov Metamorphic Islet (*Němec, 1978*). The southwestern part of the Říčany intrusion was assessed for economically viable Sn-mineralization (*Šponar and Komínek, 1985*).
- VIII. The southern contact of the Říčany intrusion has a rim of a tourmaline aplite (up to 400 m in width), with abundant tourmaline-bearing pegmatite schlieren (so-called Marginal aplite).
- IX. The central part of the Říčany intrusion is penetrated by several bodies of two-mica leucogranite (Jevany type) that is hydrothermally altered and contains macroscopically apparent fluorite crystals. It differs markedly from the Marginal aplite (6. VIII.) as there are neither tourmaline grains nor pegmatite schlieren present (*Němec, 1978*).

Interpretation of field relations

The Říčany granite forms a zoned, 'bullseye' (*Gastil et al., 1991*) body with the proportion of K-feldspar phenocrysts decreasing inwards. As this intrusion has a well-developed thermal aureole, it must have been relatively shallow (6. I.). The transgression of the Stephanian sediments over granite (6. II.) provides an important constraint on age of intrusion and consequent uplift, as the Říčany granite must have been exposed by about 290 Ma.

Unlike the metasedimentary xenoliths, which are abundant only at the contact with the Teplá-Barrandian Unit (6. III.), the MME are ubiquitous in the Říčany intrusion (6. IV.). The origin of the round K-feldspar megacrysts commonly enclosed by MME world-wide was discussed for instance by *Vernon (1986, 1990)* and *Barbarin and Didier (1991)*. Their presence suggests that the MME were not completely solid when incorporated into the acid magma and hence that the material exchange between the enclaves and host was possible. The round shape of the megacrysts could indicate resorption and mechanical rounding, which sometimes could have been followed by later re-growth from the enclave magma (*Vernon, 1990*). The importance of magma mixing in the generation of the MME is further

shown by abundant quartz xenocrysts (quartz ocelli) and resorption of both MME and surmicaceous enclaves, leaving residual biotite schlieren. The genesis of the parallel-sided zones (enclave swarms) (6.V.), similar to those in Doubek and Žernovka, has been dealt with previously (3.XI). Pegmatoid rims of some of the MME could be explained by disruption of these enclave swarms.

Formation of the Marginal aplite (6.VIII.) has been explained by degasification and degeneration of the granite magma, coupled with influx of volatiles (especially boron) from the cooling central part of the body (*Němec, 1978*). The escape of volatiles from the Říčany granite is further substantiated by the development of cassiterite mineralization in the country rocks (6.VII.) as well as by numerous pegmatite and aplite dykes at the western contact of the intrusion (6.VI.).

The Jevany leucogranite (6.IX.) is thought to represent a late differentiate of the Říčany granite (*Šmejkalová, 1960*). The magma was volatile-rich and the crystallized rock suffered weak greisenization, particularly in the strongly altered westernmost part (6.VI.), and the 'Marginal aplite' (6.VII.).

Microscopy

The (muscovite-) biotite porphyritic Říčany granite (Ri-1 to Ri-6) consists of ca. 35 % K-feldspar, 30 % plagioclase, 30 % quartz and 5 % biotite. These proportions represent estimates from several thin-sections, and are in agreement with the average modal composition of 28 % K-feldspar, 35 % plagioclase, 28 % quartz, 6 % biotite given by *Palivcová (1965)*. Apatite and opaque minerals are common accessory minerals; zircon is scarce. The average grain size of the groundmass is 0.5 - 2 mm and phenocrysts may attain up to 4 cm.

The likely order of crystallization is biotite → plagioclase, muscovite → quartz → K-feldspar. The rock is relatively fresh, with the plagioclase showing the initiation of argillitization along the cleavage planes. The K-feldspar phenocrysts are somewhat cloudy but the biotite is almost fresh. Apart from the slight undulose extinction of quartz grains, there is no evidence of post-crystallization deformation.

K-FELDSPAR K-feldspar forms anhedral to subhedral phenocrysts, which may be strongly perthitic and with pronounced cross-hatched twinning; they are sometimes zoned in terms of microcline content (triclinity) [Photo II.6.2.]. Typical of the K-feldspar is 'hourglass structure', a macroscopically obvious zoning, caused by different numbers of inclusions and, or perthite exsolution. The origin of the hourglass structure could be attributed to increasing growth rate, resulting in crystallization of less ordered K-feldspar and skeletal growth, leaving the growth pyramids of the crystal faces empty, in which the heterogeneously-nucleating impurities became concentrated (*Pivec, 1969*). Carlsbad twins are common. Cloudiness due to alteration (especially in the albite patches of perthites) is seen.

Small, round or subhedral inclusions of biotite, quartz and plagioclase are abundant. They are usually arranged into two directions, perpendicular to each other, and parallel to the cross-sections of the K-feldspar phenocrysts, implying heterogeneous nucleation (cf. *Pivec, 1970*) [Photos II.6.7.-II.6.8.]. Biotite inclusions are frequently remnants of larger flakes pushed back by the surrounding K-feldspar, and are usually rimmed by albite [Photo II.6.3.]. The K-feldspar is younger than plagioclase and probably of the same age or partly younger than quartz. At contacts with the plagioclase grains thick myrmekite rims are developed.

Dull and bright blue zones are shown in CL as is fine oscillatory zoning [Photos IL.6.7., IL.6.8.] or there are prominent zones of bright luminescence [Photo IL.6.6.]. The dull parts prevail and these are cracked and then re-healed by quartz [Photo IL.6.5.].

The prominent zone of bright blue luminescence of the K-feldspar phenocrysts [Photo IL.6.6., Fig. IL.21 b] shows only slightly lower Ab content than normal K-feldspar, and no detectable An. Similar zones from phenocrysts of the Shap granite, Cumbria, with increased An and Ba content, were interpreted as major resorption surface connected with influx of hotter mafic magma into the magma chamber (Cox, 1994). As there are no Ba data available for the Czech K-feldspars and the effects of resorption on this surface are obvious, such a link should still be considered a possibility.

QUARTZ Quartz occurs as anhedral crystals, up to 2 mm across. It shows slight undulose extinction and common sub-parallel bubble trains. It moulds on plagioclase crystals. There are also small veinlets of quartz running across the plagioclase and the K-feldspar grains. To some extent the biotite is pushed back by quartz, releasing its apatite inclusions. Quartz appears to be slightly older than the K-feldspar phenocrysts, but the crystallization intervals of the two minerals probably overlapped.

PLAGIOCLASE The plagioclase, which is albite - oligoclase, occurs as subhedral prismatic crystals, on average 1.2 - 1.9 mm across, with common albite lamellae and in places is optically discontinuously-zoned. There is no evidence of later deformation and alteration is only weakly expressed along the cleavage planes or in form of rings, concentric with the zones. In contrast, the small plagioclase crystals enclosed by the K-feldspar phenocrysts typically show a much higher degree of alteration.

The plagioclase encloses small (0.1 - 0.2 mm) flakes of muscovite, oriented in the (100) and (010) directions. Some of the muscovite occurs in almost fresh plagioclase, which implies that it may be partly of primary origin. The crystallization of this muscovite took place either before or, more likely, during the crystallization interval of the plagioclase. The resorption of plagioclase is shown at the contact with the K-feldspar and thick myrmekite rims are commonly developed. Small, round plagioclase crystals are enclosed by the K-feldspar phenocrysts and also quartz moulds on plagioclase. There are also a few euhedral plagioclases with rims of K-feldspar (antirapakivi texture; also *Pivec, 1970*). [Photo IL.6.4.]. This texture is thought to originate by juxtaposition of a near-solidus melt, rich in alkali feldspar component, with plagioclase already formed in a more mafic system; i.e. by magma mixing (*Hibbard, 1991*). However, in opinion of *Hibbard (loc.cit.)*, this texture is typical of one-feldspar granites and their enclaves. Nevertheless, it obviously implies late crystallization of K-feldspar.

The plagioclase emits a dark blue - yellow luminescence, with slight greenish hue. When altered, it becomes brownish. It is also darker at the contacts with the K-feldspar.

Apart from those enclosed within the K-feldspar, the plagioclases are of uniform oligoclase composition (An 15 - 20) and are usually chemically unzoned. If zoning is present, the difference between rims and cores is small (e.g. An 15 and An 19). The small plagioclases enclosed by the K-feldspar phenocrysts [Photo IL.6.7., Fig. IL.21 a] are variable in composition (An 12, 15, 26) but the cores of some of these plagioclases could not be analysed due to their alteration. The plagioclases are overgrown by rims of albite (An 1 - 3) of distinct dark blue luminescence, which apparently exsolved from the K-feldspar during the cooling (*also Pivec, 1969*) [Fig. IL.6.7., IL.6.8.]. The same holds for the biotite flakes overgrown by thin albite rims (see above).

BIOTITE

Biotite forms subhedral flakes which average 0.5 - 0.75 mm (up to 1.2 mm) across with a strong pleochroism: X: straw yellow, Y = Z: dark rusty-brown.

Pleochroic haloes which are very common are usually well-developed; they form around very small inclusions, which are too small to be identified by light microscopy.

The biotite is very fresh and only a few flakes with traces of chloritization were observed. As in the case with plagioclase, it lacks any evidence of a solid-state deformation.

Small apatite prisms or needles, enclosed by the biotite, are frequently observed; zircon inclusions (of dipyrarnidal habit) are, however, relatively sparse. Biotite is often associated with grains of an opaque mineral. It may also be overgrown by the primary muscovite (up to 0.2 mm across). Although small biotites are sometimes enclosed by plagioclase, biotite generally commenced crystallizing prior to plagioclase. Similarly, it is earlier than both quartz and K-feldspar. The latter encloses subhedral - euhedral biotite flakes, often with albite reaction rims.

**ACCESSORY
MINERALS**

The Říčany granite contains significant proportions of apatite, rutile, anatase, tourmaline, ilmenite, monazite and fluorite. Both zircon (of short-prismatic habit) and pyrite are rare (*Kodymová and Vejnar, 1974*). Fluorite shows conspicuous, bright dark blue luminescence. It occurs as rare tiny grains generally associated with the most altered parts of the plagioclase crystals.

ENCLAVES

Two samples of enclaves were studied: (1) Rim-3, a lobate surmicaceous enclave, with diffuse margins (6 x 3 cm) and (2) Rim-4, a grey equigranular biotite MME, with sharp contacts against the granite host. This supplements the results of the study of MME in the Říčany granite by *Palivcová et al. (1992)*, which concentrated mainly on textural characteristics, and particularly on conspicuous quartz ocelli and ovoids.

(1) The surmicaceous enclave (Rim-3) is formed by subhedral, strongly pleochroic biotite, on average 0.5 - 1 mm across, in which are numerous small but prominent pleochroic haloes around radioactive grains a few of which could be identified as zircon. Acicular apatite is also common. The habit, pleochroism and abundance of pleochroic haloes of the biotite appear to be very similar to those of the granite itself. Biotite flakes sometimes surround quartz ocelli up to 2.5 mm in size. Plagioclase and quartz have a low modal abundance, filling gaps among the biotite flakes. From the appearance of biotite and the texture of the enclave, a cumulative origin is inferred (a cumulate enclave, or autholite of *Didier and Barbarin (1991)*) rather than it being a typical surmicaceous enclave.

(2) The MME (Rim-4) is characterised by presence of partly flow-aligned, blade-shaped biotite, up to 2.5 mm long. This biotite is strongly pleochroic and full of pleochroic haloes. *Palivcová et al. (1992)* found the blade-shaped biotites of this type of MME to be similar to that of many lamprophyres; however, this habit is thought to be one of typical 'magma-mixing' textures in Mg- and K-rich systems (*e.g. Hibbard, 1991*; for details, see section on Kozárove). Plagioclase forms subhedral crystals, with weak discontinuous and often with convolute zoning, that are generally larger (~ 3 mm) than both the quartz and the K-feldspar. The plagioclase crystals often enclose round quartz and blade-shaped biotite. Smaller subhedral crystals are infrequent. The strongly cross-hatched K-feldspar is very common, occurring in form of oval-shaped grains or masses interstitial to earlier-formed minerals. The quartz is round and often enclosed by K-feldspar; it sometimes forms biotite-rimmed ocelli. Apatite, both of short-prismatic and acicular habits, is a common accessory.

The quartz ocelli are an impressive feature of MME in the Říčany granite. Some of them may be even euhedral in shape (of hexagonal outline; *Palivcová et al., 1992*). *Palivcová et al. (loc.cit.)* have rejected a magma mixing model and explained their genesis (and presence of the MME) as follows. The MME were originally pyroclastic rocks, which had enclosed xenocrysts of their wall-rocks. Pieces of these pyroclastic rocks were captured by a later sub-volcanic intrusion and, consequently, the whole complex was recrystallized. However, on the basis of the evidence from the present study the quartz ocelli are interpreted as representing a classical magma-mixing texture (*e.g. Vernon, 1990; Hibbard, 1991*). The quartz ocelli, typically rimmed by amphibole, pyroxene or biotite, are interpreted as a result of partial solution of the quartz xenocrysts in the mafic magma that extracts the latent heat from adjacent liquid. The undercooled surface of the quartz grain becomes a preferential nucleation substrate for minerals of the mafic magma (*Vernon, loc.cit.*).

It is difficult to agree with many of ideas expressed by *Palivcová et al. (1992)*, such as their rejection of basic-acid magma miscibility 'on a geological scale in plutonic conditions', ignoring the extensive evidence (experimental: *e.g. Kouchi and Sungawa, 1985; Fernandez and Barbarin, 1991; Wiebe, 1991; Blake and Koyaguchi, 1991; Koyaguchi and Blake, 1991; van der Laan and Wyllie, 1993*; geochemical and petrological: *e.g. Vernon, 1984; Castro et al., 1990, a,b; 1991 a,b; Dodge and Kistler, 1990; Lorenc, 1990; Michael, 1991*). Strong arguments for the hybrid origin of MME in the Říčany granite come from the presence of quartz ocelli, blade-shaped biotite, acicular apatite and K-feldspar xenocrysts in MME [Photo II.6.1.] as well as antirapakivi textures in the granite.

II.7. Other intrusions

In the following text, brief descriptions of additional intrusions are given [see Fig. I.4.]. These were not selected for detailed geochemical and isotopic investigation in the present study and some are representative of the durbachite suite that were subject of thesis of *Holub (1990)*, where details could be found. In due course, their nature and petrogenesis will need to be integrated with the work presented here.

II.7.1. Čertovo břemeno intrusion

The Čertovo břemeno intrusion occurs in the eastern part of the CBP [Fig. I.4.]. It is a roughly circular body with a single apophysis (the Vojice apophysis) pointing eastwards. The main rock types include porphyritic amphibole - biotite melagranite and (quartz) melasyenite (*e.g. Holub, 1978*), resembling potassium-rich magmatic rocks of the Black Forest (durbachites), Bavaria (redwizites) and Austria (the Rastenberg type). In the Čertovo břemeno intrusion, two facies could be distinguished: (1) an easterly mafic facies, and (2) a westerly leucocratic one (*Holub, 1978*). The dark facies appears to be underlain by more acidic (i.e. less dense) granitoids, possibly of the leucocratic facies or leucogranites (*Dobeš and Pokorný, 1988*).

In the W, the Čertovo břemeno mass is in contact with mainly Palaeozoic (up to mid-Devonian, *Chlupáč, 1988*) metasediments and orthogneisses (Staré Sedlo orthogneisses) [Fig. II.2.] of the Sedlčany-Krásná Hora Metamorphic Islet. The granitoids, surrounding the Čertovo břemeno intrusion, are the Sedlčany (N) and Blatná intrusions (S). The position of the so-called Dehetník type will be addressed later [II.7.9.].

The Čertovo břemeno intrusion causes a strong thermal metamorphism of the adjacent Sedlčany-Krásná Hora Metamorphic Islet, including the Staré Sedlo orthogneisses and cuts the

foliation of these (Kořler, 1993). This puts important constraints on the age of the Čertovo břemeno intrusion, as the protolith of the orthogneisses has been dated at 380 - 365 Ma and cooling after their ductile deformation is possibly as young as 340 - 330 Ma (Kořler, 1993; Kořler et al., 1993).

The Čertovo břemeno intrusion is younger than the Blatná intrusion (4.III, 4.XI) and possibly similar in age to the Sedlčany intrusion (5.II, 5.XI). Some of the tourmaline-bearing leucogranitoids, enclosing angular xenoliths of the Čertovo břemeno durbachite, for instance in the Písek area, [Photo II.7.1.] are obviously younger.

In the eastern part (the Votice apophysis), close to the contact with the Moldanubian paragneisses, Čertovo břemeno granitoids become xenolith-rich and strongly deformed [Photos II.7.2.-4.]. The deformation in this area has been studied by Lobkovic (1987).

The petrology, geochemistry and petrogenesis of the Čertovo břemeno intrusion has been dealt in context of the whole durbachite suite by Holub (1973, 1974, 1977, 1978, 1980, 1985, 1988, 1990), where additional information can be found.

II.7.2. Tábor intrusion

A roughly circular body of the Tábor syenite occurs in the southeastern part of the CBP. Its central part is composed of fine-grained biotite - pyroxene syenite with hypersthene more common than clinopyroxene, whereas the outer zone of medium-grained pyroxene - biotite, amphibole - biotite and amphibole - pyroxene - biotite syenite to melagranite has clinopyroxene > orthopyroxene (Šmejkalová, 1965; Čech, 1964; Jakeš, 1968). Towards the margins of the intrusion, biotite and amphibole form in expense of hypersthene due to retrogression of the original assemblage (Jakeš, 1968).

The Tábor intrusion is adjacent to high-grade metasediments of the Moldanubian Unit. The northern contact with the formerly-distinguished Dehetník type [II.7.9.] is tectonic (Čech, 1964; Frejvald and Jakeš, 1964).

Although there are xenoliths of pyroxene syenite that resemble that of the Tábor intrusions enclosed by the Čertovo břemeno mass (e.g. Čech, 1964), the existence of this rock type as integral part of the Čertovo břemeno intrusion itself means that unique identification of the source is not possible (Holub, 1989b; 1990).

II.7.3. Kozlovice intrusion

The SW - NE elongate Kozlovice intrusion occurs in the southwestern part of the CBP (the Klatovy apophysis) [Fig. I.4.]. The prevalent rock type is a fine-grained muscovite - biotite granodiorite with cordierite. It is in contact with high-grade Moldanubian metasediments (SE), the Klatovy intrusion (SW) and the Marginal type intrusion (NE). At its contact with the Moldanubian Unit, the granodiorite shows evidence of having assimilated a great deal of metasedimentary material and causes strong migmatization of the adjacent paragneisses (Kodym, 1951; Kodym and Suk, 1960). This migmatization and the abundance of quartz xenoliths (ovoids) in the granodiorite led Palivcová et al. (1988) to present the hypothesis that the Kozlovice intrusion was formed by in-situ granitization of the Cambrian conglomerates.

Dykes and apophyses of granodiorite, petrographically similar to the Kozlovice type, cut the Marginal type granite (Kodym and Suk, 1960; Palivcová et al., 1988) and angular xenoliths of the Marginal type granite are enclosed by Kozlovice granodiorite (Palivcová et al., loc.cit.). This evidence indicates that the Kozlovice intrusion is the younger of the two. The presence of abundant xenoliths of

Klatovy granodiorite within the Kozlovice granodiorite indicates age relationships (*Kodym and Suk, loc.cit.*).

II.7.4. Maršovice intrusion

The Maršovice intrusion occurs in the central part of the CBP [Fig. I.4.] and consists mainly of fine-grained muscovite - biotite granodiorite with cordierite. The Maršovice body is adjacent to granitoids of the Sázava (NE), Sedlčany (S) and Kozárovce (W) intrusions, as well as metasediments of the Maršovice Metamorphic Islet (W).

The Maršovice granodiorite is considered to be responsible for strong migmatization of the adjacent Maršovice and Křečovice Metamorphic Islets (*Orlov, 1940*). Little is known about its relative age in respect to the surrounding granitoid masses (*Holub, 1992*).

II.7.5. Kosova Hora intrusion

This small body of fine-grained muscovite - biotite granodiorite with cordierite (the Kosova Hora intrusion) is surrounded by the Sedlčany intrusion [Fig. II.4.]. The abundant biotite schlieren and presence of cordierite point to much assimilation of metasedimentary material (*Kodym, 1966*) or even origin by anatexis of a metasedimentary source (as a S-type granitoid, *Holub, 1992*). Nothing is known about age of the Kosova Hora intrusion (*Holub, 1992*).

II.7.6. Klatovy intrusion

The NW - SE elongate Klatovy intrusion occurs in the southwestern CBP (the Klatovy apophysis) [Fig. I.4.] and is composed mainly of a medium-grained, often porphyritic amphibole - biotite granodiorite, occasionally with pyroxene (*Kodym and Suk, 1960*). It intrudes the boundary between the Teplá-Barrandian and Moldanubian units. In addition to the metasediments, it is in contact with Marginal granite and Kozlovice granodiorite (NE).

Klatovy granodiorite caused strong thermal metamorphism of the adjacent Teplá-Barrandian metasediments (*Kodym and Suk, loc.cit.*). Xenoliths of coarse-grained granite, similar to the Marginal type, have been recorded in the Klatovy granodiorite (*Kodym and Suk, loc.cit.*). The time span between the two intrusions could have been small, as these xenoliths have diffuse margins (*Kodym, 1966*). The Klatovy intrusion is older than the Kozlovice granodiorite [II.7.3.].

II.7.7. Marginal type intrusion

The NW - SE elongate intrusion of Marginal type granite borders the southwestern contact of the CBP [Fig. I.4.]. It is a coarse-grained (amphibole) - biotite granite to granodiorite, that is often porphyritic (*Minařík and Pivec, 1977*). This intrusion is adjacent to low-grade metasediments of the Teplá-Barrandian Unit (NW), high-grade Moldanubian rocks (SW) as well as the Sázava (NE), Blatná (SE), Kozlovice and Klatovy (SW) masses.

The contact of the Marginal type granite with the Teplá-Barrandian Unit is sharp, with intense thermal metamorphism (*Kodym and Suk, 1960*). It is younger than the Sázava intrusion (I.IV., I.VII.), and older than the Blatná (4.IV.), Klatovy [II.7.6.] and Kozlovice intrusions [II.7.3.].

II.7.8. Nečín intrusion

The Nečín intrusion occurs in the northern part of the Blatná intrusion, close to the belt of basic (mainly gabbroic) rocks [Fig. II.3.]. It is a biotite (leuco-) granodiorite that forms a circular body, presumably a stock (*Kodym, 1963*), with well-developed regular jointing.

The Nečín granodiorite is remarkably uniform in composition and any enclaves are scarce. In the main Nečín quarry only a single MME, several centimetres in diameter, was found.

II.7.9. Dehetník intrusion

The so-called Dehetník type was described as rimming the contact of the Čertovo břemeno intrusion adjacent to the Moldanubian Unit [Fig. I.4.]. However it has been shown to consist of Červená granodiorite and lamproid rocks, with affinities to the Čertovo břemeno or Sedlčany intrusions (Žežulková, 1982b; Vácha, 1987; Holub and Vácha, 1989, Holub, 1992) and is not a discrete individual mass. The name is thus redundant (Žežulková, 1982b).

II.7.10. Benešov intrusion

The so-called Benešov type [Fig. II.1.] is, in fact, a very heterogeneous complex of various rock types, including quartz diorites petrographically close to the Sázava mass (I.XIV.), and granites and potassium-rich rocks with affinities to the Sedlčany granite (Holub, 1992). One of the main distinguishing features of the Benešov type was thought to be effects of a strong deformation (cataclasis). However, this cataclasis is also shown by the eastern part of the Sázava and Požáry intrusions (I.XIV., 2.VIII.), as well as adjacent rocks of the Metamorphic Islet Zone (V.Kachlák, pers.com., 1993). Further investigations are clearly required.

II.7.11. Leucogranitoids

Little is known about leucogranitoids whose bodies are too small to be plotted on Figure I.4., and which are ubiquitous throughout the (mainly eastern) CBP (Holub, 1992). As shown by Ulrych (1972), they form a heterogeneous group, which can be subdivided into several distinct suites. The need of further study is clear, as the leucogranites might have played an important role in genesis of some of the intrusions of the CBP. For instance, Holub (e.g. 1990) has proposed a hypothesis for origin of the Bohemian lamproids (including the Čertovo břemeno intrusion) that invokes hybridization between an enriched mantle-derived ultrapotassic melt and peraluminous leucogranitoids [Chapters IV.3, V.].

II.8. Discussion and implications of the field relations and petrography

II.8.1. Terminology

Based on the field and petrographic data the following terminology is adopted in remaining parts of this thesis.

- (1) The terms 'Těchnice' and Kozárovice s.s. will be used to refer to porphyritic and (essentially) even-grained facies of the Kozárovice intrusion, respectively.
- (2) The Blatná intrusion is subdivided into two major rock types, Blatná granodiorite (s.s.) and Červená granodiorite, the latter being a more mafic, amphibole-rich granodiorite with a strong foliation.
- (3) The term 'Benešov type' will be used in regional rather than petrological sense, as the petrography of that body requires a thorough investigation.
- (4) The term 'Dehetník type' is dropped.

II.8.2. Genetic constraints based on petrography and field relations

The petrographic study has shed some light on possible sources and contaminants of the parental magmas of the intrusions being investigated. The material which could have been assimilated

by the Sázava mass appears to have been mainly (meta-) basic igneous, with a negligible metasedimentary input. In contrast, the assimilation of country rocks could have been important particularly in case of the Kozárove intrusion (Solopysky, Kozárove), northern and southern parts of the Blatná mass (Hudčice, Písek, Strakonice etc.) and western part of the Sedlčany intrusion (Vápenice), i.e. mainly in those parts of masses adjacent to the Metamorphic Islet Zone or the Moldanubian Unit. For the Požáry and Říčany masses, the assimilation of the metasedimentary country-rocks (of Teplá-Barrandian Unit) could have been important only near to contacts.

An extreme case of metasedimentary involvement is represented by the cordierite-bearing (peraluminous) granodiorites of the Kozlovice, Maršovice and Kosova Hora masses, that are thought to have originated by anatexis of the metasedimentary material (S-type granitoids; Holub, 1992).

The operation of magma mixing processes is well-documented. The best examples, with actual outcrop of the products of hybridization of magmas, are at Teletín in the Sázava mass, Hudčice in the Blatná mass and at Kozárove II in the Kozárove mass. The widespread MME are also typically of hybrid character. Apart from the macroscopic evidence, the disequilibrium nature of the samples studied (granitoids as well as MME) is shown particularly by presence of discontinuous zoning, reversed zoning or calcic spikes in plagioclase, the blade-shaped habit of biotite, ocellar quartz, acicular apatite, amphibole - biotite clots (sometimes with relict pyroxene cores), occasional antirapakivi structures (Říčany granite), resorbed brown cores of amphiboles (Teletín) and resorbed biotites enclosed by euhedral amphiboles (Kozárove).

Late deformation has affected all of the intrusions studied with exception of the Říčany granite. Particularly affected was the Sázava intrusion, mainly in its eastern and western parts. In the presumed younger intrusions, the deformation is usually confined to small domains and shear zones (for instance, the Červená granodiorite, Vahlovice in the Blatná intrusion, Votice apophysis in the Čertovo břemeno intrusion).

The degree of alteration varies considerably. In places it has been severe due to late hydrothermal activity and even accompanied by mineralization (the western part of the Sázava intrusion including the Požáry trondhjemite, Hřímědice in the Kozárove intrusion and Kosova Hora in the Sedlčany mass). This alteration effectively inhibits the study of Sr (possibly also Nd) isotopes in these parts of the CBP.

II.8.3. Relative age of the intrusions in the CBP

The most likely, succession of the intrusions in the CBP is as follows (*cf.* Holub, 1992):

Sázava → Marginal (older than Klatovy and Blatná), Kozárove, Blatná (and Červená), Klatovy, → Čertovo břemeno, Sedlčany, Říčany → Jevany.

In addition, the Sázava tonalite is older than both the Požáry trondhjemite and the Mrač granite, whereas the Nečín granodiorite is likely to be younger than the Blatná mass. The formation of the Kozlovice granodiorite followed intrusion of the Klatovy and Marginal type masses. There is no evidence about the relationship between the Sedlčany granite and the intrusion of the S-type granitoids of the Maršovice and Kosova Hora masses. Nothing is known about the relative age of Tábor syenite, either.

The basic masses occurring in the Sázava, Blatná and Marginal type intrusions are partly contemporaneous with their hosts, and there must have been a number of stages of emplacement of these bodies.

II.8.4. Order of crystallization

In the previous sections, only general schemes for the order of crystallization in individual intrusions have been given. As shown by *Flood and Vernon (1988)*, the majority of the petrographic criteria extensively used for this purpose are unreliable or even invalid. The criteria of moulding, inclusion or partial inclusion of one mineral in another are considered to be especially misleading (*Flood and Vernon, loc.cit.*). The rock-forming minerals, according to the phase rule, have to crystallize since the magma becomes saturated by them right to the solidus, or until a peritectic point is reached. Thus, the majority of the rock-forming minerals in granitoids could have grossly crystallized simultaneously.

II.8.5. Cathodoluminescence

In the rocks studied, the luminescence of feldspars seems to be very similar: K-feldspars emit blue luminescence and plagioclases various shades of yellow, sometimes with greenish or bluish hue. The cathodoluminescence colours of feldspars seem to be triggered by presence of four principal activators, as shown in the following table, together with a minimum concentration for luminescence to occur (*Marshall, 1988*):

Activator	Minimum concentration (wt %)	CL colour	CL wavelength (nm)
Ti ⁴⁺	0.05 - 0.1	blue	460 ± 10
Mn ²⁺	0.0X	greenish-yellow	570 ± 5
Fe ²⁺	0.X - 1.0	greenish-yellow	550 ± 5
Fe ³⁺	> 0.1	red	700 ± 10

Theoretically, also Eu²⁺, Sm³⁺ and Dy³⁺ could activate blue or red luminescence, but, in the common granitoids, their concentrations are unlikely to reach the required thresholds (*Marshall, loc.cit.*). Red luminescence (ferric iron activated) is typical of alkaline rocks, especially of carbonatites, and was not observed anywhere in the CBP. On the other hand, even if present, the red band in the CL spectra could be difficult to recognise without an attached spectrometer (*Wenzel and Ramseyer, 1992*). As the K-feldspars cannot accommodate sufficient amounts of neither Mn²⁺ nor Fe²⁺, they usually emit bluish CL, unlike the plagioclases, with mainly bluish- or greenish-yellow luminescence. The Fe²⁺ activated luminescence of feldspars is an anomaly among other rock-forming minerals, as this element is typically a CL quencher. In the CBP, the CL has proved to be efficient tool, revealing, or at least enhancing, the oscillatory zoning, mantling relationships, alteration and leaching of feldspars. Potentially, it could be used in study of reaction rims between K-feldspars and plagioclases, including myrmekites.

The biotite and hornblende are non-luminescent, because their principal constituent, Fe²⁺, is an effective CL quencher (*Marshall, loc.cit.*).

The bright (red-) orange luminescence of calcite is caused by the Mn²⁺ activation. The required minimum concentration of 0.0X - 0.X % Mn²⁺ must increase to allow for any Fe²⁺ present, which

quenches the luminescence (*Marshall, loc.cit.*). CL is a very effective and quick method for recognition of calcite in the section. Consequently, it is useful for the identification of hydrothermal alteration that might otherwise be difficult to recognise. Therefore, the CL could be advantageous in the identification of altered samples that should be eliminated from the isotope study.

The cathodoluminescence of apatite is linked to the substitution of REE and Mn^{2+} atoms. The presence of Mn^{2+} causes yellow or yellow-green CL, which is a common luminescence of apatite from granitoid rocks (*Marshall, loc. cit.*), with granitoids of the CBP being no exception. Blue to violet luminescence is restricted mainly to carbonatites and alkaline rocks and is triggered mainly by Eu^{2+} , Sm^{3+} and Dy^{3+} and Ce^{3+} (*Marshall, 1988; Wenzel and Ramseyer, 1992*).

Generally speaking, the studied samples did not differ significantly in cathodoluminescence of their minerals and thus CL did not contribute to refinement of the subdivision of the CBP. The similar luminescence points possibly to similar activation mechanisms in all masses investigated.

Table II.1: Modal data, Central Bohemian Pluton

Data are given in volume %; presented are also QAP values for the IUGS classification (Streckeisen, 1976; Le Maitre, 1989). Data for the strongly porphyritic granitoids are shown in italics but are not considered to be reliable. (see text for discussion)

	<i>quartz</i>	<i>K-feldsp</i>	<i>plag</i>	<i>biotite</i>	<i>amphibole</i>	<i>Q</i>	<i>A</i>	<i>P</i>
	Sázava							
Sa-1	33.3	0.4	41.4	6.7	18.2	44.3	0.5	55.1
Sa-4	12.4	2.9	42.1	9.3	33.3	21.6	5.1	73.3
Sa-7	12.8	-	75.1	10.0	2.1	14.6	0.0	85.4
Sa-6	10.1	-	49.4	8.9	31.6	17.0	0.0	83.0
Sa-10	31.1	12.3	41.0	10.9	4.7	36.8	14.6	48.6
	Požáry and Nečín							
Po-1	21.0	4.7	70.1	4.2	-	21.9	4.9	73.2
Po-3	31.2	4.8	56.2	7.8	-	33.8	5.2	61.0
Ne-1	34.2	7.4	50.3	8.1	-	37.2	8.1	54.7
	Kozárovice and Těchnice							
Koz-2	16.8	11.5	43.5	10.7	17.5	23.4	16.0	60.6
Koz-4	21.9	27.4	31.1	11.6	8.0	27.2	34.1	38.7
Koz-5	17.0	31.9	35.6	12.7	2.8	20.1	37.8	42.1
Koz-6	22.4	16.2	31.4	18.7	11.3	32.0	23.1	44.9
Koz-8	16.4	18.1	37.2	15.0	13.3	22.9	25.2	51.9
Koz-12	10.1	52.1	27.7	7.9	2.2	11.2	58.0	30.8
	Blatná and Červená							
Bl-1	26.9	16.3	31.9	24.9	-	35.8	21.7	42.5
Bl-2	27.5	5.9	43.8	22.8	-	35.6	7.6	56.7
Bl-4	27.7	28.6	24.1	19.6	-	34.5	35.6	30.0
Bl-7	22.6	24.0	37.3	16.1	-	26.9	28.6	44.5
Bl-8	19.1	13.5	47.4	15.0	5.0	23.9	16.9	59.3
Cv-1	24.2	14.3	37.6	20.5	3.4	31.8	18.8	49.4
	Sedlčany							
Se-1	41.2	8.3	23.9	26.6	-	56.1	11.3	32.6
Se-2	26.0	23.2	29.2	19.5	2.1	33.2	29.6	37.2
Se-3	25.6	32.1	24.0	17.6	0.7	31.3	39.3	29.4
Se-5	27.2	30.8	22.8	17.4	1.9	33.7	38.1	28.2
Se-7	27.2	20.5	29.2	20.9	2.2	35.4	26.7	38.0
Se-9	17.7	22.2	32.5	23.2	4.4	24.4	30.7	44.9
Se-11	21.8	39.5	21.7	17.0	-	26.3	47.6	26.1
Se-12	33.4	15.4	36.1	14.5	-	39.3	18.1	42.5
	Říčany							
Ri-1	14.4	49.7	30.5	5.3	-	15.2	52.5	32.2

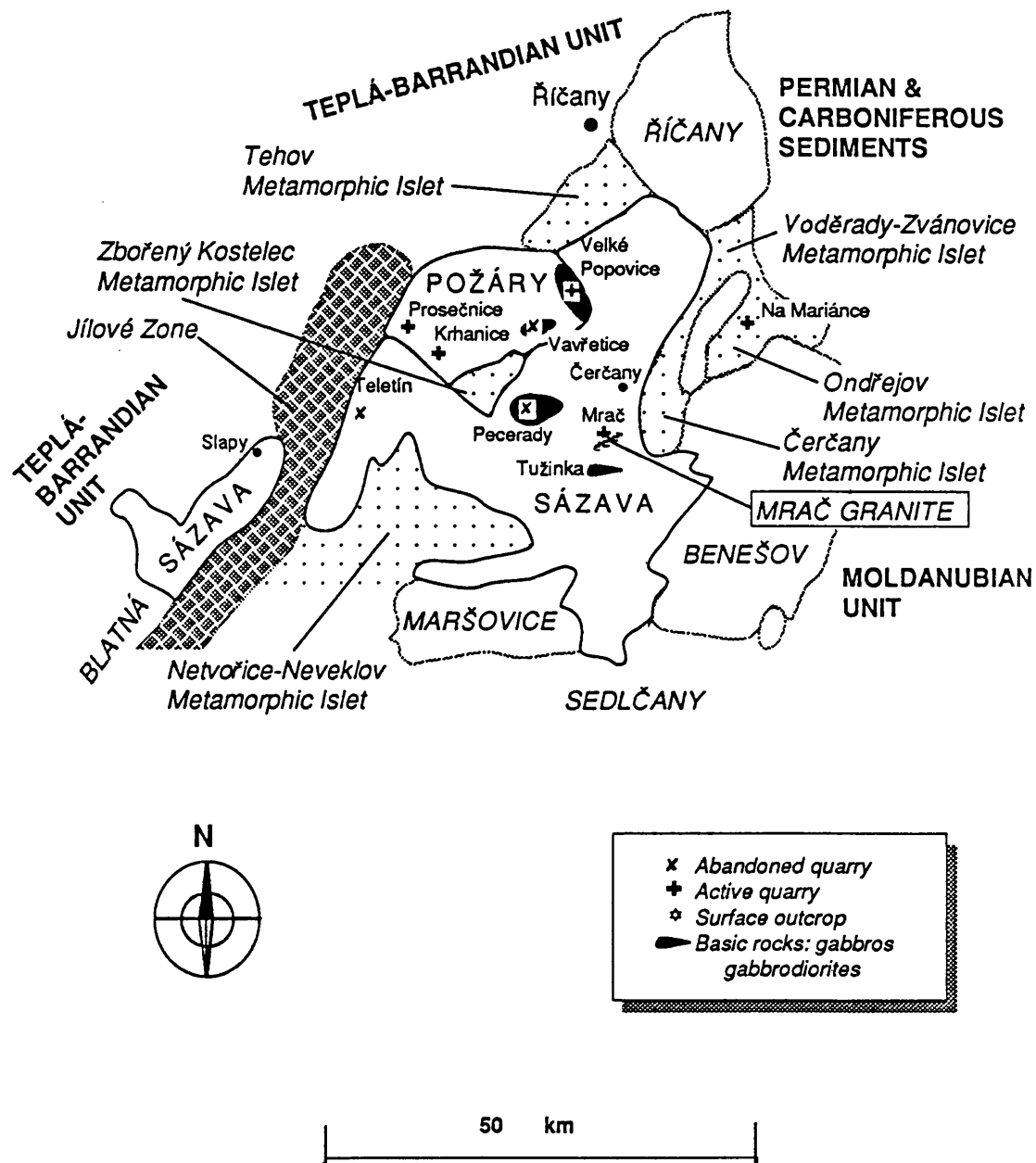


Figure II.1: Map of the Sázava and Požáry intrusions, including the main bodies of the associated basic rocks and the adjacent rock units

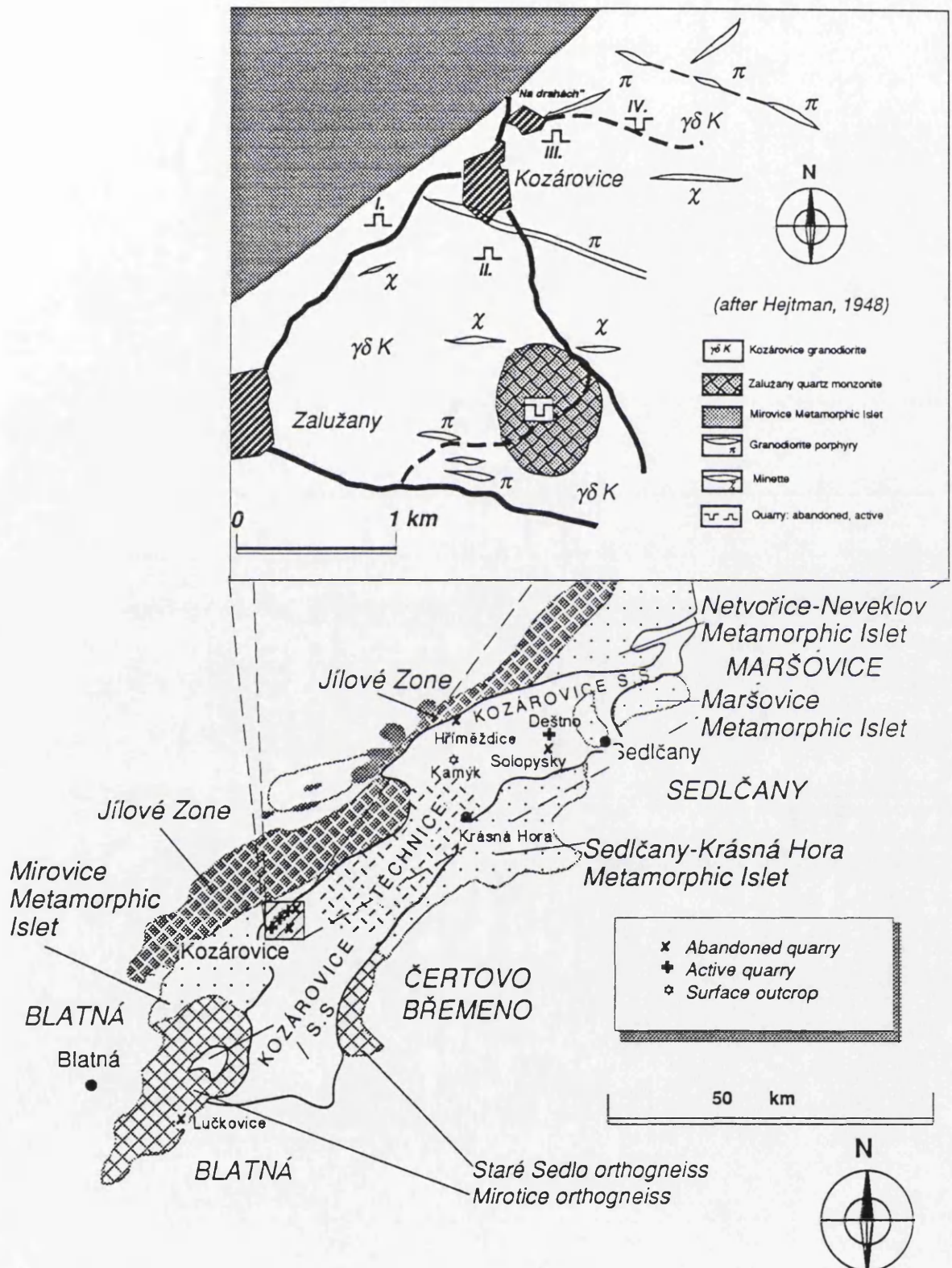


Figure II.2: Map of the Kozárovec (including Těchnice) intrusion and adjacent rock units

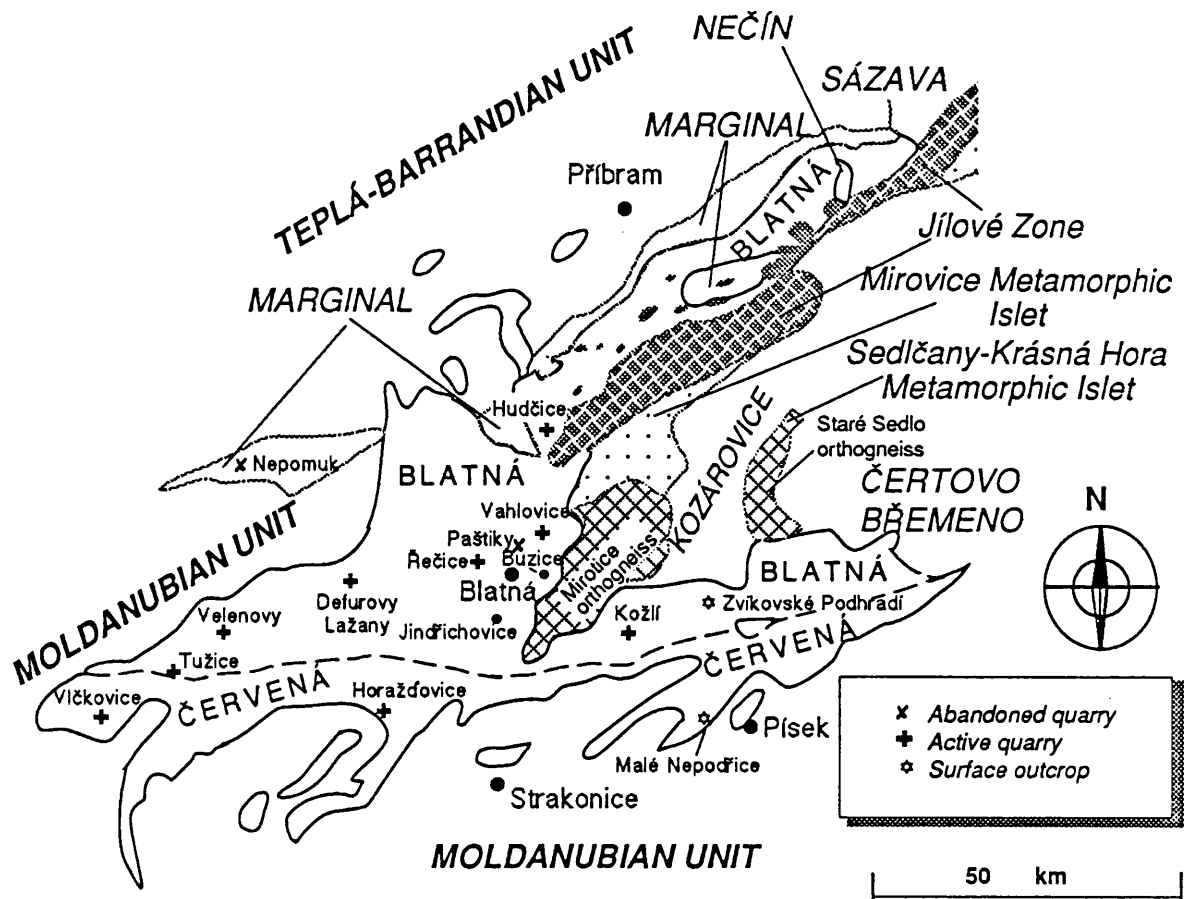


Figure II.3: Map of the Blatná (including Červená) intrusion and adjacent rock units

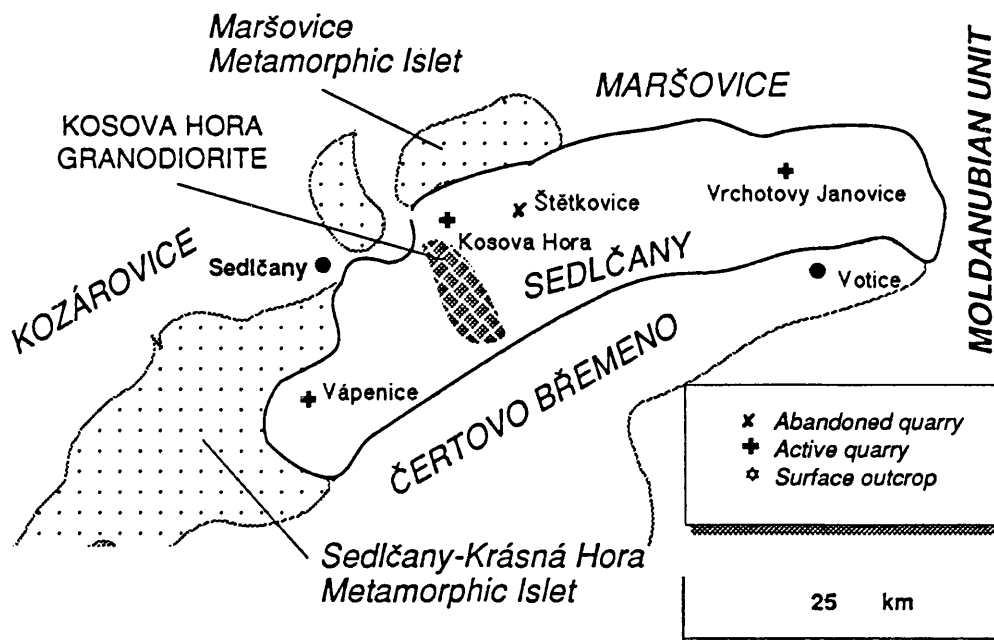
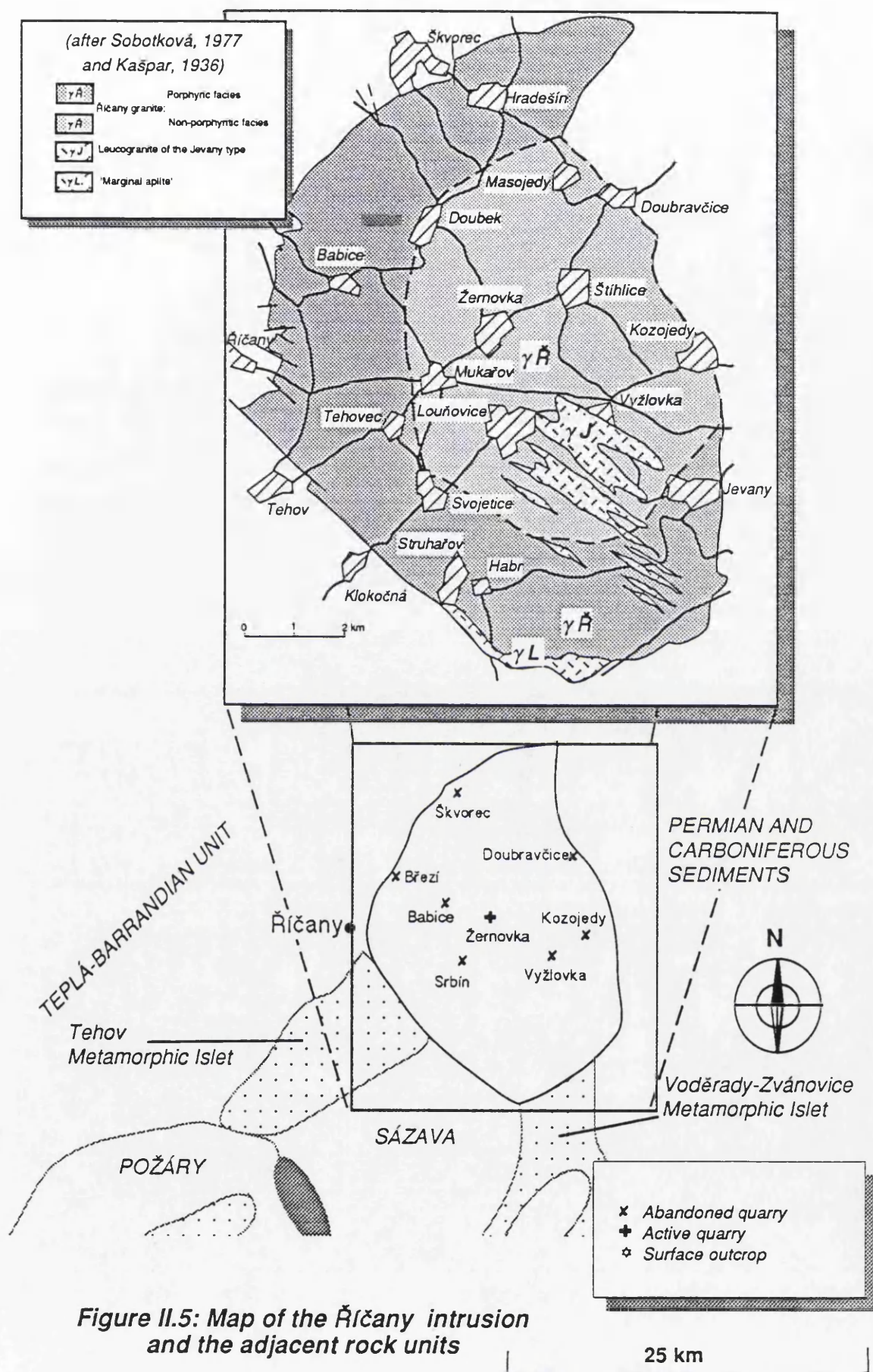


Figure II.4: Map of the Sedlčany intrusion and adjacent rock units



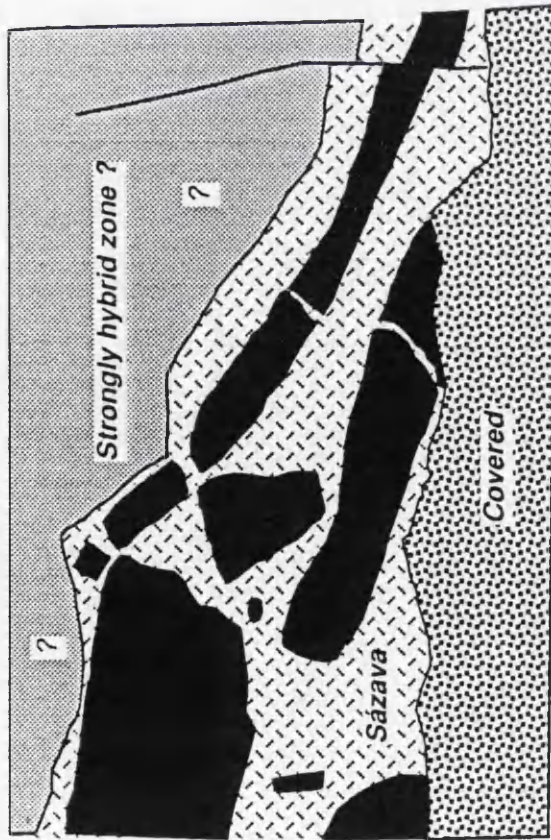
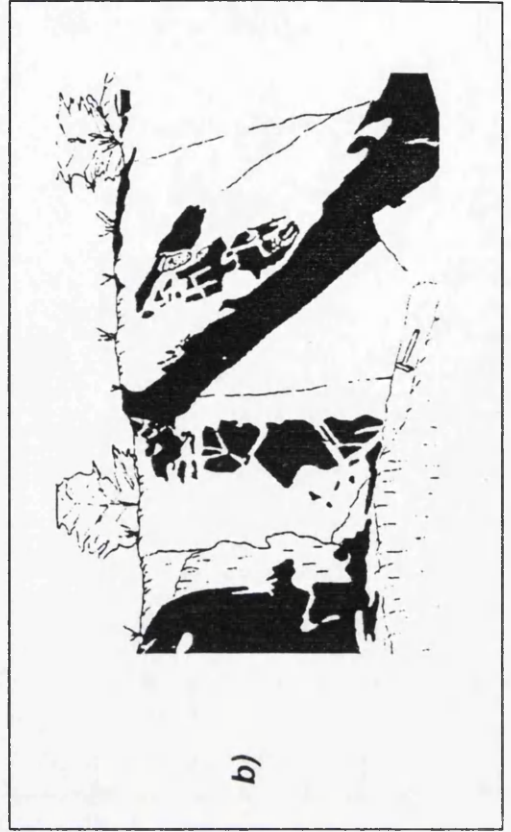
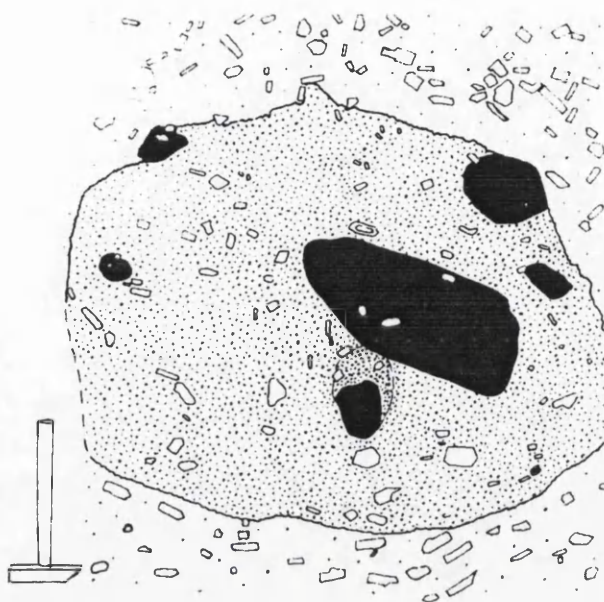


Figure II.6: Disrupted syn-plutonic dykes, Teletin; simplified from photograph of Dudek and Fedruk (1958)

Figure II.7: Syn-plutonic dykes from Cortes Island, British Columbia, Canada. (after Pitcher, 1993)

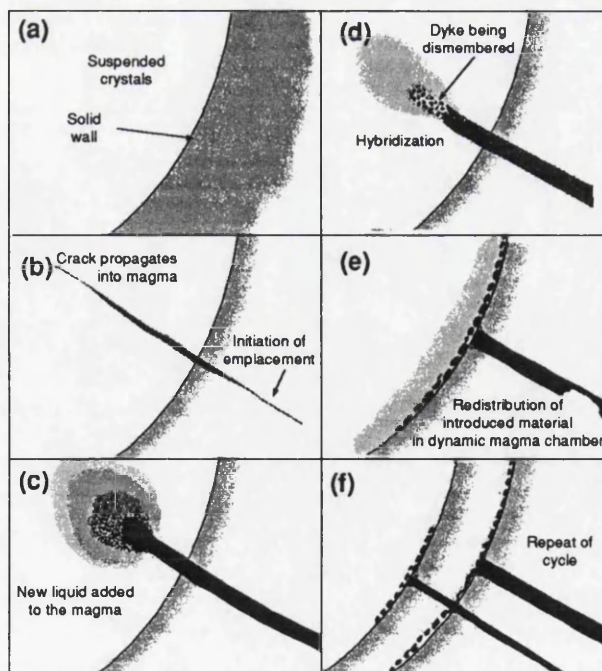
- a) A disrupted dyke cutting a fluxioned zone of more dioritic composition
- b) A less disrupted member cutting a more disrupted, earlier member of the swarm





Microdiorite enclaves enclosed by the quartz diorite itself enclosed in porphyritic granite; K-feldspar phenocrysts occur within each facies.

Figure II.8: Double enclave, Shap granite, Cumbria, England (after Pitcher, 1993).



- (a) Magma chamber, partly solidified
- (b) Propagating crack intersects the magma - solid interface
- (c) Flow of liquid through the conduit, adding to the magma already in the chamber
- (d) Mixing of both liquids and net-veining of the partly solidified dyke
- (e) Resumption of convection resumes hybrid liquids, suspended crystals and disaggregated dyke rocks are distributed parallel to the walls
- (f) Repeat of cycle

Figure II.9: Intrusion of syn-plutonic dykes and origin of the 'enclave trains' (after Hill, 1988).

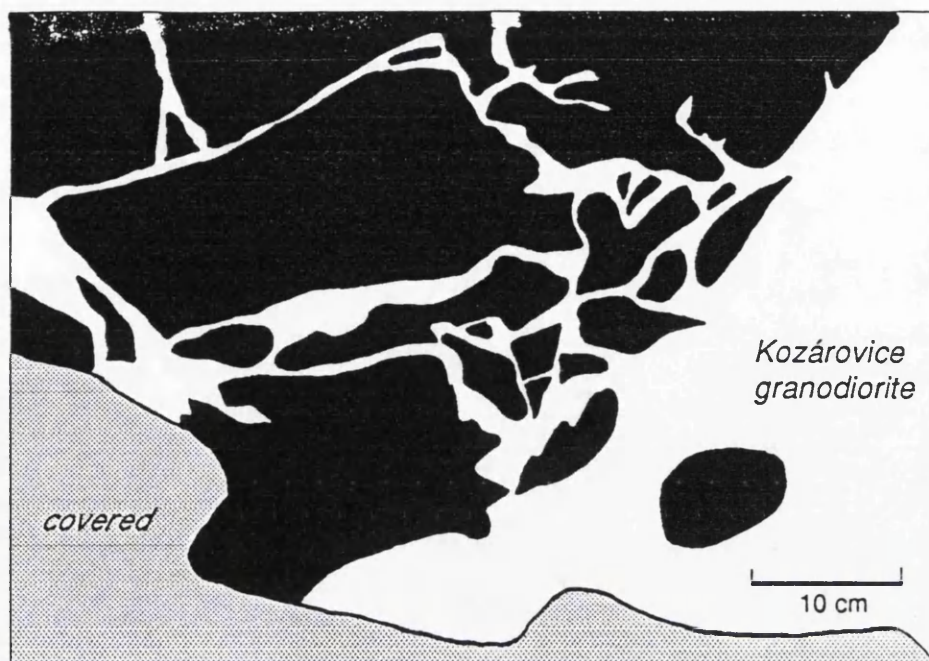


Figure II.10: Net-veining of the Kozárovec quartz monzonite by surrounding granodiorite; Kozárovec II.

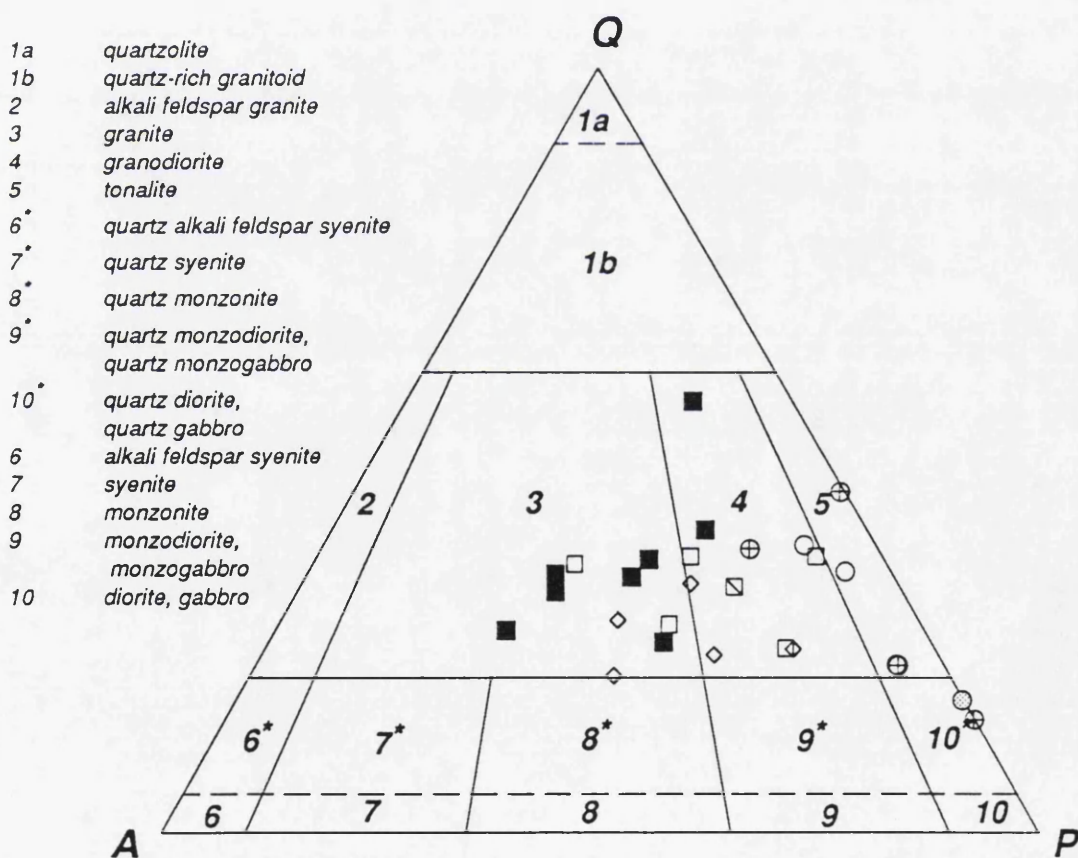


Figure II.11: The IUGS Q-A-P ternary plot for classification of magmatic rocks (Le Maitre, 1989)

Q = quartz

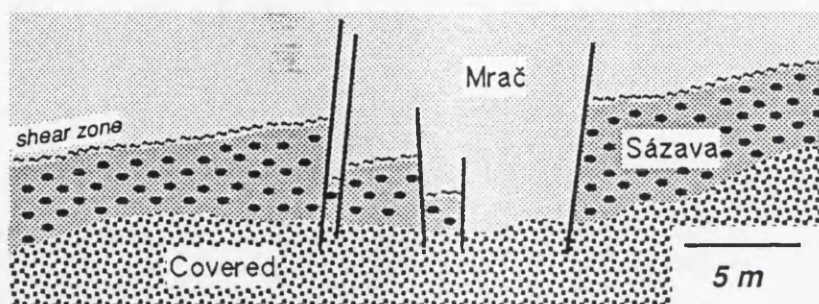
A = alkaline feldspar (K-feldspar, albite $An < 5$)

P = plagioclase

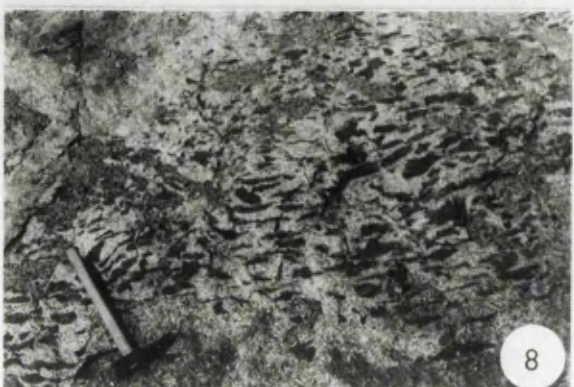
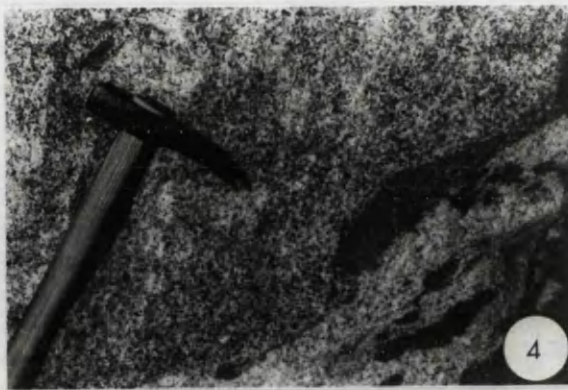
For the standard plotting symbols, see Figure I.6.

Sázava intrusion (1): field photographs

- II.1.1. Shear zone 25 cm wide forming a tectonic contact between the Sázava tonalite (bottom) and Mrač monzogranite (cf. Photo II.1.2.); the contact has been disturbed by later normal faults (see the sketch below);
Mrač, quarry, middle bench.

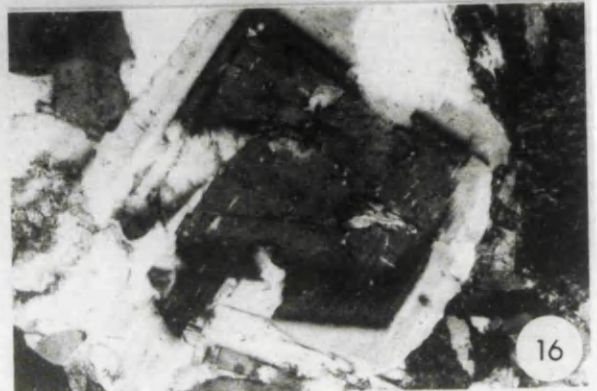
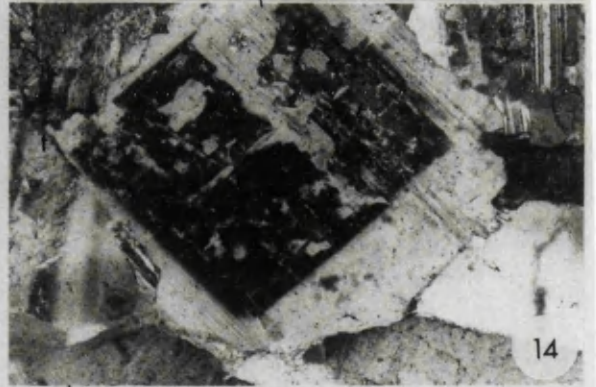
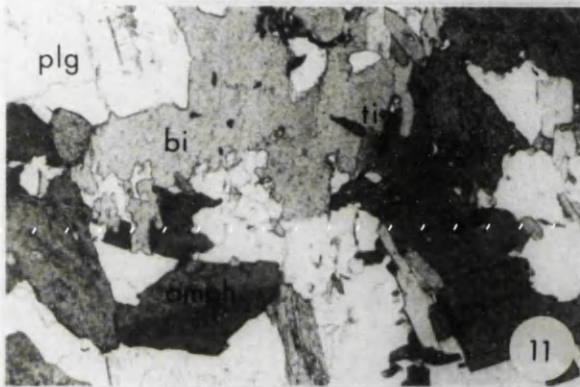
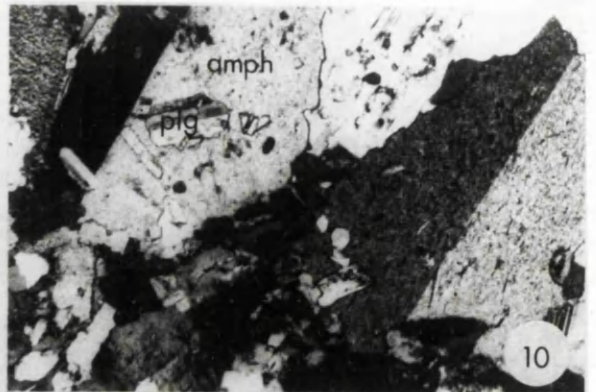
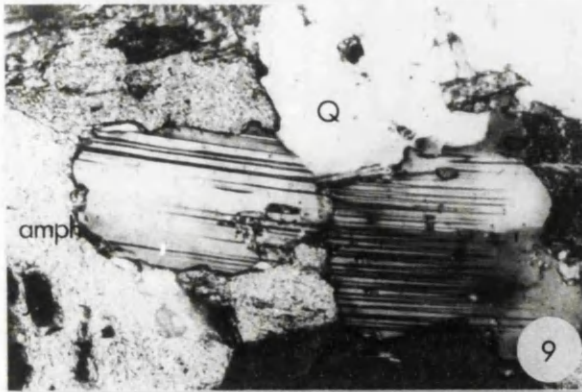


- II.1.2. Angular xenoliths of the Sázava tonalite enclosing MME in biotite monzogranite of Mrač type;
Mrač, quarry, lower bench.
- II.1.3. Požáry trondhjemite showing flow-alignment and enclosing two angular xenoliths of the Sázava tonalite which itself contains several MME;
Prosečnice, quarry.
- II.1.4. Sharp contact between the Sázava tonalite (top) and Požáry trondhjemite with no chilled margin; the MME in the Sázava intrusion is sheared along the contact and the Požáry trondhjemite includes several MME with irregular-shaped margins;
Krhanice, quarry, lower bench.
- II.1.5. Strongly flow-aligned MME of quartz dioritic composition in Sázava tonalite;
Teletín quarry, lower bench.
- II.1.6. Broken MME (cf. Photo II.1.12.) in Sázava tonalite and net-veined due to host penetration;
Teletín quarry, top bench.
- II.1.7. Bent flow-aligned MME in Sázava tonalite;
Teletín quarry, top bench.
- II.1.8. Enclave swarm next to the gabbro dyke;
Krhanice, quarry.



Sázava intrusion (2): microscopy

- II.1.9. Partially resorbed plagioclase, showing bent cleavage and surrounded by biotite, amphibole and quartz;
Sa-3, Mrač , x 20, XPL.
- II.1.10. Poikilitic simply twinned amphibole enclosing plagioclase laths and small resorbed biotite flakes;
Sa-12, Mrač , x 20, XPL.
- II.1.11. Subhedral amphibole crystals, associated with plagioclase and strongly resorbed biotite that encloses euhedral crystals of titanite;
Sa-3, Mrač , x 35, PPL.
- II.1.12. Mantled plagioclase, with resorbed bytownite-anorthite core, in matrix of strained quartz and deformed biotite;
MME Sam-7, Teletín, x 24, XPL.
- II.1.13. Patchy zoning in the core of a mantled plagioclase;
Teletín quartz diorite SaD-3, Teletín quarry, x 50, XPL.
- II.1.14. Mantled plagioclase with a protrusion of andesine rim into the bytownite - anorthite core;
Teletín quartz diorite SaD-2, Teletín quarry, x 50, XPL.
- II.1.15. Mantled plagioclase with resorbed bytownite - anorthite core overgrown by an andesine rim;
Teletín quartz diorite SaD-1, Teletín quarry, x 50, XPL.
- II.1.16. Another example of mantled plagioclase with resorbed core;
Teletín quartz diorite SaD-2, Teletín quarry, x 50, XPL.



Sázava intrusion (3): cathodoluminescence

II.1.17. Ochre plagioclases, some mantled (with bright yellow cores), that are fractured and surrounded by interstitial calcite (of bright orange CL); the non-luminescent mineral is hornblende, showing leaching (brownish patches) and calcite deposition; the yellow inclusions within the hornblende are apatite;

Sa-10, Prosečnice, CL, x 45 [cf. Fig. II.12 a]

II.1.18. Mantled plagioclase, with the bright yellow calcic core, which is partly resorbed and surrounded by the younger more sodic plagioclase with ochre-coloured luminescence; the non-luminescent minerals are biotite and hornblende;

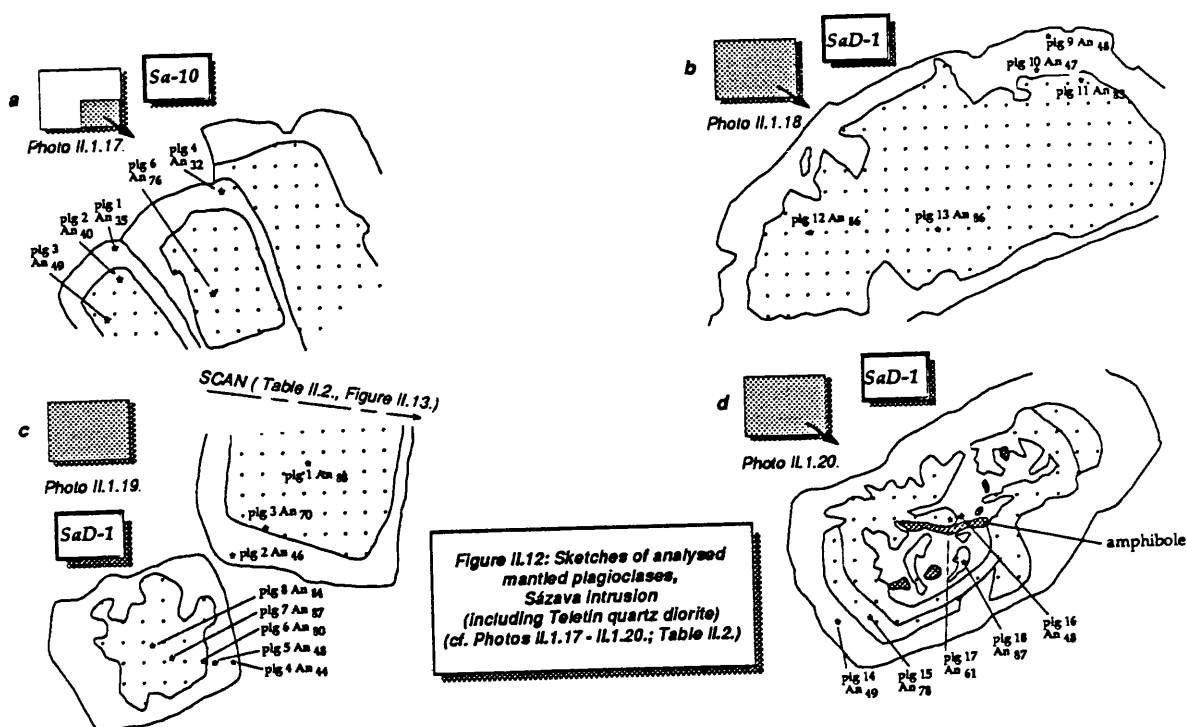
Teletín quartz diorite, SaD-1, CL, x 55 [cf. Fig. II.12 b]

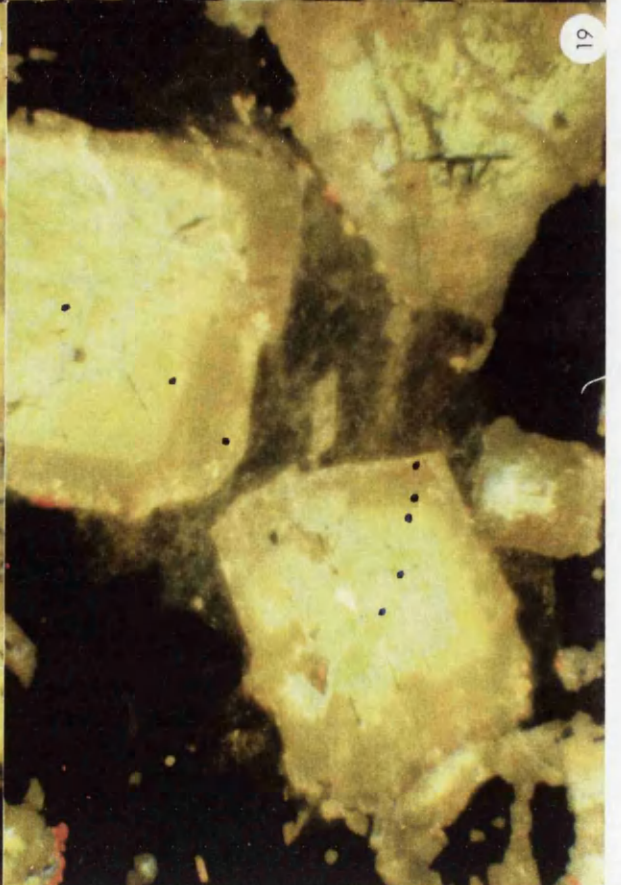
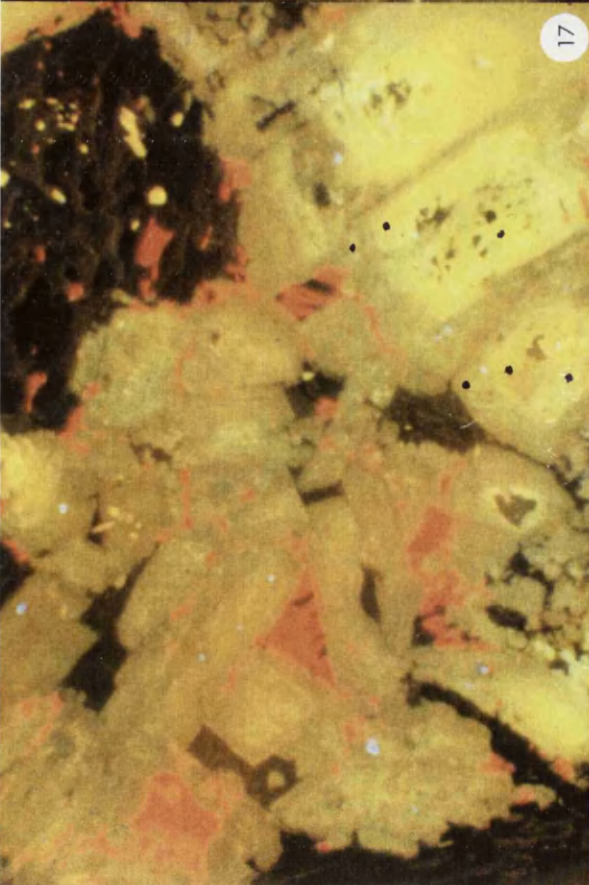
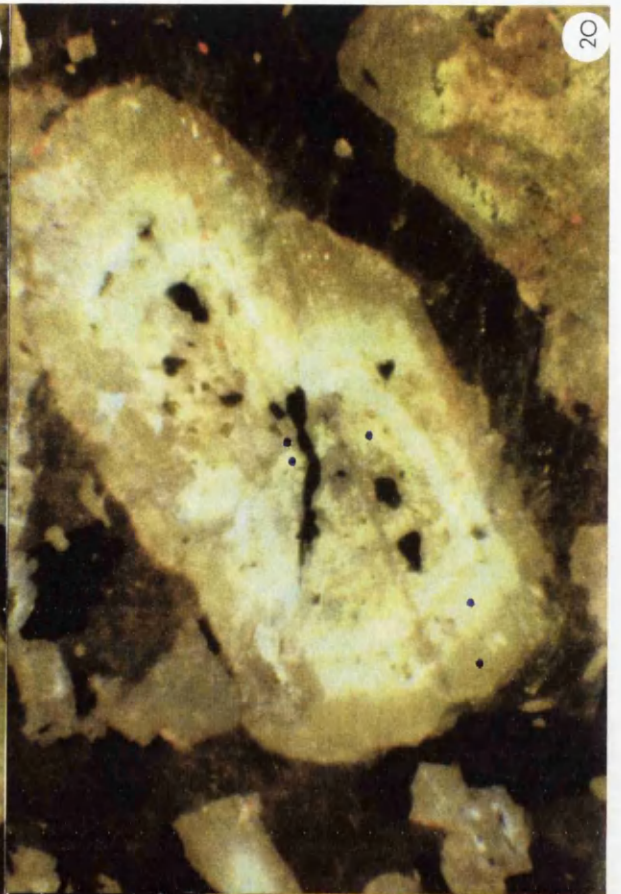
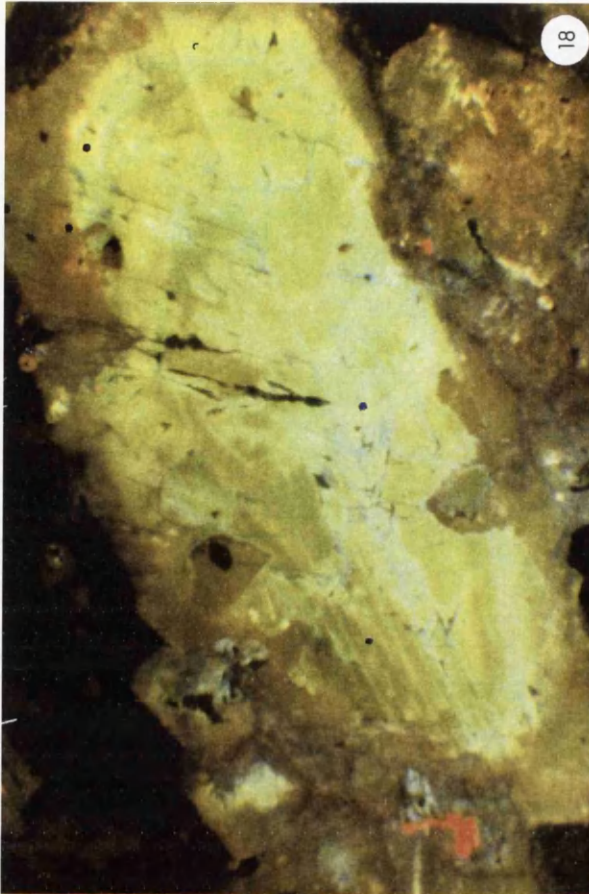
II.1.19. Mantled plagioclases, with bright yellow cores and dull ochre rims, showing different degrees of resorption;

Teletín quartz diorite, SaD-1, CL, x 45 [cf. Fig. II.12 c, II.13., Tab. II.2.]

II.1.20. Mantled plagioclase with a patchy zoned core, overgrown by a calcic spike (bright yellow) and dull ochre rim; this plagioclase encloses several round grains of amphibole;

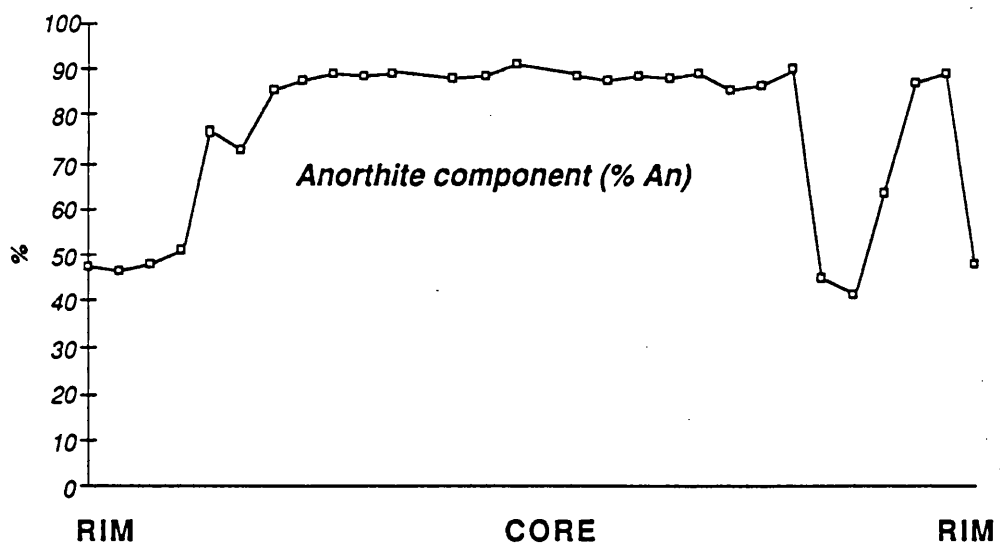
Teletín quartz diorite, SaD-1, CL, x 45 [cf. Fig. II.12 d]





**Table II.2: Traverse across mantled plagioclase,
Teletín quartz diorite (SaD-1)
[cf. Photo II.1.19, Fig. II.12 c]**

	1	2	3	4	5	6	7	8	9	10
Ab	51.9	52.6	51.2	48.1	23.0	26.8	14.3	12.4	10.8	11.0
An	47.7	46.8	48.0	51.3	77.0	72.7	85.4	87.5	89.0	88.9
Or	0.4	0.6	0.9	0.6	0.1	0.5	0.2	0.1	0.2	0.1
	11	13	14	15	17	18	19	20	21	22
Ab	10.9	11.6	11.3	8.9	11.2	12.5	11.2	11.7	10.6	14.4
An	89.1	88.3	88.6	91.0	88.7	87.5	88.8	88.1	89.3	85.6
Or	0	0.2	0.1	0.1	0.1	0	0	0.1	0.1	0.1
	23	24	25	26	27	28	29	30		
Ab	13.2	10.1	54.3	58.5	35.4	12.9	10.9	51.5		
An	86.5	89.9	45.1	41.3	63.8	87.1	89.0	48.2		
Or	0	0	0.7	0.2	0.8	0	0	0.3		



**Figure II.13: An content across mantled plagioclase, Teletín quartz diorite
[cf. Photo II.1.19., Table II.2.]**

Sázava intrusion (4): cathodoluminescence

- II.1.2.1. Strongly leached amphibole crystal (non-luminescent), with abundant worm-like inclusions of calcite (orange) and prismatic apatite (yellow), surrounded by quartz (dull brown) and plagioclase (yellow);

Sa-10, Prosečnice, CL, x 44

Požáry intrusion: cathodoluminescence

- II.2.1. Plagioclase crystals of dull ochre luminescence, the largest of them with a brighter yellow core (mantled); the gaps between the plagioclases are filled by two generations of calcite, of dull and bright orange luminescence (the brighter one appears to be the younger) and non-luminescent biotite;

Po-3, Prosečnice, CL, x 45

- II.2.2. Complex zoning in the plagioclase crystals (ochre to yellow CL); the core of the smaller of the two zoned plagioclases has suffered strong alteration (rendering the CL a brownish colour); the plagioclases are surrounded by interstitial K-feldspar (light blue); the thin dull brown rim of the plagioclases against K-feldspar could be explained due to leaching or exchange due to diffusion; the non-luminescent mineral is biotite, with yellow apatite inclusions; [cf. Fig. II.14 a]

Po-3, Prosečnice, CL, x 45

- II.2.3. Strongly brecciated oscillatory zoned plagioclases (ochre - yellow luminescence), healed by K-feldspar (light blue); the best-preserved of the plagioclases is discontinuously-zoned;

Po-3, Prosečnice, CL, x 45 [cf. Fig. II.14 b]

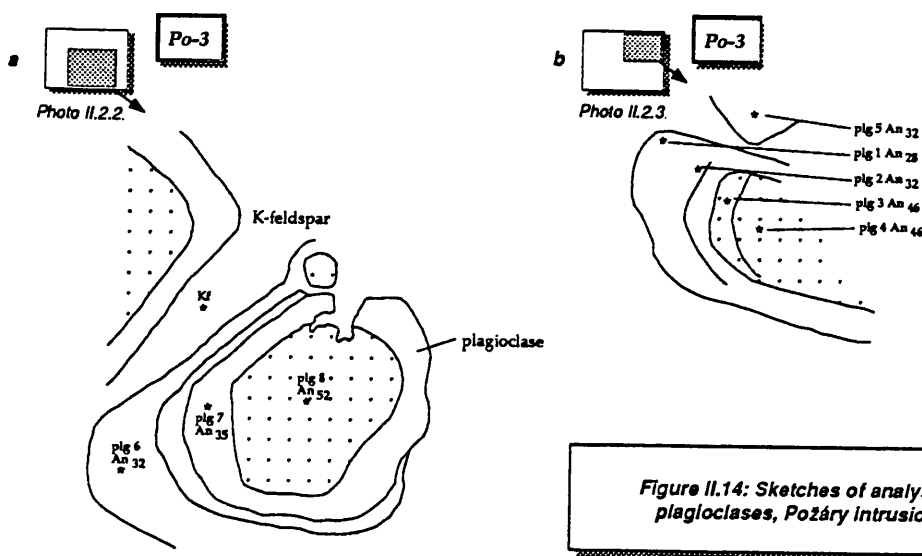
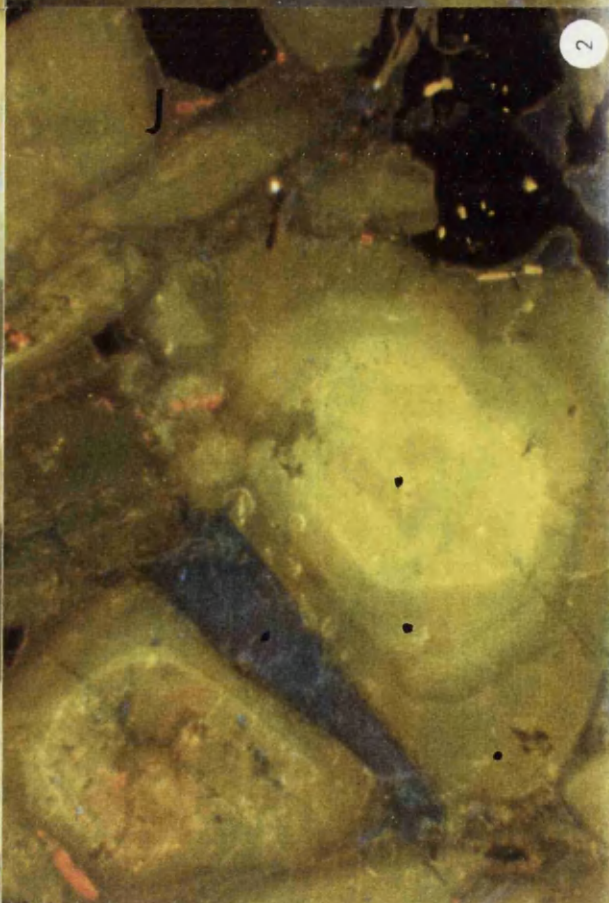
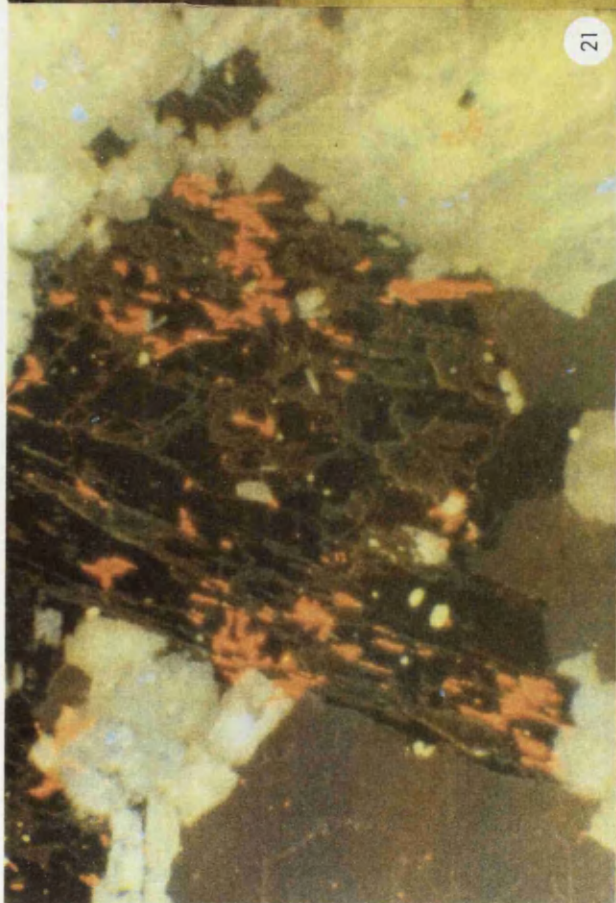


Figure II.14: Sketches of analysed plagioclases, Požáry intrusion



Kozárovec intrusion (1): field photographs

- II.3.1. Angular xenolith of a banded hornfels in sharp contact with Kozárovec granodiorite;
Solopysky, quarry

- II.3.2. Round MME, with an embayment of a granodiorite somewhat more mafic than the Kozárovec granodiorite host;
Kozárovec II, quarry

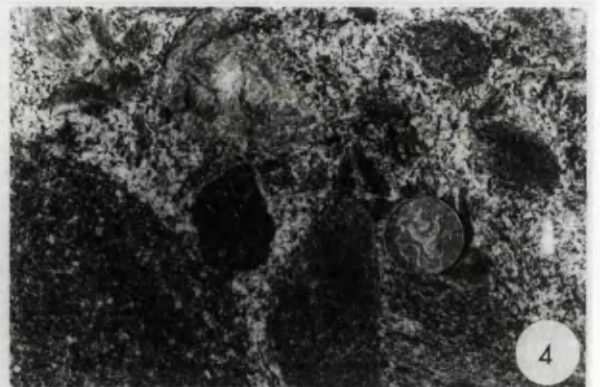
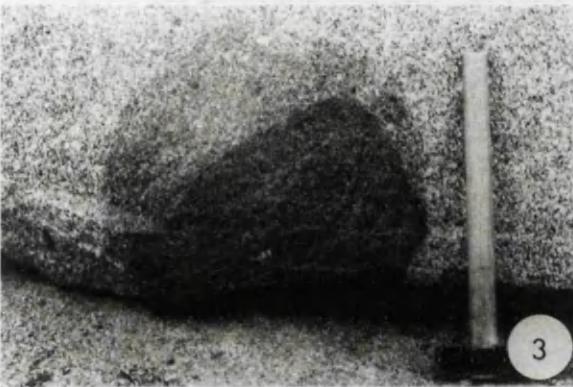
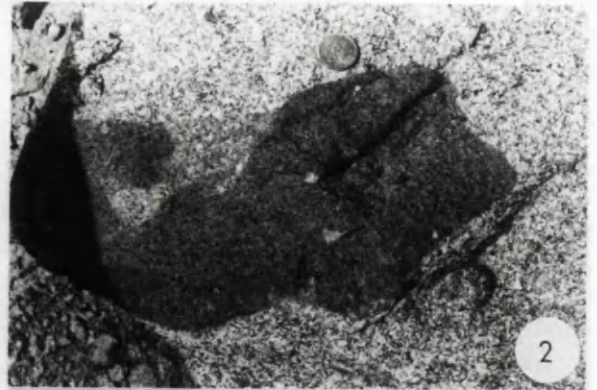
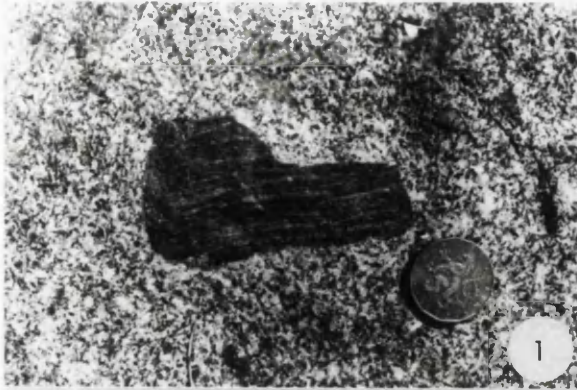
- II.3.3. MME surrounded by a zone richer in plagioclase megacrysts ('double enclave'); the contact with the host Kozárovec granodiorite is diffuse, whereas the contact between the two zones is sharp;
Kozárovec III, bottom of the quarry

- II.3.4. Polygenic enclave swarm: much contaminated Kozárovec granodiorite, full of often resorbed xenoliths of various rocks (MME, surmicaceous enclave, gneiss, calc-silicate rock);
Solopysky, bottom of the quarry

- II.3.5. Folded biotite - hornblende bands ('ladder dyke') that are generally parallel to one another; locally (right-hand side) they converge to form structures similar to cross-bedding in sediments, before wedging out; note the truncated MME next to the hammer;
Kozárovec III, lower quarry bench

- II.3.6. Close-up of II.3.5., showing the nature of the biotite - hornblende bands, and their disruption in the hinge zone of the fold;
Kozárovec III, lower quarry bench

- II.3.7. Syn-plutonic dyke of lamprophyre (?), intruding the Kozárovec granodiorite that is cut by a slightly coarser-grained granodiorite; where the boundary could be identified, a thin dark layer is present between the two masses;
Kozárovec III, quarry



Kozárove intrusion (2): microscopy & Kozárove quartz monzonite

- II.3.8. Euhedral oscillatory zoned plagioclase at contact with a strongly perthitic subhedral K-feldspar; at its outer edge the plagioclase is partly resorbed, and a thin myrmekite rim is developed;

Koz-1, Solopysky, x 20, XPL

- II.3.9. Anhedral twinned plagioclase crystal, surrounded by biotite, in which there are abundant inclusions of short-prismatic apatite; in contrast, the apatite enclosed by the plagioclase is acicular;

Koz-2, Kozárove I, x 50, XPL

- II.3.10. Poikilitic K-feldspar, enclosing euhedral crystals of amphibole (some of them in extinction), as well as partly resorbed plagioclases;

Koz-2, Kozárove I, x 20, XPL

- II.3.11. Twinned, euhedral amphibole crystal enclosing a ring of small partly resorbed biotites; the amphibole is surrounded by plagioclase and quartz;

Koz-2, Kozárove I, x 35, XPL

- II.3.12. Kozárove quartz monzonite, net-veined by granodiorite, that in places resorbs the quartz monzonite fragments; some of the contacts are diffuse;

Kozárove II, bottom of the quarry

- II.3.13. Long prismatic euhedral hornblende crystals in a matrix of K-feldspar; also present are biotite (in extinction) and abundant acicular apatite;

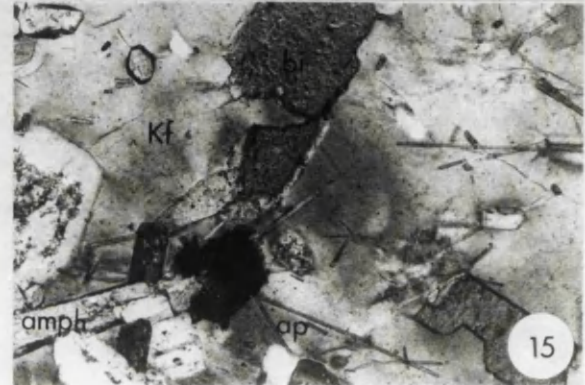
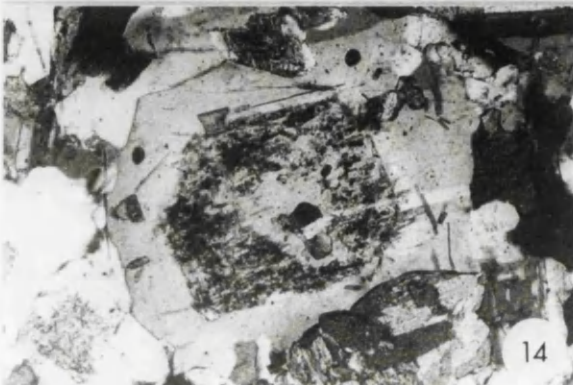
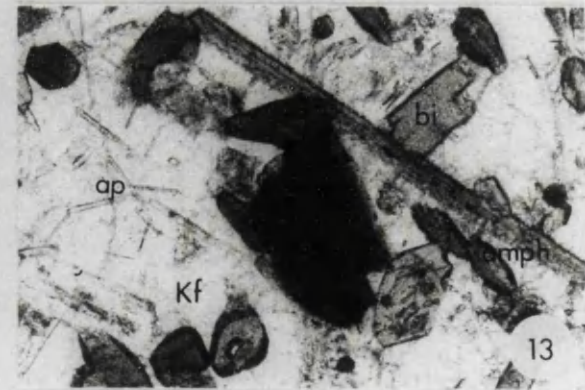
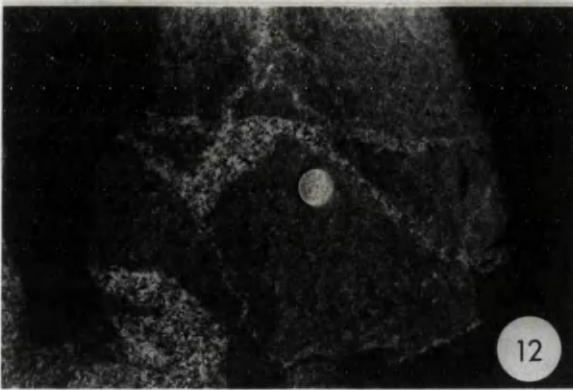
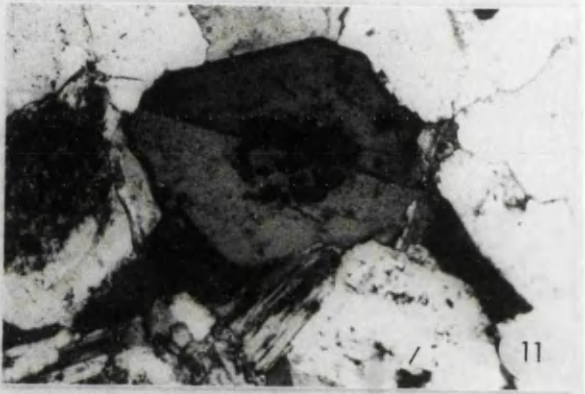
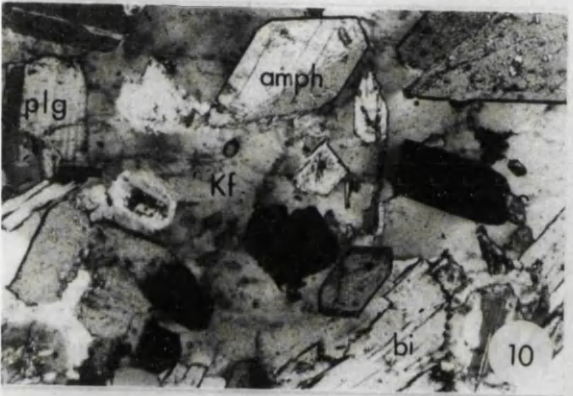
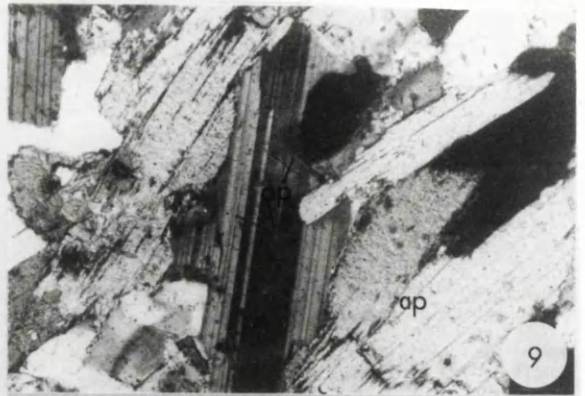
Kozárove quartz monzonite KozD-1, Kozárove II, x 80, PPL

- II.3.14. Mantled plagioclase, with an altered calcic core and abundant inclusions of hornblende and acicular apatite in the outer zone;

Kozárove quartz monzonite KozD-1, Kozárove II, x 50, XPL

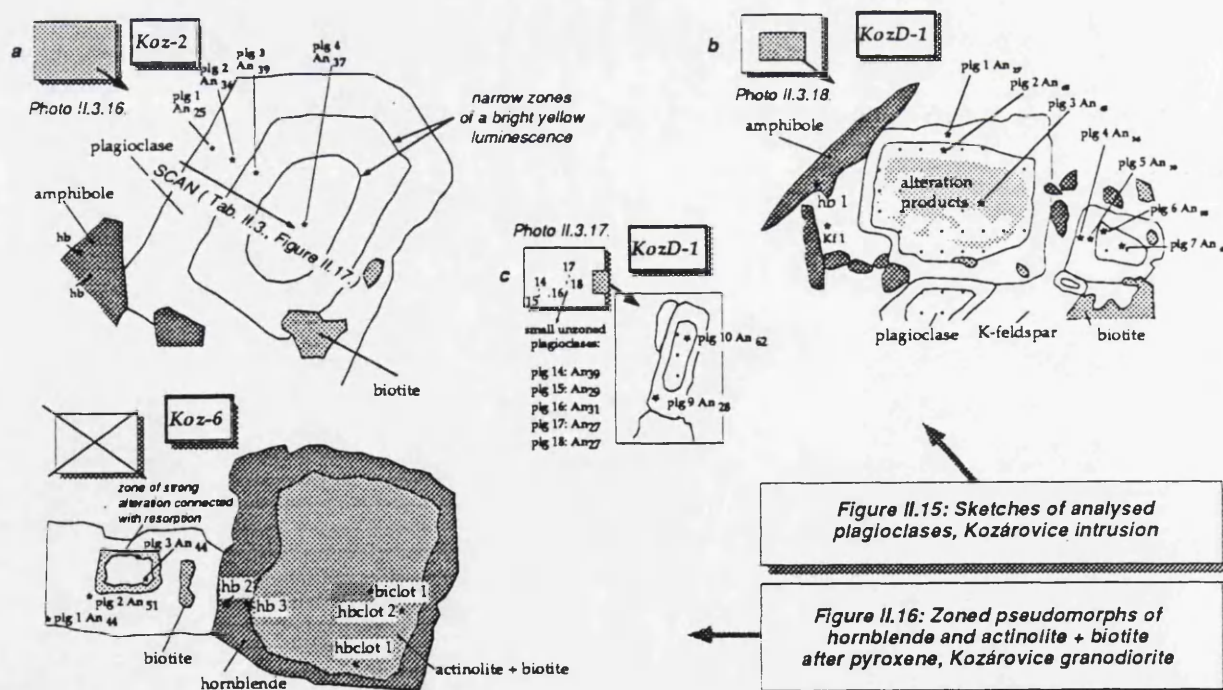
- II.3.15. Subhedral biotite flakes, together with long prismatic hornblende, mantled plagioclase and acicular apatite, in the K-feldspar matrix;

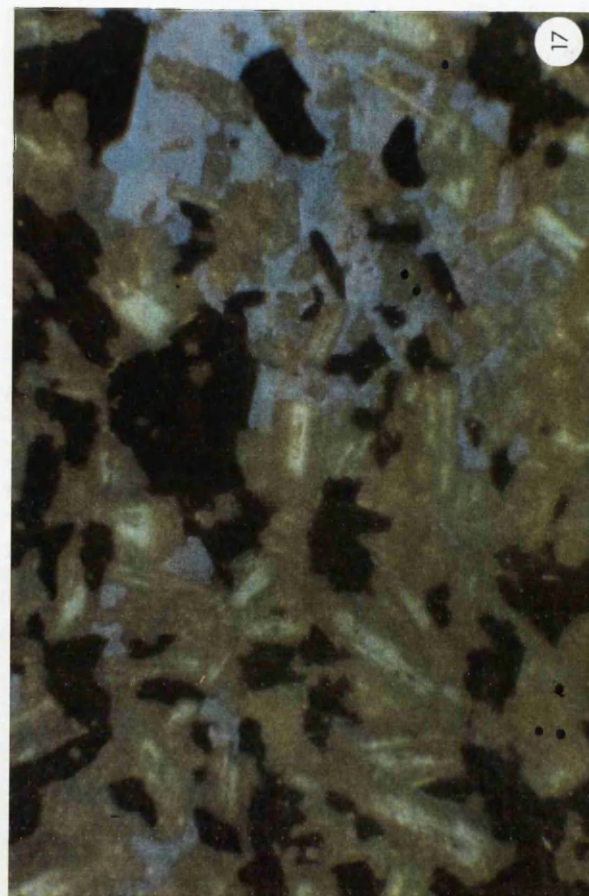
Kozárove quartz monzonite KozD-1 Kozárove II, x 50, XPL



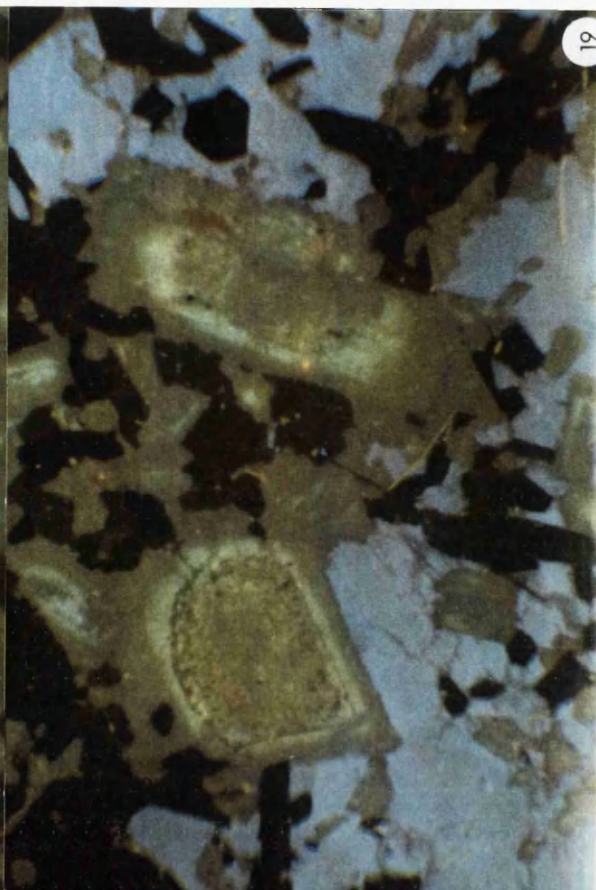
Kozárove intrusion (3): cathodoluminescence

- II.3.16. Plagioclase of ochre colour, with two resorption surfaces (brighter yellow); the plagioclase is surrounded by K-feldspar (blue), quartz (dull brown) and amphibole (non-luminescent);
Koz-2, Kozárove I, CL, x 25 [cf. Fig. II.15 a, II.17., Tab. II.3.]
- II.3.17. Abundant lath-shaped plagioclase crystals showing dull ochre luminescence, some of them mantling older bright-yellow cores; the plagioclases, together with non-luminescent amphibole and biotite, are enclosed in a large K-feldspar oikocryst (blue);
Kozárove quartz monzonite, KozD-1, Kozárove II, CL, x 45 [cf. Fig. II.15 c]
- II.3.18. Larger mantled plagioclases, with strongly altered patchy-zoned cores of generally brighter-yellow luminescence, overgrown by dull-ochre rims and surrounded by amphibole and small lath-shaped plagioclase and blue K-feldspar matrix; some of the small lath-shaped plagioclases are unzoned;
Kozárove quartz monzonite, KozD-1, Kozárove II, CL, x 45 [cf. Fig. II.15 b]
- II.3.19. Two plagioclases, with patchy-zoned cores, overgrown by bright-yellow spike and dull ochre rims together with smaller lath-shaped plagioclase crystals and amphibole, surrounded by large mass of interstitial K-feldspar;
Kozárove quartz monzonite, KozD-1, Kozárove II, CL, x 45





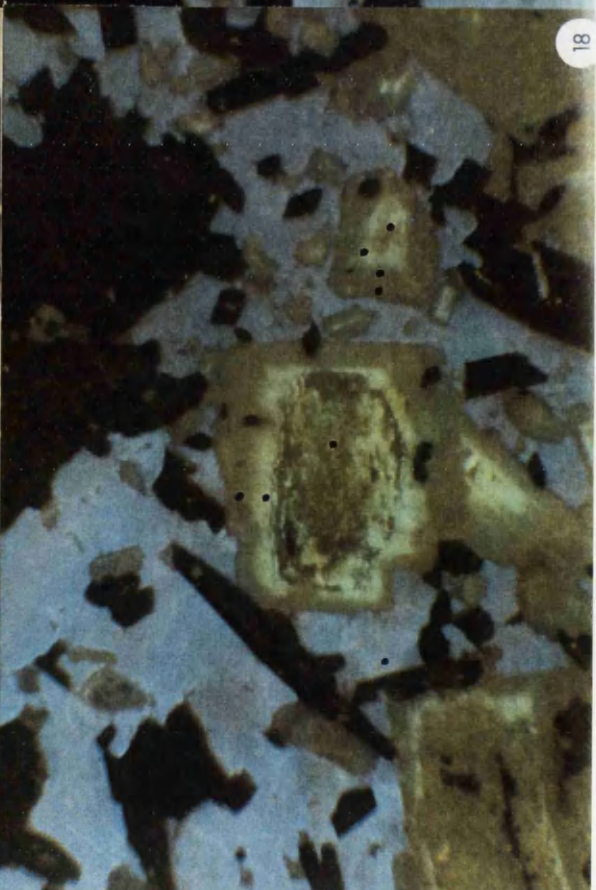
17



19



16



18

**Table II.3: Traverse across zoned plagioclase,
Kozárovice granodiorite (Koz-2)**
(cf. Photo II.3.16, Fig. II.15 a)

	1	2	3	4	5	6	9	10	11	14
Ab	74.7	75.3	73.0	71.2	69.5	67.7	62.9	62.2	63.3	64.5
An	24.4	23.0	25.0	27.3	28.6	30.3	35.4	36.3	35.4	34.9
Or	1.0	1.7	2.0	1.5	1.9	2.0	1.7	1.4	1.3	0.6
	15	17	18	19	22	23	24	26	27	28
Ab	62.2	58.3	52.8	52.0	55.5	57.8	58.1	60.5	61.2	60.0
An	36.5	38.0	46.0	46.8	43.7	40.8	40.8	38.2	37.8	38.9
Or	1.3	3.8	1.2	1.2	0.8	1.4	1.1	1.3	1.0	1.1

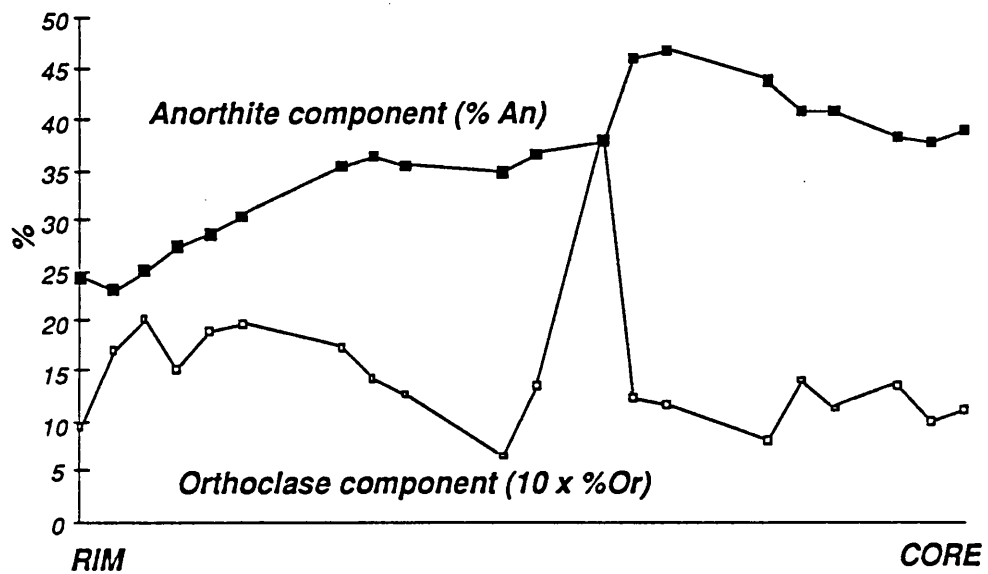
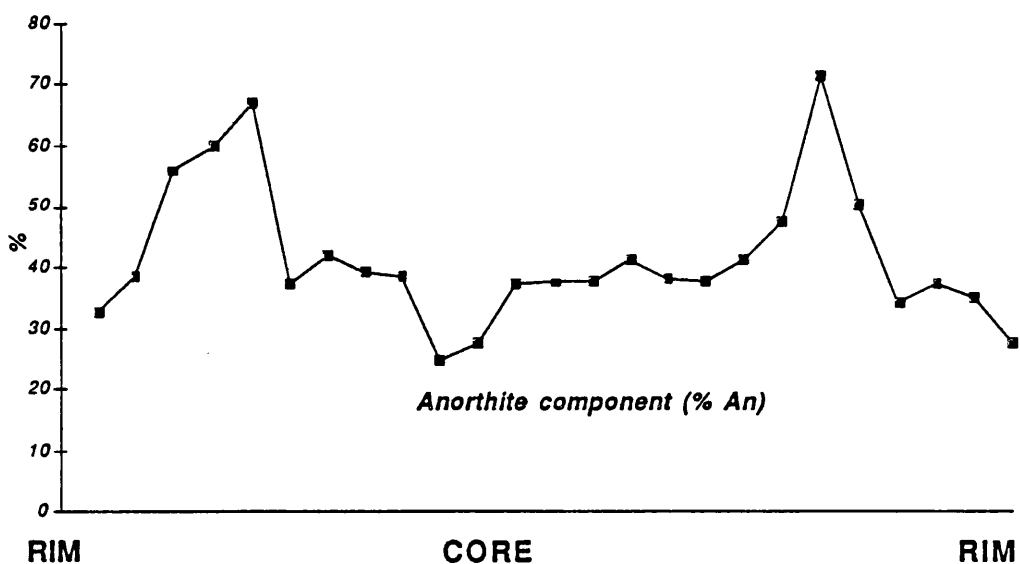


Figure II.17: Variation in An and Or from margin to core of zoned plagioclase, Kozárovice granodiorite
[cf. Photo II.3.16., Table II.3.]

**Table II.4: Traverse across zoned plagioclase,
Kozárovce quartz monzonite (KozD-1)**

	1	2	3	4	5	6	7	8	9	10
Ab	65.6	59.8	43.4	38.8	33.0	61.7	57.2	59.9	60.7	73.9
An	32.8	38.5	55.9	59.8	66.9	37.4	42.0	39.2	38.5	24.8
Or	1.6	1.7	0.7	1.4	0.1	0.9	0.8	0.9	0.8	1.3
	11	12	13	14	15	16	17	18	19	20
Ab	71.1	61.4	61.2	60.9	57.5	60.5	60.7	57.7	52.0	28.0
An	27.7	37.3	37.5	37.9	41.3	38.1	37.8	41.2	47.4	71.6
Or	1.2	1.3	1.3	1.2	1.2	1.4	1.5	1.1	0.6	0.4
	21	22	23	24	25					
Ab	48.9	64.7	61.4	64.0	71.0					
An	50.4	34.1	37.3	35.0	27.7					
Or	0.7	1.2	1.3	1.0	1.3					



**Figure II.18: Variation in An across the zoned plagioclase,
Kozárovce quartz monzonite [cf. Table II.4.]**

Blatná intrusion (1): field photographs

- II.4.1. Net-veined, fractured and partly assimilated metasedimentary xenoliths in strongly contaminated granodiorite;
Hudčice, quarry

- II.4.2. Round MME, surrounded by a thin dark reaction rim in granodiorite which is cut by an aplopegmatite vein (left);
Řečice, quarry

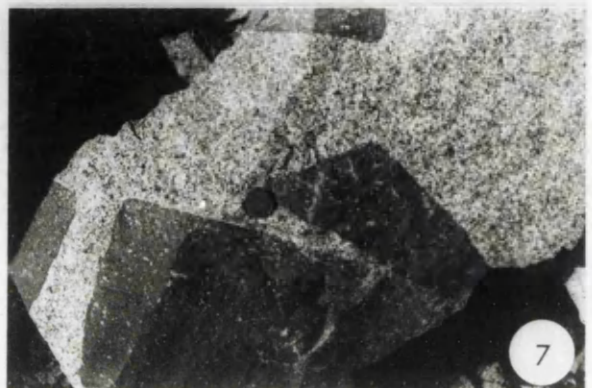
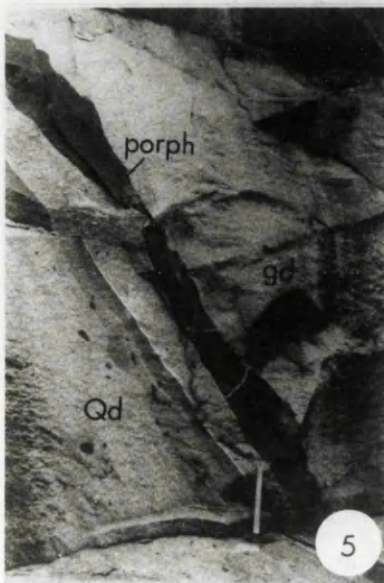
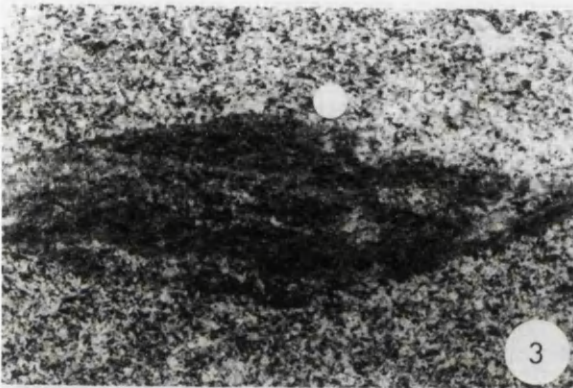
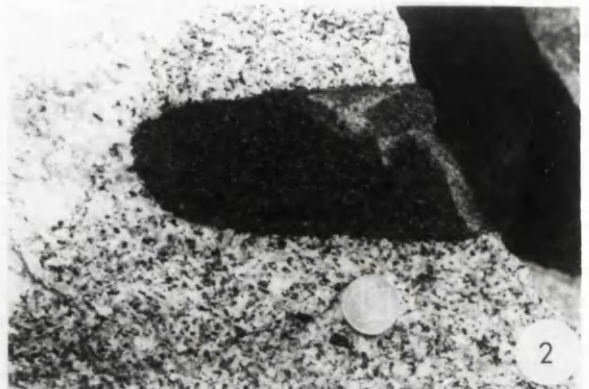
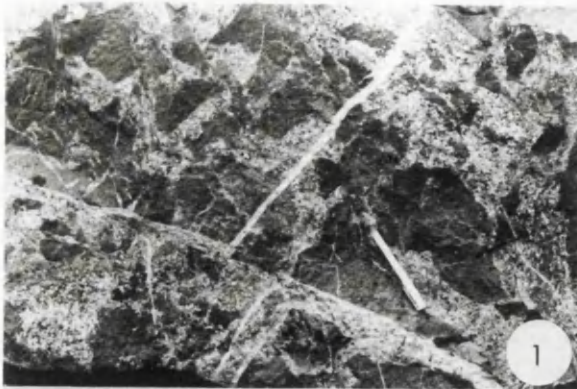
- II.4.3. MME with dimensionally-oriented minerals, partly resorbed by the host granodiorite;
Tužice, quarry

- II.4.4. Granodiorite with a relatively strong planar fabric that also affects an MME;
Vahlovice, quarry

- II.4.5. Fractured dyke of a granodiorite porphyry (dark), broken into angular xenoliths, and a quartz dioritic zone (left) that encloses many plagioclase megacrysts and scattered round enclaves of the porphyry; the quartz diorite adjacent to the dyke is rimmed by a thin (< 1 cm) aplitic band;
Hudčice, quarry

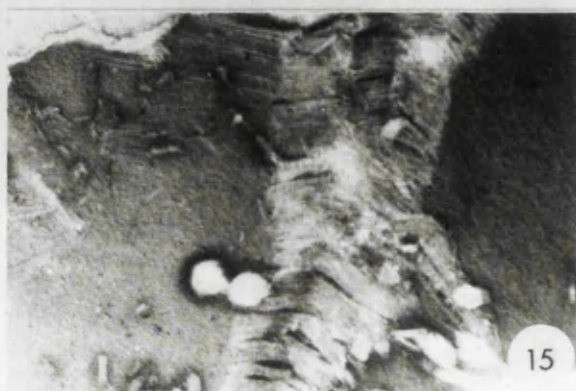
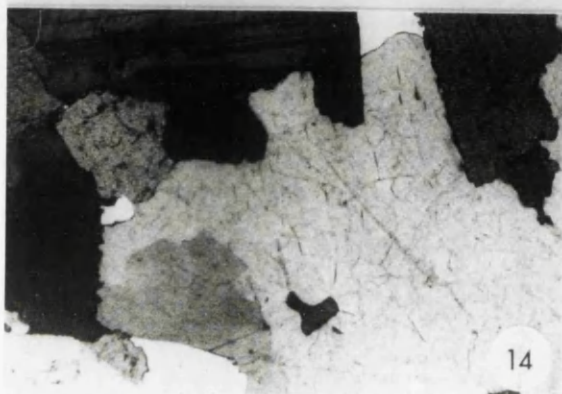
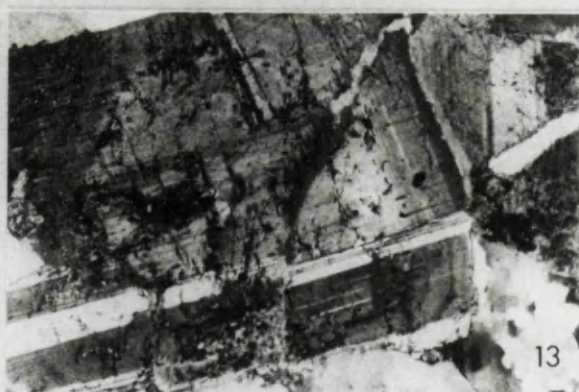
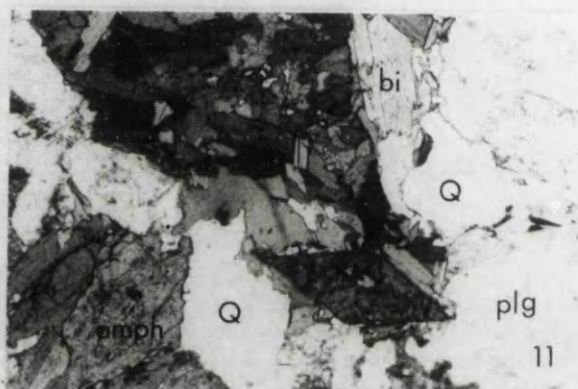
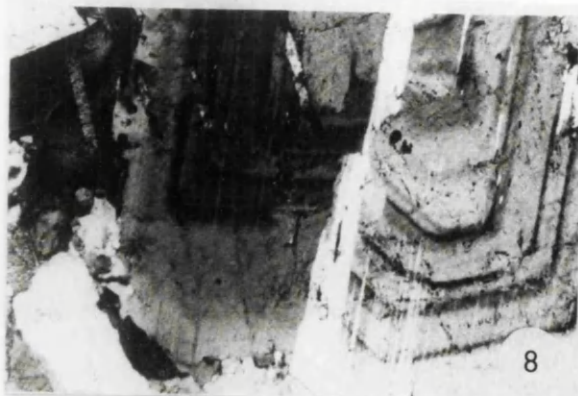
- II.4.6. Detail of the aplitic band from the previous picture [II.4.5.];
Hudčice, quarry

- II.4.7. Angular xenoliths of the quartz diorite in Blatná granodiorite host; at their contact, thin aplitic reaction rims are developed;
Hudčice, quarry



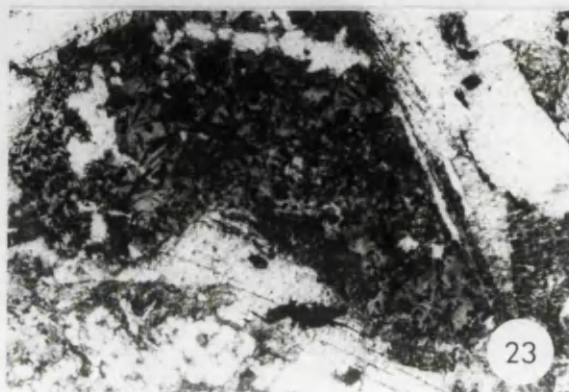
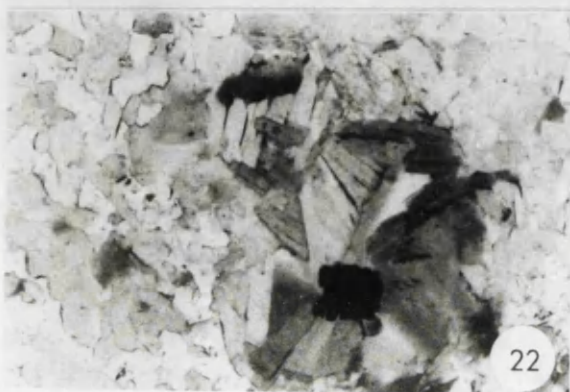
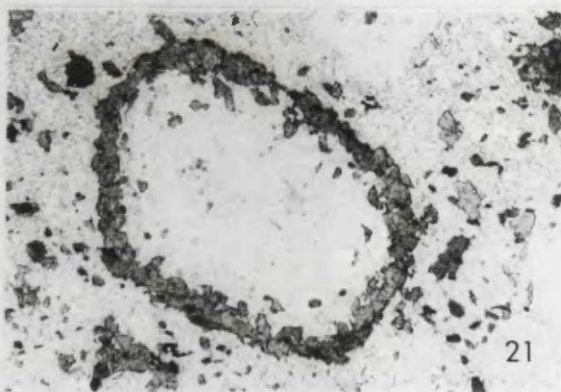
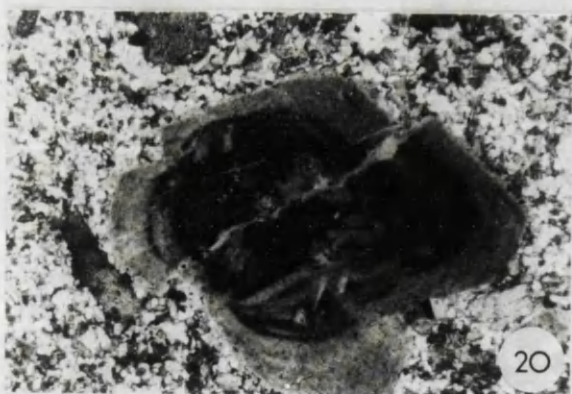
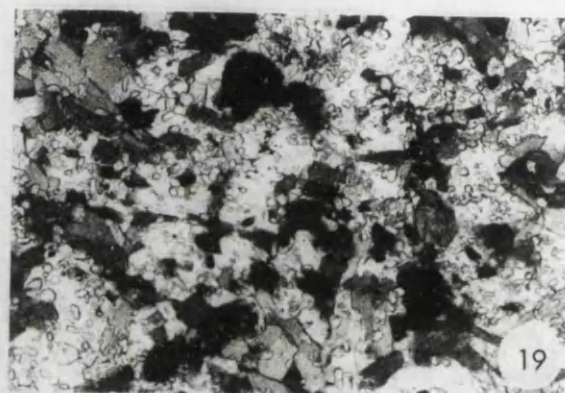
Blatná intrusion (2): microscopy

- II.4.8. Oscillatory zoning in an euhedral plagioclase crystals; the dark mineral is biotite, with a prominent inclusion of apatite;
Bl-7, Defurovy Lažany , x 20, XPL
- II.4.9. Thick myrmekite rim developed at the contact between the perthitic K-feldspar (in extinction) and plagioclase (top);
Bl-4, Paštiky, x 50, XPL
- II.4.10. K-feldspar phenocryst, with Carlsbad twinning, enclosing partly resorbed plagioclase and round quartz grains; the dark euhedral mineral, rhomboidal in shape, is titanite; the phenocryst is rimmed by zone of deformed biotite, quartz and plagioclase;
Bl-4, Paštiky , x 20, XPL
- II.4.11. Amphibole-biotite clot, enclosing two euhedral titanite crystals, surrounded by plagioclase, quartz, biotite and hornblende;
Granodiorite close to contact with a MME, Blm-7, Vahlovice, x 20, PPL
- II.4.12. Bent subhedral plagioclase crystal, occurring with biotite, another plagioclase and quartz, the latter showing strong undulose extinction;
Bl-2, Tužice, x 35, XPL
- II.4.13. Broken plagioclase crystal, with the crack healed by younger albite that also forms the rim of the plagioclase; note the strong deformation of quartz (bottom right);
Bl-8, Hudčice, x 40, XPL
- II.4.14. Strongly fractured quartz grain, surrounded by plagioclase and biotite;
Bl-7, Defurovy Lažany, x 24, XPL
- II.4.15. Detail of the kink bands in a biotite crystal, rich in inclusions of apatite;
Bl-3, Velenovy, x 106, PPL



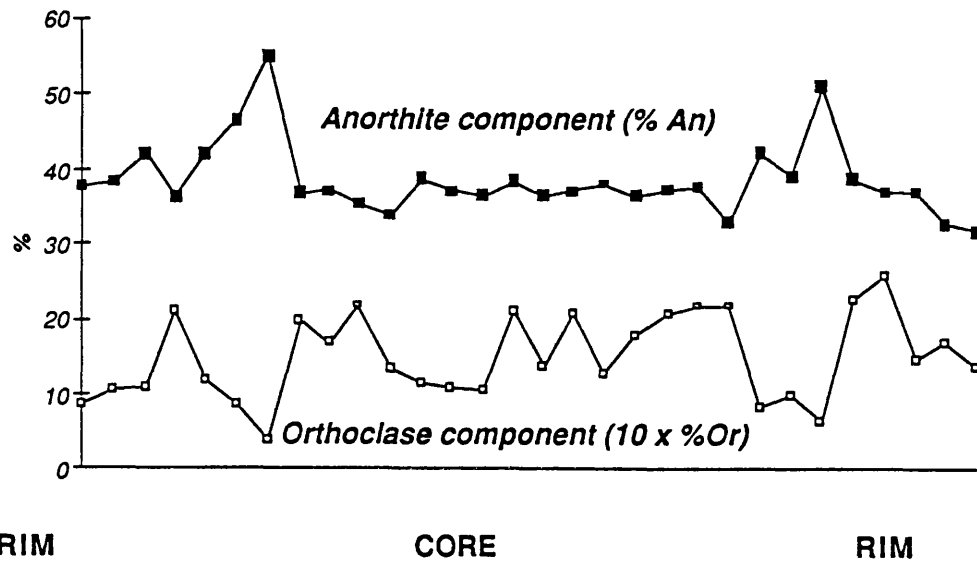
Blatná intrusion (3): microscopy

- II.4.16. Poikilitic titanite crystal, with chadacrysts of ocellar quartz; the titanite is surrounded by biotite and K-feldspar; surmicaceous enclave;
Blm-10, Defurovy Lažany, x 50, PPL
- II.4.17. Large oikocrysts of perthitic K-feldspar, enclosing biotite flakes and acicular apatite;
MME Blm-2, Tužice, x 50, XPL
- II.4.18. Large oscillatory-zoned orthite crystal growing parallel to the boundary between a finer-grained, biotite rich MME and the host Blatná granodiorite (left);
MME Blm-2, Tužice, x 20, PPL
- II.4.19. Biotite-rich MME, exceptionally rich in short-prismatic apatite;
MME Blm-7, Vahlovice, x 50, PPL
- II.4.20. Plagioclase megacryst, showing complex convolute zoning and late brittle deformation, in a fine-grained matrix;
Granodiorite porphyry, Blm-13, Hudčice quarry, x 35, XPL
- II.4.21. Quartz ocellus, surrounded by corona of tiny hornblende crystals;
Granodiorite porphyry, Blm-13, Hudčice, x 20, PPL
- II.4.22. Biotite - ore mineral spherulite;
Hudčice diorite, BID-1, Hudčice, x 70, PPL
- II.4.23. Euhedral orthite, full of elongate ore inclusions, surrounded by biotite; two light patches, enclosed by the orthite, show high interference colours, similar to calcite;
Cv-2, Malé Nepodřice, x 50, XPL



**Table II.5: Traverse across oscillatory zoned plagioclase,
Blatná granodiorite, Hudčice (Bl-8)**

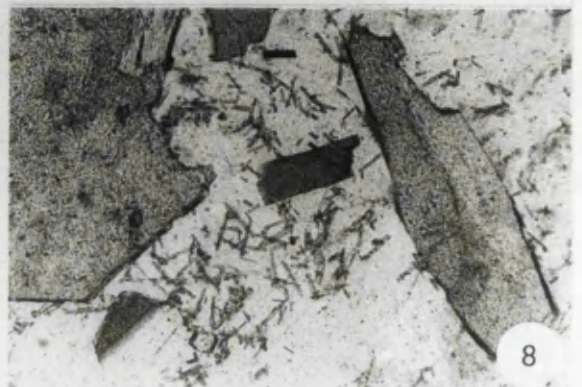
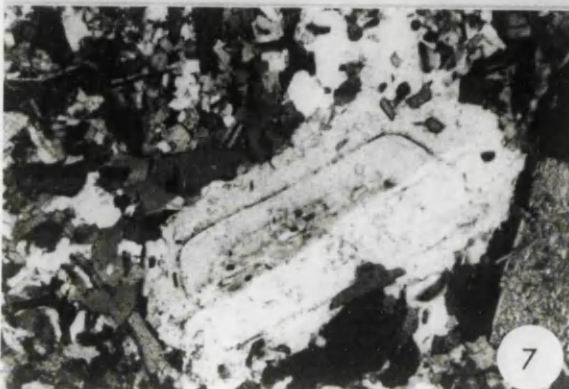
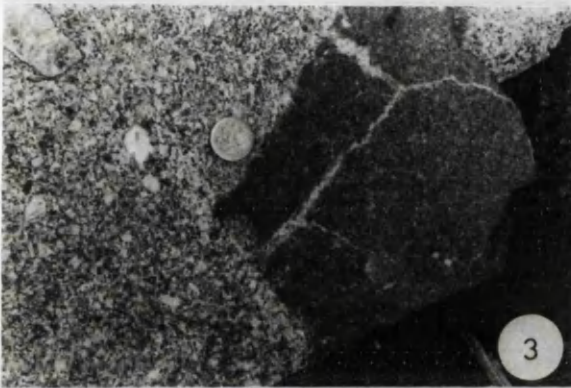
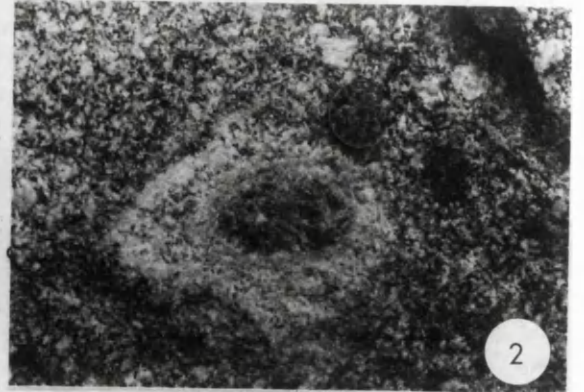
	1	2	3	4	5	6	7	8	9	10
Ab	59.7	58.7	55.1	60.1	54.9	48.6	42.7	59.9	59.9	58.7
An	37.8	38.4	42.2	36.3	42.2	46.6	55.4	36.7	37.1	35.5
Or	0.9	1.1	1.1	2.1	1.2	0.9	0.4	2.0	1.7	2.2
	11	12	13	14	15	16	17	18	19	20
Ab	59.6	58.5	60.4	60.8	58.0	60.7	59.4	59.4	59.9	58.9
An	33.9	39.0	37.1	36.5	38.7	36.4	37.3	38.3	36.6	37.4
Or	1.35	1.19	1.1	1.08	2.09	1.39	2.1	1.3	1.8	2.1
	21	22	23	24	25	26	27	28	29	30
Ab	58.7	63.2	53.9	58.3	47.1	56.5	59	60.0	63.8	65.3
An	37.8	33.0	42.4	39.4	51.1	38.8	37	37.0	32.7	31.8
Or	2.2	2.2	0.9	1.0	0.7	2.3	2.6	1.5	1.7	1.4



**Figure II.19: Variation in An and Or across oscillatory zoned plagioclase,
Blatná granodiorite [cf. Table II.5.]**

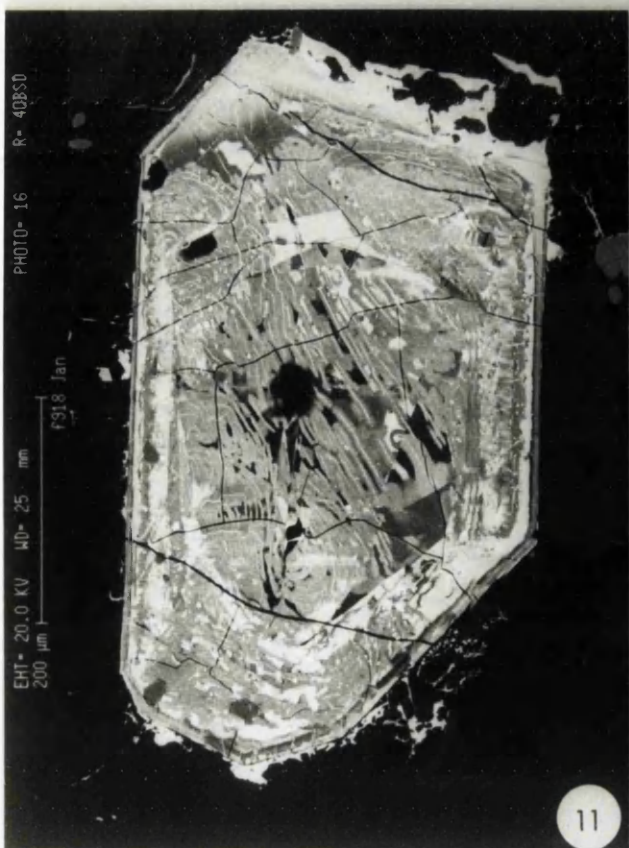
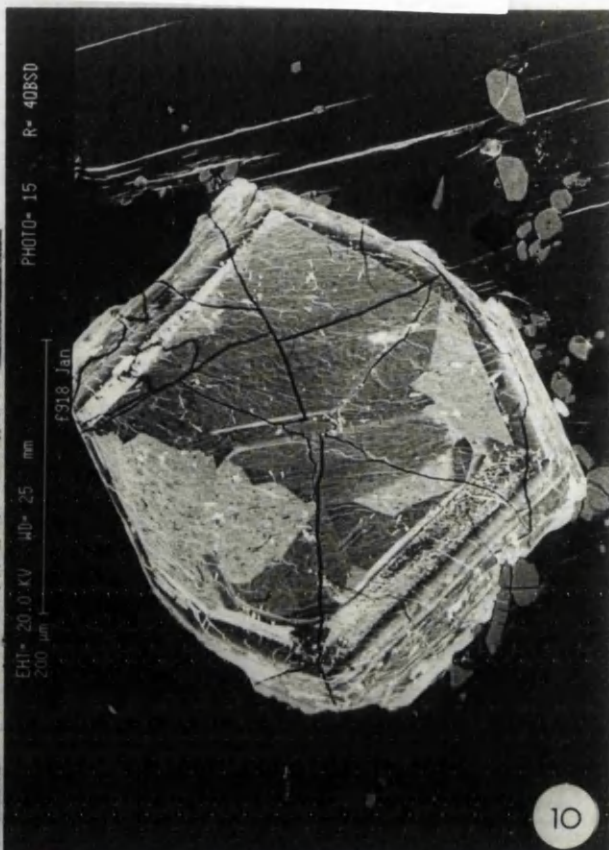
Sedlčany intrusion (1): field photographs and photomicrographs

- II.5.1. Subangular xenolith of a lime-silicate rock, with thin amphibole reaction rim; the xenolith is invaded by the host granite along the cracks;
Vápenice II, quarry
- II.5.2. Round, zoned carbonate xenolith with diffuse contacts with the surrounding granite; the marginal zone is diopside-rich, the core contains crystals of axinite (up to 0.5 cm across); the contact between the zones is sharp;
Vápenice I, bottom of the quarry
- II.5.3. Angular MME, with rare plagioclase megacrysts, broken and net-veined by the surrounding granite; note also a quartz xenolith with a thin hornblende corona (top left);
Vápenice I, quarry
- II.5.4. Subangular MME, enclosing an angular xenolith of quartz and round megacrysts of plagioclase and K-feldspar (latter about 1 cm in length), aligned roughly parallel to the elongation of the enclave;
Vápenice I, top bench of the quarry
- II.5.5. Oscillatory zoned plagioclase cores, corroded and surrounded by younger oscillatory zoned plagioclase; the matrix is composed of biotite, quartz and plagioclase;
Se-12, Kosova Hora, x 20, XPL
- II.5.6. Zoned amphibole-biotite clot, with biotite corona and mosaic of amphibole crystals in the centre;
Se-3, Vápenice I, x 50, PPL
- II.5.7. Large mantled plagioclase, surrounded by a groundmass of quartz, plagioclase, amphibole and biotite; the outer zone of the plagioclase crystal, with an obvious resorption surface, encloses abundant inclusions of acicular apatite and also biotite flakes; the apatite inclusions do not occur in the core of the plagioclase at all;
MME Sem-1, Vrchotovy Janovice, x 20, XPL
- II.5.8. Pokilitic quartz grain, enclosing three subhedral flakes of biotite (darker) and amphibole, together with abundant acicular apatite;
MME Sem-6, Vápenice I, x 50, PPL



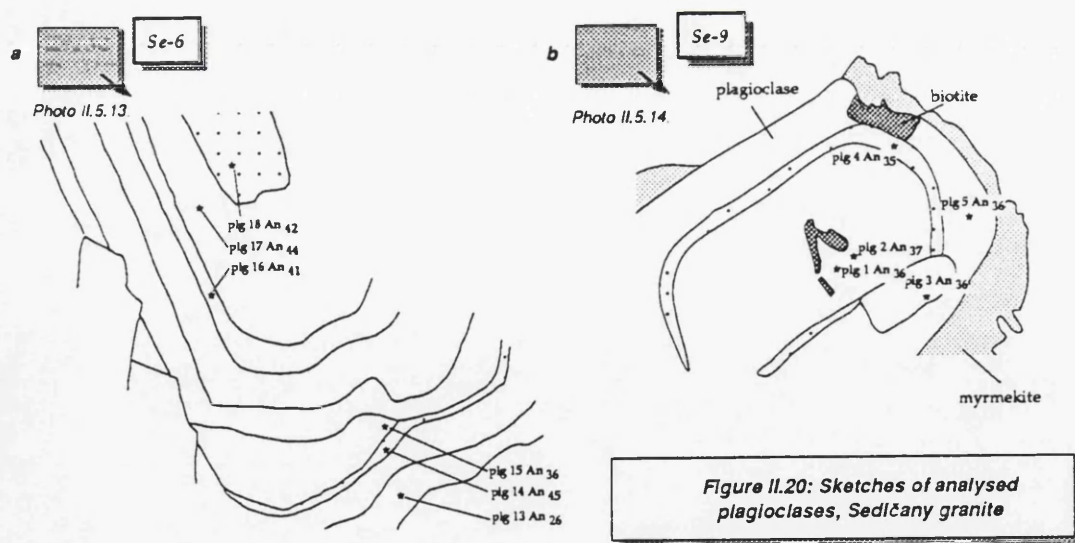
Sedlčany intrusion (2): orthite

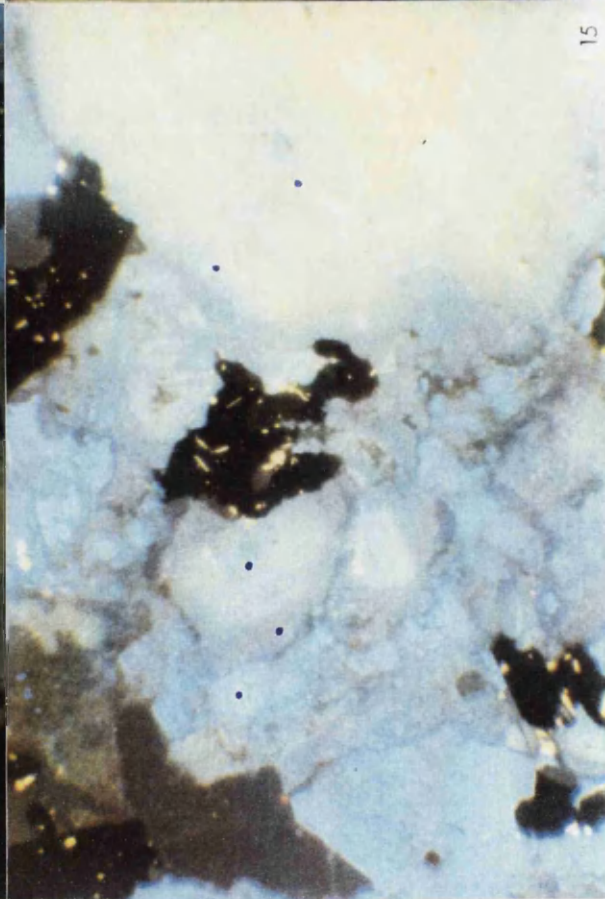
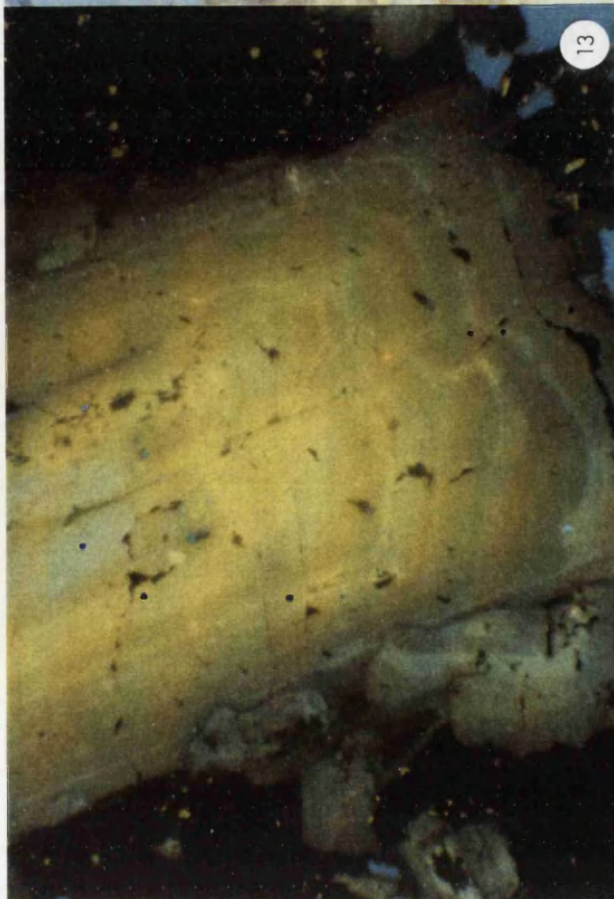
- II.5.9. Two strongly metamict (almost isotropic) euhedral orthite grains one of which is zoned; the contact with quartz is full of radial cracks; there is a pleochroic halo in the biotite flake next to the larger orthite crystal;
Se-7, Vápenice II, x 85, PPL
- II.5.10. Euhedral orthite crystal, cut parallel to the crystallographic a axis, showing sector zoning and development of radial cracks;
Se-6, Vápenice I, BSE
- II.5.11. Another grain from the same sample showing complex zoning pattern, with several resorption surfaces and abundant cracks, which originated during the metamictization, and are filled by the alteration products;
Se-6, Vápenice I, BSE
- II.5.12. Detail of the previous orthite grain;
Se-6, Vápenice I, BSE



Sedlčany intrusion (3): cathodoluminescence

- II.5.13. Large euhedral plagioclase crystal, showing yellow luminescence and fine-scale oscillatory zoning, surrounded by biotite (non-luminescent with bright yellow inclusions of apatite) and K-feldspar (blue);
Se-6, Vápenice I, x 45, CL [cf. Fig. II.20 a]
- II.5.14. Large plagioclase, with an obvious zone of brighter luminescence, enclosing several biotite flakes; the plagioclase is surrounded by blue K-feldspar and non-luminescent biotite with abundant yellow apatite inclusions; thick rims of myrmekite (of bluish-ochre luminescence) are developed at the contact between both feldspars;
Se-9, Vrchotovy Janovice, x 45, CL [cf. Fig. II.20 b]
- II.5.15. Group of yellow plagioclase grains, the largest of them with fine-scale oscillatory zoning, surrounded by light-blue interstitial K-feldspar; both feldspars are brecciated and thick reaction rims are developed at their contact (leaching? diffusion?), one of which (at the border of the large plagioclase) is myrmekitic; the non-luminescent mineral is biotite, with abundant tiny inclusions of apatite, whereas the quartz is dark brown;
Se-7, Vápenice II, x 45, CL
- II.5.16. Several euhedral plagioclase crystals, showing fine-scale oscillatory zoning, surrounded by blue K-feldspar and non-luminescent biotite with yellow apatite inclusions;
Se-6, Vápenice I, x 45, CL



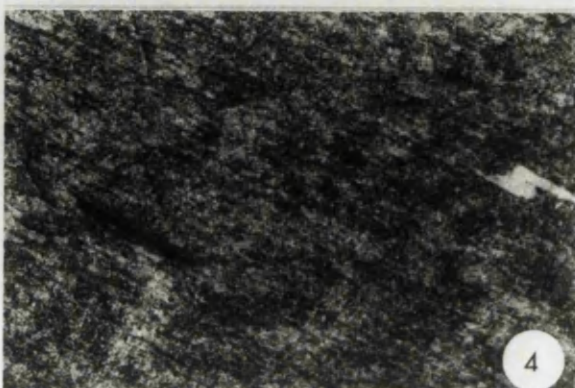
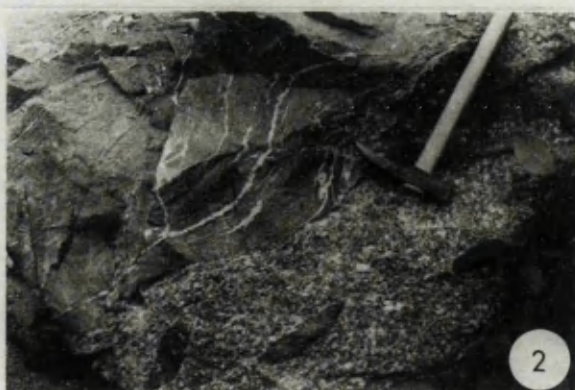
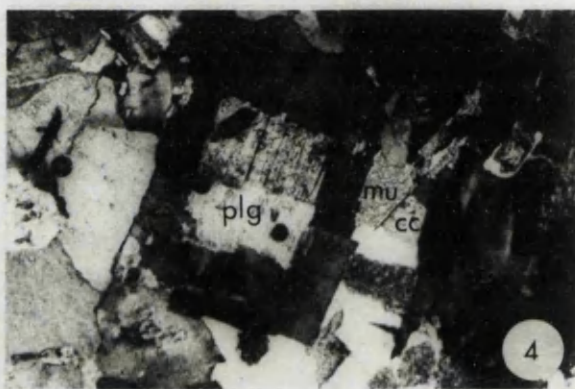
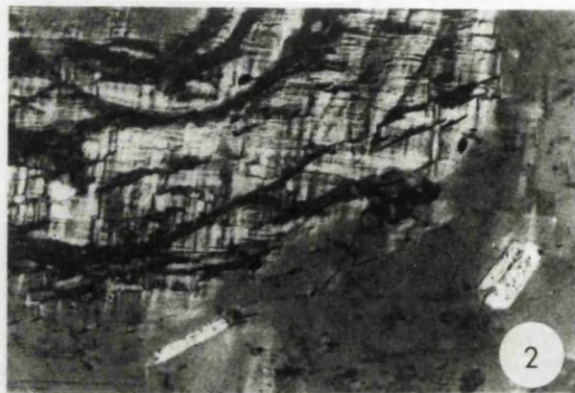
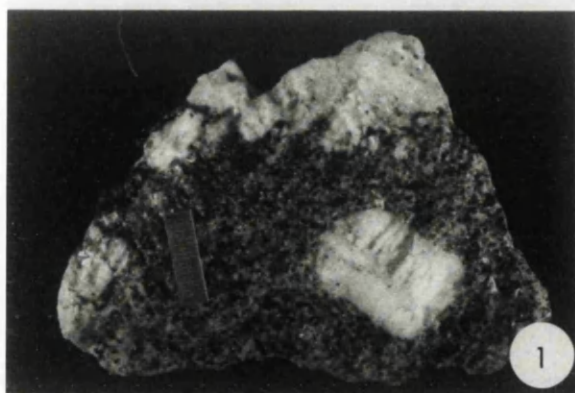


Říčany intrusion (1): field photographs and photomicrographs

- II.6.1. Round, simply-twinned K-feldspar megacryst enclosed in light MME with abundant biotite phenocrysts and quartz ocelli (there is a large quartz ocellus just below the scale); the enclave is surrounded by a fragment of the original pegmatoid rim of the MME (K-feldspar and tourmaline); scale bar = 2 cm;
Žernovka, quarry
- II.6.2. Zoned K-feldspar phenocryst, with a perthitic zone showing pronounced cross-hatched twinning; the rim encloses tiny euhedral biotite and plagioclase inclusions;
Ri-1, Žernovka, x 50, XPL
- II.6.3. Strongly resorbed biotite flake, releasing apatite inclusions, enclosed by K-feldspar phenocryst; a reaction rim of albite is developed at the contact of both minerals;
Ri-1, Žernovka, x 50, XPL
- II.6.4. Antirapakivi texture with euhedral plagioclase rimmed by simply-twinned K-feldspar; the matrix is composed of quartz and K-feldspar, with small grains of plagioclase and biotite; two euhedral muscovite flakes, associated with calcite, are also present;
Ri-7, Žernovka, x 20, XPL

Čertovo břemeno intrusion: field photographs

- II.7.1. Angular xenolith of the Čertovo břemeno melagranite enclosed by tourmaline leucogranite;
Kamenné Doly near Písek, quarry
- II.7.2. Contact between Čertovo břemeno melagranite enclosing two elongate MME and a large xenolith of Moldanubian paragneiss, which is net-veined and penetrated by the melagranite;
Votice, quarry at the railway station
- II.7.3. Tectonic contact between strongly deformed Čertovo břemeno melagranite (top-right) and adjacent Moldanubian paragneisses;
Road cut of the Tábor-Prague road, SE of Votice
- II.7.4. Strongly sheared Čertovo břemeno durbachite from immediate contact with the Moldanubian paragneisses (upper part of the Photo II.7.3.);
Road cut of the Tábor-Prague road SE, of Votice



Říčany intrusion (2): cathodoluminescence

II.6.5. Zoned K-feldspar phenocryst, with a bright blue core and a dull blue rim, cracked and rehealed by quartz; the phenocryst is surrounded by broken K-feldspars (dull blue CL), subhedral plagioclase crystals (dark bluish-yellow CL; the blue hue was exaggerated during processing); non-luminescent biotite (with yellow apatite inclusions) and dark brown quartz (also bluish due to processing); for correct CL colours, see the next pictures;

Ri-1, Žernovka, x 45, CL

II.6.6. Zoned K-feldspar phenocryst, with an obvious resorption surface marked by precipitation of a brighter-luminescent layer; small euhedral bluish-yellow crystals are plagioclase, non-luminescent mineral with yellow apatite inclusions is biotite;

Ri-1, Žernovka, x 45, CL [cf. Fig. II.21 b]

II.6.7. Detail of an oscillatory zoned K-feldspar phenocryst, enclosing abundant subhedral plagioclases of (ochre-) yellow luminescence that are overgrown by thin albite (dark-blue) rims; some of them have altered dark-brown cores;

Ri-1, Žernovka, x 45, CL [cf. Fig. II.21 a]

II.6.8. As II.6.7.

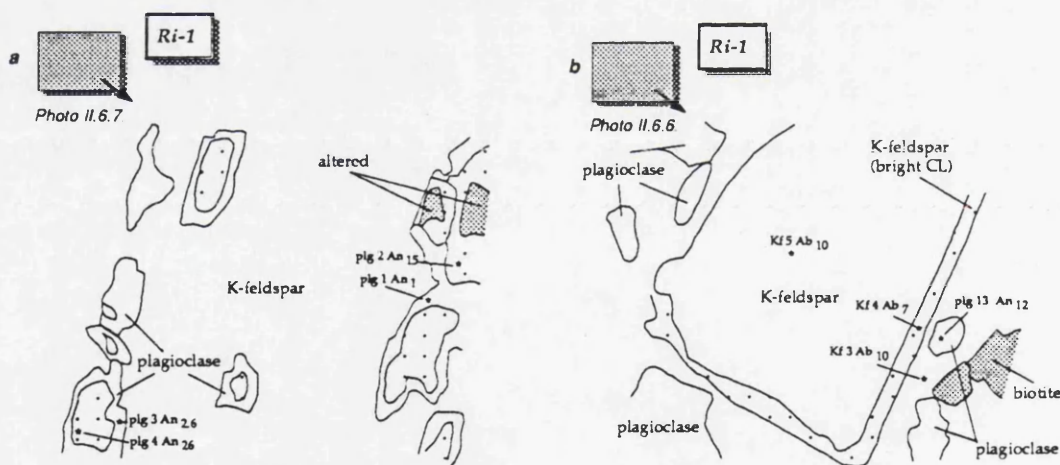
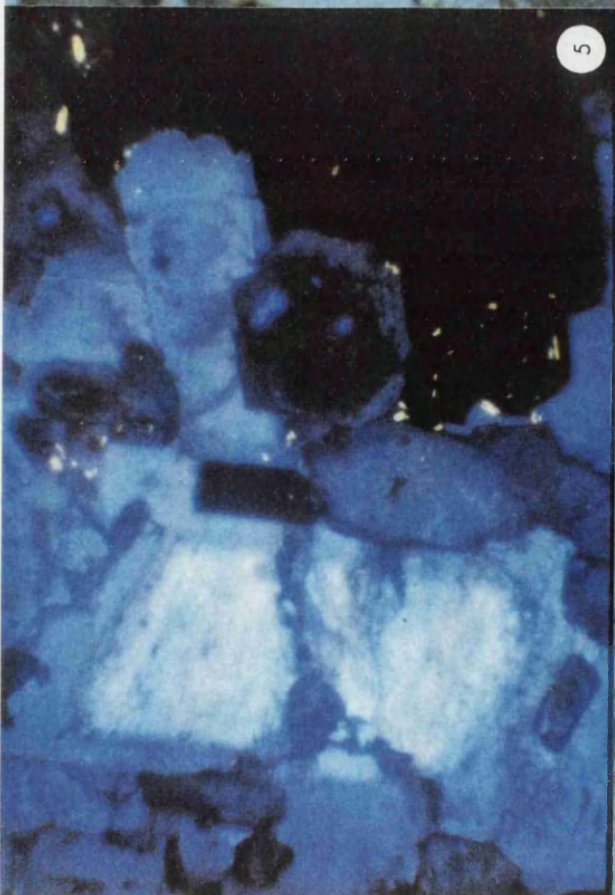
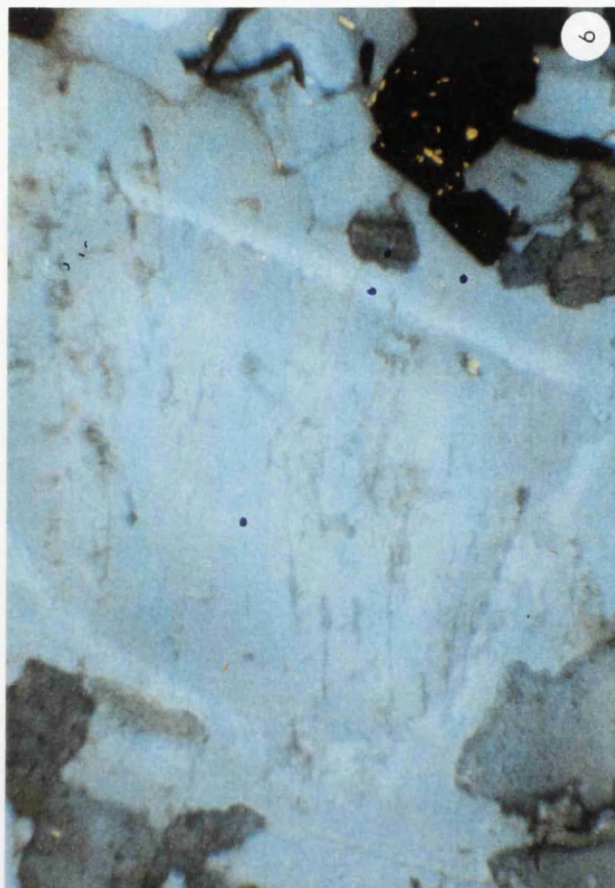


Figure II.21: Sketches of analysed feldspars, Říčany granite



III. Mineral chemistry

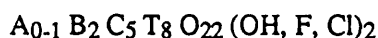
The aim of this chapter is to examine the variations in the major-element composition of the main rock-forming minerals (feldspars, biotites and amphiboles) of particular rock types in the CBP. The primary objective is to group the intrusions according to similarities in their mineral chemistry, to study the nature of the zoning of the minerals, and to assess whether the variations in mineral chemistry is an indicator of the presence of xenocrysts.

While there have been very few studies on the complete association of rock-forming minerals of a particular area or intrusion of the CBP (e.g. *Lang et al.*, 1978 for the Sázava intrusion and Teletín quartz diorite), there are many monographs concerned with particular mineral species. For instance, K-feldspar phenocrysts were studied by *Pivec* (1970); *Minařík* (1972); *Neužilová* (1973, 1978); *Minařík and Povondra* (1976); *Minařík and Pivec* (1977), whereas plagioclase was investigated by *Minařík et al.* (1978) and *Knotek and Lang* (1985) among others. Amphiboles were the subject of publications by *Poubová* (1971, 1974) and *Ulrych* (1974, 1985), biotite-hornblende pairs by *Fiala et al.* (1976) and *Minařík et al.* (1988), whereas biotite has been in focus of works by *Cimbáliková et al.* (1976, 1977).

So far, there has been a lack of coherent data covering the complete mineral paragenesis, and showing spatial variations within the studied intrusions. Because of its potential to provide invaluable petrogenetic information, new microprobe data were obtained to fill some of the gaps. Sample details are in Appendix I and the raw compositional data, together with the corresponding mineral formulae, are in Appendices VI-VIII. Recalculation of the probe analyses has been by a S language programme, *Mid as*, written by Dr. C.M.Farrow (University of Glasgow).

As the zoning patterns of the plagioclase have been discussed already [Chapter II], only a short overview is given here. The formulae of feldspars were calculated on basis of 8 oxygen equivalents.

The general formula of an amphibole may be written as (*Hawthorne*, 1985):



A = Na, K

C = Mg, Fe²⁺, Mn, Al, Fe³⁺, Ti

B = Na, Li, Ca, Mn, Fe²⁺, Mg

T = Si, Al

Several analyses of amphibole from amphibole-biotite clots were also made to assess their genesis, which is still uncertain (*Castro and Stephens*, 1992; *Bateman*, 1993b).

The amphibole formulae were calculated on basis of 23 oxygen equivalents, whereas the sum of the tetrahedral cations ($\Sigma Si + Al^{IV}$) has been assumed to be 8. As a subroutine for the estimation of the Fe³⁺/Fe²⁺ ratio of amphiboles, *Mid as* calls the FORTRAN programme *Rec amp* (*Spear and Kimball*, 1984) that utilises eight recalculation procedures as follows:

all Fe = Fe ³⁺ all Fe = Fe ²⁺ Si = 8 Si + Al = 8 $\Sigma FM = 13$ (Si + Al + Ti + Fe + Mg + Mn) $\Sigma CA = 15$ (Si + Al + Ti + Fe + Mg + Mn + Ca) $\Sigma NA = 15$ $\Sigma K = 16$	tetrahedral sites occupied only by Si, Al ^{VI} = total Al tetrahedral sites occupied only by Si and Al ^{IV} only K and Na in the A-site all Ca in the B-site all Na in the B-site no vacancies in the A-site
---	---

Midas uses, by default, the average of the lowest and highest feasible estimates (method 9 of Spear and Kimball, 1984).

Amphiboles may provide pressure constraints on the crystallization of calc-alkaline plutons. The total Al content of igneous amphiboles appears to be pressure-sensitive, forming an empirical geobarometer (Hammastrom and Zen, 1986; Hollister et al., 1987) that was later confirmed by experiments (Johnson and Rutherford, 1989; Rutter et al., 1989; Thomas and Ernst, 1990). The presence of an assemblage of quartz, K-feldspar, plagioclase, biotite, titanite, ilmenite or magnetite buffers the Al content of the coexisting amphibole (Hammastrom and Zen, 1986) and its existence is an essential prerequisite for any meaningful results. The corresponding equations of the different calibrations are:

Reference	Pressure equation	Reported error
<i>Hammastrom and Zen (1986)</i>	$P = -3.92 + 5.03 \text{ Al}$	$\pm 3 \text{ kbar}$
<i>Hollister et al. (1987)</i>	$P = -4.76 + 5.64 \text{ Al}$	$\pm 1 \text{ kbar}$
<i>Johnson and Rutherford (1989)</i>	$P = -3.46 + 4.23 \text{ Al}$	$\pm 0.5 \text{ kbar}$
<i>Thomas and Ernst (1990)</i>	$P = -6.23 + 5.34 \text{ Al}$	$\pm 1 \text{ kbar}$

On the other hand, the usefulness of the Al in amphibole geobarometer has been questioned by Blundy and Holland (1990), who found the Al^{IV} content of amphibole coexisting with plagioclase to be strongly temperature-dependent (cf. Thomas and Ernst, 1990):

$$T = \frac{0.677 P - 48.98 + Y}{-0.0429 - 0.008314 \ln K} (\pm 75 ^\circ\text{C})$$

$$K = X_{\text{Ab}}^{\text{Plag}} \frac{(\text{Si} - 4)}{(8 - \text{Si})}$$

where: T = absolute temperature

P = pressure in kbars

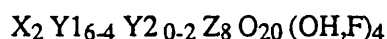
Y = plagioclase non-ideality ($Y = 0$ for $X_{\text{Ab}} > 0.5$, $Y = -8.06 + 25.5 (1 - X_{\text{Ab}})^2$ for $X_{\text{Ab}} < 0.5$)

Si = number of the silicon atoms per amphibole formula unit.

According to Blundy and Holland (1990), the geobarometers should work only at a given fixed temperature. The whole issue has recently been discussed (Blundy and Holland, 1992 a,b; Hammastrom and Zen, 1992; Poli and Schmidt, 1992; Rutherford and Johnson, 1992), but still remains controversial and is likely to remain so until more theoretical and experimental work is undertaken.

Unfortunately, there is dearth of tools providing constraints on the P - T conditions of formation of metaluminous granitoids. Thus, despite all the pitfalls, the calculations were performed on all three of the studied intrusions, which possess a suitable mineralogy, viz. Sázava, Kozárovec and Blatná. The results, however, should be viewed with caution. In the granitoid rocks, the amphibole is usually one of the earliest minerals to crystallize and thus the pressure estimates by this geobarometer will tend to be higher than the pressure at the actual emplacement level.

The theoretical formula of biotite is (Deer et al., 1992):



X = K, Na, Ca

Y₂ = Al, Fe³⁺, Ti

Y₁ = Mg, Fe²⁺, Mn

Z = Si, Al

The biotite analyses were recalculated on basis of 22 oxygen equivalents, setting the sum of tetrahedral cations ($\Sigma \text{Si} + \text{Al}^{\text{IV}}$) to 8. The algorithm of *Schumacher (1991)* has been utilised to assess the Fe^{3+} proportion, assuming a fixed $\text{Fe}^{3+}/\text{Fe}^{2+}$ ratio.

The pyroxene formulae were calculated on basis of 6 oxygen equivalents, and the Fe^{3+} proportion was estimated after *Schumacher (1991)*, assuming a constant sum of cations.

Analytical data for plagioclase, K-feldspar, biotite and amphibole are given on the following pages of the Appendix:

Intrusion	Feldspars (Appendix VI.)	Biotites (Appendix VII.)	Amphiboles (Appendix VIII.)
Sázava qtz diorite to tonalite	156 - 158	179 - 180	192 - 194
Teletín quartz diorite	158 - 159	180 - 181	194 - 197
Požáry trondhjemite	160 - 161	181 - 182	-
Kozárovice granodiorite	162 - 164	183 - 184	198 - 201
Kozárovice qtz monzonite	164 - 166	184 - 184	201 - 202
Blatná granodiorite	166 - 170	185 - 187	202 - 204
Sedlčany granodiorite	171 - 175	188 - 190	205 - 206
Říčany granite	176 - 178	191 - 191	-

III.1. Mineral chemistry of the individual intrusions

III.1.1. Sázava intrusion (including Teletín quartz diorite) [cf. Fig. II.1.]

I. Sázava quartz diorite to tonalite

As shown in the previous chapter, the composition of the Sázava plagioclase ranges from andesine to bytownite [Fig. III.1.1.]. Although the plagioclase crystals are usually unzoned (An_{45-50}), the plagioclase of the Krhanice sample (Sa-10) shows a discontinuous zoning, with andesine - labradorite cores (usually An_{40-50}) and andesine rims (An_{30-35}). The composition of the cores of mantled plagioclases from Krhanice is similar to the generally unzoned plagioclase found elsewhere in the Sázava mass (Teletín, Mráč), whereas the rim composition matches that of the unzoned plagioclase of the matrix ($\sim \text{An}_{35}$). Occasionally, more calcic cores occur ($\text{An} > 50$) which might represent relics of plagioclases of more mafic rock incorporated into the Sázava magma due to magma mixing, however limited that may have been.

The most common composition of plagioclase from the Sázava tonalite is about An_{40} , but the total range is An_{27-62} (*Minařík et al., 1978*). *Lang et al. (1978)* reported the range of plagioclase compositions from Teletín to be An_{21-45} (most commonly $\sim \text{An}_{27}$) with scarce labradorite and bytownite cores. Also *Vejnar et al. (1975)* recorded discontinuous zoning in plagioclase in MME and hybrid rocks from eastern part of the Sázava intrusion, and have attributed their presence to the operation of the hybridization processes.

Where present, the discontinuous zoning is expressed by differences in CL: the luminescence of the calcic cores is usually much brighter yellow. This fact may be linked to the presence of Mn^{2+} and

Fe^{2+} , activating greenish-yellow luminescence of plagioclase (Marshall, 1988) [Chapter II.8.5]. Although no independent microprobe data are available, the Mn^{2+} content of plagioclase is reported to increase together with An in the Sázava intrusion (Minařík et al., 1978).

K-feldspar is uniform in composition [Fig. III.1.1.], with 7 - 10 % albite component. Lang et al. (1978) recorded both higher An and Ab contents, 2.8 % and 15 % respectively, of K-feldspar from Teletín.

The biotite from the Sázava intrusion shows both high Al^{IV} and high total Fe content [Fig. III.1.2.] with Al^{IV} ranging between 2.5 - 2.7 p.f.u. and a fairly constant $100 \text{Fe}^*/(\text{Fe}^* + \text{Mg})$ ratio of ~ 55.

All the amphiboles examined are calcic amphiboles in sense of Leake (1978), because they have $(\text{Ca} + \text{Na})_{\text{B}} \geq 1.34$ and $\text{Na}_{\text{B}} < 0.67$. According to the IMA classification scheme they are mainly magnesio-hornblendes, slightly overlapping the boundary of the tschermakitic hornblende field (Mrač) [Fig. III.1.3.]. Occasionally a few of them show a somewhat higher Fe^{3+} content, corresponding to ferrian magnesio-hornblendes (Sa-10: amph 2, 3, 4 ; Sa-7: amph 10). On the basis of the older classification of Leake (1968), the majority of the Sázava amphiboles analysed by Poubová (1974) and Lang et al. (1978) were named ferro-hornblendes but in the new diagram they classify as magnesio-hornblendes. No actinolites, reported as an overgrowth on magnesio-hornblendes from the Slapy apophysis of the Sázava intrusion (Poubová and Jurek, 1976), were found. Their occurrence seems to be connected with hydrothermal alteration processes [Chapter II.1.].

Pressure estimates, based on the Al in hornblende geobarometer, are given in both Table III.1. and Figure III.1.4. Additionally, temperatures were calculated from the amphibole-plagioclase geothermometer of Blundy and Holland (1990) at pressures estimated by the above geobarometers and at an arbitrarily chosen 3 kbars. The results differ considerably for the western (Teletín, Krhanice: Sa-7, Sa-10) and eastern (Mrač: Sa-3) parts of the body and therefore they will be treated separately.

The average total Al of the amphiboles from the western part of the intrusion is 1.4 p.f.u. (without two outliers), which corresponds, according to the different calibrations, to pressures ranging from roughly 1.3 kbar (Thomas and Ernst, 1990) to 3 kbar (Hammastrom and Zen, 1986; Hollister et al., 1987); the intermediate values have been obtained after Johnson and Rutherford (1989) (2.3 kbar). Compared to the error of the geothermometer itself ($\pm 75^\circ\text{C}$), the average temperature estimates based on Blundy and Holland (1990) change little around ca. 770°C with the choice of different pressures (differences $< 30^\circ\text{C}$).

The amphiboles from the eastern part of the intrusion show significantly higher mean total Al of 1.7, corresponding to range of approximately 2.6 kbar (Thomas and Ernst, 1990) to 4.6 kbar (Hollister et al., 1987). Accordingly, the temperature estimates are higher, close to 800°C .

The spread in the data around the mean total Al (1.4 and 1.7, respectively) is considerable (equivalent to ± 1 kbar), as are the errors of the methods (± 0.5 to ± 3 kbar) and differences in the calibration equations. Despite this great uncertainty, the Sázava amphibole probably crystallized at depths of up to 10 km in the west to 17 km or somewhat less in the east.

II. Teletín quartz diorite

The common discontinuous zoning of the plagioclase from the Teletín quartz diorite points to its hybrid character, being possibly a product of magma mixing between a mafic (gabbroic) magma and the parental magma of the Sázava intrusion [Chapter II.1.]. Thus, the distribution of the An-content is strongly bimodal [Fig. III.1.1.]; the bytownite cores (An 80 - 90) are overgrown by andesine of similar composition to that of the small unzoned plagioclases of the matrix (An 40 - 50).

The compositional gap between the cores (often with patchy zoning) and the rims of the Teletín plagioclases has been mentioned by *Dudek and Fediuk (1958)* and *Lang et al. (1978)*. However, the latter authors have also recorded more sodic compositions for the rims (down to An 25) as well as more calcic cores (up to An 99), and considered the cores to be a relic of a high-temperature assemblage.

The mantling phenomena are also present in the host Sázava tonalite at the Teletín locality can be recognised, to some extent, in the host Sázava tonalite as well (see above); they are, however rare in the Sázava tonalite in Teletín (*also Lang et al., 1978*). If a major magma-mixing event took the place in the Sázava intrusion, one would anticipate, at least locally, plagioclase with reverse zoning and, or calcic spikes. As this is not the case, the most likely onset of the plagioclase crystallization in the Sázava magma, unlike in the Teletín quartz diorite, followed the magma-mixing event.

The correlation between the CL colour of studied plagioclases and their An content, caused presumably by differences in Mn^{2+} and Fe^{2+} (*Marshall, 1988*), was not verified by the microprobe study. No Mn data are available and Fe^{2+} appears to vary quite randomly, possibly because it is close to the detection limit or due to uncertainty in the $\text{Fe}^{3+}/\text{Fe}^{2+}$ estimation. Similar problems with precise determination of the minor impurities, that are crucial for the interpretation of the CL spectra, were encountered by *Marshall (1988)*.

Although no K-feldspar was found in the studied samples, an analysis of K-feldspar from the Teletín quartz diorite is given by *Lang et al. (1978)*. These data, including trace elements, are remarkably similar to those of the K-feldspar from the Sázava intrusion in the same quarry (*Lang et al., 1978*).

The compositional field for biotites from the Teletín quartz diorite largely correspond to the Sázava field [Fig III.1.2.]. The several core - rim pairs, analysed in a search for relics of the mafic end-member assemblage showed no major differences. The reason for this could be either that Fe and Mg are easily re-equilibrated in the sheet-silicates (*Vernon, 1990*) or that the biotite had not started to crystallize in the mafic end-member prior the magma-mixing event.

The composition of the calcic ($(\text{Ca} + \text{Na})_{\text{B}} \geq 1.34$ and $\text{Na}_{\text{B}} < 0.67$) amphiboles of the quartz diorite exhibits considerable variations [Fig. III.1.3.]. The small optically unzoned amphiboles are classified as magnesio-hornblendes, whereas the large ones have cores of titanian tschermakitic hornblende (amph 5), titanian tschermakite (amph 6) or ferro-tschermakitic hornblende (amph 8). The nature of the chemical zoning was studied across an optically zoned amphibole, with dark green rim and brown core [Fig. III.1.5.]. The scan revealed discontinuous zoning, with a magnesio-hornblende rim (green) and ferroan pargasite / magnesio-hastingsite core (brown). The IMA classification of the amphibole along the profile is:

Point no	IMA Classification:	Point no	IMA Classification:
1-6	magnesio-hornblende	17	titanian pargasite
7	tschermakitic hornblende	18	titanian tschermakite
8-10, 13, 16, 20	titanian ferroan pargasite	21	ferrian magnesio-hornblende
12,14	titanian magnesio-hastingsite	22-25	magnesio-hornblende

The pressure estimates based on the Al in hornblende geobarometers, presented in Tabs III.1., III.2. and on Figure III.1.4., differ dramatically for rims and cores of the zoned crystals.

The total Al content of the rims is similar to that of the amphiboles from the (western) Sázava intrusion, giving only slightly higher average pressures of 1.7 - 3.6 kbar. Accordingly, the amphibole rim - plagioclase rim pairs yield temperature of approximately 780 °C (*Blundy and Holland, 1990*), close to the value obtained for the Sázava quartz diorite - tonalite.

The amphibole cores have notably higher average total Al of about 2.3. As there is no guarantee that they have coexisted with the appropriate assemblage, the significantly higher pressure estimates of 6.1 kbar (*Thomas and Ernst, 1990*) to 8.3 kbar (*Hollister et al., 1987*) may be taken only as rough approximations. The pressure recorded by the cores may correspond to a depth of at least 20 km, possibly up to 30 km. The composition of amphibole cores, coexisting originally with calcic plagioclase (~ An₈₅; cores of mantled crystals), points to crystallization temperatures of 900 °C or higher. Such temperatures and pressures are theoretically possible, as they lie in the stability field of magmatic amphibole at $P_{H_2O} = P_{total}$ (*Gilbert et al., 1982*). In the P-T diagram compiled by *Gilbert et al. (1982)* all the amphibole-in curves for tonalitic compositions are nearly vertical and occupy the range of roughly 900 - 1000 °C over the entire pressure interval between 2 - 20 kbars.

The brown amphibole cores, with much higher Σ Al and Ti contents than the rims, evidently represent relics of a higher PT assemblage, as has been proposed by several authors (*e.g. Ulrych, 1985* and references therein) for several gabbro occurrences throughout the northern CBP. The temperature estimates for this assemblage, summarised by *Ulrych (1985)*, range between 1000 and 1200 °C. In particular, the Teletín amphiboles seem to be similar to amphiboles from the Tuzinka two-pyroxene gabbro (*Vejnar, 1972*), with matching brown magnesio-hastingsite cores and green magnesio-hornblende rims. In contrast, the brown cores of amphiboles from the Teletín 'hybrid gabbros' studied by *Lang et al. (1978)* were magnesio-hornblendes, as were their green rims, the only difference between rims and cores being higher contents of Ti, Al, and alkalis in the latter. Nevertheless, the consistently higher Ti concentration of the cores might imply that the presence of Ti, probably as Ti³⁺, could be a principal cause of the brown coloration of the amphiboles (*Ulrych et al., 1976*). The Ti content of amphiboles increases with temperature and decreasing f_{O_2} (*Gilbert et al., 1982*).

The discontinuous zoning of amphibole is consistent with the evidence for magma mixing in the origin of the from Teletín quartz diorite presented in Chapter II.1. The brown ferroan pargasite and magnesio-hastingsite cores, formed under higher P-T conditions, might have crystallized in the mafic (gabbroic?) magma at greater depth, prior the mixing. Consequently, after the magma-mixing event, they were overgrown by the green magnesio-hornblende, similar in character to the magnesio-hornblende common in the Sázava intrusion.

III.1.2. Požáry intrusion [cf. Fig. II.1.]

Distribution of the plagioclase composition of this intrusion is strongly bimodal [Chapter II.2., Fig. III.1.1.]. Mantled plagioclases have cores of andesine-labradorite (~ An₅₅ to An₆₅) overgrown by andesine rims (~ An₃₀ - 40). The An-content of unzoned matrix plagioclases matches that of the rims of the zoned crystals. There is generally a good agreement between the composition of

mantled plagioclases of the Požáry intrusion (Po-1, Po-3) and that of the Sázava mass from Krhanice (Sa-10). The rims of the latter match the composition of mantles of the Požáry plagioclases, whereas they are much less calcic than any other plagioclase anywhere else in the Sázava intrusion. However, no bytownite cores like those found in plagioclase from Sa-10 have been recorded from the Požáry intrusion.

K-feldspar shows little variation in composition, and contains about 8 - 10 % albite component.

The composition of biotite from the typical Požáry sample (i.e. sample from the type locality not showing cumulate textures; Chapter II.2.) (Po-3) differs strongly from that of the sample from Krhanice (Po-1). The former is the most iron-rich among the studied samples [Fig. III.1.2.] with $Fe^*/(Fe^*+Mg)$ fairly constant at about 70, and Al^{IV} ranging between 2.7 - 2.8 p.f.u. The latter plots close to the biotite from the Sázava intrusion, having $Fe^*/(Fe^*+Mg) \sim 60$ and Al^{IV} of 2.5 - 2.6 p.f.u. The similarity in mineral chemistry of biotite and plagioclase imply a possible genetic link between the Krhanice samples of the Požáry trondhjemite and the Sázava tonalite, rather than an affinity with the trondhjemite of the main part of the Požáry intrusion.

Of three analysed carbonates [cf. Photo II.1.17.], two are from the Sázava (Krhanice) and one from the Požáry type (Prosečnice). All of them are calcites (94.9 - 96.5 % calcite), with minor amount of rhodochrosite (1.6 - 2.4 %) and siderite (1.1 - 1.6 %) and variable proportions of the magnesite component (0.4 - 1.2 %), being the lowest in the Požáry sample.

III.1.3. Kozárovice intrusion (including Kozárovice quartz monzonite [cf. Fig. II.2])

I. Kozárovice granodiorite

The composition of plagioclase from the Kozárovice granodiorite is characterised by several maxima: (a) $\sim An_{30}$, corresponding to mantles of discontinuously-zoned crystals, (b) An_{37-47} , for optically unzoned plagioclases as well as cores of discontinuously-zoned ones, and (c) An_{50-55} , for cores of optically unzoned crystals [Fig. III.1.6.].

K-feldspar contains ca. 4 - 16 % of the albite component. The total Ab component (on mineral separates) of the Těchnice K-feldspar phenocrysts ranges between 17 and 26 %, the non-unmixed Ab component (XRD) up to 20 % and the Ba content varies between 0.42 - 1.12 % (Neužilová, 1973). This author also recorded an increase in triclinicity of the K-feldspar phenocrysts towards the SE, inferring that there had been a higher thermal gradient at the southeastern margin of the Těchnice granodiorite. This could have been caused by a younger intrusion, possibly suggesting a small age difference between the older Těchnice and younger Čertovo břemeno intrusions.

The biotite composition is uniform, with roughly equal proportions of Fe and Mg [Fig. III.1.7.]. The Al^{IV} content is more variable, ranging between 2.4 to 2.7 p.f.u. The biotite from Kozárovice II (Koz-4) has a somewhat lower Al^{IV} content.

All the amphiboles examined are calcic amphiboles in sense of Leake (1978), having $(Ca + Na)_B \geq 1.34$ and $Na_B < 0.67$. In the IMA classification diagram [Fig. III.1.8.], the amphiboles from

the Kozárovec granodiorite plot in the magnesio-hornblende field; however, the amphiboles from rims of the amphibole - biotite clots straddle the boundary with the actinolitic hornblende domain, whereas the amphiboles from the cores of the clots correspond to actinolite. These clots have $Si > 7.50$ which exceeds the limit for primary igneous crystallization suggested by *Leake (1971)*. Moreover, such a zoning appears to be in contrast to the normal trend of igneous amphiboles which increase their Si content sympathetically with that of the host magma (*Castro and Stephens, 1992*). Therefore the actinolite is interpreted as being secondary, most likely replacing clinopyroxene [cf. Chapter II.3.], possibly as a consequence of re-equilibration following a magma mixing event (*Castro and Stephens, 1992*).

Excluding the amphibole from the biotite-amphibole clots, the Al in hornblende geobarometers [Tab. III.3.; Fig III.1.9.] yield average pressures of 1.9 kbar (*Johnson and Rutherford, 1989*) to 2.4 kbar (*Hammastrom and Zen, 1986; Hollister et al., 1987*); sample Koz-6 possibly crystallized at slightly higher pressures. The estimates based on *Thomas and Ernst (1990)* appear to be too low, sometimes even negative, and never exceed 1.5 kbar. Nevertheless, the pressure of only 1.9 - 2.4 kbar according to the other calibrations implies a shallow intrusion, with amphibole crystallizing at a depth of ca. 7 - 9 km. The temperature estimates, based on *Blundy and Holland (1990)* are on average ca. 730 °C, being again slightly higher for sample Koz-6 (~ 750 - 760 °C), and decreasing for more actinolitic compositions (to 680 °C).

The relict pyroxene from the core of an amphibole from Koz-6 is $Di_{78.7} Hd_{9.3} En_{7.2}$.

II. Kozárovec quartz monzonite

The plagioclase of the Kozárovec quartz monzonite ranges from oligoclase to labradorite, commonly with discontinuous zoning [Chapter II.3., Fig. III.1.6.]. Unzoned lath-shaped crystals have uniform andesine composition (~ An 30 - 40), whereas the zoned ones contain labradorite cores (~ An 50 - 60). The cores of large rectangular plagioclases correspond to andesine (An 37 - 47), and are overgrown by labradorite spikes (An 60 - 70) and oligoclase-andesine rims (~ An 30 - 40). This provides, together with other phenomena, a clear evidence of hybrid origin of the quartz monzonite and of operation of magma mixing in the Kozárovec body [Chapter II.3.].

K-feldspar has 8.8 - 28.3 % Ab.

Biotite from the quartz monzonite shows both lower $100 Fe^*/(Fe^*+Mg)$ of 45 and lower Al^{IV} (2.3 - 2.6 p.f.u.) than the biotite of its granodiorite host [Fig. III.1.7.].

Amphiboles of the quartz monzonite cross the boundary between magnesio-hornblende and actinolitic hornblende (*Leake, 1978*) [Fig III.1.8.], and hence these are, like the amphiboles of the amphibole - biotite clots, shifted towards higher Si values compared with their host; they also have slightly higher $Mg/(Mg+Fe^{2+})$. The amphibole composition varies only a little, with the crystals lacking both chemical and optical zoning.

However, the total Al content of the amphiboles from the quartz monzonite (and amphibole - biotite clots) would correspond to a pressure of 1 kbar or less [Fig III.1.9.], but there is no evidence for the coexistence of the appropriate assemblage required for the application of the Al in hornblende geobarometers so the pressure assessed in this way cannot be valid. Moreover, as shown by the overview of experimental data by *Gilbert et al. (1982)*, amphibole is not stable in granodiorite magma at

pressures much lower than 1 kbar (at $P_{H_2O} = P_{total}$). Hence, it is possible that the amphiboles have suffered later recrystallization, causing a shift in composition towards the actinolitic hornblende. Many of them might be of secondary origin, being pseudomorphs after an older pyroxene reacting with melt after a magma-mixing event (*Castro and Stephens, 1992*) [Chapter II.3.].

III.1.4. Blatná intrusion [cf. Fig. II.3.]

Plagioclases from the Blatná granodiorite are mainly andesine (~ An 30 - 40), with a few outliers corresponding to oligoclase [Chapter II.4., Fig. III.1.10.] but at Hudčice (Bl-8) the cores are somewhat more calcic (up to An 49), the rims are andesine (~ An 30 - An 40) and there are infrequent calcic spikes in between (up to An 55). Such an abrupt change in the An content of the crystallizing plagioclase could possibly point to hybridization between the granodiorite and a syn-plutonic dyke(s) of the granodiorite porphyry [Photo II.4.5.-II.4.6.]. Other evidence for the presence of the hybrid types in this quarry is given in Chapter II.4.

The K-feldspar contains 7 - 17 % Ab. No systematic variation was found either between the composition of cores and rims of the K-feldspar phenocrysts or among K-feldspars from different localities.

In terms of their $Fe^*/(Fe^* + Mg)$ ratio of 0.45 - 0.52 [Fig. III.1.11.], the Blatná biotites are remarkably uniform. Their Al^{IV} content is slightly more variable, ranging from 2.4 to 2.7 p.f.u.

The Blatná amphiboles are magnesio-hornblendes [Fig. III.1.12.] (*Leake, 1978*) with the exception of a few cores that are edenitic hornblendes (Bl-5: amph-1, 6, 7). Cores of individual crystals tend to have higher $(Na + K)_A$ than the corresponding rims. Two distinct groups of amphiboles could be distinguished in terms of their total Al content [Fig III.1.13.]: (1) edenitic hornblende cores from Vahlovice (Bl-5) with average $\Sigma Al \sim 1.5$, and (2) the rest of the analysed amphiboles with $\Sigma Al \sim 1.25$. The following are the pressure estimates for these groups [Tab. III.4.]:

(1) The edenitic hornblende cores record the highest pressure of 1.7 kbar (*Thomas and Ernst, 1990*) to 3.6 kbar (*Hammastrom and Zen, 1986; Hollister et al., 1987*).

(2) The rest of amphiboles yield average pressures of 1.7 kbar (*Johnson and Rutherford, 1989*) to 2.3 kbar (*Hammastrom and Zen, 1986; Hollister et al., 1987*). The estimates based on *Thomas and Ernst (1990)* appear to be too low, never exceeding 0.9 kbar.

Nevertheless, the pressure of 1.7 - 2.3 kbar recorded by the main group implies a shallow intrusion (with hornblende crystallization at a depth of about 6 - 8 km), whereas the edenitic hornblende cores have possibly crystallized at a somewhat higher pressure (at a depth of up to 13 km), and might represent an earlier crystallization history of the Blatná magma, or, alternatively, xenocrysts resulting from hybridization with a foreign magma. Such an event may have been just of local importance for the NE part of the intrusion (Vahlovice). The temperature estimates, based on *Blundy and Holland (1990)*, are relatively low, on average about 720 - 730 °C, and decrease with increasing Si content to about 700 °C; they are slightly higher (~ 760 - 780 °C) for the edenitic hornblendes.

III.1.5. Sedlčany intrusion [cf. Fig. II.4.]

Plagioclase from the Sedlčany granite is uniform in composition, ranging between oligoclase and andesine [Chapter II.5., Fig. III.1.14.]. The cores of oscillatory zoned and optically unzoned crystals correspond to andesine (~ An 35 - 40), whereas the rims of the zoned ones are oligoclase (~

An 25 - 30). Also the late plagioclase, filling the fractures in older plagioclases (Se-9), is of oligoclase composition (An 19 and An 28). Slightly more calcic plagioclases are present as cores and spikes in the sample Se-6 (An 40 - 45). Plagioclases enclosed by the K-feldspar are rimmed by exsolved albite (An 1.7). Generally speaking, the composition of the Sedlčany plagioclase (apart from sample Se-6) does not vary greatly and does not point to major disturbances during the crystallization.

The K-feldspar commonly contains 8 - 15 % (up to 29 %) albite; often, the centres of the K-feldspar crystals are more Ab-rich. The Ba content was reported to be 0.23 to 0.64 % (Neužilová, 1978). The triclinicity of the Sedlčany K-feldspar is low but increases towards the contact with the Čertovo břemeno intrusion; in fact, both intrusions show a common zoning pattern, with triclinicity decreasing and K increasing from the core (of the Čertovo břemeno mass) towards the margins, especially the Votice apophysis and Sedlčany granite [Fig. I.3.-I.4.] (Neužilová, 1978). Such a pattern is in accord with a slower cooling of the core of the 'Sedlčany - Čertovo břemeno' body, implying a negligible age difference between emplacement of the two, as further supported by similarity in $2V_x$ angles of K-feldspars from Sedlčany granite and the adjacent Čertovo břemeno durbachite (of the Votice apophysis) (Neužilová, *loc.cit.*).

The $Fe^*/(Fe^*+Mg)$ ratio of biotites from the Sedlčany intrusion [Fig. III.1.15.] is uniform, varying little from 0.35, whereas the Al^{IV} ranges between 2.2 and 2.6 p.f.u. The interlayer site occupancy ($\sum X = 1.89 - 1.97$ p.f.u.) of the Sedlčany biotite is slightly higher than for the Sázava, Požáry, Kozárovce and Blatná intrusions.

The Sedlčany amphiboles are actinolitic hornblende and actinolite [Fig. III.1.16.] (Leake, 1978). The actinolite field is occupied by amphiboles from the biotite - amphibole clots (Se-6 and Se-7; Si about 7.8) and the rims some of the amphiboles of the sample Se-9 (Si ~ 7.4). Such a composition falls outside of limits of primary magmatic amphiboles of Leake (1978) and suggests a late, subsolidus crystallization. This is also the reason, apart from the absence of the required mineral assemblage, why the Al in hornblende geobarometry could not be applied to the Sedlčany amphiboles. The significance of the presence of secondary amphiboles in the Sedlčany intrusion is assessed later [Chapter III.2.3.].

III.1.6. Říčany intrusion [cf. Fig. II.5.]

Plagioclase from the Říčany granite is of uniform oligoclase composition (An 15 - 20) [Fig. III.1.17.], usually without zoning. Small plagioclases enclosed by K-feldspar phenocrysts are also oligoclase (An 12 - 26) and are overgrown by rims of albite (An 1 - 3).

K-feldspar varies only a little in its Na content (Ab 9 - 11). However, the bright blue (CL) resorbed zone on Figure II.6.6. shows slightly lower Ab 7.

The $Fe^*/(Fe^*+Mg)$ ratio of biotite from the Říčany intrusion [Fig. III.1.18.] is uniform, ranging between 0.35 - 0.4, whereas Al^{IV} is more variable (2.2 to 2.5 p.f.u.). As in the Sedlčany intrusion, the interlayer site occupancy is slightly higher ($\sum X = 1.85 - 1.93$ p.f.u.), whereas the sum of the octahedral cations ($\sum Y = 5.53 - 5.59$ p.f.u.) is both more restricted and lower than for the rest of the CBP.

III.2. Comparison of the mineral chemistry of the particular minerals

III.2.1. Plagioclase

In summary, there appears to be a trend of decreasing Ca content of plagioclase with time in the CBP. Several groups can be distinguished based on plagioclase composition as follows.

(1) *Sázava and Požáry intrusions:*

The typical Sázava plagioclase is unzoned and of andesine composition, while the plagioclase of the tonalite sample from Krhanice shows discontinuous zoning (cores of andesine sometimes with labradorite, and rims of sodic andesine). There is a pattern also followed by the Požáry trondhjemite, with frequent mantled plagioclases (cores of andesine - labradorite and rims of andesine). The composition of unzoned plagioclases from Požáry match the rims of the mantled ones. The presence of mantled plagioclase in both Sázava and Požáry intrusions in the environs of Krhanice is compatible with operation of magma mixing processes. Plagioclase of the Teletín quartz diorite is commonly discontinuously zoned, with cores of bytownite - anorthite and andesine - labradorite rims, the latter corresponding to the unzoned plagioclase of the matrix. The presence of resorbed bytownite - anorthite cores overgrown by andesine - labradorite rims points to a hybrid character of the Teletín quartz diorite [Chapter II.1.].

(2) *Kozárovice and Blatná intrusions:*

Both intrusions contain mainly normally zoned andesines, less frequently with labradorite cores or spikes (Blatná from Hudčice) that may point to some interaction with basic magma(s). The plagioclase from the Kozárovice quartz diorite contains two generations of plagioclase, (1) small lath-shaped crystals of andesine, sometimes with labradorite cores, and (2) large rectangular plagioclases, with andesine cores, overgrown by labradorite spikes and andesine rims. This is a disequilibrium texture that strongly suggests a magma-mixing origin of the quartz monzonite [Chapter II.3.].

(3) *Sedlčany intrusion:*

The most common plagioclase corresponds to andesine. In several cases, oligoclase rims and fracture infillings were observed. Plagioclases enclosed by K-feldspar phenocrysts are usually overgrown by a thin rim of exsolved albite that probably has originated in the subsolidus stage. Overall, the homogeneity of the plagioclase composition does not seem to point to major disturbances during their crystallization [Chapter II.5.].

(4) *Říčany intrusion:*

The plagioclase of this intrusion is the most sodic among the intrusions investigated, being mainly of oligoclase composition. As in the previous case, the plagioclase within the K-feldspar phenocrysts is rimmed by exsolved albite [Chapter II.6.].

III.2.2. Biotite

Biotite compositions from the individual intrusions of the Central Bohemian Pluton are compared in Figures III.2.1. and III.2.2. The first of the plots is a synthesis of the classification diagrams ($100 \text{ Fe}^*/(\text{Fe}^* + \text{Mg})$ versus Al^{IV}) that were presented earlier, as well as the fields for biotite from the Tábor and Čertovo břemeno intrusions based on Fiala *et al.* (1976) and Minařík *et al.* (1988).

The composition of the biotites follows a single trend, joining the siderophyllite and phlogopite apices as the total Fe content decreases (and Mg increases) together with Al^{IV} from Požáry trondhjemite, followed by the Sázava, Kozárovice, Blatná, Říčany, Sedlčany and Čertovo břemeno intrusions to the Tábor syenite. This trend has been explained by *Fiala et al. (1976)* either as the result of a coupled substitution of $\text{Mg} + \text{Si} \rightleftharpoons \text{Fe}^{2+} + \text{Al}^{\text{IV}}$, or of the conditions of crystallization according to the experiments of *Rutherford (1973)* because biotite tends to be more aluminous with increasing temperature and oxygen fugacity. Likewise, the iron oxidation ratio ($\text{Fe}^{3+}/\text{Fe}^{2+}$) of biotites in the CBP decreases and Mg increases as the intrusions become younger, indicating an overall drop in oxygen fugacity of the magmas with time (*Fiala et al., 1976; cf. Wones and Eugster, 1965*).

In addition to the Požáry biotite being the most Fe-rich, and the Čertovo břemeno (and Tábor) biotite the most Fe-poor, the Ti - Mg - Fe plot [Fig. III.2.2 a] reveals little difference in the Ti content of the biotite. In the Al^{VI} - Mg - Fe diagram Fig. III.2.2 b], the analyses of the Požáry biotites follow a concave-down trend, starting next to the Sázava field (at lower Fe and higher Al^{VI}) with analyses from the Krhanice quarry and ending at analyses from the typical Požáry trondhjemite at high Fe and low Al^{VI} . The biotites from the Sázava intrusion, including the Teletín quartz diorite, form a single linear trend. Analyses of Kozárovice and Blatná biotites, together with the Kozárovice quartz monzonite, cluster at about $\text{Mg} / \text{Fe} = 0.5$ and low Al^{VI} . Říčany biotites have slightly higher Fe as well as Al^{VI} than those from Sedlčany granite.

Using cluster analysis, *Fiala et al. (1976)* found that biotites from the Čertovo břemeno, Sedlčany and Tábor intrusions form a single group, isolated from the others. In general terms the other biotites show only little variation in their biotite composition and, in particular, there is no major difference in the chemistry of Blatná (s.s.) and Červená biotites on the one hand, nor Kozárovice (s.s.) and Těchnice ones on the other.

III.2.3. Amphibole

A summary of the IMA classification (*Leake, 1978*) for the calcic amphiboles detailed above together with the field of amphiboles from the Čertovo břemeno intrusion (*Minařík et al., 1988*), is given on Figure III.2.3. Many intrusions contain magnesio-hornblendes of similar composition (Sázava, Kozárovice, Blatná, rims of amphiboles from the Teletín quartz diorite), rarely crossing the boundary with tschermakitic hornblende (Sázava) or edenitic hornblende (cores of Blatná amphiboles from Vahlovice). In contrast, amphiboles from the Kozárovice quartz monzonite straddle the boundary with actinolitic hornblende, and both the Sedlčany and Čertovo břemeno amphiboles, as well as amphiboles of the amphibole - biotite clots from the Kozárovice intrusion, occupy exclusively the actinolite and actinolitic hornblende fields. The overall tendency is for an increase in Si coupled with increase in the $\text{Mg}/(\text{Mg}+\text{Fe}^{2+})$ towards presumably younger intrusions. Uniquely, the cores of amphiboles from the Teletín quartz diorite include tschermakitic hornblende, tschermakite and, in the innermost part, pargasite, ferroan pargasite and magnesio-hastingsite.

The Si and Mg-rich nature of the amphiboles from the (mela-) granites and syenites of the eastern part of the CBP (Sedlčany and Čertovo břemeno intrusions) has also been noted by *Poubová (1971, 1974)* and *Minařík et al. (1988)*.

In the diagram after *Giret et al. (1980)* [Fig. III.2.4.] the amphiboles form a single trend, characterised by a decrease in $\text{Al}^{\text{IV}} + \text{Ca}$ and an increase in $\text{Si} + \text{Na} + \text{K}$ towards the younger intrusions. In accord with Figure III.2.3., the majority of amphiboles are hornblendes, whereas both the Čertovo břemeno and Sedlčany amphiboles plot close to the actinolite field. According to *Giret et al.*

(1980), the amphiboles with low $\text{Ca} + \text{Al}^{\text{IV}}$ and high Si, Na and K are late, sometimes crystallizing even in the subsolidus (*cf. Minařík et al., 1988*).

Thus, it is more likely that the amphiboles of the Čertovo břemeno and Sedlčany intrusions (of similar composition to the amphiboles of the Kozárovce and Blatná clots) are non-magmatic (subsolidus) in origin, probably replacing older Fe - Mg phases, as shown by some of the Čertovo břemeno amphiboles which preserve relict clinopyroxene cores (*Minařík et al., 1988*). As stressed by *Minařík et al. (loc.cit.)*, the Si-rich (7.29 to 7.84 p.f.u.) Čertovo břemeno amphiboles plot outside of limits of primary magmatic amphiboles of *Leake (1978)*. This, together with other indices, such as disequilibrium Al^{IV} distribution between biotite and amphibole, points to a post-magmatic recrystallization of primary clinopyroxene and, or possibly earlier amphibole, producing actinolites and actinolitic hornblendes.

A progressive decrease in the content of alkalis coupled with an increase in Si is revealed by a plot of Si versus $(\text{Na} + \text{K})_{\text{A}}$ [Fig. III.2.5.]. The Sázava amphiboles are mainly hornblendes, whereas the amphiboles from the Teletín quartz diorite form two separate clusters, one at the boundary of the pargasite and tschermakite fields (cores of the crystals), and second in the hornblende field (rims). The other amphiboles form a single linear trend, starting with the Blatná and Kozárovce amphiboles at the edenite - hornblende boundary, followed by those of the Kozárovce quartz monzonite, to the tremolite field occupied by most of the Sedlčany amphiboles and those of the amphibole - biotite clots (of the Kozárovce and Blatná masses). The linearity and negative slope of this trend could be attributed to the $\square_{\text{A}} + \text{Si} \rightleftharpoons (\text{Na}, \text{K})_{\text{A}} + \text{Al}^{\text{IV}}$ exchange (Ed and Pg substitutions).

Pressure estimates, based on the Al in hornblende geobarometry (*Hammastrom and Zen, 1986; Hollister et al., 1987; Johnson and Rutherford, 1989; Thomas and Ernst, 1990*) are summarised on Figure III.2.6. The highest average pressure (6 - 8 kbar; range of different calibrations) has been recorded by the brown cores of the amphiboles from the Teletín quartz diorite, whereas their green rims show significantly lower ΣAl and accordingly lower pressures of 1.7 - 3.6 kbar. The ΣAl of the Sázava intrusion corresponds to a wide range of 1.5 - 4.5 kbar overlapping (at lower pressures) the fields of the Kozárovce and Blatná intrusions. Both Blatná and Kozárovce amphiboles yield a nearly identical average pressure (~ 1.7 - 2.4 kbar), which is in accord with their similar geological position of (similar age, petrography and whole-rock geochemistry) [Chapters II, IV.], although the edenitic hornblende cores from a few Blatná amphiboles record possibly slightly higher pressures (up to 2.6 kbar). Amphiboles of the Kozárovce quartz monzonite, together with those from the amphibole - biotite clots, show the lowest total Al content and failed to yield any reasonable pressure estimates, apparently due to a later re-equilibration.

The temperature estimates based on the geothermometer of *Blundy and Holland (1990)* are the highest for the cores of the amphiboles from the Teletín quartz diorite (~ 900 °C), followed by their rims and amphiboles of the Sázava intrusion (~ 770 - 800 °C), edenitic hornblende cores of the Blatná (760 - 780 °C) and Kozárovce granodiorites (~ 730 - 740 °C), and the rest of the Blatná amphiboles (~ 720 - 730 °C).

Poubová (1974) subdivided the intrusions of the Central Bohemian Pluton into three major groups, according to their amphibole composition:

Group A (actinolite-bearing):	Čertovo břemeno, Sedlčany
Group B (transitional):	Kozárovce (s.s.), Blatná (+ Červená), Klatovy

Group C (hornblende-bearing): Sázava, associated gabbros, Marginal, Těchnice.

Although there are no new microprobe data available for amphiboles from the Červená, Klatovy, Marginal and Těchnice types, there does not seem to be any significant difference between the analysed amphiboles of the proposed groups B and C, especially not in their Si and Mg content [Fig. III.2.3.]. Likewise, *Poubová (1974)* found no contrast between the trace element composition of B and C group amphiboles. Considering the analysis of the Těchnice (group C) amphibole given in *Poubová (1974)*, ($\text{Si} = 6.991$, $\text{Mg}/(\text{Mg}+\text{Fe}^{2+}) = 0.619$, $\text{Al}^{\text{T}} = 1.119$) there does not seem to be a principal difference from analysis of the Kozárovce (s.s.) (group B) amphiboles [Chapter III.1.3.]. On the other hand, the Kozárovce and Blatná amphiboles tend to have somewhat higher $(\text{Na} + \text{K})_{\text{A}}$ than those with the same Si from the Sázava mass [Fig. III.2.5.]. *Poubová (1974)* considered that group B amphiboles were typically zoned, with magnesio-hornblende cores and actinolitic rims. However, apart from in the amphibole-biotite clots and in the hybrid rocks, no actinolites or actinolitic hornblendes were found in either the Kozárovce or the Blatná intrusions. A few of the Blatná amphiboles are zoned, with cores of edenitic hornblende.

In summary, apart from the amphiboles of the hybrid rocks and of the clots, the studied intrusions can be divided into two (rather than three) major groups, based on the geochemistry of their amphiboles: (1) granitoids with magnesio-hornblendes (Sázava, Kozárovce, Blatná) and (2) granitoids with actinolites and actinolitic hornblendes (Sedlčany, Čertovo břemeno). The distribution of data in the Si versus $(\text{Na} + \text{K})_{\text{A}}$ plot [Fig. III.2.5.] suggests that the first group might consist of two subgroups, 1a (Sázava) and 1b (Blatná and Kozárovce), although the amphibole chemistry of the two appears to be generally similar. Nevertheless, the striking differences between the amphiboles of the two major groups may suggest a polygenic origin for the Central Bohemian Pluton.

III.3. Implications of the mineral chemistry

In summary, the studied intrusions divide into two major groups containing:

- a) Magnesio-hornblende and Fe-rich biotite (Sázava, Kozárovce, Blatná)
- b) Actinolite and actinolitic hornblende (higher in Si, Mg, lower in $(\text{Na} + \text{K})_{\text{A}}$) and, or Mg-rich biotite (Sedlčany, Čertovo břemeno, Říčany).

The increase in the Mg content of biotites is coupled with decrease in Fe and Al^{IV} . The amphiboles of the Teletín quartz diorite have zoned brown cores of ferroan pargasite, magnesio-hastingsite and tschermakite overgrown by green magnesio-hornblende rims. The actinolites and actinolitic hornblendes of the Sedlčany and Čertovo břemeno intrusions, as well as amphiboles from the amphibole - biotite clots (Blatná and Kozárovce) do not represent igneous amphiboles, and may have originated under subsolidus conditions (or due to re-equilibration following a magma mixing event), possibly by replacement of pyroxene.

The pressures recorded by amphiboles for most of the studied intrusions (western Sázava, Blatná, Kozárovce) are similar, being 1.5 - 3 kbar for the western Sázava and 1.7 - 2.4 kbar (Blatná and Kozárovce), corresponding to depth of about 5 - 10 km. In contrast, the pressure estimates for eastern Sázava are higher, ranging between 2.5 - 4.5 kbar (9 - 16 km). The amphibole - plagioclase geothermometer yields higher temperatures for the Sázava intrusion ($\sim 770^\circ\text{C}$ - 800°C) than for the Kozárovce and Blatná masses ($\sim 720^\circ\text{C}$ - 740°C). The brown cores of the Teletín quartz diorite are

possibly relics of a high P-T assemblage ($P = 6 - 8$ kbar; $T \sim 900$ °C), corresponding to a depth of crystallization of 20 - 30 km; their rims record similar conditions to those which are shown by the Sázava tonalite. Such a zoning pattern may be consistent with magma mixing processes.

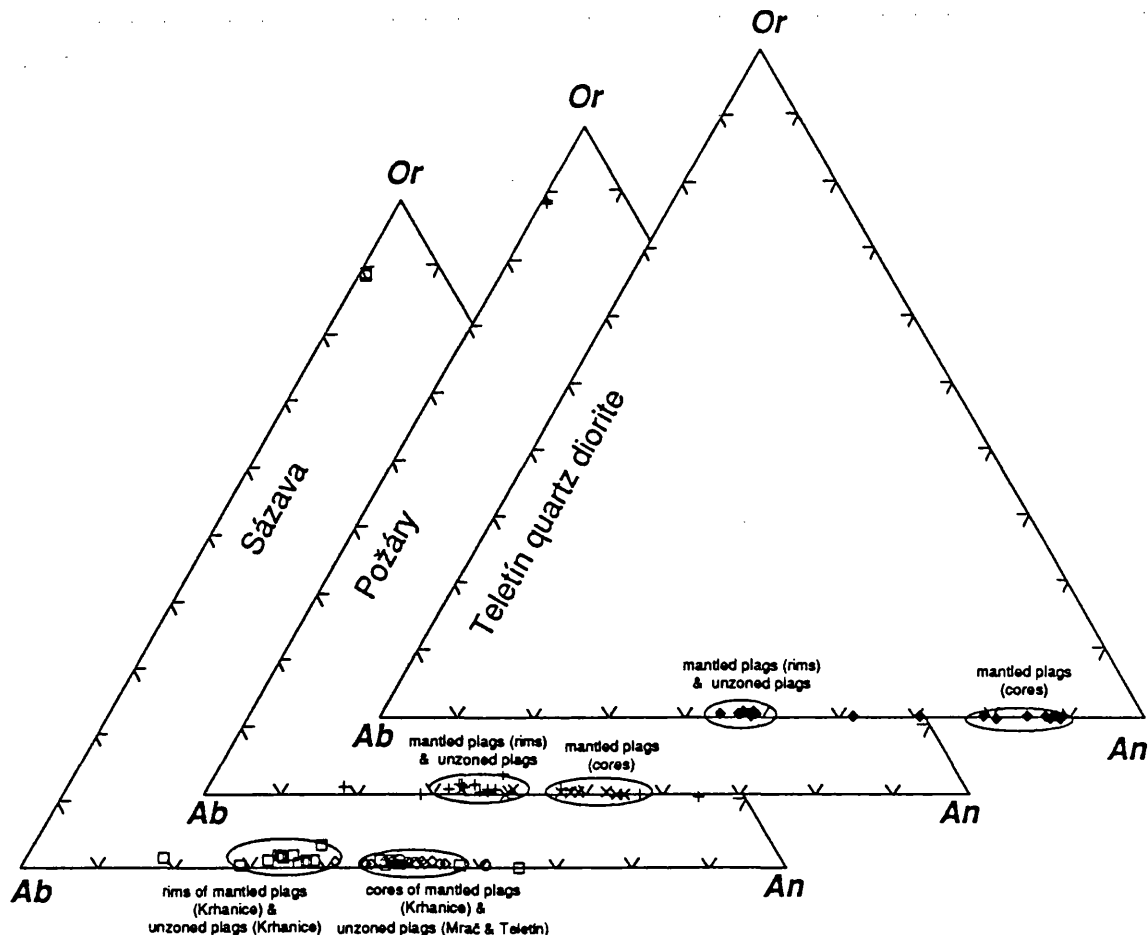


Figure III.1.1: Composition of feldspars from the Sázava (quartz diorite to tonalite), Požáry (trondhjemite) and Teletín (quartz diorite) masses in the Or - Ab - An ternary

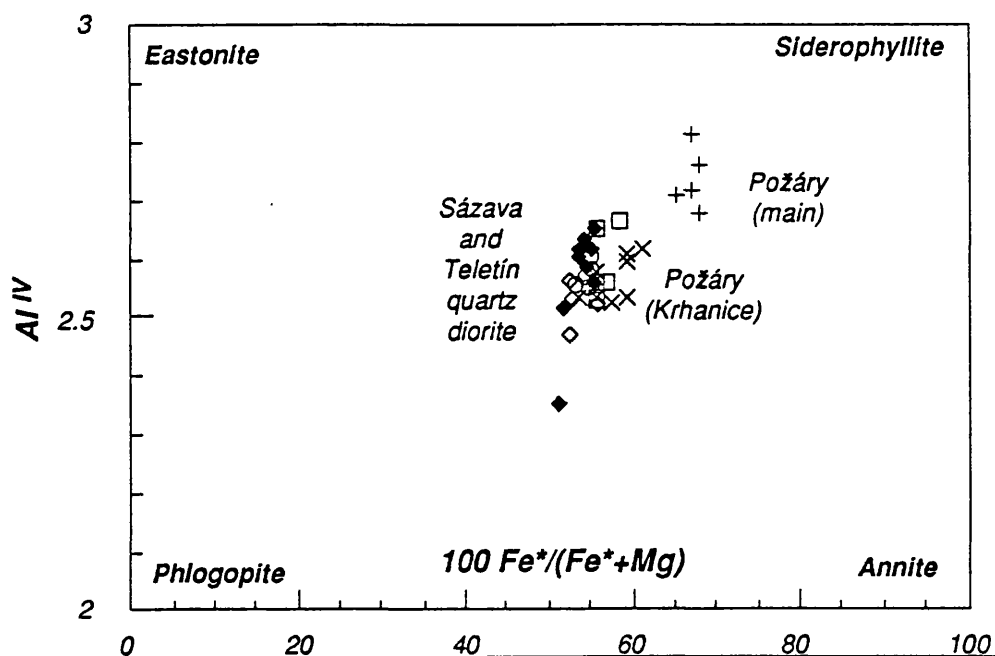


Figure III.1.2: Classification of Sázava and Požáry biotites in the $100 \text{ Fe}^*/(\text{Fe}^* + \text{Mg})$ versus Al^{IV} diagram

Sázava qtz diorite to tonalite	Teletín quartz diorite
◇ Sa-3 (Mrač)	◆ SaD-1 (Teletín)
○ Sa-7 (Teletín)	Požáry trondhjemite
□ Sa-10 (Krhanice)	× Po-1 (Krhanice)
	+ Po-3 (Prosečnice)

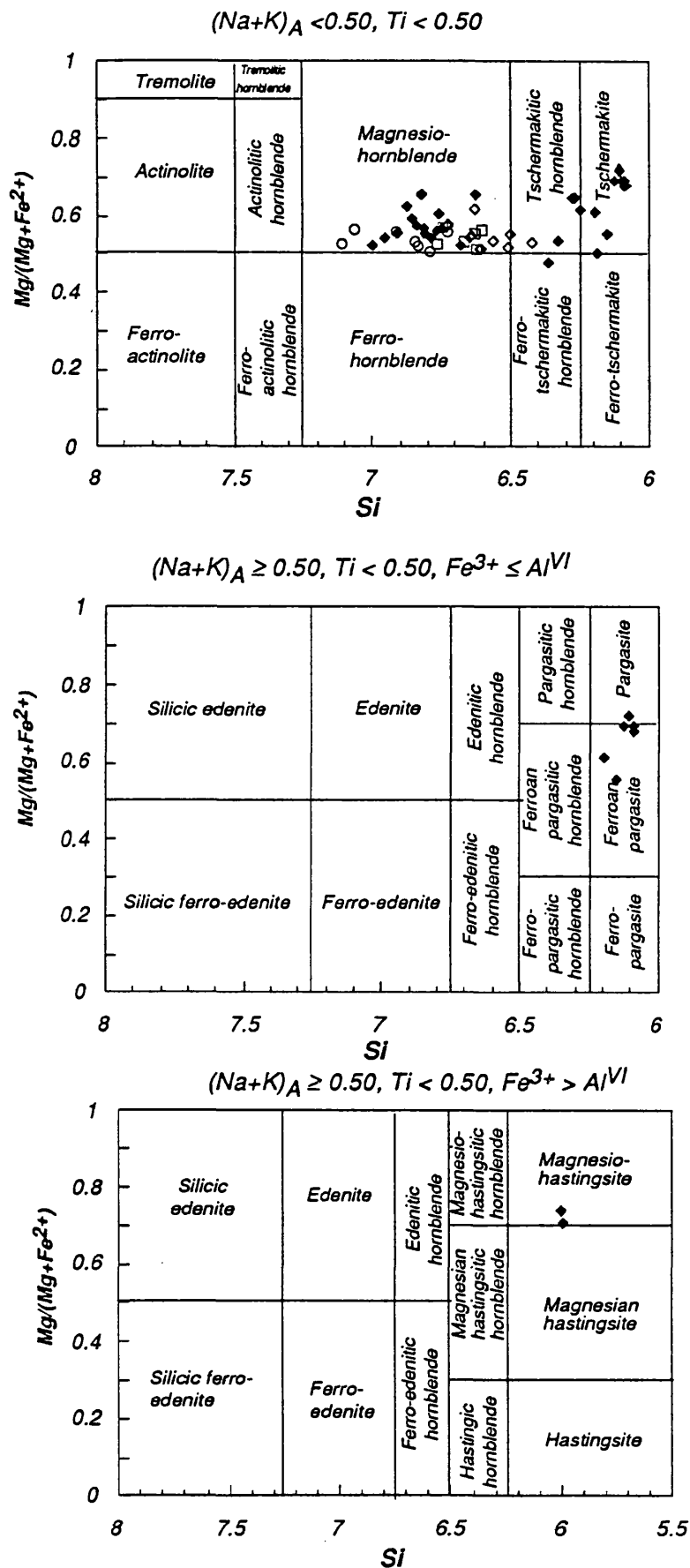


Figure III.1.3: Position in the IMA classification of amphiboles from the Sázava intrusion (including the Teletín quartz diorite) (Leake, 1978)

◇ Sa-3 ○ Sa-7 □ Sa-10 ◆ SaD-1

Table III.1: Geothermobarometry for the Sázava intrusion (including the Teletín quartz diorite) - (lower P-T assemblage)

- Aluminium in hornblende geobarometry (*Hammastrom and Zen, 1986 (H+Z); Hollister et al., 1987 (H+a); Johnson and Rutherford, 1989 (J+R); Thomas and Ernst, 1990 (T+E)*)
- Plagioclase-hornblende geothermometry (*Blundy and Holland, 1990*) was applied at the pressures determined by the previous methods and at 3 kbars.

† excluding calibration error of the methods (± 75 °C for the thermometer)

	amph		pressure (kbar)				plag		temperature (°C)				
	Si	Σ Al	H+Z	H+a	J+R	T+E	X _{Ab}	K	T _{H+Z}	T _{H+a}	T _{J+R}	T _{T+E}	T _{3.0}
Sa-3 (Mraň)													
amph 1	6.726	1.48	3.5	3.6	2.8	1.7	0.55	1.1768	779.7	778.8	790.8	808.1	787.8
amph 2	6.722	1.44	3.3	3.4	2.6	1.5	0.55	1.1714	783.7	783.1	794.3	812.3	788.7
amph 3	6.505	1.78	5.0	5.3	4.1	3.3	0.55	0.9216	806.0	802.0	821.5	834.2	838.8
amph 4	6.604	1.77	5.0	5.2	4.0	3.2	0.55	1.0259	784.8	781.1	799.8	812.5	815.8
amph 5	6.422	1.82	5.2	5.5	4.2	3.5	0.55	0.8442	822.1	817.7	838.3	850.6	858.4
amph 6	6.637	1.65	4.4	4.6	3.5	2.6	0.55	1.0641	786.6	784.0	800.0	814.7	808.2
amph 7	6.559	1.69	4.6	4.8	3.7	2.8	0.55	0.9767	801.3	798.3	815.4	829.6	826.3
amph 8	6.624	1.59	4.1	4.2	3.2	2.2	0.55	1.0488	794.7	792.7	807.3	823.1	811.2
amph 9	6.648	1.63	4.3	4.4	3.4	2.4	0.55	1.0772	786.2	783.8	799.2	814.3	805.7
amph 10	6.610	1.73	4.8	5.0	3.8	3.0	0.55	1.0327	786.8	783.5	801.3	814.6	814.4
Average			4.4	4.6	3.5	2.6			793.2	790.5	806.8	821.4	815.5
1 σ †			0.6	0.7	0.5	0.7			13.1	12.3	14.4	13.2	21.5
Sa-10 (Křhanice)													
amph 1*	6.623	1.56	3.9	4.0	3.1	2.1	0.65	1.2382	763.8	762.1	775.7	791.4	777.7
amph 4*	6.764	1.34	2.8	2.8	2.2	0.9	0.65	1.4536	749.7	750.0	758.7	777.6	747.3
amph 1	6.664	1.46	3.4	3.5	2.7	1.6	0.65	1.2961	762.5	761.7	773.1	790.4	768.9
amph 2	6.632	1.43	3.3	3.3	2.6	1.4	0.65	1.2506	771.6	771.2	782.0	799.9	775.8
amph 3	6.603	1.48	3.5	3.6	2.8	1.7	0.65	1.2111	774.4	773.5	785.4	802.6	782.1
amph 4	6.744	1.32	2.7	2.7	2.1	0.8	0.65	1.4201	755.7	756.2	764.5	783.8	751.6
Sa-7 (Teletín)													
amph 5	6.909	1.31	2.7	2.7	2.1	0.8	0.5	1.3332	768.1	768.7	776.9	796.5	763.5
amph 7	7.105	1.14	1.8	1.7	1.3	-0.2	0.5	1.7346	732.8	734.9	739.2	760.7	715.7
amph 10	6.729	1.46	3.4	3.5	2.7	1.6	0.5	1.0736	799.9	799.2	810.9	828.9	806.4
amph 11	6.791	1.49	3.6	3.7	2.9	1.7	0.5	1.1543	782.6	781.5	793.8	810.9	791.6
amph 12	6.843	1.33	2.7	2.7	2.1	0.8	0.5	1.2286	783.1	783.6	792.2	811.9	779.2
amph 13	7.058	1.08	1.5	1.3	1.1	-0.5	0.5	1.6231	749.0	751.6	754.8	777.5	727.3
amph 15	6.827	1.44	3.3	3.4	2.6	1.4	0.5	1.2050	778.3	777.7	788.8	806.7	783.1
Average			3.0	3.0	2.3	-			767.0	767.1	776.6	795.3	766.9
1 σ †			0.7	0.8	0.6	-			17.7	16.9	19.0	17.9	25.6
SaD-1 (rims) (Teletín quartz diorite)													
amph 1	6.997	1.38	3.0	3.0	2.4	1.1	0.5	1.4940	742.0	742.0	751.4	769.6	742.2
amph 2	6.676	1.60	4.1	4.3	3.3	2.3	0.5	1.0106	801.1	798.9	814.0	829.6	819.0
amph 3	6.813	1.42	3.2	3.2	2.5	1.3	0.5	1.1849	783.4	783.0	793.6	812.0	786.4
amph 4	6.779	1.56	3.9	4.0	3.1	2.1	0.5	1.1380	780.3	778.6	792.4	808.4	794.5
amph 7	6.95	1.28	2.5	2.4	1.9	0.6	0.5	1.4048	761.0	761.9	769.3	789.4	753.6
scan 1	6.807	1.44	3.3	3.3	2.6	1.4	0.5	1.1769	783.1	782.6	793.6	811.6	787.7
scan 2	6.811	1.45	3.4	3.4	2.7	1.5	0.5	1.1818	781.4	780.7	792.0	809.8	786.9
scan 3	6.747	1.48	3.5	3.6	2.8	1.7	0.5	1.0960	793.7	792.7	805.0	822.4	802.1
scan 4	6.904	1.53	3.8	3.9	3.0	1.9	0.5	1.3253	753.2	751.9	764.6	780.7	764.6
scan 5	6.869	1.43	3.3	3.3	2.6	1.4	0.5	1.2690	769.1	768.6	779.3	797.2	772.9
scan 6	6.837	1.44	3.3	3.4	2.6	1.5	0.5	1.2195	775.7	775.1	786.2	804.0	780.7
scan 21	6.621	1.59	4.1	4.2	3.3	2.3	0.5	0.9506	814.5	812.4	827.5	843.5	832.1
scan 22	6.815	1.54	3.8	3.9	3.1	2.0	0.5	1.1872	773.1	771.5	784.9	801.1	786.0
scan 23	6.854	1.43	3.3	3.3	2.6	1.4	0.5	1.2447	772.6	772.2	783.0	800.9	776.7
scan 24	6.757	1.52	3.7	3.8	3.0	1.9	0.5	1.1085	788.9	787.5	800.5	817.3	799.8
scan 25	6.765	1.54	3.8	3.9	3.0	2.0	0.5	1.1198	785.3	783.8	797.2	813.6	797.7
Average			3.5	3.6	2.8	1.7			778.7	777.7	789.7	806.9	786.4
1 σ †			0.4	0.5	0.4	0.5			17.7	17.2	18.6	18.0	22.5

Table III.2: Geothermobarometry for the Teletín quartz diorite
(higher PT-assemblage)

(for explanation see Table III.1.)

	amph		pressure (kbar)				plag		temperature (°C)				
	Si	Σ Al	H+Z	H+a	J+R	T+E	X _{Ab}	K	T _{H+Z}	T _{H+a}	T _{J+R}	T _{T+E}	T _{8.0}
SaD-1 (cores)													
amph 5	6.266	2.23	7.5	8.0	6.1	5.9	0.15	0.1960	870.0	857.5	901.2	907.1	858.0
amph 6	6.185	2.30	7.7	8.2	6.3	6.1	0.15	0.1806	893.0	879.7	925.6	930.7	884.9
scan 7	6.326	2.04	6.3	6.7	5.2	4.7	0.15	0.2083	876.5	867.4	903.1	914.6	838.8
scan 8	6.149	2.35	7.9	8.5	6.5	6.3	0.15	0.1741	899.9	885.7	933.7	937.6	897.2
scan 9	6.190	2.49	8.6	9.3	7.1	7.1	0.15	0.1815	868.9	853.0	905.1	905.2	883.1
scan 10	6.081	2.39	8.1	8.7	6.7	6.5	0.15	0.1627	918.2	903.1	953.6	956.3	921.0
scan 12	5.995	2.30	7.7	8.2	6.3	6.1	0.15	0.1493	960.8	946.7	995.4	1000.7	952.6
scan 13	6.087	2.41	8.2	8.8	6.7	6.7	0.15	0.1637	913.6	898.2	949.3	951.6	918.9
scan 14	5.993	2.41	8.2	8.8	6.7	6.7	0.15	0.1490	947.9	932.1	984.6	987.0	953.2
scan 16	6.091	2.47	8.5	9.2	7.0	7.0	0.15	0.1643	905.4	889.2	942.2	942.9	917.5
scan 17	6.105	2.38	8.0	8.7	6.6	6.5	0.15	0.1665	911.7	896.9	946.6	949.7	912.7
scan 18	6.243	2.22	7.3	7.8	5.9	5.6	0.15	0.1915	882.5	870.5	913.1	920.1	865.4
scan 20	6.123	2.42	8.2	8.9	6.8	6.7	0.15	0.1696	900.9	885.7	936.3	938.5	906.4
amph 8	6.355	2.00	6.1	6.5	5.0	4.4	0.15	0.2147	871.6	863.1	897.2	909.6	829.5
Average			7.7	8.3	6.3	6.1			901.5	887.8	934.8	939.4	895.7
1σ			0.7	0.8	0.6	0.8			28.0	26.9	30.3	28.8	38.1

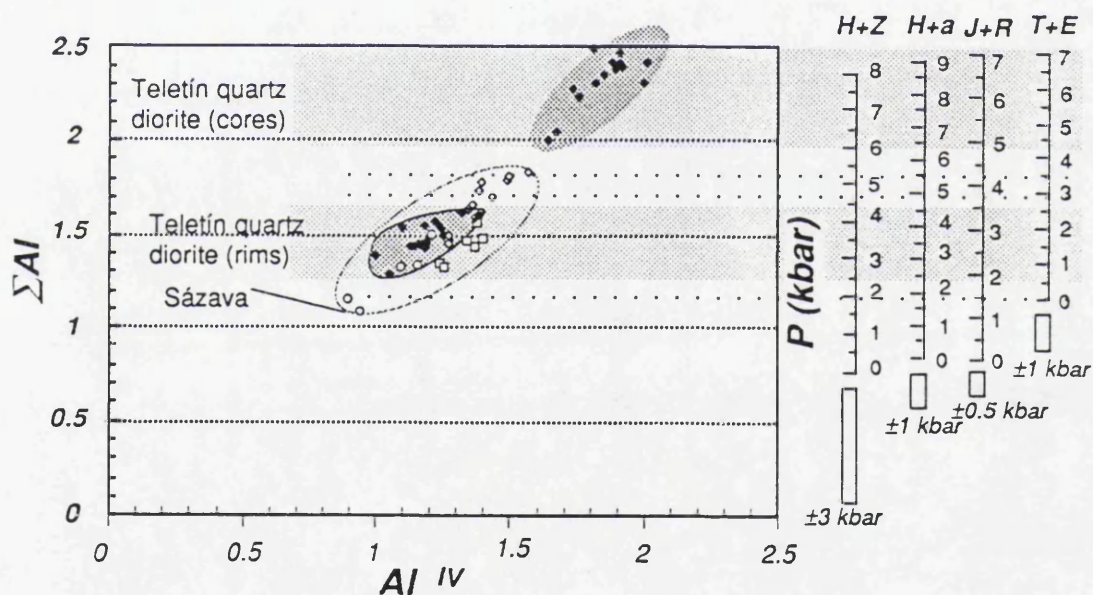


Figure III.1.4: Al^{IV} versus Σ Al plot of amphiboles, Sázava intrusion

Sázava qtz diorite to tonalite	Teletín quartz diorite
◇ Sa-3 (Mrač)	◆ SaD-1 (Teletín)
○ Sa-7 (Teletín)	
□ Sa-10 (Krhanice)	

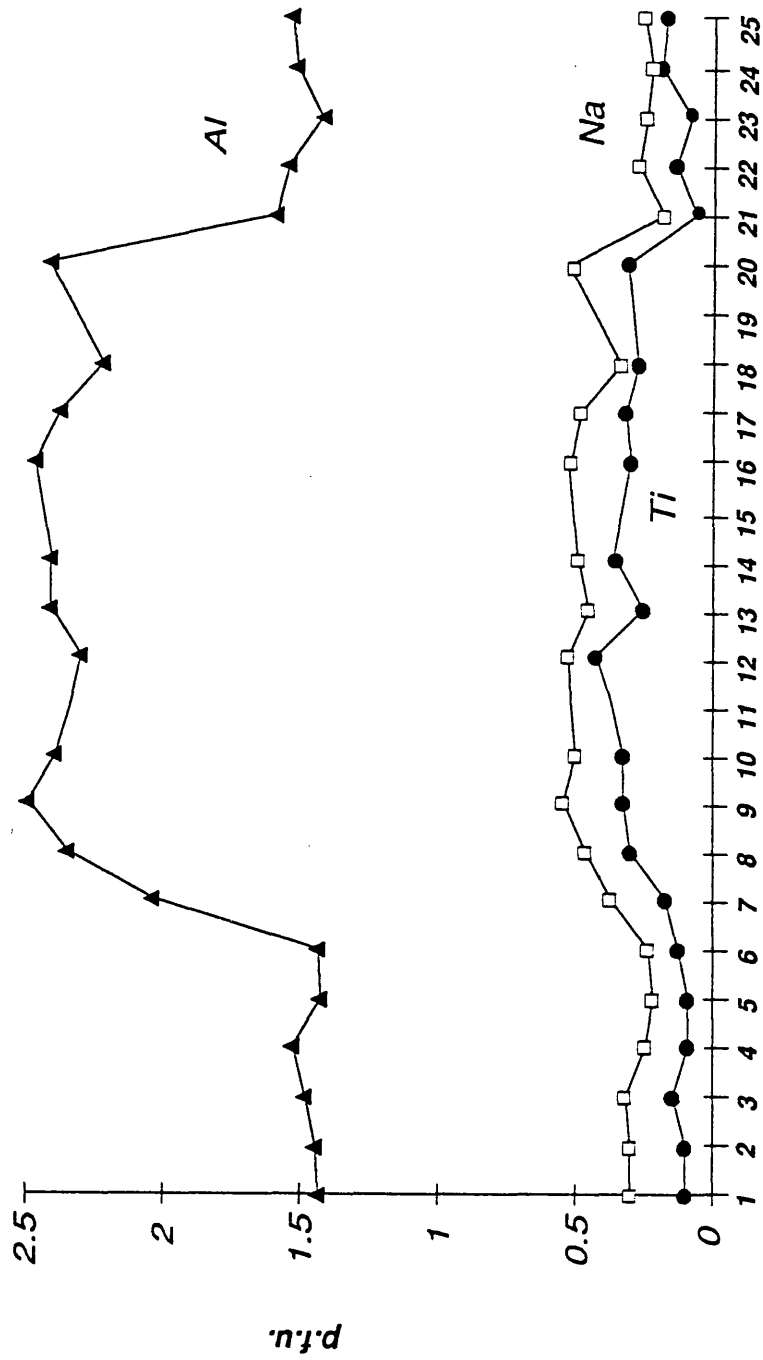


Figure III.1.5: Scan across a zoned amphibole, Teletín quartz diorite (SaD-1)

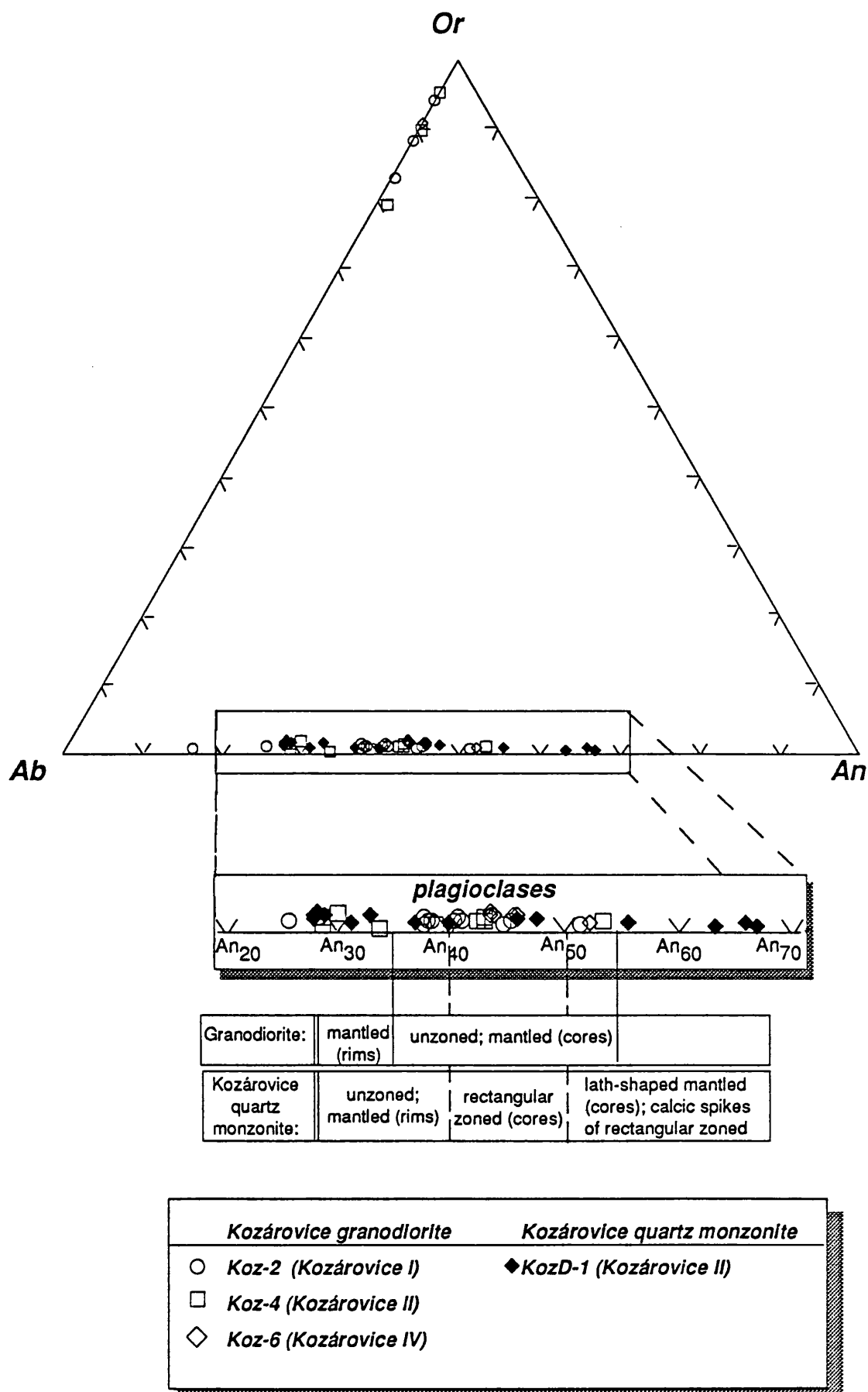


Figure III.1.6: Composition of the Kozárovec feldspars in the Or-Ab-An ternary diagram

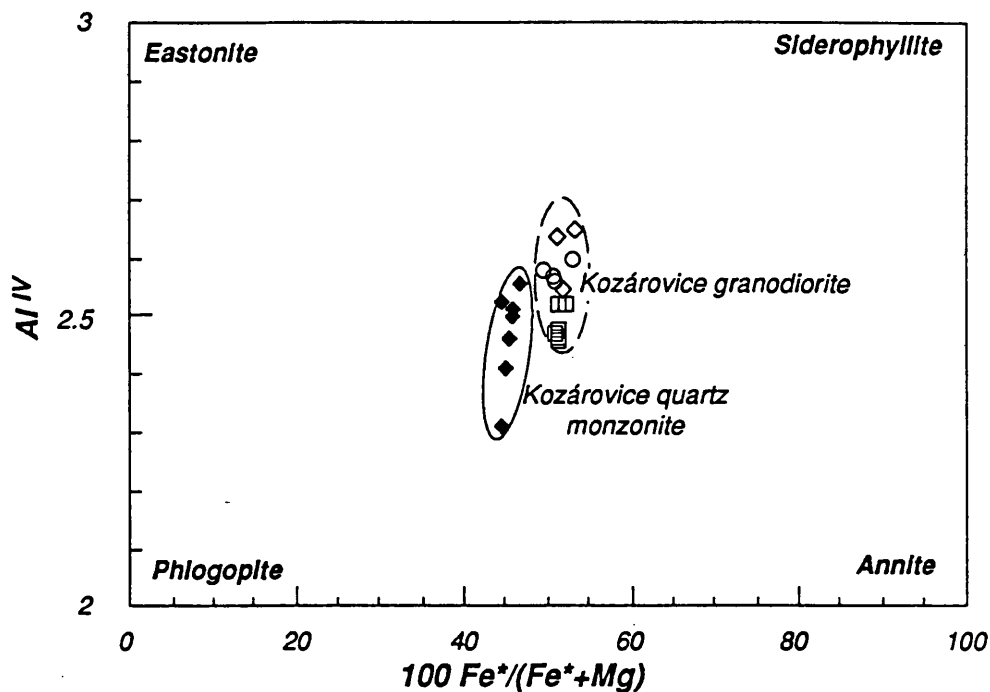


Figure III.1.7: Classification of the Kozárove biotites in the 100 Fe⁺/(Fe⁺ + Mg) versus Al^{IV} diagram

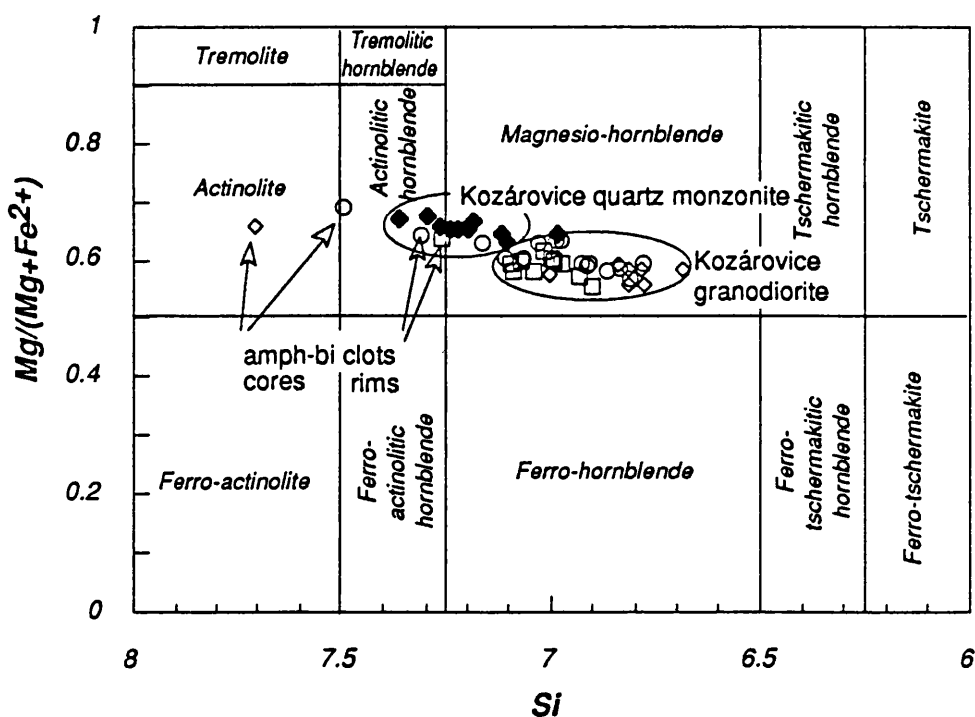


Figure III.1.8: Position of the Kozárove amphiboles in the classification diagram of Leake (1978)

Kozárove granodiorite	Kozárove quartz monzonite
○ Koz-2 (Kozárove I)	◆ KozD-1 (Kozárove II)
□ Koz-4 (Kozárove II)	
◇ Koz-6 (Kozárove IV)	

Table III.3: Geothermobarometry for the Kozárovec intrusion
(excluding amphibole - biotite clots and the Kozárovec quartz monzonite;
for explanation see Table III.1.)

	amph		pressure (kbar)				plag		temperature (°C)				
	Si	Σ Al	H+Z	H+a	J+R	T+E	X _{Ab}	K	T _{H+Z}	T _{H+a}	T _{J+R}	T _{T+E}	T _{2.5}
Koz-2 (Kozárovec I)													
amph 1	6.831	1.35	2.9	2.9	2.3	1.0	0.6	1.4530	749.2	749.4	758.3	777.0	754.7
amph 2	6.922	1.32	2.7	2.7	2.1	0.8	0.6	1.6261	731.2	731.7	739.8	758.6	734.2
amph 3	6.906	1.35	2.9	2.8	2.2	1.0	0.6	1.5928	732.8	733.0	741.7	760.2	737.9
amph 4	6.971	1.30	2.6	2.6	2.0	0.7	0.6	1.7330	721.5	722.2	729.7	748.7	723.0
amph 5	6.805	1.41	3.2	3.2	2.5	1.3	0.6	1.4089	750.8	750.5	760.6	778.5	760.5
amph 6	6.780	1.37	3.0	3.0	2.4	1.1	0.6	1.3671	758.8	758.9	768.4	786.9	766.1
amph 7	7.106	1.05	1.4	1.2	1.0	-0.6	0.6	2.0840	707.3	710.1	712.6	-	691.8
amph 8	6.987	1.22	2.2	2.1	1.7	0.3	0.6	1.7687	723.8	725.2	731.1	751.3	719.4
amph 9	7.061	1.13	1.8	1.6	1.3	-0.2	0.6	1.9570	712.4	714.5	718.6	-	702.2
amph 10	7.026	1.17	2.0	1.8	1.5	0.0	0.6	1.8638	718.2	720.0	724.8	-	710.4
Koz-4 (Kozárovec II)													
amph 2*	6.973	1.22	2.2	2.1	1.7	0.3	0.6	1.7367	726.6	728.0	734.0	754.2	722.6
amph 3*	7.261	0.94	0.8	0.5	0.5	-1.2	0.6	2.6481	676.9	680.5	680.7	-	654.1
amph 1	7.044	1.19	2.0	1.9	1.6	0.1	0.6	1.9099	712.6	714.2	719.5	739.8	706.3
amph 2	6.995	1.22	2.2	2.1	1.7	0.3	0.6	1.7873	721.9	723.3	729.2	749.3	717.6
amph 3	7.093	1.16	1.9	1.8	1.4	0.0	0.6	2.0461	703.1	704.9	709.5	-	694.8
amph 4	6.999	1.17	2.0	1.8	1.5	0.0	0.6	1.7971	724.3	726.1	731.0	-	716.7
amph 5	6.933	1.34	2.8	2.8	2.2	0.9	0.6	1.6495	726.8	727.1	735.7	754.1	731.7
amph 6	7.096	1.09	1.6	1.4	1.2	-0.4	0.6	2.0549	707.1	709.5	712.8	-	694.1
Koz-6 (Kozárovec IV)													
amph 1	6.815	1.45	3.4	3.4	2.7	1.5	0.6	1.4250	745.7	745.0	756.0	773.2	758.3
amph 2	6.838	1.34	2.8	2.8	2.2	0.9	0.6	1.4654	748.1	748.4	757.1	775.9	753.1
amph 3	6.685	1.44	3.3	3.4	2.6	1.5	0.6	1.2252	774.9	774.3	785.4	803.2	787.4
amph 4	6.779	1.40	3.1	3.1	2.5	1.2	0.6	1.3658	757.1	756.8	766.9	785.0	766.3
amph 5	6.785	1.40	3.1	3.1	2.4	1.2	0.6	1.3755	756.1	755.9	765.8	784.0	765.0
amph 6	6.815	1.34	2.8	2.8	2.2	0.9	0.6	1.4248	753.7	754.0	762.7	781.6	758.3
Average			2.4	2.4	1.9	-			730.9	731.8	738.8	-	730.3
1σ			0.7	0.8	0.6	-			22.6	21.6	24.3	-	31.6

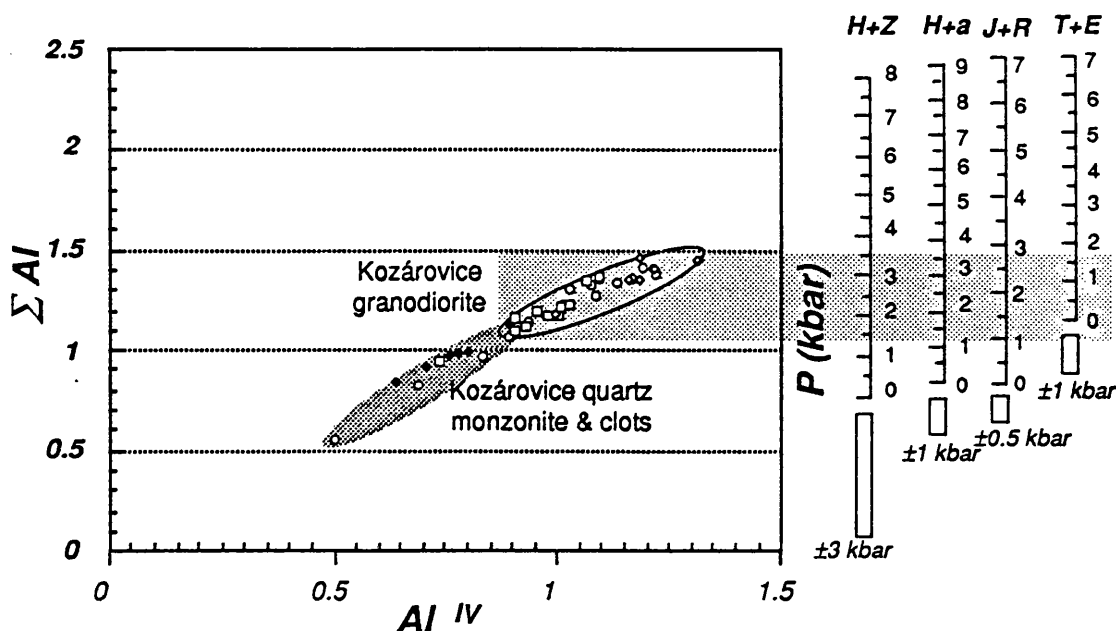


Figure III.1.9: Al^{IV} versus ΣAl plot of amphiboles, Kozárovec intrusion

○Koz-2 (Kozárovec I) □Koz-4 (Kozárovec II) ◇Koz-6 (Kozárovec IV)

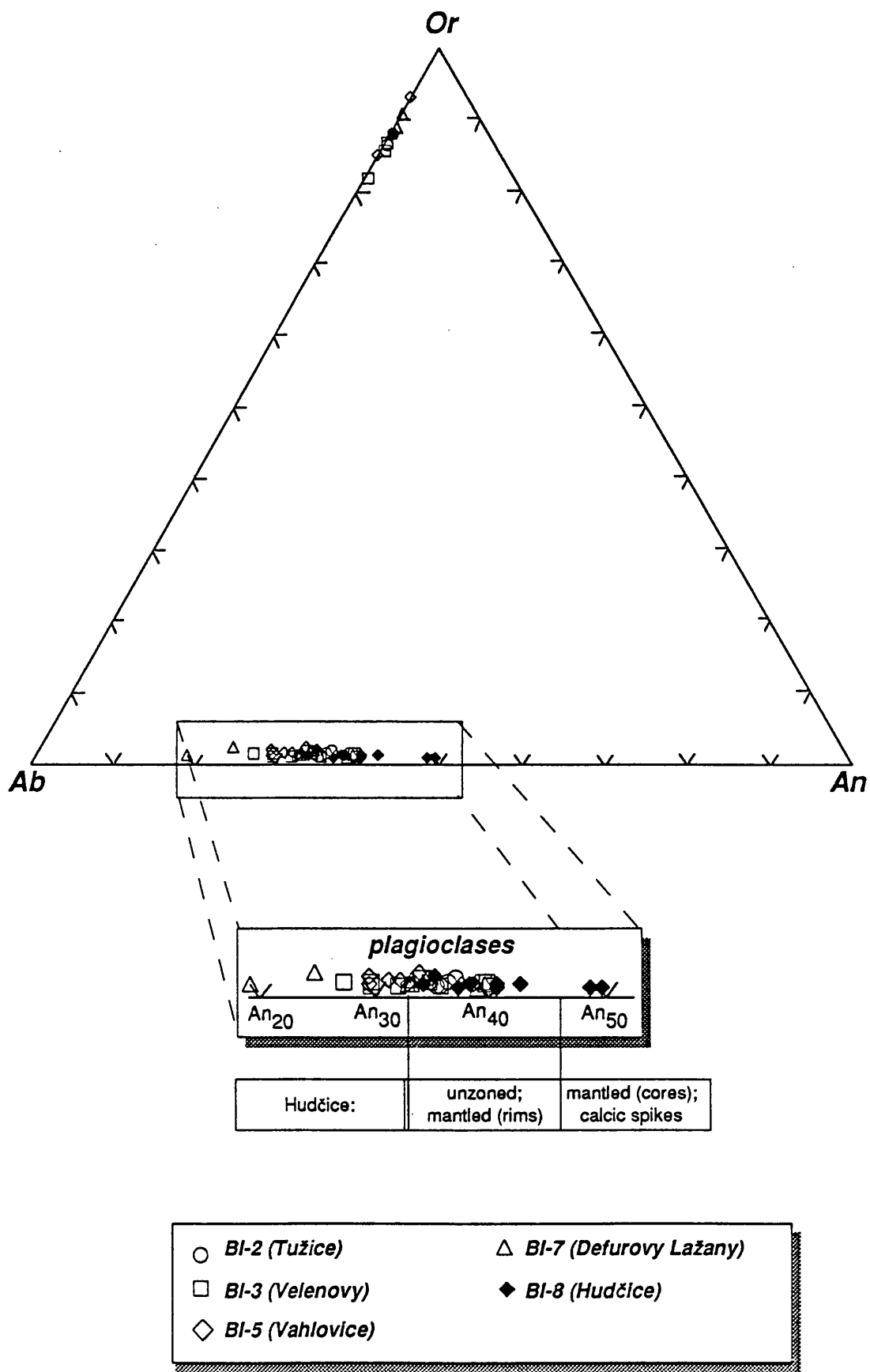


Figure III.1.10: Composition of the Blatná feldspars in the Or-Ab-An ternary diagram

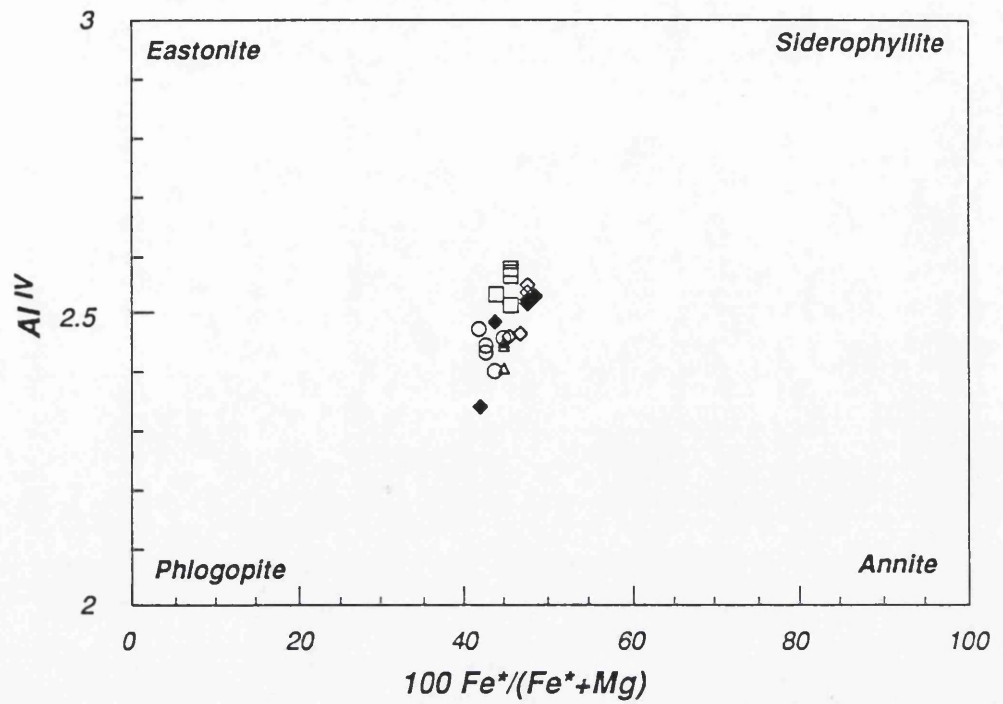


Figure III.1.11: Classification of the Blatná biotites in the $100 \text{ Fe}^*/(\text{Fe}^* + \text{Mg})$ versus Al^{IV} diagram

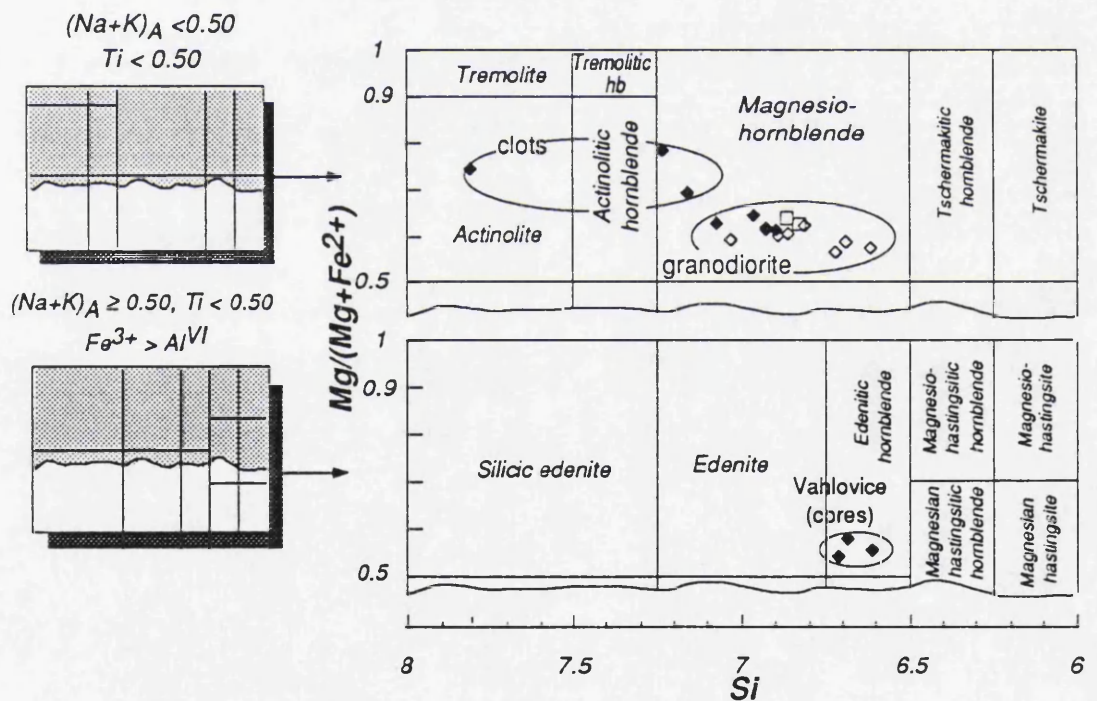


Figure III.1.12: Position of the Blatná amphiboles in the classification diagram of Leake (1978)

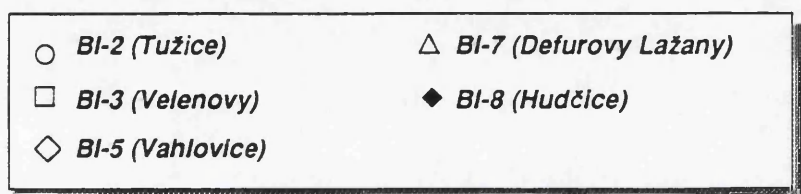


Table III.4: Geothermobarometry for the Blatná intrusion
(excluding amphibole - biotite clots and the Kozárovec quartz monzonite;
for explanation see Table III.1.)

	amph		pressure (kbar)				plag		temperature (°C)				
	Si	Σ Al	H+Z	H+a	J+R	T+E	X _{Ab}	K	T _{H+Z}	T _{H+a}	T _{J+R}	T _{T+E}	T _{2.5}
Bl-3 (Velenov)													
amph 1	6.826	1.34	2.8	2.8	2.2	0.9	0.65	1.5650	736.6	737.0	745.5	764.2	741.1
amph 2	6.864	1.24	2.3	2.2	1.8	0.4	0.65	1.6389	735.2	736.4	742.9	762.9	732.8
Bl-5 (Vahlovice)													
amph 2	6.813	1.34	2.8	2.8	2.2	0.9	0.65	1.5397	739.2	739.5	748.1	766.8	744.0
amph 3	6.859	1.29	2.6	2.5	2.0	0.6	0.65	1.6281	733.1	733.9	741.4	760.7	734.0
amph 4	6.928	1.22	2.2	2.1	1.7	0.3	0.65	1.7758	722.7	724.1	730.1	750.2	718.7
amph 5	6.892	1.25	2.4	2.3	1.8	0.4	0.65	1.6970	728.8	729.9	736.5	756.3	726.7
amph 8	7.029	1.15	1.9	1.7	1.4	-0.1	0.65	2.0288	705.2	707.1	711.5	-	696.2
Bl-8 (Hudčice)													
amph 1	6.898	1.30	2.6	2.5	2.0	0.7	0.65	1.7085	724.1	724.8	732.3	751.4	725.5
amph 2	6.964	1.15	1.9	1.7	1.4	-0.1	0.65	1.8587	719.8	721.7	726.3	-	710.9
amph 3	7.072	1.03	1.2	1.0	0.9	-0.8	0.65	2.1526	703.8	706.8	708.8	-	686.5
amph 4	6.929	1.20	2.1	2.0	1.6	0.2	0.65	1.7776	724.1	725.7	731.2	751.6	718.6
Average			2.3	2.2	1.7	-			724.8	726.1	732.2	-	721.4
1σ			0.47	0.53	0.40	-			11.82	11.13	12.90	-	17.91
Bl-5 (cores) (Vahlovice)													
amph 1	6.690	1.46	3.4	3.5	2.7	1.6	0.65	1.3344	757.2	756.4	767.7	784.9	770.8
amph 6	6.616	1.53	3.8	3.9	3.0	1.9	0.65	1.2292	767.6	766.2	779.2	795.5	786.7
amph 7	6.718	1.48	3.5	3.6	2.8	1.7	0.65	1.3776	749.4	748.5	760.2	776.9	764.7
Average			3.6	3.6	2.8	1.7			758.1	757.0	769.0	785.8	774.1
1σ			0.18	0.20	0.15	0.19			9.15	8.91	9.58	9.33	11.39

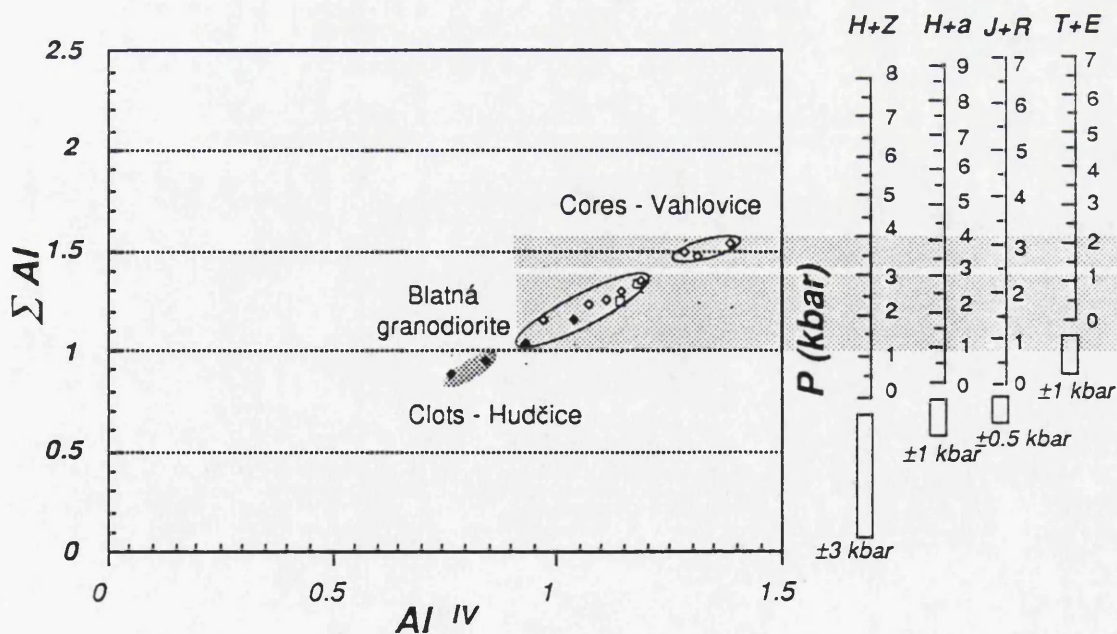


Figure III.1.13: Al^{IV} versus ΣAl plot of amphiboles, Blatná intrusion

○ Bl-2 (Tužice) □ Bl-3 (Velenov) ◇ Bl-5 (Vahlovice) ◆ Bl-8 (Hudčice)

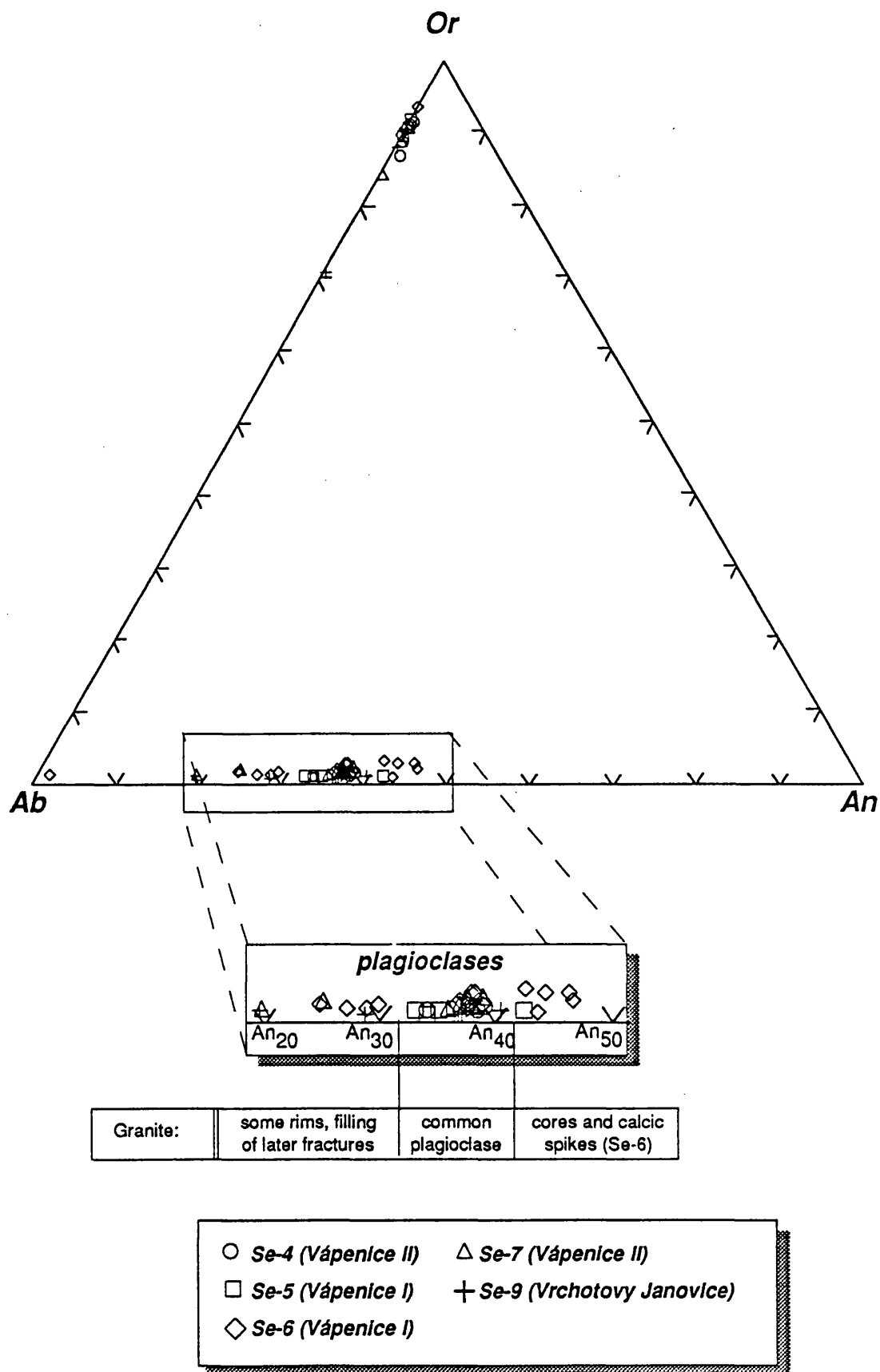


Figure III.1.14: Composition of the Sedlčany feldspars in the Or-Ab-An ternary diagram

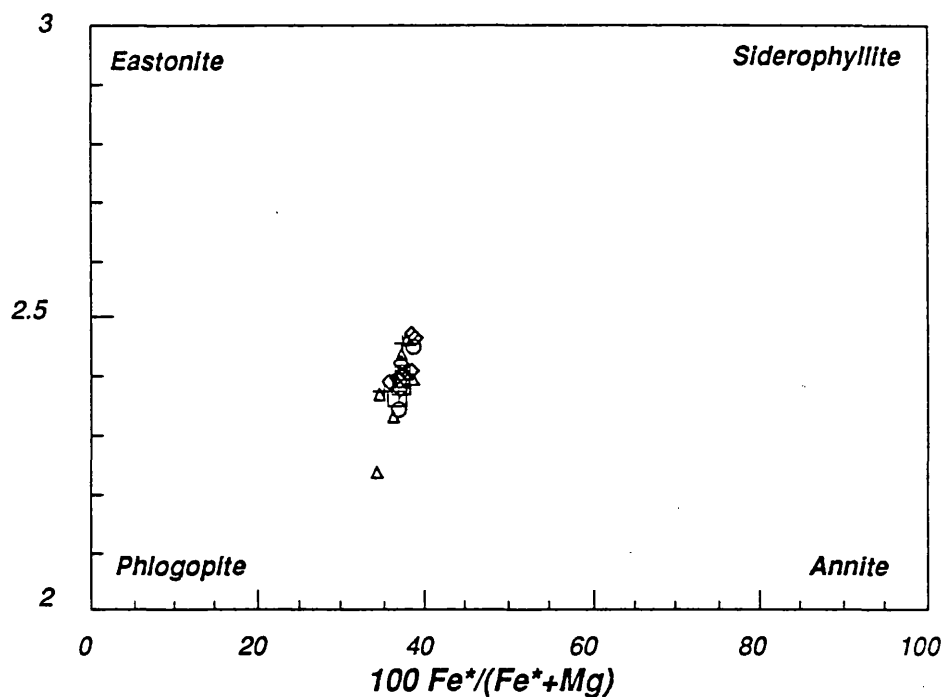


Figure III.1.15: Classification of the Sedlčany biotites in the $100 \text{ Fe}^*/(\text{Fe}^* + \text{Mg})$ versus Al^{IV} diagram

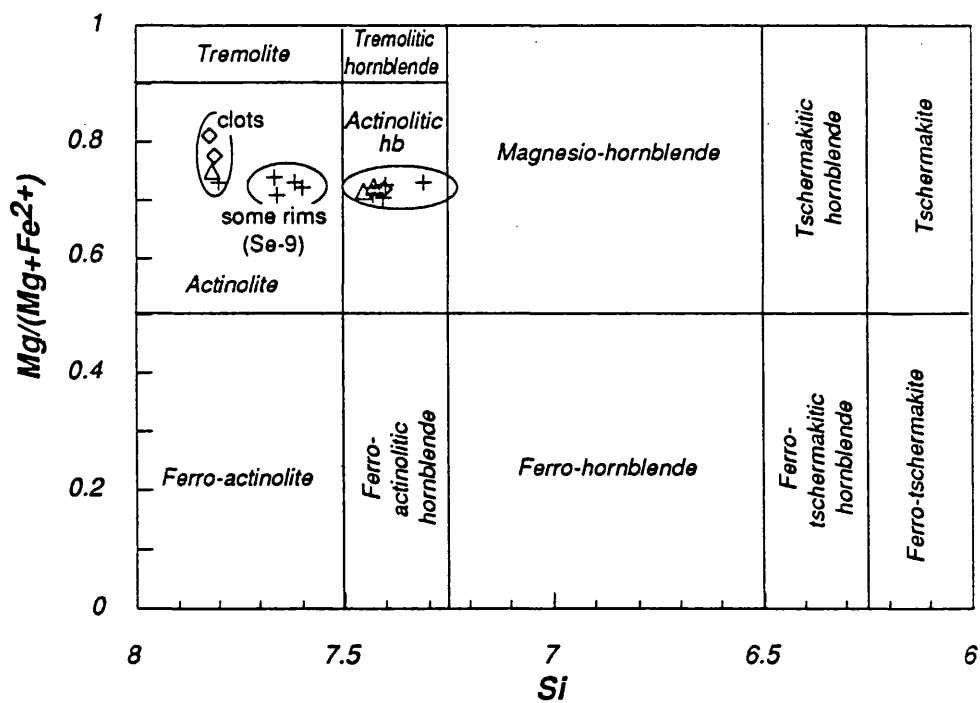


Figure III.1.16: Position of the Sedlčany amphiboles in the classification diagram of Leake (1978)

- | | |
|----------------------|-----------------------------|
| ○ Se-4 (Vápenice II) | △ Se-7 (Vápenice II) |
| □ Se-5 (Vápenice I) | + Se-9 (Vrchotovy Janovice) |
| ◇ Se-6 (Vápenice I) | |

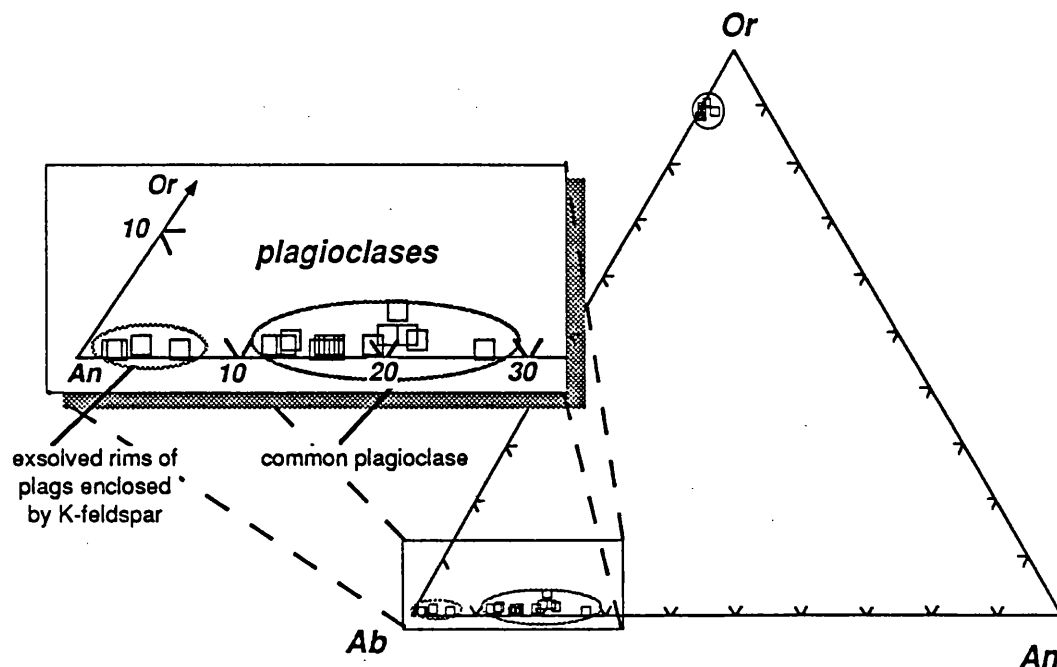


Figure III.1.17: Composition of the Říčany feldspars in the Or-Ab-An ternary diagram

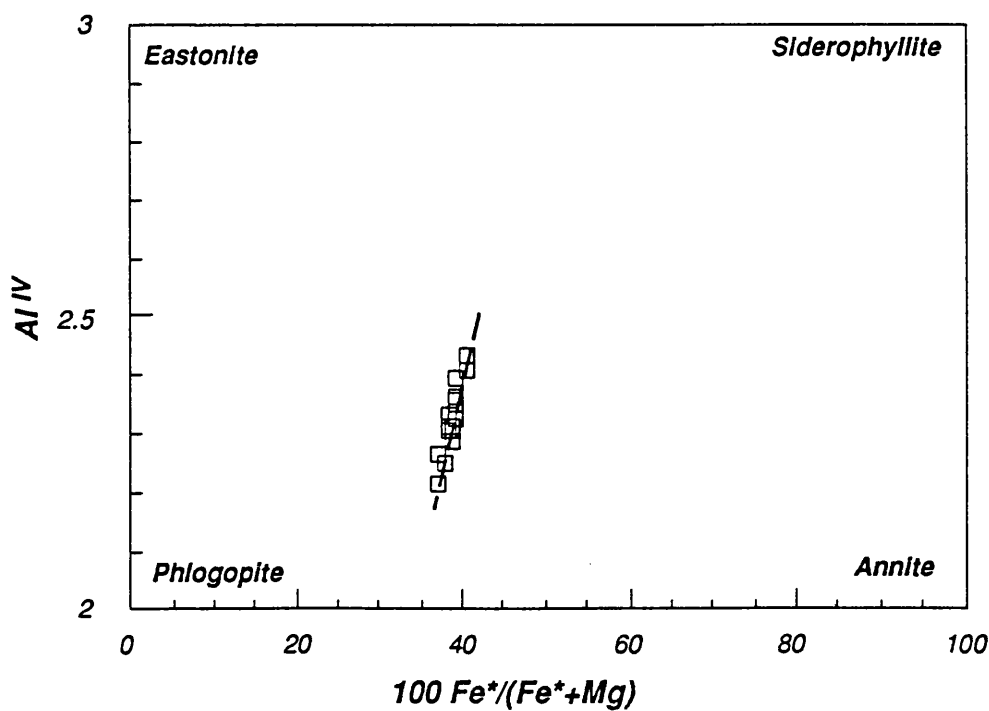
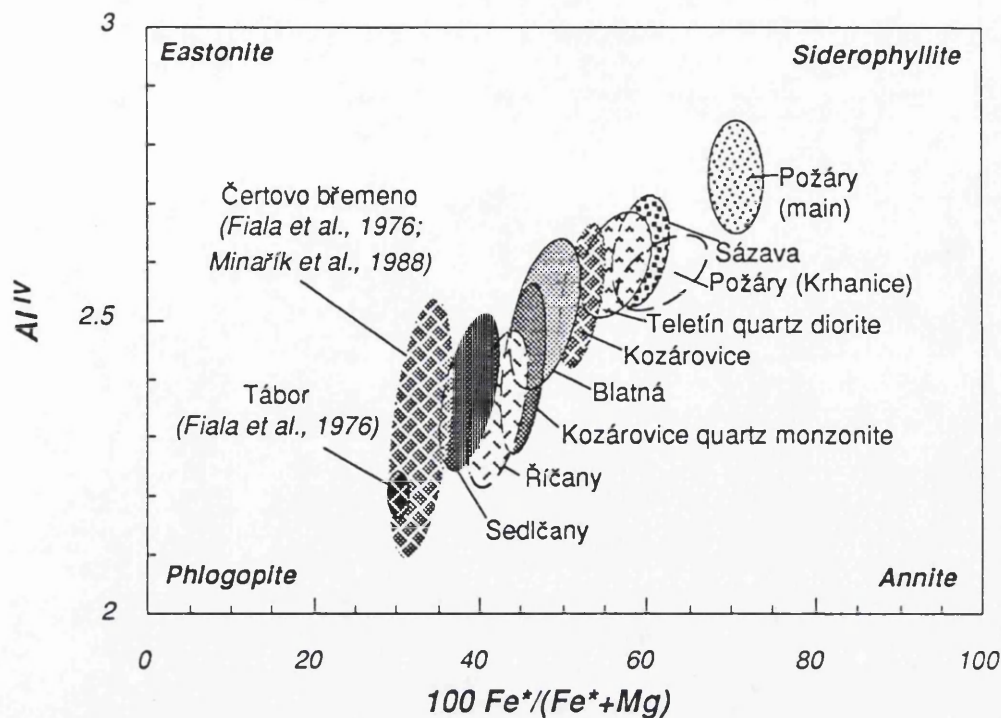
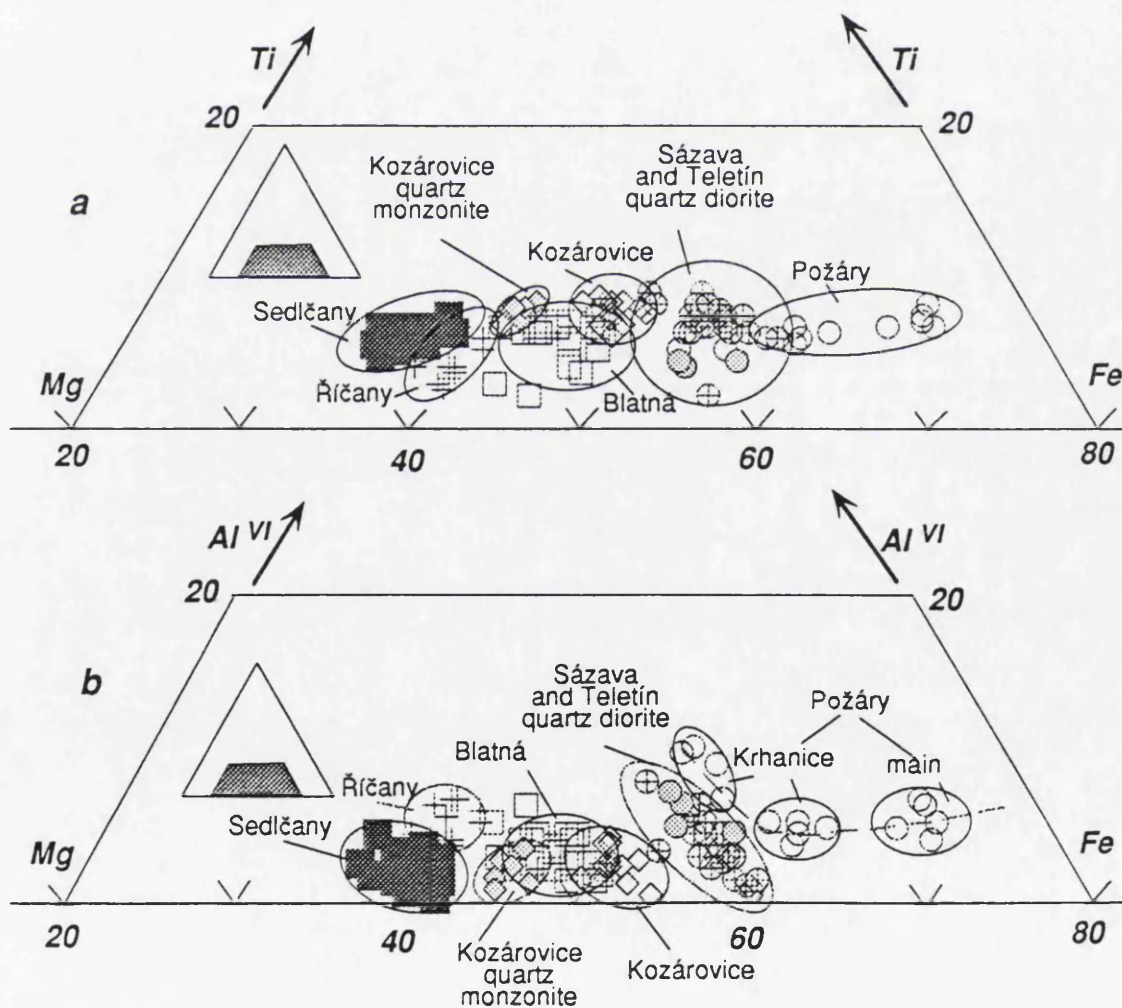


Figure III.1.18: Classification of the Říčany biotites in the $100 \text{ Fe}^*/(\text{Fe}^* + \text{Mg})$ versus Al^{IV} diagram



**Figure III.2.1: Summary of biotite classification,
Central Bohemian Pluton**



**Figure III.2.2: Composition of biotites,
Central Bohemian Pluton**

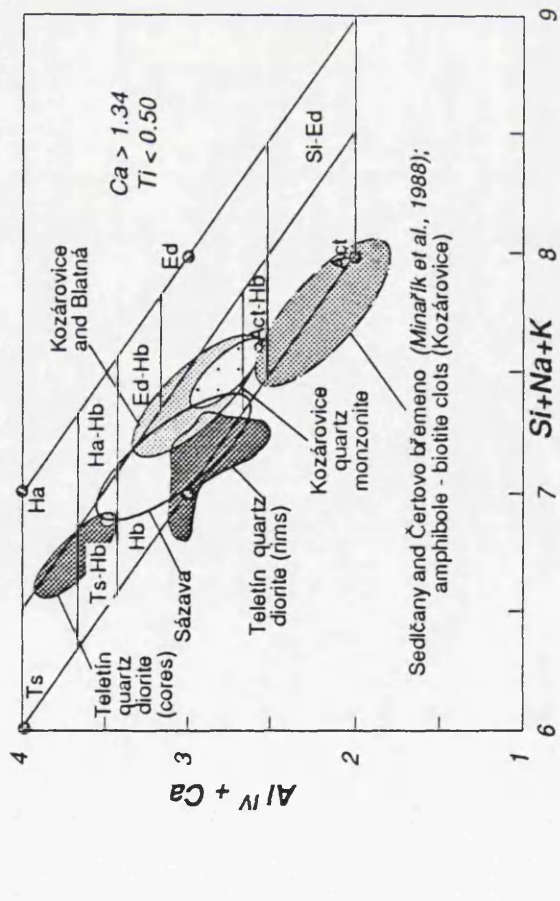
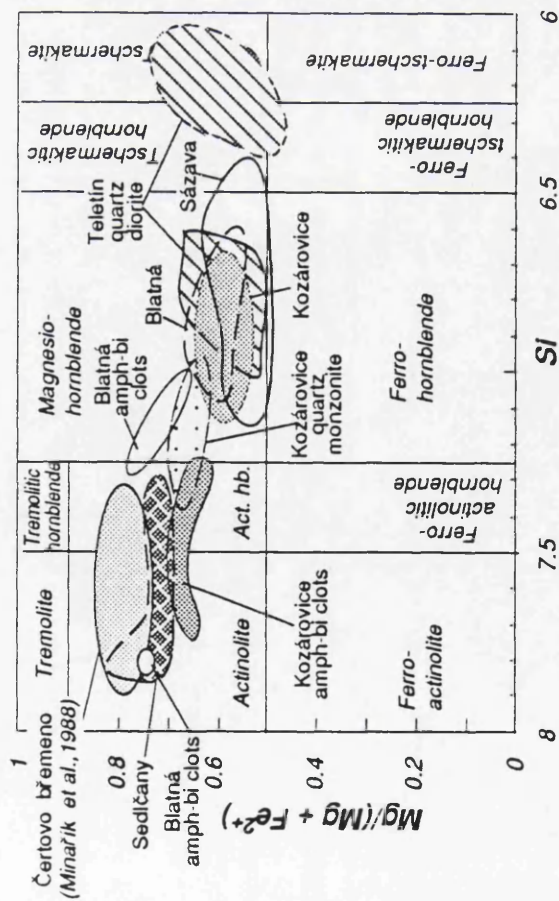


Figure III.2.3: Summary of classification of analysed amphiboles, Central Bohemian Pluton (after Leake, 1978)

Figure III.2.4: Position of studied amphiboles in the diagram of Giret et al. (1980)

- Ts Tschermakite
- Ts-Hb Tschermakititic hornblende
- Ed Edenite
- Hb Hornblende
- Act-Hb Actinolitic hornblende
- Ha Hastingsite
- Ha-Hb Hastingsitic hornblende
- Ed-Hb Edenitic hornblende
- Act Actinolite
- Si-Ed Silicic edenite

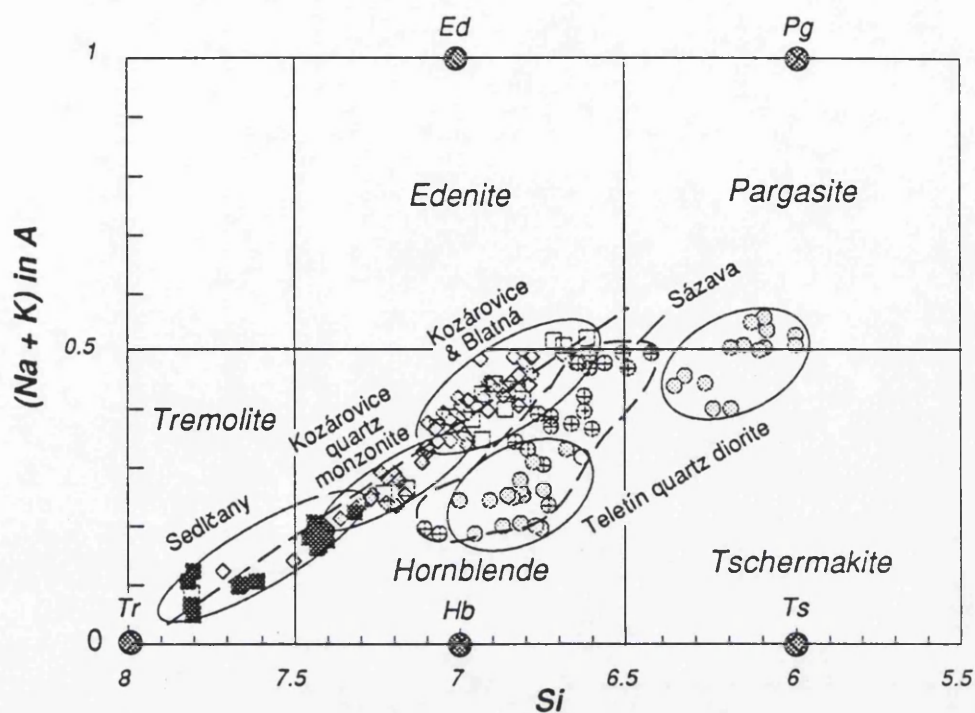


Figure III.2.5: Chemical variation of calcic amphiboles, Central Bohemian Pluton (after Deer et al., 1992)

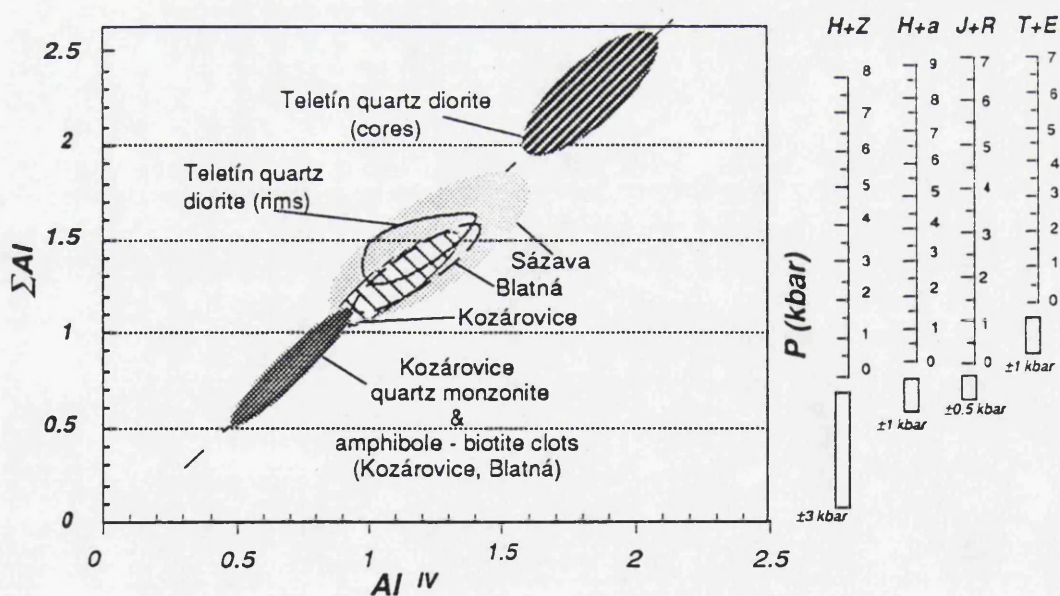


Figure III.2.6: 'Aluminium in hornblende' geobarometry, as applied to amphiboles from the Central Bohemian Pluton

- H+Z: Hammarstrom and Zen (1986)
H+a: Hollister et al. (1987)
J+R: Johnson and Rutherford (1989)
T+R: Thomas and Ernst (1990)

IV. Whole-rock geochemistry

Since the pioneering work of *Oriov* (1935), the whole-rock geochemistry of the CBP has attracted much attention. The available information about petrography, geochemistry and petrogenesis was integrated by *Steinöcher* (1969) and *Vejnar* (1973). With the advancement of analytical techniques, trace elements became more and more important (*Vejnar*, 1974b; *Tanton et al.*, 1977; *Mirafit et al.*, 1979; *Bouška et al.*, 1984). Summaries of the major and trace element geochemistry of the granitoids of the CBP are given in *Vejnar* (1973, 1974b) and *Jakeš* (1977). Further works, utilising statistical and computer methods for the compositional analysis of granitoids are given by *Rajlich and Viedlmač* (1983) and *Machart* (1989, 1992). Most recently, a critical review of the geochemical characters and a subdivision of the CBP based on major elements was presented by *Holub* (1989a, 1992) and of the lamproid rocks (the Čertovo břemeno suite and associated rocks of the Blatná suite) by *Holub* (1990). The geochemical characters of the dyke rocks associated with the CBP have been studied by *Němec* (e.g. 1974, 1988) and *Žalutková* (1982a). Integrated geochemical and geophysical information can be found in unpublished reports of the uranium programme (e.g. *Sebatková*, 1977).

The aims of this section are to present a large body of new data, and on the basis of it, and previous data, to give an overview of the major and trace element composition of the particular rock types of the CBP. This will lead towards a classification scheme based on the recognition of suites of similar geochemical nature. These suites are investigated in terms of the intra- and inter-suite variations in both major [Chapter IV.1] and trace [Chapter IV.2.] elements, their geochemical constraints on their petrogenesis are sought [Chapter IV.3.] together with their likely genetic affinities [Chapter IV.4.]. Sample details of analysed specimens are set out in Appendix I.

IV.1. Major elements

The major element data and the normative values are given in Appendix II. The normative calculations were performed using an IBM PC program *Norman* written by the author (Appendix A.3). Unless stated otherwise, the plotting symbols are the standard ones (Fig. 1.6, and end of this chapter).

In order to preserve the homogeneity of the data set, no extra analyses were incorporated from the literature. The only exception is the unpublished data for the Sedlčany granite from the MSc. thesis of *Svojilka* (1983), which were obtained in the same laboratory (University of Glasgow) by identical methods. Additionally, several major-element and REE analyses were used from the MSc. thesis of *Janoušek* (1991) (the Říčany granite) that compare well with the rest of the dataset for this intrusion. The problems arising from the compilation of data from different laboratories have been addressed, for instance, by *Holub* (1992).

The next remark concerns the usage of triangular plots. As pointed out by *Rollinson* (1993), among others, three variables, forced to a total of 100 %, tend to be strongly correlated due to the well-known closure (constant-sum) effect (*Chayes*, 1950; *Rollinson*, 1992). However important information can still be recovered from triangular plots, if one is aware of this drawback.

□ Sázava suite:

- ⊕ Sázava tonalite and quartz diorite
- Basic rocks associated with Sázava intrusion
- Teletín quartz diorite
- Požáry trondhjemite and Nečín granodiorite

□ Blatná suite:

- Mrač monzogranite
- ◇ Kozárovice (s.s.) granodiorite
- ⊕ Těchnice granodiorite (porphyritic Kozárovice)
- ◇ Kozárovice quartz monzonite
- ◆ Zalužany quartz monzonite
- ◆ Lučkovice monzonite
- Blatná (s.s.) granodiorite
- Hudčice diorite
- ▣ Červená granodiorite
- Mafic microgranular enclave, Červená granodiorite
- △ Klatovy granodiorite
- ▽ Marginal monzogranite

□ Čertovo břemeno suite:

- Sedlčany monzogranite
- Čertovo břemeno monzogranite to quartz syenite
- ◆ Tábor quartz syenite

□ Říčany suite:

- + Říčany granite
- × Jevany leucogranite
- ◆ Mafic microgranular enclaves, Říčany intrusion

Standard plotting symbols

☐ Sázava suite:

- ⊕ *Sázava tonalite and quartz diorite*
- ⊗ *Basic rocks associated with Sázava intrusion*
- ⊙ *Teletín quartz diorite*
- *Požáry trondhjemite and Nečín granodiorite*

☐ Blatná suite:

- ⊘ *Mrač monzogranite*
- ◇ *Kozárovce (s.s.) granodiorite*
- ⊕ *Těchnice granodiorite (porphyritic Kozárovce)*
- ◆ *Kozárovce quartz monzonite*
- ◆ *Zalužany quartz monzonite*
- ⊞ *Lučkovice monzonite*
- ☐ *Blatná (s.s.) granodiorite*
- ▒ *Hudčice diorite*
- ▣ *Červená granodiorite*
- ▤ *Mafic microgranular enclave, Červená granodiorite*
- △ *Klatovy granodiorite*
- ▽ *Marginal monzogranite*

☐ Čertovo břemeno suite:

- *Sedlčany monzogranite*
- *Čertovo břemeno monzogranite to quartz syenite*
- ◆ *Tábor quartz syenite*

☐ Říčany suite:

- ⊕ *Říčany granite*
- × *Jevany leucogranite*
- ⊕ *Mafic microgranular enclaves, Říčany intrusion*

Standard plotting symbols

IV. Whole-rock geochemistry

Since the pioneering work of *Orlov (1935)*, the whole-rock geochemistry of the CBP has attracted much attention. The available information about petrography, geochemistry and petrogenesis was integrated by *Steinöcher (1969)* and *Vejnar (1973)*. With the advancement of analytical techniques, trace elements became more and more important (*Vejnar, 1974b; Tauson et al., 1977; Minařík et al., 1979; Bouška et al., 1984*). Summaries of the major and trace element geochemistry of the granitoids of the CBP are given in *Vejnar (1973, 1974b)* and *Jakeš (1977)*. Further works, utilising statistical and computer methods for the compositional analysis of granitoids are given by *Rajlich and Vlašimský (1983)* and *Machart (1989, 1992)*. Most recently, a critical review of the geochemical characters and a subdivision of the CBP based on major elements was presented by *Holub (1989a, 1992)* and of the lamproid rocks (the Čertovo břemeno suite and monzonitic rocks of the Blatná suite) by *Holub (1990)*. The geochemical characters of the dyke rocks associated with the CBP have been studied by *Němec (e.g. 1974, 1988)* and *Žežulková (1982a)*. Integrated geochemical and geophysical information can be found in unpublished reports of the uranium prospection (*e.g. Sobotková, 1977*).

The aims of this section are to present a large body of new data, and on the basis of it, and previous data, to give an overview of the major and trace element composition of the particular rock types of the CBP. This will lead towards a classification scheme based on the recognition of suites of similar geochemical nature. These suites are investigated in terms of the inter- and intra-suite variations in both major [Chapter IV.1] and trace [Chapter IV.2.] elements, then geochemical constraints on their petrogenesis are sought [Chapter IV.3.] together with their likely geotectonic affiliation [Chapter IV.4.]. Sample details of analysed specimens are set out in Appendix I.

IV.1. Major elements

The major element data and the normative values are given in Appendix III. The normative calculations were performed using an IBM PC program *Norman* written by the author [Appendix II.]. Unless stated otherwise, the plotting symbols are the standard ones [Fig. L6. and end of this chapter].

In order to preserve the homogeneity of the data set, no extra analyses were introduced from the literature. The only exception is the unpublished data for the Sedlčany granite from the MSc. thesis of *Svojtka (1993)*, which were obtained in the same laboratory (University of Glasgow) by identical methods. Additionally, several major-element and REE analyses were used from the MSc. thesis of *Janoušek (1991)* (the Říčany granite) that compare well with the rest of the dataset for this intrusion. The problems arising from the compilation of data from different laboratories have been addressed, for instance, by *Holub (1992)*.

The next remark concerns the usage of triangular plots. As pointed out by *Rollinson (1993)*, among others, three variables, forced to a total of 100 %, tend to be strongly correlated due to the well-known closure (constant-sum) effect (*Chayes, 1960; Rollinson, 1992*). However important information can still be recovered from triangular plots, if one is aware of this drawback.

IV.1.1. Major-element-based subdivision of the CBP

The AFM diagram ($A = \text{Na}_2\text{O} + \text{K}_2\text{O}$, $F = \text{FeO}^*$, $M = \text{MgO}$) [Fig. IV.1.1.] is a classic petrological tool for the genetic classification of igneous suites. The evolution of a magma in terms of its AFM characteristics appears to be controlled by oxidation state which, in turn, influences the onset of the magnetite crystallization. Early magnetite crystallization in open (oxidising) systems tends to buffer the low F values (Bowen trend), whereas closed (reducing) system crystallization usually leads to a steep AFM trend (Fenner trend) (Wilson, 1993). These trends are commonly referred to as calc-alkaline and tholeiitic, respectively (Irvine and Baragar, 1971). However, many of the alkaline suites typically show a tendency to iron enrichment and thus the term "tholeiitic" should be restricted to compositions lacking K-feldspar and biotite (Bowden *et al.*, 1984). Among the granitoids of the Central Bohemian Pluton, two main AFM trends were recognised by Vejnar (1973), one steep (Požáry, Nečín, Sázava and associated mafic rocks), the other one (the rest of the rock types) significantly shallower. However, as can be seen on the present AFM diagram [Fig. IV.1.1.], at least four distinct suites can be distinguished, being:

- (1) *Sázava suite*
(Sázava, associated mafic rocks, Požáry, Nečín),
- (2) *Blatná suite*
(Kozárovce s.s., Těchnice, Blatná, Červená, Klatovy, Mrač, Marginal),
- (3) *Čertovo břemeno suite*
(Čertovo břemeno, Tábor and Sedlčany),
- (4) *Říčany suite*
(Říčany and Jevany).

The Sázava, Blatná and Čertovo břemeno suites form progressively shallower calc-alkaline trends. As the Říčany and Jevany granites fall close to the A apex, their relation to the other suites is uncertain, and, therefore, they will be treated as a separate suite. This Říčany suite is unlikely to belong to the tholeiitic trend, due to presence of biotite and K-feldspar (Bowden *et al.*, 1984) but no definite answer can be given from the AFM diagram only. The classification, based on behaviour in the AFM ternary plot, will be used throughout this thesis, as it groups together those intrusions with geochemical affinities such that broad chemical characteristics of the CBP may be more readily discernible. This approach is analogous to the suite classification as used by A.J.R. White and co-workers in the Lachlan Fold Belt of Australia (*e.g.* White and Chappell, 1988; White, 1990). Each suite ought to have its own identity in terms of chronology, modal and chemical composition, textures, enclaves and dyke-swarm population (Pitcher, 1993). The usefulness of this subdivision, especially for readers not familiar with the Czech terminology, will be obvious from the forthcoming text as it simplifies the plethora of names of individual intrusive bodies. The suites are named after the most 'typical' member (*viz.* Sázava, Blatná, Čertovo břemeno, Říčany).

As the quality of the modal analyses of porphyritic types has not been satisfactory [Chapter II.], additional options to characterise the petrographic inter- and intra-suite variations were considered. In the Q'-ANOR diagram of Streckeisen and Le Maitre (1979) [Fig. IV.1.2.; cf. Fig. II.11.] both the Q' and ANOR parameters are calculated from the normative mineralogy: $Q' = 100 Q / (Q + \text{Or} + \text{Ab} + \text{An})$ and $\text{ANOR} = 100 \text{An} / (\text{Or} + \text{An})$. Among others, the CIPW norm (Hutchison, 1974) has been chosen, as the Q'-ANOR plot for the studied rocks appears to be a best approximation of the modal classification (*also* Bowden *et al.*, 1984). Moreover, no H_2O^+ data are available (only LOIs), and

therefore any calculation taking into account the water content would be meaningless. Thus, the normative calculations involving biotite and, or hornblende in the norm (e.g. the Granite mesonorm: *Mielke and Winkler, 1979* or the CIPW norm with hornblende and biotite: *Hutchison, 1974*) were not used.

On the Q'-ANOR diagram, the studied granitoids are classified as follows:

Sázava suite	
Sázava intrusion (main)	mainly tonalite and quartz diorite
Teletín quartz diorite	quartz diorite
Basic rocks	quartz gabbro (quartz diorite), gabbro (diorite)
Požáry intrusion	tonalite
Nečín intrusion	granodiorite
Blatná suite	
Mrač intrusion	monzogranite
Kozárovice intrusion (main)	granodiorite and quartz monzonite
Blatná intrusion (including Červená)	granodiorite
Klatovy and Marginal type intrusions	granodiorite and monzogranite
Zalužany and Kozárovice quartz monzonite	quartz monzonite
Lučkovice intrusion	monzonite
Čertovo břemeno suite	
Sedlčany intrusion	monzogranite
Čertovo břemeno intrusion	monzogranite, quartz syenite or alkali feldspar syenite
Tábor intrusion	quartz syenite to quartz monzonite
Říčany suite	
Říčany and Jevany intrusions	mainly syenogranite

Actually, the Požáry intrusion should be classified as trondhjemite, corresponding to a tonalite with less than 10 % mafic minerals (*Le Maitre, 1989*).

IV.1.2. Harker plots

Analyses of each of the four major suites have been plotted on simple bivariate plots of SiO₂ versus major element oxides (Harker plots) [Figs. IV.1.3.-6.] that remain, despite the recent discussion concerning the spurious correlation caused by the constant sum effect (*Cox et al., 1979; Rollinson, 1993 and references therein*), one of the major tools for study of granitoids.

The Harker plots for the Sázava suite [Fig. IV.1.3.] show a strong negative correlation between SiO₂ and MgO, CaO and total Fe₂O₃ (Fe₂O₃*), as well as a positive correlation between SiO₂ and both K₂O and Na₂O. There is also, to some extent, a tendency of TiO₂ and P₂O₅ to decrease with increasing degree of fractionation. Within the Sázava intrusion, the lowest SiO₂ is that of the sample Sa-4, whereas the highest one is shown by the samples Sa-10 and Sa-11.

The Blatná suite [Fig. IV.1.4.] exhibits negative correlation between SiO₂ and Fe₂O₃*, MnO, MgO, CaO, P₂O₅ and, to some extent, also TiO₂, whereas Al₂O₃ remains more-or-less constant, and K₂O does not show any simple trend at all. The Harker plot for Na₂O was too scattered and is not shown. Among the Kozárovice samples, the lowest SiO₂ is that of Koz-9, and the highest SiO₂ is

shown by Koz-5. In many of the plots, the Kozárovec quartz monzonite (KozD-1) forms an integral part of the Kozárovec trend, plotting between the samples Gbl-1 (Lučkovice), Zal-1 (Zalužany) and the Kozárovec granodiorite (e.g. Fe_2O_3^* , MnO, MgO, CaO). In plots of Al_2O_3 and MgO sample Gbl-2 is not plotted, as it would distort the scaling. Within the Blatná intrusion, the lowest SiO_2 is that of the Červená granodiorite (Cv-3), followed by the amphibole-bearing analyses of the Blatná s.s. (e.g. Bl-2, Bl-8) and the analysis of the biotite facies with the highest SiO_2 content (Bl-4).

The Harker plots of the Čertovo břemeno suite [Fig. IV.1.5.] can be characterised by an overall negative correlation between SiO_2 and other oxides, in particular TiO_2 , Fe_2O_3^* , MgO, CaO and P_2O_5 . Several of the plots show a major inflection for the Sedlčany intrusion, whose trend is typically subhorizontal. The Čertovo břemeno and Tábor analyses behave as a coherent group on several of the plots (TiO_2 , Fe_2O_3 , CaO). The lowest SiO_2 is shown by the sample Cb-3. The subhorizontal trends for the Sedlčany intrusion start with samples from the western part of the body (Vápenice; Se-3 and Se-6) and end at the samples of the biotite facies from the central part of the body (Kosova Hora; Se-11 and Se-12). The only exception is the plot of SiO_2 versus Na_2O , which shows a considerable scatter for the Sedlčany granite.

Little can be said about the Harker plots of the Říčany suite [Fig. IV.1.6.] as they fail to define simple trends. However, it is worth noting the restricted range of SiO_2 concentration (~ 69 - 72 %), with the lowest SiO_2 for the samples from Žernovka in the centre of the intrusion (Ri-6) and the highest values for the samples from Březí at the western margin (Ri-21).

IV.1.3. Major-element character of the studied suites

The following paragraphs deal with the inter-suite variations in major elements and normative major-element based values.

The A / CNK vs. A / NK plot (molar $\text{Al}_2\text{O}_3 / (\text{CaO} + \text{Na}_2\text{O} + \text{K}_2\text{O})$ versus molar $\text{Al}_2\text{O}_3 / (\text{Na}_2\text{O} + \text{K}_2\text{O})$) shows the character of granitoids in terms of their alumina saturation [Fig. IV.1.7.]. Generally speaking, the Sázava and Čertovo břemeno suites are mainly metaluminous, whereas the Blatná, and, to larger extent, the Říčany suite tend to be more peraluminous. In the Sázava suite, the analyses of the Sázava intrusion and associated mafic rocks are metaluminous, whereas the Požáry trondhjemite plots within the peraluminous domain. In the Blatná suite, the lowest A / CNK (corresponding to the metaluminous field) is that of the Kozárovec granodiorite and monzonitic rocks, whereas the rest of the suite is mainly peraluminous, with the highest A / CNK for the Mrač granite. The more mafic members of the Čertovo břemeno suite are mainly metaluminous (Čertovo břemeno and Tábor intrusions) but the Sedlčany granite straddles the boundary of the peraluminous domain. The Říčany suite (particularly the Říčany granite s.s.) is almost exclusively peraluminous as demonstrated by presence of a variable proportion of primary muscovite [Chapter II.6.].

Similar conclusions about the alumina saturation can be drawn on the basis of the ACF plot (White, 1990) ($A = \text{Al} - \text{Na} - \text{K}$; $\text{Ca} = \text{Ca} - 3.3 * P$, i.e. calcium corrected for apatite; $F = \text{Mg} + \text{Fe}^{2+}$) [Fig. IV.1.8.]. Moreover, the diagram indicates a trend of decreasing calcium content from the Sázava suite, through the Blatná to the Čertovo břemeno and Říčany suites. The majority of the rock types plot in the fields of hornblende-bearing and biotite only granitoids, generally in a good agreement with their modal mineralogy. The Požáry (Sázava suite), Mrač and Marginal (Blatná suite), as well as Říčany s.s. (Říčany suite) intrusions fall into the (peraluminous) field of the granitoids bearing at least one of the following peraluminous minerals: cordierite, garnet, andalusite, or muscovite. However, apart from anatectic, strongly peraluminous granitoids that are not dealt with this thesis (the Kosova Hora,

Maršovice and Kozlovice intrusions), no cordierite, garnet or andalusite is present in the CBP. The peraluminous character of some of the granitoids studied could be possibly linked to a metasedimentary source; however, no sedimentary parentage is necessarily required for the peraluminous magmas (Miller, 1985; cf. Chapter IV.3.).

The variation of the calcium content between the suites suggested on Figure IV.1.8. is more clearly shown on a plot of MgO vs. CaO [Fig. IV.1.9 a]. Although there is a trend within each suite of decreasing CaO with decreasing MgO (increasing degree of fractionation), at a given MgO the CaO content differs, with the Sázava suite having the highest CaO and the Čertovo břemeno the lowest. All trends converge towards the low MgO - CaO domain, occupied by the Říčany suite. In the plot of SiO₂ vs. K₂O [Fig. IV.1.9 b], the rock types studied again form tight clusters, but in this case dependent on K₂O concentrations (cf. Holub, 1992). The relatively low potassium content of the Sázava suite classifies it as being largely calc-alkaline, whereas the Blatná suite is high-potassium calc-alkaline and both Čertovo břemeno and Říčany suites, together with the monzonitic rocks of the Blatná suite, are shoshonitic in character. The discrimination boundaries are from *Peccerillo and Taylor (1976)*. The progressively increasing K₂O content with age is observed during evolution of granitoids from Andean type continental margin settings (e.g. *Wilson, 1989*). The distinctive character of the four granitoid suites in the CBP can also be demonstrated by means of the CaO - Na₂O - K₂O ternary diagram of *Condie (1981)* [Fig. IV.1.10.]. The decrease in CaO from Sázava through Blatná to Čertovo břemeno and Říčany suites is coupled with an increase in the K₂O / Na₂O ratio corresponding to the increase in K₂O seen on Figure IV.1.9 b. The Sázava suite forms a trend similar to the tholeiitic one; in contrast the rest of the rocks form part of a broadly calc-alkaline trend. The increase in the K₂O content with time observed in the CBP resembles that shown in orogenic zones connected with ageing of a subduction zone (*Holub, 1992*).

From the preceding text and Appendix III. it is apparent that the Sázava suite is characterised by high FeO (except Požáry and Nečín), Fe₂O₃, CaO, Na₂O/K₂O (>1) and FeO/Fe₂O₃, whereas its K₂O content is low. The Blatná suite has high FeO/Fe₂O₃, and intermediate CaO, Na₂O, K₂O and Na₂O/K₂O. The Čertovo břemeno suite shows high K₂O, MgO, P₂O₅ and low Na₂O, CaO and Na₂O/K₂O (<<1). The Říčany suite has high K₂O and low FeO, MgO, CaO, Na₂O/K₂O and FeO/Fe₂O₃.

The P - Q diagram (calculated in millications; see Appendix III.) of *Debon and Le Fort (1983,1988)* can be used for classification of both rock types and magmatic associations [Fig. IV.1.11.]. The *P* parameter represents the proportion of K-feldspar to plagioclase ($P = K - (Na + Ca)$) and *Q* the quartz content ($Q = Si / 3 - (K + Na + 2 * Ca / 3)$). On this diagram, the rocks of the Sázava suite are classified mainly as tonalite, quartz diorite or quartz monzodiorite (Sázava intrusion), tonalite and granodiorite (Požáry and Nečín intrusions) as well as gabbro (diorite) and quartz diorite (basic rocks). The great majority of the Blatná suite plots in the adamellite domain, with the mafic rocks belonging to quartz monzonite and monzonite. The Sedlčany and part of the Čertovo břemeno intrusions (Čertovo břemeno suite) are of granitic composition, as is the Říčany suite. The rest of the Čertovo břemeno and Tábor intrusions are quartz syenite. There is an obvious discrepancy in comparison with *Streckeisen and LeMaitre's (1979)* classification, as majority of their granodiorites fall into the adamellite field of the P - Q plot. This was attributed by *Debon and Le Fort (1988)* to the somewhat broader definition of their adamellite field compared with the monzogranite field of *Streckeisen's* classification.

Figure IV.1.12. shows the B - A diagram of *Debon and Le Fort (1988)*, where $A = Al - (K + Na + 2 * Ca)$ and $B = Fe + Mg + Ti$; B is proportional to the amount of dark minerals. This diagram is used to express the aluminous character and, consequently, the characteristic mineral assemblage. The subdivision based on this diagram corresponds well to the observed mineralogy [cf. Chapter II.]. Thus, part of the Požáry samples (Sázava suite), the Mrač intrusion (Blatná suite) and the majority of the Říčany suite plot in the II. domain (biotite prevailing over muscovite), the rest of the Požáry and Nečín intrusions (Sázava suite), the Klatovy, Marginal and part of Blatná granodiorite (Blatná suite), and majority of the Sedlčany granite (Čertovo břemeno suite) plot in the III. domain (biotite only) and the rest of the samples in the IV. domain (other mafic phases, e.g. amphibole, orthopyroxene, clinopyroxene and, or olivine also present). The trend with deep roots in the IV. domain is termed *cafemic* by *Debon and Le Fort (1988)*; it means that the majority of the Sázava suite (excluding the Požáry and Nečín intrusions), Čertovo břemeno suite (Čertovo břemeno and Tábor intrusions) and the amphibole-bearing rock types of the Blatná suite (Kozárovce, Červená and the amphibole-bearing facies of Blatná s.s.) represent *cafemic* associations. The rest of the Blatná suite (biotite facies of the Blatná intrusion, Klatovy and Marginal) with the Sedlčany granite (Čertovo břemeno suite) are *alumino-cafemic*. The Požáry (Sázava suite) and Mrač (Blatná suite) intrusions, as well as the whole of the Říčany suite represent *aluminous* associations.

The B ($B = Fe + Mg + Ti$) vs. $Mg / (Fe + Mg)$ diagram of *Debon and Le Fort (1988)* is used to distinguish between ferriferous and magnesian associations [Fig. IV.1.13.]. Amongst the rocks of the CBP, the majority of the Sázava suite is an example of a ferriferous association, whereas the rest of the rock types plot clearly above the dividing line in the magnesian associations field. In particular, the Čertovo břemeno suite has a high $Mg / (Fe + Mg)$ ratio.

The Q - B - F and K / (Na + K) - B plots serve for the further classification of aluminous associations [Figs IV.1.14.-15.]. The Q - B - F plot expresses the balance of dark minerals, feldspars ($F = 555 - (Q + B)$) and quartz. Additionally, five subtypes are distinguished according to the A parameter ($A = Al - (K + Na + 2 Ca)$; Appendix III.): very low aluminous ($A < 10$), low aluminous ($10 \leq A < 20$), moderately aluminous ($20 \leq A < 40$), high aluminous ($40 \leq A < 60$) and very high aluminous ($A \geq 60$). The Požáry and Nečín intrusions (Sázava suite) are quartz-rich, mesocratic to subleucocratic, sodic and very low to moderately aluminous. The Mrač granite (Blatná suite) is quartz-rich, mesocratic, and highly aluminous. The Říčany suite is quartz-poor, mainly subleucocratic, or leucocratic (the Jevany intrusion), potassic to sodi-potassic (the Říčany intrusion) or sodi-potassic to sodic (the Jevany intrusion), and mainly moderately aluminous.

The alkali balance is evaluated by the comparison with the model compositions presented in the Table 1 of *Debon and Le Fort (1988)*. This comparison has been summarised, along with the overall result of *Debon - Le Fort's* classification applied to the granitoids of the CBP, and given in the following table.

Cafemic associations		
Sázava	Tholeiitic ?	Ferriferous
Kozárovce	Calc-alkaline	Magnesian
Čertovo břemeno	Light subalkaline potassic	Magnesian
Tábor	Light subalkaline potassic	Magnesian
Blatná (amph-bearing) and Červená	Calc-alkaline	Magnesian

Alumino-cafemic associations				
Blatná (biotite facies)	Calc-alkaline		Magnesian	
Klatovy	Calc-alkaline		Magnesian	
Marginal	Calc-alkaline		Magnesian	
Sedlčany	Light subalkaline potassic		Magnesian	
Aluminous associations				
Požáry & Nečín	Sodic	Quartz-rich	Mesocratic-subleucocratic	Very low-moderately aluminous
Mrať	Potassic	Quartz-rich	Mesocratic	Highly aluminous
Říčany	Potassic	Quartz-poor	Subleucocratic	Moderately aluminous
Jevany	Sodipotassic	Quartz-poor	Leucocratic	Moderately aluminous

IV.2. Trace elements

This section starts with a brief description of the changes in trace element concentration during the course of fractionation (with SiO_2 used as a fractionation index). After that, the inter- and intra-suite variations in trace element abundance are demonstrated. This section is subdivided according to different trace element groups (LILE, HFSE, transition metals, REE). The corresponding data are in Appendices III. and IV.

IV.2.1. Bivariate plots with SiO_2

The bivariate plots with SiO_2 as the abscissa are used to demonstrate the variations of trace element concentration with fractionation of individual rock suites [Figs IV.2.1-IV.2.4.]. The plots for the Sázava suite show positive correlations between SiO_2 and Rb, Ba, Zr and La, as well as a good negative correlation with Y [Fig. IV.2.1.]. The Blatná suite exhibits negative correlations especially between SiO_2 and Sr, Ba, Cr and Ni, and positive correlation of SiO_2 with Rb [Fig. IV.2.2.]. The Čertovo břemeno suite is characterised by strong negative correlations between SiO_2 and Sr, Ba, Cr, Co and, to some extent, also Zr and Ce [Fig. IV.2.3.]. In the Říčany suite, there is a broad trend of decreasing Sr (except Jevany intrusion), Zr, La, Ce and Th as well as increasing Rb with SiO_2 [Fig. IV.2.4.].

IV.2.2. Inter- and intra-suites variation of the trace elements

The main statistical characteristics of the trace element distribution are presented in the form of box and whiskers plots [Fig. IV.2.5.]. The box represents 50 % of the population, the horizontal line inside it is the median. With help of this plot, it is very simple to visualise the shape of the distribution. The Sázava suite (Sázava s.s., Požáry and Nečín intrusions) typically has relatively high Sr and Y (except for Požáry and Nečín), and low Ba, Rb, Zr, Nb, La, Ce and Cr contents. The Blatná suite has high Y and low Ce, whereas its Ba, Rb, Zr, La, Cr and Nb are intermediate. The Čertovo břemeno suite has high contents of Rb, Zr and Cr; within this suite, the Tábor intrusion is characterised by high Ba, Sr, La and Ce that are generally intermediate in the Čertovo břemeno suite. The Říčany suite is characterised by high Rb, Sr (Jevany) and Zr (Říčany s.s.) but low Ba, Cr, La, Ce and Y.

Large Ion Lithophile elements (LILE)

The Rb-Sr plot shows the variation in Rb content between the various rock suites, especially the low contents of the Sázava and Blatná suites, which provide a good discriminating tool for these suites [Fig. IV.2.6.]. The approximate ranges of the Rb and Sr concentrations are:

- *Sázava suite*: 30 - 90 ppm and 200 - 600 ppm, respectively
(without the Nečín intrusion, the Sr range is 380 - 600 ppm),
- *Blatná suite*: 130 - 220 ppm and 180 - 520 ppm
(Kozárovice, Blatná and Červená themselves have a Sr concentration range of 340-520 ppm),
- *Čertovo břemeno and Říčany suites*: 210 - 440 ppm and 190 - 500 ppm
(the Jevany granite overlaps the boundary with the Blatná suite due to its higher Sr concentration of 500 - 740 ppm and lower Rb concentration of 190 - 260 ppm).

Some of the Rb - Sr correlation trends will be discussed later [Chapter IV.3.] as they are of petrogenetic importance.

On the K-Rb plot, the granitoids show a progressive increase in both K and Rb in the succession of Sázava - Blatná - Čertovo břemeno - Říčany suites [Fig. IV.2.7.]. The K/Rb ratio decreases in the same direction. Thus the average K/Rb ratio of the Sázava suite rocks is about 250 - 200, whereas that of the Říčany suite is between 100 - 150 (*cf. Minařík et al., 1979*).

There is also striking inter-suite difference in the Cs content which is generally low for the Sázava and Blatná suites but high for both the Čertovo břemeno and Říčany suites [Appendix V.] (*cf. Minařík et al., 1979; Bouška et al., 1984*). Likewise, based on the K/Rb, and Ba/Cs ratios that are indicative of geochemical differentiation, *Minařík et al., (1979)* have distinguished two groups of rock in the CBP: (1) Sázava and Blatná suites (Ba/Cs > 100), (2) Čertovo břemeno and Říčany suites, leucogranites (Ba/Cs < 100). The strong correlation between Cs and K₂O in the rocks of the CBP has been noticed by *Vejnar (1974 b)*.

High Field Strength elements (HFSE)

The granitoids of the Sázava suite have low concentrations of HFSE except Y [Tab. IV.1.], especially of Ta and Nb [Fig. IV.2.8 b]. Such a depletion in Ta, Nb (and Ti) is typical of volcanic arc settings, as these elements are thought to be retained by secondary titanites in the subducted slab (*Saunders et al., 1991; Foley and Wheller, 1990*). The significance of this so-called TNT (Ti - Nb - Ta) anomaly will be discussed further in the section on the geotectonic setting [Chapter IV.4.]. The Blatná suite has higher HFSE concentrations than the Sázava suite, although there is some overlap. The Čertovo břemeno suite has the highest HFSE concentrations among the samples studied; in particular, its Zr content is very high (up to 410 ppm; Fig. IV.2.8 a), but Y is intermediate between the Sázava and Blatná suites on the one hand, and the Říčany suite on the other hand. The HFSE content of the Říčany suite is transitional between that of the Blatná and Čertovo břemeno suites (for the Říčany granite s.s.) but its Y is very low. The Jevany intrusion is close to the Blatná suite in terms of the HFSE signature. Generally speaking, both Zr and Nb contents increase successively in the Sázava → Blatná → Říčany → Čertovo břemeno suites [Figs. IV.2.8 a-b].

Important constraints on the behaviour of accessory zircon during the crustal anatexis are provided by the zircon saturation model of *Watson and Harrison (1983)*:

$$\ln D_{\text{Zr}}^{\text{zircon/melt}} = -3.8 - 0.85 (M - 1) + \frac{12900}{T}$$

Where: $D_{\text{Zr}}^{\text{zircon/melt}}$ = concentration ratio of Zr in the stoichiometric zircon to that in the melt

T = absolute temperature M = cation ratio $\frac{(\text{Na} + \text{K} + 2 \text{Ca})}{(\text{Al} + \text{Si})}$

This equation can be used to calculate a zircon saturation temperature, provided there is no relict zircon present (no inheritance) and that the source was capable of providing sufficient Zr to saturate the melt. Besides that, the likelihood of the presence of inherited zircon cores could be assessed, which is an information important for the U - Pb geochronology (*e.g. Pidgeon and Aftalion, 1978; Chappell et al., 1987; Paterson et al., 1992 a,b*). It is also possible to constrain the Zr concentration of the source rocks, prior to and after the melt extraction. Schematically this approach is shown by Figure IV.2.9. from *Watson and Harrison (1984)* who have distinguished two cases, with the Zr concentration of the source higher and lower, respectively, than the calculated saturation level. In the first case, the melt is saturated in Zr throughout the melting event, and its Zr content is buffered at a constant level, independent of the degree of melting; the amount of Zr retained by the residuum increases with increasing degrees of partial melting. In the second case, however, the melt is saturated in Zr only for a limited time span until the Zr in the source is exhausted, and, as a consequence, the melt extracted becomes gradually more and more Zr-depleted.

The results of calculations are presented in Table IV.2. The Zr concentration in the stoichiometric zircon was assumed to be 49.8 %, and both the expected Zr concentrations at 750 °C and saturation temperatures corresponding to the observed Zr concentration are given. The temperature 750 °C has been chosen as it corresponds to the granite minimum in the water-saturated granite system (at 8 kbars) and that magmas much colder than that are unlikely to reach shallow crustal levels as they tend to crystallize en route (*Whitney, 1988*). For the Sázava intrusion and the associated basic rocks, as well as the Lučkovice monzonite, the actual Zr content is much lower than the calculated saturation level at 750 °C. Moreover, much higher liquidus temperatures are expected for tonalites (~ 1100 °C at 2 % water content; *Pitcher, 1993*). Thus, these granitoids were unlikely to have been saturated in Zr at higher degrees of partial melting and this is supported by the incompatible behaviour of Zr in the Sázava suite [Fig. IV.2.1.]. This has two important consequences: (1) their sources were Zr-poor, and therefore all the Zr was probably exhausted during the melting, resulting in an essentially Zr-free residuum, and (2) no zircon inheritance is likely to be encountered in these intrusions.

The calculations on the majority of the Blatná suite (Blatná s.s., Kozárovce, Červená, Klatovy and Marginal), as well as the Jevany leucogranite (Říčany suite) yield saturation temperatures that may correspond to the temperatures at the peak of anatexis, but caution should be exercised in their interpretation. For instance, the settling of zircon crystals may dramatically change the Zr concentration of both melt and cumulates, as may both assimilation and hybridization processes. The accessory phases could also be physically isolated from the melt as inclusions within a residual major mineral, although this process has been shown to be relatively unimportant in granite petrogenesis (*Watson et al., 1989*). As suggested by the Zr saturation calculations, these granitoids may contain only little of an inherited zircon component. The Mrač granite shows much higher Zr saturation temperatures that may point to the presence of a significant inheritance or to a higher temperature of the parental magma. The remaining intrusions, especially Čertovo břemeno, Tábor, and Říčany, have been saturated in Zr throughout their crystallization history, as this element behaves compatibly [Figs. IV.2.3.-IV.2.4.], as

an essential structural constituent (ESC; cf. *Evans and Hanson, 1993*). These intrusions may contain zircons with a relatively high proportion of inherited component, as indicated by their high Zr. This is indeed the case for both Čertovo břemeno and Sedlčany zircons (*J. Košler, pers.com., 1994*). Alternatively, temperatures of parental magmas of these intrusions had to be significantly higher than 800 °C.

Transition metals

Figures IV.2.8 c-e show that the Sázava suite is characterised by low contents of transition metals (cf. *Bouška et al., 1984*), in particular Cr and Ni. Relatively low Ni and Cr of the basic rocks associated with the Sázava suite is particularly diagnostic and has been explained by late recrystallization processes (*Vejnar, 1974b*). On the other hand, the basic rocks are characterised by high Co and Sc (*Bouška et al., 1984*) [Fig. IV.2.8 e]. The concentration of Ni in the Blatná suite is generally comparable with that of the Sázava suite, although it is much higher in the Lučkovice monzonite. Likewise, Cr and Co tend to be rather low, except for some of the monzonitic rocks. The Čertovo břemeno suite is characterised by high contents of all transition metals, most notably Cr and Ni, whereas Co and Sc are somewhat lower than in the Sázava suite (*Bouška et al., 1984*). The Říčany suite is poor in all transition metals (Cr, Ni, Co, Sc; cf. *Bouška et al., 1984*).

Rare Earth Elements (REE)

The Rare Earth Element concentration data and values normalised by the CI chondrite (*Boynton, 1984*) are given in Appendix V, and are plotted on Figures IV.2.10. and IV.2.11. Note that Eu^* is a value extrapolated between Sm_N and Gd_N :

$$\log(Eu^*) = \frac{(\log Sm_N + \log Gd_N)}{2}$$

$$Eu^* = \sqrt{Sm_N \cdot Gd_N}$$

Thus, the Eu / Eu^* ratio is proportional to the magnitude of the Eu anomaly; this is said to be positive if $Eu / Eu^* > 1$. The symbol used for the total REE concentration is ΣREE .

Sázava suite

In the Sázava suite [Fig. IV.2.10 a], the Sázava intrusion has $\Sigma REE \sim 100 - 150$ ppm (samples Sa-4 and Sa-7), but the Požáry samples (Po-1 and Po-4) have significantly lower ΣREE of $\sim 40 - 85$. The sample Sa-4 with its negative Eu anomaly ($Eu / Eu^* = 0.7$) differs from the others, which show a coupled decrease in ΣREE and increase in the magnitude of the *positive* Eu anomaly. Thus the sample Sa-4 of the Sázava intrusion has $Eu / Eu^* = 0.7$, whereas the Požáry trondhjemite (sample Po-1) has $Eu / Eu^* = 3.1$. The Teletín quartz diorite SaD-1 shows no Eu-anomaly at all. The Požáry samples have U-shaped REE patterns, and are more LREE enriched ($Ce_N / Yb_N = 15 - 16.6$) than Sázava s.s. ($Ce_N / Yb_N = 4.5 - 7.2$).

Blatná suite

The Kozárovice intrusion (Kozárovice granodiorite: samples Koz-2 and Koz-6, Těchnice granodiorite: Koz-12, Kozárovice quartz monzonite: KozD-1) shows very limited variation in REE abundance with $\Sigma REE \sim 150$ ppm; all patterns have a slight negative Eu anomaly ($Eu / Eu^* \sim 0.8$), as well as only limited enrichment of LREE over HREE ($Ce_N / Yb_N = 10$) [Fig. IV.2.10 b]. A similar

pattern at higher total REE concentration ($\Sigma\text{REE} = 230$ ppm) is shown by the Zalužany monzonite (Zal-1). However, the sample of Zalužany monzonite (10A) analysed by *Bowes and Košler (1993)* had significantly lower ΣREE of 164 ppm.

The Lučkovice monzonite [Fig. IV.2.10 b] has $\Sigma\text{REE} \sim 150$ ppm, a slight negative or no Eu anomaly at all ($\text{Eu} / \text{Eu}^* = 1.0$ for Gbl-1 and 0.8 for Gbl-2) and low LREE enrichment ($\text{Ce}_\text{N} / \text{Yb}_\text{N} = 9.9$ and 7.1 respectively). The Lučkovice sample (11C) of *Bowes and Košler (1993)* had higher total REE content ($\Sigma\text{REE} = 220$ ppm) as well as slightly higher magnitude of the Eu anomaly ($\text{Eu} / \text{Eu}^* = 0.7$).

The overall affinity of the Mrač granite to the Blatná suite is confirmed by its REE pattern [Fig. IV.2.10 b; Mrc-1]: $\Sigma\text{REE} \sim 150$ ppm, $\text{Eu} / \text{Eu}^* = 0.6$, $\text{Ce}_\text{N} / \text{Yb}_\text{N} \sim 17$.

The Blatná intrusion possesses variable ΣREE of 154 - 244 ppm; the Červená granodiorite (Cv-1) and samples of the amphibole - biotite facies of Blatná s.s. (Bl-2, Bl-7, Bl-8) are generally significantly richer in the REE [Fig. IV.2.10 c]. A negative Eu anomaly is well developed ($\text{Eu} / \text{Eu}^* = 0.5$ for Cv-1, and $\text{Eu} / \text{Eu}^* = 0.7$ for the rest of the samples). The LREE / HREE ratio is low ($\text{Ce}_\text{N} / \text{Yb}_\text{N} \sim 10$) with exception of the sample Bl-2 ($\text{Ce}_\text{N} / \text{Yb}_\text{N} = 23.2$).

Čertovo břemeno suite

The Sedlčany granite (Se-1, Se-5, Se-9) is characterised by high abundance of REE ($\Sigma\text{REE} \sim 215$ ppm), a negative Eu anomaly ($\text{Eu} / \text{Eu}^* = 0.7$) and a slightly higher enrichment of LREE over HREE ($\text{Ce}_\text{N} / \text{Yb}_\text{N} \sim 13$) than the Blatná suite [Fig. IV.2.11 a].

The durbachite of the Čertovo břemeno intrusion (mafic facies, Cb-3) exhibits both higher ΣREE (274 ppm) and LREE enrichment ($\text{Ce}_\text{N} / \text{Yb}_\text{N} = 13.6$), but only a slight negative Eu anomaly ($\text{Eu} / \text{Eu}^* = 0.8$). The REE patterns of this sample and the minette (Mi-1) are virtually identical [Fig. IV.2.11 a].

The Tábor syenite (Ta-1) has the highest total REE among the rocks studied ($\Sigma\text{REE} = 300$ ppm), a relatively steep REE profile ($\text{Ce}_\text{N} / \text{Yb}_\text{N} = 15.5$), and a negative Eu anomaly ($\text{Eu} / \text{Eu}^* = 0.7$) [Fig. IV.2.11 b]. *Bowes and Košler (1993)* have published three REE analyses from the Tábor intrusion, of melasyenite, syenogabbro and biotitite. The melasyenite showed the same magnitude of Eu anomaly as Ta-1, but lower ΣREE of 240 ppm; the syenogabbro had no Eu anomaly, being possibly the least influenced by the fractional crystallization processes. In contrast, the biotitite possessed a very pronounced negative anomaly ($\text{Eu} / \text{Eu}^* = 0.3$). The REE patterns are less steep ($\text{Ce}_\text{N} / \text{Yb}_\text{N} \sim 13$ for the melasyenite and biotitite, and about 10 for the syenogabbro). The ΣREE of biotitite is very high ($\Sigma\text{REE} = 375$ ppm).

Říčany suite

The relatively low but variable REE content (ΣREE 80 to 153 ppm) of the Říčany granite (Ri-1, Ri-2, Ri-5, Ri-6) is possibly related to the relative scarcity of accessory phases which are the main contributors to the whole rock REE budget [Fig. IV.2.11 c.] (*Fourcade and Allègre, 1981; Gromet and Silver, 1983; Sawka, 1988*). This granite has a variable magnitude of the Eu anomaly ($\text{Eu} / \text{Eu}^* = 0.7 - 0.9$) and among the other granitoid types the highest LREE enrichment (up to $\text{Ce}_\text{N} / \text{Yb}_\text{N} = 20$) and the lowest content of HREE. The sample of the Jevany leucogranite (Je-3) has low $\Sigma\text{REE} = 55$ and a slight positive Eu anomaly ($\text{Eu} / \text{Eu}^* = 1.2$).

The overall differences in the REE distribution between the Blatná, Čertovo břemeno and Říčany suites compared to an analysis from the Sázava intrusion (Sa-4) can be seen from Figure

IV.2.12. and Table IV.3. The REE patterns of the granodiorites of the Blatná suite are steeper than those from the Sázava suite with higher LREE and lower HREE contents. The Kozárovec granodiorite tends to have lower LREE and higher HREE than Blatná s.s., although there is considerable overlap. Likewise, the analyses of the Čertovo břemeno suite show higher LREE and lower HREE than the Sázava sample, resulting in higher LREE / HREE enrichment. The patterns of the Říčany suite, and that of the Jevany granite in particular, are strongly depleted in the HREE compared to Sa-4. The Σ REE of the Říčany suite is significantly lower than that of the Blatná and Čertovo břemeno suites, and the Říčany REE patterns are characterised by an extreme LREE / HREE enrichment. This trend of increasing LREE / HREE ratio in the succession Sázava - Blatná - Čertovo břemeno - Říčany suites has also been reported by *Bouška et al. (1984)*.

IV.3. Petrogenetic constraints based on whole-rock geochemistry

The causes of the geochemical variation within each distinct suite are now assessed using major and trace element modelling.

The major element modelling is based on the general least-squares mixing equation of *Bryan et al. (1969)*. The calculations were performed by the *MacGPP* package (version 2 for Macintosh) of *Geist and McBirney (1992)*. Those oxides which were not determined or which had very low concentrations in all the studied minerals and rocks (MnO and P₂O₅) were omitted; total iron content (Fe₂O₃*) was used instead of the separate FeO and Fe₂O₃. Typical mineral analyses for each particular intrusion were chosen; the choice of whole-rock end-members was based on the Harker plots [Figs IV.1.3 - 6.] and the R₁ vs. R₂ plot [Fig. IV.3.1.] of *De la Roche et al. (1980)* and *Batchelor and Bowden (1985)*. In the least-squares calculations, the percentage of the individual minerals has a positive value, if added to the parental magma (crystal accumulation and, or assimilation), and a negative one, if removed from it (fractional crystallization). The quality of the model is assessed by the sum of squares of the residuals (R²), with R² = 0 for the ideal fit; R² < 1 considered to be acceptable. It is worth noting, that the quality of the fit depends also on the number of suspected fractionating minerals, as the more phases that are involved in calculations, the better the fit tends to be.

As a next step, LILE data were used to verify the feasibility of the major-element based model. The Rb - Sr - Ba data were plotted in logarithmic co-ordinates, so that exponential fractional crystallization trends converted into linear ones.

According to the Rayleigh law (*Hanson, 1978*):
$$\frac{C_L}{C_0} = F^{(D-1)}$$

$$\log(c_L) = \log(c_0) + (D - 1)\log(F)$$

where: F = the fraction of melt remaining in the system, c_0 = original concentration of a trace element, c_L = concentration of this element in the fractionating melt, and D = bulk partition coefficient.

In all diagrams, the vectors corresponding to the shift in the liquid composition following 10 % fractionation ($F = 0.9$) of the main rock-forming minerals, as well as of assemblages corresponding to the major-element models, are plotted. Wherever applicable, REE were also utilised to further test the petrogenetic model. The partition coefficients are listed in Table IV.4. (mainly from *Hanson, 1978* for LILE and both *Henderson, 1982* and *Sawka, 1988* for REE) Some of the plotting was done by the programme *NewPet* by Dr. Daryl Clarke, Memorial University, Newfoundland.

Wherever, as an alternative, the magma-mixing scenario is invoked, it is verified by the mixing test (*Fourcade and Allègre, 1981; Castro et al., 1990a*). Its principle is that the samples related by magma mixing should plot on a straight line in a diagram of $c_a - c_b$ versus $c_h - c_b$ [e.g. Fig. IV.3.2.] (c_a : % oxide in the acid end-member, c_b : % oxide in the basic end-member, and c_h : that in the hybrid) with the slope being equivalent to the proportion of the component *a*. The theoretical proportions obtained in this way are then tested on trace element data by comparison of calculated and observed trace-element contents of the suspected hybrid (*Castro et al., 1990a*).

IV.3.1. The Sázava suite

The Harker plots for the Sázava suite [Fig. IV.1.3.] show a negative correlation of SiO₂ with Fe₂O₃*, MgO, CaO and TiO₂ and a positive correlation with Na₂O and K₂O. This is compatible with fractionation dominated by amphibole and (calcic) plagioclase. A major role for biotite and K-feldspar fractionation is unlikely in view of the positive correlation between SiO₂ and K₂O, Rb and Ba [Figs IV.1.3., IV.2.1.], as well as the low modal proportion of K-feldspar in the Sázava intrusion [Tab. II.1.] and its late position in the mineral succession (forming interstitial crystals: Chapter II.1.). The importance of amphibole crystallization is further substantiated by decreasing Σ REE with fractionation (Sa-4, Sa-7, Po-4; Fig. IV.2.10 a) and the compatible behaviour of Y as seen on the SiO₂ - Y plot [Fig. IV.2.1.]. Moreover, the trend of the Sázava intrusion in the R₁ vs. R₂ diagram [Fig. IV.3.1.] is compatible with largely amphibole crystallization, together with fairly calcic plagioclase and a minor contribution from biotite and K-feldspar.

The aim of the major element modelling was to find out what fractionating assemblage would drive the melt composition from silica-poor samples of the Sázava intrusion (Sa-4) to the more silicic ones (Sa-11), and to check whether the Požáry magma could have been derived from the Sázava parent solely by fractional crystallization. The results of the least-squares modelling [Tab. IV.5. A] show, that the composition similar to Sa-11 could be produced from Sa-4 by extensive (84 %) fractionation of amphibole (50 %), calcic plagioclase (An₅₄; 42 %) and biotite (6 %) with a negligible proportion of K-feldspar (2.5 %). The fit of the model is good ($R^2 = 0.23$) and the output is almost identical with that produced with an arbitrarily chosen sample from the middle of the silica range (Sa-12). The latter model required 69 % fractionation of 52 % amphibole, 43 % plagioclase and 5 % biotite ($R^2 = 0.76$; not shown).

The degree of fractionation may be estimated independently using a strongly incompatible element (i.e. if $D \sim 0$; e.g. *Rollinson, 1993*)

$$\frac{c_L}{c_0} \sim \frac{1}{F}$$

where: c_L = concentration of a trace element in melt, c_0 = initial concentration of this element in melt, F = fraction of the melt remaining.

In the Sázava intrusion, such incompatible behaviour is shown particularly by Ba [Fig. IV.2.1.] For the current models, the degree of fractionation calculated is 74 % and 62 %, respectively; this is comparable with figures derived from major-elements (84 % and 69 %).

The fractionation from the silica-rich end of the Sázava array (Sa-11) to the silica-rich Požáry sample (Po-5) is shown by the trend B [Tab. IV.5.]. Although the fit is not particularly good ($R^2 = 0.87$), the model suggests 32 % fractionation of equal amounts (41 %) of plagioclase (An₃₆) and amphibole, with 17 % of biotite. The calculated Na₂O is too high and CaO too low, possibly as a

consequence of choosing too calcic a composition for the plagioclase; however, more sodic plagioclase is not common in the Požáry intrusion [Chapter III.1.3.]. A Zr-based (incompatible in the Požáry intrusion; cf. Fig. IV.2.1) estimate of the degree of fractionation is 54 %, being significantly higher than the result of the least-squares modelling (32 %) which could point to non-ideality of its behaviour, or to the presence of cumulative zircon in the Požáry rocks. However, no other trace element can be used instead as the others all show compatible or less incompatible behaviour [Fig. IV.2.1].

On the basis of structural evidence [Chapters II.1-II.2.] it was argued that the sample Po-1 from the Požáry trondhjemite had possibly originated by plagioclase accumulation. Its biotite is similar in composition to that of the Sázava mass, rather than to biotite of the Požáry intrusion proper [Chapter III.1.3.], and this sample is displaced from others on many plots [e.g. Fig. IV.1.2., IV.3.1.]. If this is the case, it could have originated from two possible parents, either the Požáry trondhjemite or the SiO₂ rich members of the Sázava intrusion (like Sa-11; Fig. IV.1.3.). As there are REE data available for sample Po-4, it has been chosen as a parental composition for the major-element based modelling [Tab IV.5 C]. The model (with a reasonable fit, $R^2 = 0.64$) implies 72 % accumulation of mainly plagioclase (87 %), with minor contributions from biotite (7 %) and K-feldspar (6 %). There is a striking similarity between the calculated composition of the cumulate and the actual modal percentage of Po-1 recalculated to 100 % without quartz (plagioclase 88.7 %, K-feldspar 5.9 % and biotite 5.3 %; cf. Tab. II.1.). The least-squares modelling with Sa-11 as parent also resulted in a good fit for an assemblage of 78 % plagioclase, 11 % K-feldspar and 11 % quartz ($R^2 = 0.56$) [Tab IV.5 D].

The granitoids from localities in the western part of the Sázava body (Teletín, Krhanice and Prosečnice), and from the Požáry intrusion, have suffered considerable hydrothermal alteration, as shown by optical microscopy and CL [Chapter II.2.]. These rocks are therefore not the best candidates for trace element modelling, especially not using highly-mobile elements like Rb, and so the LILE-based approach was therefore not applied.

In contrast, the REE are thought to be fairly resistant to the hydrothermal alteration (Hanson, 1980) although some authors warn against indiscriminate use of the REE in petrogenetic modelling, as REE appear to be mobile in the form of complexes, especially in F- and CO₂-rich fluids (Humphris, 1984). The extent to which the REE patterns will be influenced is principally a function of the composition of the rock, the fluid, and the ability of the secondary minerals to accommodate the REE released by alteration. As none of the rocks of the Sázava suite contains significant amounts of fluorite, the major involvement of F-rich fluids in its genesis can be ruled out. In contrast, the presence of secondary calcite confirms the role for CO₂-rich fluids. Yet petrogenetic information may be recovered from the REE data, provided the alteration was not very severe (Hanson, 1980). The development of a positive Eu anomaly in samples Po-1 and Po-4 [Fig. IV.2.10 a], unique in the CBP, may be connected with one of the following processes (Cullers and Graf, 1984) :

- Plagioclase accumulation;
- Rayleigh fractional crystallization of a hornblende-dominated assemblage;
- Partial melting with hornblende as a residual phase.

The *average* trace-element composition of the cumulate for Rayleigh crystallization is:

$$C_{s,a} = C_o \frac{1-FD}{1-F} \quad (\text{Haskin, 1984}).$$

The hypothesis formulated earlier in the text that the sample Po-1 could have been produced from Po-4 by extensive accumulation of 87 % plagioclase, 7 % biotite, 6 % K-feldspar was tested by REE modelling based on this equation [Fig. IV.3.3 a]. The calculated REE patterns, after up to 90 % accumulation, show a good fit for the LREE, but the HREE are too depleted and the Eu anomaly is too high. If, however, limited accumulation of accessory phases, which strongly fractionate mid- and heavy REE is invoked (0.1 % zircon and 0.3 % apatite), the fit of the data is reasonable and the cumulative origin of Po-1 from the Požáry trondhjemite cannot be discounted. The REE modelling of accumulation from the Sázava parent could not be performed, as there are no REE data available for Sa-11. However, if its REE pattern showed higher Σ REE and a lower positive (or even negative) Eu anomaly than Po-4, then the fit of the REE modelling would tend to be better.

In contrast to Po-1, sample Po-4 does not exhibit textural and chemical characteristics compatible with a (largely) cumulative origin [Chapter II.2.] and its Eu anomaly is only slightly smaller ($\text{Eu} / \text{Eu}^* = 2.0$). The purely cumulative origin of the Požáry trondhjemite (apart from Po-1) from the Sázava magma is unlikely, as it would require the fractional crystallization of the Sázava magma to be driven towards less silicic compositions [cf. IV.1.3.]. If the cumulates were to have a chemical composition similar to the Požáry samples, the fractionating assemblage would have to have a high quartz content as the Požáry trondhjemite is more silica-rich than its feldspars. This necessity of early crystallization of a plagioclase - quartz assemblage without a significant proportion of amphibole, together with the observed absence of amphibole in the Požáry trondhjemites, is not in accord with evidence of simultaneous crystallization of plagioclase and amphibole in the Sázava intrusion [Chapter II.1.] and does not seem likely in a tonalitic liquid. This is not to deny a role for plagioclase accumulation in the Sázava suite.

Concerning the fractional crystallization model, the crystallizing assemblages calculated on the basis of the major elements have a high proportion of amphibole. The decreasing Σ REE and Y contents with fractionation in the Sázava suite also imply a major role for either amphibole or some accessory mineral-controlled fractional crystallization, as only these phases have partition coefficients for REE generally higher than 1. As shown by the REE modelling [Fig. IV.3.3 b], 30 - 50 % of amphibole-dominated (54 % amphibole, 40 % plagioclase, 6 % biotite; i.e. an assemblage similar to that calculated from major elements; cf., model A) fractionation produces REE patterns similar to the Požáry samples, but only for REE from Eu to Yb (HREE). Conversely, no LREE depletion (relative to the parent), similar to that observed for the Požáry trondhjemite, could result from fractional crystallization of hornblende only [Fig. IV.3.3 b]. For this reason, involvement of an additional phase, which strongly fractionated the LREE, is necessary (cf. *Martin, 1987; Evans and Hanson, 1993*). Such minerals are orthite and titanite (*Sawka, 1988*). Both of them do occur in the granitoids in question, and even their limited crystallization may cause drastic changes in the LREE / HREE ratio of magma. Addition of 0.1 % orthite to the fractionating assemblage dramatically improves the fit [Fig. IV.3.3 c]. If titanite were involved in the calculations, a much higher proportion would be needed (0.5 %) and a large amount of apatite (1 %) would need to be added to compensate for depletion in mid- and heavy REE [Tab. IV.4]. On this basis, the combined amphibole - plagioclase - orthite model is preferred, although some apatite had to fractionate to explain the gradually decreasing P_2O_5 with fractionation in the Sázava suite [Fig. IV.1.3.]. The origin of strikingly similar REE patterns of trondhjemites from Finland was also explained by fractional crystallization of amphibole > plagioclase and biotite assemblage from a tonalitic parent (*Arth et al., 1978*).

The partial melting of amphibolite, eclogite or garnet amphibolite is also capable of generating trondhjemites with low total REE contents, high LREE / HREE ratios and pronounced positive Eu anomalies because of presence in the residue of amphibole and, or garnet (*Cullers and Graf, 1984 and references therein*). The REE patterns observed for the Požáry samples resemble those modelled as melts of basaltic parents leaving an amphibolite residuum (*cf. Hanson, 1980, fig. 5*) although at somewhat higher ΣREE . They are also similar to the trondhjemite argued to have originated by small degrees of partial melting of amphibolite (*Rapp et al., 1991, fig. 6c*). The occurrence of the Sázava suite in the proximity of metabasites of both the Jílové Zone and Metamorphic Islet Zone [Chapter II.1.] may support an origin by melting similar rocks at depth. However, the uncertainties in partition coefficients, source composition, residual mineralogy and degree of melting make any quantitative modelling of partial melting process difficult (*cf. Arth et al., 1978; Rollinson, 1993*). The origin of the Požáry trondhjemite either by partial melting of a tholeiitic basalt or by fractionation of a hypothetical, K-poor magma, has been proposed by *Holub (1990)*. In his opinion, the Sázava magma could not have corresponded to the parental liquid for the fractionation model. However, in view of the modelling done earlier in this chapter, it may be a viable hypothesis.

Considerable microstructural and mineral chemistry evidence for the hybrid origin of the Teletín quartz diorite (SaD 1 - 3) has already been given [Chapters II.1., III.1.2.] and this hypothesis is now to be addressed by the mixing test for major elements (*Fourcade and Allègre, 1981; Castro et al., 1990a*). The model assumes an origin for SaD-2 by mixing of the Sázava tonalite (Sa-1) with a gabbro (Gbs-2). As there are few petrographic constraints on the composition of both end-members, the compositions on a straight line in the R_1 vs. R_2 plot [Fig. IV.3.1.] resulting in the best fit (regression coefficient, $R = 0.975$) were chosen. In this model, 84 % of the Sázava tonalite is required to be present in the mixture [Fig. IV.3.2 a]. General support for this model is given by the trace element data, although Zr and Ba are significantly higher in the quartz diorite than suggested by the modelling. However, the composition of the mafic end-member is not known exactly and it could even be some rock type which either does not crop out at all, or was not analysed. It ought to be stressed that the preceding modelling implies, rather than involvement of these particular end-members, the overall geochemical viability of the mixing scenario for the origin of the Teletín quartz diorite. Thus it is apparent from the R_1 - R_2 plot [Fig. IV.3.1.] that the acid end-member for two remaining samples (SaD-1 and SaD-3) appears to be closer to Sa-2 rather than Sa-1.

An analogous magma mixing origin for the whole compositional range of the Sázava intrusion does not seem to be feasible, as the associated basic rocks do not form a continuum with the Sázava samples [e.g. CaO, MgO; Fig. IV.1.3.; Cr, Y; Fig. IV.2.1.; B - Mg / (Mg + Fe) plot; Fig. IV.3.1.; R_1 - R_2 plot; Fig. IV.3.1.] or do not have low enough SiO_2 . The peraluminous nature of the Požáry trondhjemite can be readily accounted for by the fractional crystallization model, as this is an attribute typical of strongly fractionated granitoids of metaluminous suites that have crystallized a great proportion of a metaluminous mineral, such as amphibole (*Miller, 1985; Debon and Le Fort, 1988*). However, the peraluminous character may also point to genesis either by partial melting of amphibolite (due to reactions amphibole \rightarrow clinopyroxene + olivine + melt, and, or garnet \rightarrow clinopyroxene + melt; *Miller, 1985*), or by the operation of late alteration processes, responsible for the crystallization of peraluminous secondary minerals, such as muscovite [Chapter II.2.], but this is not considered being likely.

In summary, the derivation of the Sázava and Požáry granitoids is compatible with extensive fractional crystallization of an amphibole > plagioclase > biotite assemblage, with a minor proportion of orthite. An alternative hypothesis is partial melting of amphibolite or eclogite, with amphibole and, or, garnet in the residuum. In fact, both processes are not mutually exclusive, as shown by the study of *Martin (1987)* of tonalitic gneisses in Finland - following combined major and trace element modelling, the proposed genesis of these gneisses was by partial melting of tholeiitic garnet-bearing amphibolites, followed by fractional crystallization of amphibole, plagioclase, ilmenite and orthite. In the genesis of the Sázava suite, plagioclase accumulation (e.g. Po-1) and magma mixing (Teletín quartz diorite) are likely to have occurred on the basis of both the chemical and the petrographic evidence.

IV.3.2. The Blatná suite

If a fractional crystallization model is invoked, the Harker plots for the Blatná suite with strong negative correlations between SiO_2 and Fe_2O_3^* , MnO, MgO, CaO and TiO_2 imply fractionation dominated by ferromagnesian phase(s) and possibly plagioclase [Fig. IV.1.4.]. A major role for the K-feldspar and biotite does not agree with rather scattered SiO_2 - K_2O plot, which lacks a negative correlation, and by late crystallization of the K-feldspar in these granitoids [Chapters II.3.-II.4.]. On the other hand, some involvement of these phases is likely in view of the negative correlation between SiO_2 and Ba [Fig. IV.2.2.].

In order to specify the possible crystallizing assemblage and to quantify the degree of fractionation, least-squares modelling has been applied to the Kozárovice samples. The presumed parents, Koz-9 and Koz-1 with the lowest SiO_2 [Fig. IV.1.4.] and R_1 [Fig. IV.3.1.] values, might have evolved to the most silicic members (Koz-5 and Koz-8) by fractional crystallization of a mainly amphibole - plagioclase - K-feldspar assemblage with small contribution from biotite [Tab. IV.6.]. Thus, Koz-5 can be derived from Koz-9 by 39 % fractional crystallization of 47 % amphibole, 24 % plagioclase (An_{50}), 23 % K-feldspar and 6 % biotite ($R^2 = 0.45$) [Tab. IV.6 A]. The sample Koz-8 could have originated from the same parent by 33 % fractionation of 43 % amphibole, 26 % plagioclase (An_{50}), 23 % K-feldspar and 8 % biotite ($R^2 = 0.39$) [Tab. IV.6 B]. If more sodic plagioclase is involved in the calculations, the fit is not so good as the modelled daughter compositions become strongly Na_2O -depleted. If sample Koz-1 is invoked as a parent, comparable models with even better fits ($R^2 = 0.27$ and 0.20) result [Tab. IV.6 C, D]. The fractionating assemblage is analogous, and the required degree of fractionation consistent, in all four cases. Therefore, crystallization seems to have proceeded in the following succession (the degree of fractionation relative to Koz-9 is given in brackets): Koz-9 (0 %), Koz-1 (12 %), Koz-8 (33 %), Koz - 5 (~ 40 %).

In order to test the feasibility of the major-element models A - D, the corresponding vectors were plotted on the Ba - Sr diagram [Fig. IV.3.4 a]. All four modelled trends are subparallel and in good agreement with the data. In comparison with the major-element-based models, however, the appropriate degree of fractionation (up to ~ 25 % for the assemblage A) appears to be significantly lower in all the cases.

The Kozárovice REE patterns are very uniform, and, moreover, there is no information on the REE composition of presumed end-members [Fig. IV.2.10 b], so no quantitative REE modelling could be performed. However, if assemblage A is considered (for $F = 0.6$), the following values of the bulk distribution coefficient (D) are obtained: $D_{\text{La}} = 0.48$, $D_{\text{Ce}} = 0.79$, $D_{\text{Eu}} = 2.06$, $D_{\text{Lu}} = 2.88$, resulting in enrichment by about 1.1 - 1.3 x in the LREE and depletion by 0.6 - 0.4 x in mid- and HREE. This is

within the range of observed REE compositions for the Kozárove intrusion, and fractionation of such an assemblage would maintain an almost constant size of the Eu anomaly.

The strong linear correlation on the Harker plots for the Kozárove intrusion [Fig. IV.1.4.] may be compatible with the operation of another petrogenetic process, namely mixing (*e.g.* Castro *et al.*, 1990a). In the broad sense, it might represent mixing of magmas, restite unmixing, and, or, assimilation of the country rocks. Although, strictly speaking, the presence of linear trends on the Harker plots does not necessarily imply the involvement of mixing (Wall *et al.*, 1987), the magma mixing origin of at least the quartz monzonite from the quarry Kozárove II (KozD-1) by interaction between a monzonitic melt and the Kozárove granodiorite is likely because of the microstructural and field evidence [Chapters II.3.-III.1.5.]. On the Harker plots, KozD-1 often falls onto a straight line connecting the granodiorite samples with the monzonitic rocks (Zalužany, Zal-1, and Lučkovice, Gbl-1 and Gbl-2) [Figs. IV.1.4., IV.2.2.], but plots of SiO₂ versus K₂O, Rb, Zr, La, Ce and Ni suggest that the Lučkovice monzonite is the more likely end-member of the two. Thus, the parents chosen for the mixing test (Fourcade and Allègre, 1981; Castro *et al.*, 1990a) [Fig. IV.3.5 a-b] were the most silicic Kozárove granodiorite (Koz-5) and the Lučkovice monzonite (Gbl-1). The model fits very well the major elements ($R = 0.994$), suggesting that about 60 % of the granodiorite is necessary to be mixed with the monzonite to give the quartz monzonite [Fig. IV.3.5 a]. The trace element data, in general do not seem to contradict this hypothesis, either [Fig. IV.3.5 b], although the predicted contents of some of the compatible elements (Ni, Zn, Cu, Pb) and, to some extent, La and Y, are somewhat different from those observed. Nevertheless, the exact composition of the basic end-member is not known, and there is no information about variations of the suspected hybrid either, as only a single analysis is available. The elevated Zn, Cu and Pb contents in the sample could point to later hydrothermal activity, as these elements occur commonly in the hydrothermal fluids and the content of REE can be dramatically changed by a small-scale fractionation, especially of accessory minerals (*e.g.* Fourcade and Allègre, 1981; Sawka, 1988; Evans and Hanson, 1993).

As has been suggested on the basis of the textural evidence [Chapter II.3.], there is a possibility that the monzonitic magma (similar to the Lučkovice monzonite) also contributed to the genesis of the Kozárove granodiorite itself, at least in surroundings of the village of Kozárove. The mixing test (end-members Gbl-1 and Koz-5 as in the previous case, potential hybrids Koz-2 and Koz-4 from the Kozárove quarries closest to the occurrence of the hybrid quartz monzonite stock) fits well the major element ($R = 0.998$ and $R = 0.995$) as well as the trace element data [Fig. IV.3.5 c-d] requiring 88 % of the acid magma to be involved.

Although the evidence for wall-rock assimilation has been documented in the field, mainly in the northern part of the body (*e.g.* Šolopysky; Chapter II.3.) the great majority of the geochemical variation can be explained by other processes, namely fractional crystallization and magma mixing.

In summary, the variations in geochemistry of the Kozárove intrusion could have been caused by up to 40 % fractional crystallization of an amphibole-dominated (~ 40 - 55 %) assemblage, with about 25 - 30 % plagioclase, 15 - 25 % K-feldspar and 5 - 15 % biotite; the closest to the parental composition appears to be sample Koz-9 from northern part of the body. There is also a well-documented role of magma-mixing in the Kozárove intrusion, at least in genesis of quartz monzonitic (KozD-1), and arguably also of granodioritic rocks around the village of Kozárove.

Based on the field relations and geochemical affinities [Chapters II.4., IV.1.-IV.2.], the Červená granodiorite is likely to be an integral part of the Blatná intrusion, and so the possible genesis

of both Blatná (s.s.) and Červená granodiorites are examined together. For the least-squares modelling of fractional crystallization [Tab. IV.6 E-H] two SiO₂-poor end-members were chosen, one of Červená granodiorite (Cv-3) and one of an amphibole-bearing Blatná granodiorite (Bl-8); the most silicic samples Bl-4 and Bl-1 represent the end-products. If Cv-3 is used as a parent, sample Bl-4 can be produced by 36 % fractional crystallization of 52 % plagioclase (An₃₈), 31 % biotite and 17 % amphibole ($R^2 = 0.797$) [Tab. IV.6 E]. Similar cumulate mineralogy results from 32 % fractionation of Cv-3 to give Bl-1 (47 % plagioclase, 28 % biotite and 25 % amphibole) [Tab. IV.6 F] but the fit is better ($R^2 = 0.521$). K-feldspar appears unlikely to play a major role, as the models required only a negligible *positive* amount (assimilation or accumulation?) of K-feldspar, and, accordingly, its proportion has been set to zero. Calculations with Cv-1 as the parent were also performed, but they did not give reasonable fits, although they did allow for limited K-feldspar fractionation (7 - 9 %). For example, 34 % fractionation of 42 % plagioclase, 34 % amphibole, 16 % biotite and 9 % K-feldspar is needed to produce composition similar to Bl-1 from Cv-1 ($R^2 = 1.15$) [Tab. IV.6 G]. If an assemblage without K-feldspar is calculated (not shown), 30 % fractionation of 46 % plagioclase, 32 % amphibole and 22 % biotite is required. Although R^2 is too high (1.19), this assemblage, as well as the extent of fractionation is similar to the model involving Cv-3 [cf. Tab. IV.6 F].

Modelling of the genesis of Bl-4 from the amphibole-bearing Blatná granodiorite (Bl-8) [Tab. IV.6 H] is compatible with 25 % fractional crystallization of 45 % plagioclase, 40 % amphibole, 11 % biotite and 5 % K-feldspar ($R^2 = 0.232$). Sample Bl-1 could be modelled from the Bl-8 parent by 20 % fractionation of 33 % plagioclase, 60 % amphibole, 7 % K-feldspar and no biotite ($R^2 = 0.082$) [Tab. IV.6 I].

The Ba - Sr plot suggests that the assemblages H and I could not account for the variation observed within the Blatná suite [Fig. IV.3.4 b]. On the other hand, models E - G appear to be generally consistent with the Ba - Sr data, although the degree of fractionation estimated on their basis is lower than that calculated from major elements.

The fact that the REE patterns of the Blatná suite [Fig. IV.2.10 c] differ significantly between the amphibole-rich types (Cv-1 and Bl-8) and others in their total REE content, implies the necessity of fractionation of phases reducing the bulk REE, such as amphibole (*Haskin, 1984*). On the other hand, slight decrease in the depth of the Eu anomaly is consistent with a roughly balanced contribution of feldspar fractionation compared to that of the phases contributing to a positive Eu-anomaly (amphibole, clinopyroxene and apatite). Thus, if amphibole is to be a cumulus phase, its proportion should be slightly higher than about half that of plagioclase (*Hanson, 1980*). On this basis, model I with almost twice as much amphibole as feldspar appears to be unrealistic. However, models E (similar to F), H and I require to be tested quantitatively.

As there are no REE data available for Cv-3, the pattern for Cv-1 has been used instead for this modelling of fractionation of the Červená granodiorite. Although the fit of major-element models based on Cv-1 was not satisfactory, the degree of fractionation and the fractionating assemblages for both parents seem to be sufficiently close to allow such a replacement. The first model tested [Fig. IV.3.6 a] was Cv-1 producing Bl-4 by 30 - 40 % of fractionation of a plagioclase-dominated assemblage E [Tab. IV.6.]. Inevitably, an additional phase, which strongly fractionates the LREE has to be involved (cf. section on the Sázava suite); the most likely is orthite, a mineral that is present in the analysed rocks [Chapter II.4.]. After the introduction of 0.1 % orthite the model fits well [Fig. IV.3.6 a]. The following two models assumed the amphibole-bearing Blatná granodiorite as a parent and cumulate

with a much higher proportion of amphibole. The first of them [Fig. IV.3.6 b], involving 20 - 30 % fractionation of assemblage 'H' with 0.1 % orthite, fits reasonably at 20 % of fractionation, although the HREE appear to be too depleted by the abundant amphibole. Assemblage 'T' can produce REE patterns similar to the biotite facies of the Blatná intrusion at only very low degrees of fractionation (< 10 %; Fig. IV.3.2 c) as the negative Eu anomaly quickly disappears and reverses to a positive one due to the high proportion of crystallizing amphibole (60 %). The degree of fractionation in this case compares unfavourably with 20 % fractionation required by the least-squares model.

In addition to the above mechanisms, the role of country-rock assimilation in the history of the Blatná intrusion is unequivocal (Hudčice and Zavlekov localities; Chapter II.4.), but appears to be only of local importance.

In summary, the variation in the Blatná intrusion (Blatná s.s. and Červená granodiorites) could be explained by up to 35 % fractionation of mainly plagioclase (~ 45 - 50 %), amphibole (15 - 25 %), biotite (~ 30 %) and orthite (~ 0.1 %) from a parent similar to the Červená granodiorite.

One of the viable scenarios for the origin of the Blatná suite as a whole (Blatná s.s., Červená, Kozárovce s.s., Těchnice) may be mixing between a basic melt and a magma similar to the most silicic granodiorites of the biotite facies of the Blatná granodiorite. The relatively high K_2O [Fig. IV.1.9 b] as well as the low CaO [Fig. IV.1.9 a] and $Fe_2O_3^*$ of the Kozárovce and Blatná granodiorites imply that the mafic end-member in this process was K-rich, precluding a role for the Sázava mass or associated mafic rocks in the genesis of the Blatná suite. The most obvious candidate are the monzonitic rocks associated with the Kozárovce suite, notably the Lučkovice monzonite (Gbl-1). This model has been invoked already by Machart (1992), who has established 5 petrochemical types of granitoids within the Blatná suite based on cluster analysis of the major element data. He has stressed that the whole compositional spectrum of the Blatná suite could have originated by hybridization of a magma corresponding to the biotite facies of the Blatná intrusion by monzonitic rocks similar to the Lučkovice or Zalužany masses, possibly accompanied by limited contamination by metasediments of the Moldanubian Unit and, or the Metamorphic Islet Zone. Such a model could explain the linear trends on the Harker plots [Fig. IV.1.4], some binary SiO_2 - trace elements plots [Fig. IV.2.2.] and the R_1 - R_2 plot [Fig. IV.3.1.].

The results of the mixing tests performed on the Blatná suite (end-members: Gbl-1, Bl-1; cf. Fig. IV.3.1.) are given on Figure IV.3.5. e-p. The fits of major elements are good ($R^2 > 0.99$ in all cases). Thus, the Kozárovce quartz monzonite (KozD-1) can represent a mixture of about equal proportions of the granodiorite (56 %) and monzonite (44 %) [Fig. IV.3.5 e-f]. The samples Koz-2 and Koz-4 may contain 80 % of the acidic end-member [Fig. IV.3.5. g-h], whereas samples of the Těchnice granodiorite need about 85 % [Fig. IV.3.5 i-j]. With the exception of KozD-1 (Y, Ni, Pb, Cu), all the trace elements match satisfactorily the observed patterns. Based on the major element data, the least silicic samples of the Kozárovce granodiorite (Koz-1 and Koz-9) required 63 and 68 % of the acid end-member ($R^2 = 0.997$ in both cases) but the fit of trace elements, Zr and REE in particular, was poor (not shown). In the genesis of the least silicic sample of the Blatná intrusion (Cv-3 of the Červená granodiorite) about 75 % of the acidic end-member is required. The fit of both major [Fig. IV.3.5 k] and trace elements [Fig. IV.3.5 l] is excellent. The sample of amphibole-bearing Blatná (Bl-2) requires 80 % of the granodioritic component [Fig. IV.3.5 m]; however the LREE and Pb fail the test [Fig. IV.3.5 n]. Its REE pattern with a strong LREE enrichment [Fig. IV.2.10 c], is rather exceptional amongst the samples of the Blatná intrusion. The sample Bl-8 may contain 85 % of the acidic

component [Fig. IV.3.5 o], but the model does not fit well for Y, Pb and Rb [Fig. IV.3.5 p]. For both Bl-2 and Bl-8, however, subsequent fractionation may have altered the original abundances of some of the trace elements after the mixing took place. It is, however, significant that the great majority of the others is compatible with the test. Thus, the whole-rock geochemistry does not appear to be inconsistent with the magma mixing scenario; the main line of evidence, however, comes from the radiogenic isotopes as they are not influenced by crystal fractionation [Chapter V.3.], and so can potentially distinguished between open- and closed-system processes.

Another possibility, supported by presented modelling, is a combination of both scenarios. The Blatná suite may have primarily originated by magma mixing between monzonitic (similar to the Lučkovice monzonite) and granodioritic melts (close to the biotite facies of the Blatná intrusion). In this model the Kozárovec quartz monzonite would contain about 55 % of the acidic component, whereas the least evolved samples of the Kozárovec intrusion require about 65 % (?) and the Blatná intrusion 75 %. Subsequently, these hybrid parental magmas could have undergone fractional crystallization of 40 - 55 % amphibole, 25 - 30 % plagioclase, 15 - 25 % K-feldspar or 5 - 15 % biotite (Kozárovec intrusion) and of 15 - 25 % amphibole, 45 - 50 % plagioclase, ~ 30 % biotite and minor proportion of orthite (Blatná intrusion).

In summary, variation in the Blatná suite can be explained by magma mixing between monzonitic and granodioritic melts, or by closed-system fractional crystallization of amphibole > plagioclase + K-feldspar > biotite (Kozárovec) or plagioclase > biotite > amphibole > orthite (Blatná) assemblages. Also possible is a scenario involving both models. However, wall-rock assimilation seems to be only of a limited importance.

IV.3.3. The Čertovo břemeno suite

The subhorizontal trends for the Sedlčany intrusion on the Harker plots [Fig. IV.1.5.], especially SiO₂ versus TiO₂, Fe₂O₃, CaO and K₂O, do not allow for extensive fractionation of K-feldspar, biotite, amphibole, and calcic plagioclase. However, the negative correlation of SiO₂ with Ba and, to some extent, Rb and Sr [Fig. IV.2.3.] is compatible with limited fractionation of mainly K-feldspar and biotite. On the R₁ - R₂ plot [Fig. IV.3.1.], the Sedlčany samples form a prominent horizontal trend which may be due to fractionation of Fe-rich biotite, possibly with a significant contribution from K-feldspar and relatively sodic plagioclase; the Mg-rich nature of the Sedlčany biotite [Chapter III.1.7.], however, precludes fractionation controlled solely by this mineral.

For the major-element modelling, the SiO₂-poor samples Se-3 and Se-6 were taken as parents, and SiO₂-rich Se-11 and Se-12 as end-products [cf. Fig. IV.3.1.; Tab. IV.7 A-D]. The sample Se-12 can be modelled from Se-3 by 11 % fractional crystallization of 35 % plagioclase (An₄₂), 28 % K-feldspar, 22 % biotite and 15 % amphibole ($R^2 = 0.27$; Tab. IV.7 A). In contrast, modelling of Se-11 from Se-3 did not produce a good fit ($R^2 = 1.94$); in this case, the fractionating assemblage had higher proportion of plagioclase at lower proportion of K-feldspar [Tab. IV.7 B]. Modelling with Se-6 as a parent and Se-12 as a daughter resulted in a much better fit; it could have evolved by 14 % fractional crystallization of 34 % plagioclase, 35 % K-feldspar, 17 % biotite and 15 % amphibole to give a composition similar to Se-12 ($R^2 = 0.13$; Tab. IV.7 C), whereas Se-11 may be produced by 10 % fractionation of 45 % plagioclase, 31 % K-feldspar, 14 % amphibole and 10 % biotite ($R^2 = 0.65$; Tab. IV.7 D).

On the Rb - Sr plot [Fig. IV.3.7 a], the majority of samples (excluding two outliers) plot into two clusters: the lowest Sr values are shown by those from Vrchotovy Janovice; samples from Kosova Hora and Vápenice have gradually increasing Sr concentrations (i.e. in the Sedlčany body there appears to be a progressive increase in Sr westwards). All three trends (A, C and D) appear to disagree with the observed variation. However, on basis of the Ba - Sr plot [Fig. IV.3.7 b], none of the assemblages A, C, D can be rejected although the necessary degree of fractionation is consistently slightly lower than in the previous case (up to 10 %), but it is comparable to results of the major element modelling.

The REE data, unfortunately, do not allow any modelling to be performed, as the REE curves are very similar to each other [Fig. IV.2.11 a]. Moreover, the small degree of fractionation (~ 10 - 15 %) would imply a negligible difference between both parent and daughter compositions and thus seriously complicate formulation of an accurate REE-based model.

Some of the variation in the Sedlčany granite could have been caused by assimilation processes, that are likely to have been accompanied by fractional crystallization (AFC: *DePaolo, 1981*). Both quarries in Vápenice, and, to some extent, also in Kosova Hora, contain many xenoliths from the adjacent Sedlčany - Krásná Hora Metamorphic Islet [Chapter II.5.]. Many of them are carbonates (one of the most important rock types in the Islet), which are commonly partially dissolved by the surrounding magma and in this way could have contributed to the Sr content that is somewhat higher in the Vápenice samples than in the rest of the Sedlčany intrusion.

The linearity of the Harker plots for Říčany and Čertovo břemeno suites [Figs. IV.1.5.-6.], and the fact that the least evolved members of the Čertovo břemeno suite lie on a line which intersects the Říčany trend part way along (close to Ri-2) on the R_1 vs. R_2 plot [Fig. IV.3.1.], may indicate that both of them may be related by magma mixing, possibly of 'durbachitic' and 'granitic' (Říčany s.s.) components (*cf. Batchelor and Bowden, 1985*). Likewise, on the basis of major and trace elements *Holub (1978, 1990)* argued that the different members of the durbachite suite can be derived by hybridization of durbachites with leucogranites such as those present within the CBP or the S-type granites such as the Eisgarn intrusion of the Moldanubian Pluton, Czech Republic. From the table of expected end-member compositions of the Bohemian durbachite suite (*Holub, 1990*) [Tab. IV.8.] it is apparent that the geochemistry of the Říčany granite makes it a possible candidate for the acidic end-members. This model can be assessed by the mixing test [Fig. IV.3.8.] with presumed end-members, chosen on basis of the R_1 vs. R_2 plot, being the most mafic Čertovo břemeno durbachite (Cb-3) and slightly fractionated Říčany granite (Ri-2). All the mixing models show reasonable fits for the major element data ($R = 0.87$ to 0.998), and generally also for the trace element data, although the fit of the sample Ta-1 is the poorest, with higher calculated Nb, Ni and Th than is observed in the actual sample. The proportion of the acid end-member varies from 15 % (Tábor: Ta-1), through 41 - 44 % (Čertovo břemeno: Cb-1, Cb-2) to 62 % (Sedlčany: Se-3). On the other hand, some of the plots are not consistent with such a simplistic interpretation (*cf. A/CNK-A/NK, Fig. IV.1.7., P - Q, Fig. IV.1.11.; Rb - Sr, Fig. IV.2.6.*) casting doubts on the validity of such a model. Much needed additional information is provided by the Sr - Nd isotopes [Chapter V.3.].

In summary, the parental magma of the Sedlčany granite could have been produced either by magma mixing of about 40 % of the durbachitic component (similar to the sample Cb-3 of the Čertovo břemeno intrusion), and 60 % of the acidic magma (leucogranite or granite with some characteristics of the Říčany granite), or by fractional crystallization from the Čertovo břemeno parent. Subsequently, the

magma was modified by a limited degree of fractional crystallization (< 15 %) of an assemblage consisting of about 35 % plagioclase (andesine), 35 % K-feldspar, 15 % biotite and 15 % amphibole. Part of the variation, especially in the western part of the Sedlčany body, may be attributed to assimilation (AFC) of metasedimentary (carbonate ?) rocks of the adjacent Sedlčany - Krásná Hora Metamorphic Islet.

IV.3.4. The Říčany suite

The Harker plots for the Říčany granite do not offer much scope for genetic considerations as the SiO₂ content does not change greatly in the Říčany intrusion [Fig. IV.1.6.]. The ill-defined trends of decreasing Sr and Ba as well as of increasing Rb with SiO₂ [Fig. IV.2.4.] may be compatible with fractional crystallization of a mainly K-feldspar - plagioclase assemblage with a little biotite. Likewise, the subhorizontal trend observed on the R₁ vs. R₂ plot [Fig. IV.3.1.] implies fractional crystallization of one or more of the following minerals: K-feldspar, sodic plagioclase, Fe-rich biotite. The involvement of Fe-rich biotite can be ruled out, as the biotite is phlogopitic in the Říčany intrusion [Chapter III 1.8.].

Due to the restricted range in SiO₂ content, Zr has been used as the fractionation index for the Říčany suite, as the plots with Zr on the abscissa are characterised by a relatively low scatter and significant variation [Fig. IV.3.10.]. This element shows a negative correlation with SiO₂, and, therefore, the Zr axis is reversed. There are trends of slightly decreasing K₂O, Na₂O and CaO with differentiation in the Říčany granite, whereas Fe₂O₃* does not change at all [Fig. IV.3.10 a]. Both Sr and Ba decrease markedly with fractionation, but Rb slightly increases [Fig. IV.3. b-c]. Trends of rapidly decreasing Sr and Ba with increasing Rb and little change in SiO₂, Al₂O₃, Na₂O and K₂O in course of fractionation have been documented in the Lachlan Fold Belt granites in Australia and are considered to be characteristic of evolved granites fractionating K-feldspar-dominated assemblages (White, 1990; Chappell and White, 1992).

The limited difference in major element composition between presumed end-members, the lack of coherent trends on the Harker plots, and low range of SiO₂ in particular, do not favour major element-based least squares modelling on the Říčany granite.

The Říčany intrusion exhibits a progressive decrease in Rb coupled with an increase in both Ba and Sr from the marginal porphyritic facies towards the innermost non-porphyritic one, and the Jevany leucogranite [Fig. IV.3.9., Chapter II 6.]. However, as shown by the fractional crystallization vectors of rock-forming minerals, the fractionating assemblage would have to be dominated by amphibole to produce such trends. This mineral is, however, completely absent both in the granite and in its enclaves [Chapter II]. An alternative is that the pluton is reversely zoned with the more evolved compositions occurring at the margins.

On the basis of Figure IV.3.10., the SiO₂ - Ba, SiO₂ - Sr [Fig. IV.2.4.], Rb - Sr [Fig. IV.3.9 a], Ba - Sr [Fig. IV.3.9 b] and R₁ - R₂ plots [Fig. IV.3.1.], the observed geochemical variations (a decrease in K₂O, Ba and Sr, as well as a slight increase in Rb towards the margins of the intrusion) can be explained by ~ 20 % K-feldspar-dominated fractionation [Fig. IV.3.9]. This could not have taken place in situ, but in a deeper magma chamber prior to intrusion, because otherwise a normally-zoned pluton would have been formed. The existence of a deep magmatic reservoir beneath the Říčany intrusion is compatible with the presence of a major negative gravity anomaly [cf. Fig. I.2.], extending from the town of Říčany as far as Kutná Hora (Orel, 1975), 40 km to the E (the so-called Říčany - Kutná Hora batholith). Subsequently, the reverse zoning could have been achieved at high-

level either by mixing (including assimilation and, or, periodical influx of fresh, little-fractionated magma into the centre of the intrusion), or emplacement in at least three separate batches (porphyritic and non-porphyritic facies, Jevany leucogranite). Unfortunately, no information on the relationship between the porphyritic and normal facies of the Říčany granite is available due to lack of exposure [Chapter II.6.].

An alternative model for the origin of reversely-zoned plutons, proposed for the Lacorne Complex in Québec by *Bourne and Danis (1987)* [Fig. IV.3.11.], uses a hypothetical horizontally-zoned magma diapir. In this model the layer of the acid magma (1, 2) breaks its already crystallized crust (3), tapping the underlying more mafic magma (4) which tends to form the core of the newly-formed daughter magma diapir (5, 6). Such a scenario has been reproduced experimentally (see references in *Bourne and Danis, 1987*), and is possibly realistic for zoned plutons with a high density contrast between the centre and margins; thus such a model does not seem to be applicable to the Říčany granite where both central and marginal facies are similar in composition.

Reversely-zoned plutons may also be generated by wall-rock contamination, as suggested by *Gastil et al. (1991 and the references therein)*. For the Říčany body, this might be consistent with its more peraluminous character and higher boron content towards the margins (*Němec, 1978*), as the country rocks are predominantly shales; however the increase in A / CNK and B could be explained solely by increasing degrees of fractionation of the melt. Wall-rock assimilation, however, appears to be rather exceptional in upper crustal conditions, as with operation of this process the contact zones of the majority of the granitic plutons would be likely to freeze quickly (*Pitcher, 1993*). More importantly, the most probable contaminant, represented by the adjacent Teplá - Barrandian shales (CR-1 and CR-9), has lower SiO₂ and Rb, together with higher Al₂O₃, Fe₂O₃*, MgO and Na₂O than the Říčany granite. Accordingly its assimilation cannot account either for the trend of outwards increasing SiO₂ and Rb coupled with decreasing Al₂O₃ and Na₂O, or for the virtually constant Fe₂O₃* and MgO throughout the Říčany intrusion [cf. Fig. IV.1.6, IV.3.10 a-b].

The origin of reverse zoning in the Grizzly Peak cauldron, Colorado, has been explained by rearrangement of a stratified magma column during emplacement (*Fridrich and Mahood, 1984*). Following their scenario, progressive less-evolved magma from successively deeper levels in a stratified magma chamber would have risen into core of the Říčany intrusion, displacing more evolved magma towards the margins [Fig. IV.3.12 a]. Such an emplacement pattern would be preserved by rapid solidification or volatile loss (cf. *Fridrich and Mahood, 1984*) as otherwise it would be probably destroyed by subsequent convection. There is, indeed, evidence of volatile loss in the marginal parts of the intrusion (*Němec, 1978; see below*)

If the granite body were intruded as essentially separate batches, then there is a space problem. The most likely emplacement mechanism would be stoping or cauldron subsidence, which are considered to be important especially for late, high-level plutons (*Pitcher, 1979*) and cauldron subsidence can account for the origin of reverse zoning in plutons (*Pitcher, 1993* and Fig. IV.3.12 b). In the stoping model, the fresh batches of magma, coming from a continuously fractionating magma chamber, work their way upwards by breaking up and possibly also digesting the country rock as the pluton advances outwards [Fig. IV.3.12 c]. The zoned pluton resulting from such a process would have a steep xenolith-rich margin composed of the most evolved volatile-rich magma (*B.E. Leake, pers.com., 1993*), although the presence of a large number of xenoliths is not crucial, as they may have been removed to the bottom of the magma chamber (*Pitcher, 1979*). In reality, the steep margins of the Říčany intrusion (*Kodym, 1925*), with abundant pegmatite veins and country-rock xenoliths

(Palivcová *et al.*, 1992), seem to be compatible with such a view, as is also the presence of marginal aplite, bordering the southwestern contact of the body [Chapter II.6.]. The marginal aplite differs from the Jevany leucogranite by the presence of tourmaline and abundance of pegmatite schlieren. As shown by Němec (1978), B, Be and Sn concentrations also increase outwards in the Říčany intrusion, as do the amounts of tourmaline and cassiterite. Němec (1978) has formulated a model for the origin of the Marginal aplite by degasification of the granite magma from which a great deal of the volatiles escaped into the permeable country rocks (mainly shales).

Unlike the negative Eu anomaly of the Říčany granite [Chapter IV.2.] caused probably by K-feldspar-dominated fractionation in depth, the low HREE contents may provide evidence of garnet and/or zircon in the residuum although some of the HREE depletion could be attributed to a zircon fractionation in the deep reservoir (cf. the SiO_2 - Zr plot, Fig. IV.2.4.). Overall, the Říčany REE patterns [Fig. IV.2.11 c] resemble those modelled by Hanson (1980) for liquids derived from metasedimentary parents, in particular that originating by 40 % partial melting of greywacke leaving an amphibolite residuum (cf. Hanson, 1980, fig. 7). Similar patterns, however, will probably also result from the melting of large volumes of heterogeneous continental crust under granulite facies conditions (Hanson, 1980). The peraluminous nature of the granite may be consistent with an origin from a metasedimentary precursor, although the peraluminous composition could also be generated by partial melting of metaluminous igneous rocks or fractional crystallization of metaluminous minerals (Miller, 1985). More importantly, the whole-rock geochemical characteristics of the Říčany granite fulfil all but one of criteria set out by Miller (1985) for pelite-derived magmas (i.e. $\text{Na}_2\text{O} < 3.5 - 4 \%$, $\text{CaO} < 2 \%$, $\text{SiO}_2 > 65 \%$, $\text{Rb} > 100 \text{ ppm}$, $\text{Sr} < 300 - 400 \text{ ppm}$, $\text{Ba} < 600 - 1000 \text{ ppm}$, $\text{Rb} / \text{Ba} > 0.25$; cf. Appendices III. and IV.). The only exception is the normative corundum (C; CIPW norm), that rarely exceeds $\sim 3 \%$ in the studied samples, which compares with $\text{C} > 5 \%$ required for the pelitic parentage (Miller, 1985).

The REE pattern of the Jevany leucogranite with its significantly lower ΣREE than that of the Říčany granite and a slight positive Eu anomaly [Fig. IV.2.11 c] is in accord with an origin of the leucogranite from an aqueous fluid rather than by differentiation of a parental magma similar to the Říčany granite (Hanson, 1980, fig. 8). The position of the Jevany leucogranite at the least-evolved end of the Říčany array in the R_1 - R_2 , Ba - Sr and Rb - Sr diagrams is compatible with such an explanation.

In summary, the Říčany granite represents a geochemically evolved, high level, reversely-zoned pluton. Its parental magma, originating probably by anatexis of metasedimentary material, developed through K-feldspar fractionation in a crustal reservoir below the present level of exposure. The origin of the reverse zoning can be explained by a high-level emplacement either as a single batch from a horizontally-stratified magma chamber, or in several batches associated with cauldron subsidence and, or, stoping. The Jevany leucogranite does not appear to represent a highly-differentiated version of the Říčany granite, but possibly had crystallized from an aqueous liquid derived from the same parental melt.

IV.4. Tectonic affiliations of the granitoids

The whole-rock geochemistry of the granitoids reflects, to different degrees, that of their sources, and thus also the geotectonic setting in which they originated. In turn, the geotectonic information may provide further constraints on possible and impossible sources, subdivision and relative age relationships within the CBP.

Major element data have been used by *Maniar and Piccoli (1989)* to assess the likely tectonic environment of granitoids [Figs. IV.4.1-IV.4.2.]. They distinguished the following associations:

<i>IAG</i>	Island Arc Granitoids	<i>CAG</i>	Continental Arc Granitoids
<i>CCG</i>	Continental Collision Granitoids	<i>POG</i>	Post-orogenic granitoids
<i>RRG</i>	Rift-related Granitoids	<i>OP</i>	Oceanic Plagiogranites
<i>CEUG</i>	Continental Epeirogenic Uplift Granitoids.		

Two of the diagrams of *Maniar and Piccoli (1989)*, SiO_2 - K_2O and SiO_2 - Al_2O_3 are not shown, as the K_2O content of most of the analysed samples is $> 1\%$ (and they therefore do not classify as *OP* on the SiO_2 - K_2O plot; cf. Fig. IV.1.9 b). Furthermore, as SiO_2 is generally lower than 70% (with the exception of a few of the most acid rocks from the Říčany and Požáry intrusions), the discrimination by means of the SiO_2 - Al_2O_3 plot was not applicable; the favourable analyses fell at the intersection of the *IAG* + *CAG* + *CCG* and *POG* fields (cf. fig. 10b of *Maniar and Piccoli, 1989*). On the plot of SiO_2 vs. $\text{FeO}^* / (\text{FeO}^* + \text{MgO})$ [Fig. IV.4.1 a], all the rocks from the CBP plot into the field of *IAG* + *CAG* + *CCG* (Group I. of *Maniar and Piccoli, 1989*) as they do in the MgO vs. FeO^* plot [Fig. IV.4.1 b]. In contrast, in the CaO - $(\text{FeO}^* + \text{MgO})$ plot this is not the case [Fig. IV.4.2 a]. The majority of the Čertovo břemeno suite (Čertovo břemeno, Tábor and half the Sedlčany samples) fall into the *RRG* + *CEUG* (Group II.) field, apparently due to the low FeO^* and high MgO at low CaO of the durbachites [cf. Fig. IV.9 a].

Discrimination within both groups is done by means of the A / CNK vs. A / NK plot [Fig. IV.4.2 b]. Both Blatná and Sázava suites can be considered to be *CAG* or *IAG*, even though the Sázava suite shows considerable scatter in the northwestern sector of the A / CNK - A / NK diagram. The affinity of the Čertovo břemeno suite is also unclear on this diagram, especially for the mafic members (Čertovo břemeno s.s. and Tábor intrusions) but the Sedlčany analyses plot mainly into the *CAG* field. The Říčany suite, with A / CNK generally > 1.15 , is a typical *CCG*. The A / CNK versus A / NK plot that is of great importance in the classification of *Maniar and Piccoli (1989)*, does not satisfactorily discriminate between the distinct genetic groups, and there are many samples in the CBP dataset, that do not plot in *any* of the designed fields.

In summary, the Sázava and Blatná suites may be continental- or island-arc-related granitoids (*CAG*, *IAG*), whereas the Říčany suite could have been generated during continental collision (*CCG*). *Maniar and Piccoli (1989)* indicate that the *CAG* and *IAG* are typically biotite (\pm amphibole \pm pyroxene) quartz diorites, tonalites, granodiorites and granites, whereas the *CCG* are muscovite - biotite granites, sometimes with other peraluminous phase(s) present. Thus the major-element discrimination of these suites is in accord with the observed petrography [Chapter II.]. Although a clear discrimination is not apparent for the Čertovo břemeno suite based on this major-element

approach, the presence of quartz syenites could suggest either *RRG* or *CEUG* affinities but the ambiguity in the geochemical signature of this suite may point either to a mixed source [Chapter IV.3.] or to the limitations in the approach of *Maniar and Piccoli (1989)*.

Using the R_1 ($R_1 = 4 \text{ Si} - 11 (\text{Na} + \text{K}) - 2 (\text{Fe}^{2+} + \text{Fe}^{3+} + \text{Ti})$) vs. R_2 plot ($R_2 = 6 \text{ Ca} + \text{Mg} + \text{Al}$) of *De la Roche et al. (1980)*, it is possible to highlight the tectonic affinities of the granitoid suites as well as the importance of fractional crystallization, mixing and partial melting processes in their history (*Bachelor and Bowden, 1985*) [Fig IV.4.3., cf. Fig. IV.3.1., Chapter IV.3.]. In this diagram, the oldest rock types of the Sázava suite occupy mainly the *Pre-plate collision* field 2 with some of the Požáry trondhjemites and basic rocks crossing the boundary into the *Mantle plagiogranites* field 1. The Blatná suite granitoids are significantly shifted towards the boundary with the *Post-collision uplift* field 3 that is occupied by the rocks of the Čertovo břemeno suite. The analyses of the Říčany suite fall into the field of *Synorogenic anatectic magmatism*. (6). However, as *Batchelor and Bowden (1985)* have pointed out, there is an inevitable overlap between other suites and suite 6, as all granitoids evolve towards minimum melting compositions. Their figure 4 shows a great number of sub-alkaline late orogenic plutons, which were otherwise assigned to the field 4, plotting in field 6: such a scenario is possible for the Říčany suite granitoids. The decrease in both R_1 and R_2 of the most mafic members of all four suites in the sequence Sázava - Blatná - Čertovo břemeno - Říčany follows the source trend of *Batchelor and Bowden (1985)*, which is thought to represent a shift in the composition of successive intrusions within an igneous complex (or orogeny) towards progressively more silicic and alkaline compositions. In geochemical terms, the rocks plotting in the field 2 (Sázava and Blatná suites) belong to either the trondhjemitic or calc-alkaline series, field 3 corresponds to the high-K calc-alkaline series (Čertovo břemeno suite), field 4 to the subalkaline monzonitic series and field 6 to the anatectic two-mica series (either possibly Říčany suite).

On the Y versus Nb discrimination diagram of *Pearce et al. (1984)* [Fig. IV.4.4 a], the studied samples are classified as *VAG* (Volcanic Arc Granites) and *syn-COLG* (Syn-Collisional Granites). The Y+Nb versus Rb plot [Fig IV.4.4 b] is potentially capable of discriminating between the two settings: the Sázava suite falls into the *VAG* field, the Blatná suite analyses cluster closer to the boundary with the *syn-COLG* field, and both the Čertovo břemeno and Říčany suites belong to the *syn-COLG* field. Such a conclusion is fully in agreement with the discrimination in the Yb - Ta diagram [Fig IV.4.4 c]. It is worth noting that there is no way of distinguishing post-collisional granites on these plots due to the geochemical variability of their possible sources, resulting in a lack of a coherent trace-element signature (cf. *Pearce et al., 1984*). Thus, the post-collisional granitoids plotted in the Y + Nb versus Rb diagram (in the original paper) spread over both *VAG* and *syn-COLG* fields.

Of relevance to the potassic rocks (i.e. to both the Čertovo břemeno and Říčany suites) is the classification scheme of *Müller et al. (1992)*, which was originally developed for the study of volcanic rocks [Fig. IV.4.5.]. The first three of the them [a-c] show clearly that neither the Čertovo břemeno nor Říčany suites have the *WIP* (Within-Plate) character, a conclusion apparent from the earlier diagrams [Figs IV.4.3., IV.4.4.]. In contrast, the following two plots are in obvious disagreement with each other [Figs IV.4.5 d-e]. Although both suites are classified as *CAP* (Continental Arc related) on the Zr/TiO_2 - $\text{Ce}/\text{P}_2\text{O}_5$ plot [Fig. IV.4.5 d], on the Zr^{*3} - Nb^{*50} - $\text{Ce}/\text{P}_2\text{O}_5$ ternary diagram [Fig. IV.4.5 e] the Čertovo břemeno suite falls into the *PAP* (Post-collisional Arc) field. On the original Zr/TiO_2 - $\text{Ce}/\text{P}_2\text{O}_5$ diagram of *Müller et al. (1992, fig. 7d)*, there is considerable overlap between the volcanic rocks from the continental arc and post-collisional arc settings; in particular many analyses of

The high Ga / Al ratio, thought to be characteristic of the A-type granitoids, may be attributed to a high F content of the Říčany magma (0.10 - 0.19 % after *Tauson et al.*, 1977). Gallium tends to form GaF_6^{3-} complexes in the melt, whereas Al tends to be incorporated into (An-rich) residual plagioclase (*Collins et al.*, 1982; *Whalen et al.*, 1987). Thus the Říčany intrusion does not appear to be a typical A-type granitoid.

The classification scheme of *Pearce et al.* (1984) is not the only one which utilises HFSE elements (in combination with LILE) as a powerful tool for judging the geotectonic setting. *Harris et al.* (1986) used the Rb - Hf - Ta ternary plot [Fig. IV.4.9.] to distinguish four principal settings. They numbered the granitoid groups sequentially, as they would occur in a normal orogenic cycle:

- Group I.* Volcanic arc granitoids, pre-dating the collision; typically calc-alkaline gabbros to biotite granites,
- Group II.* Syn-orogenic (leuco-) granitoids; S-types containing muscovite and tourmaline and having over 70% of silica,
- Group III.* High-level calc-alkaline plutons, similar in character to the Group I., and
- Group IV.* Minor, post-tectonic intrusions, typically alkaline or shoshonitic in character.

In this diagram, the Sázava and Blatná suites fall mainly into the Volcanic-arc field (Group I.), unlike the Čertovo břemeno and Říčany suites, which plot mainly in the Post-collisional field (Group III.). However, the Čertovo břemeno sample Cb-3 plots in the Group I. field, suggesting that the setting of the Čertovo břemeno suite was possibly transitional between the post-collisional and arc settings. The position of the Tábor sample in the Group II. field appears to be misleading, as it is by no means a S-type leucogranite with muscovite and tourmaline (see above; cf. Chapter II.7.2.).

Although the various discrimination diagrams do not give unequivocal indications of the tectonic setting of the individual suites, for each suite certain affinities seem more likely than others. The Sázava suite may have originated in a volcanic (continental) arc environment, as suggested by its calc-alkaline nature and a pronounced Nb-Ta trough on the ORG-normalised spiderdiagrams [Fig. IV.4.6]. The Blatná suite has also a signature of volcanic-arc related granitoids but on the basis of it being more potassic and having a higher $\text{K}_2\text{O} / \text{Na}_2\text{O}$ ratio than the Sázava suite it have probably originated in a mature volcanic arc environment.

There is a striking difference between previous two suites (Sázava and Blatná) and both the Čertovo břemeno and Říčany suites. The Čertovo břemeno suite, which is shoshonitic in character, probably originated in a post-collision uplift setting, or in a setting transitional between the volcanic arc and post-collisional. As an alternative, its geochemistry could account for mixing of material derived from both sources. The peraluminous Říčany suite, geochemically transitional between shoshonitic and high-potassium calc-alkaline series, seems to have originated by anatexis of metasedimentary material in a collision-related environment post-dating the collision event. It is important to note that none of the intrusions shows a within-plate signature, but in almost all of them, there is, to a different extent, an indication of volcanic-arc component.

A note of caution is to be added here: in the CBP, which probably developed within a short time interval [Chapter I., Appendix IX.], the distinct geochemical affinities of the individual suites may point to a distinct parentage of the observed magma rather than to a change in the tectonic environment. For instance, magmas with a volcanic-arc signature may be either generated in the appropriate geotectonic setting, or their character can be inherited from the source, represented by earlier, arc-

related rocks. Additionally, mixing of several components (either within the source or of melts from distinct sources), may further complicate the situation.

IV.5. Implications of the whole-rock geochemistry

In the preceding text, the studied granitoids of the Central Bohemian Pluton have been subdivided into four suites, each having distinct behaviour in the AFM ternary. These four suites, viz. Sázava, Blatná, Čertovo břemeno and Říčany, differ in their major and trace element signatures, likely genesis and probable geotectonic setting.

Sázava suite

The calc-alkaline Sázava suite is the least geochemically differentiated of the suites studied. The rocks of this suite are characterised by low Ba/Cs, LREE/HREE, low content of HFSE (apart from Y), transition metals and REE (Požáry intrusion in particular), as well as by high K/Rb and a pronounced Nb-Ta trough. The basic rocks associated with the Sázava suite are generally low in Ni and Cr, whereas Co and Sc are high.

A genetic model of origin of both the Sázava and Požáry intrusions invokes melting of amphibolite or eclogite with amphibole and, or garnet (Požáry intrusion) in the residue. Subsequently, this magma underwent extensive fractionation of an amphibole > plagioclase > biotite > orthite assemblage. The Požáry intrusion, composed mainly of trondhjemitic, may correspond to the last, strongly differentiated derivatives of the Sázava magma. In this way, the trondhjemitic could have attained their leucocratic and peraluminous character, as well as their low Σ REE and positive Eu anomalies.

The basic rocks appear to have, at least partly, an independent position within the Sázava suite, as they do not form a compositional continuum with the other members. On the other hand, they are responsible for some of the variation within the Sázava intrusion, being involved in the production of the hybrid quartz diorites in the western part of the Sázava body (Teletín). The geochemistry of the Sázava suite points to a magmatic arc setting.

Blatná suite

The Blatná suite possesses a high-K calc-alkaline character for the more acidic members, but the associated monzonitic rocks are shoshonitic in character. The suite is metaluminous to peraluminous and is characterised by intermediate ratios of Ba/Cs, K/Rb, LREE/HREE, as well as contents of HFSE, REE and transition metals (except for the monzonitic rock types).

The geochemical signature as well as the field relations suggest an origin for the compositional variation of both the Kozárovec and Blatná intrusions by mixing between the monzonitic rocks (similar to the Lučkovice monzonite) and the most acidic magma of the biotite facies of the Blatná intrusion. These magmas have subsequently evolved by fractional crystallization of amphibole > plagioclase + K-feldspar > biotite (Kozárovec) or plagioclase > biotite > amphibole and orthite (Blatná). Alternatively, each of the suites could have been produced purely by either magma mixing of similar end-members or fractional crystallization of assemblages as above. Locally, wall-rock assimilation may have been important in portions adjacent to the Metamorphic Islet Zone and, or the Moldanubian Unit. The geochemistry of the Blatná suite is compatible with an origin in a mature volcanic arc or a setting transitional between arc and one that is collision-related.

Table IV.1: HFSE content of particular rock suites, CBP

Rock suite	Hf (ICP-MS)	Ta (ICP-MS)	Nb (XRF)	Y (XRF)	Zr (XRF)
Sázava	2 - 5 †	0.2, 0.3 (Požáry) † 0.5 - 1.1 (Sázava s.s.)	4 - 11	5 - 45	50 - 180
Blatná	3 - 13 ‡	0.7 - 1.7 ‡	5 - 18	2 - 48	120 - 230
Čertovo břemeno	4, 13	1.7, 1.8	11 - 23	12 - 26	230 - 410
Říčany	7 - 9	1.4 (Jevany), 2.3 - 2.8 (Říčany s.s.)	13 - 21	b.d. - 13	90 - 160 (Jevany), 160 - 250 (Říčany s.s.)

† no data for Ta or Hf from Nečín were obtained; ‡ no data available for the Marginal and Klatovy types

Table IV.2: Zircon saturation calculations (Watson and Harrison, 1983)

(shown are Zr concentration, $\Sigma \text{Cat} = \text{Si} + \text{Ti} + \text{Al} + \text{Fe}^{2+} + \text{Fe}^{3+} + \text{Ca} + \text{Na} + \text{Mg}$, $M = (\text{Na} + \text{L} + 2 \text{Ca}) / (\text{Al} \cdot \text{Si})$, saturated concentration of Zr at 750°C (ppm) and saturation temperature corresponding to the observed Zr concentration)

Sample	Zr (ppm)	ΣCat	M	Zr sat @750°C	T (°C)	Sample	Zr (ppm)	ΣCat	M	Zr sat @750°C	T (°C)
Sázava suite						Blatná suite					
Sázava						Kozárovce					
Sa-1	76	1.680	2.013	180	686	Koz-1	161	1.639	1.866	159	753
Sa-2	55	1.713	2.448	261	639	Koz-2	216	1.673	1.769	146	785
Sa-4	56	1.694	2.720	329	626	Koz-4	201	1.655	1.634	131	788
Sa-7	57	1.644	1.821	153	677	Koz-5	201	1.674	1.658	133	787
Sa-10	79	1.717	1.865	159	698	Koz-6	218	1.654	1.685	136	792
Sa-11	74	1.660	1.664	134	706	Koz-8	221	1.643	1.679	136	793
Sa-12	95	1.669	1.968	173	705	Koz-9	251	1.644	1.981	175	782
Sa-13	146	1.691	1.685	136	758	Koz-10	148	1.672	1.688	137	759
Average	80	1.684	2.023	191	687	Koz-11	156	1.651	1.698	138	762
1 σ	30	0.025	0.374	69	41	Koz-12	211	1.657	1.529	119	800
Gabbros						Koz-13	139	1.659	1.593	126	760
Gbs-1	76	1.741	4.823	1964	541	Average	193	1.656	1.707	140	778
Gbs-2	27	1.745	2.714	327	582	1 σ	36	0.012	0.126	16	17
Gbs-3	72	1.699	2.128	199	676	Zalužany					
Gbs-4	43	1.751	3.682	744	562	Zal-1	251	1.642	2.643	308	736
Average	54	1.734	3.337	808	590	Blatná					
1 σ	24	0.024	1.180	805	59	Bl-1	177	1.655	1.390	106	795
Požáry						Bl-2	188	1.652	1.584	125	786
Po-1	128	1.701	1.668	135	748	Bl-3	188	1.662	1.392	106	800
Po-3	159	1.702	1.461	113	781	Bl-4	171	1.655	1.471	114	786
Po-4	180	1.691	1.256	95	807	Bl-5	209	1.656	1.502	117	801
Po-5	162	1.688	1.214	91	801	Bl-6	163	1.673	1.341	102	792
Average	157	1.696	1.400	108	784	Bl-7	149	1.633	1.446	111	776
1 σ	22	0.007	0.209	20	27	Bl-8	169	1.674	1.716	140	767
Nečín						Average	177	1.658	1.480	115	788
Ne-1	115	1.683	1.373	105	759	1 σ	18	0.013	0.122	12	12
Ne-2	101	1.686	1.304	99	754	Červená					
Average	108	1.685	1.339	102	756	Cv-1	226	1.643	1.879	161	780
1 σ	10	0.002	0.049	4	4	Cv-2	157	1.67	1.572	124	771
						Cv-3	146	1.678	1.606	127	763
						Average	176	1.664	1.686	137	772
						1 σ	43	0.018	0.168	20	8

Table IV.2: Zircon saturation calculations (*cont.*)*(for explanation, see previous page)*

Sample	Zr (ppm)	Σ Cat	M	Zr sat @750°C	T (°C)	Sample	Zr (ppm)	Σ Cat	M	Zr sat @750°C	T (°C)
Blatná suite						Čertovo břemeno suite					
Mrač						Tábor					
Mrc-1	200	1.630	1.226	92	819	Ta-1	390	1.604	2.024	182	818
Mrc-2	211	1.647	1.190	90	827	Ta-2	305	1.624	2.130	199	788
Average	205	1.639	1.208	91	823	Ta-3	405	1.613	1.783	148	841
1 σ	8	0.012	0.025	2	6	Average	367	1.614	1.979	176	816
Lučkovice						1 σ	54	0.010	0.178	26	27
Gbl-1	62	1.666	3.825	840	576	Říčany suite					
Gbl-2	77	1.783	5.080	2440	531	Říčany					
Average	70	1.725	4.453	1640	553	Ri-1	240	1.653	1.287	97	831
1 σ	11	0.083	0.887	1131	32	Ri-2	246	1.648	1.559	123	812
Marginal						Ri-3	239	1.636	1.403	107	822
Mg-1	115	1.630	1.335	101	762	Ri-4	246	1.643	1.455	112	820
Mg-2	152	1.654	1.209	97	789	Ri-5	219	1.639	1.420	109	812
Average	133	1.642	1.313	99	776	Ri-6	238	1.644	1.294	98	830
1 σ	26	0.017	0.032	3	19	Ri-7	268	1.614	1.145	86	854
Klatovy						Ri-8	224	1.634	1.246	94	828
Kl-1	171	1.652	1.431	110	789	Ri-9	224	1.637	1.277	96	826
Kl-2	128	1.657	1.262	95	777	Ri-10	214	1.660	1.252	94	823
Average	150	1.655	1.347	103	783	Ri-11	193	1.589	1.060	80	829
1 σ	30	0.004	0.120	10	9	Ri-12	196	1.507	1.238	93	816
Čertovo břemeno suite						Ri-13	215	1.634	1.243	94	824
Sedlčany						Ri-14	217	1.642	1.264	95	824
Se-1	237	1.610	1.567	123	808	Ri-15	237	1.596	1.165	88	840
Se-3	260	1.627	1.561	123	817	Ri-18	187	1.632	1.178	89	817
Se-4	269	1.631	1.530	120	823	Ri-19	187	1.609	1.197	90	815
Se-5	283	1.606	1.619	129	820	Ri-20	163	1.629	0.988	75	819
Se-6	269	1.619	1.466	113	828	Ri-22	166	1.648	1.115	84	811
Se-7	283	1.618	1.424	109	836	Average	217	1.626	1.252	95	824
Se-8	259	1.646	1.450	112	825	1 σ	28	0.034	0.138	11	10
Se-9	256	1.639	1.413	108	827	Jevany					
Se-10	266	1.618	1.347	102	836	Je-1	149	1.641	1.353	103	783
Se-11	274	1.648	1.280	97	844	Je-2	137	1.624	1.293	98	780
Se-12	259	1.596	1.419	109	828	Je-3	164	1.614	1.061	80	814
Se-13	240	1.633	1.402	107	822	Je-4	139	1.638	1.416	108	773
Se-14	315	1.625	1.401	107	848	Je-5	94	1.616	1.222	92	754
Se-15	229	1.617	1.364	104	821	Average	137	1.627	1.269	96	781
Se-16	249	1.632	1.388	106	827	1 σ	26	0.012	0.137	11	22
Average	263	1.624	1.442	111	827						
1 σ	21	0.014	0.092	9	10						
Čertovo břemeno											
Cb-1	291	1.582	1.518	118	831						
Cb-2	294	1.631	1.943	170	799						
Cb-3	405	1.599	2.380	246	794						
Cb-4	282	1.622	1.705	139	813						
Cb-5	299	1.630	1.366	104	846						
Average	314	1.613	1.782	155	817						
1 σ	51	0.022	0.398	57	22						

Table IV.5: Least-squares modelling; major elements, Sázava suite

A	PARENT	plg2 An ⁵⁴	bi3 ²	amph7	KF3	DAUGHTER ¹
	Sa-4	Sa-3	Sa-3	Sa-3	Sa-10	Sa-11
SiO ₂	49.94	53.41	35.32	45.35	61.46	64.16
TiO ₂	0.75	0.00	2.11	1.39	0.00	0.48
Al ₂ O ₃	17.58	29.48	15.31	9.47	19.39	15.89
Fe ₂ O ₃ *	8.81	0.08	21.94	16.71	0.03	5.46
MgO	4.89	0.00	9.05	9.82	0.00	2.14
CaO	9.52	11.27	0.01	11.92	0.01	4.96
Na ₂ O	2.72	5.05	0.10	1.08	0.75	3.36
K ₂ O	1.54	0.12	9.81	1.02	15.78	1.79

A	PARENT ³	DAUGHTER ³	DAUGHTER ³ CALCULTD	WEIGHTED RESIDUALS
SiO ₂	52.15	65.31	65.18	0.13
TiO ₂	0.78	0.49	0.48	0.01
Al ₂ O ₃	18.36	16.18	16.19	-0.01
Fe ₂ O ₃ *	9.20	5.55	5.37	0.19
MgO	5.11	2.18	2.58	-0.41
CaO	9.94	5.05	4.94	0.11
Na ₂ O	2.84	3.42	3.47	-0.05
K ₂ O	1.61	1.82	1.79	0.03

A	SOLUTION ⁴	CUMULATE ⁵
Sa-4	1	
plg	-0.353	42.107
KF	-0.021	2.531
bi	-0.047	5.612
amph	-0.417	49.751
Sa-11	0.161	R ² = 0.233

B	PARENT	bi3	plg7 An ³⁶	amph7	DAUGHTER
	Sa-11	Sa-3	Sa-10	Sa-3	Po-5
SiO ₂	64.16	35.32	56.69	45.35	71.42
TiO ₂	0.48	2.11	0.00	1.39	0.30
Al ₂ O ₃	15.89	15.31	27.62	9.47	15.04
Fe ₂ O ₃ *	5.46	21.94	0.11	16.71	2.64
MgO	2.14	9.05	0.00	9.82	0.52
CaO	4.96	0.01	7.69	11.92	3.67
Na ₂ O	3.36	0.10	7.07	1.08	1.08
K ₂ O	1.79	9.81	0.21	1.02	1.79

B	PARENT	DAUGHTER	DAUGHTER CALCULTD	WEIGHTED RESIDUALS
SiO ₂	65.31	72.91	72.66	0.25
TiO ₂	0.49	0.31	0.26	0.05
Al ₂ O ₃	16.18	15.35	15.16	0.20
Fe ₂ O ₃ *	5.55	2.69	2.92	-0.22
MgO	2.18	0.53	0.46	0.07
CaO	5.05	3.75	3.53	0.21
Na ₂ O	3.42	2.63	3.42	-0.78
K ₂ O	1.82	1.83	1.59	0.24

B	SOLUTION	CUMULATE
Sa-11	1	
bi	-0.055	17.154
plg	-0.132	41.392
amph	-0.132	41.454
Po-5	0.682	R ² = 0.874

¹ Original whole-rock analyses of presumed parent and daughter [Appendix III.]

² Mineral analyses [Appendices VI.-VIII.]

³ Parent and daughter analyses recalculated to 100 %, solution vector (calculated daughter)

⁴ Amount of particular minerals removed (parent = 1), 1 - total multiplied by 100 corresponds to degree of fractionation (here 83.9 %)

⁵ Percentage of individual minerals in the cumulate

Table IV.5: Least-squares modelling; major elements, Sázava suite (cont.)

C	PARENT	bi1	plg2 An54	KF3	DAUGHTER
	Po-4	Po-1	Sa-3	Sa-10	Po-1
SiO ₂	70.17	35.54	53.41	61.46	62.46
TiO ₂	0.28	2.93	0.00	0.00	0.28
Al ₂ O ₃	15.35	17.00	29.48	19.39	20.41
Fe ₂ O ₃ *	2.02	19.26	0.08	0.03	1.91
MgO	1.32	8.60	0.00	0.00	0.87
CaO	3.77	0.03	11.27	0.01	6.26
Na ₂ O	2.73	0.07	5.05	0.75	4.03
K ₂ O	1.82	9.41	0.12	15.78	1.92

C	PARENT	DAUGHTER	DAUGHTER CALCULTD	WEIGHTED RESIDUALS
SiO ₂	72.00	63.64	64.05	-0.41
TiO ₂	0.29	0.29	0.26	0.02
Al ₂ O ₃	15.75	20.80	21.04	-0.24
Fe ₂ O ₃ *	2.07	1.95	1.85	0.10
MgO	1.35	0.89	1.06	-0.17
CaO	3.87	6.38	6.39	-0.02
Na ₂ O	2.80	4.11	3.50	0.60
K ₂ O	1.87	1.96	1.84	0.11

C	SOLUTION	CUMULATE
Po-4	1	
bi	0.052	7.115
plg	0.629	86.794
KF	0.044	6.091
Po-1	1.724	R ² = 0.644

D	PARENT	plg4 An39	quartz	KF3	DAUGHTER
	Sa-11	Po-1	stochiom	Sa-10	Po-1
SiO ₂	64.16	57.16	100.00	61.46	62.46
TiO ₂	0.48	0.04	0.00	0.00	0.28
Al ₂ O ₃	15.89	27.01	0.00	19.39	20.41
Fe ₂ O ₃ *	5.46	0.15	0.00	0.03	1.91
MgO	2.14	0.00	0.00	0.00	0.87
CaO	4.96	8.10	0.00	0.01	6.26
Na ₂ O	3.36	6.68	0.00	0.75	4.03
K ₂ O	1.79	0.26	0.00	15.78	1.92

D	PARENT	DAUGHTER	DAUGHTER CALCULTD	WEIGHTED RESIDUALS
SiO ₂	65.31	63.64	64.66	-0.02
TiO ₂	0.49	0.29	0.20	0.09
Al ₂ O ₃	16.18	20.80	20.81	-0.02
Fe ₂ O ₃ *	5.55	1.95	2.09	-0.13
MgO	2.18	0.89	0.79	0.10
CaO	5.05	6.38	5.90	0.48
Na ₂ O	3.42	4.11	4.65	-0.54
K ₂ O	1.82	1.96	1.92	0.04

D	SOLUTION	CUMULATE
Sa-11	1	
plg	1.382	78.250
KF	0.193	10.912
Q	0.191	10.832
Po-1	2.766	R ² = 0.563

Table IV.6: Least-squares modelling; major elements, Blatná suite

A	PARENT	plg10 An50	Kf1	bi4	amph6	DAUGHTER
	Koz-9	Koz-2	Koz-4	Koz4	Koz4	Koz-5
SiO ₂	59.22	54.13	63.01	35.60	45.95	65.53
TiO ₂	0.63	0.04	0.00	3.80	1.04	0.45
Al ₂ O ₃	15.49	29.96	19.35	14.66	7.55	15.43
Fe ₂ O ₃ *	5.09	0.05	0.08	18.14	14.49	3.57
MgO	3.83	0.00	0.00	10.02	11.29	2.14
CaO	5.35	10.49	0.04	0.03	11.79	3.76
Na ₂ O	2.55	5.53	1.05	0.12	1.29	3.25
K ₂ O	4.13	0.11	14.93	9.39	0.86	4.14

A	PARENT	DAUGHTER	DAUGHTER CALCULTD	WEIGHTED RESIDUALS
SiO ₂	61.50	66.69	66.85	-0.16
TiO ₂	0.65	0.46	0.59	-0.13
Al ₂ O ₃	16.09	15.70	15.84	-0.13
Fe ₂ O ₃ *	5.29	3.63	3.37	0.26
MgO	3.98	2.18	2.57	-0.39
CaO	5.56	3.83	3.76	0.07
Na ₂ O	2.65	3.31	2.91	0.40
K ₂ O	4.29	4.21	4.11	0.10

A	SOLUTION	CUMULATE
Koz-9	1	
plg	-0.094	24.291
KF	-0.090	23.350
bi	-0.022	5.579
amph	-0.181	46.780
Koz-5	0.614	R ² = 0.453

B	PARENT	plg10 An50	Kf1	bi4	amph6	DAUGHTER
	Koz-9	Koz-2	Koz-4	Koz4	Koz4	Koz-8
SiO ₂	59.22	54.13	63.01	35.60	45.95	64.65
TiO ₂	0.63	0.04	0.00	3.80	1.04	0.54
Al ₂ O ₃	15.49	29.96	19.35	14.66	7.55	15.38
Fe ₂ O ₃ *	5.09	0.05	0.08	18.14	14.49	4.05
MgO	3.83	0.00	0.00	10.02	11.29	2.56
CaO	5.35	10.49	0.04	0.03	11.79	4.30
Na ₂ O	2.55	5.53	1.05	0.12	1.29	2.49
K ₂ O	4.13	0.11	14.93	9.39	0.86	4.00

B	PARENT	DAUGHTER	DAUGHTER CALCULTD	WEIGHTED RESIDUALS
SiO ₂	61.50	65.99	65.68	0.31
TiO ₂	0.65	0.55	0.58	-0.03
Al ₂ O ₃	16.09	15.70	15.63	0.06
Fe ₂ O ₃ *	5.29	4.13	3.89	0.24
MgO	3.98	2.61	2.99	-0.38
CaO	5.56	4.39	4.29	0.10
Na ₂ O	2.65	2.54	2.82	-0.28
K ₂ O	4.29	4.08	4.11	-0.02

B	SOLUTION	CUMULATE
Koz-9	1	
plg	-0.086	26.278
KF	-0.075	22.928
bi	-0.024	7.479
amph	-0.142	43.315
Koz-8	0.673	R ² = 0.392

C	PARENT	plg10 An50	Kf1	bi4	amph6	DAUGHTER
	Koz-1	Koz-2	Koz-4	Koz4	Koz4	Koz-5
SiO ₂	60.18	54.13	63.01	35.60	45.95	65.53
TiO ₂	0.60	0.04	0.00	3.80	1.04	0.45
Al ₂ O ₃	15.43	29.96	19.35	14.66	7.55	15.43
Fe ₂ O ₃ *	4.81	0.05	0.08	18.14	14.49	3.57
MgO	3.36	0.00	0.00	10.02	11.29	2.14
CaO	4.91	10.49	0.04	0.03	11.79	3.76
Na ₂ O	2.64	5.53	1.05	0.12	1.29	3.25
K ₂ O	3.99	0.11	14.93	9.39	0.86	4.14

C	PARENT	DAUGHTER	DAUGHTER CALCULTD	WEIGHTED RESIDUALS
SiO ₂	62.74	66.69	66.93	-0.24
TiO ₂	0.63	0.46	0.52	-0.06
Al ₂ O ₃	16.09	15.70	15.83	-0.12
Fe ₂ O ₃ *	5.01	3.63	3.52	0.11
MgO	3.50	2.18	2.35	-0.17
CaO	5.12	3.83	3.80	0.03
Na ₂ O	2.75	3.31	2.93	0.38
K ₂ O	4.16	4.21	4.13	0.09

C	SOLUTION	CUMULATE
Koz-1	1	
plg	-0.075	26.556
KF	-0.054	18.986
bi	-0.026	9.035
amph	-0.128	54.422
Koz-5	0.718	R ² = 0.271

Table IV.6: Least-squares modelling; major elements, Blatná suite (cont.)

D	PARENT		plg10 An50		Kf1		b14		amph6		DAUGHTER	
	Koz-1	Koz-2	Koz-4	Koz-4	Koz-4	Koz-4	Koz-4	Koz-4	Koz-4	Koz-8	Koz-8	Koz-8
SiO ₂	60.18	54.13	63.01	35.60	45.95	64.65						
TiO ₂	0.60	0.04	0.00	3.80	1.04	0.54						
Al ₂ O ₃	15.43	29.96	19.35	14.66	7.55	15.38						
Fe ₂ O ₃ *	4.81	0.05	0.08	18.14	14.49	4.05						
MgO	3.36	0.00	0.00	10.02	11.29	2.56						
CaO	4.91	10.49	0.04	0.03	11.79	4.30						
Na ₂ O	2.64	5.53	1.05	0.12	1.29	2.49						
K ₂ O	3.99	0.11	14.93	9.39	0.86	4.00						

D	PARENT	DAUGHTER	DAUGHTER CALCULTD	WEIGHTED RESIDUALS
SiO ₂	62.74	65.99	65.75	0.24
TiO ₂	0.63	0.55	0.52	0.03
Al ₂ O ₃	16.09	15.70	15.63	0.07
Fe ₂ O ₃ *	5.01	4.13	4.02	0.11
MgO	3.50	2.61	2.80	-0.18
CaO	5.12	4.39	4.32	0.07
Na ₂ O	2.75	2.54	2.84	-0.30
K ₂ O	4.16	4.08	4.12	-0.03

D	SOLUTION	CUMULATE
Koz-1	1	
plg	-0.066	30.925
KF	-0.035	16.693
bi	-0.029	13.676
amph	-0.082	38.707
Koz-8	0.788	R ² = 0.201

E	PARENT		amph1		plg 3An38		b11		DAUGHTER	
	Cv-3	Bl-5	Bl-7	Bl-7	Bl-7	Bl-7	Bl-7	Bl-7	Bl-4	Bl-4
SiO ₂	61.86	45.75	57.49	36.04	68.73					
TiO ₂	0.73	1.14	0.00	3.35	0.45					
Al ₂ O ₃	16.17	7.02	26.69	14.59	13.91					
Fe ₂ O ₃ *	4.57	14.77	0.02	17.02	2.63					
MgO	3.58	11.73	0.00	11.28	1.98					
CaO	3.98	11.89	8.04	0.03	2.78					
Na ₂ O	2.94	1.16	7.02	0.11	2.95					
K ₂ O	3.56	0.78	0.16	9.61	3.91					

E	PARENT	DAUGHTER	DAUGHTER CALCULTD	WEIGHTED RESIDUALS
SiO ₂	63.52	70.61	71.09	-0.48
TiO ₂	0.75	0.46	0.41	0.06
Al ₂ O ₃	16.60	14.29	14.57	-0.28
Fe ₂ O ₃ *	4.69	2.70	2.53	0.17
MgO	3.68	2.03	2.37	-0.33
CaO	4.09	2.86	2.77	0.08
Na ₂ O	3.02	3.03	2.50	0.53
K ₂ O	3.66	4.02	3.76	0.25

E	SOLUTION	CUMULATE
Cv-3	1	
amph	-0.062	17.065
plg	-0.189	51.846
bi	-0.113	31.089
Bl-4	0.635	R ² = 0.797

F	PARENT		amph1		plg 3An38		b11		DAUGHTER	
	Cv-3	Bl-5	Bl-7	Bl-7	Bl-7	Bl-7	Bl-7	Bl-7	Bl-1	Bl-1
SiO ₂	61.86	45.75	57.49	36.04	67.77					
TiO ₂	0.73	1.14	0.00	3.35	0.49					
Al ₂ O ₃	16.17	7.02	26.69	14.59	14.90					
Fe ₂ O ₃ *	4.57	14.77	0.02	17.02	2.70					
MgO	3.58	11.73	0.00	11.28	1.80					
CaO	3.98	11.89	8.04	0.03	2.71					
Na ₂ O	2.94	1.16	7.02	0.11	2.99					
K ₂ O	3.56	0.78	0.16	9.61	3.94					

F	PARENT	DAUGHTER	DAUGHTER CALCULTD	WEIGHTED RESIDUALS
SiO ₂	63.52	69.65	69.94	-0.28
TiO ₂	0.75	0.50	0.47	0.04
Al ₂ O ₃	16.60	15.31	15.52	-0.20
Fe ₂ O ₃ *	4.69	2.77	2.53	0.24
MgO	3.68	1.85	2.27	-0.42
CaO	4.09	2.79	2.70	0.09
Na ₂ O	3.02	3.07	2.72	0.35
K ₂ O	3.66	4.05	3.86	0.19

F	SOLUTION	CUMULATE
Cv-3	1	
amph	-0.082	25.224
plg	-0.151	46.579
bi	-0.092	28.179
Bl-1	0.675	R ² = 0.521

Table IV.6: Least-squares modelling; major elements, Blatná suite (cont.)

G	PARENT	KF2	amph1	plg 3An38	bi1	DAUGHTER
	Cv-1	B1-7	B1-5	B1-7	B1-7	B1-1
SiO ₂	62.88	62.99	45.75	57.49	36.04	67.77
TiO ₂	0.76	0.00	1.14	0.00	3.35	0.49
Al ₂ O ₃	16.15	18.83	7.02	26.69	14.59	14.90
Fe ₂ O ₃ *	4.39	0.01	14.77	0.02	17.02	2.70
MgO	3.49	0.00	11.73	0.00	11.28	1.80
CaO	4.44	0.05	11.89	8.04	0.03	2.71
Na ₂ O	2.62	0.98	1.16	7.02	0.11	2.99
K ₂ O	3.67	15.10	0.78	0.16	9.61	3.94

G	PARENT	DAUGHTER	DAUGHTER CALCULTD	WEIGHTED RESIDUALS
SiO ₂	63.90	69.65	69.99	-0.34
TiO ₂	0.77	0.50	0.65	-0.15
Al ₂ O ₃	16.41	15.31	15.64	-0.32
Fe ₂ O ₃ *	4.46	2.77	2.48	0.30
MgO	3.55	1.85	2.18	-0.33
CaO	4.51	2.79	2.89	-0.11
Na ₂ O	2.66	3.07	2.25	0.82
K ₂ O	3.73	4.05	3.92	0.13

G	SOLUTION	CUMULATE
Cv-1	1	
KF	-0.030	8.719
plg	-0.142	41.566
bi	-0.055	16.119
amph	-0.115	33.597
B1-1	0.658	R ² = 1.151

H	PARENT	amph1	plg 3An38	bi1	KF2	DAUGHTER
	B1-8	B1-5	B1-7	B1-7	B1-7	B1-4
SiO ₂	64.63	45.75	57.49	36.04	62.99	68.73
TiO ₂	0.67	1.14	0.00	3.35	0.00	0.45
Al ₂ O ₃	14.80	7.02	26.69	14.59	18.83	13.91
Fe ₂ O ₃ *	4.07	14.77	0.02	17.02	0.01	2.63
MgO	2.78	11.73	0.00	11.28	0.00	1.98
CaO	4.25	11.89	8.04	0.03	0.05	2.78
Na ₂ O	2.93	1.16	7.02	0.11	0.98	2.95
K ₂ O	3.48	0.78	0.16	9.61	15.10	3.91

H	PARENT	DAUGHTER	DAUGHTER CALCULTD	WEIGHTED RESIDUALS
SiO ₂	66.21	70.61	70.71	-0.10
TiO ₂	0.69	0.46	0.63	-0.16
Al ₂ O ₃	15.16	14.29	14.35	-0.06
Fe ₂ O ₃ *	4.17	2.70	2.85	-0.15
MgO	2.85	2.03	1.74	0.29
CaO	4.35	2.86	2.96	-0.10
Na ₂ O	3.00	3.03	2.77	0.26
K ₂ O	3.57	4.02	3.99	0.03

H	SOLUTION	CUMULATE
B1-8	1	
amph	-0.097	39.515
KF	-0.012	4.927
plg	-0.111	44.877
bi	-0.026	10.680
B1-4	0.753	R ² = 0.23

I	PARENT	amph1	plg 3An38	KF2	DAUGHTER
	B1-8	B1-5	B1-7	B1-7	B1-1
SiO ₂	64.63	45.75	57.49	62.99	67.77
TiO ₂	0.67	1.14	0.00	0.00	0.49
Al ₂ O ₃	14.80	7.02	26.69	18.83	14.90
Fe ₂ O ₃ *	4.07	14.77	0.02	0.01	2.70
MgO	2.78	11.73	0.00	0.00	1.80
CaO	4.25	11.89	8.04	0.05	2.71
Na ₂ O	2.93	1.16	7.02	0.98	2.99
K ₂ O	3.48	0.78	0.16	15.10	3.94

I	PARENT	DAUGHTER	DAUGHTER CALCULTD	WEIGHTED RESIDUALS
SiO ₂	66.21	69.65	69.62	0.03
TiO ₂	0.69	0.50	0.67	-0.17
Al ₂ O ₃	15.16	15.31	15.30	0.01
Fe ₂ O ₃ *	4.17	2.77	2.83	-0.06
MgO	2.85	1.85	1.67	0.18
CaO	4.35	2.79	2.87	-0.08
Na ₂ O	3.00	3.07	2.97	0.10
K ₂ O	3.57	4.05	4.05	0.00

I	SOLUTION	CUMULATE
B1-8	1	
plg	-0.066	32.619
KF	-0.14	6.977
amph	-0.121	60.403
B1-1	0.799	R ² = 0.082

Table IV.7: Least-squares modelling; major elements, Sedlčany granite

A	PARENT Se-3	bi1 Se-6	plg3An42 Se-5	KF1 Se-5	amph4 Se-9	DAUGHTER Se-12
SiO ₂	65.15	36.85	56.61	62.99	50.82	68.47
TiO ₂	0.55	2.95	0.02	0.02	0.36	0.51
Al ₂ O ₃	14.73	14.15	26.82	18.69	4.15	14.74
Fe ₂ O ₃ *	2.83	15.16	0.07	0.06	12.47	2.58
MgO	2.67	13.82	0.00	0.02	14.71	2.36
CaO	2.40	0.00	8.63	0.01	11.22	2.14
Na ₂ O	2.98	0.08	6.51	0.89	0.89	2.74
K ₂ O	5.60	10.03	0.22	15.35	0.37	5.50

A	PARENT	DAUGHTER	DAUGHTER CALCULTD	WEIGHTED RESIDUALS
SiO ₂	67.22	69.14	68.80	0.34
TiO ₂	0.57	0.51	0.54	-0.03
Al ₂ O ₃	15.20	14.88	14.74	0.14
Fe ₂ O ₃ *	2.92	2.60	2.58	0.02
MgO	2.76	2.38	2.39	-0.01
CaO	2.48	2.16	2.18	-0.02
Na ₂ O	3.07	2.77	3.12	-0.35
K ₂ O	5.78	5.55	5.64	-0.09

A	SOLUTION	CUMULATE
Se3	1	
bi	-0.025	22.322
KF	-0.031	27.451
plg	-0.040	35.274
amph	-0.017	14.952
Se-12	0.888	R ² = 0.266

B	PARENT Se-3	bi1 Se-6	plg3An42 Se-5	KF1 Se-5	amph4 Se-9	DAUGHTER Se-11
SiO ₂	65.15	36.85	56.61	62.99	50.82	68.27
TiO ₂	0.55	2.95	0.02	0.02	0.36	0.51
Al ₂ O ₃	14.73	14.15	26.82	18.69	4.15	15.02
Fe ₂ O ₃ *	2.83	15.16	0.07	0.06	12.47	2.68
MgO	2.67	13.82	0.00	0.02	14.71	2.69
CaO	2.40	0.00	8.63	0.01	11.22	2.13
Na ₂ O	2.98	0.08	6.51	0.89	0.89	2.05
K ₂ O	5.60	10.03	0.22	15.35	0.37	5.56

B	PARENT	DAUGHTER	DAUGHTER CALCULTD	WEIGHTED RESIDUALS
SiO ₂	67.22	69.02	68.13	0.89
TiO ₂	0.57	0.52	0.55	-0.04
Al ₂ O ₃	15.20	15.19	14.79	0.39
Fe ₂ O ₃ *	2.92	2.71	2.78	-0.07
MgO	2.76	2.72	2.61	0.11
CaO	2.48	2.15	2.23	-0.08
Na ₂ O	3.07	2.07	3.02	-0.94
K ₂ O	5.78	5.62	5.88	-0.25

B	SOLUTION	CUMULATE
Se-3	1	
bi	-0.014	22.470
KF	-0.007	11.130
plg	-0.036	56.488
amph	-0.006	9.913
Se-11	0.936	R ² = 1.936

C	PARENT Se-6	bi1 Se-6	plg3An42 Se-5	KF1 Se-5	amph4 Se-9	DAUGHTER Se-12
SiO ₂	65.11	36.85	56.61	62.99	50.82	68.47
TiO ₂	0.51	2.95	0.02	0.02	0.36	0.51
Al ₂ O ₃	14.97	14.15	26.82	18.69	4.15	14.74
Fe ₂ O ₃ *	2.59	15.16	0.07	0.06	12.47	2.58
MgO	2.82	13.82	0.00	0.02	14.71	2.36
CaO	2.38	0.00	8.63	0.01	11.22	2.14
Na ₂ O	2.63	0.08	6.51	0.89	0.89	2.74
K ₂ O	5.58	10.03	0.22	15.35	0.37	5.50

C	PARENT	DAUGHTER	DAUGHTER CALCULTD	WEIGHTED RESIDUALS
SiO ₂	67.41	69.14	69.19	-0.05
TiO ₂	0.53	0.51	0.52	0.00
Al ₂ O ₃	15.50	14.88	14.93	-0.05
Fe ₂ O ₃ *	2.68	2.60	2.37	0.24
MgO	2.92	2.38	2.64	-0.25
CaO	2.46	2.16	2.11	0.05
Na ₂ O	2.72	2.77	2.72	0.04
K ₂ O	5.78	5.55	5.53	0.02

C	SOLUTION	CUMULATE
Se-6	1	
bi	-0.023	16.501
KF	-0.047	34.601
plg	-0.047	34.362
amph	-0.020	14.535
Se-12	0.863	R ² = 0.130

**Table IV.7: Least-squares modelling; major elements, Sedlčany granite
(cont.)**

D	PARENT	bi1	plg3An42	KF1	amph4	DAUGHTER
	Se-6	Se-6	Se-5	Se-5	Se-9	Se-11
SiO ₂	65.11	36.85	56.61	62.99	50.82	68.27
TiO ₂	0.51	2.95	0.02	0.02	0.36	0.51
Al ₂ O ₃	14.97	14.15	26.82	18.69	4.15	15.02
Fe ₂ O ₃ *	2.59	15.16	0.07	0.06	12.47	2.68
MgO	2.82	13.82	0.00	0.02	14.71	2.69
CaO	2.38	0.00	8.63	0.01	11.22	2.13
Na ₂ O	2.63	0.08	6.51	0.89	0.89	2.05
K ₂ O	5.58	10.03	0.22	15.35	0.37	5.56

D	PARENT	DAUGHTER	DAUGHTER CALCULTD	WEIGHTED RESIDUALS
SiO ₂	67.41	69.02	68.55	0.48
TiO ₂	0.53	0.52	0.54	-0.03
Al ₂ O ₃	15.50	15.19	14.97	0.21
Fe ₂ O ₃ *	2.68	2.71	2.59	0.12
MgO	2.92	2.72	2.84	-0.12
CaO	2.46	2.15	2.12	0.03
Na ₂ O	2.72	2.07	2.65	-0.58
K ₂ O	5.78	5.62	5.74	-0.12

D	SOLUTION	CUMULATE
Se-6	1	
bi	-0.010	9.751
KF	-0.032	31.441
plg	-0.045	44.765
amph	-0.014	14.043
Se-11	0.899	R ² = 0.65

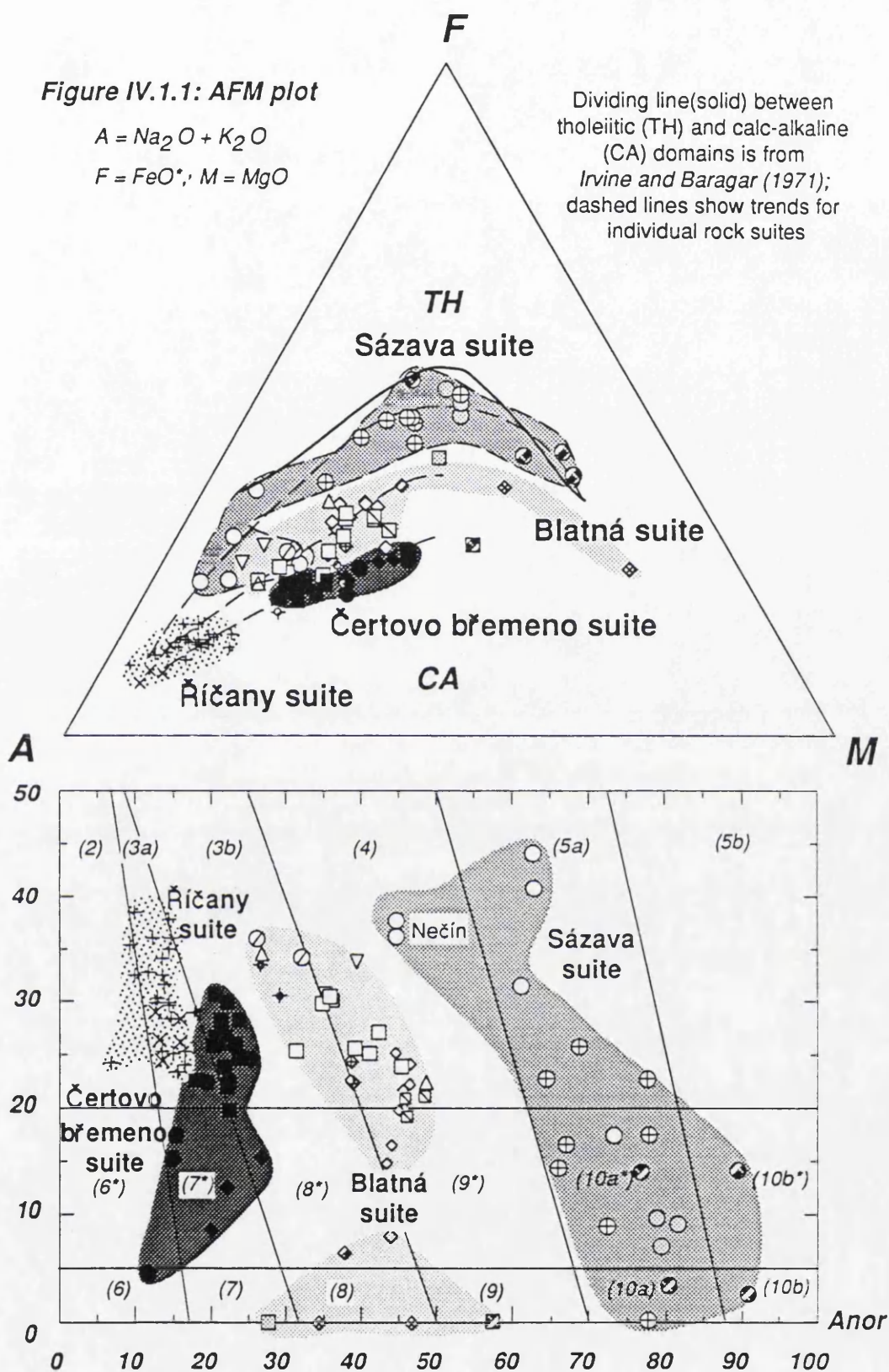
Table IV.8: Theoretical compositions of two end-members of the Bohemian durbachite suite (*Holub, 1990*) compared to an analysis of the Říčany granite

	Mafic end-member	Acid end-member	Říčany granite (Ri-2)
SiO ₂	51.5 - 54	72 - 75.5	70.72
TiO ₂	1.2 - 1.4	0.1 - 0.3	0.23
Al ₂ O ₃	13 - 14	12 - 14	13.97
FeO *	6.5 - 7.3	0.45 - 1.3	1.54
MnO	0.10 - 0.12	0.01 - 0.03	0.01
MgO	8.5 - 9.5	0.2 - 0.5	1.12
CaO	4.5 - 5.0	0.7 - 1.5	1.27
Na ₂ O	1.5 - 2.0	2.7 - 3.3	3.32
K ₂ O	6.2 - 7.2	5.0 - 6.5	5.29
P ₂ O ₅	1.2 - 1.4	0.05 - 0.20	0.17
V	80 - 100	20	-
Cr	500 - 600	0 - 20	47
Ni	160 - 200	10	30
Zn	100 - 130	20 - 50	37
Rb	380 - 420	300 - 420	346
Sr	440 - 540	170 - 270	372
Zr	470 - 520	40 - 150	246
Cs	17 - 22	(40)	55.3
Ba	2100 - 2700	100 - 500 (1000?)	1015
Ce	110 - 130	75 - 105	68.3
Th	15 - 50	25 - 45 (10 - 45)	35
U	10 - 20	10 - 30	26

Figure IV.1.1: AFM plot

$A = \text{Na}_2\text{O} + \text{K}_2\text{O}$
 $F = \text{FeO}^*$; $M = \text{MgO}$

Dividing line(solid) between
 tholeiitic (TH) and calc-alkaline
 (CA) domains is from
 Irvine and Baragar (1971);
 dashed lines show trends for
 individual rock suites



**Figure IV.1.2: Q'-ANOR classification diagram;
 after Streckeisen and Le Maitre (1979)**

(2) alkali feldspar granite
 (3a) syenogranite
 (3b) monzogranite

(4) granodiorite
 (5) tonalite

(6*) quartz alkali feldspar syenite
 (7*) quartz syenite
 (8*) quartz monzonite
 (9*) quartz monzodiorite, quartz monzogabbro
 (10*) quartz diorite, quartz gabbro, quartz anorthosite

(6) alkali feldspar syenite
 (7) syenite
 (8) monzonite
 (9) monzodiorite, monzogabbro
 (10) diorite, gabbro, anorthosite

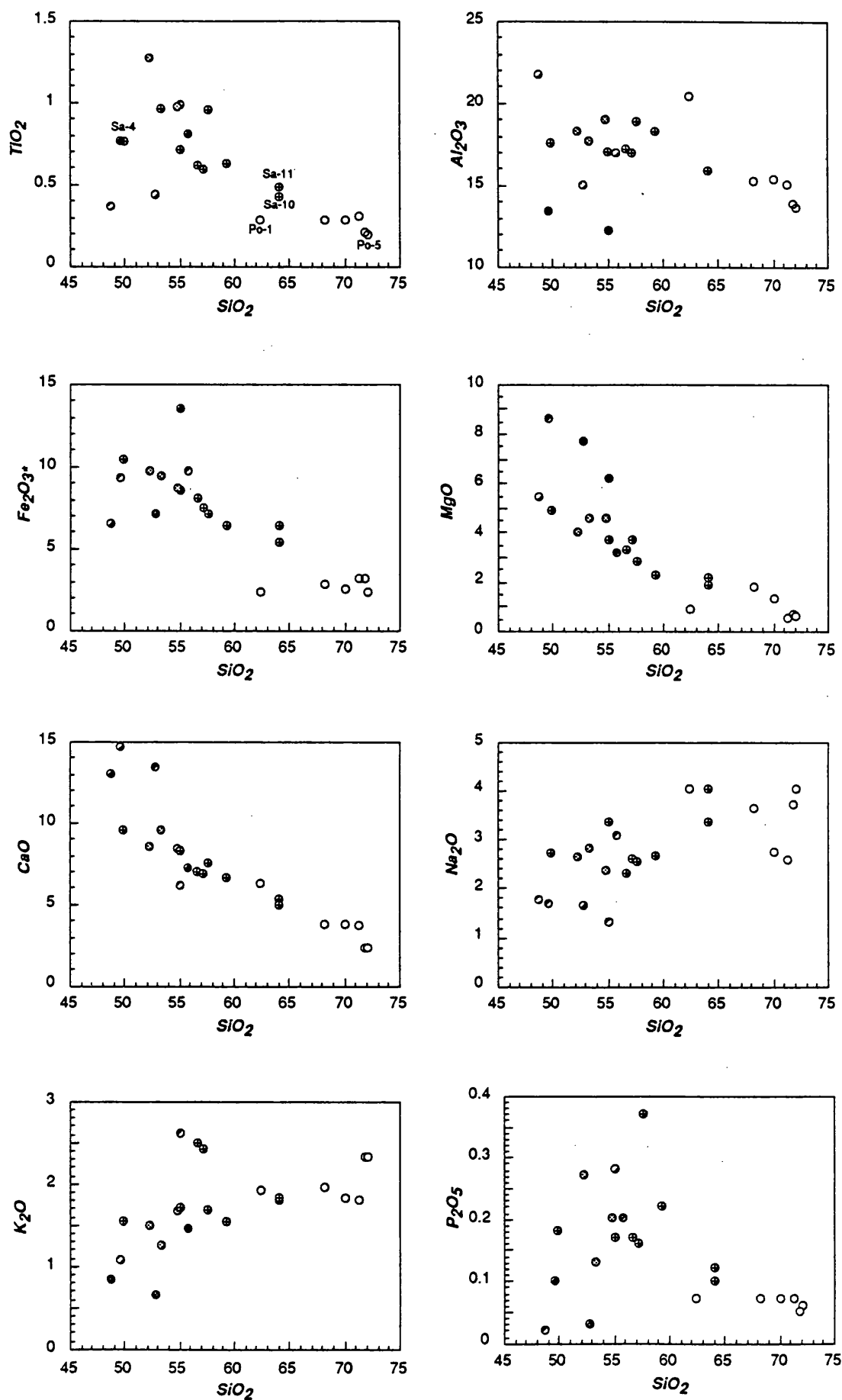


Figure IV.1.3: Harker plots for the Sázava suite

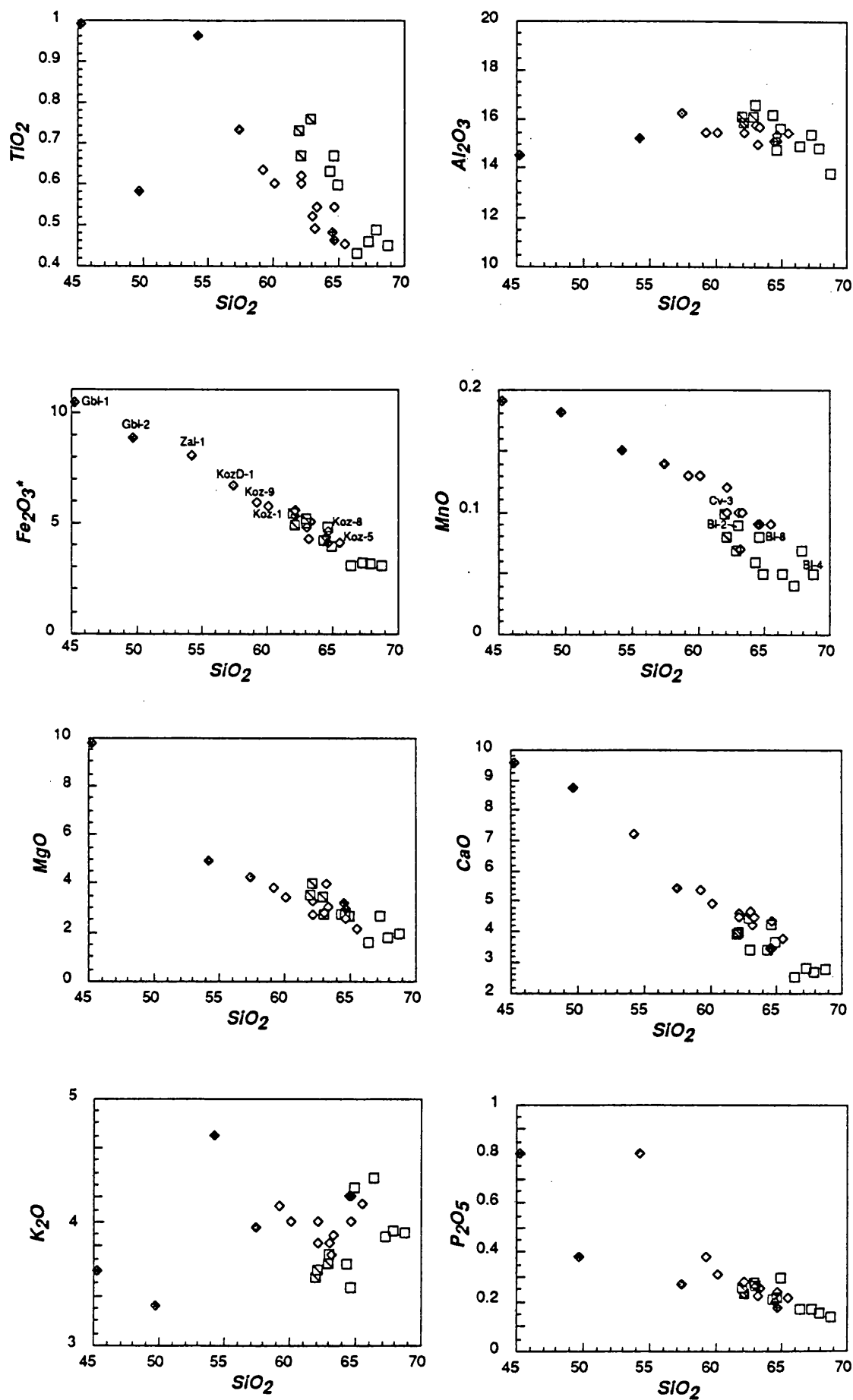


Figure IV.1.4: Harker plots for the Blatná suite

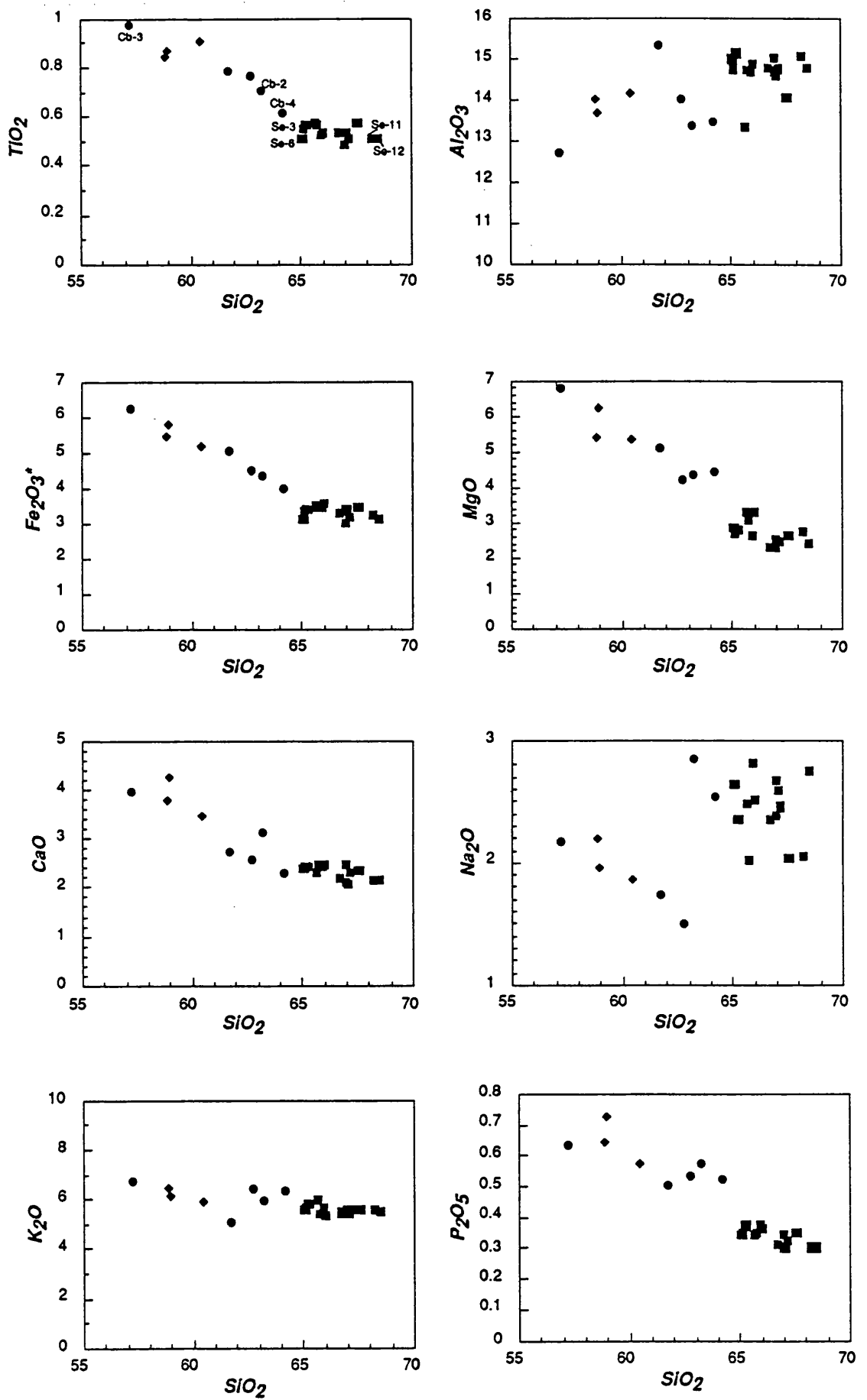


Figure IV.1.5: Harker plots for the Čertovo břemeno suite

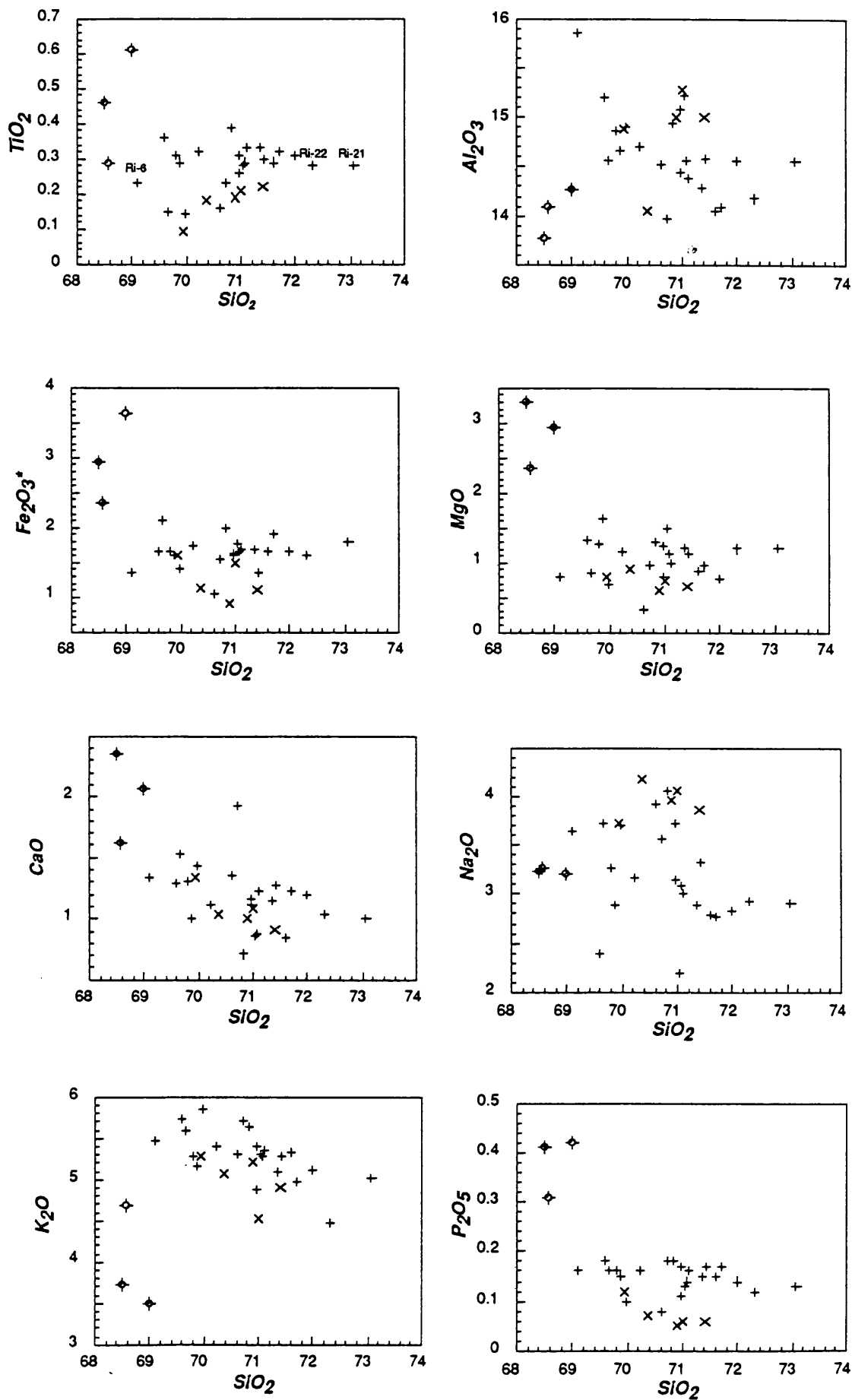


Figure IV.1.6: Harker plots for the Říčný suite

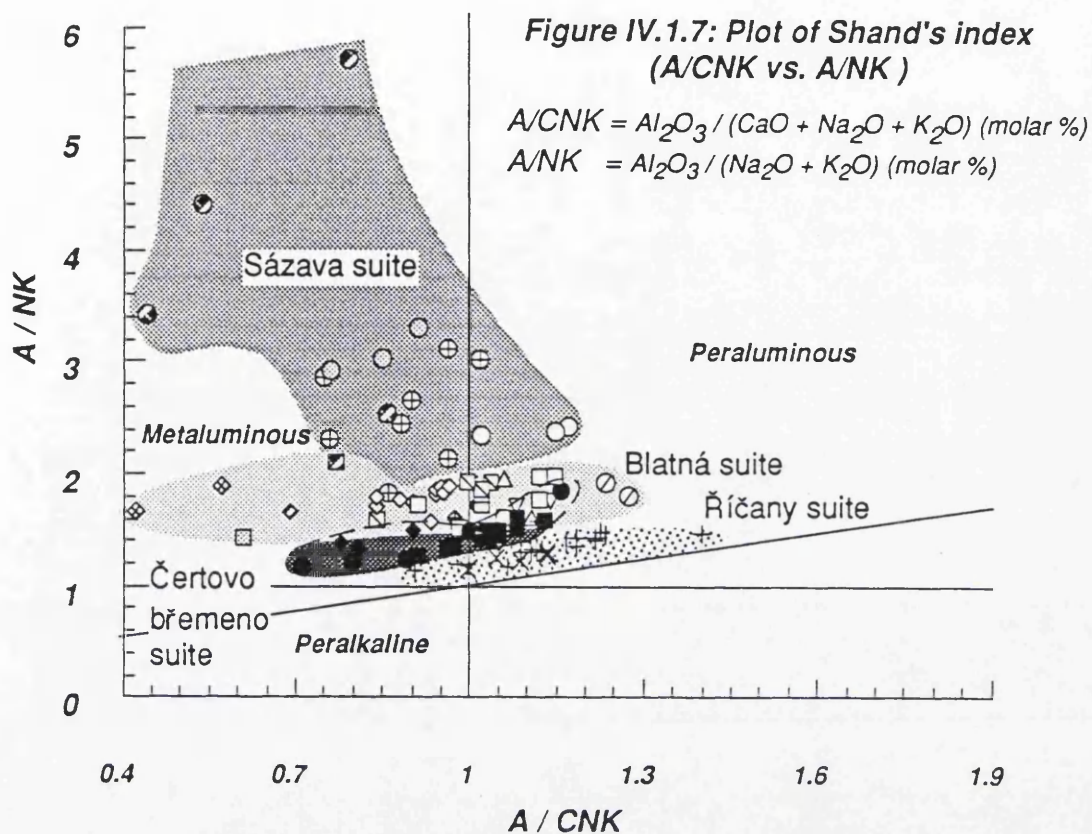
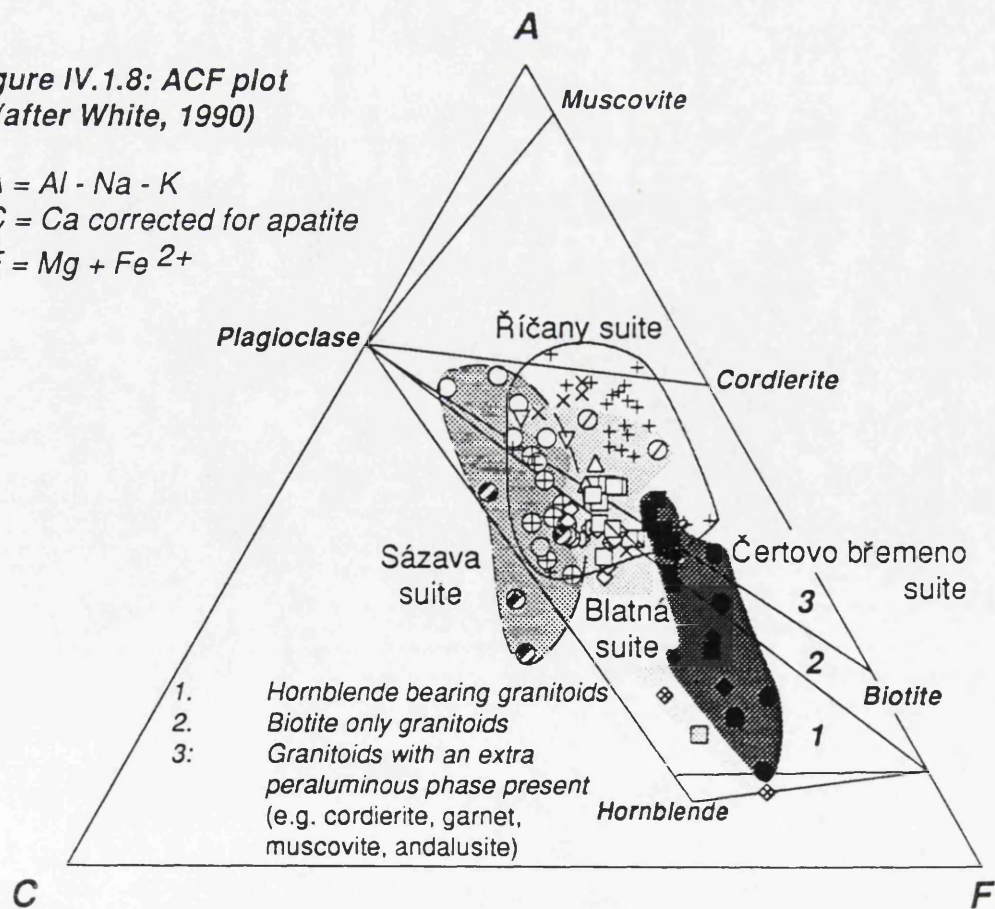


Figure IV.1.8: ACF plot (after White, 1990)

$A = Al - Na - K$
 $C = Ca \text{ corrected for apatite}$
 $F = Mg + Fe^{2+}$



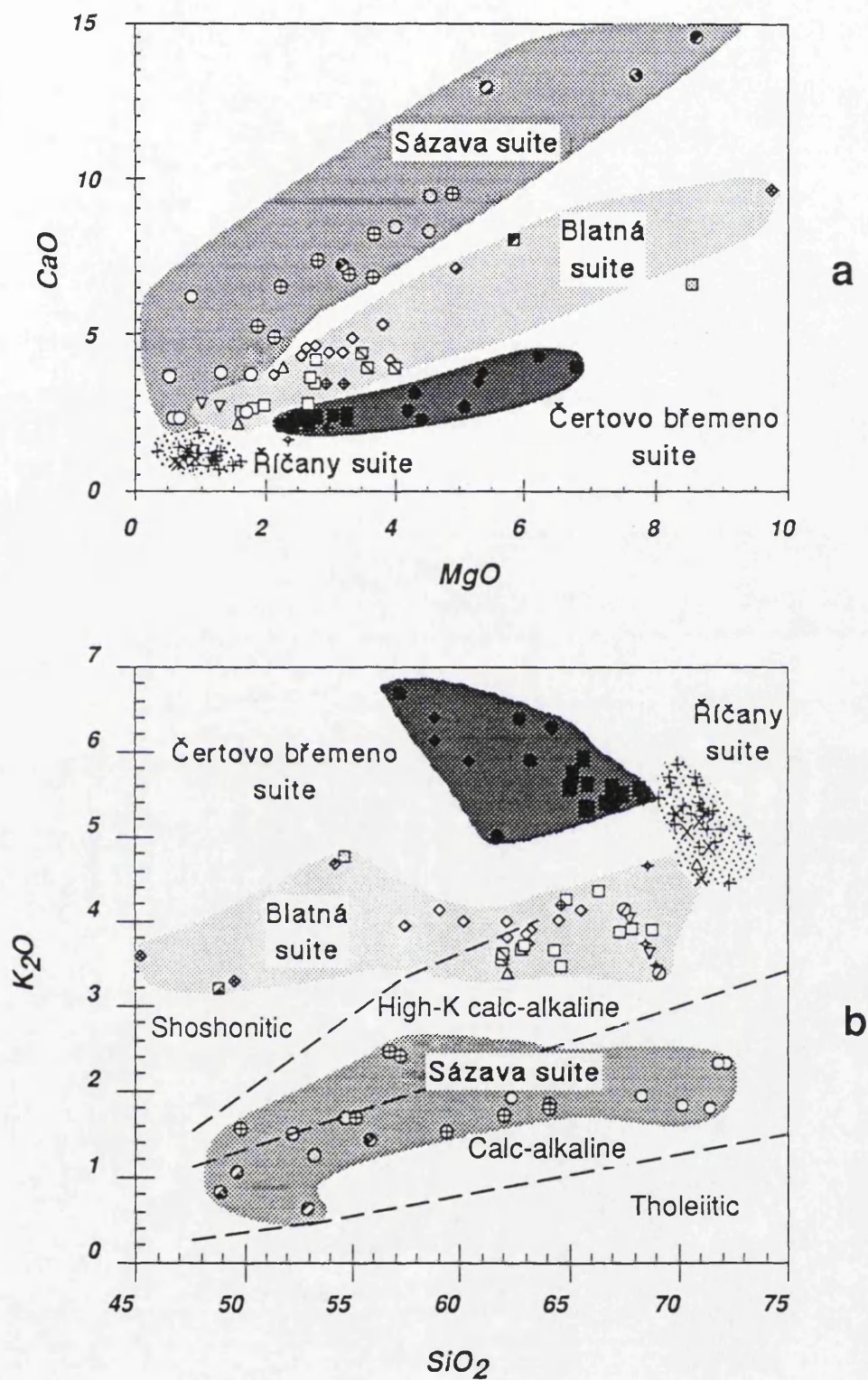


Figure IV.1.9: Major element characteristics of granitoids from the CBP

The spread of the Sázava, Blatná, Čertovo břemeno and Říčany suites is shown

The tholeiitic, calc-alkaline, high-K calc-alkaline and shoshonitic field boundaries are from *Peccerillo and Taylor (1976)*

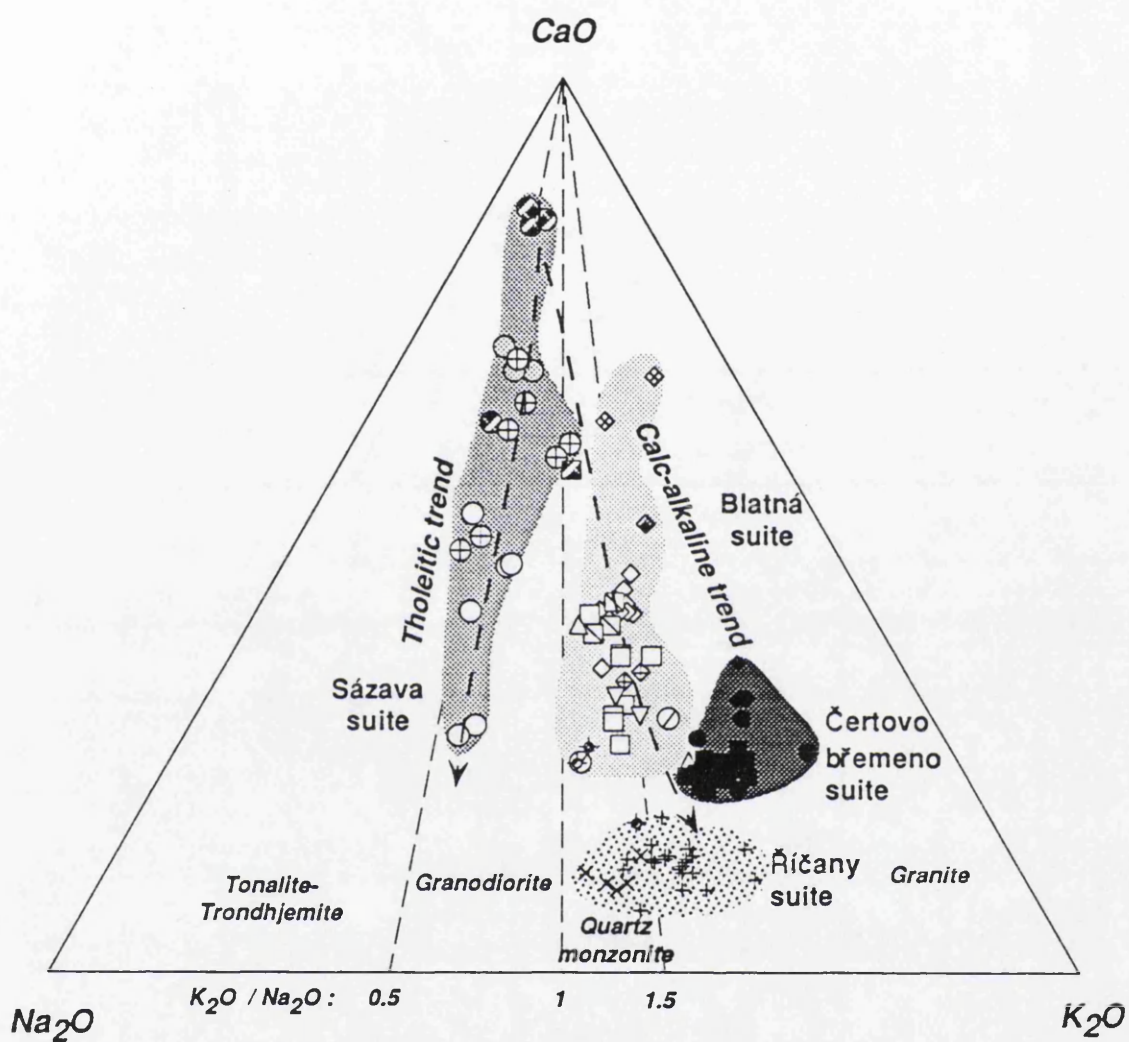


Figure IV.1.10: $\text{CaO} - \text{Na}_2\text{O} - \text{K}_2\text{O}$ ternary diagram (after Condie, 1981)

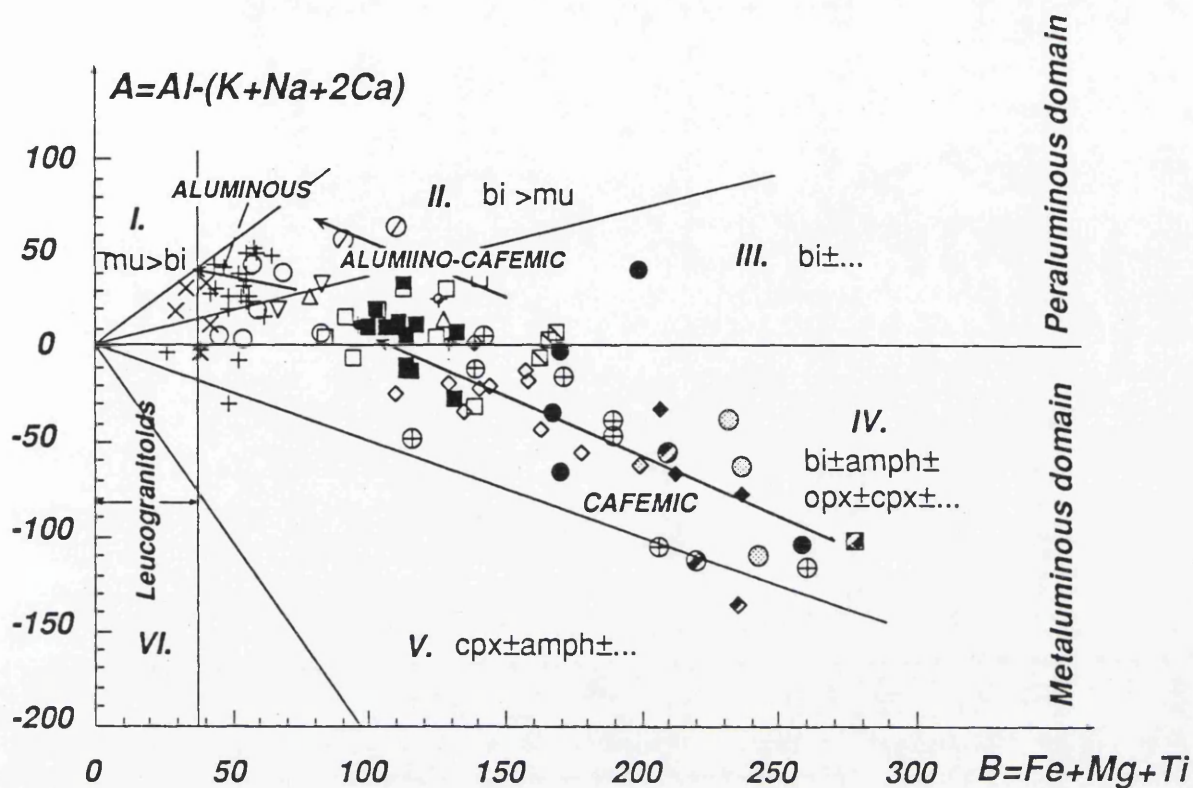


Figure IV.1.12: The B - A ("characteristic minerals") plot of Debon and Le Fort (1988)

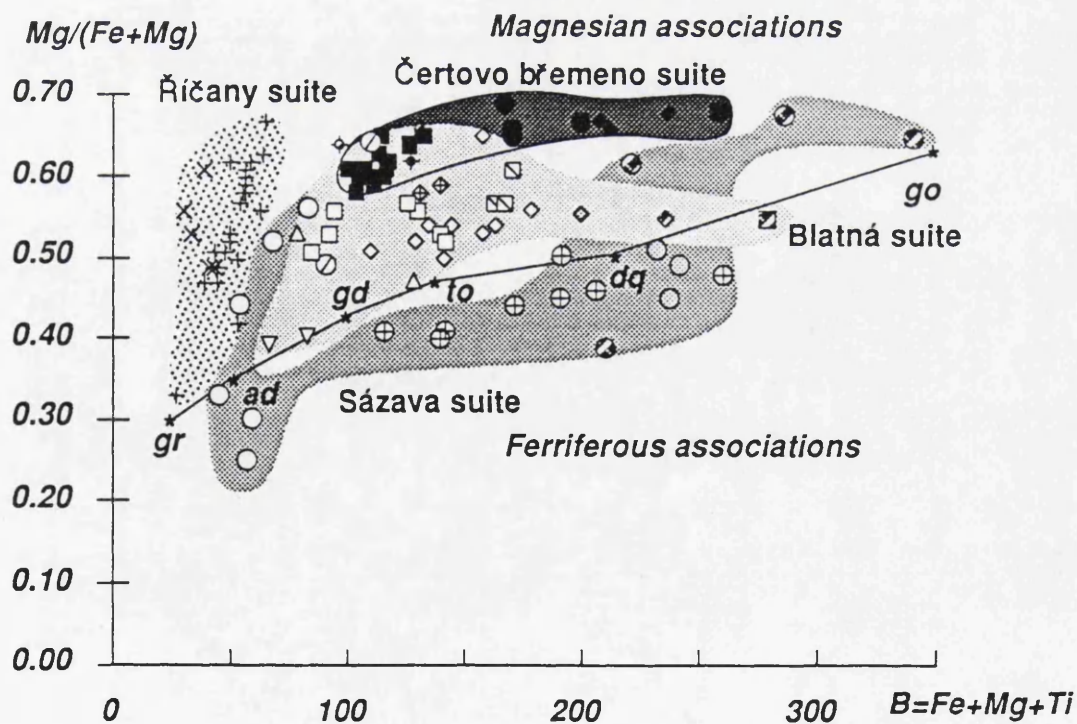


Figure IV.1.13: Plot of B versus $Mg / (Fe + Mg)$ of Debon and Le Fort (1988)

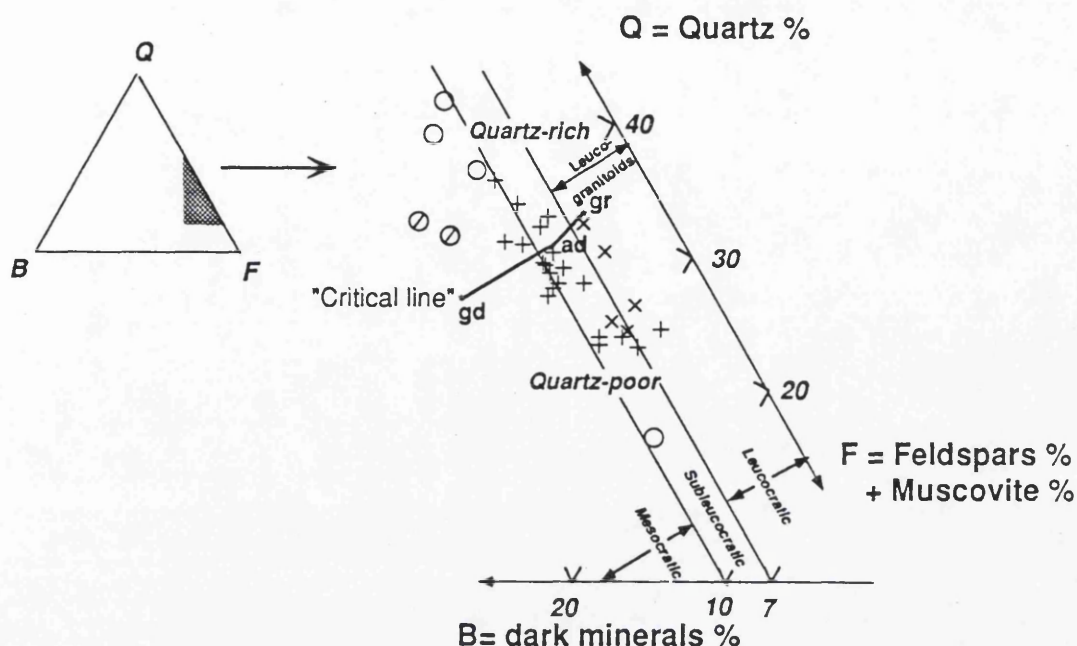


Figure IV.1.14: The Q - B - F diagram (quartz - dark minerals - feldspars)
(after Debon and Le Fort, 1988)

Only the peraluminous intrusions are plotted, i.e. Požáry and Nečín (Sázava suite),
Mrač (Blatná suite), Říčany and Jevany (Říčany suite)

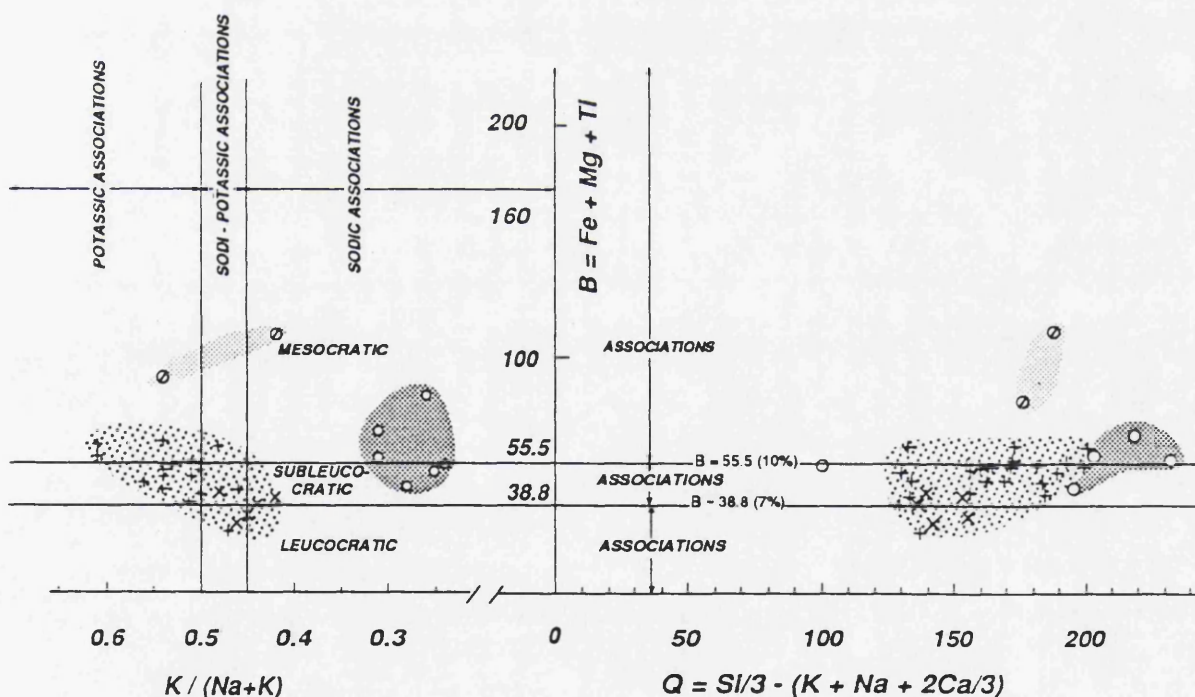


Figure IV.1.15: Classification of aluminous associations using
B as function of Q and K / (Na+K)
(after Debon and Le Fort, 1988)

Only the peraluminous intrusions are plotted, i.e. Požáry and Nečín (Sázava suite),
Mrač (Blatná suite), Říčany and Jevany (Říčany suite)
The dividing lines $B = 55.5$ and $B \sim 38.8$ also show the corresponding
percentage of dark minerals (cf. the previous diagram)

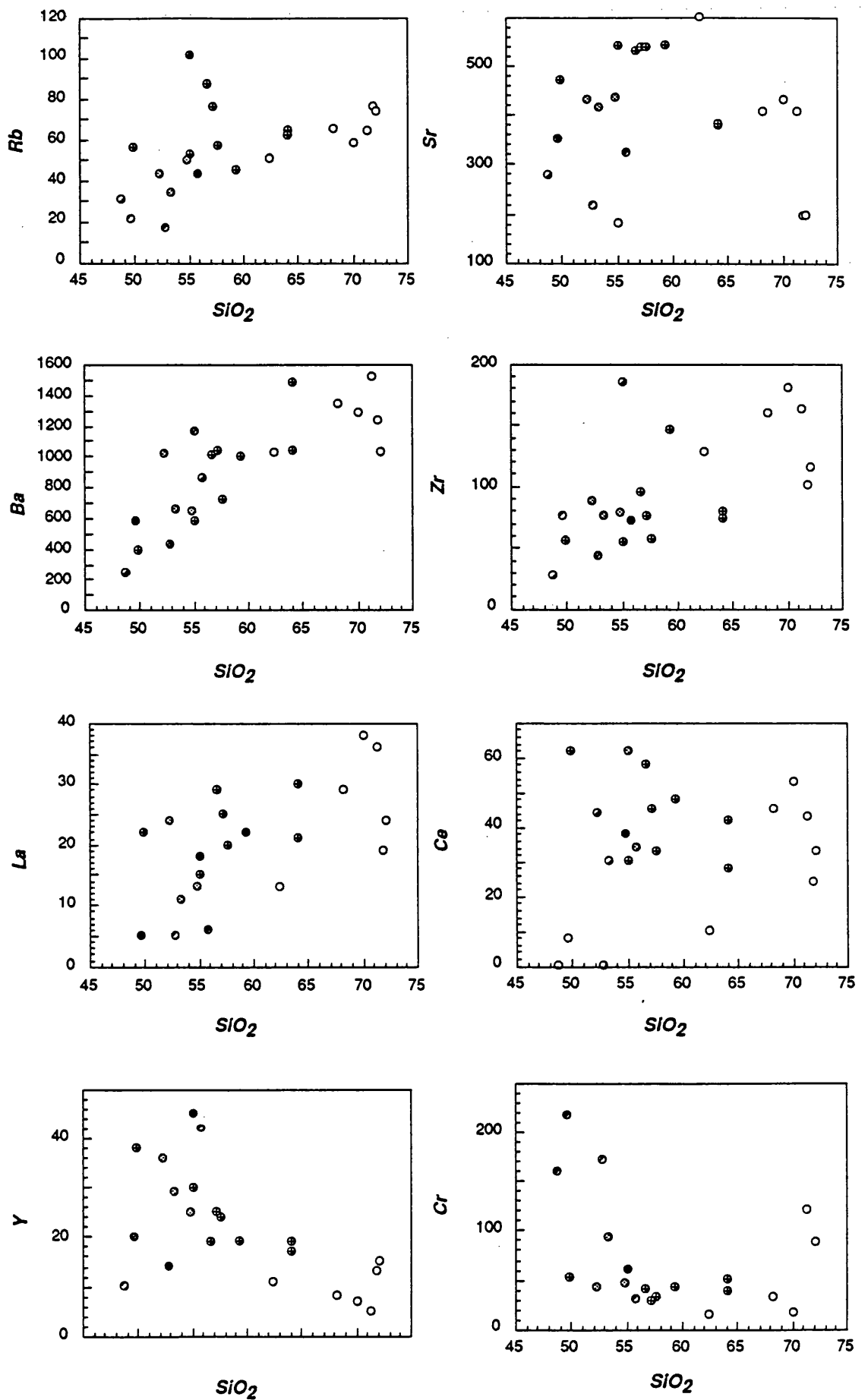


Figure IV.2.1: Bivariate plots of SiO_2 vs. trace elements for the Sázava suite

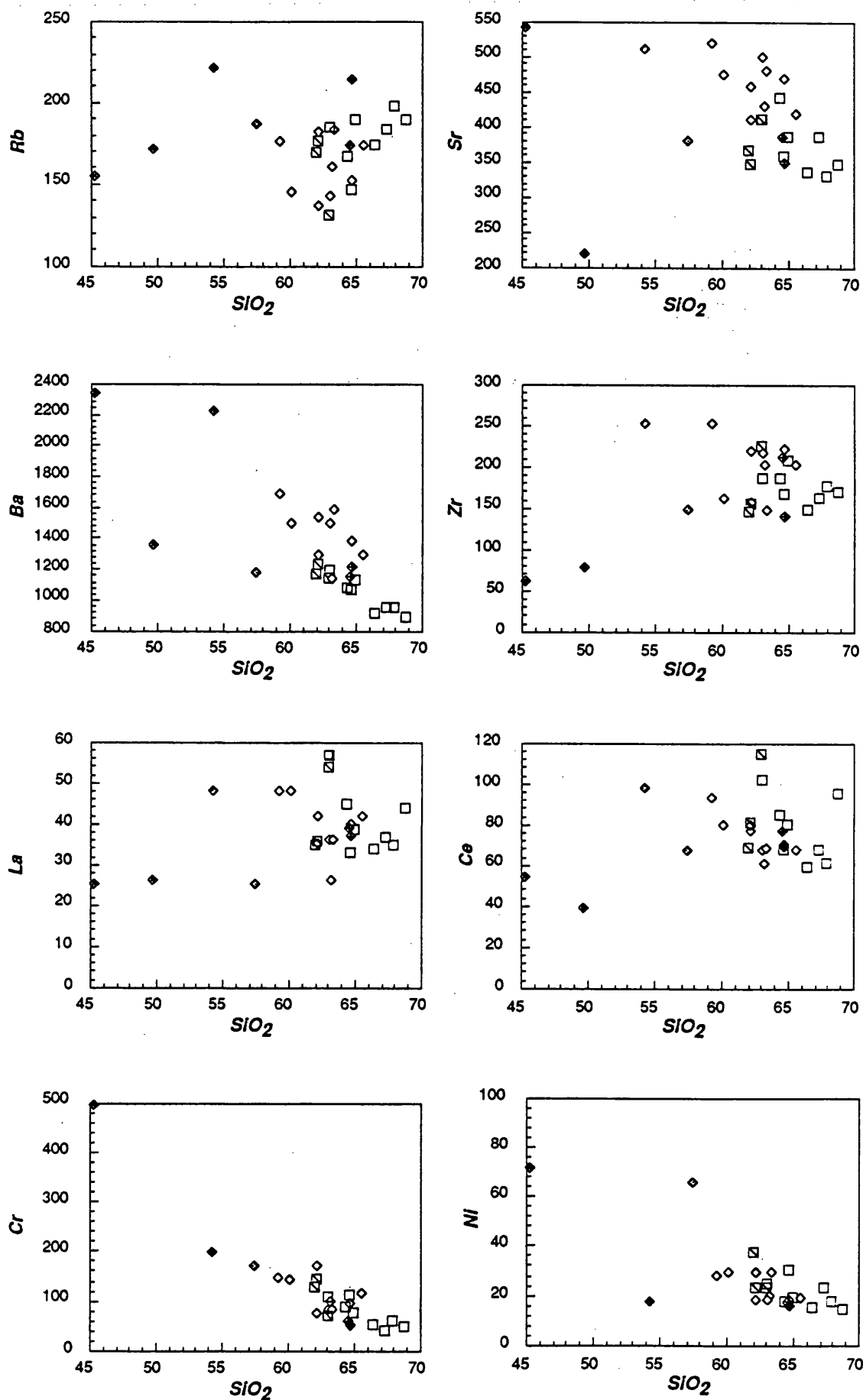


Figure IV.2.2: Bivariate plots of SiO_2 vs. trace elements for the Blatná suite

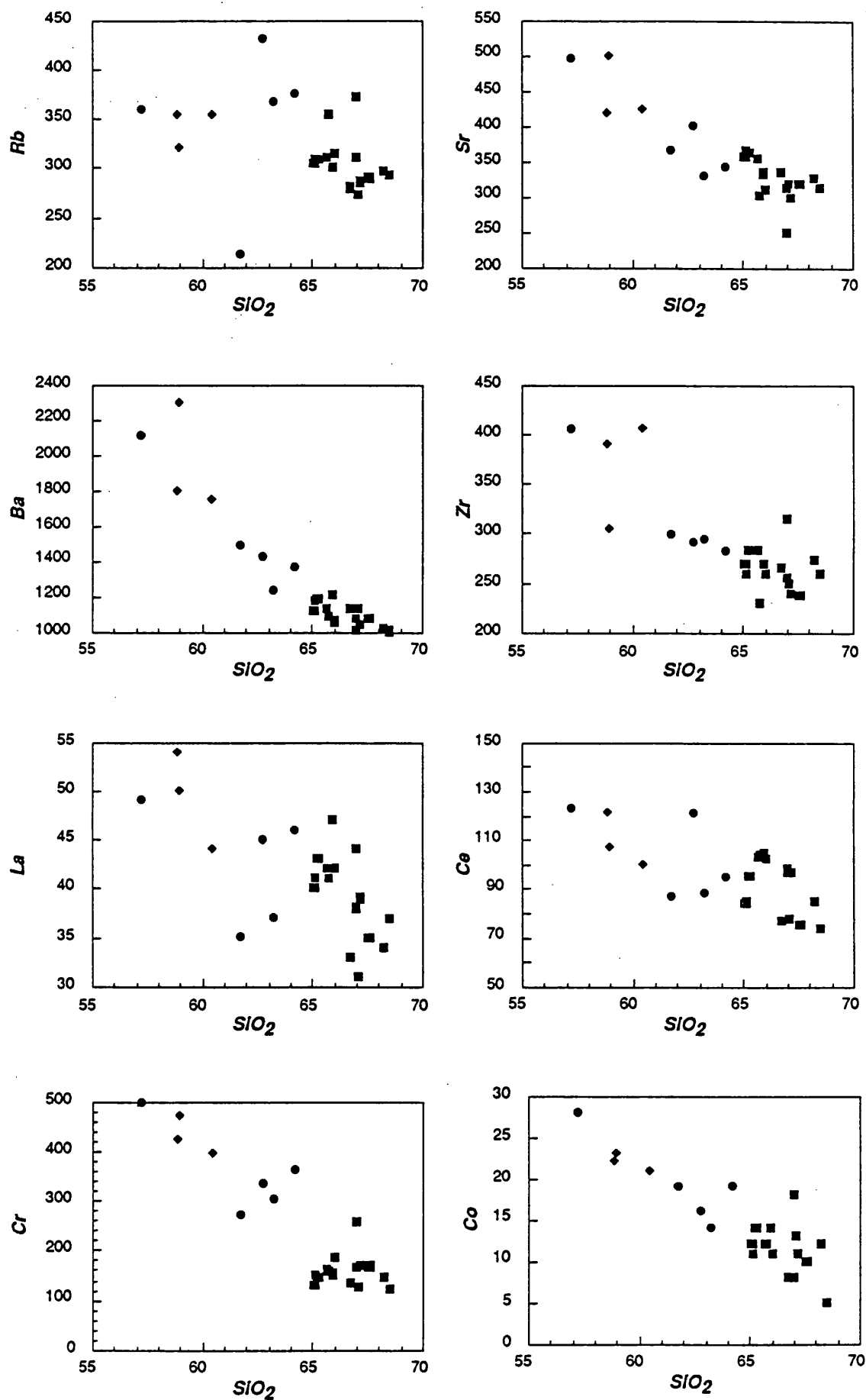


Figure IV.2.3: Bivariate plots of SiO_2 vs. trace elements for the Čertovo břemeno suite

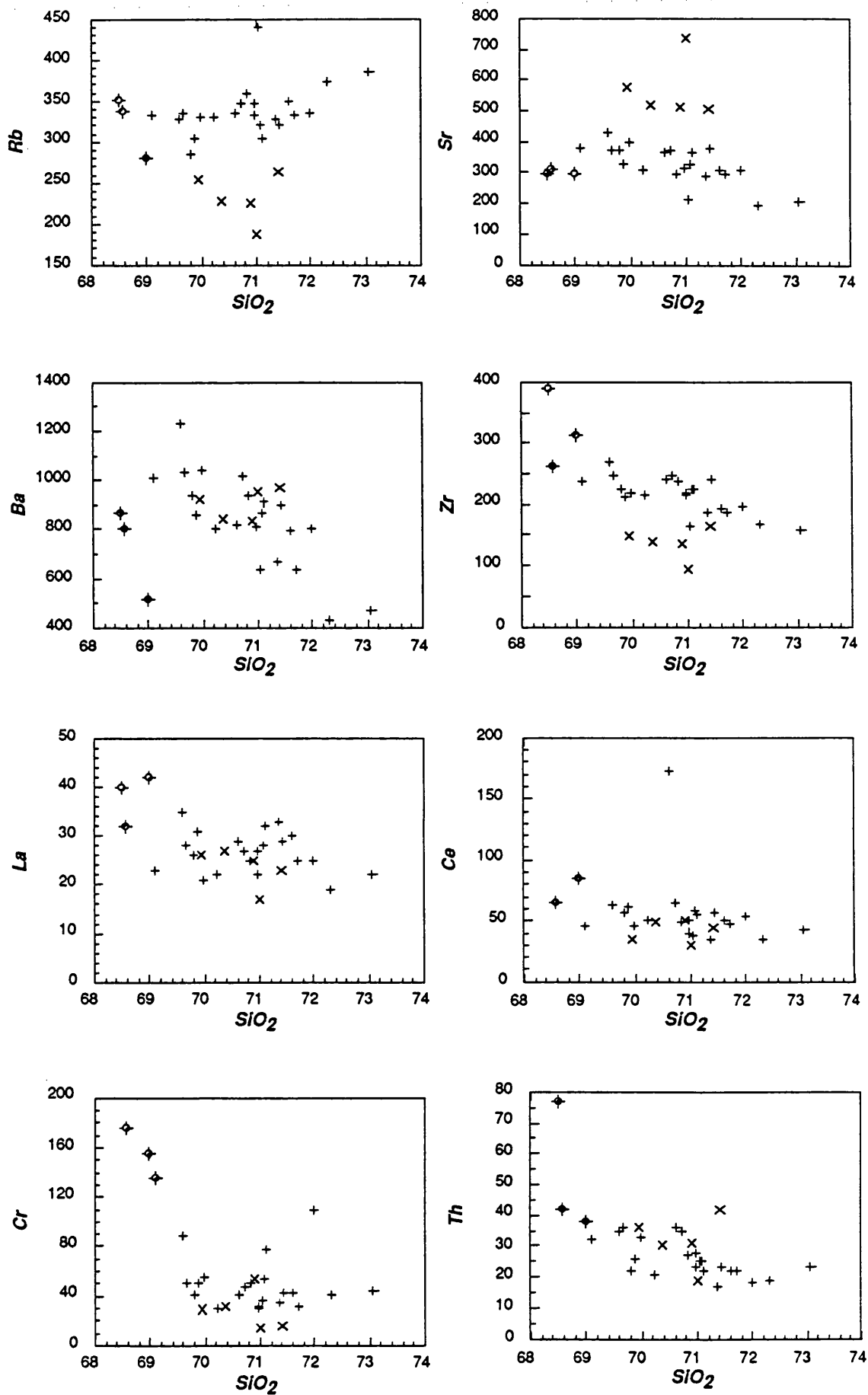


Figure IV.2.4: Bivariate plots of SiO_2 vs. trace elements for the Říčany suite

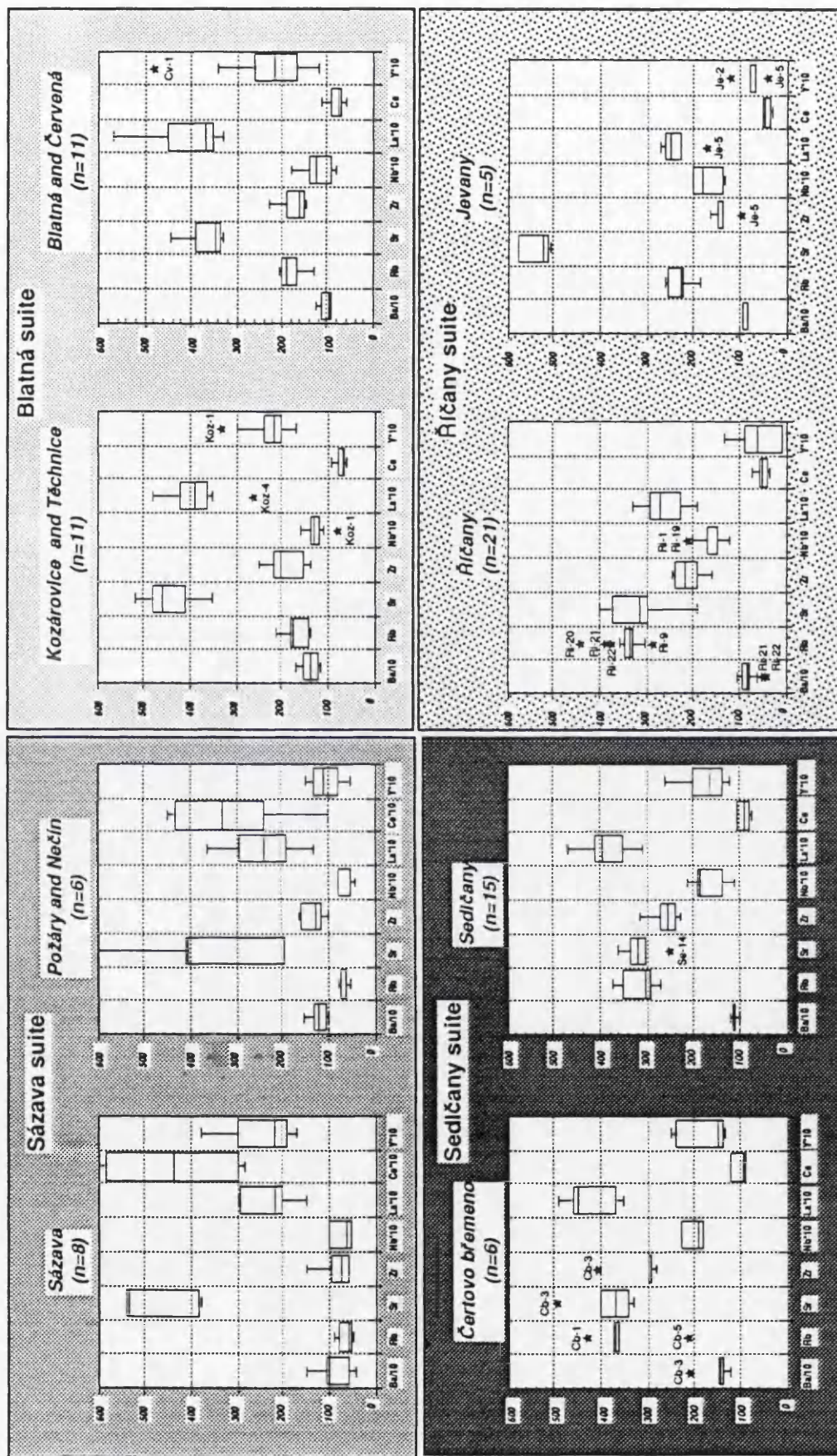


Figure IV.2.5: Trace element composition range of selected intrusions

Note the different scale for the elements:

Ba is divided by 10, whereas Nb, La, Ce (only for the Sázava suite) and Y are multiplied by 10

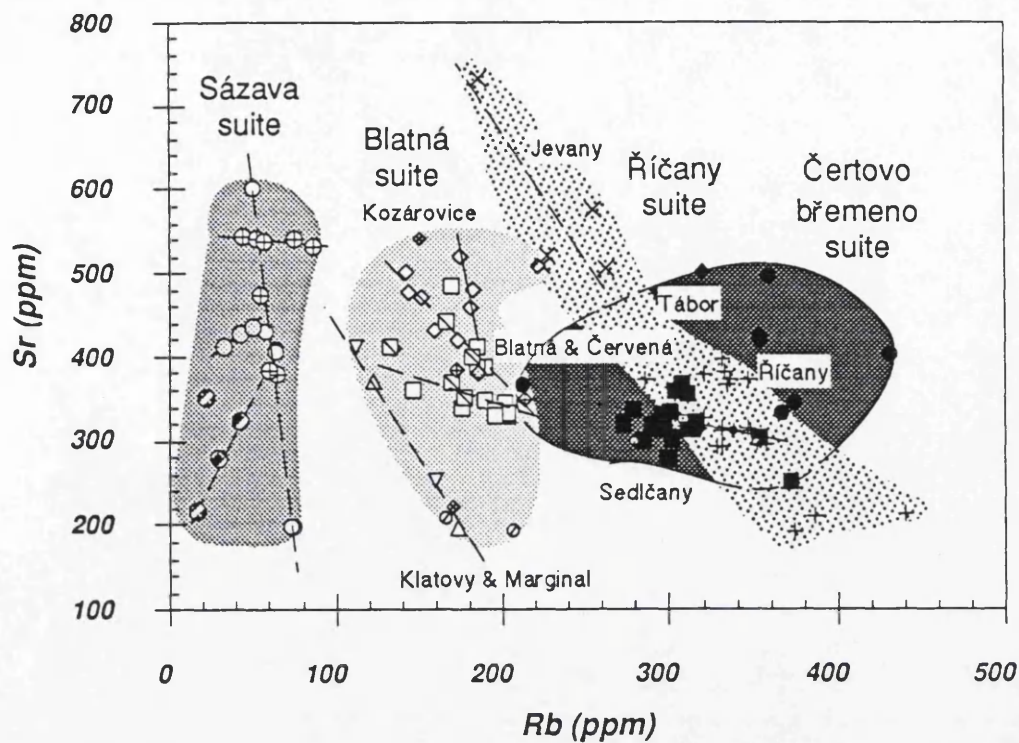


Figure IV.2.6: Rb versus Sr diagram for the rocks of the CBP

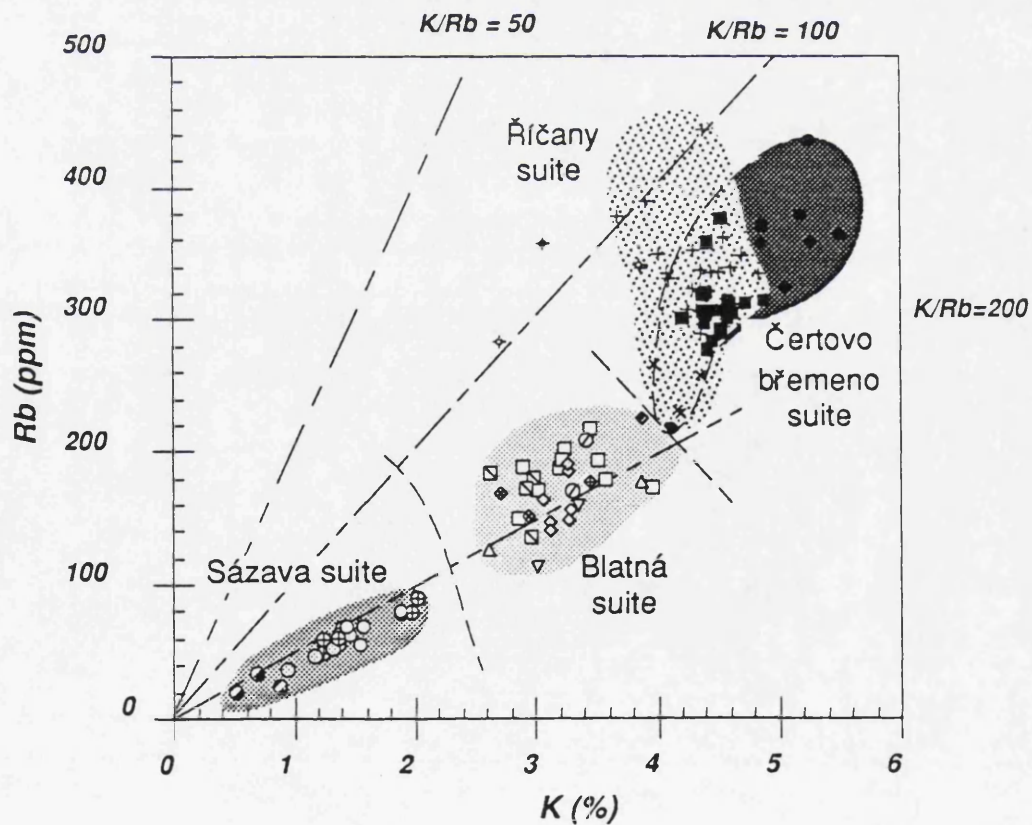


Figure IV.2.7: K versus Rb diagram for the rocks of the CBP

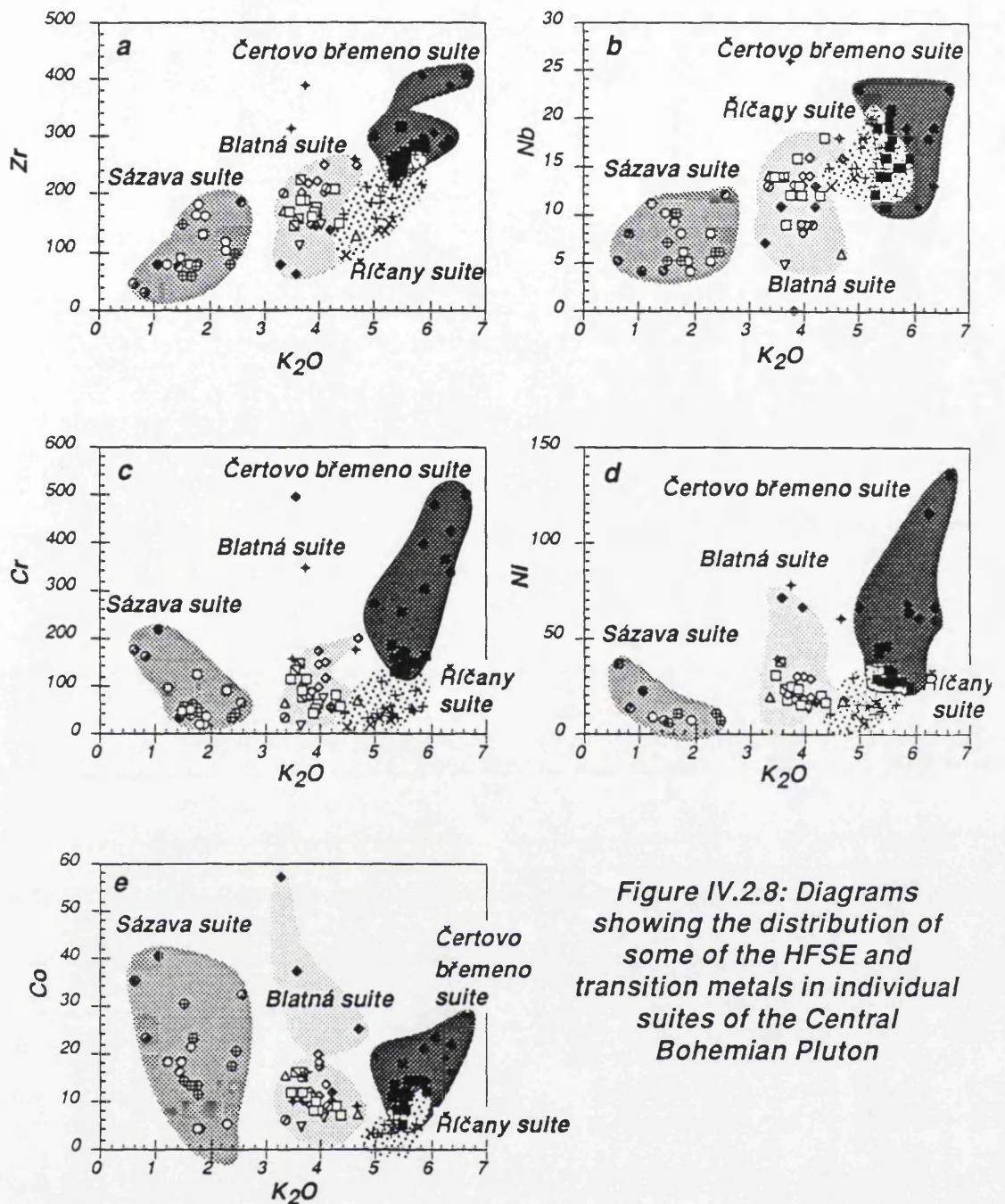


Figure IV.2.8: Diagrams showing the distribution of some of the HFSE and transition metals in individual suites of the Central Bohemian Pluton

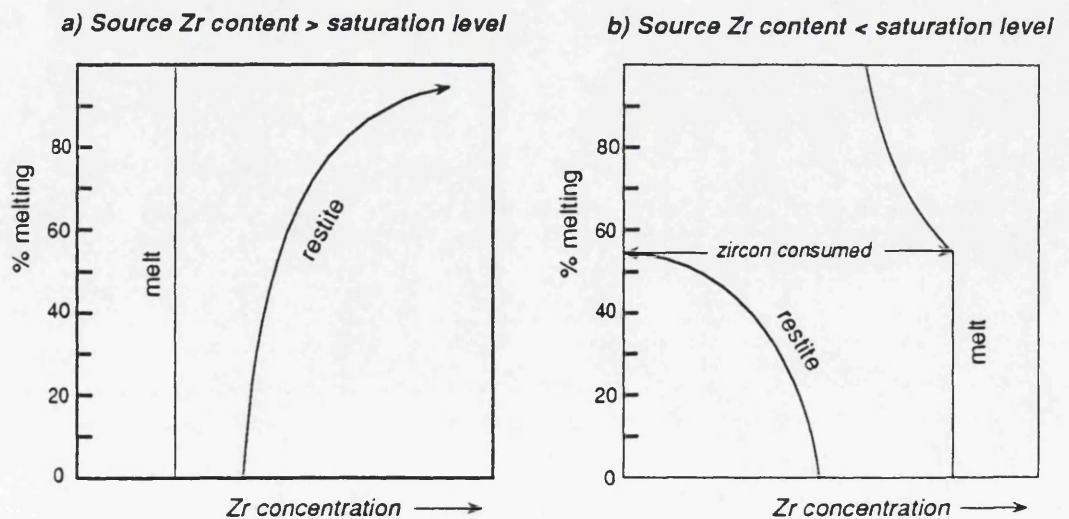


Figure IV.2.9: Variation in Zr content of melts and restites with degree of melting of a crustal source (after Watson and Harrison, 1984)

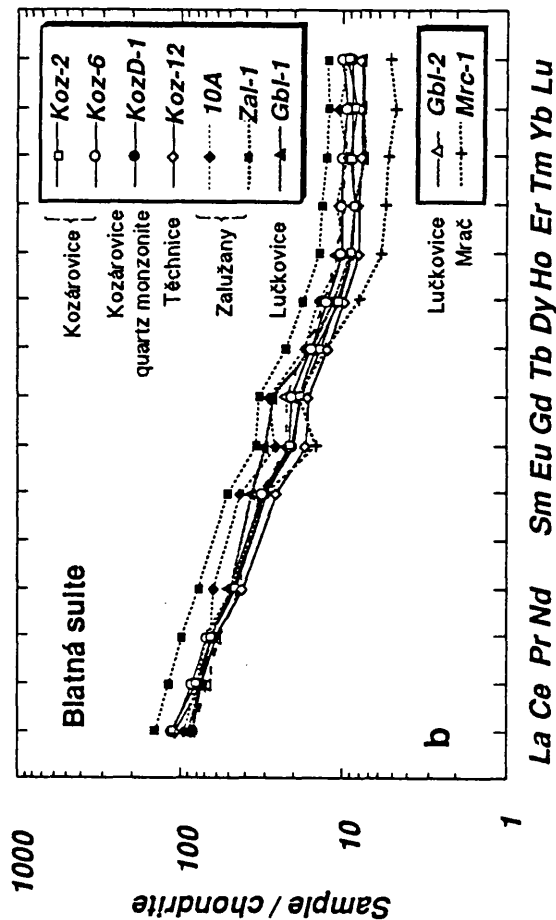
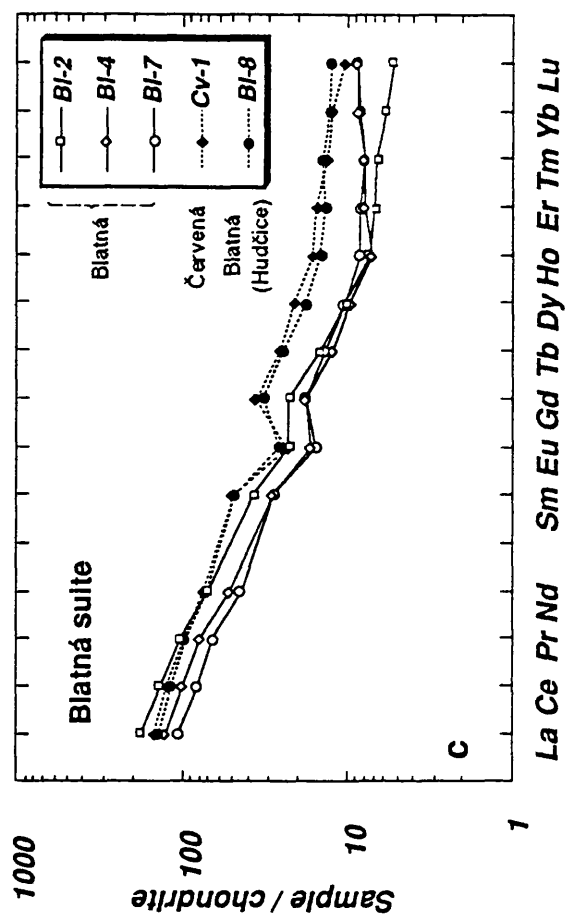
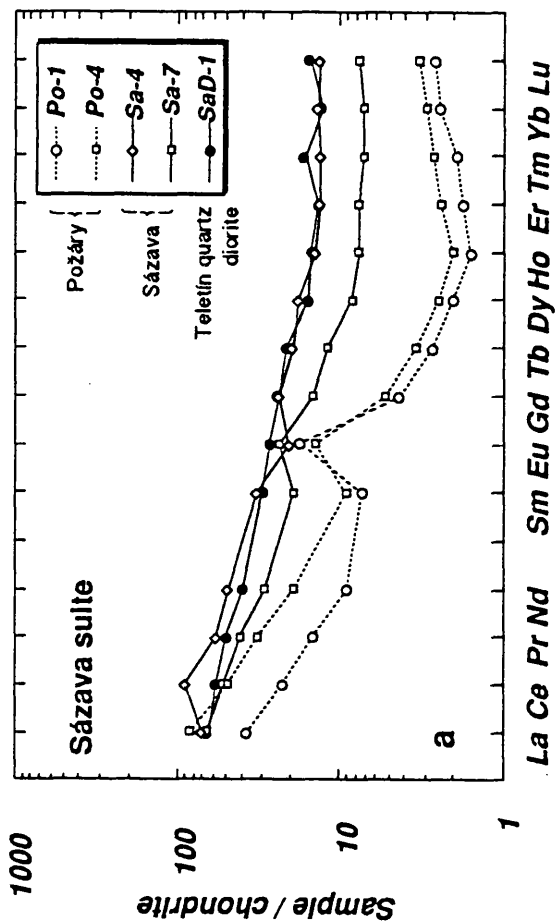


Figure IV.2.10: Rare Earth Element patterns for the Sázava and Blatná suites

The analysis of sample 10A is from Bowes and Košler (1993)

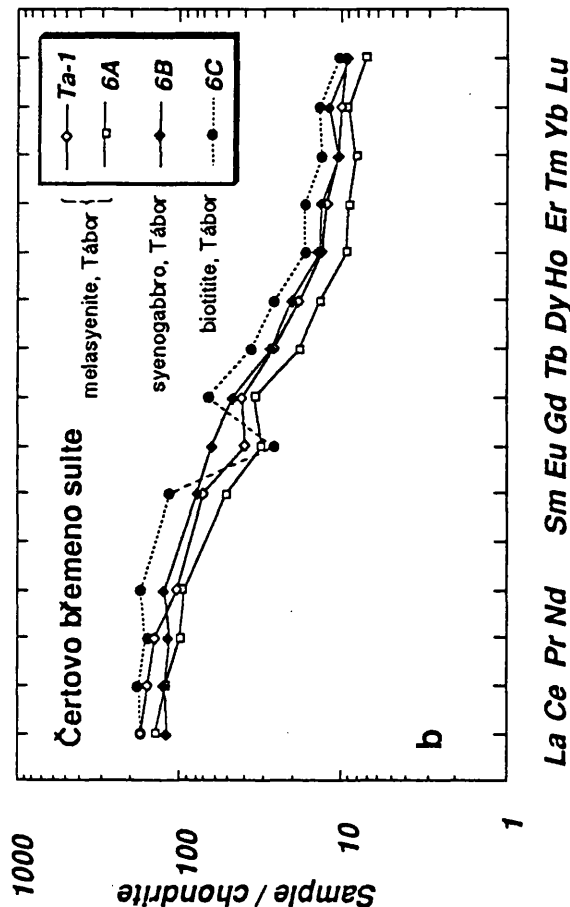
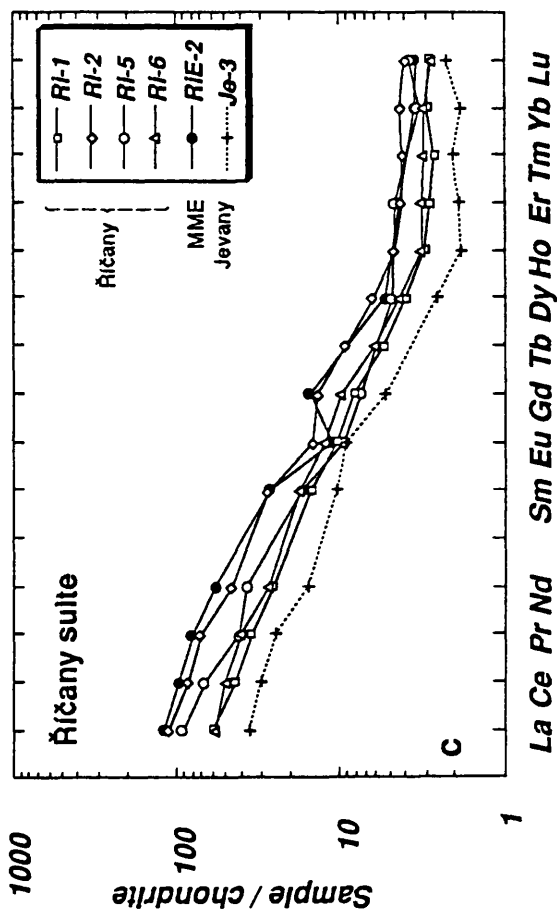
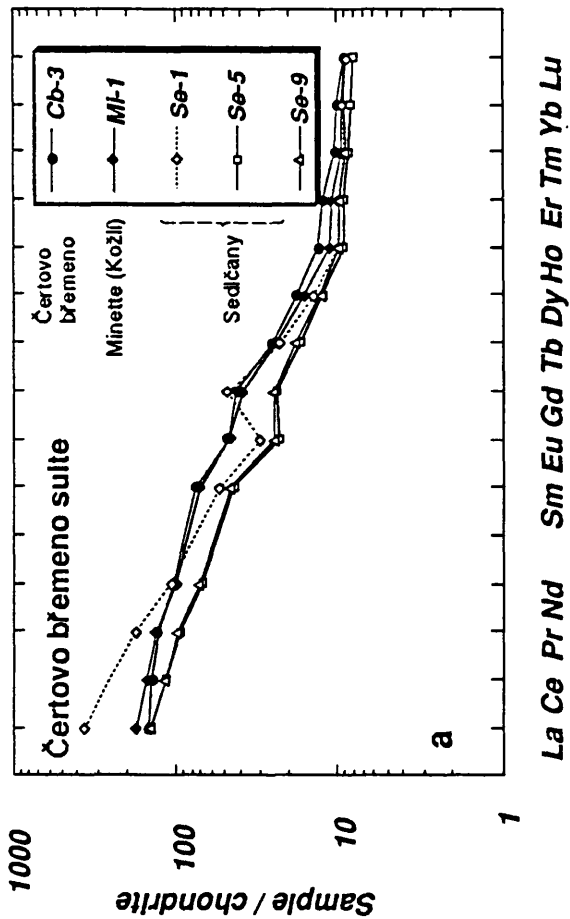


Figure IV.2.11: Rare Earth Element patterns for the Čertovo břemeno and Říčany suites
Analyses of samples 6A-6C are from Bowes and Kosler (1993); ŘI-5 and ŘIE-2 from Janoušek (1991)

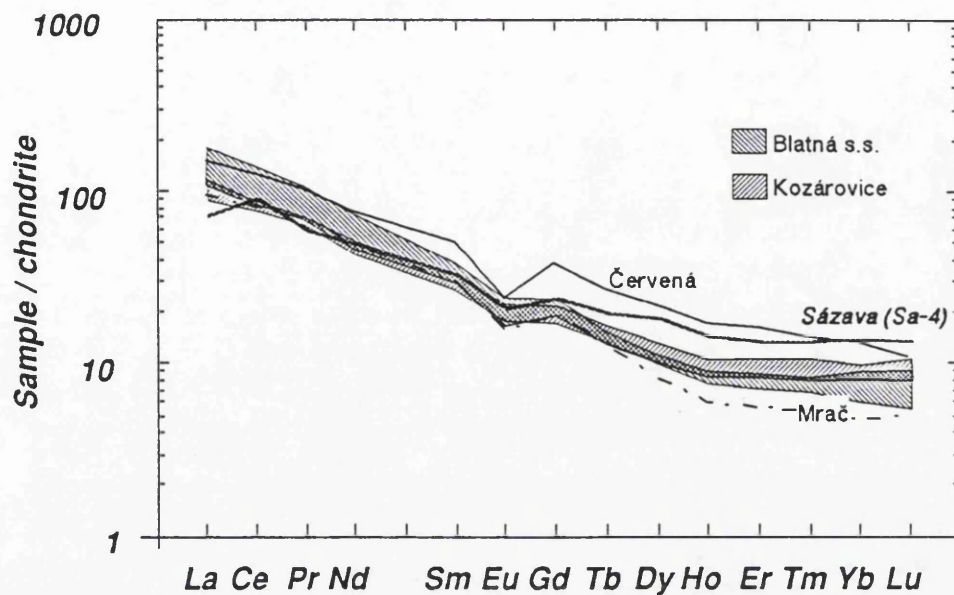
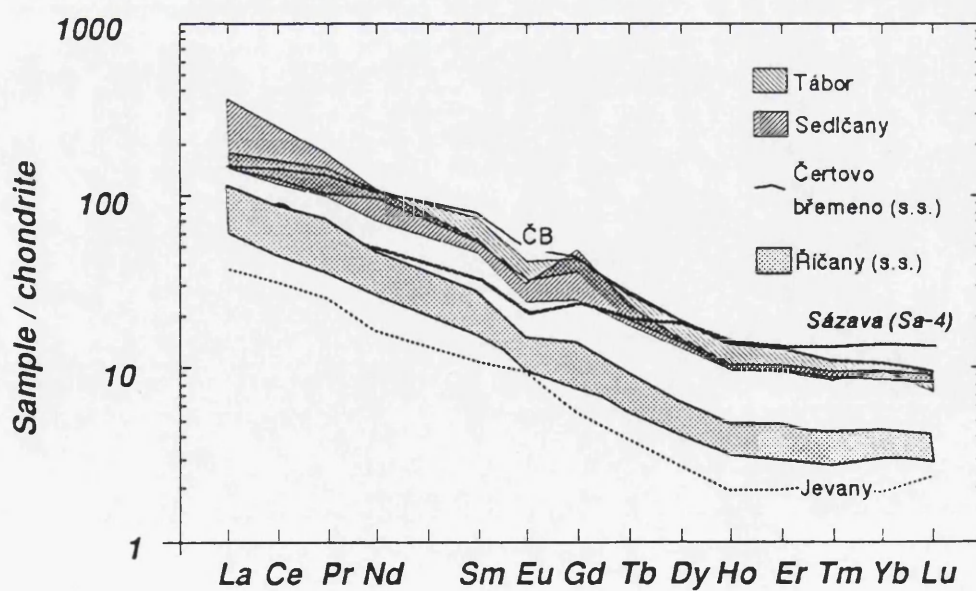


Figure IV.2.12: Comparison of Rare Earth Element patterns for the Blatná, Čertovo břemeno and Říčany suites (compilation of the previous figures; the pattern of the Sázava sample Sa-4 is shown for reference)



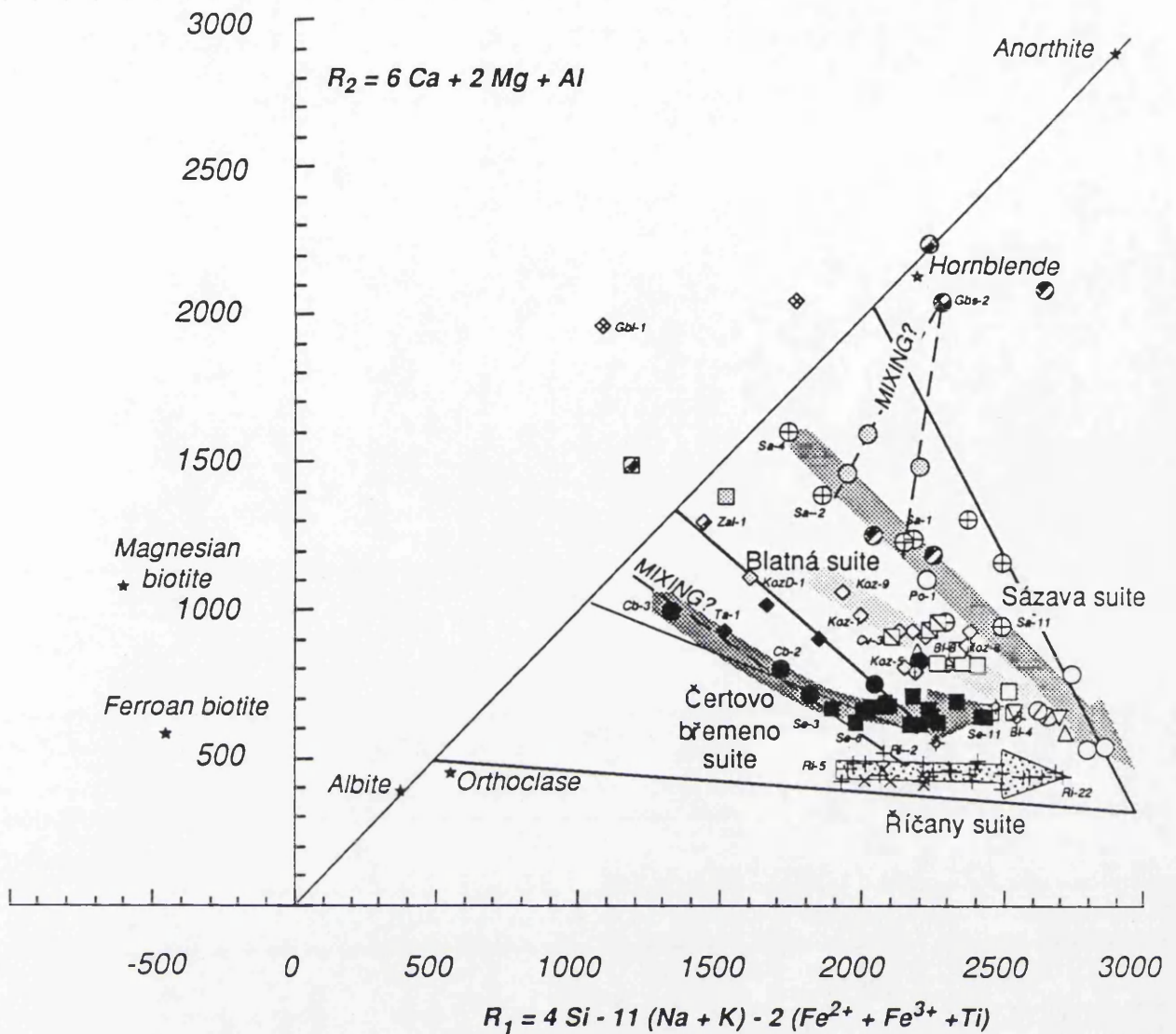


Figure IV.3.1: Plot of R_1 versus R_2 values of De la Roche et al. (1980) (after Batchelor and Bowden, 1985) (petrogenetic implications)

The diagram shows the main fractionation trends, as well as two possible mixing lines, one between a gabbro Gbs-2 and the Sázava magma, the second between a durbachite, similar to Cb-3, and the Říčný granite

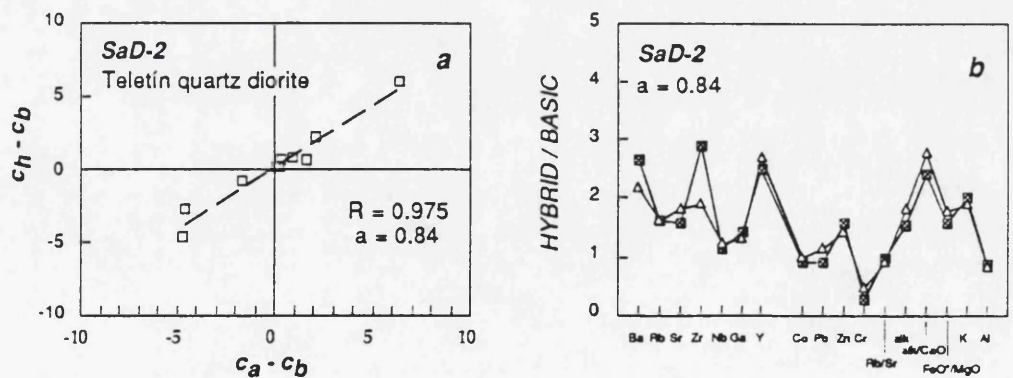
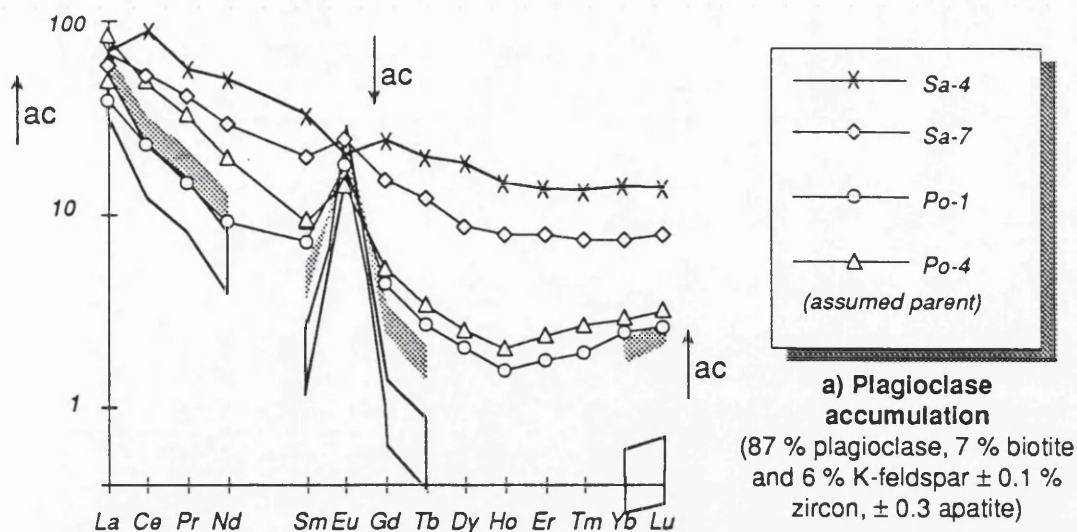


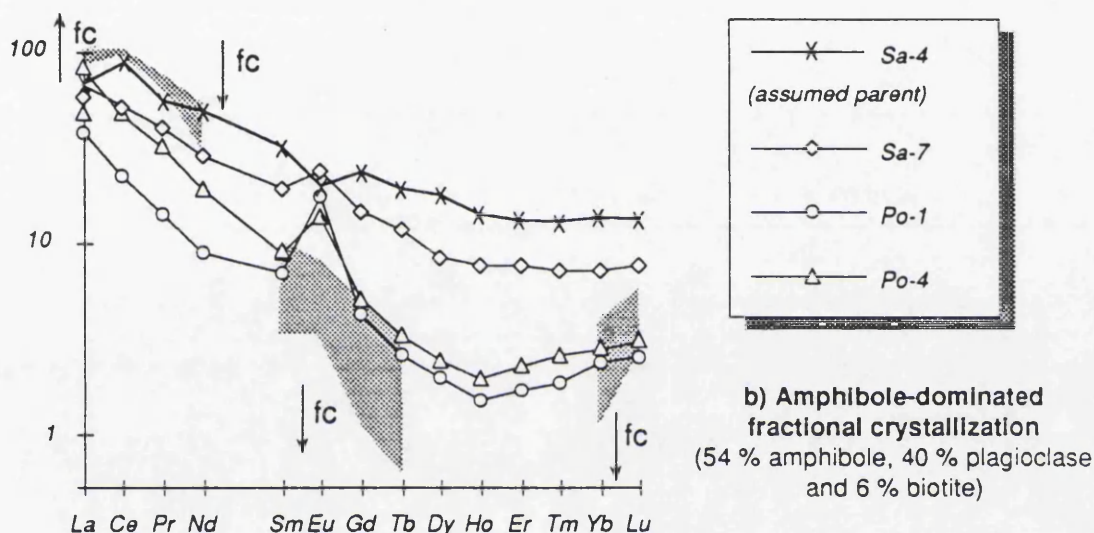
Figure IV.3.2: Mixing test for the Teletín quartz diorite

The selected end-members were gabbro Gbs-2 (B) and sample Sa-1 of the Sázava intrusion

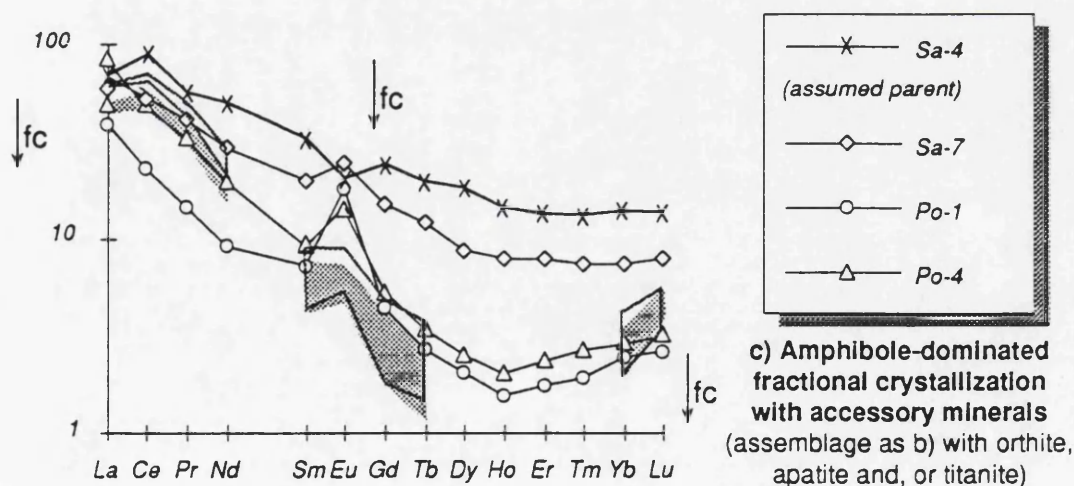
The trace element diagrams compare the actual composition of the hybrids (filled squares) with the calculated compositions (hollow triangles) using proportions from the mixing test for major elements a = fraction of felsic magma in the mixing, R = correlation coefficient, $alk = \text{Na}_2\text{O} + \text{K}_2\text{O}$



The average composition of the solid following up to 50 - 90 % accumulation of 87 % plagioclase, 7 % biotite and 6 % K-feldspar (outlined) and of the same assemblage with 0.1 % zircon and 0.3 % apatite (hatched). The arrows show the development of the cumulate.



Hatched area corresponds to the liquid composition following 30 % - 50 % fractional crystallization ($F = 0.7 - 0.5$) of 54 % amphibole, 40 % plagioclase and 6 % biotite.



The diagram shows fields for the liquid composition after 30 - 40 % fractional crystallization of 54 % amphibole, 40 % plagioclase, 6 % biotite and 0.1 % orthite (hatched) and 20 - 30 % fractional crystallization of 54 % amphibole, 40 % plagioclase, 6 % biotite, 1 % apatite and 0.5 % titanite (outlined).

Figure IV.3.3: REE modelling for the Sázava suite

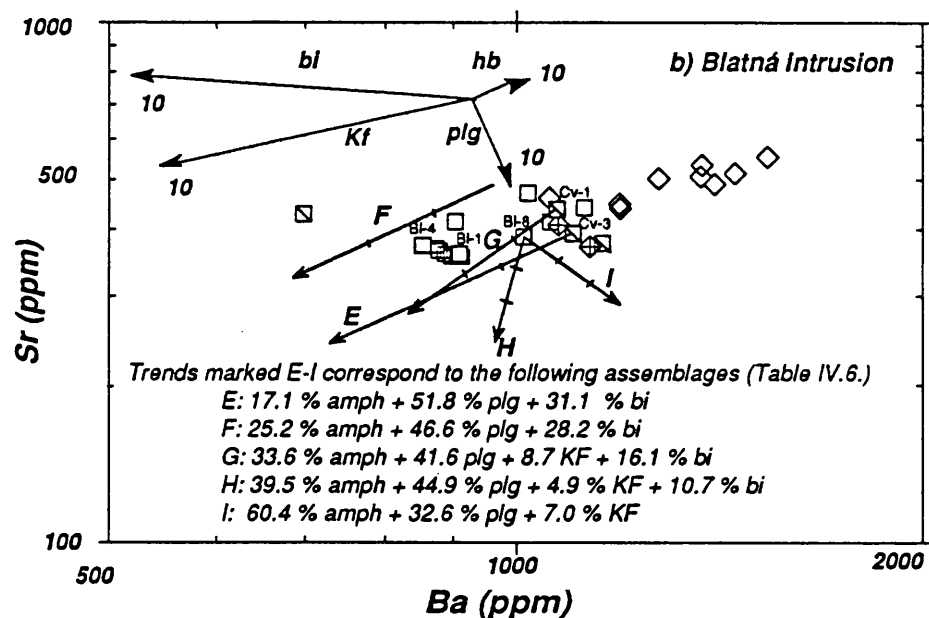
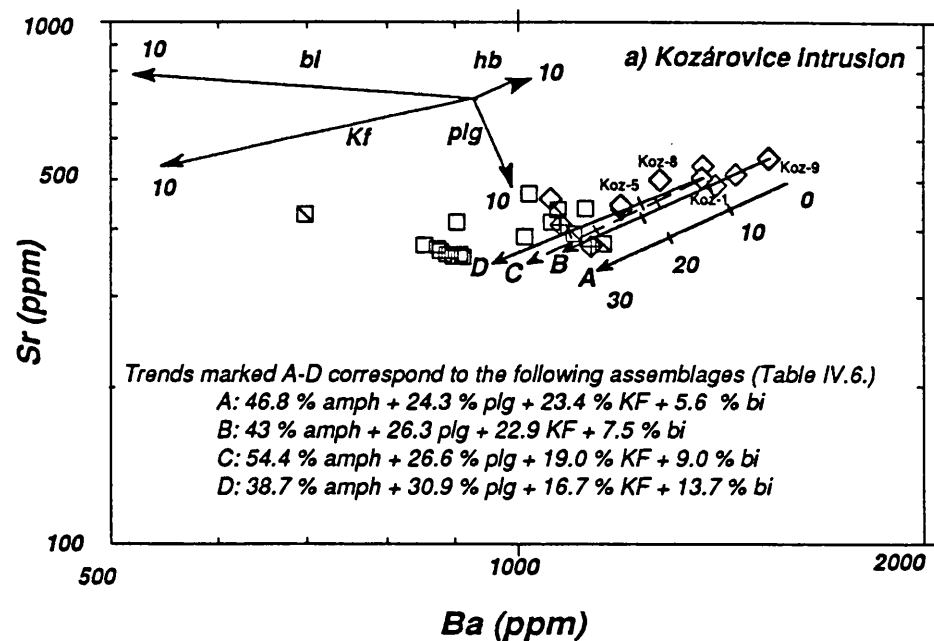


Figure IV.3.4: Fractional crystallization modelling for the Blatná suite (Blatná s.s., Červená, Kozárovce, Těchnice)

Vectors labelled bi, Kf, hb, plg correspond to 10 % fractionation of the appropriate rock-forming minerals (i.e. $F=0.9$); the other vectors correspond to up to 30% fractionation (with tick marks for each 10 %) of assemblages calculated by the least-squares method from majors (A - I).

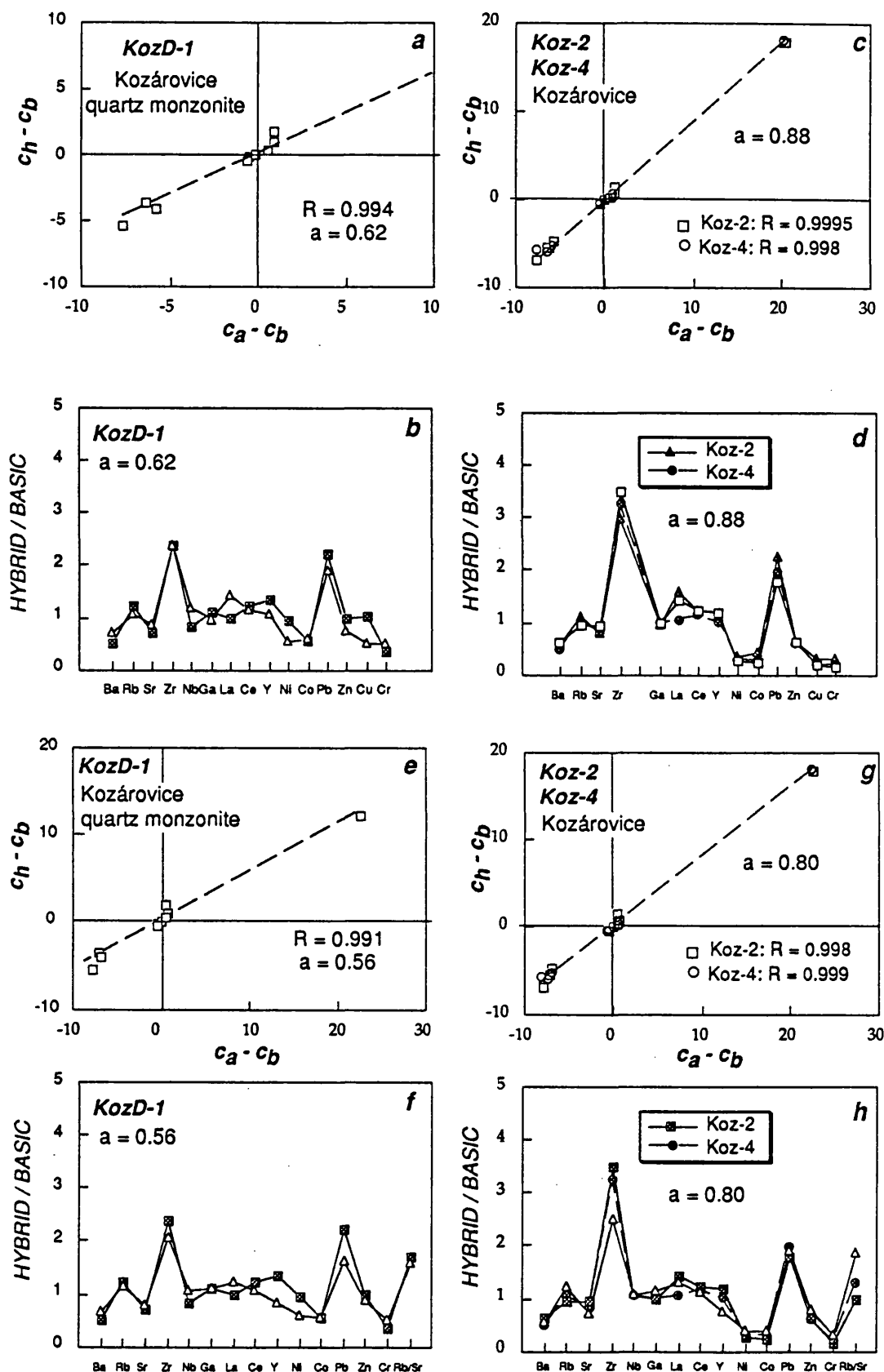


Figure IV.3.5: Mixing tests for the Blatná suite

The selected end-members were Lučkovice monzonite Gbl-1 (B) and Kozárove granodiorite Koz-5 (A) (figs. a-d), and Lučkovice monzonite Gbl-1 (B) and Blatná granodiorite Bl-1 (A) (figs e-h).

The trace element diagrams compare the actual composition of the hybrids (filled symbols) with calculated compositions (empty symbols) using proportions from the mixing test for major elements; a = fraction of felsic magma in the mixing, R = correlation coefficient

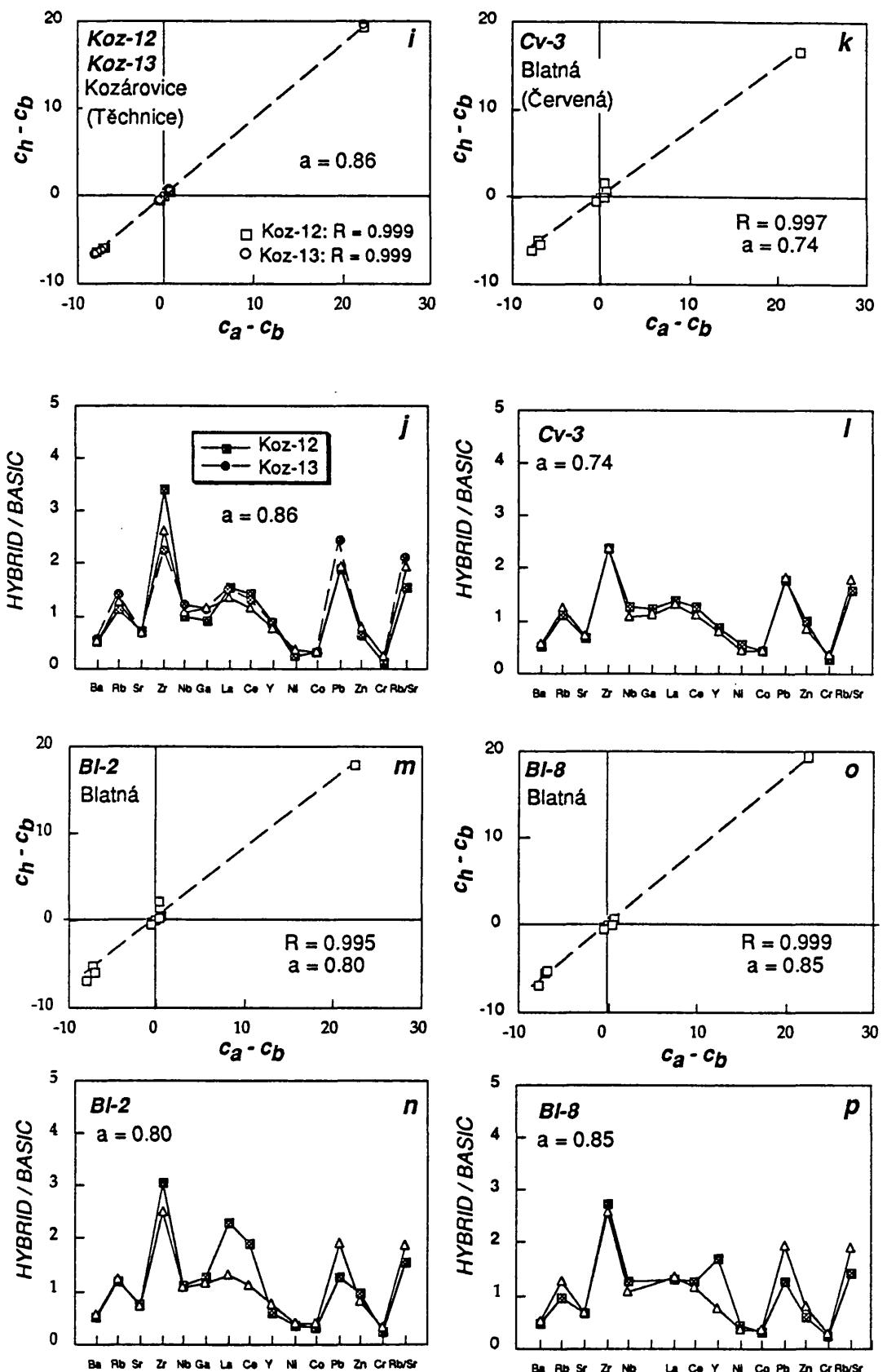
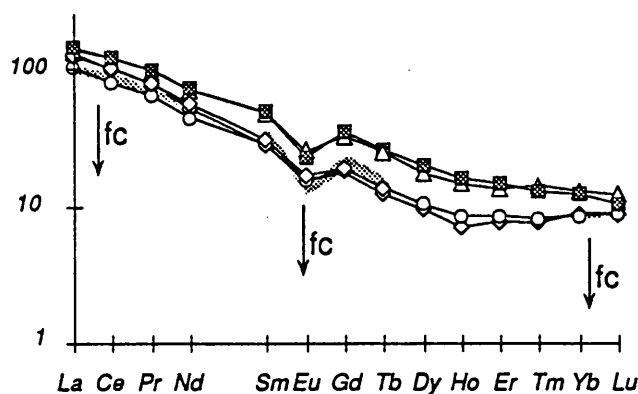


Figure IV.3.5: Mixing tests for the Blatná suite

The selected end-members were Lučkovice monzonite Gbl-1 (B) and Blatná granodiorite BI-1 (A).

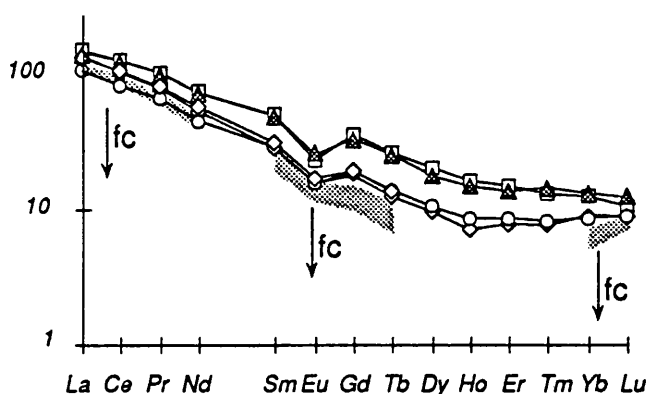
The trace element diagrams compare the actual composition of the hybrids (filled symbols) with calculated compositions (empty symbols) using proportions from the mixing test for major elements; a = fraction of felsic magma in the mixing, R = correlation coefficient



—■— Cv-1
(assumed parent)
—◇— BI-4
—○— BI-7
—△— BI-8

a) Plagioclase-dominated fractional crystallization, Červená as a parent (Model E of Tab. IV.6. with 0.1 % orthite)

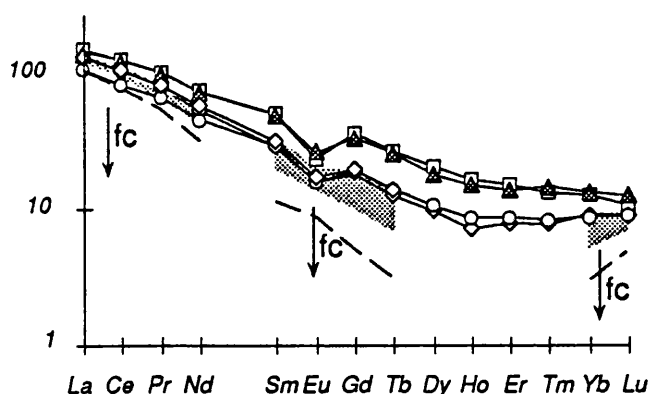
Hatched area corresponds to the liquid composition following 30 % - 40 % fractional crystallization ($F = 0.7 - 0.6$) of 52 % plagioclase, 31 % biotite, 17 % amphibole and 0.1 % orthite.



—△— BI-8
(assumed parent)
—◇— BI-4
—○— BI-7
—□— Cv-1

b) Plagioclase-amphibole-dominated fractional crystallization, amphibole-bearing Blatná as a parent (Model H of Tab. IV.6. with 0.1 % orthite)

Hatched area represents the liquid composition following 20 % - 30 % fractional crystallization of 45 % plagioclase, 40 % amphibole, 11 % biotite, 5 % K-feldspar and 0.1 % orthite.



—△— BI-8
(assumed parent)
—◇— BI-4
—○— BI-7
—□— Cv-1

c) Amphibole-dominated fractional crystallization, amphibole-bearing Blatná as a parent (Model I of Tab. IV.6. with 0.1 % orthite)

The diagram shows the field for the liquid composition following 10 - 20 % fractional crystallization of 60 % amphibole, 33 % plagioclase, 7 % K-feldspar and 0.1 % orthite (hatched) and 30 % fractional crystallization of the same assemblage (dashed line).

Figure IV.3.6: REE modelling for the Blatná suite

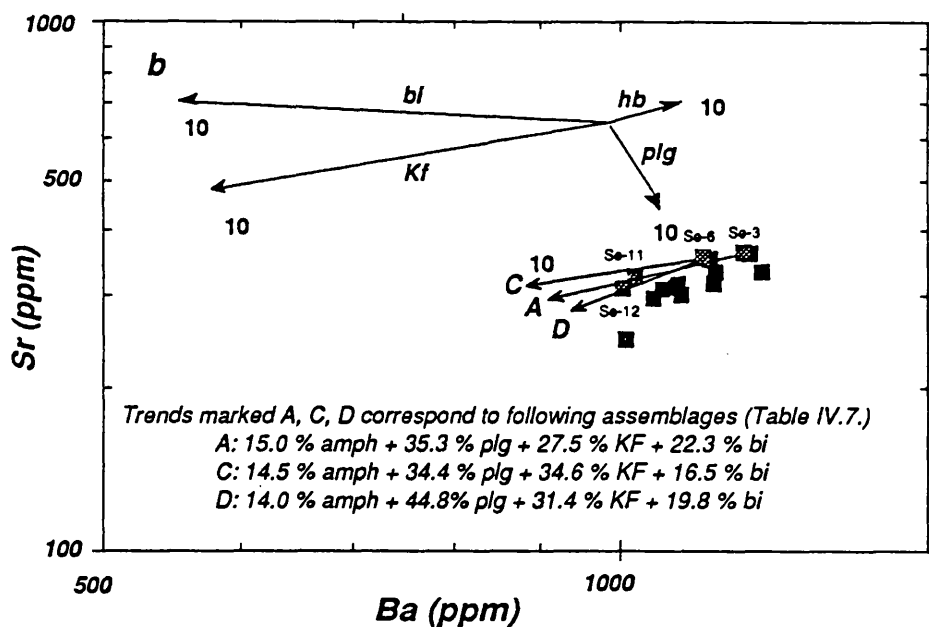
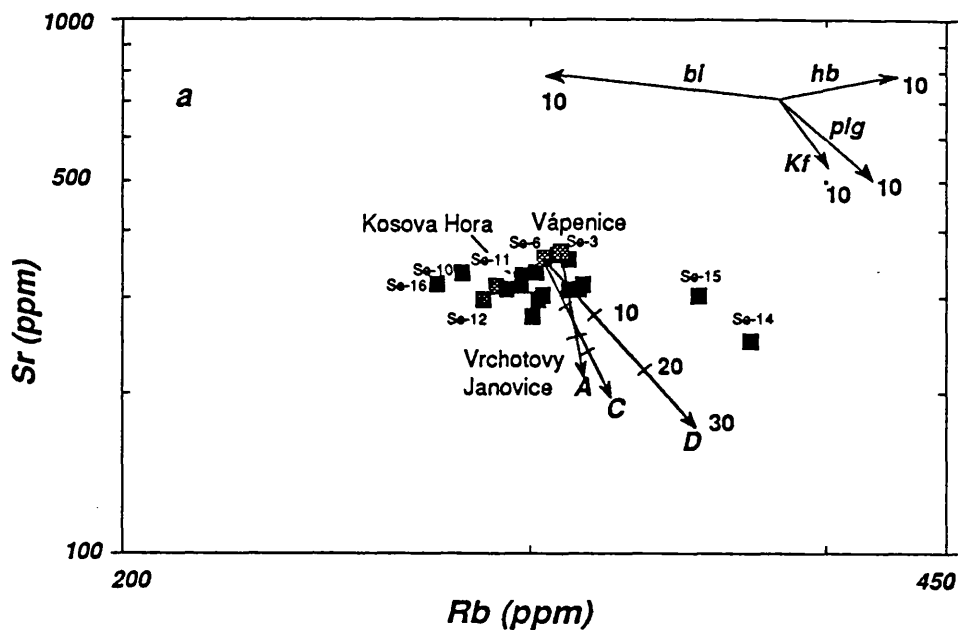


Figure IV.3.7: Fractional crystallization modelling for the Sedlčany granite

Vectors labelled *bi*, *Kf*, *hb*, *plg* correspond to 10 % fractionation of the appropriate rock-forming minerals (i.e. $F=0.9$); the other vectors correspond to up to 30% fractionation (with tick marks for each 10 %) of assemblages calculated by the least-squares method from majors (A, C, D).

Additional Rb-Sr data are from Svojtka (1993).
 The end-members are highlighted by shading

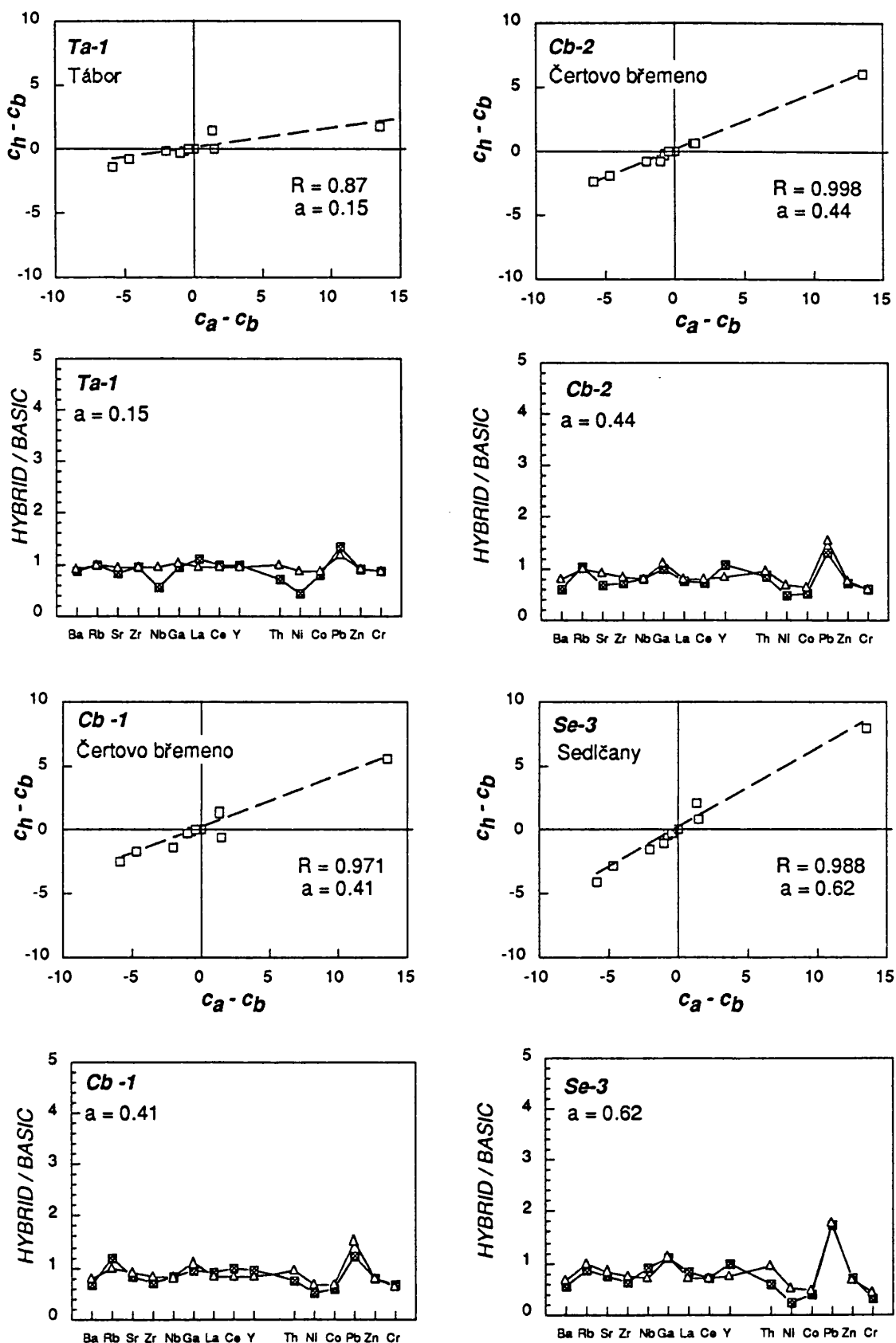


Figure IV.3.8: Mixing test for the Čertovo břemeno and Říčany suites

The selected end-members were samples Cb-3 (B) of the dark facies of the Čertovo břemeno and Ri-2 (A) of the Říčany intrusion. The trace element diagrams compare the actual composition of the hybrids (filled squares) and the calculated compositions (empty triangles) using the proportions calculated from major elements
 a = fraction of acid magma in the mixing, R = correlation coefficient

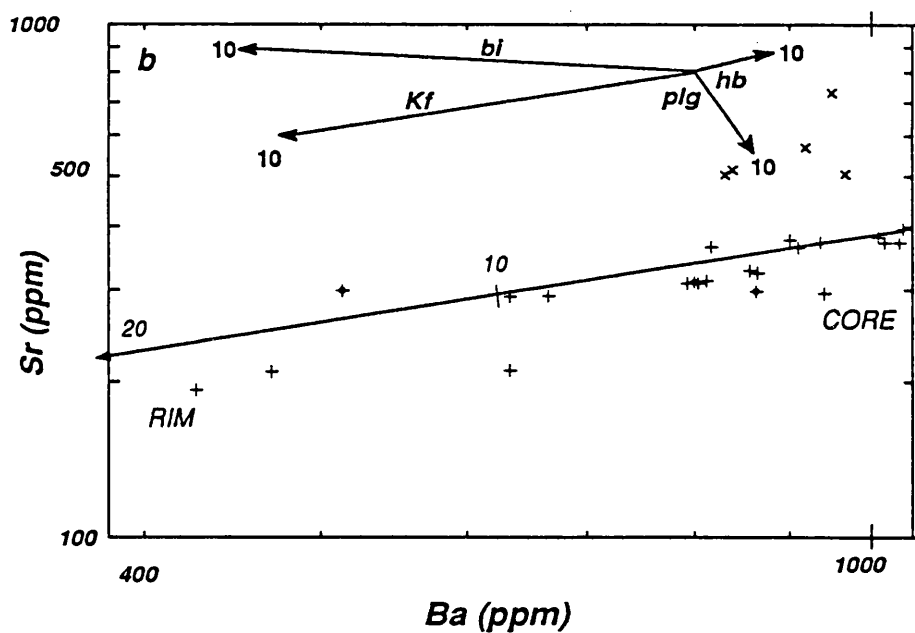
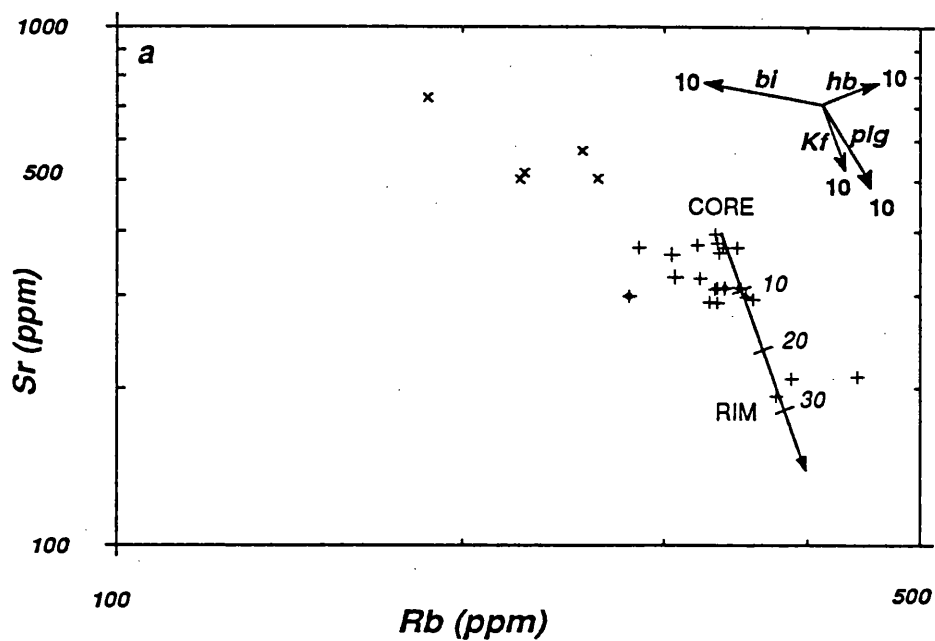


Figure IV.3.9: Fractional crystallization modelling for the Říčany suite

Labelled vectors correspond to 10% fractionation (i.e. $F=0.9$) of the rock-forming minerals; those not labelled show effects of up to 30% fractionation of K-feldspar

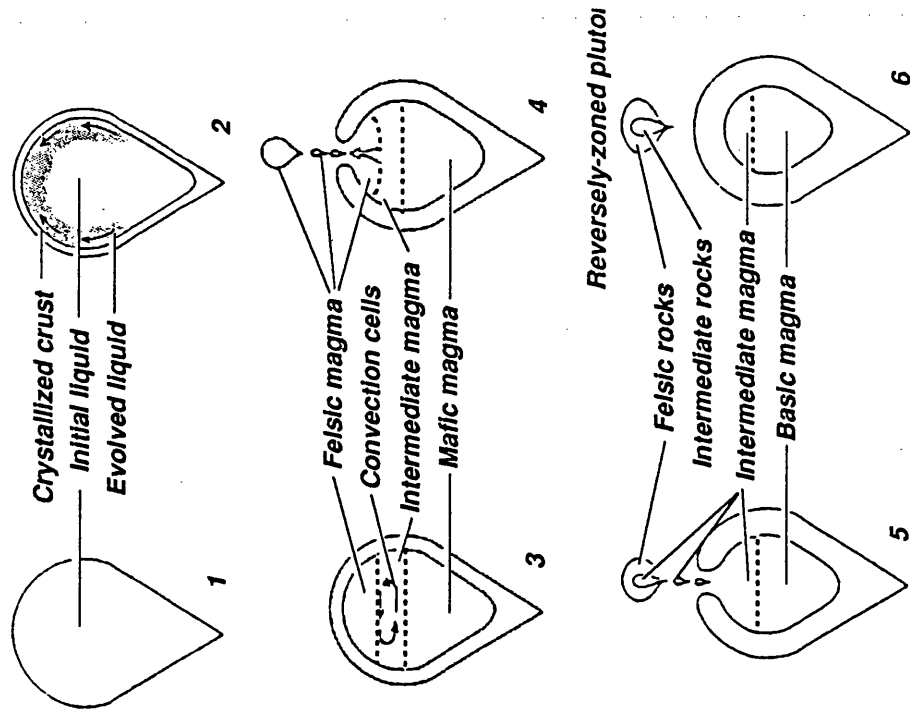


Figure IV.3.11: Cartoon illustrating one of the possible scenarios for the origin of reversely-zoned plutons: The Lacorne Complex, Québec (after Bourne and Danis, 1987)
For explanation, see the text

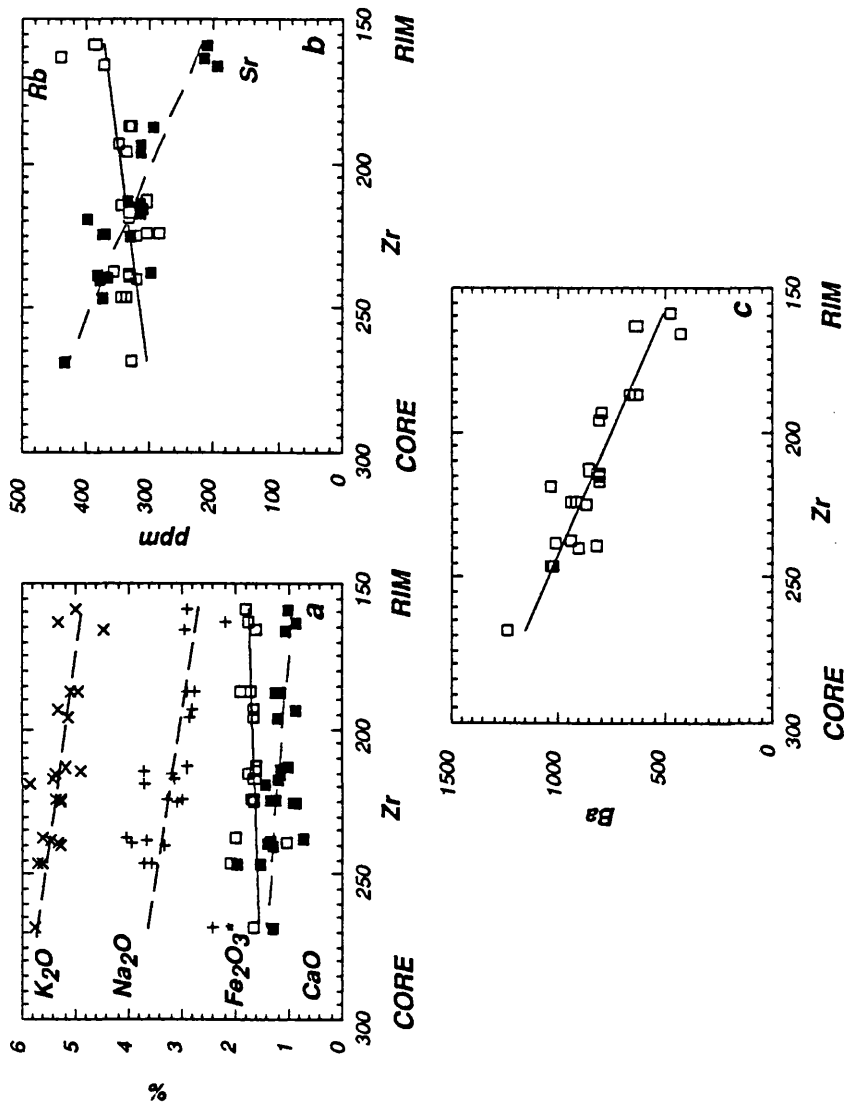


Figure IV.3.10: Binary plots showing the inverse nature of the zoning in the Říčaný granite (excluding the Jevany leucogranite)

Note inversion of the Zr axes

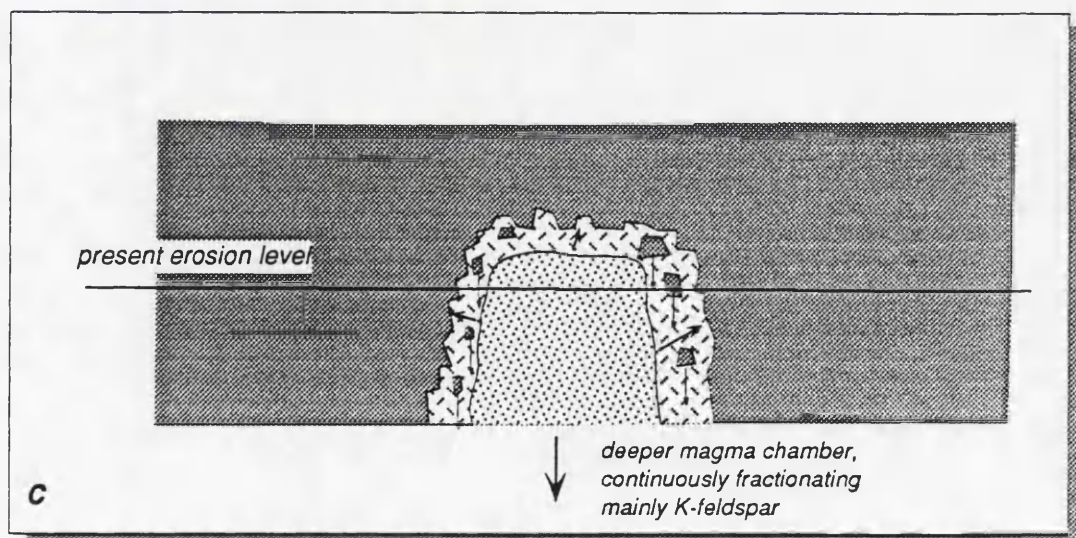
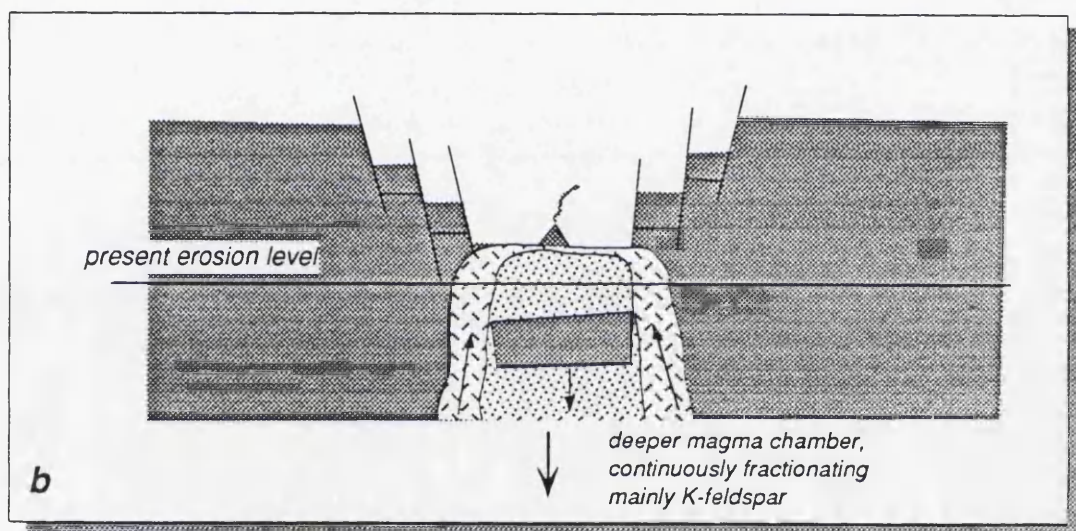
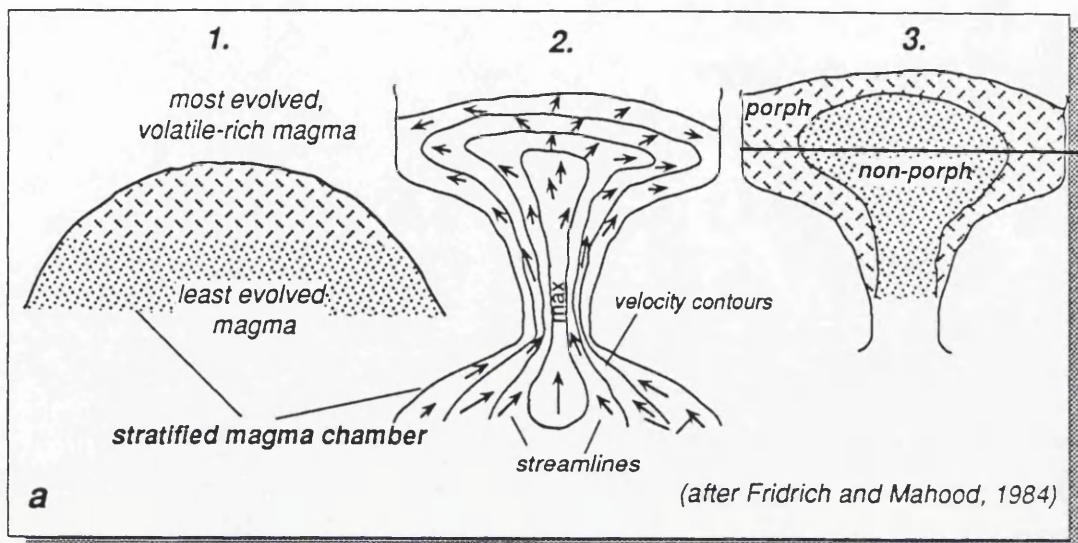


Figure IV.3.12: Possible origin of the reverse zoning in the Rířany intrusion
 (a) emplacement as a single batch from a compositionally-zoned magma chamber,
 (b) in several batches following cauldron subsidence, or (c) accompanied by stoping
 (for discussion, see text)

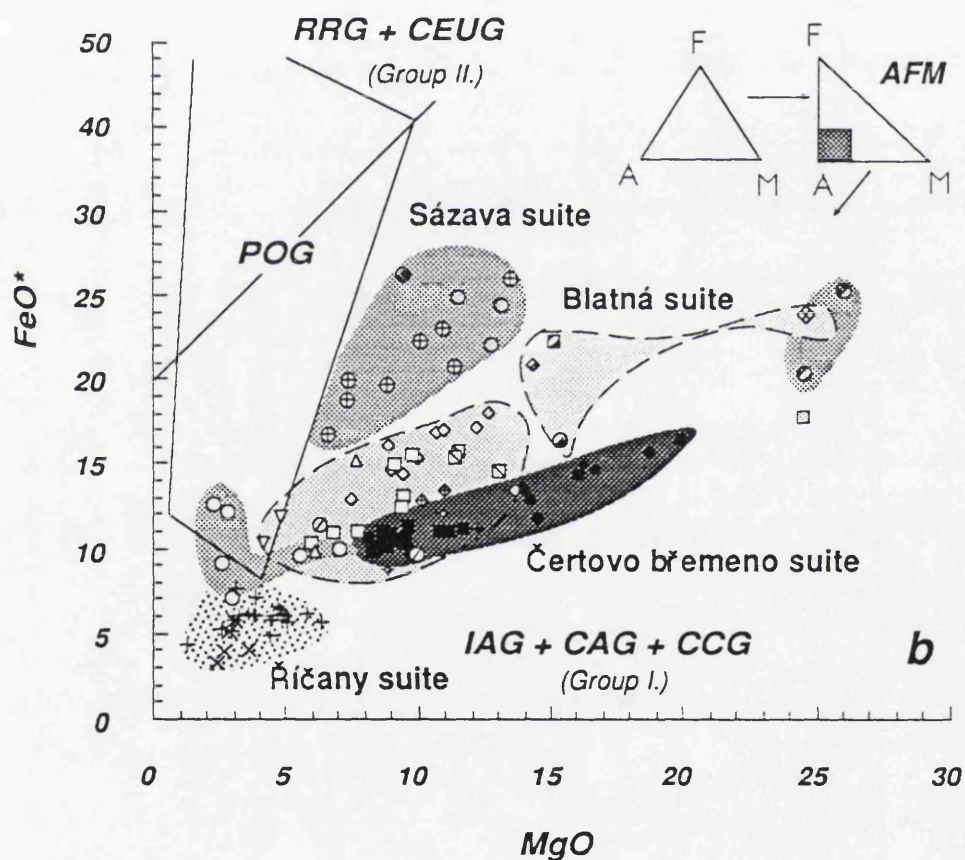
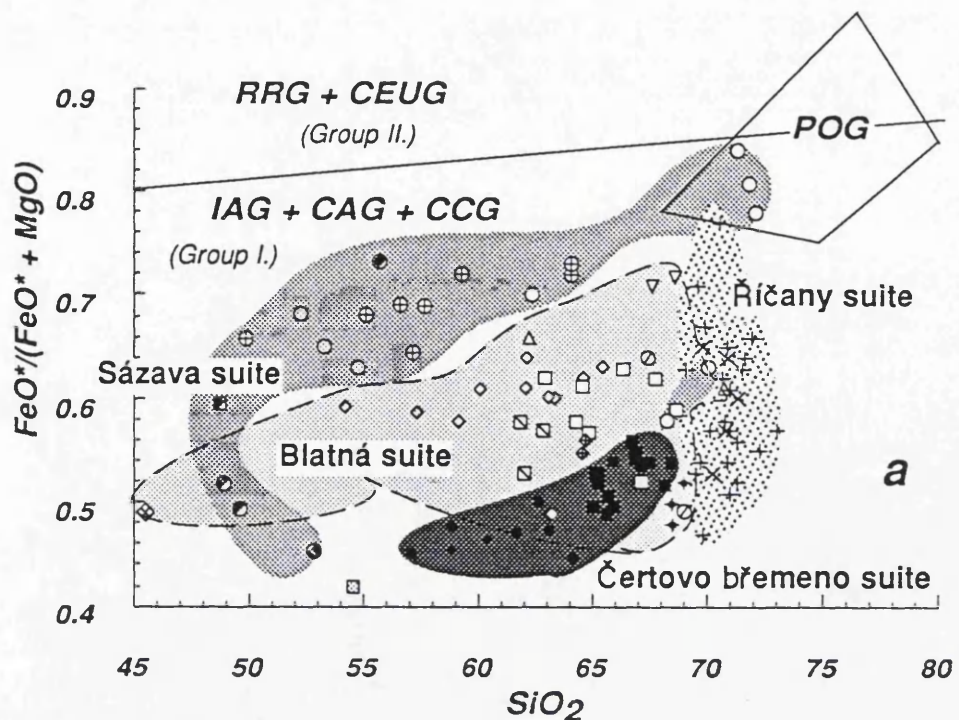


Figure IV.4.1: Tectonic discrimination of granitoids of the CBP (after Maniar and Piccoli, 1989)

IAG	Island Arc Granitoids	CAG	Continental Arc Granitoids
CCG	Continental Collision Granitoids	POG	Post-Orogenic Granitoids
RRG	Rift-Related Granitoids	CEUG	Continental Epeirogenic Granitoids
OP	Oceanic Plagiogranites		

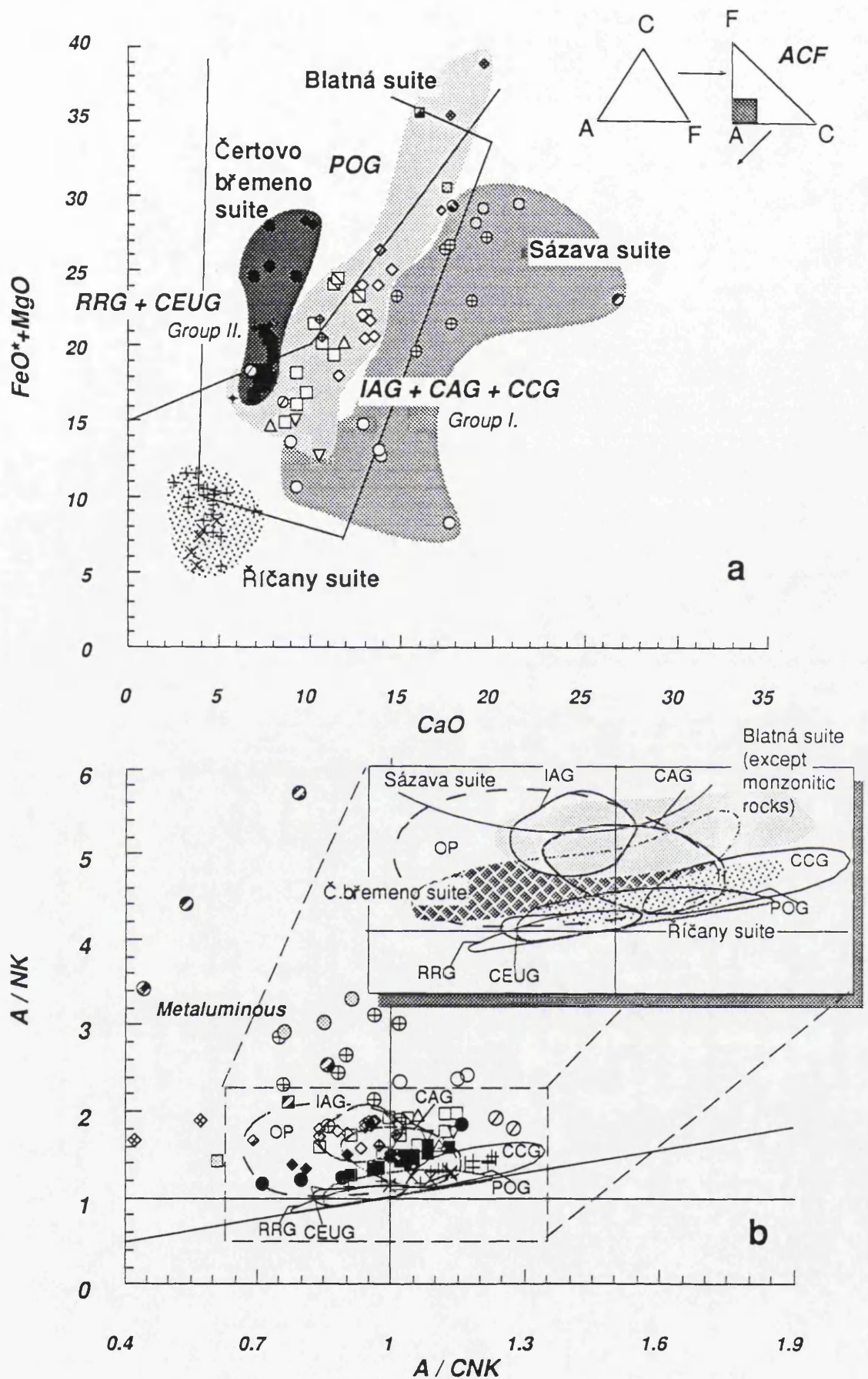
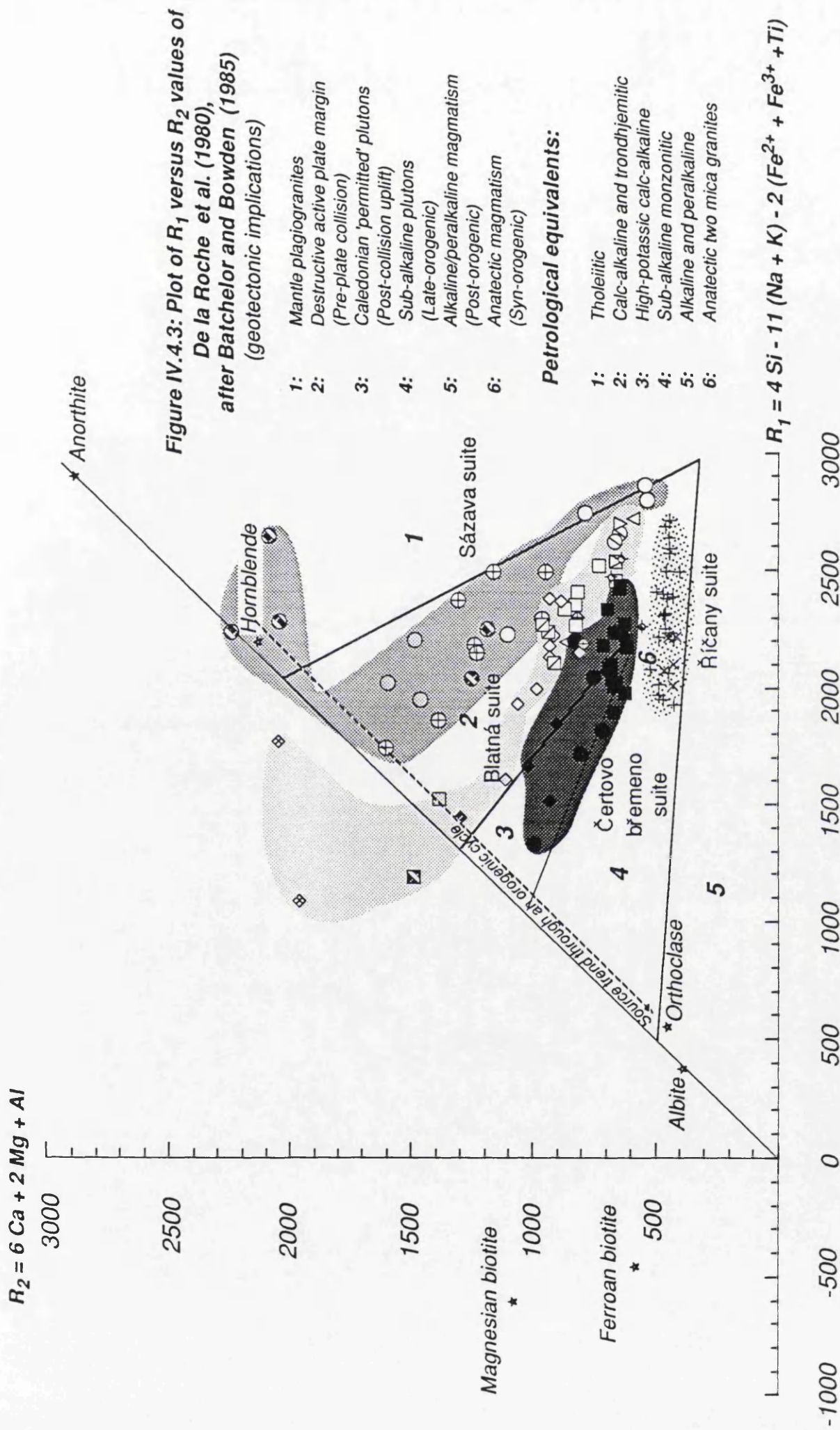


Figure IV.4.2: Tectonic discrimination of granitoids of the CBP (after Maniar and Piccoli, 1989)



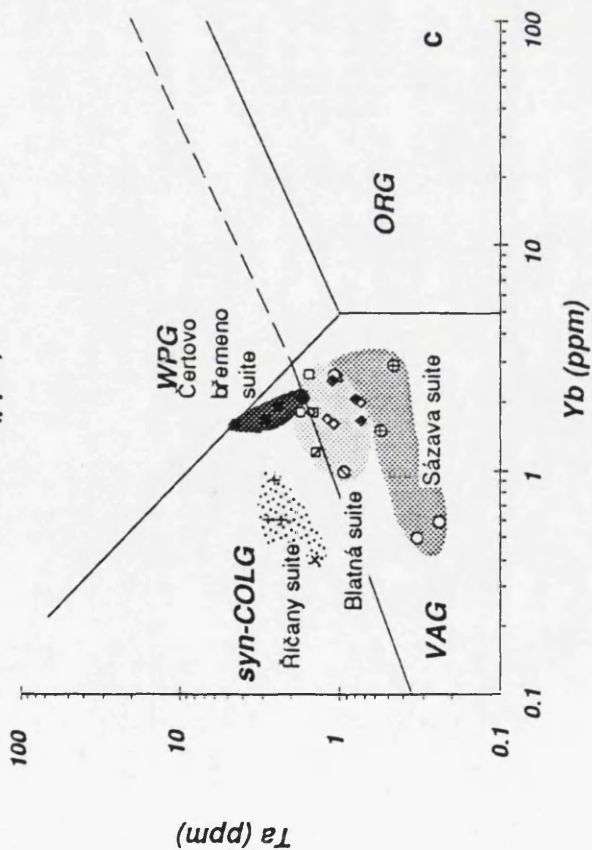
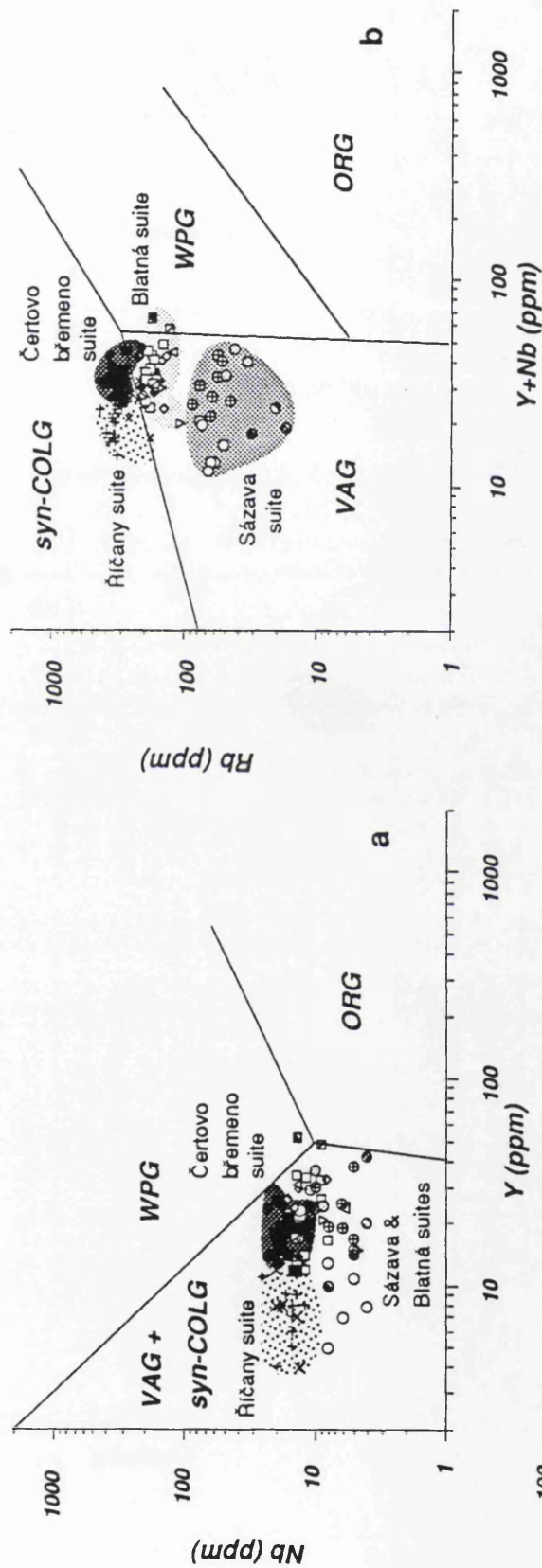
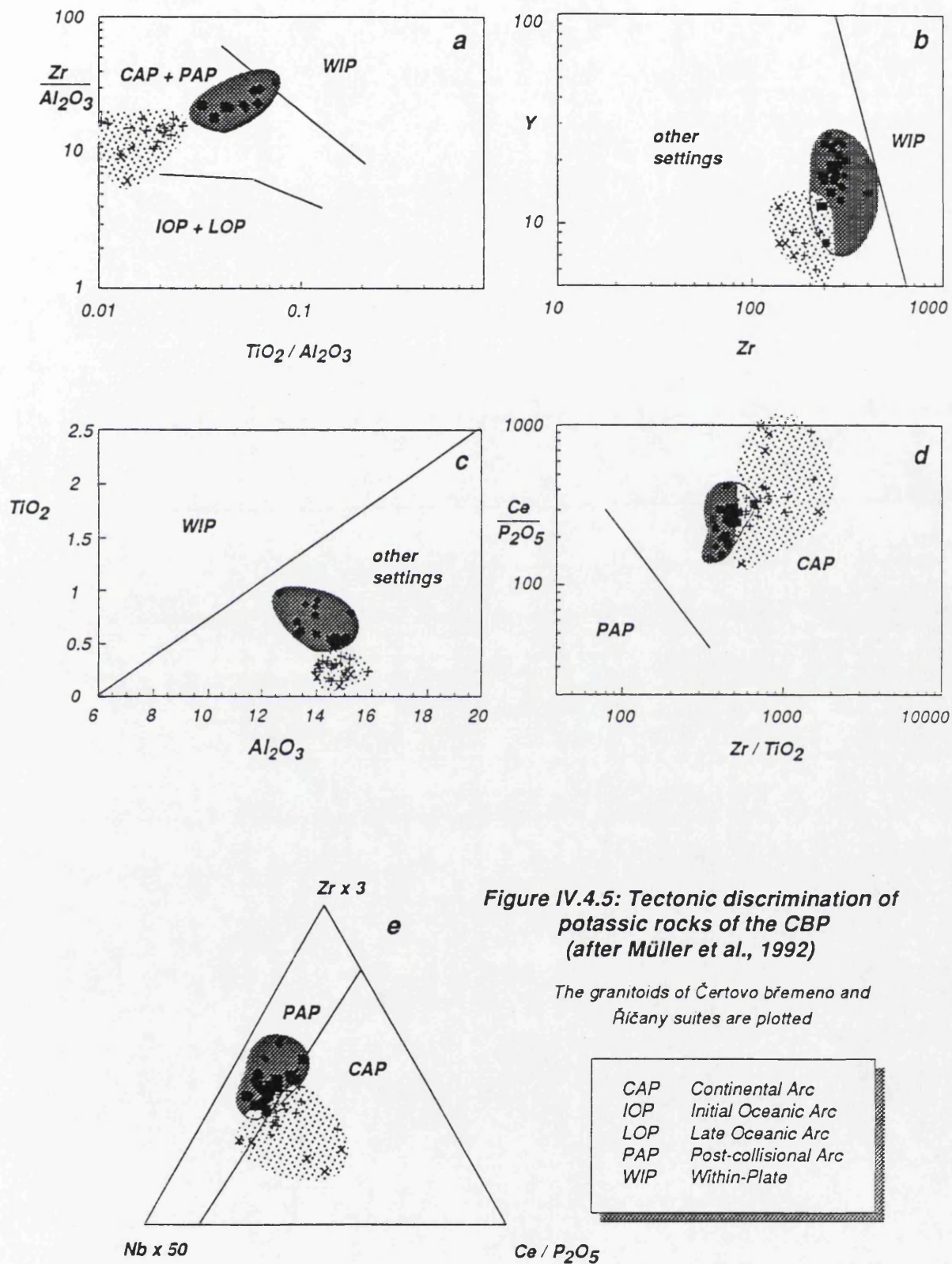


Figure IV.4.4: Tectonic classification of granitoids of the CBP (after Pearce et al., 1984)

ORG Ocean Ridge Granites
VAG Volcanic Arc Granites
WPG Within Plate Granites
syn-COLG Syn-Collisional Granites



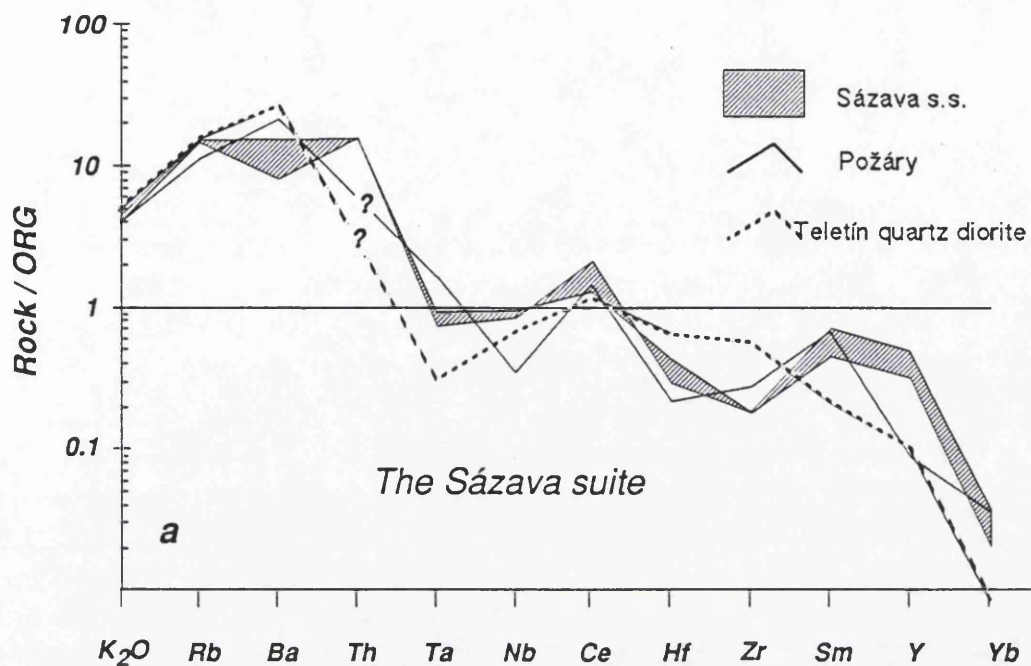
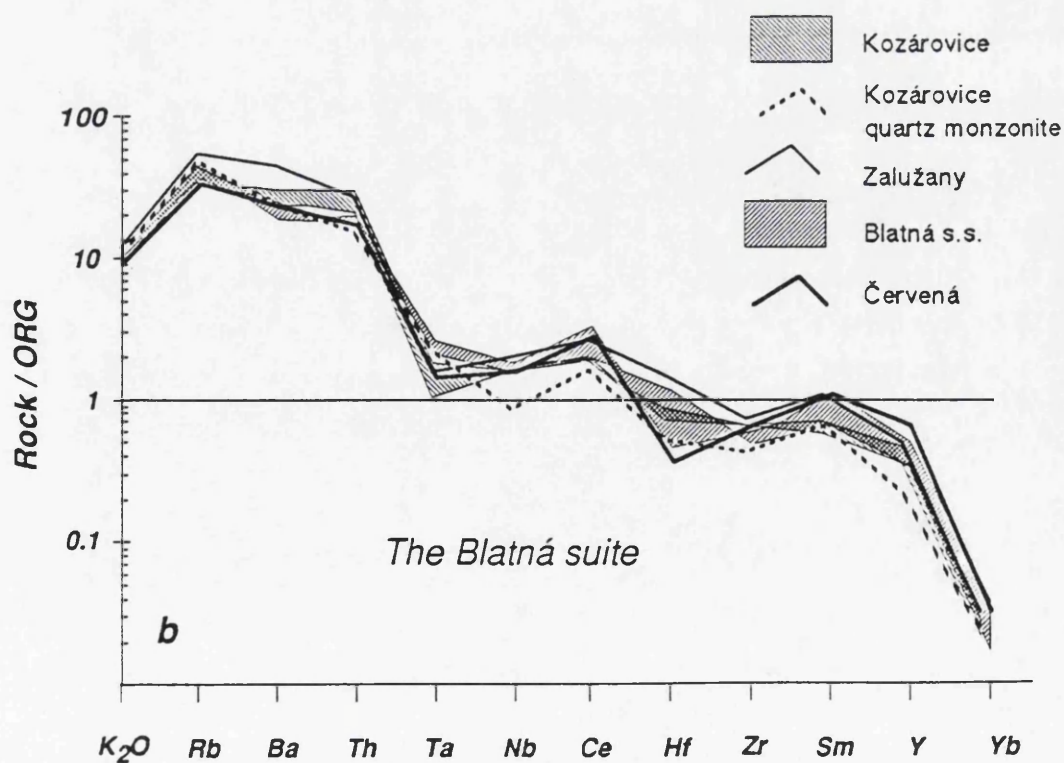


Figure IV.4.6: Ocean Ridge Granite (ORG; Pearce et al., 1984) normalised spiderdiagrams for the Central Bohemian Pluton
(Question marks: below detection limit)



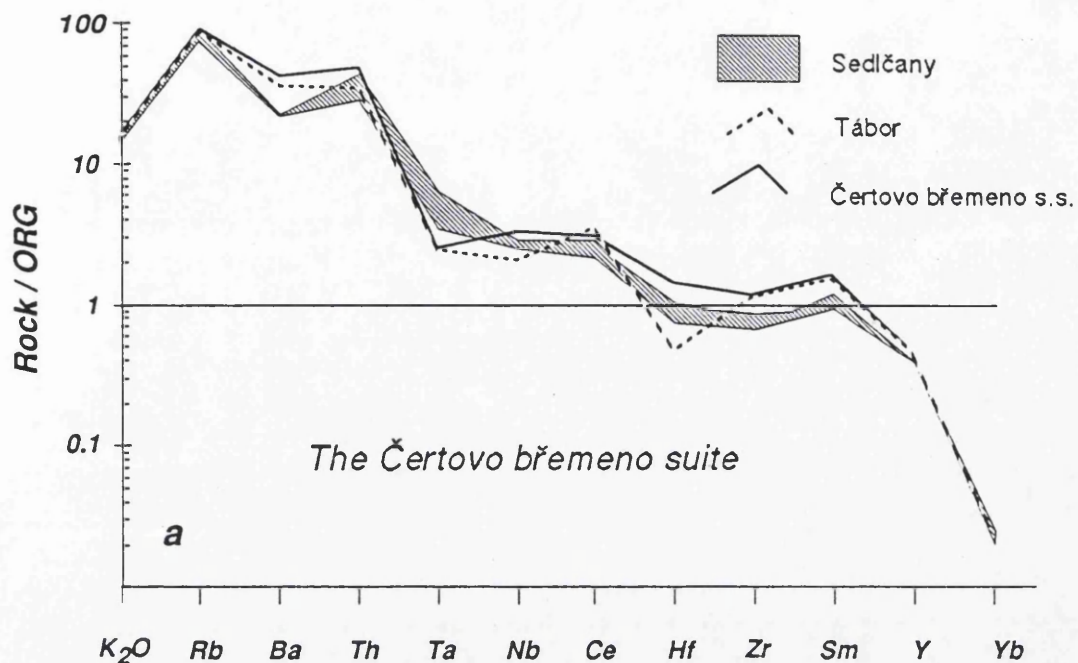
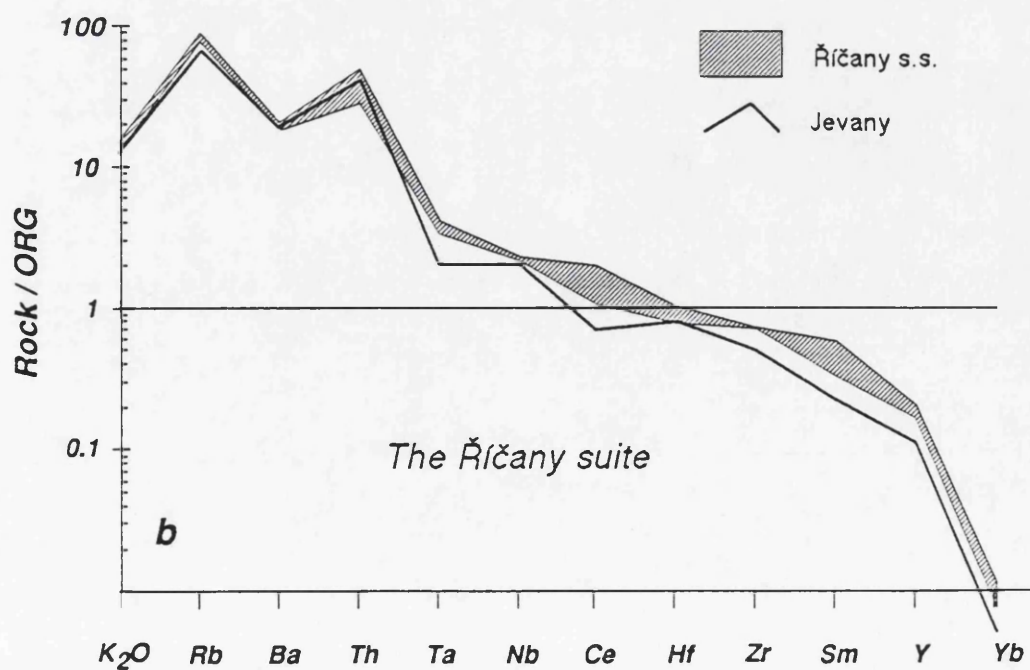


Figure IV.4.7: Ocean Ridge Granite (ORG; Pearce et al., 1984) normalised spiderdiagrams for the Central Bohemian Pluton



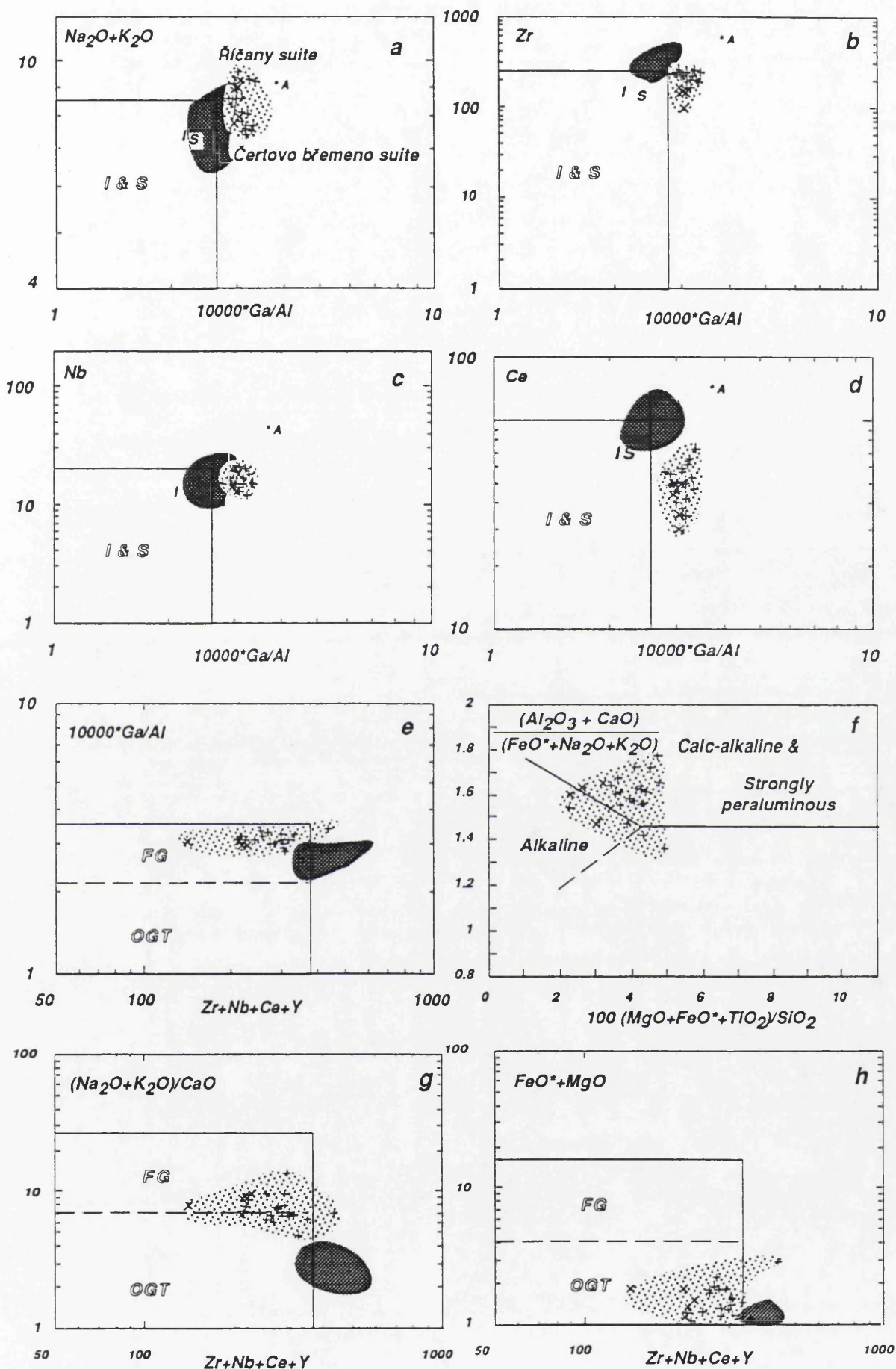


Figure IV.4.8: A-type discrimination diagrams
(a-d, g-h: Whalen et al., 1987; f: Sylvester, 1989; e: Eby, 1990)

Averages of felsic I-, felsic S- and A-type granitoids are also shown (Whalen et al., 1987) as are fields of I- and S-types (I&S), fractionated I- and S-types (FG), and normal ones (OGT). Analyses of the *Říčany* granite and, for comparison, the *Čertovo břemeno* suite, are also plotted.

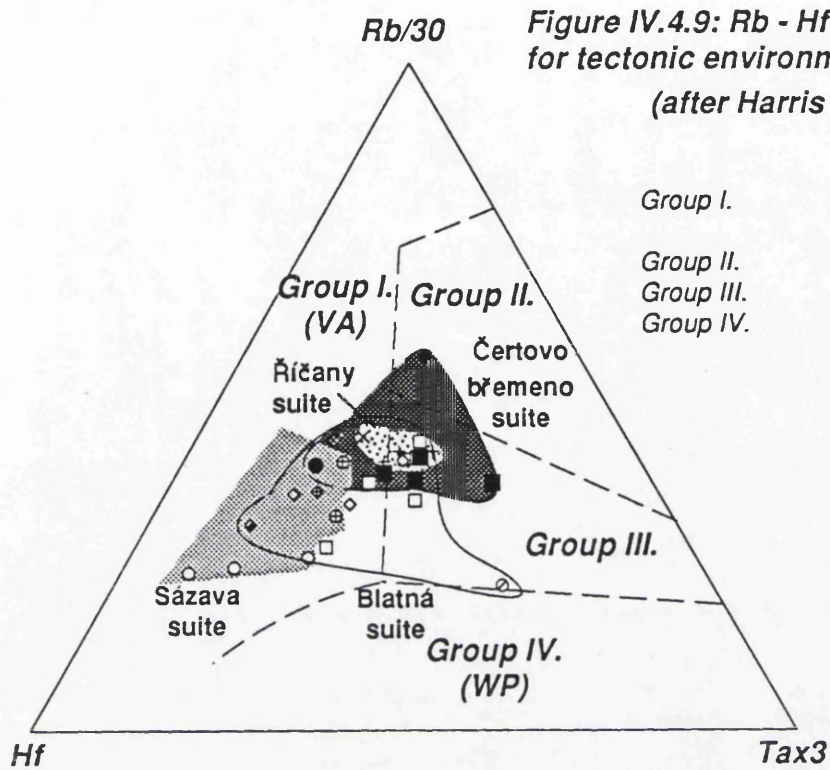


Figure IV.4.9: Rb - Hf - Ta triangular plot for tectonic environment discrimination (after Harris et al., 1986)

- | | |
|------------|--------------------------------|
| Group I. | Pre-collisional (Volcanic arc) |
| Group II. | Syn-collisional |
| Group III. | Post-collisional |
| Group IV. | Within-plate |

V. Sr-Nd isotope geochemistry and petrogenetic implications

Additional constraints on the petrogenesis of the studied granitoids have been provided by the whole-rock Sr-Nd isotope study. The goal was to distinguish between possible and impossible sources and contaminants of the parental magmas of the intrusions being investigated. Details of the methods used are in Appendix II.

For the calculations, the following IBM PC software has been utilised:

- **ISOCHRON** PASCAL programme for the calculation of isochrons and plotting the improved isochron diagrams (Pronost, 1990);
- **ISOPLOT** Qbasic programme, used for some of the model calculations (Ludwig, 1994);
- **BTRAP** Qbasic programme written by the author and used for model calculations and determining ages (Dierckx and Efron, 1983; Kalbeek and deGroot, 1986; for details see Appendix II).

Decay constants used were $\lambda_{238} = 1.55 \times 10^{-11} \text{ yr}^{-1}$ (Stetler and Jäger, 1977) and $\lambda_{147}^{147}\text{Sm} = 6.54 \times 10^{-12} \text{ yr}^{-1}$ (Stetler and Jäger, 1977).

V.1. Theoretical background

V.1.1. Epilim values and model ages

The present-day Sr and Nd isotope ratios (after 0) were age-corrected to the presumed age of the majority of the intrusions at 330 Ma (with an index of 330) (Chapter I.3., Appendix IX.) and the correction has been used to express the Nd isotope ratios relative to the Chondritic Uniform Reservoir (CHUR) (DePaolo, 1988):

$$(1) \quad \epsilon_{\text{Nd}}^{330} = \left(\frac{\left(\frac{^{143}\text{Nd}}{^{144}\text{Nd}} \right)_{\text{SA}} \cdot \left(\frac{^{143}\text{Nd}}{^{144}\text{Nd}} \right)_{\text{CHUR}}^{330}}{\left(\frac{^{143}\text{Nd}}{^{144}\text{Nd}} \right)_{\text{CHUR}}^{330}} - 1 \right) \cdot 10^4$$

where:

$$\left(\frac{^{143}\text{Nd}}{^{144}\text{Nd}} \right)_{\text{CHUR}}^{330} = 0.512638 \quad \left(\frac{^{147}\text{Sm}}{^{144}\text{Nd}} \right)_{\text{CHUR}}^{330} = 0.1967 \quad (\text{Jacobsen and Wasserburg, 1980})$$

In order to evaluate the influence of the uncertainty of the age on calculation of the Sr and Nd initial ratios, the samples with the highest $^{87}\text{Rb}/^{86}\text{Sr}$ (R15-1) and $^{147}\text{Sm}/^{144}\text{Nd}$ (Gbl-2) were recalculated for ages ± 20 Ma. The resulting departures were ± 0.00092 for the $^{87}\text{Sr}/^{86}\text{Sr}$ and ± 0.15 for the $\epsilon_{\text{Nd}}^{330}$ values, being comparable with size of the plotting symbols (Fig. V.3.1). Moreover, it is not likely that ages differ from 330 Ma by more than ± 20 Ma for the studied intrusions (Chapters I.3., II., Appendix IX. I, apart from possibly only the oldest (Sázava) and youngest (Řečany).

The Nd model ages were calculated using the two-stage model of *Liew and Rahn* (1983) which accounts for the fact that a great deal of granitoids contain a significant proportion of a crustally-derived material. In the following formulae, the indexes DM, CC, SA refer to depleted mantle, average crustal reservoir and the sample, respectively, T = two-stage Nd model age, t = crystallisation age of the sample, 0 refers to the present day.

□ Sázava suite:

- ⊕ Sázava tonalite and quartz diorite
- Basic rocks associated with Sázava intrusion
- Teletín quartz diorite
- Požáry trondhjemite and Nečín granodiorite

□ Blatná suite:

- Mrač monzogranite
- ◇ Kozárovec (s.s.) granodiorite
- ⊕ Těchnice granodiorite (porphyritic Kozárovec)
- ◇ Kozárovec quartz monzonite
- ◆ Zalužany quartz monzonite
- ◆ Lučkovice monzonite
- Blatná (s.s.) granodiorite
- Hudčice diorite
- Červená granodiorite
- Mafic microgranular enclave, Červená granodiorite
- △ Klatovy granodiorite
- ▽ Marginal monzogranite

□ Čertovo břemeno suite:

- Sedlčany monzogranite
- Čertovo břemeno monzogranite to quartz syenite
- ◆ Tábor quartz syenite

□ Říčany suite:

- + Říčany granite
- × Jevany leucogranite
- ◆ Mafic microgranular enclaves, Říčany intrusion

Standard plotting symbols

□ Sázava suite:

- ⊕ Sázava tonalite and quartz diorite
- ⊗ Basic rocks associated with Sázava intrusion
- ⊙ Teletín quartz diorite
- Požáry trondhjemite and Nečín granodiorite

□ Blatná suite:

- ⊘ Mrač monzogranite
- ◇ Kozárovice (s.s.) granodiorite
- ⊕ Těchnice granodiorite (porphyritic Kozárovice)
- ◇ Kozárovice quartz monzonite
- ◆ Zalužany quartz monzonite
- ⊞ Lučkovice monzonite
- Blatná (s.s.) granodiorite
- ▨ Hudčice diorite
- ▧ Červená granodiorite
- ⊞ Mafic microgranular enclave, Červená granodiorite
- △ Klatovy granodiorite
- ▽ Marginal monzogranite

□ Čertovo břemeno suite:

- Sedlčany monzogranite
- Čertovo břemeno monzogranite to quartz syenite
- ◆ Tábor quartz syenite

□ Říčany suite:

- + Říčany granite
- × Jevany leucogranite
- ⊕ Mafic microgranular enclaves, Říčany intrusion

Standard plotting symbols

V. Sr-Nd isotope geochemistry and petrogenetic implications

Additional constraints on the petrogenesis of the studied granitoids have been provided by the whole-rock Sr-Nd isotope study. The goal was to distinguish between possible and impossible sources and contaminants of the parental magmas of the intrusions being investigated. Details of the methods used are in Appendix II.

For the calculations, the following IBM PC software has been utilised:

- * ISOCHRON PASCAL programme for the calculation of isochrons and plotting the 'improved isochron diagrams' (*Provost, 1990*);
- * ISOPLOT QuickBasic programme, used for some of the model calculations (*Ludwig, 1993*);
- * BTRAP QuickBasic programme written by the author and used for model calculations and Bootstrap method of determining ages (*Diaconis and Efron, 1983; Kalsbeek and Hansen, 1989*); for details see Appendix II.

Decay constants used were $\lambda(^{87}\text{Rb}) = 1.42 \times 10^{-11} \text{ yr}^{-1}$ (*Steiger and Jäger, 1977*) and $\lambda(^{147}\text{Sm}) = 6.54 \times 10^{-12} \text{ yr}^{-1}$ (*Lugmair and Marti, 1978*).

V.1. Theoretical background

V.1.1. Epsilon values and model ages

The present-day Sr- and Nd-isotope ratios (denoted by index '0') were age-corrected to the presumed age of the majority of the intrusions in the CBP - 330 Ma (with an index of '330') [Chapter I.3., Appendix IX.] and the ϵ -notation has been used to express the Nd-isotope ratios relative to the Chondritic Uniform Reservoir (CHUR) (*DePaolo, 1988*):

$$(1) \quad \epsilon_{\text{Nd}}^{330} = \left(\frac{\left(\frac{^{143}\text{Nd}}{^{144}\text{Nd}} \right)_{\text{SA}}^{330} - \left(\frac{^{143}\text{Nd}}{^{144}\text{Nd}} \right)_{\text{CHUR}}^{330}}{\left(\frac{^{143}\text{Nd}}{^{144}\text{Nd}} \right)_{\text{CHUR}}^{330}} \right) \cdot 10^4$$

where:

$$\left(\frac{^{143}\text{Nd}}{^{144}\text{Nd}} \right)_{\text{CHUR}}^0 = 0.512638 \quad \left(\frac{^{147}\text{Sm}}{^{144}\text{Nd}} \right)_{\text{CHUR}}^0 = 0.1967 \quad (\text{Jacobsen and Wasserburg, 1980}).$$

In order to evaluate the influence of the uncertainty of the age on calculation of the Sr and Nd initial ratios, the samples with the highest $^{87}\text{Rb}/^{86}\text{Sr}$ (RiE-1) and $^{147}\text{Sm}/^{144}\text{Nd}$ (Gbl-2) were recalculated for ages ± 20 Ma. The resulting departures were ± 0.00092 for the $^{87}\text{Sr}/^{86}\text{Sr}$ and ± 0.15 for the $\epsilon_{\text{Nd}}^{330}$ values, being comparable with size of the plotting symbols [Fig. V.3.]. Moreover, it is not likely that ages differ from 330 Ma by more than ± 20 Ma for the studied intrusions [Chapters I.3., II., Appendix IX.], apart from possibly only the oldest (Sázava) and youngest (Říčany).

The Nd model ages were calculated using the two-stage model of *Liew and Hofmann (1988)* which accounts for the fact that a great deal of granitoids contain a significant proportion of a crustally-derived material. In the following formulae, the indexes DM, CC, SA refer to depleted mantle, average crustal reservoir and the sample, respectively. T = two-stage Nd model age, t = crystallization age of the sample, 0 refers to the present day.

From Figure V.1:

$$(2) \quad \left(\frac{^{143}\text{Nd}}{^{144}\text{Nd}}\right)_{\text{CC}}^{\text{T}} = \left(\frac{^{143}\text{Nd}}{^{144}\text{Nd}}\right)_{\text{DM}}^{\text{T}}$$

$$(3) \quad \left(\frac{^{143}\text{Nd}}{^{144}\text{Nd}}\right)_{\text{CC}}^0 - \left(\frac{^{147}\text{Sm}}{^{144}\text{Nd}}\right)_{\text{CC}}^0 (e^{\lambda T} - 1) = \left(\frac{^{143}\text{Nd}}{^{144}\text{Nd}}\right)_{\text{DM}}^0 - \left(\frac{^{147}\text{Sm}}{^{144}\text{Nd}}\right)_{\text{DM}}^0 (e^{\lambda T} - 1)$$

$$(4) \quad T = \frac{1}{\lambda} \ln \left(\frac{\left(\frac{^{143}\text{Nd}}{^{144}\text{Nd}}\right)_{\text{CC}}^0 - \left(\frac{^{143}\text{Nd}}{^{144}\text{Nd}}\right)_{\text{DM}}^0}{\left(\frac{^{147}\text{Sm}}{^{144}\text{Nd}}\right)_{\text{CC}}^0 - \left(\frac{^{147}\text{Sm}}{^{144}\text{Nd}}\right)_{\text{DM}}^0} + 1 \right)$$

For the crustal evolution line:

$$(5) \quad \left(\frac{^{143}\text{Nd}}{^{144}\text{Nd}}\right)_{\text{CC}}^t = \left(\frac{^{143}\text{Nd}}{^{144}\text{Nd}}\right)_{\text{CC}}^0 - \left(\frac{^{147}\text{Sm}}{^{144}\text{Nd}}\right)_{\text{CC}}^0 (e^{\lambda t} - 1)$$

similarly, for the sample evolution line:

$$(6) \quad \left(\frac{^{143}\text{Nd}}{^{144}\text{Nd}}\right)_{\text{SA}}^t = \left(\frac{^{143}\text{Nd}}{^{144}\text{Nd}}\right)_{\text{SA}}^0 - \left(\frac{^{147}\text{Sm}}{^{144}\text{Nd}}\right)_{\text{SA}}^0 (e^{\lambda t} - 1)$$

and because:

$$(7) \quad \left(\frac{^{143}\text{Nd}}{^{144}\text{Nd}}\right)_{\text{CC}}^t = \left(\frac{^{143}\text{Nd}}{^{144}\text{Nd}}\right)_{\text{SA}}^t$$

we can write (5, 6):

$$(8) \quad \left(\frac{^{143}\text{Nd}}{^{144}\text{Nd}}\right)_{\text{CC}}^0 = \left(\frac{^{143}\text{Nd}}{^{144}\text{Nd}}\right)_{\text{SA}}^0 - \left(\frac{^{147}\text{Sm}}{^{144}\text{Nd}}\right)_{\text{SA}}^0 (e^{\lambda t} - 1) + \left(\frac{^{147}\text{Sm}}{^{144}\text{Nd}}\right)_{\text{CC}}^0 (e^{\lambda t} - 1)$$

$$(9) \quad \left(\frac{^{143}\text{Nd}}{^{144}\text{Nd}}\right)_{\text{CC}}^0 = \left(\frac{^{143}\text{Nd}}{^{144}\text{Nd}}\right)_{\text{SA}}^0 - (e^{\lambda t} - 1) \left(\left(\frac{^{147}\text{Sm}}{^{144}\text{Nd}}\right)_{\text{SA}}^0 - \left(\frac{^{147}\text{Sm}}{^{144}\text{Nd}}\right)_{\text{CC}}^0 \right)$$

From (4, 9) we finally get :

$$(10) \quad T = \frac{1}{\lambda} \ln \left(\frac{\left(\frac{^{143}\text{Nd}}{^{144}\text{Nd}}\right)_{\text{SA}}^0 - (e^{\lambda t} - 1) \left(\left(\frac{^{147}\text{Sm}}{^{144}\text{Nd}}\right)_{\text{SA}}^0 - \left(\frac{^{147}\text{Sm}}{^{144}\text{Nd}}\right)_{\text{CC}}^0 \right) - \left(\frac{^{143}\text{Nd}}{^{144}\text{Nd}}\right)_{\text{DM}}^0}{\left(\frac{^{147}\text{Sm}}{^{144}\text{Nd}}\right)_{\text{CC}}^0 - \left(\frac{^{147}\text{Sm}}{^{144}\text{Nd}}\right)_{\text{DM}}^0} + 1 \right)$$

$$\text{where: } \begin{aligned} \left(\frac{^{143}\text{Nd}}{^{144}\text{Nd}}\right)_{\text{DM}}^0 &= 0.513151 & \left(\frac{^{147}\text{Sm}}{^{144}\text{Nd}}\right)_{\text{DM}}^0 &= 0.219 \\ \left(\frac{^{147}\text{Sm}}{^{144}\text{Nd}}\right)_{\text{CC}}^0 &= 0.12 & & (\text{Liew and Hofmann, 1988}). \end{aligned}$$

Caution should be taken in interpretation of the Nd model ages. Clearly, for granitoids with a significant contribution from polygenic crustal material, either in the source, or acquired by open-system processes like assimilation or magma mixing, the Nd model ages do not correspond to the crust-formation event (Arndt and Goldstein, 1987). Schematically this idea is documented in Figure

V.2, where the Nd model age ($T_{\text{MIX}}^{\text{DM}}$) of granite from a mixed source (older mantle-derived granite B and younger mantle-derived component A) falls between model ages T_B^{DM} and T_A^{DM} , being a function of their proportions. Additionally, major fractionation of LREE-rich phases like orthite (Pimentel and Charnley, 1991) [Chapter IV.3.] or monazite (Turpin et al., 1990) may radically change the Sm / Nd ratio, which is violation of the basic assumption for calculation of the Nd model ages. The two-stage model for calculation of Nd-model ages (Liew and Hofmann, 1988), unlike the single-stage one, takes into account potential changes in Sm/Nd ratio which may occur during intra-crustal melting and, or, fractional crystallization processes at the time of granite production.

V.1.2. Mixing of two isotope systems

The equations for mixing of two Sr-isotopically distinct components A and B, in proportions f and $1 - f$, respectively, were given by Faure (1986) (M denotes the mixture):

$$(11) \quad \text{Sr}_M = \text{Sr}_A f + \text{Sr}_B (1 - f)$$

$$(12) \quad \left(\frac{^{87}\text{Sr}}{^{86}\text{Sr}}\right)_M = \left(\frac{^{87}\text{Sr}}{^{86}\text{Sr}}\right)_A \frac{\text{Sr}_A f}{\text{Sr}_M} + \left(\frac{^{87}\text{Sr}}{^{86}\text{Sr}}\right)_B \frac{\text{Sr}_B (1 - f)}{\text{Sr}_M}$$

$$(13) \quad \left(\frac{^{87}\text{Sr}}{^{86}\text{Sr}}\right)_M = \frac{\text{Sr}_A \text{Sr}_B \left(\left(\frac{^{87}\text{Sr}}{^{86}\text{Sr}}\right)_B - \left(\frac{^{87}\text{Sr}}{^{86}\text{Sr}}\right)_A \right)}{\text{Sr}_M (\text{Sr}_A - \text{Sr}_B)} + \frac{\text{Sr}_A \left(\frac{^{87}\text{Sr}}{^{86}\text{Sr}}\right)_A - \text{Sr}_B \left(\frac{^{87}\text{Sr}}{^{86}\text{Sr}}\right)_B}{\text{Sr}_A - \text{Sr}_B}.$$

From (13), an equation for the calculation of Sr_A from the isotope ratios and Sr concentrations of both component B and the mixture (Sr_B , Sr_M) can be derived (no knowledge of f is required):

$$(14) \quad \text{Sr}_M \left(\frac{^{87}\text{Sr}}{^{86}\text{Sr}}\right)_M (\text{Sr}_A - \text{Sr}_B) = \text{Sr}_A \text{Sr}_B \left(\left(\frac{^{87}\text{Sr}}{^{86}\text{Sr}}\right)_B - \left(\frac{^{87}\text{Sr}}{^{86}\text{Sr}}\right)_A \right) + \text{Sr}_M \text{Sr}_A \left(\frac{^{87}\text{Sr}}{^{86}\text{Sr}}\right)_A - \text{Sr}_M \text{Sr}_B \left(\frac{^{87}\text{Sr}}{^{86}\text{Sr}}\right)_B$$

$$(15) \quad \text{Sr}_A \left(\text{Sr}_M \left(\frac{^{87}\text{Sr}}{^{86}\text{Sr}}\right)_M + \text{Sr}_B \left(\frac{^{87}\text{Sr}}{^{86}\text{Sr}}\right)_A - \text{Sr}_B \left(\frac{^{87}\text{Sr}}{^{86}\text{Sr}}\right)_B - \text{Sr}_M \left(\frac{^{87}\text{Sr}}{^{86}\text{Sr}}\right)_A \right) = \text{Sr}_M \text{Sr}_B \left(\left(\frac{^{87}\text{Sr}}{^{86}\text{Sr}}\right)_M - \left(\frac{^{87}\text{Sr}}{^{86}\text{Sr}}\right)_B \right)$$

$$(16) \quad \text{Sr}_A = \frac{\text{Sr}_M \text{Sr}_B \left(\left(\frac{^{87}\text{Sr}}{^{86}\text{Sr}}\right)_M - \left(\frac{^{87}\text{Sr}}{^{86}\text{Sr}}\right)_B \right)}{\text{Sr}_M \left(\left(\frac{^{87}\text{Sr}}{^{86}\text{Sr}}\right)_M - \left(\frac{^{87}\text{Sr}}{^{86}\text{Sr}}\right)_A \right) + \text{Sr}_B \left(\left(\frac{^{87}\text{Sr}}{^{86}\text{Sr}}\right)_A - \left(\frac{^{87}\text{Sr}}{^{86}\text{Sr}}\right)_B \right)}.$$

The proportion of component A can be calculated from the following equation (Faure, 1986) derived from (13):

$$(17) \quad f = \frac{\left(\frac{^{87}\text{Sr}}{^{86}\text{Sr}}\right)_M \text{Sr}_M - \left(\frac{^{87}\text{Sr}}{^{86}\text{Sr}}\right)_B \text{Sr}_B}{\left(\frac{^{87}\text{Sr}}{^{86}\text{Sr}}\right)_A \text{Sr}_A - \left(\frac{^{87}\text{Sr}}{^{86}\text{Sr}}\right)_B \text{Sr}_B}.$$

V.2. Sr-Nd isotope results

Sr - Nd whole-rock isotope data for the CBP granitoids are presented in Table V.1. Initial ratios have been calculated using an age of 330 Ma (*van Breemen et al., 1982*). These results, together with additional data for the Blatná intrusion (*van Breemen et al., 1982; Košler, 1993*) are plotted onto a $(^{87}\text{Sr}/^{86}\text{Sr})_{330}$ versus $\epsilon_{\text{Nd}}^{330}$ diagram [Fig. V.3.]. Most of the CBP data form a shallow-dipping trend with the total range of $(^{87}\text{Sr}/^{86}\text{Sr})_{330} = 0.7051 - 0.7129$, and $\epsilon_{\text{Nd}}^{330} = +0.2$ to -8.9 , similar to the other granitoids within the Hercynian belt (*e.g. Bernard-Griffiths et al., 1985; Liew and Hofmann, 1988; Liew et al., 1989; Pin and Duthou, 1990*). Apart from the Sázava intrusion, none of the rocks analysed has positive $\epsilon_{\text{Nd}}^{330}$ values, in contrast to some of the orthogneisses of the Metamorphic Islet Zone, preserved as roof pendants in the CBP (*Košler, 1993*). Each of the suites, however, forms a well-defined cluster of restricted Sr - Nd isotopic composition.

The lowest $(^{87}\text{Sr}/^{86}\text{Sr})_{330}$ and highest $\epsilon_{\text{Nd}}^{330}$ values are shown by samples of the Sázava suite: 0.7051 and $+0.1$ to -0.3 respectively. The gabbro (Gbs-5) has very low $(^{87}\text{Sr}/^{86}\text{Sr})_{330} = 0.7011$ compared to $(^{87}\text{Sr}/^{86}\text{Sr})_{330}$ of CHUR (0.7043). This sample, showing much higher Rb and lower Sr than other gabbros, has probably suffered a late hydrothermal alteration, documented by microstructural study of other samples from the same quarry (Krhánek, Chapter II.1.)

Intrusions from the Blatná suite have significantly higher $(^{87}\text{Sr}/^{86}\text{Sr})_{330}$ and lower $\epsilon_{\text{Nd}}^{330}$ values than the Sázava suite. The Kozárovec granodiorite has $(^{87}\text{Sr}/^{86}\text{Sr})_{330} = 0.7073 - 0.7083$ and $\epsilon_{\text{Nd}}^{330} = -3.7$ to -5.3 ; the Lučkovice monzonite has $(^{87}\text{Sr}/^{86}\text{Sr})_{330} = 0.7077 - 0.7081$ and $\epsilon_{\text{Nd}}^{330} = -3.1$ to -3.4 ; the Blatná and Červená masses have analogous values of $0.7086 - 0.7092$ and -5.3 to -6.5 (including the data of *van Breemen et al., 1982 and Košler, 1993*). The samples from the Říčany granite have higher $(^{87}\text{Sr}/^{86}\text{Sr})_{330}$ (0.7102 - 0.7108) and lower $\epsilon_{\text{Nd}}^{330}$ values (-6.2 to -7.7) than the Blatná suite. The Nd isotopic composition of a mafic microgranular enclave (MME) from the Říčany granite ($\epsilon_{\text{Nd}}^{330} = -8.9$) shows disequilibrium with its host ($\epsilon_{\text{Nd}}^{330} = -7.4$), whereas its initial Sr ratio is in equilibrium ($(^{87}\text{Sr}/^{86}\text{Sr})_{330} = 0.7106$). The most evolved Sr - Nd isotopic signature is that of the Sedlčany granite, with $(^{87}\text{Sr}/^{86}\text{Sr})_{330} = 0.7126 - 0.7128$ and $\epsilon_{\text{Nd}}^{330} = -7.2$ to -7.8 . A similar composition is shown by two widely separated dykes of minette that cut the Blatná suite; these have high initial Sr isotope ratios of $0.7127 - 0.7129$ and low $\epsilon_{\text{Nd}}^{330}$ values of -6.9 and -7.2 .

The fields of country rocks are also plotted on Figure V.3.; these comprise orthogneisses from the Metamorphic Islet Zone (*Košler, 1993*), Proterozoic and Lower Palaeozoic volcanic rocks of the Teplá-Barrandian Unit and the Jílové Zone (*Veress, 1992*), and granulites (*Valbracht et al., 1994; Wendt et al., 1994*), metasediments (*Gorokhov et al., 1977; Köhler and Müller-Sohnius, 1980 and references therein; Liew and Hofmann, 1988; Scharbert and Veselá, 1990; present text*), and eclogites (*Brueckner et al., 1991; Beard et al., 1992*) of the Moldanubian Unit.

The initial Sr and Nd isotopic composition of the Sázava intrusion overlaps the field of volcanic rocks from the Teplá-Barrandian Unit and Metamorphic Islet Zone (*Veress, 1992*) whereas the Říčany and Sedlčany intrusions have similar initial ratios to the Moldanubian metasediments of *Liew and Hofmann (1988)*. Overall, the earlier intrusions of the CBP show lower initial Sr and higher initial Nd isotopic ratios than the later ones.

V.3. Discussion

V.3.1. Comparison with other Hercynian granitoids in Europe

I. Sr-Nd isotopic data

A comparison between the initial Sr ratios and initial ϵ_{Nd} values of Hercynian granitoids is given in Figure V.4. In addition to results from the CBP, data are also shown for granitoids from the Austrian part of the Moldanubian Pluton (*Liew et al., 1989*), the Massif Central in France (*Pin and Duthou, 1990; Turpin et al., 1990; Shaw et al., 1993*), the Querigut massif in the Pyrenees (*Ben Othman et al., 1984*), the Odenwald and Spessart massifs in Germany (*Liew and Hofmann, 1988*), the Gredos massif in Spain (*Moreno-Ventas, 1991*), as well as the fields of minettes and kersantites, mainly from the Armorican massif and Massif Central (*Turpin et al., 1988*).

With the exception of the Sázava suite, the granitoids of the CBP fall into the broad field of the granitoids of the Moldanubian Pluton (*Liew et al., 1989*), whereas the Sázava intrusion has a Sr - Nd signature similar to the quartz diorites from Limousin, Massif Central (*Shaw et al., 1993*). The isotopic composition of the Kozárovice granodiorite resembles that of the I-type granites of the Moldanubian Pluton (e.g. Weinsberg), whereas the K-rich rocks of the durbachite suite from the Czech part of this Pluton (the Jihlava and Třebíč intrusions; *Scharbert and Veselá, 1990*) have almost identical $(^{87}\text{Sr}/^{86}\text{Sr})_i$ ratios to the Sedlčany granite, whose Sr - Nd isotopic signature is much more evolved than that of the potassium-rich rocks in Austrian part of the Moldanubian Pluton (the Rastenberg intrusion). Although the Říčany granite has some geochemical affinities with the S-type Eisgarn granite of the Moldanubian Pluton (*M. Klečka, pers. com., 1990*), the latter typically has a higher $(^{87}\text{Sr}/^{86}\text{Sr})_i$ ratio of $\sim 0.717 - 0.718$ (*Liew et al., 1989; Scharbert and Veselá, 1990*).

The minettes cutting the CBP have similar Sr - Nd isotopic signatures to the Sedlčany intrusion; these values, however, are much more evolved than those for the minettes and kersantites from the western part of the Hercynian belt (*Turpin et al., 1988*).

The frequently-observed negative correlation between $(^{87}\text{Sr}/^{86}\text{Sr})_i$ and ϵ_{Nd}^i in granitoids, is often attributed to an increasing sensitivity of the more fractionated (Sr-poor) rocks to crustal contamination processes involving high $^{87}\text{Sr}/^{86}\text{Sr}$ contaminants (e.g. *Allègre and Ben Othman, 1980; McCulloch and Chappell, 1982; DePaolo, 1988; Pin and Duthou 1990*). The overall trend of data from the CBP would therefore appear to be compatible with progressive contamination, with time, of a primary magma with an isotopic composition similar to Bulk Earth or depleted mantle by the metasediments or granulites of the Moldanubian Unit [Fig. V.3.]. The granitoids of the CBP, however, can not have been derived by simple binary mixing (including magma mixing and bulk assimilation) between 'mantle' and 'crustal' components for several reasons: (1) there is an absence of members with intermediate isotopic compositions, (2) the most peraluminous and acidic Říčany granite plots in the middle of the 'mixing trend', (3) the Sázava and Blatná suites, despite having gabbroic rocks with similar SiO_2 contents, have significantly different isotopic compositions, and (4) the more mafic Sedlčany granite and the minettes, that appear to represent relatively pristine mantle-derived melts (*Holub, 1990*), are close to the field of the presumed contaminant. This is not to deny that binary mixing may have been an important process in causing the variation along parts of the main trend, notably the linear array formed by the Kozárovice samples (see below). The paucity of positive ϵ_{Nd}^i values throughout the Hercynian belt, as well as the evolved nature of the Sr - Nd isotopic composition of minettes and kersantites (*Turpin et al., 1988*), however, precludes a substantial role for depleted

mantle as a source of Hercynian magmas (*cf. Liew and Hofmann, 1988, Liew et al., 1989; Pin and Duthou, 1990*).

The diagram of $1/\text{Sr}$ versus $(^{87}\text{Sr}/^{86}\text{Sr})_i$ [Fig. V.5.] shows the data for the CBP and the Moldanubian Pluton (*Liew et al. 1989; Scharbert and Veselá, 1990*), together with fields for their country rocks at 330 Ma (see above for references). Apart from the Kozárovec intrusion, the CBP granitoids form sub-horizontal arrays, indicative of closed-system fractionation processes with a negligible role for mixing with material of distinct Sr isotopic signature (*Wendt, 1993*).

The geochemical and isotopic evidence therefore suggest that the main trend observed on Figure V.5. is more likely to point to a diversity of sources and processes in the genesis of the CBP rather than to a single high-level crustal contamination process. The causes of the isotopic composition of each of the suites are discussed in the following sections.

Some of the analyses of the Eisgarn granite from the territory of Czech Republic (of the so-called Bílý Kámen variety; *Scharbert and Veselá, 1990*) form a mixing array between low- $(^{87}\text{Sr}/^{86}\text{Sr})_i$ (~ 0.705), high-Sr (~ 500 ppm) and high- $(^{87}\text{Sr}/^{86}\text{Sr})_i$ (0.717-0.718), low-Sr (60 ppm) components (*cf. Arakawa, 1990*). The high Sr-contents of this facies of the Eisgarn intrusion were originally interpreted as being due to extensive alteration (*Scharbert and Veselá, 1990*). However, if we assume that the magma which formed the bulk of the Eisgarn mass had high $(^{87}\text{Sr}/^{86}\text{Sr})_i$, then the less radiogenic Sr-isotopic signature of the contaminant precludes a fluid derived from the surrounding S-type granitoids and metasediments, pointing to a mantle source or a source similar to the Moldanubian I-type granitoids (e.g. the Freistadt granite with similar age and Sr = 460 ppm; *Liew et al., 1989 and references therein*). However, magma-mixing with a similar I-type melt cannot be ruled out without careful textural and geochemical study.

II. Neodymium model ages

The box and whiskers plot of the two-stage Nd depleted mantle model ages for the CBP granitoids shows three maxima, at about 1.05 Ga for the Sázava suite, 1.45 Ga for the Blatná suite, and 1.6 Ga for the Sedlčany and Říčany suites [Fig. V.6.]. This compares well with the overall pattern for the European Hercynides, with at least 50 % of the model ages for each data set falling in range of 1.25 - 1.65 Ga (all data recalculated after *Liew and Hofmann, 1988*). The only exceptions are the relatively unevolved quartz diorites from Limousin, Massif Central (*Shaw et al., 1993*), which have a mean model age of 1 Ga, and the rocks of the Sázava suite. The sample of a mafic microgranular enclave from the Říčany granite is an outlier, having a Nd-model age of ~ 1.75 Ga, similar to several analysed granitoids from the Massif Central.

The observed model ages for the majority of the CBP granitoids, and in the Hercynian belt in general, do not appear to correspond to a major crust-forming event, as there is little geochronological evidence of ca. 1.0 - 1.8 Ga igneous activity in the European Hercynides (*Peucat et al., 1988; Gebauer et al., 1989; Pin and Duthou, 1990; Gebauer and Friedl, 1994*). Thus, the model ages may rather represent average crustal residence ages of the Hercynian crust reflecting mixtures of Archaean (> 2.5 Ga) and Late Proterozoic (~ 0.6 Ga) sources (*Gebauer et al., 1989; Pin and Duthou, 1990; Wendt et al., 1993*).

V.3.2. Petrogenetic implications

I. Sázava suite

The relatively primitive major and trace element geochemistry [Chapter IV.], the least evolved Sr - Nd isotope signature, and the abundance of mafic microgranular enclaves and absence of surmicaceous enclaves imply a major role for mantle-derived material in the genesis of the Sázava suite. The geochemical character (metaluminous, $K_2O \ll Na_2O$, $(^{87}Sr/^{86}Sr)_i \sim 0.704$, $\epsilon_{Nd}^i \sim 0$) corresponds to a typical I-type granitoid (e.g. McCulloch and Chappell, 1982), and could be compatible with an origin by the dehydration melting of hornblende (Whitney, 1988). The Sr - Nd isotope geochemistry of the Sázava intrusion points to one of the following models: (1) crystallization from mantle-derived melts, with the mantle component having an isotopic composition close to that of Bulk Earth, (2) melting of the adjacent metabasites of the Jílové Zone or Metamorphic Islet Zone, or (3) mixing between melts derived from these two sources. The similar isotopic characteristics of the Limousin quartz diorite in the French Massif Central were explained by melting of subduction-enriched mantle, and subsequent contamination by lower crustal rocks (Shaw *et al.*, 1993). Although such a model could apply to the Sázava suite, the local metabasites, which have an appropriate Sr - Nd isotope signature (Veress, 1992), may potentially provide a fertile source of tonalitic and trondhjemitic magma at depth (Rapp *et al.*, 1991; Martin, 1987). The model of origin of the Sázava suite by melting of metabasic rocks is in agreement with the conclusions drawn on basis of the REE data [Chapter IV.3.1.].

The temperature required for the vapour-absent melting of hornblende ($> 900^\circ C$) is higher than that for the dehydration melting of muscovite ($650 - 750^\circ C$) and biotite ($750 - 850^\circ C$), as well as the presumed temperature of the normal lower crust ($500 - 700^\circ C$; Whitney, 1988). Accordingly, in order to melt amphibolite an extra heat source is needed. In the case of the CBP the simplest possibility is that of a major basic body underplating the pre-existing continental crust in a manner proposed by Huppert and Sparks (1988). This model supposes a period of initial basaltic magmatism that heats up the base of the crust and initiates its melting. Mixing between the mafic and tonalitic magmas might occur subject to favourable physical conditions (e.g. Huppert and Sparks 1988). A corresponding model of infracrustal melting has been proposed by Chappell and Stephens (1988) for the origin of Australian I-type granitoids from meta-igneous material underplated by mafic melts.

This scenario is consistent with temperatures close to $900^\circ C$ recorded by the amphibole-plagioclase pairs in the Teletín quartz diorite [Chapter III.1.1.]. It also accounts for the occurrence of abundant mafic bodies in the northern CBP, as well as for the genesis of numerous mafic microgranular enclaves and a quartz diorite (Teletín) in the western part of the Sázava body through magma mixing of the basic magma with the Sázava tonalite. The hybrid character of both the quartz diorite and mafic microgranular enclaves is supported by microtextural evidence and both mineral chemistry and whole-rock geochemistry [Chapters II - IV.]. The presence of a major basic body below the western part of the Sázava intrusion is consistent with a strong positive gravity anomaly in the area (e.g. Marek and Palivcová, 1968).

The Sázava suite shows affinities to a subduction-related setting [Chapter IV.4.], especially by its calc-alkaline character, pronounced Nb-Ta anomaly, and the abundance of associated basic rocks (also Palivcová, 1984). The operation of Hercynian subduction in the area of the CBP, albeit earlier, is further substantiated by the geochemistry of the orthogneisses in the Metamorphic Islet Zone, spatially associated with the CBP (Košler, 1993).

One possible model for the generation of the Sázava suite is illustrated in Figure V.7. The hydrous fluids, released from the subducted slab, carry substantial amount of LILE and leave behind insoluble HFSE (Saunders *et al.*, 1991). This influx of volatiles causes melting of overlying mantle wedge, and generates basic magmas (a) that intrude and underplate the crust composed of rocks similar to the metabasites of the Jílové Zone or Metamorphic Islet Zone. The emplacement of hot basic magmas causes an increase in temperature and, consequently, widespread generation of more acidic melts (*cf.* Huppert and Sparks, 1988). At this stage, homogeneous magmas are produced by mixing of basic and acid magmas and the resulting tonalitic melt intrudes into higher level (b). The crystallizing tonalite is locally invaded by basic syn-plutonic dykes, the margins of these dykes may chill against the tonalite and the tonalite, in turn, is mobilised by the temperature increase and volatile influx (c). The thermal and density instability of the magma chamber causes convection and disruption of these syn-plutonic bodies, accompanied by magma mingling and mixing. As a result, both round and sub-angular MME, the latter possibly representing relics of the chilled margin (d; *cf.* Castro *et al.*, 1990 a,b; 1991 a,b), were generated.

A similar model for the genesis of tonalitic magmas at Andinotype margins has been formulated by Pitcher (1993). In his view, the magmatic material that underplates the lower crust, generated from the mantle wedge above a subduction zone, itself becomes a source of tonalitic magmas, being remelted as a consequence of tectonic relaxation and uplift.

In any of these scenarios the Požáry trondhjemite may represent either a small-degree melt fraction of a similar metabasic source, or, more likely, a late differentiate of the Sázava magma [Chapter IV.3.1.].

II. Blatná suite

The variation of the Blatná suite on both the $(^{87}\text{Sr}/^{86}\text{Sr})_{330} - \epsilon_{\text{Nd}}^{330}$, and $1/\text{Sr} - (^{87}\text{Sr}/^{86}\text{Sr})_i$ diagrams [Figs. V.3, V.5.] is consistent with open system behaviour. The linear relationship between $1/\text{Sr}$ and $(^{87}\text{Sr}/^{86}\text{Sr})_i$ corresponds to a mixing line (Faure, 1986; Wendt, 1993) and renders the Kozárovec granodiorite unsuitable for Rb - Sr dating, as the assumption of a constant $(^{87}\text{Sr}/^{86}\text{Sr})_i$ is not fulfilled. This could have been the result of either mixing between different magmas of the suite with distinct isotopic signatures, or crustal contamination of a more mafic magma. The whole-rock geochemistry [Chapter IV.3.2.] indicates that the parental basic magma to the suite was unlike that of the Sázava suite, and had probably an isotopic and chemical composition close to that of the Lučkovice monzonite. In both cases the evolved end-member had to have $(^{87}\text{Sr}/^{86}\text{Sr})_{330} > 0.709$ and $\epsilon_{\text{Nd}}^{330} < -6$. In the preceding text [Chapter IV.3.2.] it has been argued that the variation in the Blatná suite could have originated by mixing between shoshonitic magmas chemically similar to the Lučkovice monzonite and the most acidic Blatná granodiorite. The analysed sample of the Lučkovice monzonite Gbl-1 has low SiO_2 (45.3 %), and high mg (molar $\text{Mg}/(\text{Mg} + \text{Fe}^{2+} + \text{Fe}^{3+})$) (65) and Cr (496 ppm), and thus its composition may be close to that of a primary, mantle-derived melt (*cf.* Rock, 1991). If this is the case, then the mantle source of the Lučkovice monzonite had to be enriched in LILE and LREE compared to that of the Sázava suite. On basis of the Sr isotopes, van Breemen *et al.* (1982) and Bendl and Vokurka (1989) explained the genesis of the Blatná granodiorite by mixing of mantle- and crustally-derived components.

Following Sr-isotope modelling, Bendl and Vokurka (1989) estimated that 50 - 70 % of Moldanubian material ($\text{Sr} = 155$ ppm, $(^{87}\text{Sr}/^{86}\text{Sr})_{331} = 0.7167$) mixed with a basaltic depleted mantle-derived melt ($\text{Rb} = 26$ ppm, $\text{Sr} = 1007$ ppm, $(^{87}\text{Sr}/^{86}\text{Sr})_0 = 0.70312$) to produce the Blatná

granodiorite ($\text{Sr} = 331 \text{ ppm}$, $(^{87}\text{Sr}/^{86}\text{Sr})_{331} = 0.7072$). They presented two equations [effectively Equations 12-13.], of which one is, however, redundant as there is only one variable (f) involved. After recalculation, the mafic end-member gives $(^{87}\text{Sr}/^{86}\text{Sr})_{331} = 0.70277$, and, subsequently, $f_A = 0.79$ for both equations. This does not fall into the reported range 0.5 - 0.7 of *Bendl and Vokurka (1989)* and thus it is not clear, how this value was obtained. Moreover, these authors have assumed depleted mantle-derived end-member that does not seem to be the case.

A mixing test (*Fourcade and Allègre, 1981; Castro et al., 1990a*) performed in Chapter IV.3.2. has indeed confirmed the feasibility of hybridization between the most evolved Blatná granodiorite (from Řečice) and the Lučkovice monzonite in order to produce the Kozárovec granodiorite that is intermediate between the two. Based on this major-element-based modelling, at least 65 % of the acid end-member is needed to generate the Kozárovec granodiorite, whereas the Sr-Nd isotope-based modelling [Equation 17] requires about 60 % [Fig. V.8.]. Such a small difference may be accounted for by the likelihood of operation of fractional crystallization in both the Kozárovec and Blatná intrusions [Chapter IV.3.2.]. Assimilation may also explain the scatter in the Sr-Nd isotopic compositions. Sample Koz-6 is displaced towards lower $(^{87}\text{Sr}/^{86}\text{Sr})_{330}$ and higher $\epsilon_{\text{Nd}}^{330}$ values, suggesting the role of a third component, possibly derived from the adjacent Metamorphic Islet Zone, although essentially different from the analysed Proterozoic shale from the Teplá - Barrandian Unit [Fig. V.8.].

If the isotopic variation observed in the Blatná suite were to be caused by crustal contamination of a mantle-derived magma similar to the Lučkovice monzonite, then the data array on Figure V.3. suggests that the crustal component could have been represented either only by rocks of the Moldanubian Unit or a mixture between these and metasedimentary lithologies of the Teplá-Barrandian Unit. The sole involvement of shales of the Teplá-Barrandian Unit with low $\epsilon_{\text{Nd}}^{330} = -7.8$ but intermediate $(^{87}\text{Sr}/^{86}\text{Sr})_{330} = 0.707 - 0.708$ [Fig. V.3.] is ruled out. The uncertainty in the composition of the contaminant, however, precludes carrying out quantitative AFC modelling.

In summary, the isotopic variation within the Blatná suite reflects open system processes (crustal contamination and, or, magma mixing), with the Lučkovice monzonite representing the least evolved member of the suite. Both crustal contamination and magma mixing were operative in the Kozárovec intrusion, as documented by field observation of country-rock assimilation [Chapter II.3.] as well as structural and chemical evidence for the hybrid origin of the Kozárovec quartz monzonite [Chapters III.1.3., IV.3.2.].

The preferred model is magma mixing involving different proportions of a moderately enriched ($(^{87}\text{Sr}/^{86}\text{Sr})_{330} \sim 0.708$, $\epsilon_{\text{Nd}}^{330} \sim -3$) mantle component which was close in isotopic composition to the more basic rocks of the suite (Lučkovice monzonite) with either an isotopically evolved metasedimentary component, possibly of Moldanubian provenance, or with a more evolved magma of the Blatná intrusion producing the parental magma of the Kozárovec ($\sim 60 - 70$ % of the acid end-member) and Blatná ($\sim 70 - 80$ %) granodiorites. These have evolved by AFC giving the whole compositional spectrum of both intrusions.

III. Čertovo břemeno suite

The Sedlčany granite and both analysed minettes lie within a tightly constrained field on Figures V.3. and V.5. The initial Sr isotopic composition is within the range of that shown by the durbachitic rocks of the Moldanubian Pluton (*Scharbert and Veselá, 1990*), providing evidence of a uniform source and a limited role for high-level contamination in these magmas. Their very evolved Sr - Nd

isotope signature implies either significant crustal contamination of a more depleted magma, or the involvement of a LILE-enriched mantle source. The Sr - Nd isotopic data could be explained by (1) closed system fractionation of a mantle-derived parental magma similar to the minettes giving rise to the Sedlčany granite, (2) contamination of depleted mantle-derived magmas at depth producing an isotopically homogeneous magma from which the minettes and the Sedlčany granite both crystallized, or (3) contamination of an enriched mantle-derived melt by crustal material of similar Sr - Nd isotope signature.

The two minettes appear to represent almost pristine mantle-derived melts as they have mg = 71 and 75, Cr = 504 and 486 ppm, Co = 28 and 30 ppm, and Ni = 235 and 127 ppm, values that correspond to those in primary mantle-derived melts (65 - 80, 200 - 500, 25 - 80, and 90 - 700 ppm, respectively, given by *Rock, 1991; cf. Holub, 1990*). If these rocks were derived from the mantle, their evolved Sr - Nd isotopic signature could have been acquired either by subsequent assimilation of the continental crust during ascent, or they could reflect the isotopic composition of the mantle source. As the minettes have relatively high Nd and Sr concentrations, the proportion of material derived from the country rocks of the adjacent Moldanubian Unit (mostly metasediments with $(^{87}\text{Sr}/^{86}\text{Sr})_{330}$ typically ≤ 0.717) would have to be excessive as shown by modelling using simple two-component mixing (*Faure, 1986*). If it is assumed that the minette with $(^{87}\text{Sr}/^{86}\text{Sr})_{330} = 0.7127$ and Sr = 350 ppm originally had a Sr isotopic composition similar to Bulk Earth ($(^{87}\text{Sr}/^{86}\text{Sr})_{330} = 0.704$), and the contaminant was a paragneiss of the Moldanubian Unit ($(^{87}\text{Sr}/^{86}\text{Sr})_{330} = 0.717$; Sr = 250 ppm), then 96 % crustal contamination is required [Equations 16-17]. Even using the extreme case of contamination by a hypothetical metasediment with 250 ppm and highly radiogenic Sr ($(^{87}\text{Sr}/^{86}\text{Sr})_{330} = 0.730$), this still requires 47 % assimilation. Such a high degree of contamination is unrealistic in the upper crust because of thermal constraints (*e.g. DePaolo, 1981*) and it would inevitably drastically change the whole-rock geochemistry of the minette. If AFC-style processes involving plagioclase or clinopyroxene fractionation were operative then the amount of contamination would have to be even greater. Crustal contamination of a similar mantle-derived magma by the surrounding granodiorites of the Kozárovec and Blatná intrusions can be discounted, as these show more primitive Sr - Nd isotopic compositions than the minettes. Furthermore, it is unlikely that both minettes, which are from localities about 20 km apart and which cut different intrusions, assimilated exactly the same amount of material required to produce identical Sr - Nd isotope ratios. In summary, the isotopic composition of the minettes may reflect an enriched mantle source.

There is considerable evidence that the upper mantle is heterogeneous on a small scale due to metasomatism by fluids rich in incompatible elements, or by small melt fractions incapable of separating from the mantle residuum. On cooling such metasomatic melts are thought to form phlogopite and K-richterite rich veins which are less refractory than their surrounding mantle (*Roden and Murthy, 1985; Peccerillo, 1992*). Incompatible-element-enriched mantle is thought to play an important role in genesis of K-rich magmas (*e.g. Hawkesworth and Vollmer, 1979; van Kooten, 1981; Wilson, 1989; Foley and Wheller, 1990; Rock, 1991; Peccerillo, 1992*), and such a source has indeed been suggested for the potassic rocks of the Bohemian massif - the so-called durbachite suite and lamprophyres (*Holub, 1990*). The Sr - Nd isotopic composition of the minettes from the CBP could correspond to unaltered enriched mantle values. Mantle-derived K-rich volcanic rocks having $(^{87}\text{Sr}/^{86}\text{Sr})_i = 0.7096$ and $(^{143}\text{Nd}/^{144}\text{Nd})_i = 0.5122$ have been documented from the Italian Volcanic Province (*Hawkesworth and Vollmer, 1979*), and primitive, mantle-derived diamond-bearing lamprophyres may even attain $^{87}\text{Sr}/^{86}\text{Sr} = 0.73$ and $\epsilon_{\text{Nd}} = -25$ (*Rock, 1991*). This continental potassic

volcanism requires a source in the sub-continental mantle, which had been previously invaded by an incompatible element-enriched metasomatic component. The origin of this component could be either from old sub-continental lithosphere, subducted sediments or subducted "megacrysts" of oceanic crust with sediments introduced straight into mantle (Nelson *et al.*, 1986 and references therein). Thus mantle metasomatism is capable of producing the extreme isotopic enrichments seen in certain K-rich rocks.

The presence of enriched mantle within the Hercynian belt has been invoked in several studies, for instance, to explain the petrogenesis of the minettes and kersantites in the French Hercynides (Turpin *et al.*, 1988), granitoids and peridotite xenoliths from the Massif Central (Pin and Duthou, 1990 and references therein), and peridotites from the Ivrea Zone in the Italian Alps (Voshage *et al.*, 1987). In the latter case, the peridotites were metasomatised by K-rich fluids, possibly derived from a metasedimentary source. The Ivrea Zone phlogopite-bearing peridotites had $^{87}\text{Sr}/^{86}\text{Sr} \sim 0.706$ and $\epsilon_{\text{Nd}} \sim -5.3$ at the time of the metasomatic event. Likewise, the proposed origin of the ultrapotassic lamprophyres from the western Alps has been explained by partial melting of enriched mantle, strongly metasomatised by crustal-derived fluids associated with subduction processes (Venturelli *et al.*, 1984). There is evidence for mid-Devonian to early Carboniferous subduction being operative in the area of the CBP (see section on the Sázava suite), which may have introduced K-rich fluids into the mantle wedge. The parental mantle of the Bohemian durbachites could have been previously depleted by extraction of basaltic melt, causing a decrease in CaO and Sr, and increase in SiO_2 , MgO and Cr, prior to the LILE enrichment event(s) (Holub, 1990).

Given that the minettes and the Sedlčany granite have identical Sr - Nd isotopic compositions, it is possible that the parental magma of this granite originated from a similar enriched mantle source. In this case the Sedlčany granite may have been derived from a parental magma similar to the minettes through closed system fractional crystallization.

An alternative hypothesis for the origin of some of the syenite porphyries in the CBP (part of the Čertovo břemeno suite) by magma mixing between a largely mantle-derived minette magma with granitic melt has been formulated by Němec (1988). Likewise, Holub (1988, 1990) argued that the different members of the durbachite suite could have been derived by hybridization of an enriched-mantle component with leucogranites such as those present within the CBP or the S-type granites such as the Eisgarn intrusion of the Moldanubian Pluton [Chapter IV.3.3.]. The samples from the Čertovo břemeno and Sedlčany intrusions could be produced by variable mixing of similar components [Chapter IV.3.3.]. Unfortunately, there are no isotope data available for the leucogranites. Nevertheless, if these S-type granitic rocks represent crustal anatectic melts of the local metasediments, then they may show little Sr - Nd isotopic contrast to the rocks of the Čertovo břemeno suite [Fig. V.3.]. Although this would be in accord with the observed Sr - Nd isotopic data, it precludes any Sr - Nd isotope-based assessment of the mass balance between both components. The similarity in Sr isotopic composition between the rocks of the Čertovo břemeno suite and those of durbachites elsewhere in the Bohemian massif (the Jihlava and Třebíč masses of the Moldanubian Pluton; Scharbert and Veselá, 1990) implies that such a process may have been widespread in this area. As these Moldanubian intrusions, together with the minettes and the Sedlčany granite, cover almost the entire compositional range of rocks with durbachitic affinities, their similar Sr isotopic ratios provide evidence against mixing (magma mixing or assimilation) of two Sr-isotopically different components being responsible for their genesis.

The Čertovo břemeno suite, including the minettes, is likely to have originated from strongly enriched ($(^{87}\text{Sr}/^{86}\text{Sr})_{330} \sim 0.7128$, $\epsilon_{\text{Nd}}^{330} \sim -7$) mantle derived magmas. The mantle was probably metasomatised prior to the melting by a metasedimentary component, possibly subduction-related. These primary magmas may have evolved through closed-system fractionation, or have interacted with S-type leucogranitic magmas of similar isotopic composition that were derived from the Moldanubian Unit.

IV. Říčany suite

An origin for the Říčany granite by fractional crystallization of the Čertovo břemeno suite would account for similarities in the whole-rock geochemistry between the two suites [Chapter IV.] and presence of MME of durbachitic character [Chapter II.6.], but is not consistent with the significant differences in Sr - Nd isotopic compositions.

In view of the Sr-Nd data, it is possible that the Říčany suite could have been produced through contamination of the rocks of the Čertovo břemeno suite (or minettes) by metasediments of the Teplá-Barrandian Unit. However high-level contamination of a durbachite-like melt by metasedimentary material with low $(^{87}\text{Sr}/^{86}\text{Sr})_{330}$ (<0.710), similar to analysed shales of the Teplá-Barrandian Unit, is not considered likely because the shales have too low SiO_2 and too high TiO_2 , FeO^* , MgO and CaO [cf. also Chapter IV.3.4.]. A contamination process involving these components could only be applicable were the contamination to occur prior to fractionation, and if only the most evolved magmas were subsequently emplaced at the present erosion level.

The Říčany suite is also unlikely to represent a highly contaminated version of the Blatná suite, as on the K_2O - SiO_2 plot [Fig. IV.1.9 b] the fields of the Říčany and Blatná suites neither overlap nor intersect; the most evolved Říčany rocks still have higher K_2O than the those of the Blatná suite. Furthermore, both suites show distinct trends on several other plots, for instance P - Q [Fig. IV.1.11.], B-Mg/(Fe+Mg) [Fig. IV.1.13.] and R_1 - R_2 [Fig. IV.3.1.].

The peraluminous nature of even the least evolved Říčany granite may be consistent with derivation from a peraluminous source such as metasediments of the Moldanubian Unit or the peraluminous leucocratic granulites which are also part of this unit. The Sr - Nd isotopic composition of the Říčany granite falls within the field of the metasediments of the Moldanubian Unit (*Liew and Hofmann 1988*), and close to that of the peraluminous leucocratic granulites occurring at Blanský les, southern Bohemia (Fig. V.3., *Valbracht et al., 1994*). Its genesis can therefore be explained by derivation from these Moldanubian lithologies, or from a mixture of the Moldanubian and Teplá-Barrandian units with a high proportion of the former.

The presence of abundant mafic microgranular enclaves in the Říčany granite suggests interaction of the granitic melt with basic magmas. Such magmas may have provided the heat necessary to promote melting of the Moldanubian crust. However their major direct involvement is unlikely, considering the major negative gravity anomaly in the area (*Orel, 1975*; Fig. I.2.).

In summary, the parental melts of the Říčany suite are most likely to have been produced by partial melting of peraluminous lithologies within the Moldanubian Unit, although an origin by mixing between magmas resembling the Čertovo břemeno suite and metasediments of the Teplá-Barrandian Unit cannot be ruled out. This magma has undergone a high degree of (K-feldspar-dominated) fractionation in a deep magma chamber [Chapter IV.3.4.], prior high-level intrusion. The reverse zoning of the Říčany intrusion has been achieved at this stage either by emplacement in a single batch

of magma from a compositionally zoned magma chamber, or in several batches in connection with cauldron subsidence or stoping [Fig. IV.3.12.].

V.3.3. Summary

The Sr - Nd isotopic compositions of granitic rocks from the CBP are comparable with those of other Hercynian occurrences, notably from the Moldanubian Pluton and the Massif Central. The older intrusions have more depleted Sr - Nd compositions and calc-alkaline geochemistry, but there is a conspicuous shift towards K-rich calc-alkaline and shoshonitic rocks with more evolved isotopic signatures in the later suites. Unlike the temporal control, there does not seem to be a major spatial control on the distribution of the main geochemical suites within the CBP. The main process responsible for such an evolution is interpreted to be enrichment of the mantle by an incompatible-element-enriched and, or, high $^{87}\text{Sr}/^{86}\text{Sr}$ component, possibly associated with an earlier subduction environment. The observed geochemical variation also probably reflects distinct crustal sources for the individual suites.

The Sázava suite could have originated by re-melting of metabasites of the Metamorphic Islet Zone or Jílové Zone, by partial melting of a mantle source with an isotopic composition similar to Bulk Earth, or by mixing of mantle-derived melt with crustally-derived tonalitic magmas.

Variation within the Blatná suite can be modelled by mixing between a moderately enriched ($(^{87}\text{Sr}/^{86}\text{Sr})_{330} \sim 0.708$, $\epsilon_{\text{Nd}}^{330} \sim -3$) mantle component, close in isotopic composition to the more basic rocks of the suite (Lučkovice monzonite) with either an isotopically evolved metasedimentary component, possibly of Moldanubian provenance, or with more evolved magma of the Blatná intrusion.

The Čertovo břemeno suite and the minettes originated from strongly enriched ($(^{87}\text{Sr}/^{86}\text{Sr})_{330} \sim 0.7128$, $\epsilon_{\text{Nd}}^{330} \sim -7$) mantle-derived magmas. These may have evolved through closed-system fractionation, or have interacted with S-type (leuco-)granitic magmas of similar isotopic composition that were derived from the Moldanubian Unit.

The parental melts of the Říčany suite are most likely to have been produced by partial melting of peraluminous lithologies within the Moldanubian Unit, although an origin by mixing between magmas resembling the Čertovo břemeno suite and metasediments of the Teplá-Barrandian Units cannot be ruled out.

The two-stage Nd model ages increase from the assumed oldest to the youngest intrusions: ~ 1.05 Ga for the Sázava suite, ~ 1.45 Ga for the Blatná suite and 1.65 Ga for both Říčany and Čertovo břemeno suites. The data for the Blatná, Čertovo břemeno and Říčany suites represent typical 'Hercynian' values, and are likely to point to an mixed source (Archaean and Late Proterozoic components) rather than a major crustal-formation event, whereas the lower $T_{\text{Nd}}^{\text{DM}}$ of the Sázava intrusion is similar to that of the quartz diorites of Limousin, the Massif Central and is not compatible with a major involvement of a mature metasedimentary material.

V.4. Towards a petrogenetic model of the CBP

In the extensive literature about the CBP, many petrogenetic theories have been presented, some of which have been discussed already elsewhere in this thesis. Accordingly they are mentioned only briefly here.

The oldest hypothesis, based on whole rock geochemistry, is that of *Orlov (1935)* who proposed that magmatic fractionation was operative throughout the CBP and showed that there are

important geochemical and also possibly genetic differences between the western (~ Sázava and Blatná suites) and eastern (Čertovo břemeno suite) parts of the CBP. Likewise, *Steinöcher (1969)* assumed differentiation of a single, tonalitic, basalt-derived magma similar to that of the Sázava intrusion, with, however, contributions from crustally-derived potassic magmas. *Vejnar (1973)* suggested that the granite - granodiorite suite of the CBP (Sázava and Blatná suites) originated by crustal contamination and recrystallization of pre-Hercynian tholeiitic volcanic and subvolcanic rocks, whereas the durbachite suite (Čertovo břemeno suite) corresponded to Hercynian minimum crustal melts. An upper crustal source of the geochemically evolved Čertovo břemeno suite has also been recently proposed by *Bouška et al. (1984)*, whereas fractionation of small-degree (< 1 %) mantle-derived melts by multiple freezing-remelting cycles has been invoked by *Bowes and Košler (1993)*. *Rajlich and Vlačinský (1983)* proposed a petrogenetic model, involving diffusional differentiation of a large, hypothetical batholith beneath the present CBP. In their view, by means of such differentiation, driven by the thermal contrast between the colder Barrandian and hot Moldanubian units, it was possible to derive both granodioritic and durbachitic melts, the latter enriched by MgO, P₂O₅ and K₂O.

In view of the Sr-Nd isotope data presented in this thesis, and without considering any other problems involved in the model of *Rajlich and Vlačinský (1983)* (sluggish diffusion in granitic melts, possibility of convection and subsequent rehomogenization of the magma, lack of geophysical evidence for the presence of a large granitic reservoir underlying the CBP, etc.; see *Holub, 1990*), any kind of closed-system process generating the whole compositional spectrum of the CBP can be rejected, although closed-system processes were possibly important in a number of individual intrusions.

The genetic model of *Afanasjev et al. (1977)* involved regional-scale anatexis under amphibolite-facies conditions, followed by the upward migration and emplacement of the anatectic melt in the north-western sector of the CBP (e.g. Sázava intrusion), whereas the actual melting zone is thought to be preserved in the south-eastern segment (durbachites). As an alternative they invoked a hypothesis of in-situ recrystallization producing the whole CBP. The concept of an origin for the Červená and Čertovo břemeno intrusions by in-situ metasomatism of metasediments has been formulated by *Röhlichová (1964 a,b)*. *Vlačinský et al. (1992)* defended their model of a metasomatic origin for the CBP (e.g. *Palivcová, 1965; Palivcová et al., 1988, 1989 a,b, 1992*). They proposed that the majority of the granitoids in the CBP had originated by isochemical in-situ granitization of sediments, volcanic and subvolcanic rocks. This process was considered to have been operative under amphibolite-facies conditions at a shallow level (< 700 °C and < 0.8 kbar according to *Palivcová et al., 1989b*; cf. Chapter III.), with heat provided by transpressional movements.

Many phenomena which suggest that all the intrusions studied were, at some time in their history, magmas, mobile and capable of inducing thermal metamorphism on, and assimilating their country rocks have been described in Chapter II. and these negate the metasomatic model. The explanation of the mafic enclaves as boulders produced by the erosional disintegration of volcanic bodies or volcanic products (e.g. bombs) prior to the granitization (*Vlačinský et al., 1992*) and the statement that "neither experimental nor geological facts support mixing of magmas" (*Vlačinský et al., 1992, page 33*) ignore completely the overwhelming experimental, field and geochemical evidence to the contrary [cf. Chapter II. and citations therein]. As shown in Chapters II.-V. the structural, geochemical and isotopic data point towards an important role for magma-mixing in the CBP, whereas Chapter IV.3. suggests that fractional crystallization was also important. It is difficult to imagine any metasomatic process that would result in Sr-Nd isotopic ratios that are very similar within each intrusion but differ considerably between different ones [Chapter V.].

Magma-mixing models have been previously applied to explain the origin of the Čertovo břemeno suite and minettes (Němec, 1988; Holub, 1988, 1990), as well as the K-rich granitoids of the southern CBP (Blatná suite, van Breemen *et al.*, 1982; Bendl and Vokurka, 1989; Machart, 1989, 1992) [Chapters IV.3., V.III.]. The operation of magma mixing in the genesis of both the Blatná and Čertovo břemeno suites is indeed invoked in the genetic model presented in the following paragraphs.

In geotectonic terms, the shift towards K-rich calc-alkaline and shoshonitic compositions in the CBP may be compatible with a transition from a magmatic-arc to a post-collisional setting. The operation of subduction in this part of the Bohemian Massif in mid-late Devonian has been inferred from geochemistry of orthogneisses from the Metamorphic Islet Zone (Košler, 1993). Based on the ~ 40 Ma time gap between the age of protolith of orthogneisses (~ 369 Ma) and the age of the Blatná granodiorite (~ 331 Ma), as well as the more evolved Sr-Nd signature of the Blatná granodiorite [Fig. V.3.], Košler (1993), argued that the protolith of the orthogneisses was a product of an independent magmatic phase from the granitoids of the CBP themselves. As demonstrated in Chapters I.3., II.4. and Appendix IX., the rocks of the Blatná suite do not appear to be amongst the earliest amongst unmetamorphosed granitoids of the CBP as the Sázava suite may be significantly older than ~ 330 Ma. The subduction could have been rather short-lived; for instance, in the French Massif Central, it has been suggested that subduction was operative between ~ 370 - 350 Ma and was responsible for the production of the rocks of the Limousin Tonalite Belt (Shaw *et al.*, 1993). In any case, the generation of calc-alkaline magmas may post-date the *cessation* of the processes by as much as 30 - 50 Ma depending on availability of the water (Bonin, 1990). Additionally, there are many geochemical affinities between the orthogneisses (Staré Sedlo and Mirovice) and the Sázava suite, most importantly the Sr-Nd isotope ratios [Fig. V.3.] and thus there is no apparent reason to treat these orthogneisses separately from the rest of the CBP just on basis of their higher age and strong deformation. Paterson and Tobisch (1988) presented an excellent example of several pre-tectonic plutons from the same locality and of similar age some of which showed pronounced foliation, whereas the others were virtually undeformed. Thus, the question of the relationship of the Sázava suite to the orthogneisses cannot be fully resolved until detailed geochronological information on the former is available.

Alternatively, the volcanic-arc-like geochemical signature of both the orthogneisses and the Sázava suite might have been inherited from their source that could itself be volcanic-arc-related. One of the models invoked earlier on for the genesis of the Sázava suite [Chapter V.3.2.] involved melting of the metabasic rocks of the Jílové Zone that are, indeed, considered to have originated in an island-arc setting (Waldhausrová, 1984; Fediuk, 1992a).

If subduction was operative in the area of the CBP early in the development of the Hercynian belt, the influx of LILE-enriched and HFSE-depleted volatiles into a mantle wedge above the subduction zone might have promoted melting and generation of basaltic calc-alkaline magmas, that, in turn, provided heat for infracrustal melting yielding the tonalitic magmas of the Sázava suite. Such a volatile influx may have also been responsible for widespread metasomatism of the mantle beneath the CBP. This metasomatized mantle, later reactivated, may have contributed as a major source to basic shoshonitic magmas (similar in isotopic composition to the studied monzonitic rocks and minettes) that were to become basic end-members involved in genesis of Blatná and Čertovo břemeno suites, respectively.

The generation of late post-collision magmas is often attributed to melting LILE-enriched mantle wedge above (fossil) subduction zones, possibly modified by contamination with melts from the lower

crust (*Harris et al.*, 1986) and melting of these anomalous mantle compositions may be connected to adiabatic decompression in the upper mantle (*Harris et al.*, 1986). In this way, the mantle wedge metasomatised by slab-derived fluids during the subduction stage could have been remelted due to asthenospheric upwelling following crustal extension and uplift, to produce shoshonitic magmas.

Clearly, time was needed for this anomalous source with elevated Rb/Sr to develop the $^{87}\text{Sr}/^{86}\text{Sr}$ ratio observed in the Čertovo břemeno suite. Assuming that the subduction-induced mantle metasomatism was early Hercynian (~ 380 Ma), a time span of some 50 Ma (to 330 Ma) was available for this source to evolve from a Sr isotopic composition close to the Bulk Earth ($^{87}\text{Sr}/^{86}\text{Sr} \sim 0.7045$) to that of the minettes ($^{87}\text{Sr}/^{86}\text{Sr} \sim 0.7128$). Simple calculations show that the mantle source would have to have had $^{87}\text{Rb}/^{86}\text{Sr}$ of 11.7. *Ellam and Hawkesworth* (1988) suggested that melting of mantle rocks at destructive margins generating basaltic magmas does not result in a major fractionation in Rb/Sr. Considering that the minettes have $^{87}\text{Rb}/^{86}\text{Sr} = 3 - 3.5$, and assuming that they experienced little subsequent fractional crystallization, the enrichment of the source of the Čertovo břemeno suite solely due to the subduction related to the Hercynian orogen can be discounted: a longer time interval is needed if subduction-related enrichment were to have been operative.

An island-arc setting for the ~ 600 Ma old volcanic rocks of the Jílové Zone has been proposed by *Waldhausrová* (1984) and this has been given support by the identification of boninites within it (*Fediuk*, 1992a). A similar calculation for the 270 Ma interval between 600 - 330 Ma gives $^{87}\text{Rb}/^{86}\text{Sr} = 2.2$, i.e. similar to that of the minettes. Thus Proterozoic subduction-related fluids may have significantly contributed to the mantle enrichment responsible for the Sr isotopic signature of the Čertovo břemeno suite. The mantle reservoir enriched by the Proterozoic subduction could have become an integral part of the local lithospheric mantle which would preserve it from being destroyed were subduction operative during the Hercynian orogeny, as well. Alternatively, the enriched mantle source of the shoshonitic magmas could have corresponded to lithospheric mantle with a relatively high time-integrated Rb/Sr ratio, that may have developed beneath ancient (*Gebauer et al.*, 1989; *Wendt et al.*, 1993; *Gebauer and Friedl*, 1994) basement beneath the Moldanubian Unit.

The mantle end-member of the Blatná suite was probably much less enriched ($(^{87}\text{Sr}/^{86}\text{Sr})_{330} \sim 0.708$, $\epsilon_{\text{Nd}}^{330} \sim -3$), than that of the Čertovo břemeno suite ($(^{87}\text{Sr}/^{86}\text{Sr})_{330} \sim 0.7128$, $\epsilon_{\text{Nd}}^{330} \sim -7$). Because of the probably nearly coeval development of these two suites [Chapters I, II], and their relatively low $^{87}\text{Rb}/^{86}\text{Sr}$ (< 3.5), it is unlikely that differences in $(^{87}\text{Sr}/^{86}\text{Sr})_{330}$ between both basic end-members were caused by delayed melting of an otherwise homogeneous enriched mantle source. Instead, different proportions of the enriched component in the source of both suites ought to be considered, either being a consequence of mixing within the mantle of distinct components, or of source inhomogeneity. Moreover, for the Blatná suite, the amount of mantle-derived shoshonitic melt was likely to be subordinate to that of the crustal component, in contrast to the Čertovo břemeno suite, that appears to be mantle-dominated.

The heat introduced by emplacement of the shoshonitic magmas might have been, at least partly, responsible for the anatexis of the crustal rocks (partly or fully of Moldanubian provenance) and both magmas could have interacted with each other producing abundant K-rich MME which are especially abundant within the Červená granodiorite [Chapter II.4.]. Therefore, the Blatná and Čertovo břemeno suites may have been generated by similar processes, both being formed by mixing of (variously) enriched mantle with a crustal component(s). Such a model resembles that of *Harmon et al.* (1984) and *Rock and Hunter* (1987) for the genesis of British Late Caledonian granitoids in which basic, mantle-derived magmas have acted both as parents, undergoing crustal contamination, and heat

sources, facilitating melting. Similarly, *Fowler (1988)* argued that the whole compositional spectrum of lamprophyres, syenites and Newer Granites in the Scottish Highlands might have been generated by mixing of various proportions of shoshonitic, (subduction-related ?) and crustally-derived components.

In contrast to the other three suites, the peraluminous Říčany suite has most probably originated largely by anatexis of Moldanubian metasedimentary rocks.

In summary, the low-K calc-alkaline Sázava suite appears to correspond to granitoids typical of subduction settings, with classic examples found in the Andean batholiths and Sierra Nevada Batholith (California), or, in the classification scheme of *Barbarin (1990a)*, to H_{CA} (Hybrid Continental Arc) granitoids. The higher K, mainly crustally-dominated Blatná suite, and especially the mantle-dominated shoshonitic Čertovo břemeno suite seem to belong to the H_{LO} (Hybrid Late Orogenic) group of *Barbarin (1990a)*, that is usually associated with relaxation and uplift following a collision event, like late Caledonian granitoids of Scotland including the appinite suite (*Barbarin, 1990a; Bowes and Košler, 1993*). The Říčany suite appears to have affinities to the 'subalkaline' group of French authors (*Barbarin, 1990a, and references therein*), as it shares some features with the alkaline granites (e.g. mode of emplacement) like the Ploumanac'h complex in Brittany (*cf. Palivcová, 1992*). Such subalkaline granitoids typically develop in a transitional environment between late orogenic compressional and extensional regimes (*Barbarin, 1990a*).

The time range of the CBP intrusions now needs to be established from geochronological studies. This would help further integration of this granitoid complex into the overall evolution of the Hercynian orogenic belt and extend the knowledge obtained by the combined field, petrographic and geochemical study presented in this thesis.

Table V.1: Sr - Nd isotopic data, Central Bohemian Pluton and its country rocks

Sample	Rb (ppm)	Sr (ppm)	$^{87}\text{Rb}/^{86}\text{Sr}$	$^{87}\text{Sr}/^{86}\text{Sr}$	2 s.e.	$(^{87}\text{Sr}/^{86}\text{Sr})_{330}$	Sm (ppm)	Nd (ppm)	$^{147}\text{Sm}/^{144}\text{Nd}$	$^{143}\text{Nd}/^{144}\text{Nd}$	2 s.e.	$(^{143}\text{Nd}/^{144}\text{Nd})_{330}$	$\epsilon_{\text{Nd}}^{330}$	$T_{\text{CHUR}}^{\text{Nd}}$ (Ga)	$T_{\text{DM}}^{\text{Nd}}$ (Ga)
Sázava suite															
Sázava															
Sa-1	76†	555.8	0.3955	0.70700	3	0.70514	4.57	24.2	0.1188	0.512476	6	0.512219	0.1	0.32	1.04
Sa-3	55†	606.1	0.2627	0.70638	3	0.70514	6.66	33.9	0.1189	0.512479	7	0.512222	0.2	0.31	1.03
Gabbro, Křhanice															
Gbs-5	101†	116.7	2.4987	0.71279	3	0.70105	8.45	36.8	0.1386	0.512498	6	0.512199	-0.3	0.37	1.07
Blatná suite															
Kozárovce															
Koz-2	164.1	486.9	0.9767	0.71258	4	0.70799	5.91	31.7	0.1128	0.512210	7	0.511966	-4.8	0.78	1.42
Koz-4	174.5	437.6	1.1544	0.71367	3	0.70825	5.36	28.9	0.1121	0.512186	5	0.511944	-5.3	0.82	1.46
Koz-5	181.9	410.3	1.2838	0.71434	4	0.70831	5.04	26.7	0.1141	0.512187	7	0.511941	-5.3	0.83	1.46
Koz-6	146.7	417.7	1.0167	0.71209	3	0.70732	6.23	33.4	0.1127	0.512267	7	0.512024	-3.7	0.67	1.34
Koz-12	172.9	398.5	1.2564	0.71373	4	0.70783									
Lučkovice															
Gbl-1	138.2	547.5	0.7305	0.71114	4	0.70771	6.39	31.7	0.1217	0.512316		0.512053	-3.1	0.66	1.29
Gbl-2	171†	221.3	2.2389	0.71863	4	0.70811	6.09	26.9	0.1366	0.512334	7	0.512039	-3.4	0.77	1.31
Blatná and Červená															
Bl-2	185†	439.1	1.2189	0.71434	3	0.70862	6.85	43.8	0.0946	0.512101	7	0.511897	-6.2	0.80	1.53
Cv-1	132†	404.6	0.9438	0.71362	4	0.70918	10.83	50.1	0.1307	0.512225	6	0.511943	-5.3	0.96	1.46
Čertovo břemeno suite															
Sedlčany															
Se-1	310.9	313.9	2.8703	0.72615	3	0.71267	8.26	40.0	0.1253	0.512114	7	0.511843	-7.2	1.12	1.61
Se-5	314.4	339.0	2.6879	0.72543	3	0.71280	7.88	40.2	0.1186	0.512103	8	0.511847	-7.2	1.05	1.61
Se-9	308.1	307.8	2.9016	0.72620	3	0.71257	8.17	40.2	0.1228	0.512080	10	0.511815	-7.8	1.15	1.65
Říčany suite															
Říčany															
Ri-1	310.7	374.1	2.4058	0.72154	3	0.71024	4.06	24.1	0.1020	0.512053	6	0.511833	-7.4	0.94	1.63
Ri-2	326.9	360.2	2.6299	0.72267	3	0.71031	4.98	29.0	0.1005	0.512035	6	0.511818	-7.7	0.96	1.65
Ri-4	319.2	377.7	2.4483	0.72216	4	0.71066	4.59	27.9	0.0995	0.512062	11	0.511847	-7.1	0.90	1.61
Ri-5	310.4	399.5	2.2510	0.72134	4	0.71077	3.83	23.6	0.0980	0.512074	14	0.511862	-6.8	0.87	1.58
Ri-6	317.3	386.6	2.3776	0.72186	3	0.71069	4.56	28.1	0.0980	0.512068	7	0.511856	-7.0	0.88	1.59
Ri-10	322.9	322.4	2.9034	0.72431	3	0.71067	4.40	26.5	0.1005	0.512075	9	0.511858	-6.9	0.89	1.59
Ri1-1	330.4	297.9	3.2142	0.72571	4	0.71062	12.59	71.0	0.1071	0.511989	6	0.511758	-8.9	1.10	1.74

Table V.1: Sr - Nd isotopic data, Central Bohemian Pluton and its country rocks (cont.)

Sample	Rb (ppm)	Sr (ppm)	$^{87}\text{Rb}/^{86}\text{Sr}$	$^{87}\text{Sr}/^{86}\text{Sr}$ 2 s.e.	$(^{87}\text{Sr}/^{86}\text{Sr})_{330}$	Sm (ppm)	Nd (ppm)	$^{147}\text{Sm}/^{144}\text{Nd}$	$^{143}\text{Nd}/^{144}\text{Nd}$ 2 s.e.	$(^{143}\text{Nd}/^{144}\text{Nd})_{330}$	$\epsilon_{\text{Nd}}^{330}$	$T_{\text{CIUR}}^{\text{Nd}}$ (Ga)	$T_{\text{DM}}^{\text{Nd}}$ (Ga)		
Minettes															
Mi-1	421.8	354.1	3.4540	0.72907	4	0.71285	12.60	61.7	0.1235	0.512113	7	0.511846	-7.2	1.09	1.61
Mi-2	350†	333.7	3.0408	0.72700	4	0.71272	16.25	75.9	0.1293	0.512140	7	0.511861	-6.9	1.13	1.58
Teplá-Barrandian Unit															
CR-1	110†	80.4	3.9709	0.72596	3	0.70730	3.3	17.3	0.1156	0.512061	19	0.511644	-7.8	1.09	1.65
CR-9	100†	83.7	3.4486	0.72419	2	0.70799									
CR-10	32†	209.4	0.4340	0.70807	4	0.70603									
Moldanubian Unit															
CR-4	44†	723.4	0.1736	0.70898	4	0.70816									
CR-5	160†	86.4	5.3717	0.74670	4	0.72147									
CR-7	118†	195.5	1.7499	0.72173	4	0.71351									
JT-23	125†	163.1	2.2316	0.72493	5	0.71445									
JT-27	98†	143.9	1.9710	0.72632	3	0.71706									
JT-28	182†	154.3	3.4226	0.73300	4	0.71693									

Isotopic ratios with subscript '330' are age-corrected to 330 Ma; $\epsilon_{\text{Nd}}^{330}$ values and $T_{\text{CIUR}}^{\text{Nd}}$ model ages calculated using Bulk Earth parameters given by *Jacobsen and Wasserburg (1980)*.
 $T_{\text{DM}}^{\text{Nd}}$ are two-stage Nd model ages based on *Liew and Hofmann (1988)*.

† Rb concentrations determined by XRF rather than by isotope dilution.

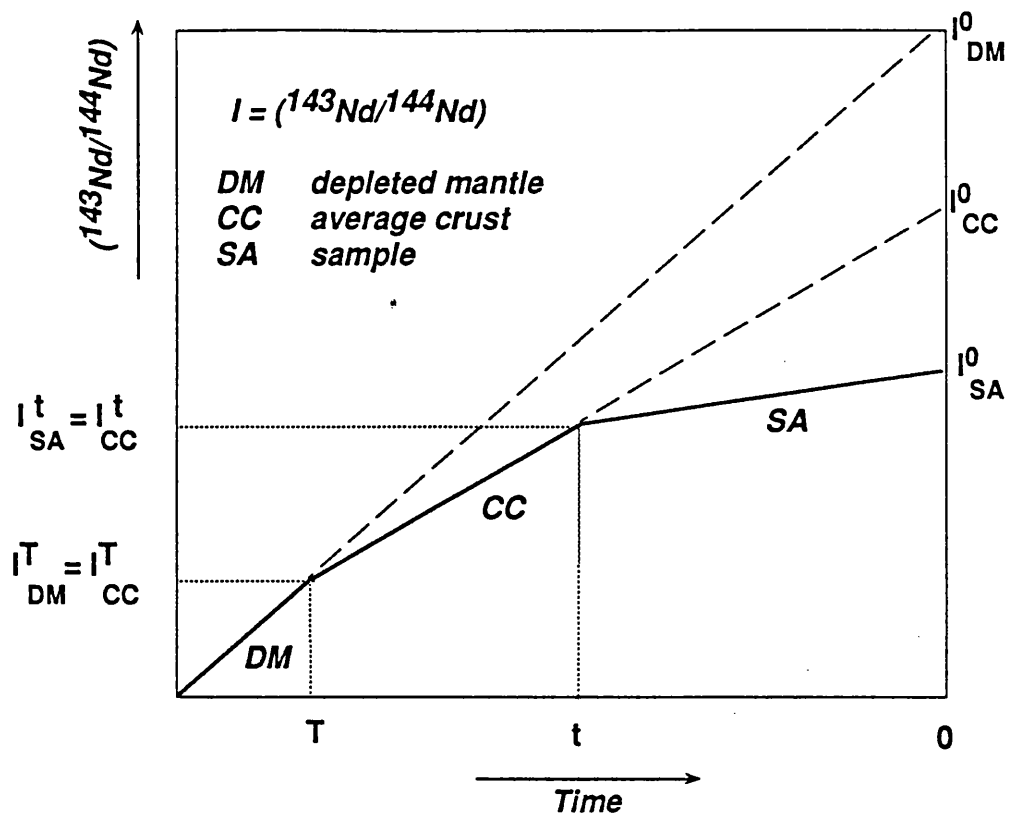


Figure V.1: Derivation of the two-stage model Nd age
(Liew and Hofmann, 1988)

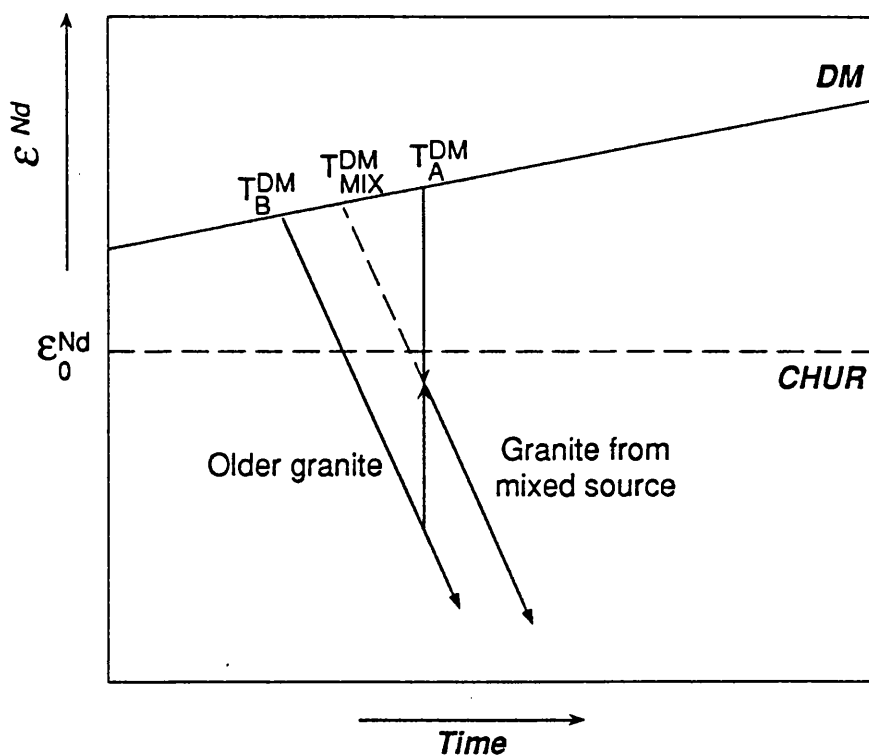


Figure V.2: Diagram illustrating why the Nd model ages of rocks from mixed sources do not correspond to crust-formation events (after Arndt and Goldstein, 1987)

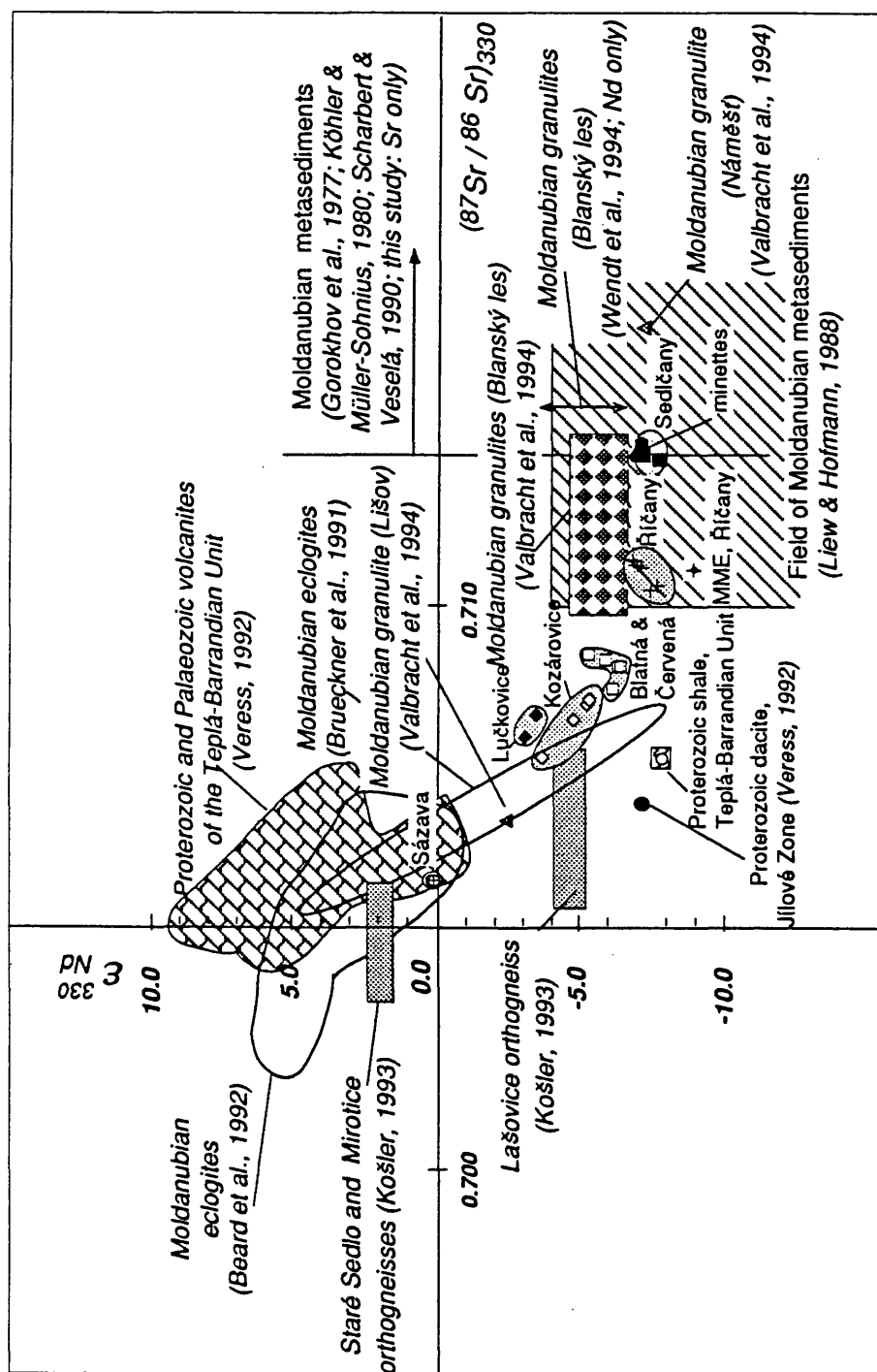


Figure V.3: ($^{87}\text{Sr}/^{86}\text{Sr}$)₃₃₀ versus $\epsilon_{\text{Nd}}^{330}$ plot of the granitoids of the CBP and their country rocks
(age-corrected to the age of the Blatná intrusion; van Breemen et al., 1982);
Part of the data for the Blatná granodiorite is from van Breemen et al. (1982) and Košler (1993)

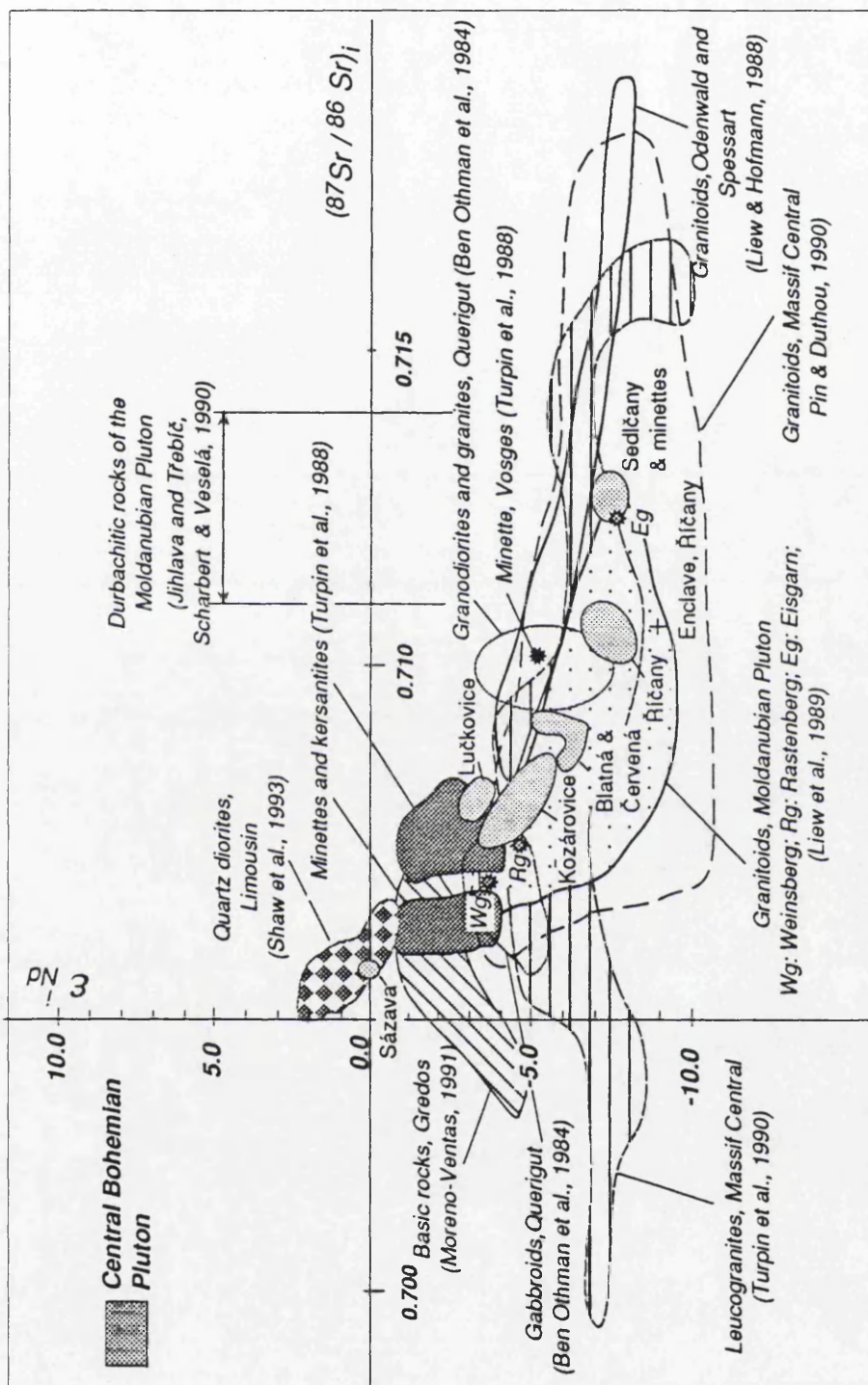


Figure V.4: Comparison of the $(^{87}\text{Sr}/^{86}\text{Sr})_i$ versus ϵ_{Nd} data for other Hercynian granitoids and lamprophyres with data for the granitoids of the CBP

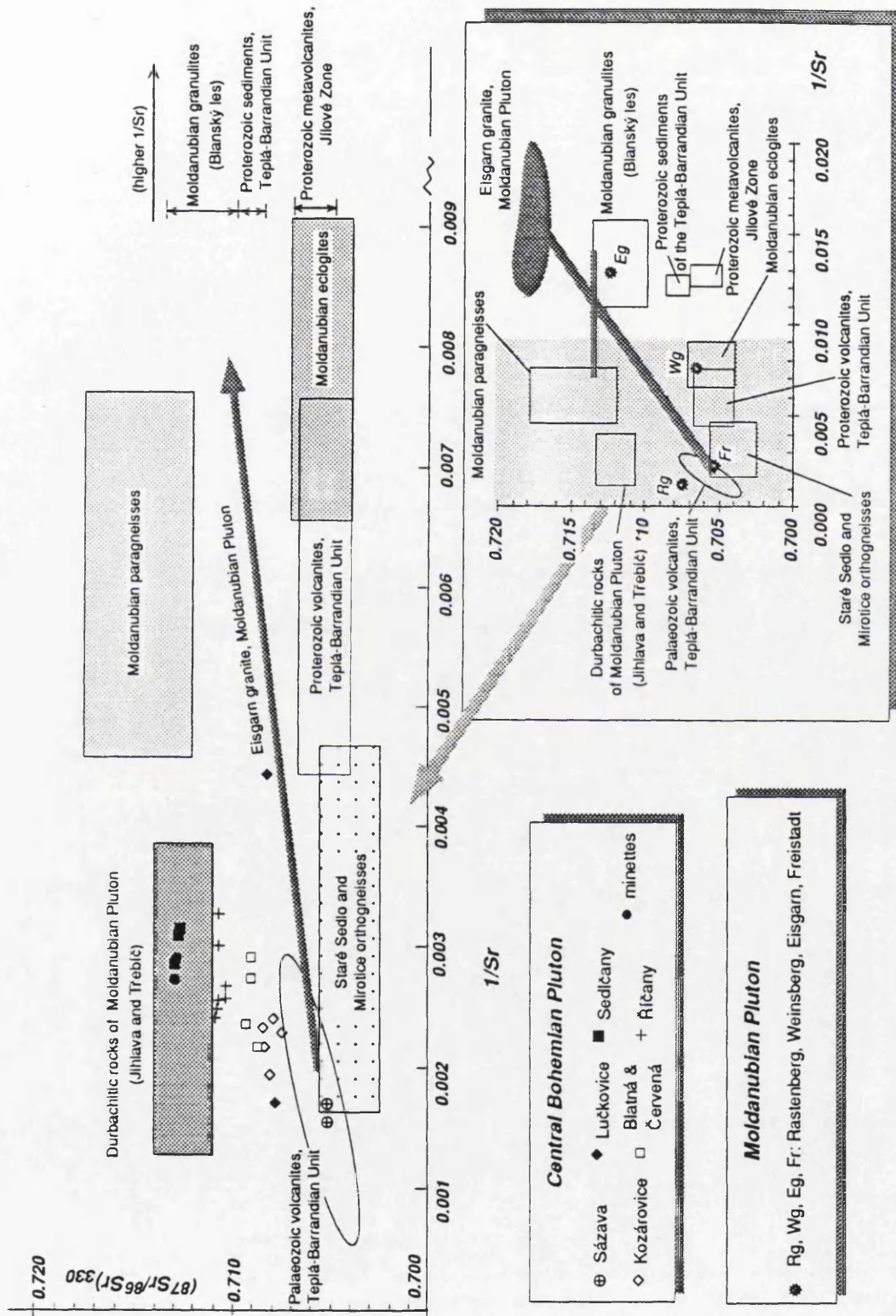


Figure V.5: $1/Sr$ versus $(^{87}Sr/^{86}Sr)_{330}$ plot of rocks of the CBP and their country rocks, together with the data for granitoids from the Moldanubian Pluton
See Figures V.3-V.4. and text for references

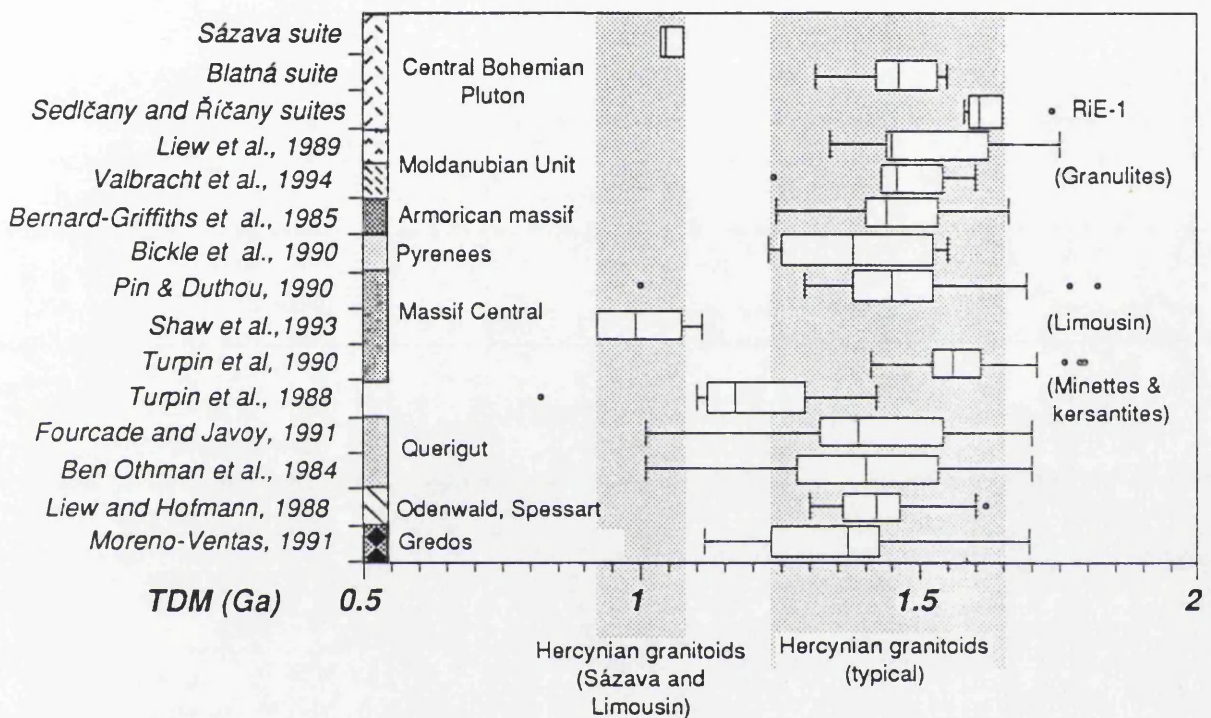
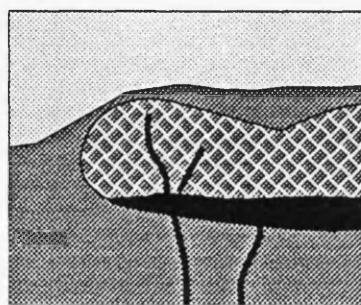
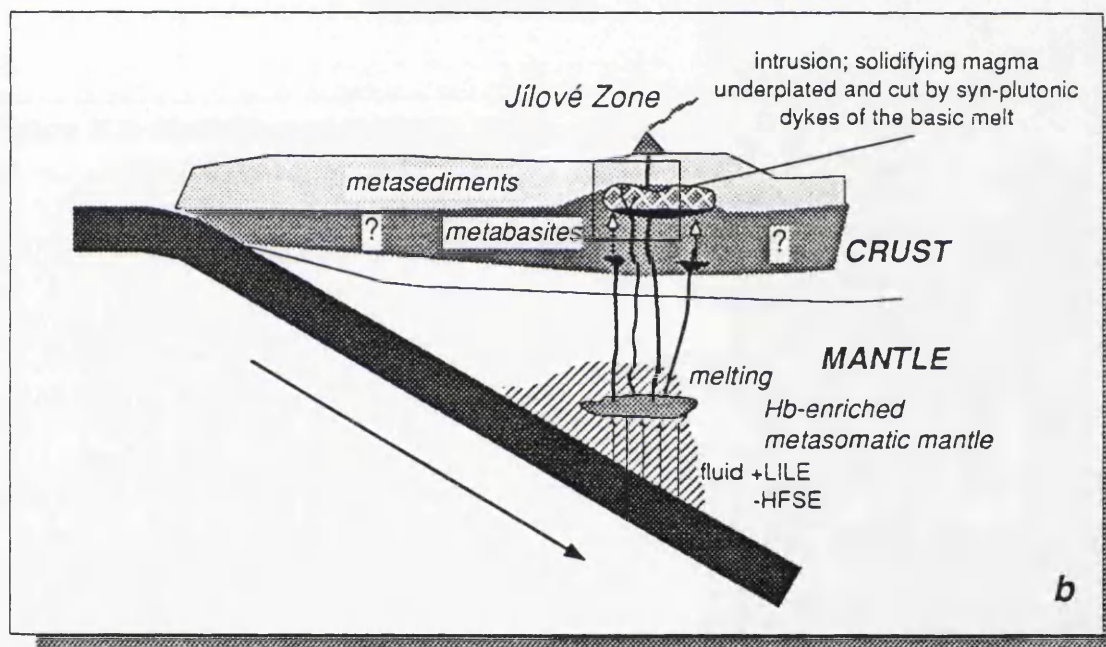
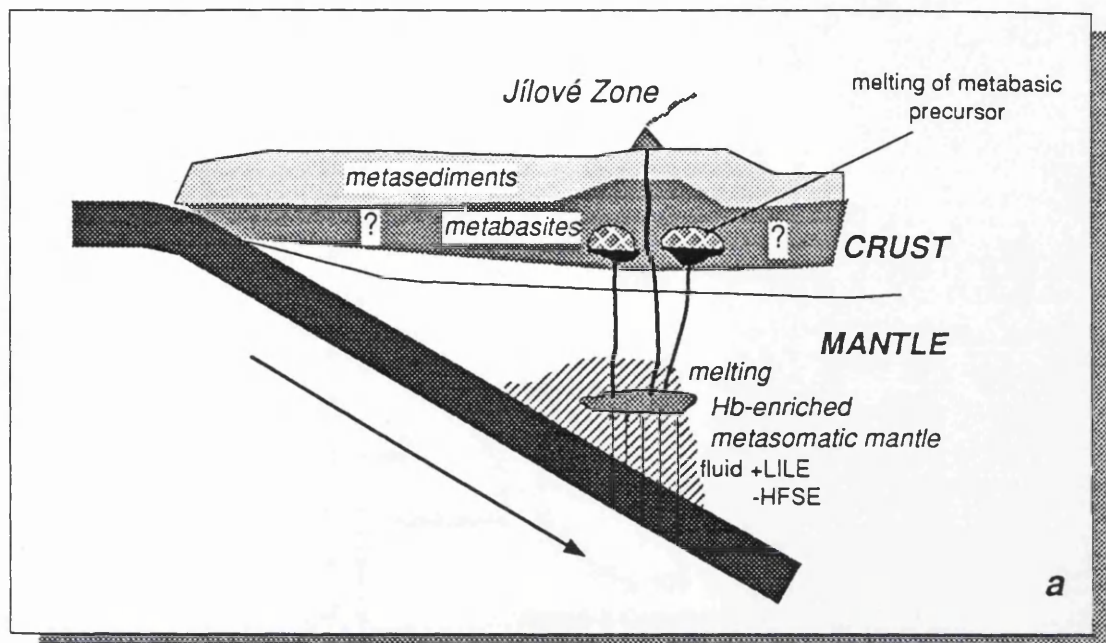
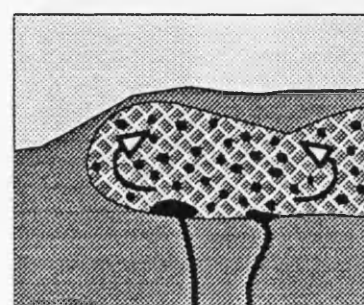


Figure V.6: Compilation of two-stage (Liew and Hofmann, 1988) depleted mantle Nd model ages for granitoids from the European Hercynides



Intrusion of syn-plutonic dykes



Their disruption and origin of abundant MME

Figure V.7: Schematic model for the origin of the Sázava suite
(for discussion, see text)

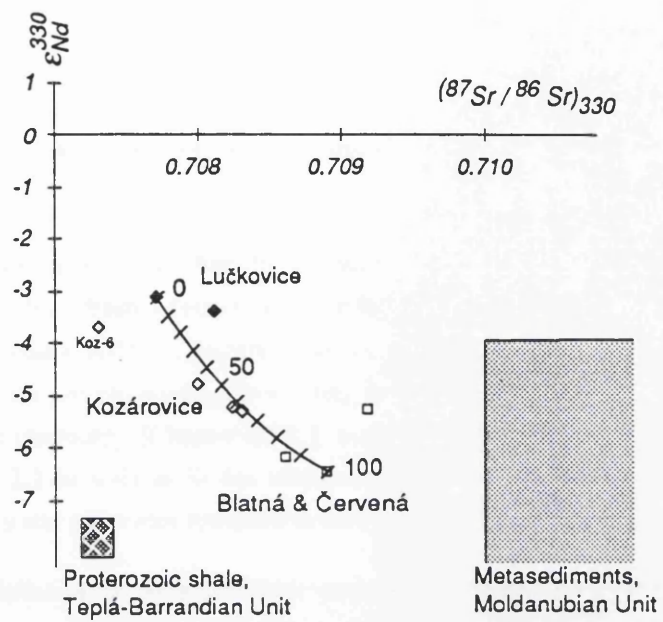


Figure V.8: Modelling of a simple binary mixing for the rocks of the Blatná suite
 Presumed end-members are the Blatná granodiorite from Řečice
 (van Breemen et al., 1982; Košler, 1993) and Lučkovice monzonite (Gbl-1);
 tick marks show percentage of the granodiorite in the mixture

VI. Conclusions

The new petrographic, mineral and whole-rock geochemical data on selected intrusions of the Central Bohemian Pluton, Czech Republic, covering most of the compositional and chronological spectrum of the granitoids, place important constraints on the sources and processes that were operative in their history.

I. The granitoids of the CBP belong to at least five distinct suites: Sázava (gabbro, quartz diorite, tonalite, trondhjemite and granodiorite) Blatná (quartz monzonite, granodiorite, granite), Čertovo břemeno (melasyenite and melagranite), Říčany (granite), and an extra group of S-type anatectic granitoids that was not subject of the present study. They differ from each other in respect of their petrography [Chapter II.], mineral chemistry [Chapter III.2.], major and trace element whole-rock geochemistry [Chapters IV.1., IV.2.] as well as Sr-Nd isotopic signatures [Chapter V.2.]. These differences point to range of sources and processes involved in their genesis [Chapters V.3.2., V.4.].

II. The individual intrusions differ in the nature of their enclaves, implying differences in their emplacement and crystallization history. The Sázava intrusion contains abundant mafic microgranular enclaves (MME), no surmicaceous enclaves and virtually no metasedimentary xenoliths [Chapter II.1.], and therefore the metasedimentary input had to be of limited importance. This could, however, have been significant at the margins of the Požáry intrusion [Chapter II.2.]. The abundance of MME, the field relations in the Teletín quarry, and the microtextural evidence, particularly the presence of mantled plagioclases, discontinuous zoning in the amphiboles and acicular apatite in both the Teletín quartz diorite and the MME [Chapter II.1.], point to contemporaneous basic magmatic activity and the interaction between basic and acid magmas.

III. The Blatná suite, especially the Kozárovce and Červená granodiorites, also contains abundant MME, along with surmicaceous enclaves and metasedimentary xenoliths [Chapters II.3., II.4.]. The presence of both surmicaceous enclaves and locally very abundant metasedimentary xenoliths (e.g. Solopysky in the Kozárovce and Hudčice in the Blatná intrusions) implies a considerable metasedimentary input, at least near to the Metamorphic Islet Zone and Moldanubian Unit. There is evidence of contemporaneity between the Kozárovce granodiorite and shoshonitic magma represented by monzonitic rocks and lamprophyres, the most important being net-veining of the Kozárovce quartz monzonite, the presence of syn-plutonic lamprophyre dykes and disequilibrium textures in both quartz monzonite and host granodiorite, including mantled plagioclases, quenched textures, resorbed biotite flakes enclosed by amphibole crystals and amphibole-biotite pseudomorphs retaining relic pyroxene cores [Chapter II.3.].

IV. The Sedlčany granite [Chapter II.5.] contains common metasedimentary xenoliths and both mafic microgranular and surmicaceous enclaves pointing to a mixed mantle-crustal parentage.

V. For the zoned Říčany mass, the importance of hybridization of the granitic magma with more basic ones is shown by the presence within the enclaves of K-feldspar phenocrysts, quartz xenocrysts (ocelli) and blade-shaped biotite, as well as rare antirapakivi textures and resorbed K-feldspar phenocrysts observed in the granite itself. Surmicaceous enclaves are abundant throughout, whereas metasedimentary xenoliths are common only near the margins of the intrusion.

VI. Relative age of intrusion, inferred from contact relationships, decreases in the succession Sázava - Marginal - Kozárovce, Blatná, Klatovy - Čertovo břemeno, Sedlčany, Říčany - Jevany intrusions. There is also evidence for the Sázava tonalite being older than both the Požáry trondhjemite and the Mrač granite [Chapter II.8.3.]. The majority of the CBP granitoids were probably emplaced at a narrow time interval around ~ 330 Ma and geological evidence excludes the occurrence of granitoid bodies younger than ~ 290 Ma [Chapters I, II; Appendix IX.]

VII. Late brittle deformation has affected all of the studied intrusions, with exception of the Říčany granite [Chapter II.]. In particular the Sázava intrusion has been affected in its eastern and western parts, whereas in the younger intrusions the deformation is usually confined to small domains and shear zones. Likewise, the degree of alteration is very variable, being the most severe in the western part of the Sázava intrusion and the Požáry intrusion.

VIII. In terms of the mineral chemistry, there is a striking difference between the Sázava and Blatná suites on the one hand and the Říčany and Čertovo břemeno suites on the other [Chapter III.2.]. The former contains hornblende and relatively Fe-rich biotite, whereas typical for the latter are actinolite and actinolitic hornblende (originating, the most likely, from a primary pyroxene in subsolidus conditions) and Mg-rich biotite. Based on the Al in hornblende geobarometer, the majority of the amphiboles studied (Sázava, Blatná, Kozárovce intrusions) crystallized at depths ca. 5 - 10 km. In contrast, the brown cores of the Teletín amphiboles may have originated at much greater depths, possibly as much as 30 km. The amphibole - plagioclase geothermometer yields temperature estimates of ~ 770 °C - 800 °C for the Sázava intrusion, and ~ 720 °C - 730 °C for both the Blatná and Kozárovce intrusions; these are compatible with the zircon saturation calculations [Chapter IV.2.2.].

IX. Each of the suites, and each of the individual intrusions alike, show a restricted range of the Sr-Nd isotopic ratios [Chapter V.2.1.]. The total observed range of $(^{87}\text{Sr}/^{86}\text{Sr})_{330} = 0.7051 - 0.7129$ and $\epsilon_{\text{Nd}}^{330} = +0.2 - -8.9$ is comparable with granitoids from other parts of the Hercynian belt, notably from the Moldanubian Pluton and the French Massif Central. The lack of positive ϵ_{Nd}^i values suggests very limited involvement of a depleted mantle component in the petrogenesis of the studied rocks. Moreover, there is a conspicuous trend towards isotopically more evolved compositions with time (in the succession Sázava, Blatná, Říčany and Čertovo břemeno suites) that is interpreted as being due to enrichment of the mantle by an incompatible element enriched and, or high $^{87}\text{Sr}/^{86}\text{Sr}$ component, possibly associated with an earlier (late Proterozoic ?) subduction environment [Chapters IV.4., V.4.].

X. There are several maxima of two-stage $T_{\text{DM}}^{\text{Nd}}$ model ages: ~ 1.05 Ga for the Sázava suite, ~ 1.45 Ga for the Blatná suite and 1.65 Ga for both Říčany and Čertovo břemeno suites. The data falling into range 1.25 - 1.65 Ga represent typical 'Hercynian' values, and are likely to point to a mixed source (Archaean and Late Proterozoic components) rather than a major crust-formation event [Chapter V.3.1.]. The lower $T_{\text{DM}}^{\text{Nd}}$ of the Sázava intrusion is similar to that of the quartz diorites from Limousin in the French Massif Central.

XI. The low-K calc-alkaline Sázava suite may have originated by re-melting of metabasites of the adjacent Jílové Zone or the Metamorphic Islet Zone, by partial melting of a mantle source with an isotopic composition similar to Bulk Earth, or by mixing of magmas derived by both processes. Abundant basic rocks, associated with the Sázava suite, have probably acted as heat sources as well as

one of the major components in the generation of the Sázava intrusion. The major and trace-element plots [Chapters IV.1.-IV.2.] and subsequent modelling [Chapter IV.3.1.] are compatible with extensive fractional crystallization of a mainly amphibole - plagioclase assemblage, with a minor contribution from biotite and orthite. The Požáry intrusion, being peraluminous and showing low ΣREE and high positive Eu anomalies, may have been derived from the Sázava parent largely by fractional crystallization (with some crystal accumulation) or, alternatively, by small-scale melting of a metabasic parent. The mixing tests performed on the Teletín quartz diorite are compatible with its genesis by hybridization of about 80 % of the Sázava tonalite with 20 % of a gabbroic melt.

XII. The variation within the high-K calc-alkaline Blatná suite can be modelled by mixing between moderately enriched ($(^{87}\text{Sr}/^{86}\text{Sr})_{330} \sim 0.708$, $\epsilon_{\text{Nd}}^{330} \sim -3$) mantle component, close in composition to monzonitic rocks of the suite (Lučkovice monzonite), with either an isotopically evolved metasedimentary component (most likely of Moldanubian provenance) or with the most acidic magma of the Blatná intrusion. This is also supported by modelling based on the whole-rock (major, trace and isotopic) geochemistry [Chapters IV.3.2., V.3.2.]. If the most evolved compositions within the Blatná intrusion are chosen as an acidic end-member, about 60 - 70 % and 70 - 80 % of it is needed to produce the least evolved members of the Kozárovec and Blatná suites, respectively. As shown by the major and trace-element data [Chapter IV.3.2.], these parental magmas have possibly evolved by fractional crystallization (or rather AFC) of amphibole > plagioclase + K-feldspar >> biotite (Kozárovec) or plagioclase > biotite > amphibole > orthite (Blatná) assemblages.

XIII. The Čertovo břemeno suite, including the minettes, originated from strongly enriched ($(^{87}\text{Sr}/^{86}\text{Sr})_{330} \sim 0.7128$, $\epsilon_{\text{Nd}}^{330} \sim -7$) mantle-derived magmas [Chapter IV.3.3.]. These may have evolved through closed-system fractionation, or have interacted with S-type leucogranitic magmas of similar isotopic composition and that may have been derived from the Moldanubian Unit. If the latter is the case, for the Sedlčany intrusion, the proportion of the basic end-member could have been close to 40 % [Chapter IV.3.3.]. Subsequently, the Sedlčany magma probably evolved by limited degrees of fractional crystallization (< 15 %) or AFC of plagioclase - K-feldspar > biotite - amphibole assemblage.

XIV. Overall, the processes which produced the most mafic members of the Blatná and Čertovo břemeno suites appear to have been similar [Chapter V.4.]. These shoshonitic basic rocks, generated from an isotopically heterogeneous source, acted as parents, undergoing contamination by the crustal material, as well as a heat source facilitating its melting.

XV. The parental magmas of the Říčany suite are most likely to have been produced by partial melting of peraluminous lithologies within the Moldanubian Unit leaving garnet in residuum [Chapter V.3.2.], although an origin by mixing between magmas resembling the Čertovo břemeno suite and metasediments of the Teplá-Barrandian Unit cannot be ruled out. Whole-rock compositional data [Chapter IV.3.4.] show that it is a reversely-zoned body, and imply K-feldspar-dominated fractionation in a deep magma-chamber prior to high-level intrusion. The reverse zoning could have been achieved either by emplacement of the magma in a single batch from a stratified magma chamber, or in several batches following cauldron subsidence or stopping. The Jevany leucogranite does not appear to have evolved by fractionation of the Říčany magma [Chapter IV.3.4.].

XVI. In summary, the main genetic processes responsible for the variation within the studied granitoids seem to be magma-mixing and fractional crystallization, the latter, to some extent, also accompanied by wall-rock assimilation (AFC) [Chapter V.4.]. There is firm petrological [Chapter II.] and geochemical [Chapter IV.3.] evidence for operation of hybridization processes, most importantly in the Sázava (Teletín) and Kozárovec intrusions.

XVII. The age and geochemical constraints are compatible with a progression with time from calc-alkaline magmas (Sázava suite) towards K-rich calc-alkaline (Blatná suite) and shoshonitic compositions (Čertovo břemeno and Říčany suites), that is interpreted as a transition from a magmatic arc to a post-collision uplift setting. Alternatively, the volcanic-arc-like signature of the Sázava and also the Blatná suites may have been inherited from the source region [Chapters IV.4., V.4.] .

XVIII. The presented dataset points to a widespread role for the enriched mantle component in the genesis of granitoids in this part of the Hercynian belt. It shows that caution should be exercised in making implicit presumption that the negative correlation in the $(^{87}\text{Sr}/^{86}\text{Sr})_i$ versus ϵ_{Nd}^i diagram is caused by crustal contamination.

This thesis represents, in many respects, a pilot study and clearly much more work needs to be undertaken to elucidate the petrogenesis of the CBP. Most importantly, accurate geochronological information is needed. The whole-rock Rb-Sr method does not seem to be suitable for this purpose due to the frequently-encountered limited spread in the $^{87}\text{Rb}/^{86}\text{Sr}$ ratios, and, or evidence of open-system behaviour (hydrothermal alteration, magma mixing, AFC) [Chapters II., IV.3., V.3.2.]. Potentially U-Pb and Ar-Ar isotopic systems may provide vital constraints on the crystallization ages and cooling history of the individual intrusions. Also more detailed information on mineral chemistry is needed, particularly concerning spatial variations within each intrusion, together with more whole-rock geochemical analyses for both the granitoids and their country rocks. Sets of integrated data, analogous to that presented here, need to be obtained for other intrusions of the studied suites as well as for the whole group of anatectic, S-type leucogranitoids. There is also gap in Sr-Nd isotopic information on the Čertovo břemeno intrusion and associated leucogranites that so far inhibits formulation of an accurate petrogenetic model for this intrusion. The data and ideas presented in thesis represent a basis for these additional studies.

Appendix I. List of samples

In Appendix I. is given list of the analysed samples, containing the sample number, rock type and locality. Sample numbers used are presented along with the original ones (field numbers or as assigned by others): J-1 to 35 are from *Bouška et. al. (1984)* and were made available by Dr. E. Jelínek, Charles University, Prague; JT-21, JT-27 and JT-28 were donated by Dr. M. Klečka from the Geological Institute, Czech Academy of Science and R-1 to R-16 by Dr. V. Vaňková, Geophysical Institute, Czech Academy of Science; Z-1 to Z-7, S-1 and V-1 are from the MSc. thesis of *Janoušek (1991)*. Location of the sampled outcrops is shown on **Figure VII.1**.

Appendix I: List of samples, Central Bohemian Pluton (cont.)

Blatná suite

Sample	Orig ID	Petrography	Locality
Mrač intrusion			
Mrc-1		biotite granite	Mrač
Mrc-2	J-29	biotite granite	Mrač
Kozárovce intrusion			
Koz-1		bi-amph granodiorite	Solopysky, 2.5 km WSW of Sedláčany
Koz-2		bi-amph granodiorite	Kozárovce, 10 km E of Břežnice
Koz-4		amph-bi granodiorite	Kozárovce
Koz-5		amph-bi granodiorite	Kozárovce
Koz-6		porph amph-bi granodiorite	Kozárovce
Koz-8		amph-bi granodiorite	Kamýk n/V.
Koz-9		bi-amph granodiorite	Hřimědice, 5 km NNE of Kamýk
Koz-10	J-15	bi-amph granodiorite	Kozárovce
Koz-11	J-16	bi-amph granodiorite	Solopysky
Koz-12	Te-1	porph amph-bi granodiorite	Kamýk n/V.
Koz-13	J-17	porph amph-bi granodiorite	Těchovice
Monzonitic rocks associated with the Kozárovce intrusion			
KozD-1	Koz-3	bi-amph quartz monzonite	Kozárovce
Zal-1	Koz-7	px - bi-amph quartz monzonite	Zalužany, 8.5 km ESE of Břežnice
Gbl-1		px-bi-amph monzonite	Lučkovice, 9 km E of Blatná
Gbl-2		(px)-bi-amph monzonite	Lučkovice
Blatná intrusion			
Bl-1		(amph)-bi granodiorite	Řečice, 2 km NW of Blatná
Bl-2		(amph)-bi granodiorite	Tužice, 13 km WNW of Horažďovice
Bl-3		amph-bi granodiorite	Velenov, 12 km NW of Horažďovice
Bl-4		bi granodiorite	Pařitky, 2.5 km NE of Blatná
Bl-5		(porph) amph-bi granodiorite	Vahlovice, 5 km NE of Blatná
Bl-6	J-13	(amph)-bi granodiorite	Řečice
Bl-7		bi granodiorite	Defurovy Lázně, 15 km SW of Blatná
Bl-8		amph-bi granodiorite	Hudčice, 3 km SW of Břežnice
BlD-1	Bl-9	amph-bi diorite	Hudčice
Cv-1		amph-bi granodiorite	Vičkovice, 18 km W of Horažďovice
Cv-2	J-3	amph-bi granodiorite	Malé Nepodřice, 4 km W of Písek
Cv-3	J-4	amph-bi granodiorite	Horažďovice
CvE-1	Cv-2	bi - amph MME	Vičkovice

Appendix I: List of samples, Central Bohemian Pluton (cont.)

Blatná suite (cont.)

Sample	Orig ID	Petrography	Locality
Marginal type intrusion			
Mg-1	J-21	porph amph-bi granite	Raděnice, 7 km SE of Příbram
Mg-2	J-22	porph amph-bi granite	Nepomuk, 22 km NW of Blatná
Klatovský intrusion			
Kl-1	J-20	porph amph-bi granodiorite (amph)-bi granodiorite	Klatovy, NE suburb of the city
Kl-2	J-20		Klatovy Disused quarry, E suburb of the city ('Pražské předm.'). 500 m SW elevation of 446 m see Kl-1

Čertovo břemeno suite

Sample	Orig ID	Petrography	Locality
Sedláčany intrusion			
Se-1		(amph-) bi granite	Vrchotovy Janovice, 6 km NW of Vočice
Se-3		amph-bi granite	Vápenice, 4.5 km S of Sedláčany
Se-4		amph-bi granite	Vápenice
Se-5		amph-bi granite	Vápenice
Se-6		amph-bi granite	Vápenice
Se-7		amph-bi granite	Vápenice
Se-8		amph-bi granite	Vrchotovy Janovice
Se-9		(amph-) bi granite	Vrchotovy Janovice
Se-10		biotite granite	Kosova Hora, 3.5 km ESE of Sedláčany
Se-11		biotite granite	Kosova Hora
Se-12		biotite granite	Kosova Hora
Se-13		amph-bi granite	Bořená Hora
Se-15	J-18	amph-bi granite	Vrchotovy Janovice
Se-16	J-19	bi oolite granite	Kosova Hora
Se-1	Se-2	amph-bi MME	Bořená Hora, 4 km NNE of Sedláčany
Čertovo břemeno intrusion			
Cb-1		porph amph-bi melagranite	Zvíkovské Podhradí, 12 km N of Písek
Cb-2		porph amph-bi qtz syenite	Vepice, 8 km NW of Milevsko
Cb-3		porph bi-amph syenite	Chyšky, 9 km NE of Milevsko
Cb-4	J-1	porph amph-bi qtz syenite	Petrovice, 11 km WNW of Milevsko
Cb-5	J-2	porph amph-bi melagranite	Vočice Quarry, 2 km WSW of the centre of the town, at railway station

Appendix I: List of samples, Central Bohemian Pluton (cont.)

Čertovo břemeno suite (cont.)

Sample	Orig ID	Petrography	Locality	Tábor intrusion
Ta-1		px-bi quartz syenite	Klokoty, W suburb of Tábor	Disused quarry, 100 m S of Klokoty monastery, in the Vltava river valley
Ta-2		px-bi quartz syenite	Dražičky, 5 km WSW of Tábor	Quarry, 700 m E of chapel in Dražičky, 1200 m NW of chapel in Slapy
Ta-3	J-5	px-bi quartz monzonite	Klokoty	Disused quarry, see Ta-1
Minettes				
Mi-1	Bl-10	minette	Kožlí, 11.5 km SE of Blatná	Quarry, 200 m NE of chapel, SW slopes of the Ostrý hill
Mi-2	Koz-10	minette	Zalužany	Disused quarry called 'V selci', 1 km NE of church in Zalužany

Říčany suite

Sample	Orig ID	Petrography	Locality	Říčany intrusion
Ri-1		porph (mu)-bi granite	Žernovka, 8 km ENE of Říčany	Quarry, 1 km NW of bus stop, forest 'Horka'
Ri-2	Z-1	porph (mu)-bi granite	Žernovka	Quarry, see Ri-1
Ri-3	Z-2	porph (mu)-bi granite	Žernovka	Quarry, see Ri-1
Ri-4	Z-4†	porph (mu)-bi granite	Žernovka	Quarry, see Ri-1
Ri-5	Z-5†	porph (mu)-bi granite	Žernovka	Quarry, see Ri-1
Ri-6	Z-7†	porph (mu)-bi granite	Žernovka	Quarry, see Ri-1
Ri-7	J-25	porph (mu)-bi granite	Žernovka	Quarry, see Ri-1
Ri-8	R-7	porph (mu)-bi granite	Žernovka	Quarry, see Ri-1
Ri-9	R-8	porph (mu)-bi granite	Žernovka	Quarry, see Ri-1
Ri-10	S-1	porph (mu)-bi granite	Žernovka	Quarry, see Ri-1
Ri-11	R-12	porph (mu)-bi granite	Srbín, 6 km ESE of Říčany	Disused quarry, 400 m SSW of bus stop; flooded quarry at Srbín-Svojetice road
Ri-12	R-13	porph (mu)-bi granite	Srbín	Disused quarry, see Ri-10
Ri-13	R-3	porph (mu)-bi granite	Srbín	Disused quarry, see Ri-10
Ri-14	R-4	porph (mu)-bi granite	Babice, 4 km NE of Říčany	Disused quarry, 600 m SE of the bus stop Babice
Ri-15	R-14	porph (mu)-bi granite	Babice	Disused quarry, see Ri-13
Ri-16	R-16	porph (mu)-bi granite	Kozojedy, 3 km W of Kostelec n/C. L.	
Ri-17	R-15	porph (mu)-bi granite	Doubravčice, 6 km NW of Kostelec n/C. L.	
Ri-18	R-5	porph (mu)-bi granite	Doubravčice	see Ri-16
Ri-19	R-6	porph (mu)-bi granite	Škvorec, 7 km NE of Říčany	Disused quarry
Ri-20	J-26	porph (mu)-bi granite	Škvorec	Disused quarry, see Ri-18
Ri-21	R-1	porph (mu)-bi granite	Březi, 3 km NE of Říčany	Disused quarry
			Březi	Disused quarry

Appendix I: List of samples, Central Bohemian Pluton (cont.)

Říčany suite (cont.)

Sample	Orig ID	Petrography	Locality	Říčany intrusion (cont.)
Ri-22	R-2	porph (mu)-bi granite	Březi	Disused quarry
RIE-1	Z-3	bi MME	Žernovka	Quarry, <i>see Ri-1</i>
RIE-2	Z-6	bi MME	Žernovka	Quarry, <i>see Ri-1</i>
RIE-3	R-9	bi MME	Žernovka	Quarry, <i>see Ri-1</i>
Jevany intrusion				
Je-1	V-1	mu-bi leucogranite	Vyžlovka, 9 km E of Říčany	Disused quarry, 400 m SW of the restaurant in Vyžlovka
Je-2	Ri-2	mu-bi leucogranite	Vyžlovka	Disused quarry, <i>see Je-1</i>
Je-3	J-27	mu-bi leucogranite	Vyžlovka	Disused quarry, <i>see Je-1</i>
Je-4	R-10	mu-bi leucogranite	Vyžlovka	Disused quarry, <i>see Je-1</i>
Je-5	R-11	mu-bi leucogranite	Vyžlovka	Disused quarry, <i>see Je-1</i>

† These samples contain a great deal of K-feldspar phenocrysts from accumulations around the MME [cf. Chapter II.]

Country rocks of the CBP

Sample	Orig ID	Petrography	Locality	Teplá-Barrandian Unit
CR-1		Proterozoic shale	Dobříš	Disused quarry, called 'Jezírka', 1750 m SW of chateau in Dobříš
CR-9		Proterozoic shale	Vrané n/V., 9 km NW of Jilové	Rock outcrop, 600 m NE of railway station, left bank of the Vltava river
CR-10		Proterozoic acidic tuff	Davle, 7 km W of Jilové	Disused quarry, 50 m SW of church in Davle, at the new road bridge
Moldanubian Unit				
CR-2		garnet-biotite kinzigite	Kuš, 17 km NW of Český Krumlov	Disused excavation site at elevation 768 m, 900 m NE of chapel
CR-3		mu-bi (ortho?) gneiss	Zátoň, 9 km SSE of Český Krumlov	Road cut, 1500 m NW of chapel in Zátoň, NE of the private bridge over Vltava river
CR-4		bi-amph orthogneiss	Rájov, 5 km NE of Český Krumlov	Rock outcrop, 1300 m SW of Zlatá Koruna monastery, SW of road bridge
CR-5		grnt bi-mu micascist	Chýnov, 10 km E of Tábor	Quarry 'Pod Pacovou horou', 3200 m NE of chapel in Chýnov
CR-7		biotite paragneiss	Miličín, 7 km SSE of Votice	Quarry, 300 m S of the top of Kalvárie hill
CR-8		bi oolite orthogneiss	Postupice, 9 km NW of Vlašim	Quarry, 1800 m NW of chapel in Postupice
CR-11	JT-21	paragneiss	Hněvkovice, 3 km SSE of Týn n/V.	Dam building site
CR-12	JT-27	paragneiss	Hněvkovice	<i>see CR-11</i>
CR-13	JT-28	paragneiss	Hněvkovice	<i>see CR-11</i>

For the trace elements, pressed pellets containing 6 g of the rock powder and 1 g of RO 214/1 (fenol formaldehyde) resin were prepared (*Leake et al., 1969*). All the trace elements were analysed using a Mo tube, except Nb, which was analysed with a Cr tube. Correction for absorption utilising the incoherently scattered Compton peak (*Harvey and Atkin, 1982*) has been applied. The detection limits for the XRF are summarised in the following table:

	detection limit (ppm)		detection limit (ppm)		detection limit (%)
Ba	12.3	Th	11.5	SiO ₂	0.086
Rb	1.7	Ni	4.8	TiO ₂	0.018
Sr	1.5	Co	3.2	Al ₂ O ₃	0.087
Zr	2.7	Pb	11.6	Fe ₂ O ₃	0.045
Nb	7.3	Zn	1.8	MnO	0.012
Ga	2.4	Cu	4.4	MgO	0.165
La	3.9	Cr	1.9	CaO	0.006
Ce	3.2			Na ₂ O	0.155
Y	1.4	S	7.1	K ₂ O	0.002
U	9.4			P ₂ O ₅	0.008

The performance of the Glasgow XRF instrument is frequently checked using standards, including international ones:

7500	G-GR	granite	Glasgow	7560	G-MA	marble	Glasgow	8550	SGR-1	shale	USGS
7510	G-GN	gneiss	Glasgow	7570	G-SL	slate	Glasgow	8560	STM-1	neph syenite	USGS
7520	G-TR	trachyte	Glasgow	7580	G-SS	staurolite	Glasgow	8800	T-1	tonalite	USGS
7530	G-TH	tholeiite	Glasgow			schist		9210	GR	granite	CRPG
7540	G-DO	dolerite	Glasgow					9220	GH	granite	CRPG

Below are given their recommended values together with average (\bar{x}) and standard deviation (σ) obtained in course of this project ('<' means below detection limit, '-' not determined, or not applicable):

	7500 n=4			7510 n=4			7530 n=2			7540 n=3			7560 n=2		
	\bar{x}	σ		\bar{x}	σ		\bar{x}	σ		\bar{x}	σ		\bar{x}	σ	
Zr	125	100	23	110	108	6	264	250	6	145	165	56	14	36	8
Y	8	9	0	7	8	2	45	44	1	30	31	1	4	6	1
Sr	860	870	17	305	308	6	540	527	6	610	595	14	50	46	1
Rb	80	80	6	28	28	5	25	24	2	37	36	4	6	6	4
Pb	25	30	7	5	<12	-	7	<12	-	3	<12	-	1	<12	-
Ga	18	21	4	16	16	1	23	24	1	21	23	1	1	<2	-
Zn	36	36	6	33	35	2	144	144	2	98	93	1	5	-	-
Cu	5	26	27	10	16	7	20	28	3	107	121	3	-	<4	-
Ni	6	10	4	48	49	5	24	21	4	53	50	4	0	-	-

	7500 n=5			7510 n=5			7530 n=1			7540 n=1			7560 n=2		
	\bar{x}	σ		\bar{x}	σ		\bar{x}	σ		\bar{x}	σ		\bar{x}	σ	
Co	3	5	2	5	6	1	44	40	-	40	44	-	0	<3	-
Cr	16	12	3	133	129	4	20	31	-	28	40	-	0	<2	-
Ce	30	31	4	22	13	6	110	101	-	48	49	-	4	<3	-
Ba	1245	1241	68	580	569	32	760	776	-	660	667	-	40	60	-
La	18	21	2	12	11	2	50	45	-	27	28	-	1	5	-

	8550 n=3			8560 n=3			9210 n=2			9220 n=2			8800 n=1		
	\bar{x}	σ		\bar{x}	σ		\bar{x}	σ		\bar{x}	σ		\bar{x}	σ	
Nb	5	9	2	270	202	3	22	16	4	85	59	47	12	12	-

	Plasma Quad PQ1	Plasma Quad PQ2
	<i>Sample introduction</i>	
Method	Liquid nebulisation	Liquid nebulisation
Uptake rate	1.0 ml min ⁻¹	0.8 ml min ⁻¹
	<i>Plasma</i>	
RF power	Forward 1300 W Reflected < 5 W	Forward 1350 W Reflected < 5 W
Gas controls: Auxiliary	0.55 l min ⁻¹	0.75 l min ⁻¹
Coolant	14.0 l min ⁻¹	14.0 l min ⁻¹
Nebuliser	0.73 l min ⁻¹	0.90 l min ⁻¹
Nebuliser	Meinhart: concentric type	De Galan V-groove
Spray chamber	Scott type double bypass, water cooled	Scott type double bypass, water cooled
	<i>Ion sampling</i>	
Sampling cone	Nickel, 1.0 mm orifice	Nickel, 1.0 mm orifice
Skimmer cone	Nickel, 0.75 mm orifice	Nickel, 0.75 mm orifice
Sampling distance	10 mm from load coil	10 mm from load coil
	<i>Vacuum</i>	
Expansion stage	2.4 mbar	2.5 mbar
Intermediate stage	< 1 x 10 ⁻⁴ mbar	2 x 10 ⁻⁴ mbar
Analyser stage	4.6 x 10 ⁻⁶ mbar	2 x 10 ⁻⁶ mbar
	<i>Data acquisition</i>	
Acquisition time	60 s	30 s
Acquires per sample	3	3

Ru, Re and In were used as internal standards. Measured masses were: ¹³⁹La, ¹⁴⁰Ce, ¹⁴¹Pr, ¹⁵²Sm, ¹⁵³Eu, ¹⁵⁷Gd, ¹⁵⁸Gd, ¹⁵⁹Tb, ¹⁵²Dy, ¹⁶⁵Ho, ¹⁶⁶Er, ¹⁶⁹Tm, ¹⁷⁴Yb, ¹⁷⁵Lu, ⁷¹Ga, ⁸⁹Y, ⁹⁰Zr, ⁹¹Zr, ¹⁷⁷Hf, ¹⁷⁸Hf, ¹⁸¹Ta.

The accuracy of the method has been checked against two international granitoid standards, GPS-1 and G-2, that were processed like any other samples. The recommended values (Govindaraju, 1989), together with obtained concentrations are presented in the table. The accuracy was satisfactory for majority of the elements, but Zr and Hf show concentrations several times lower than the recommended value, pointing to problems with zircon dissolution. This is rather surprising in view of the reasonable correlation between the Zr data obtained from the same samples from the XRF and ICP-MS, showing that the microwave dissolution is generally capable of dissolving (or equilibrating) zircons. The content of Hf, of which zircon is the main host, should therefore be viewed with some caution, although they may be reasonable considering Figure VII.2. The serious discrepancy in determination of Zr and Hf in the standard powders is enigmatic, and may point to a human error.

	GSP-1	n=1	G-2	n=1
La	184	150.9	89	60.2
Ce	399	374.1	160	194.0
Pr	52	49.9	18	13.3
Nd	196	173.6	55	39.8
Sm	26.3	23.8	7.2	6.1
Eu	2.33	2.7	1.4	1.6
Gd	12.1	18.7	4.3	6.1
Tb	1.34	1.6	0.48	0.4
Dy	5.5	7.1	2.4	2.0
Ho	1.01	0.8	0.4	0.2
Er	2.7	2.4	0.92	0.7
Tm	0.38	0.2	0.18	0.1
Yb	1.7	1.2	0.8	0.4
Lu	0.214	0.1	0.11	0.1
	GSP-1	n=3	G-2	n=2
Ga	23	23.8	23	23.6
Y	26	28.5	11	10.8
Nb	27.9	29.1	12	13.2
Cs	1.02	1.2	1.34	1.7
Ta	0.97	0.9	0.88	0.8
Zr	530	49.8	309	71.0
Hf	15.5	1.2	7.9	1.7

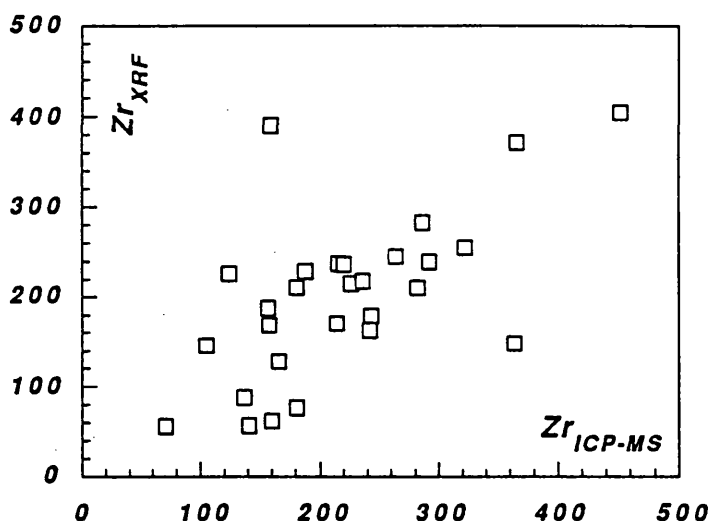


Figure VII.2. Comparison between Zr concentrations determined using the XRF and ICP-MS techniques

2.8. Sr and Nd isotopes

2.8.1 Chemistry

I. Sample Dissolution

Samples were dissolved in PFA teflon screw-top beakers (Saville) using 10mls 40% HF and 1ml 14M HNO₃ on a hotplate overnight. The beakers were removed, cooled, and then the solution was dried down under lamps. The residue was then dissolved in 3 mls 14M HNO₃ overnight on a hotplate, and dried down as before. The residue was now dissolved in 8 mls 6M HCl overnight on a hotplate. After cooling, a weighed aliquot of about 1/3 the volume of the solution was taken, to which was added weighed quantities of ¹⁴⁵Nd and ¹⁴⁹Sm spikes for isotope dilution determination of Sm and Nd concentrations. The remaining 2/3 aliquot was used for the determination of the isotopic composition of both Sr and Nd. ⁸⁷Rb and ⁸⁴Sr spikes were also added to this solution for the determination of Rb and Sr concentrations by isotope dilution analysis. Both solutions were dried down and the final residues each taken up in 2 mls 2.5M HCl.

II. Column chemistry

Sr and the REE were separated using standard cation exchange chromatography techniques. The sample was transferred to a centrifuge tube and any residue was centrifuged off. The solution was then loaded onto a preconditioned cation exchange column containing 10 mls Bio-Rad AG50W x 8, 200-400 mesh resin. The sample was washed in with 2 * 1 ml 2.5M HCl. For samples where Rb and Sr were to be collected 29 mls 2.5M HCl were eluted, followed by collection of Rb in 7 mls 2.5M HCl; this was then evaporated to dryness. 10 mls 2.5M HCl was then eluted. The Sr fraction was collected with a further 10 mls 2.5M HCl, and evaporated to dryness. Sr blanks were less than 2 ng. For Sm and Nd spiked samples the Sr fraction did not need to be collected, and so 56 mls 2.5M HCl were eluted.

The REE were separated by further eluting 20 mls 2.5M HCl and 10 mls 3M HNO₃. The next 26 mls 3M HNO₃ were collected, and evaporated to dryness.

Sm and Nd were isolated from Ba and the other REE using 3 columns.

Column 1 (initial Ba clean-up):

The residue from the REE fraction from the Sr columns was dissolved in 1 ml of a solution of 75% CH₃COOH - 25% 5M HNO₃ (hereafter called 75/25). This was loaded onto a column containing 8ml of Bio-Rad AG1 x8, 200-400 mesh anion exchange resin which had been preconditioned with 5 mls of a solution of 90% CH₃COOH - 10% 5M HNO₃ (90/10). The sample was washed in with 2 * 1 ml 90/10 solution, and then eluted with 50 mls 90/10 solution. The REE's were collected with 15 mls 0.05M HNO₃, and evaporated to dryness.

Column 2 (Sm and Nd separation):

The residue from column 1 was dissolved in 1 ml of "orange cocktail". This cocktail consisted of 75% CH₃OH - 25% orange cocktail mix: the mix is made of 1336 mls H₂O - 406 mls CH₃COOH - 256 mls 5M HNO₃. The sample was loaded onto a column containing 8 ml of Bio-Rad AG1 x8, 200-400 mesh anion exchange resin which had been preconditioned with 5 mls "orange cocktail". This column was encased in a water jacket through which water kept at 25°C by a thermostatically-controlled water bath was circulated. The sample was washed in with 2 * 1 ml "orange cocktail", and eluted with 10 mls "orange cocktail". For spiked samples the next 17 mls "orange cocktail" were collected which contained the Sm fraction; this was evaporated to dryness. A further 12 mls "orange cocktail" were then eluted. For unspiked samples 29 mls "orange cocktail" were eluted. The next 29 mls "orange cocktail" containing the Nd fraction were then collected, and the solution evaporated to dryness.

Column 3 (final Ba clean-up):

The residue from the Nd fraction from column 2 (both spiked and unspiked) was dissolved in 1 ml 75/25 solution, and loaded onto a column containing 5 ml of Bio-Rad AG1 x8, 200-400 mesh anion exchange resin which had been preconditioned with 3 mls 90/10 solution. The sample was washed in with 2 * 1 ml of 90/10 solution and eluted with 15 mls 90/10 solution. The Nd was collected with 10 mls 0.05M HNO₃, and evaporated to dryness.

Sm and Nd blanks were less than 0.2 ng.

2.8.2. Mass Spectrometry***Rb***

Rb samples were run on single collector VG MM30 thermal ionisation mass spectrometer. Rb samples were dissolved in a few ml of RO H₂O in a glass spitzer, loaded onto a Ta side filament of an outgassed triple Ta filament assembly, and carefully dried down so as to avoid the sample bubbling up on the filament. Beams were managed to give a peak intensity of about 5 pA ⁸⁷Rb. Peak intensities were corrected for zero and dynamic memory.

Sr

Sr samples were run on a single collector VG 54E thermal ionisation mass spectrometer. Sr samples were dissolved in 1ml 1M H₃PO₄ and were loaded onto a single outgassed Ta filament. A small current is passed through the filament to dry the sample which is then increased slowly until the H₃PO₄ fumes off and the filament glows dull red. Sr beams were managed to give an intensity of 1.5 pA ⁸⁶Sr. Peak intensities were corrected for zero, dynamic memory and Rb interference (if necessary). The ⁸⁷Sr/⁸⁶Sr ratio was corrected for mass fractionation using ⁸⁶Sr/⁸⁸Sr = 0.1194. Repeat analysis of NBS 987 Sr standard gave ⁸⁷Sr/⁸⁶Sr = 0.71023 ± 4 (2s.d.).

Nd

Nd analyses were performed on a VG Sector 54-30 thermal ionisation mass spectrometer with 8 Faraday collectors. Nd samples were dissolved in water and loaded on the Ta side filaments of an outgassed triple filament assembly with a Re centre filament. The sample was dried very carefully at 0.5A. For Nd isotopic composition runs beams were managed to give a ^{144}Nd intensity of 10pA with a centre filament current of 4 A. Data were acquired in multi-dynamic mode (to avoid inter-collector gain calibration uncertainties) using a 5 collector peak jumping routine. The data were collected in 12 blocks of 10 collection routines/block, giving 120 ratios in total. Each collection routine comprised 4 cycles; after each cycle the magnet was switched to place a different isotope into any given collector. The integration time for each cycle within a collection routine was 5 seconds with a 2 second wait time between each cycle to allow the magnet to settle. $^{143}\text{Nd}/^{144}\text{Nd}$ ratios were corrected for mass fractionation using $^{146}\text{Nd}/^{144}\text{Nd} = 0.7219$. Peak intensities were corrected for background and the ^{144}Nd peak was corrected for Sm interference. During the course of this study the JM Nd standard gave $^{143}\text{Nd}/^{144}\text{Nd} = 0.511500 \pm 10$ (2s.d.).

For Nd isotope dilution runs the ^{143}Nd beam intensity was 0.5 pA. The analyses were performed in static mode, with 3 blocks of 10 cycles being collected. The integration time for each cycle was 5 seconds. Peak intensities are corrected for zero and Sm interference (where necessary).

Sm

Sm analyses were also performed on the Sector 54-30 instrument. Loading techniques were the same as those for Nd. Sm beams were managed to give a ^{149}Sm beam intensity of 0.5 pA. The analyses were performed in static mode, with 3 blocks of 10 cycles being collected. The integration time for each cycle was 5 seconds. Peak intensities are corrected for background. Measured Sm/Nd ratios are considered to be better than 0.15% (2 s.d.)

2.9. Software

For the purposes of handling the data gathered in the course of this project, two Microsoft QuickBasic programmes were developed: BTRAP for age and model calculations with the Rb-Sr isotope data and NORMAN for normative recalculations of the major element data. Both of them run on IBM PC compatible computers; BTRAP will run only on computers with EGA or VGA cards and needs 150 kB of file space, whereas NORMAN requires EGA, VGA or Hercules graphic cards and 250 kB. Both programmes are menu-driven and thus relatively easy to use. The software is available on request for the cost of the shipment and media but, as it is still under development, no documentation is available yet.

2.9.1. BTRAP

The main aim in this case was to implement the bootstrap algorithm (*Diaconis and Efron, 1983*) that can be used for the calculation of isochrons (*Kalsbeek and Hansen, 1989*) and for checking the homogeneity of Rb-Sr isotope data. This computer-intensive algorithm calculates repeatedly conventional isochrons (*York, 1966, 1967, 1969*) for combinations (with repetition) randomly chosen from the available data. There are

$$\frac{(n + n - 1)!}{n! (n - 1)!}$$

such non-identical combinations, giving, for instance, 1716 non-identical bootstrap samples for $n = 7$ (*Kalsbeek and Hansen, 1989*). After data acquisition, the frequency distribution curves are plotted. The

datasets correspond to isochrons should result in a Gaussian-like distribution curve of the calculated age, with the median corresponding to the time of closure of the Rb-Sr system. Poorly-defined isochrons, errorchrons and mixing lines produce different types of frequency curves, often bi- or polymodal.

BTRAP reads data from an ASCII file (compatible with the *.SR files used by ISOCHRON.EXE of *Provost, 1990*) [Fig. VII.3.]. Currently, the data can be also used to compute conventional isochrons (*York, 1969*) and the distribution-free alternative of *Vugrinovich (1981)*. Isochrons can be plotted, and model calculations (initial ratios, CHUR model ages, ϵ -values etc.) can be performed. The BOOTSTRAP data can be generated, the distribution curves viewed and the data saved into a raw ASCII data file that can be later re-processed for a neater output or further analysis by a statistical package.

Four simple Rb-Sr calculators are provided with input from the keyboard, which give initial ratios, CHUR model ages, ϵ -values, $^{87}\text{Rb}/^{86}\text{Sr}$ ratios (from Rb/Sr), and perform simple binary mixing calculations.

There is much to be improved in terms of the usability of this programme, most importantly the routines for printing the graphics, new isochron calculation schemes and statistical tools for the re-processing of the bootstrap spectra. The current version does not take into account the error-correlation between $^{87}\text{Rb}/^{86}\text{Sr}$ and $^{87}\text{Sr}/^{86}\text{Sr}$ ratios.

2.9.2. NORMAN

NORMAN performs basic normative calculations [Fig. VII.4.], including the Granite Mesonorm (*Mielke and Winkler, 1979*), Köhler-Raaz's values (*Köhler and Raaz, 1951*), CIPW norm (*Hutchison, 1974, 1975*), Niggli's Catanorm (*Hutchison, 1974*), and recalculation using the millications of French authors (*Debon and Le Fort, 1983, 1988; De la Roche et al., 1980*). Apart from these so-called standard functions [Fig. VII.5.], it is possible also to implement user-defined functions, in the form of formulae entered in an ASCII file [Fig. VII.6.]. Other user-defined as well as standard functions can be called from within the user-defined function using arithmetic operators and constants (like atomic weights), that are stored in a separate file.

The input for this programme is either from a file in the DBASE format (*.DBF), or from the keyboard. The results can be browsed, printed on any dot-matrix printer or saved in either DBASE or ASCII file (comma-, semicolon- and space-delimited) for further processing by spreadsheet or graphics packages.

The primary objective was to build a core module, handling the main input / output operations, leaving the user only to code the calculation algorithm itself. These algorithms are stored in small, stand-alone modules. Thus writing of these standard functions is straightforward, and can be done by anybody with limited knowledge of the QuickBasic language, whereas the user-defined functions do not require any knowledge of programming at all. The advantage of this approach should be that the calculation process is more transparent, and if needs be, the geochemist can easily tailor the algorithms used (the programme is not a 'black box' anymore). Additionally, this approach should also encourage others to produce additional modules.

The programme is to be further improved, especially by the implementation of new import formats (most importantly ASCII) and the speed of the interpretation of the user-defined functions. Moreover, no saving of changes made to the original data set is currently possible.

THE MAIN MENU:

1. Age and Model Calculations
2. Bootstrap- Data Collecting
3. Bootstrap- File Processing
4. Rb/Sr Calculator
5. Load Screen
6. Options Change
7. Help
8. Program Exit

Strontium data filename (*.sr) ?
pluton

1	1	9.059	.061	.7504	.0009
2	2	4.679	.041	.7288	.0019
3	3	1.567	.023	.7168	.0006
4	B4	3.828	.014	.7235	.001
5	5	2.894	.032	.7199	.0008
6	B7	10.41	.1	.7565	.001

Numbers of samples

1. Next CHUR Calculation
2. Print
3. Previous Menu

1 2
B7

1. Initial Ratios and ϵ Values
2. Age From Initial Ratio
3. CHUR Model Age

Model age for CHUR having ages

Sample ID

Presumed Initial Ratio?
0.710

Previous Menu

3816

1				
2				
3				
B4				
5				
B7				

Input file: blatna.sr

1. Print Screen
2. Zoom
3. Previous Menu

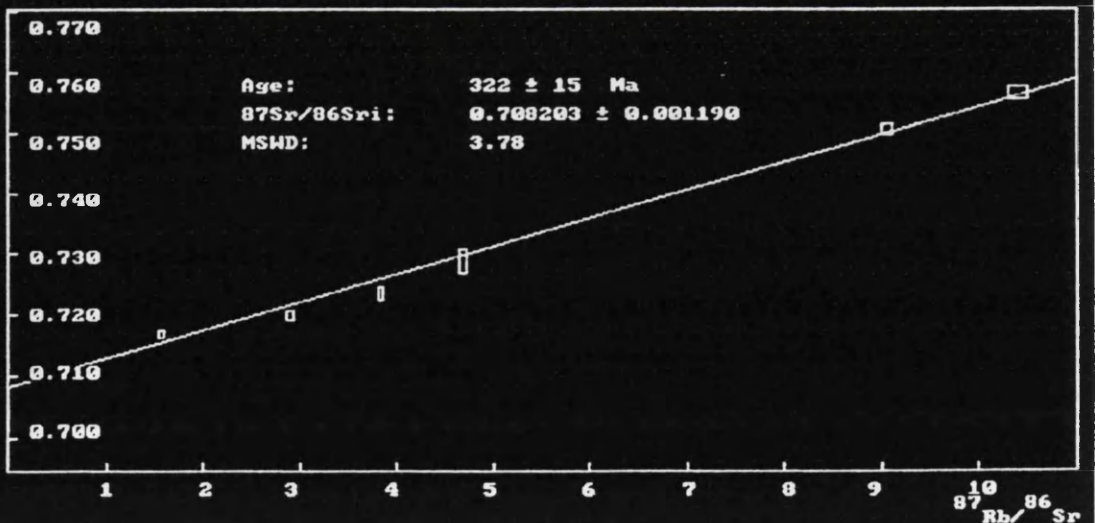


Figure VII.3: Typical session with the programme BTRAP: main menu, the model calculations and the isochron plot

The Main menu

- Load data: *.DBF
- Edit/Keyboard entry
- Calculations
- Show the results
- Print all the results
- Save the results
- Customize
- Exit to DOS

Calculations

- Granit.nezonorm
- Kohler-Raaz
- CIPW
- CIPW with Hb & Bi
- Niggli (Katanorm)
- De La Roche
- Debon-Le Fort
- Millications
- User defined
- Main menu

Muf Software (C) 1990-1993 presents

Norman: Petrochemical calculator

The file in usage:

c:\vojta\qb\norman\data\PLUTON.DBF

Q	146.000
P	-54.000
A	6.000
B	125.000
F	284.000
(Na+K)	170.000
K/(Na+K)	0.535
Mg/(Fe+Mg)	0.573
Q(quartz)	26.306
B(dark n.)	22.523
F(feldsp)	51.171

Sample: bl-5

Show the results

- Recall
- Delete
- Print
- Backward
- Forward
- Go to
- Main menu

Sample name: 7. of 112

bl-2_

	P	A	B	F
j-10	-153.000	-11.000	130.000	277.000
j-11	-145.000	-38.000	190.000	260.000
j-12	-170.000	6.000	142.000	201.000
po-2	-186.000	-48.000	116.000	313.000
sa-1	-155.000	-47.000	190.000	264.000
sa-2	-219.000		206.000	285.000
sa-4	-225.000		260.000	252.000
sa-7	-172.000		169.000	292.000
sa-6	-204.000		237.000	245.000
sa-9	-190.000		232.000	229.000
j-29	-32.000		91.000	282.000
sa-5	-40.000		84.000	296.000
j-18	5.000		126.000	272.000
j-19	-6.000	11.000	111.000	293.000
kh-1	-6.000	11.000	100.000	311.000
se-1	-22.000	-12.000	114.000	326.000
se-10	0	21.000	103.000	299.000
se-11	14.000	35.000	113.000	273.000
se-12	-15.000	14.000	101.000	325.000
se-13	-3.000	11.000	106.000	299.000

Esc...Menu

(Ctrl+) Arrows, PgUp, PgDn, Home, End

Samples 81 - 100

Figure VII.4: Example of a session with the programme NORMAN: main menu, and two output screens for the calculations after Debon and Le Fort (1989)

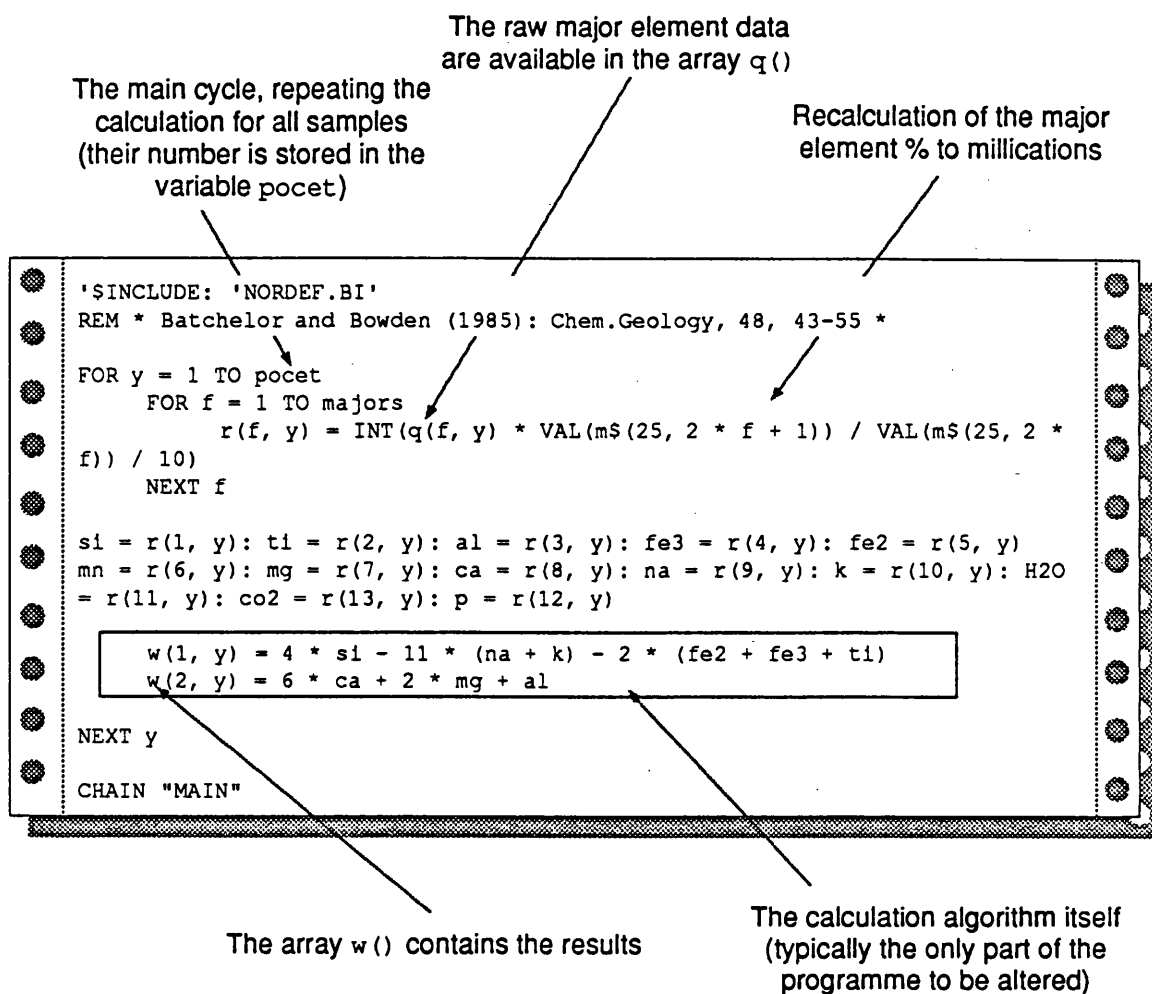


Figure VII.5: Listing of one of the standard functions of the programme NORMAN (LAROCH.EXE)

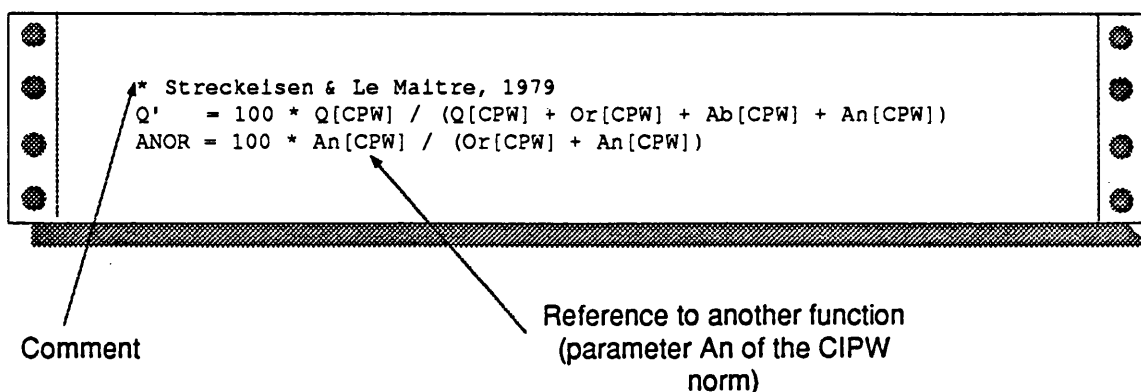


Figure VII.6: Example of an user-defined function of the programme NORMAN for calculating the Q' - ANOR parameters of Streckeisen and Le Maitre, 1979 (PKC.DEF)

<p>Appendices III.-V. Whole-rock geochemistry, the Central Bohemian Pluton</p>

Appendix III. Major elements

Appendix IV. Trace elements (XRF)

Appendix V. Trace elements (ICP-MS)

In Appendix III. are given major element data (in wt %) together with some normative values, whose meaning is explained on the next page. In Appendix IV. are summarised trace element concentrations determined by XRF (in ppm, b.d. = below detection limit). Appendix V. contains trace elements that were obtained using ICP-MS, i.e. mainly REE. Concentrations of Ga, Y and Nb are shown for comparison only, as XRF data, available for all the samples, were preferred. For REE, the index 'N' (like Nd_N) means chondrite normalised values (*Boynton, 1984*), whereas asteriks (*) denotes an extrapolated value (Eu*). See Appendix II. for details about analytical techniques.

Appendix III: Major element data and normative values

(XRF except for FeO and LOI)

Sample Locality	Ne-1 Nečín	Ne-2 Nečín
	Nečín	Nečín
SiO ₂	72.18	71.91
TiO ₂	0.19	0.20
Al ₂ O ₃	13.58	13.82
FeO	1.56	2.29
Fe ₂ O ₃	0.54	0.57
MnO	0.07	0.08
MgO	0.58	0.67
CaO	2.31	2.30
Na ₂ O	4.01	3.71
K ₂ O	2.32	2.32
P ₂ O ₅	0.06	0.05
S	b.d. [†]	-
LOI	0.76	0.53
Total	98.16	98.45
Q	195	203
P	-121	-112
A	6	20
B	45	59
F	315	293
(Na+K)	178	169
K/(Na+K)	0.28	0.29
Mg/(Fe+Mg)	0.33	0.30
quartz	35.14	36.58
dark m.	8.11	10.63
feldsp.	56.76	52.79
R ₁	2788	2856
R ₂	540	549
A	70.68	63.45
F	22.84	29.50
M	6.48	7.05
A	53.61	53.61
F	22.07	25.46
C	24.32	20.92
Q'	36.20	37.73
ANOR	44.67	44.70
FeO*	2.05	2.80
Fe/(Fe+Mg)	0.78	0.81
A/NK	1.49	1.60
A/CNK	1.02	1.08
A	88.35	85.11
F	9.08	12.02
M	2.57	2.87
A	80.13	77.47
F	10.57	13.55
C	9.30	8.98

Intrusion to which the sample belongs or petrography if not applicable

Major element data (%)
LOI: loss on ignition

Debon and La Fort (1988)
 $Q = Si/3 - (K + Na + 2/3 \cdot Ca)$
 $P = K - (Na + Ca)$
 $A = Al - (K + Na + 2 Ca)$
 $B = Fe^{2+} + Fe^{3+} + Mg + Ti$
 $F = 555 - (Q + B)$
quartz, dark m., feldsp. = Q, B, F recalculated to 100 % ($\Sigma = 100\%$) (millications)

De la Roche et al. (1980)
 $R_1 = 4 Si - 11 (Na+K) - 2 (Fe^{2+} + Fe^{3+} + Ti)$
 $R_2 = 6 Ca + 2 Mg + Al$ (millications)

$A = Na_2O + K_2O$ $F = FeO$
 $M = MgO$ (wt %; $\Sigma = 100\%$)

White (1990)
 $A = Al - Na - K$ $C = Ca - 3.3 P$
 $F = Mg + Fe^{2+}$ (millications)

Streckeisen and Le Maitre (1979)
 $Q' = 100 Q / (Q + Or + Ab + An)$
 $ANOR = 100 An / (Or + An)$ (CIPW)

Manlar and Piccoli (1989)
 $Fe/(Fe+Mg) = FeO^*/(FeO^* + MgO)$
 $A/NK = Al_2O_3 / (Na_2O + K_2O)$
 $A/CNK = Al_2O_3 / (CaO + Na_2O + K_2O)$
 $A = Al_2O_3 + Na_2O + K_2O$
 $F = FeO^*$
 $M = MgO$ ($\Sigma = 100\%$)
 $A = Al_2O_3 + Na_2O + K_2O$
 $F = FeO^* + MgO$
 $C = CaO$ ($\Sigma = 100\%$)
(all wt % except A/NK and A/CNK: molar %)

[†] b.d. below detection limit
- not determined
FeO* total Fe as FeO

Appendix III. Major element data and normative values

Sázava suite

Sample	Sa-1	Sa-2	Sa-4	Sa-7	Sa-10	Sa-11	Sa-12	Sa-13	SaD-1	SaD-2
Locality	Mrač	Mrač	Mrač	Teletín	Krhanice	Prosečnice	Mrač	Teletín	Teletín	Teletín
	Sázava	Sázava	Sázava	Sázava	Sázava	Sázava	Sázava	Sázava	diorite	diorite
SiO ₂	57.24	55.17	49.94	57.73	64.21	64.16	56.71	59.36	52.34	54.86
TiO ₂	0.59	0.71	0.75	0.95	0.42	0.48	0.61	0.62	1.27	0.97
Al ₂ O ₃	16.91	17.00	17.58	18.82	15.68	15.89	17.20	18.28	18.24	18.99
FeO	5.46	5.26	7.65	5.43	3.60	4.44	4.99	4.53	7.20	6.56
Fe ₂ O ₃	1.31	2.66	1.93	1.00	1.19	1.46	2.47	1.29	1.65	1.36
MnO	0.16	0.16	0.24	0.12	0.13	0.13	0.16	0.12	0.17	0.18
MgO	3.66	3.67	4.89	2.82	1.86	2.14	3.29	2.23	4.02	4.53
CaO	6.83	8.22	9.52	7.47	5.29	4.96	6.97	6.57	8.49	8.36
Na ₂ O	2.60	3.36	2.72	2.54	4.03	3.36	2.30	2.66	2.64	2.36
K ₂ O	2.41	1.70	1.54	1.67	1.81	1.79	2.48	1.54	1.49	1.66
P ₂ O ₅	0.16	0.17	0.18	0.37	0.12	0.10	0.17	0.22	0.27	0.20
S	0.02	0.02	0.05	0.06	0.02	0.01	0.02	0.08	0.01	0.03
LOI	0.70	0.55	0.67	0.76	0.65	0.63	0.63	-	0.66	-
Total	98.05	98.66	97.66	99.73	99.01	99.55	98.01	97.50	98.45	100.06
Q	101	64	43	115	126	151	105	132	73	94
P	-155	-219	-225	-180	-186	-158	-145	-170	-204	-190
A	-47	-105	-116	-14	-48	-10	-38	6	-61	-37
B	190	206	260	171	116	139	190	142	237	232
F	264	285	252	269	313	265	260	281	245	229
(Na+K)	135	144	121	117	168	146	127	119	117	111
K/(Na+K)	0.38	0.25	0.27	0.30	0.23	0.26	0.42	0.28	0.27	0.32
Mg/Fe+Mg	0.50	0.46	0.48	0.44	0.41	0.40	0.45	0.41	0.45	0.51
quartz	18.20	11.53	7.75	20.72	22.70	27.21	18.92	23.78	13.15	16.94
dark m.	34.23	37.12	46.85	30.81	20.90	25.05	34.23	25.59	42.70	41.80
feldsp.	47.57	51.35	45.41	48.47	56.40	47.75	46.85	50.63	44.14	41.26
R ₁	2138	1860	1737	2368	2286	2492	2174	2489	1938	2191
R ₂	1237	1391	1600	1305	963	945	1243	1170	1461	1490
A	32.73	30.88	22.98	31.51	47.21	39.48	31.28	34.65	24.53	24.61
F	43.37	46.71	50.64	47.38	37.76	44.11	47.19	46.95	51.59	47.65
M	23.91	22.40	26.38	21.11	15.04	16.41	21.53	18.40	23.88	27.73
A	40.84	38.11	36.32	48.24	42.55	45.12	43.68	51.02	41.12	42.86
F	34.64	33.13	36.88	27.89	29.45	31.37	31.35	25.16	34.12	33.44
C	24.52	28.76	26.80	23.88	28.00	23.51	24.97	23.82	24.76	23.71
Q'	14.37	9.00	0.00	17.34	22.88	25.77	16.43	22.55	6.84	9.71
ANOR	65.76	72.35	77.42	77.83	64.40	68.49	66.64	77.39	79.20	78.73
FeO*	6.64	7.65	9.39	6.33	4.67	5.75	7.21	5.69	8.68	7.78
Fe/Fe+Mg	0.64	0.68	0.66	0.69	0.72	0.73	0.69	0.72	0.68	0.63
A/NK	2.46	2.31	2.86	3.14	1.83	2.13	2.66	3.03	3.06	3.34
A/CNK	0.88	0.76	0.75	0.96	0.86	0.96	0.90	1.02	0.85	0.91
A	68.03	66.08	60.47	71.57	76.72	72.72	67.67	73.95	63.78	65.14
F	20.61	22.93	25.99	19.67	16.65	19.89	22.20	18.72	24.76	22.04
M	11.36	10.99	13.54	8.76	6.63	7.40	10.13	7.34	11.46	12.82
A	56.13	53.02	47.86	58.08	64.55	62.08	55.71	60.80	51.35	52.67
F	26.37	27.22	31.28	23.08	19.59	23.29	26.62	21.42	29.16	28.19
C	17.49	19.76	20.86	18.84	15.87	14.63	17.67	17.77	19.49	19.14

Appendix III. Major element data and normative values (cont.)

Sázava suite (cont.)

Sample	SaD-3	Gbs-1	Gbs-2	Gbs-3	Gbs-4	Gbs-5	Po-1	Po-2	Po-4	Po-5
Locality	Teletín	Pecorady	Vavřetice	Brtnice	Popovice	Krhanice	Krhanice	Proseč-nice	Proseč-nice	Proseč-nice
Intrusion	diorite	gabbro	gabbro-diorite	gabbro-diorite	gabbro	gabbro	Požáry	Požáry	Požáry	Požáry
SiO ₂	53.34	49.63	48.85	55.80	52.90	55.17	62.46	68.30	70.17	71.42
TiO ₂	0.96	0.76	0.36	0.80	0.43	0.98	0.28	0.28	0.28	0.30
Al ₂ O ₃	17.65	13.34	21.67	16.98	14.99	12.14	20.41	15.29	15.35	15.04
FeO	5.20	3.22	2.74	6.22	2.28	9.58	1.65	2.12	2.12	2.41
Fe ₂ O ₃	3.60	5.69	3.41	2.79	4.55	2.78	0.43	0.40	0.11	0.47
MnO	0.19	0.17	0.12	0.25	0.14	0.38	0.05	0.04	0.06	0.05
MgO	4.56	8.59	5.40	3.16	7.69	6.19	0.87	1.77	1.32	0.52
CaO	9.49	14.64	12.98	7.22	13.40	6.12	6.26	3.76	3.77	3.67
Na ₂ O	2.81	1.67	1.76	3.07	1.64	1.31	4.03	3.63	2.73	2.58
K ₂ O	1.24	1.07	0.83	1.45	0.64	2.60	1.92	1.95	1.82	1.79
P ₂ O ₅	0.13	0.10	0.02	0.20	0.03	0.28	0.07	0.07	0.07	0.07
S	0.01	0.03	0.06	0.02	0.05	-	0.18	0.00	0.00	0.01
LOI	0.80	0.92	1.32	0.86	0.85	-	0.65	0.50	0.62	0.49
Total	99.99	99.83	99.52	98.82	99.59	97.53	99.26	98.12	98.43	98.82
Q	66	24	42	94	67	136	101	176	218	232
P	-234	-292	-270	-197	-278	-96	-201	-143	-116	-110
A	-109	-337	-112	-55	-251	-77	5	8	40	44
B	242	339	220	210	285	334	54	83	68	57
F	247	192	293	251	203	85	400	296	269	266
(Na+K)	117	77	75	130	67	97	171	158	127	121
K/(Na+K)	0.22	0.30	0.24	0.24	0.21	0.57	0.24	0.26	0.31	0.31
Mg/(Fe+Mg)	0.49	0.65	0.62	0.39	0.68	0.48	0.44	0.56	0.52	0.25
quartz	11.89	4.32	7.57	16.94	12.07	24.50	18.20	31.71	39.28	41.80
dark m.	43.60	61.08	39.64	37.84	51.35	60.18	9.73	14.95	12.25	10.27
feldsp.	44.50	34.59	52.79	45.23	36.58	15.32	72.07	53.33	48.47	47.93
R ₁	2014	2227	2281	2033	2621	2247	2226	2732	3216	3339
R ₂	1586	2253	2077	1257	2102	1198	1108	787	767	709
A	23.75	13.93	18.77	27.54	13.95	17.63	67.18	56.77	56.25	56.58
F	49.50	42.40	42.09	53.20	39.00	54.47	23.00	25.23	27.43	36.68
M	26.75	43.67	39.14	19.26	47.05	27.91	9.82	18.01	16.32	6.73
A	39.46	26.37	46.52	41.28	33.06	26.53	59.76	50.45	57.69	61.18
F	31.93	36.76	22.83	33.51	32.33	54.12	11.60	26.20	20.60	16.35
C	28.61	36.87	30.65	25.21	34.61	19.36	28.64	23.35	21.71	22.47
Q'	8.89	3.72	3.02	14.16	14.40	19.90	17.48	31.49	40.80	44.03
ANOR	81.31	80.28	90.86	76.74	89.33	56.01	72.95	61.23	62.91	62.66
FeO*	8.44	8.34	5.81	8.73	6.37	12.08	2.04	2.48	2.22	2.83
Fe/Fe+Mg	0.65	0.49	0.52	0.73	0.45	0.66	0.70	0.58	0.63	0.84
A/NK	2.96	3.42	5.71	2.56	4.42	2.44	2.34	1.89	2.38	2.43
A/CNK	0.76	0.44	0.79	0.86	0.54	0.75	1.02	1.02	1.15	1.17
A	62.54	48.71	68.40	64.39	55.12	46.76	90.07	83.08	84.90	85.27
F	24.32	25.26	16.38	26.15	20.34	35.20	6.96	9.87	9.47	12.45
M	13.14	26.02	15.22	9.46	24.54	18.04	2.97	7.05	5.63	2.28
A	49.11	33.75	50.07	52.94	38.61	39.69	74.20	72.26	73.14	73.43
F	29.42	35.53	23.13	29.28	31.44	45.18	8.18	14.72	13.01	12.68
C	21.48	30.72	26.79	17.78	29.95	15.13	17.62	13.02	13.86	13.88

Appendix III. Major element data and normative values (cont.)

Blatná suite

Locality	Mrc-1	Mrc-2	Koz-1	Koz-2	Koz-4	Koz-5	Koz-6	Koz-8	Koz-9	Koz-10
	Mrač	Mrač	Solo- pysky	Kozáro- vice I	Kozáro- vice II	Kozáro- vice III	Kozáro- vice IV	Kamýk	Hřimež- dice	Zalužany
	Mrač	Mrač	Kozáro- vice	Kozáro- vice	Kozáro- vice	Kozáro- vice	Kozáro- vice	Kozáro- vice	Kozáro- vice	Kozáro- vice
SiO ₂	69.13	67.50	60.18	63.14	63.24	65.53	62.21	64.65	59.22	63.35
TiO ₂	0.46	0.49	0.60	0.52	0.49	0.45	0.62	0.54	0.63	0.54
Al ₂ O ₃	15.64	15.93	15.43	15.76	14.98	15.43	15.42	15.38	15.49	15.69
FeO	2.32	2.54	4.42	3.51	2.69	2.34	3.37	2.72	4.07	3.25
Fe ₂ O ₃	0.38	0.61	0.83	0.81	1.29	1.46	1.83	1.60	1.43	1.45
MnO	0.06	0.04	0.13	0.10	0.07	0.09	0.10	0.09	0.13	0.10
MgO	2.72	1.71	3.36	2.78	3.93	2.14	3.21	2.56	3.83	2.98
CaO	1.98	2.56	4.91	4.65	4.18	3.76	4.43	4.30	5.35	4.44
Na ₂ O	3.09	2.30	2.64	2.99	2.39	3.25	2.48	2.49	2.55	2.69
K ₂ O	3.38	4.15	3.99	3.82	3.73	4.14	3.82	4.00	4.13	3.89
P ₂ O ₅	0.43	0.16	0.31	0.26	0.22	0.21	0.23	0.24	0.38	0.25
S	0.01	0.03	0.01	-	-	0.01	0.05	b.d.	0.04	0.02
LOI	0.71	0.73	0.72	0.50	0.50	0.53	0.83	0.63	0.47	0.65
Total	100.31	98.75	97.52	98.84	97.71	99.34	98.60	99.20	97.72	99.29
Q	188	182	105	118	145	126	131	142	95	129
P	-63	-32	-88	-98	-73	-84	-78	-72	-89	-83
A	65	58	-43	-34	-12	-24	-17	-17	-56	-20
B	110	91	163	135	157	110	158	129	178	144
F	257	282	287	302	253	319	266	284	282	282
(Na+K)	172	162	170	177	156	193	161	165	170	170
K/(Na+K)	0.42	0.54	0.50	0.46	0.51	0.46	0.50	0.52	0.52	0.49
Mg/Fe+Mg	0.64	0.49	0.54	0.54	0.65	0.51	0.53	0.52	0.56	0.54
quartz	33.87	32.79	18.92	21.26	26.13	22.70	23.60	25.59	17.12	23.24
dark m.	19.82	16.40	29.37	24.32	28.29	19.82	28.47	23.24	32.07	25.95
feldsp.	46.31	50.81	51.71	54.41	45.59	57.48	47.93	51.17	50.81	50.81
R ₁	2648	2614	1989	2125	2374	2149	2219	2370	1921	2230
R ₂	650	666	990	937	931	810	928	883	1063	927
A	54.59	57.34	43.74	49.24	44.03	56.05	43.37	49.13	42.10	46.62
F	22.46	27.46	34.09	30.65	27.70	27.71	34.53	31.49	33.76	32.27
M	22.95	15.20	22.17	20.10	28.27	16.23	22.10	19.38	24.14	21.11
A	51.96	55.64	37.08	40.32	40.22	42.64	41.38	44.16	35.97	41.82
F	38.32	28.82	40.47	36.12	39.47	33.24	37.05	32.82	40.76	36.01
C	9.72	15.54	22.44	23.56	20.31	24.12	21.56	23.02	23.26	22.17
Q'	35.80	34.34	16.46	19.56	24.06	22.40	22.13	25.09	14.72	21.65
ANOR	25.99	32.21	43.92	44.77	46.46	38.45	46.55	44.53	43.28	45.57
FeO*	2.66	3.09	5.17	4.24	3.85	3.65	5.02	4.16	5.36	4.55
Fe/Fe+Mg	0.49	0.64	0.61	0.60	0.49	0.63	0.61	0.62	0.58	0.60
A/NK	1.79	1.92	1.78	1.74	1.88	1.57	1.88	1.83	1.79	1.82
A/CNK	1.27	1.23	0.88	0.90	0.96	0.93	0.95	0.95	0.84	0.94
A	80.42	82.34	72.12	76.28	73.06	79.75	72.53	76.50	70.70	74.72
F	9.68	11.37	16.89	14.33	13.33	12.77	16.75	14.55	17.08	15.28
M	9.89	6.29	10.99	9.40	13.61	7.48	10.72	8.95	12.21	10.00
A	75.02	75.26	62.15	65.92	63.82	70.49	63.18	66.49	60.40	65.03
F	18.26	16.14	24.02	20.50	23.53	17.90	23.93	20.43	25.03	22.00
C	6.72	8.61	13.83	13.58	12.64	11.61	12.89	13.07	14.57	12.97

Appendix III. Major element data and normative values (cont.)

Blatná suite (cont.)

Sample	Koz-11	Koz-12	Koz-13	KozD-1	Zal-1	Gbl-1	Gbl-2	Bl-1	Bl-2	Bl-3
Locality	Solo- pysky Kozáro- vice	Kamýk Těchnice	Těchnice Těchnice	Kozáro- vice II quartz monzonite	Zalužany Zalužany	Lučkovi- ce gabbro	Lučkovi- ce gabbro	Rečice Blatná	Tužice Blatná	Velenov Blatná
SiO ₂	62.24	64.60	64.74	57.44	54.22	45.27	49.73	67.77	63.00	64.30
TiO ₂	0.60	0.48	0.46	0.73	0.96	0.99	0.58	0.49	0.76	0.63
Al ₂ O ₃	15.88	15.18	15.12	16.22	15.24	14.47	8.89	14.90	16.64	16.23
FeO	4.21	2.79	2.74	4.08	-	6.96	5.08	2.43	4.06	3.37
Fe ₂ O ₃	0.63	1.21	1.08	2.17	7.98	2.67	3.15	0.51	0.51	0.47
MnO	0.12	0.09	0.09	0.14	0.15	0.19	0.18	0.07	0.09	0.06
MgO	2.65	3.19	2.92	4.28	4.94	9.76	19.25	1.80	2.74	2.75
CaO	4.61	3.43	3.46	5.43	7.17	9.55	8.69	2.71	3.46	3.47
Na ₂ O	2.56	2.60	2.92	3.17	2.44	2.29	0.96	2.99	2.62	2.59
K ₂ O	3.99	4.20	4.20	3.95	4.70	3.60	3.31	3.94	3.74	3.67
P ₂ O ₅	0.28	0.20	0.17	0.27	0.80	0.80	0.38	0.16	0.27	0.21
S	0.02	-	0.01	0.03	0.02	0.03	0.04	0.02	0.03	0.04
LOI	0.47	0.71	0.62	0.64	0.75	1.25	1.12	0.68	0.45	0.53
Total	98.26	98.68	98.52	98.55	99.37	97.83	101.36	98.47	98.37	98.33
Q	123	145	135	68	36	-12	72	164	144	153
P	-80	-56	-67	-115	-107	-168	-116	-60	-68	-68
A	-21	3	-10	-62	-136	-206	-237	16	38	32
B	141	139	130	199	235	384	595	91	141	129
F	291	271	290	288	284	183	-112	300	270	273
(Na+K)	168	173	183	186	179	150	101	180	164	162
K/(Na+K)	0.51	0.51	0.49	0.45	0.56	0.51	0.69	0.47	0.48	0.48
Mg/Fe+Mg	0.50	0.59	0.58	0.56	0.55	0.65	0.81	0.53	0.52	0.56
quartz	22.16	26.13	24.32	12.25	6.49	-2.16	12.97	29.55	25.95	27.57
dark m.	25.41	25.05	23.42	35.86	42.34	69.19	107.21	16.40	25.41	23.24
feldsp.	52.43	48.83	52.25	51.89	51.17	32.97	-20.18	54.05	48.65	49.19
R ₁	2170	2290	2183	1601	1439	1091	1976	2449	2257	2404
R ₂	933	821	806	1106	1304	1787	2052	668	826	820
A	46.86	49.03	51.78	40.84	37.07	23.55	13.58	59.64	46.70	48.90
F	34.18	27.97	26.99	34.61	37.28	37.43	25.18	24.96	33.18	29.63
M	18.96	23.00	21.23	24.55	25.65	39.02	61.24	15.49	20.12	21.48
A	41.88	41.68	40.20	34.24	34.18	21.39	9.53	47.67	47.45	47.68
F	36.13	39.43	39.28	42.27	34.80	54.31	71.44	33.37	36.36	35.00
C	21.99	18.89	20.51	23.49	31.02	24.30	19.04	19.96	16.19	17.32
Q*	19.99	24.48	22.40	7.97	6.46	0.00	0.00	29.67	25.10	27.04
ANOR	45.96	38.76	38.81	44.03	37.62	46.61	34.21	34.75	41.07	42.21
FeO*	4.78	3.88	3.71	6.03	7.18	9.36	7.91	2.89	4.52	3.79
Fe/Fe+Mg	0.64	0.55	0.56	0.58	0.59	0.49	0.29	0.62	0.62	0.58
A/NK	1.86	1.72	1.62	1.71	1.67	1.89	1.72	1.62	1.99	1.97
A/CNK	0.94	1.01	0.97	0.84	0.69	0.58	0.42	1.06	1.14	1.12
A	75.13	75.67	77.03	69.36	64.87	51.57	32.64	82.32	76.01	77.46
F	16.00	13.35	12.86	17.93	20.81	23.71	19.63	10.89	14.93	13.06
M	8.88	10.98	10.11	12.72	14.32	24.72	47.74	6.79	9.06	9.47
A	65.08	67.67	68.79	59.72	53.71	41.52	26.85	74.69	68.21	69.19
F	21.55	21.76	20.51	26.39	29.09	39.00	55.42	16.04	21.53	20.13
C	13.38	10.56	10.70	13.89	17.21	19.48	17.73	9.27	10.26	10.68

Appendix III. Major element data and normative values (cont.)

Blatná suite (cont.)

Locality	Bl-4 Pastiky Blatná	Bl-5 Vahlo- vice Blatná	Bl-6 Rečice Blatná	Bl-7 Defur. Lažany Blatná	Bl-8 Hudečice Blatná	BlD-1 Hudečice diorite	Cv-1 Vlčkovice Červená	Cv-2 M.Nepod- řice Červená	Cv-3 Horaž- dovice Červená	CvE-1 Vlčkovice enclave
SiO ₂	68.73	64.88	67.23	66.38	64.63	54.62	62.88	62.03	61.86	48.80
TiO ₂	0.45	0.60	0.46	0.43	0.67	0.66	0.76	0.67	0.73	1.22
Al ₂ O ₃	13.91	15.70	15.48	15.01	14.80	12.98	16.15	15.94	16.17	17.76
FeO	2.32	2.93	2.48	2.36	3.92	5.23	3.90	3.91	4.18	7.48
Fe ₂ O ₃	0.54	0.70	0.49	0.47	0.54	1.06	0.88	0.62	0.81	1.16
MnO	0.05	0.05	0.04	0.05	0.08	0.14	0.07	0.08	0.10	0.16
MgO	1.98	2.70	2.65	1.61	2.78	8.54	3.49	4.01	3.58	5.80
CaO	2.78	3.68	2.84	2.56	4.25	6.67	4.44	3.99	3.98	8.04
Na ₂ O	2.95	2.46	2.74	3.23	2.93	2.33	2.62	2.62	2.94	2.98
K ₂ O	3.91	4.28	3.89	4.36	3.48	4.79	3.67	3.62	3.56	3.21
P ₂ O ₅	0.14	0.30	0.17	0.17	0.22	0.50	0.28	0.24	0.26	0.56
S	0.02	0.02	0.02	0.01	0.02	b.d.	0.03	0.05	0.05	0.08
LOI	0.55	0.52	0.67	0.37	0.53	0.39	0.38	0.58	0.61	0.55
Total	98.33	98.83	99.17	97.01	98.86	97.91	99.54	98.37	98.82	97.80
Q	170	146	168	141	139	47	133	135	125	11
P	-62	-54	-56	-57	-97	-92	-86	-79	-90	-171
A	-5	6	31	5	-31	-160	-4	9	4	-102
B	94	125	113	84	139	306	162	169	166	278
F	291	284	274	330	277	202	260	251	264	266
(Na+K)	178	170	171	197	169	177	163	162	171	164
K/(Na+K)	0.47	0.54	0.49	0.47	0.44	0.58	0.48	0.48	0.44	0.41
Mg/Fe+Mg	0.56	0.57	0.62	0.51	0.53	0.71	0.57	0.61	0.57	0.55
quartz	30.63	26.31	30.27	25.41	25.05	8.47	23.96	24.32	22.52	1.98
dark m.	16.94	22.52	20.36	15.14	25.05	55.14	29.19	30.45	29.91	50.09
feldsp.	52.43	51.17	49.37	59.46	49.91	36.40	46.85	45.23	47.57	47.93
R ₁	2528	2347	2512	2176	2327	1514	2265	2230	2103	1178
R ₂	664	829	733	642	876	1384	962	936	913	1492
A	58.90	51.85	54.34	63.34	47.15	32.60	43.46	42.40	43.37	30.17
F	24.09	27.38	23.94	23.22	32.41	28.31	32.42	30.36	32.75	41.55
M	17.00	20.77	21.72	13.44	20.45	39.10	24.12	27.25	23.88	28.27
A	42.56	45.28	47.44	46.02	38.56	16.55	41.95	40.80	40.91	32.72
F	36.61	35.44	35.86	34.32	39.08	60.61	38.30	41.51	40.99	44.10
C	20.83	19.28	16.70	19.66	22.36	22.85	19.75	17.69	18.10	23.18
Q*	30.42	25.49	29.93	25.36	23.91	0.00	21.21	21.06	19.28	0.00
ANOR	35.79	39.18	36.08	31.02	45.19	27.64	48.22	46.00	46.17	57.44
FeO*	2.81	3.56	2.92	2.78	4.41	6.18	4.69	4.47	4.91	8.52
Fe/Fe+Mg	0.59	0.57	0.52	0.63	0.61	0.42	0.57	0.53	0.58	0.60
A/NK	1.53	1.81	1.78	1.50	1.72	1.44	1.95	1.94	1.86	2.12
A/CNK	0.98	1.02	1.12	1.02	0.91	0.61	0.99	1.03	1.02	0.77
A	81.27	78.19	79.87	83.73	74.69	57.72	73.28	72.35	72.76	62.58
F	10.98	12.40	10.55	10.31	15.52	17.76	15.32	14.57	15.75	22.27
M	7.75	9.41	9.57	5.96	9.79	24.52	11.40	13.08	11.49	15.15
A	73.30	69.30	72.44	76.47	64.97	48.44	64.00	64.02	64.52	51.71
F	16.89	19.33	18.25	14.86	22.01	35.48	23.34	24.47	24.16	30.93
C	9.81	11.37	9.31	8.66	13.02	16.07	12.66	11.52	11.33	17.36

Appendix III. Major element data and normative values (cont.)

Blatná suite (cont.)

Čertovo břemeno suite

Locality	Kl-1	Kl-2	Mg-1	Mg-2	Se-1	Se-3	Se-4	Se-5	Se-6	Se-7
	Klatovy	Klatovy	Radětice	Nepomuk	Vrch. Janovice	Vápenice I	Vápenice II	Vápenice I	Vápenice I	Vápenice II
	Klatovy	Klatovy	Marginal	Marginal	Sedláčany	Sedláčany	Sedláčany	Sedláčany	Sedláčany	Sedláčany
SiO ₂	62.32	70.88	68.75	67.76	67.58	65.15	65.93	65.70	65.11	65.29
TiO ₂	0.67	0.35	0.28	0.41	0.57	0.55	0.52	0.57	0.51	0.56
Al ₂ O ₃	16.66	14.45	14.94	15.72	14.03	14.73	14.64	13.31	14.97	15.11
FeO	3.95	2.24	1.70	2.78	2.64	2.56	2.57	2.60	2.33	2.59
Fe ₂ O ₃	0.65	0.29	1.00	0.53	0.48	0.53	0.55	0.57	0.49	0.48
MnO	0.08	0.07	0.08	0.07	0.06	0.07	0.08	0.06	0.05	0.06
MgO	2.30	1.57	1.02	1.30	2.61	2.67	2.58	3.26	2.82	2.74
CaO	4.03	2.19	2.94	2.77	2.34	2.40	2.40	2.30	2.38	2.41
Na ₂ O	2.92	2.38	2.70	2.66	2.03	2.98	2.81	2.48	2.63	2.34
K ₂ O	3.38	4.70	3.68	4.08	5.51	5.60	5.62	5.92	5.58	5.75
P ₂ O ₅	0.19	0.08	0.07	0.10	0.35	0.35	0.37	0.34	0.34	0.37
S	0.03	0.00	0.01	0.01	0.02	0.02	0.03	0.01	0.01	0.02
LOI	0.53	0.65	0.69	0.56	0.46	0.57	0.53	0.53	0.52	0.55
Total	97.71	99.85	97.87	98.75	98.68	98.18	98.63	97.65	97.74	98.27
Q	132	190	182	170	164	118	127	131	130	136
P	-94	-16	-61	-48	9	-20	-15	5	-9	3
A	17	28	24	37	8	-12	-9	-27	7	12
B	128	78	66	83	115	116	114	131	114	117
F	295	287	307	302	276	321	314	293	311	302
(Na+K)	166	177	165	173	183	215	210	206	203	198
K/(Na+K)	0.43	0.56	0.47	0.50	0.64	0.55	0.57	0.61	0.58	0.62
Mg/Fe+Mg	0.47	0.53	0.40	0.41	0.60	0.61	0.60	0.65	0.65	0.62
quartz	23.78	34.23	32.79	30.63	29.55	21.26	22.88	23.60	23.42	24.50
dark m.	23.06	14.05	11.89	14.95	20.72	20.90	20.54	23.60	20.54	21.08
feldsp.	53.15	51.71	55.32	54.41	49.73	57.84	56.58	52.79	56.04	54.41
R ₁	2193	2715	2685	2529	2407	1888	1995	2017	2022	2079
R ₂	866	593	655	666	649	672	667	667	683	682
A	47.96	63.49	63.80	59.66	57.03	60.06	59.89	56.86	59.49	58.40
F	34.53	22.43	26.00	28.83	23.23	21.26	21.78	21.07	20.08	21.82
M	17.51	14.08	10.20	11.51	19.74	18.69	18.33	22.07	20.43	19.78
A	47.25	49.89	56.16	53.52	40.70	35.11	36.55	26.93	39.74	41.65
F	32.93	32.75	21.52	27.94	44.56	48.42	47.26	56.96	45.06	43.86
C	19.82	17.37	22.32	18.54	14.75	16.47	16.19	16.11	15.20	14.49
Q'	22.34	34.50	34.14	31.30	29.84	19.70	21.78	22.54	22.38	23.87
ANOR	48.42	27.13	39.38	35.18	22.26	22.52	22.22	18.04	22.52	21.92
FeO*	4.53	2.50	2.60	3.26	3.07	3.04	3.06	3.11	2.77	3.02
Fe/Fe+Mg	0.66	0.61	0.72	0.71	0.54	0.53	0.54	0.49	0.50	0.52
A/NK	1.97	1.61	1.77	1.79	1.51	1.34	1.37	1.27	1.44	1.50
A/CNK	1.06	1.11	1.08	1.14	1.03	0.96	0.97	0.91	1.02	1.05
A	77.06	84.10	85.49	83.13	79.15	80.33	80.34	77.31	80.57	80.11
F	15.22	9.77	10.42	12.06	11.27	10.47	10.67	11.08	9.63	10.43
M	7.72	6.13	4.09	4.81	9.58	9.20	8.98	11.61	9.80	9.46
A	67.88	77.47	76.47	75.40	72.89	74.20	74.14	71.45	74.41	73.95
F	20.21	14.65	12.98	15.30	19.20	18.17	18.14	20.98	17.95	18.37
C	11.91	7.88	10.55	9.30	7.91	7.64	7.71	7.57	7.64	7.68

Appendix III. Major element data and normative values (cont.)

Čertovo břemeno suite (cont.)

Sample Locality	Se-8 Vrchot. Janovice Sedláčany	Se-9 Vrchot. Janovice Sedláčany	Se-10 Kosova Hora Sedláčany	Se-11 Kosova Hora Sedláčany	Se-12 Kosova Hora Sedláčany	Se-13 Bořena Hora Sedláčany	Se-14 Kosova Hora Sedláčany	Se-15 Vrchot. Janovice Sedláčany	Se-16 Kosova Hora Sedláčany	SeE-1 Bořena Hora HME
SiO ₂	66.00	66.98	66.77	68.27	68.47	67.21	66.98	65.77	67.11	62.15
TiO ₂	0.53	0.53	0.53	0.51	0.51	0.51	0.48	0.56	0.53	0.70
Al ₂ O ₃	14.85	14.99	14.77	15.02	14.74	14.73	14.68	14.69	14.55	14.59
FeO	2.46	2.53	2.54	2.39	2.43	2.51	2.30	2.81	2.70	3.56
Fe ₂ O ₃	0.82	0.54	0.43	0.53	0.39	0.35	0.43	0.34	0.37	0.79
MnO	0.07	0.05	0.06	0.06	0.05	0.07	0.07	0.07	0.06	0.10
MgO	3.26	2.49	2.26	2.69	2.36	2.45	2.28	3.05	2.45	3.76
CaO	2.47	2.45	2.17	2.13	2.14	2.28	2.08	2.45	2.07	2.84
Na ₂ O	2.50	2.38	2.34	2.05	2.74	2.45	2.66	2.01	2.58	2.56
K ₂ O	5.33	5.58	5.42	5.56	5.50	5.51	5.50	5.36	5.37	6.04
P ₂ O ₅	0.36	0.34	0.31	0.30	0.30	0.32	0.30	0.35	0.30	0.51
S	0.02	0.02	0.02	0.02	0.01	0.01	0.02	0.02	0.02	0.02
LOI	0.43	0.52	0.60	0.64	0.61	0.63	0.45	0.48	0.52	0.48
Total	99.09	99.40	98.21	100.17	100.25	99.03	98.24	97.96	98.63	98.10
Q	143	147	153	169	150	150	144	157	151	100
P	-12	-3	0	14	-9	-3	-6	5	-6	-6
A	9	11	21	35	8	11	11	21	14	-27
B	132	111	103	113	104	106	100	126	111	162
F	280	297	299	273	301	299	311	272	293	293
(Na+K)	194	195	191	184	205	196	203	179	197	211
K/(Na+K)	0.58	0.61	0.60	0.64	0.57	0.60	0.58	0.64	0.58	0.61
Mg/Fe+Mg	0.65	0.60	0.58	0.63	0.60	0.61	0.61	0.64	0.59	0.61
quartz	25.77	26.49	27.57	30.45	27.03	27.03	25.95	28.29	27.21	18.02
dark m.	23.78	20.00	18.56	20.36	18.74	19.10	18.02	22.70	20.00	29.19
feldsp.	50.45	53.51	53.87	49.19	54.23	53.87	56.04	49.01	52.79	52.79
R ₁	2169	2228	2262	2430	2226	2239	2159	2329	2203	1694
R ₂	715	674	629	648	633	648	621	696	621	772
A	54.80	59.11	59.94	57.80	61.58	60.14	62.16	54.45	59.18	51.71
F	22.38	22.40	22.61	21.77	20.78	21.34	20.47	23.02	22.58	25.68
M	22.82	18.49	17.46	20.43	17.64	18.51	17.37	22.53	18.24	22.61
A	39.25	42.65	44.64	45.73	40.45	41.87	41.83	42.14	40.72	29.32
F	46.38	41.89	41.18	41.42	44.52	43.15	43.41	44.18	45.45	55.59
C	14.37	15.46	14.18	12.84	15.03	14.97	14.76	13.68	13.83	15.09
Q'	24.69	26.06	28.09	30.55	26.06	26.55	25.76	28.11	26.70	14.72
ANOR	23.92	23.15	21.44	20.76	21.03	22.07	20.46	23.75	20.75	22.70
FeO*	3.20	3.02	2.93	2.87	2.78	2.82	2.69	3.12	3.03	4.27
Fe/Fe+Mg	0.50	0.55	0.56	0.52	0.54	0.54	0.54	0.51	0.55	0.53
A/NK	1.50	1.51	1.52	1.60	1.41	1.47	1.42	1.61	1.45	1.36
A/CNK	1.03	1.04	1.08	1.13	1.03	1.04	1.04	1.08	1.05	0.92
A	77.84	80.65	81.29	80.29	81.72	81.14	82.14	78.16	80.41	74.28
F	10.97	10.60	10.56	10.17	9.89	10.10	9.66	11.04	10.84	13.68
M	11.19	8.75	8.15	9.54	8.39	8.76	8.20	10.81	8.76	12.04
A	71.75	74.26	75.38	74.64	75.94	75.02	76.42	71.91	74.87	68.08
F	20.43	17.82	17.36	18.33	16.99	17.44	16.62	20.10	18.24	23.58
C	7.81	7.93	7.26	7.03	7.07	7.54	6.96	7.99	6.89	8.34

Appendix III. Major element data and normative values (cont.)

Čertovo břemeno suite (cont.)

Sample Locality	Cb-1 Zvíkov. Podhradí Čertovo břemeno	Cb-2 Vepřice Čertovo břemeno	Cb-3 Chyšky Čertovo břemeno	Cb-4 Petro- vice Čertovo břemeno	Cb-5 Votice Čertovo břemeno	Ta-1 Klokoty Tábor	Ta-2 Slapy- Dražický Tábor	Ta-3 Klokoty Tábor	Mi-1 Kozlí minette	Mi-2 Zaluzany minette
SiO ₂	62.76	63.23	57.22	64.25	61.75	58.93	58.94	60.51	57.82	57.19
TiO ₂	0.76	0.70	0.97	0.61	0.78	0.84	0.86	0.90	0.87	1.37
Al ₂ O ₃	13.99	13.34	12.67	13.45	15.30	14.01	13.65	14.11	12.77	12.84
FeO	3.44	3.26	3.56	2.96	4.04	3.93	-	3.59	4.11	4.26
Fe ₂ O ₃	0.65	0.70	2.25	0.67	0.53	1.05	5.75	1.15	1.56	1.31
MnO	0.07	0.07	0.08	0.07	0.08	0.09	0.09	0.10	0.11	0.09
MgO	4.20	4.32	6.78	4.42	5.07	5.36	6.22	5.33	7.70	9.23
CaO	2.56	3.11	3.95	2.28	2.70	3.75	4.25	3.45	3.63	4.14
Na ₂ O	1.49	2.84	2.16	2.53	1.73	2.19	1.95	1.86	1.76	0.69
K ₂ O	6.39	5.91	6.68	6.29	5.01	6.39	6.12	5.89	6.07	7.10
P ₂ O ₅	0.53	0.57	0.63	0.52	0.50	0.64	0.72	0.57	0.65	0.93
S	0.03	0.04	0.04	0.02	0.02	0.05	0.05	0.03	0.04	-
LOI	0.67	0.45	0.66	0.61	2.23	0.44	0.12	0.63	-	-
Total	97.53	98.53	97.65	98.68	99.74	97.67	98.72	98.12	97.10	99.15
Q	134	97	59	113	149	75	83	109	91	95
P	42	-22	2	11	2	-2	-9	3	7	55
A	-2	-65	-103	-34	42	-66	-77	-32	-66	-69
B	170	170	258	167	199	212	237	207	279	321
F	251	288	238	275	207	268	235	239	185	139
(Na+K)	184	217	212	216	162	207	193	185	186	173
K/(Na+K)	0.74	0.58	0.67	0.62	0.65	0.66	0.67	0.68	0.69	0.87
Mg/Fe+Mg	0.65	0.66	0.68	0.69	0.67	0.66	0.68	0.67	0.71	0.75
quartz	24.14	17.48	10.63	20.36	26.85	13.51	14.95	19.64	16.40	17.12
dark m.	30.63	30.63	46.49	30.09	35.86	38.20	42.70	37.30	50.27	57.84
feldsp.	45.23	51.89	42.88	49.55	37.30	48.29	42.34	43.06	33.33	25.05
R ₁	2035	1710	1320	1810	2195	1511	1655	1845	1652	1728
R ₂	752	805	1004	721	838	934	1025	906	1016	1147
A	48.93	51.59	41.69	52.49	41.28	45.60	41.46	43.77	37.21	34.69
F	24.99	22.94	26.34	21.20	27.67	25.91	26.58	26.12	26.20	24.22
M	26.08	25.47	31.97	26.31	31.05	28.49	31.96	30.10	36.59	41.10
A	32.84	18.61	11.91	21.32	38.69	22.22	25.98	28.46	17.87	18.80
F	55.09	63.75	70.12	66.15	51.06	60.91	53.54	56.56	68.45	68.75
C	12.07	17.64	17.96	12.53	10.25	16.87	20.48	14.98	13.68	12.45
Q*	22.46	15.32	4.64	17.52	24.79	8.66	12.62	15.46	8.65	7.31
ANOR	19.65	15.07	11.53	15.40	25.49	20.14	22.36	26.82	20.09	20.72
FeO*	4.02	3.89	5.58	3.56	4.52	4.87	5.17	4.62	5.51	5.44
Fe/Fe+Mg	0.49	0.47	0.45	0.45	0.47	0.48	0.45	0.46	0.42	0.37
A/NK	1.49	1.21	1.17	1.23	1.85	1.33	1.39	1.50	1.35	1.46
A/CNK	1.00	0.80	0.71	0.89	1.16	0.81	0.78	0.90	0.79	0.79
A	72.67	72.90	63.50	73.61	69.69	68.82	65.59	68.71	60.92	58.44
F	13.37	12.84	16.49	11.78	14.28	14.85	15.62	14.54	16.31	15.41
M	13.96	14.26	20.02	14.61	16.03	16.33	18.78	16.75	22.77	26.15
A	66.97	66.12	56.87	68.45	64.21	61.76	58.13	61.99	55.02	52.31
F	25.19	24.57	32.69	24.54	27.93	27.98	30.49	28.23	35.29	37.19
C	7.84	9.31	10.44	7.01	7.87	10.25	11.37	9.78	9.69	10.50

Appendix III. Major element data and normative values (cont.)

Říčany suite

Sample Locality	RI-1 Zernov- ka Říčany	RI-2 Zernov- ka Říčany	RI-3 Zernov- ka Říčany	RI-4 Zernov- ka Říčany	RI-5 Zernov- ka Říčany	RI-6 Zernov- ka Říčany	RI-7 Zernov- ka Říčany	RI-8 Zernov- ka Říčany	RI-9 Zernov- ka Říčany	RI-10 Srbín Říčany
SiO ₂	71.43	70.72	70.61	69.67	69.98	69.10	69.59	71.12	69.80	70.98
TiO ₂	0.30	0.23	0.16	0.15	0.14	0.23	0.36	0.33	0.31	0.26
Al ₂ O ₃	14.58	13.97	14.52	14.56	14.90	15.85	15.21	14.38	14.86	15.08
FeO	0.99	0.84	0.84	0.77	0.59	0.84	1.25	1.25	1.24	0.27
Fe ₂ O ₃	0.26	0.78	0.29	1.40	0.87	0.59	0.26	0.29	0.28	1.36
MnO	0.01	0.04	0.04	0.03	0.01	0.01	0.03	0.03	0.03	0.04
MgO	1.12	0.96	0.33	0.84	0.68	0.79	1.32	0.98	1.26	0.79
CaO	1.27	1.93	1.35	1.53	1.43	1.34	1.29	1.23	1.30	1.12
Na ₂ O	3.32	3.57	3.92	3.72	3.70	3.65	2.40	3.01	3.27	3.72
K ₂ O	5.29	5.70	5.30	5.59	5.86	5.46	5.73	5.35	5.29	4.88
P ₂ O ₅	0.17	0.18	0.08	0.16	0.10	0.16	0.18	0.16	0.16	0.11
S	b.d.	-	-	-	-	-	0.01	b.d.	b.d.	-
LOI	0.41	1.21	1.66	0.98	1.06	1.39	0.55	0.46	0.53	1.52
Total	99.15	100.13	99.10	99.40	99.32	99.41	98.18	98.59	98.33	100.13
Q	162	134	137	130	129	133	172	169	154	156
P	-18	-28	-37	-28	-20	-26	22	-5	-17	-36
A	21	-30	-2	-7	-1	29	53	27	27	32
B	49	49	26	52	38	42	58	49	56	44
F	344	372	392	373	388	380	325	337	345	355
(Na+K)	219	236	239	239	243	234	199	211	218	224
K/(Na+K)	0.51	0.51	0.47	0.50	0.51	0.50	0.61	0.54	0.51	0.46
Mg/Fe+Mg	0.62	0.52	0.33	0.42	0.47	0.51	0.62	0.53	0.60	0.49
quartz	29.19	24.14	24.68	23.42	23.24	23.96	30.99	30.45	27.75	28.11
dark m.	8.83	8.83	4.68	9.37	6.85	7.57	10.45	8.83	10.09	7.93
feldsp.	61.98	67.03	70.63	67.21	69.91	68.47	58.56	60.72	62.16	63.96
R ₁	2305	2068	2050	1962	1945	2008	2406	2374	2211	2225
R ₂	471	524	444	487	474	486	500	456	491	447
A	78.60	78.75	86.57	76.44	82.32	80.83	74.36	77.04	75.67	79.02
F	11.17	13.10	10.34	16.66	11.82	12.16	13.57	13.92	13.19	13.72
M	10.22	8.16	3.10	6.90	5.86	7.01	12.07	9.03	11.14	7.26
A	52.47	36.51	52.10	45.95	50.10	60.00	59.00	54.35	52.00	63.89
F	32.78	34.30	22.62	30.94	25.94	24.32	29.81	31.78	34.26	20.69
C	14.74	29.20	25.28	23.10	23.96	15.68	11.19	13.87	13.74	15.42
Q'	29.84	25.35	25.24	24.08	23.44	25.11	32.63	31.65	28.46	29.60
ANOR	14.24	13.50	16.47	16.48	15.68	14.79	13.36	13.79	14.74	14.37
FeO*	1.22	1.54	1.10	2.03	1.37	1.37	1.48	1.51	1.49	1.49
Fe/Fe+Mg	0.52	0.62	0.77	0.71	0.67	0.63	0.53	0.61	0.54	0.65
A/NK	1.30	1.16	1.19	1.20	1.20	1.33	1.50	1.34	1.34	1.32
A/CNK	1.08	0.90	0.99	0.97	0.99	1.10	1.22	1.11	1.10	1.12
A	90.82	90.28	94.32	89.27	92.26	92.03	89.27	90.13	89.49	91.20
F	4.79	5.99	4.37	7.59	5.18	5.05	5.68	5.99	5.70	5.75
M	4.39	3.73	1.31	3.14	2.56	2.91	5.05	3.88	4.81	3.04
A	86.52	83.98	89.51	84.44	87.54	87.70	85.08	85.94	85.25	87.43
F	8.74	9.04	5.40	10.15	7.35	7.59	10.22	9.41	10.02	8.43
C	4.74	6.97	5.09	5.41	5.12	4.71	4.70	4.65	4.73	4.14

Appendix III. Major element data and normative values (cont.)

Říčany suite (cont.)

Sample	Ri-11	Ri-12	Ri-13	Ri-14	Ri-15	Ri-16	Ri-17	Ri-18	Ri-19	Ri-20
Locality	Srbín	Srbín	Babice	Babice	Kozojedy	Doubrav- dice	Doubrav- dice	Skvorec	Skvorec	Březi
	Říčany	Říčany	Říčany	Říčany	Říčany	Říčany	Říčany	Říčany	Říčany	Říčany
SiO ₂	71.62	71.99	70.22	70.98	70.83	69.86	71.09	71.71	71.36	71.04
TiO ₂	0.29	0.31	0.32	0.31	0.39	0.29	0.29	0.32	0.33	0.28
Al ₂ O ₃	14.05	14.56	14.71	14.44	14.94	14.67	14.57	14.10	14.28	15.22
FeO	1.08	1.33	1.17	1.15	1.16	1.07	1.08	1.36	1.21	1.43
Fe ₂ O ₃	0.46	0.19	0.43	0.35	0.71	0.41	0.45	0.40	0.35	0.17
MnO	0.03	0.04	0.01	0.04	0.03	0.01	0.04	0.03	0.02	0.04
MgO	0.88	0.78	1.17	1.25	1.29	1.63	1.13	0.95	1.22	1.50
CaO	0.84	1.19	1.12	1.16	0.71	1.00	0.87	1.23	1.14	0.86
Na ₂ O	2.79	2.83	3.17	3.15	4.05	2.88	3.09	2.76	2.89	2.19
K ₂ O	5.33	5.11	5.39	5.40	5.63	5.16	5.27	4.96	5.10	5.31
P ₂ O ₅	0.15	0.14	0.16	0.17	0.18	0.15	0.14	0.17	0.15	0.13
S	b.d.	b.d.	b.d.	b.d.	b.d.	b.d.	b.d.	b.d.	b.d.	0.01
LOI	0.72	0.85	0.56	0.50	0.74	0.67	0.54	0.58	0.60	0.66
Total	98.24	99.32	98.43	98.90	100.66	97.80	98.56	98.57	98.65	98.84
Q	184	186	160	163	133	173	172	189	182	200
P	8	-4	-8	-8	-24	-1	-4	-6	-5	27
A	43	45	33	24	16	49	42	39	39	85
B	47	44	54	55	62	64	53	52	55	63
F	324	325	341	337	360	318	330	314	318	292
(Na-K)	203	199	216	217	251	203	212	194	201	184
K/(Na-K)	0.56	0.54	0.53	0.53	0.48	0.54	0.53	0.54	0.54	0.61
Mg/Fe-Mg	0.51	0.47	0.58	0.61	0.56	0.67	0.57	0.50	0.59	0.63
quartz	33.15	33.51	28.83	29.37	23.96	31.17	30.99	34.05	32.79	36.04
dark m.	8.47	7.93	9.73	9.91	11.17	11.53	9.55	9.37	9.91	11.35
feldsp.	58.38	58.56	61.44	60.72	64.86	57.30	59.46	56.58	57.30	52.61
R ₁	2485	2557	2246	2313	1917	2393	2376	2584	2489	2678
R ₂	401	449	460	465	429	469	431	448	460	462
A	77.38	77.68	75.84	75.90	75.81	72.37	76.17	74.30	74.43	70.87
F	14.24	14.69	13.79	13.00	14.09	12.95	13.53	16.55	14.21	14.96
M	8.39	7.63	10.37	11.10	10.10	14.67	10.30	9.14	11.36	14.17
A	59.95	60.57	53.84	51.22	43.06	55.03	57.28	57.61	55.13	62.38
F	30.53	26.74	33.98	35.98	48.42	35.71	33.25	29.79	33.06	30.95
C	9.52	12.69	12.19	12.80	8.52	9.26	9.47	12.60	11.82	6.67
Q*	35.27	34.98	29.84	30.31	24.23	32.77	32.52	35.93	34.01	38.45
ANCR	9.19	14.18	12.41	12.70	6.59	11.55	9.85	14.55	13.43	9.82
FeC*	1.49	1.50	1.56	1.46	1.80	1.44	1.48	1.72	1.52	1.58
Fe/Fe-Mg	0.63	0.66	0.57	0.54	0.58	0.47	0.57	0.64	0.56	0.51
A/NK	1.36	1.43	1.33	1.31	1.17	1.42	1.35	1.42	1.39	1.63
A/CNK	1.18	1.18	1.12	1.10	1.06	1.21	1.18	1.16	1.16	1.39
A	90.33	90.80	89.51	89.44	88.85	88.10	89.76	89.10	89.03	88.05
F	6.09	6.06	5.99	5.70	6.49	5.58	5.81	7.02	6.10	6.13
M	3.59	3.15	4.50	4.86	4.66	6.32	4.42	3.88	4.88	5.81
A	87.34	86.64	85.81	85.58	86.63	84.81	86.81	84.84	85.15	85.21
F	9.35	8.78	10.06	10.11	10.87	11.46	9.90	10.38	10.49	11.56
C	3.31	4.58	4.13	4.32	2.50	3.73	3.29	4.78	4.36	3.23

Appendix III. Major element data and normative values (cont.)

Říčany suite (cont.)

Sample	R1-21	R1-22	R1E-1	R1E-2	R1E-3	Je-1	Je-2	Je-3	Je-4	Je-5
Locality	Březi	Březi	Zernovka	Zernovka	Zernovka	Vyzlovka	Vyzlovka	Vyzlovka	Vyzlovka	Vyzlovka
	Říčany	Říčany	MME	MME	MME	Jevany	Jevany	Jevany	Jevany	Jevany
SiO ₂	73.07	72.32	68.51	68.56	69.00	69.94	70.91	71.41	70.37	71.01
TiO ₂	0.28	0.28	0.46	0.29	0.61	0.09	0.19	0.22	0.18	0.21
Al ₂ O ₃	14.56	14.18	13.78	14.09	14.26	14.88	15.01	15.01	14.05	15.28
FeO	1.23	1.12	1.97	1.19	2.67	0.32	0.64	0.84	0.92	1.05
Fe ₂ O ₃	0.42	0.37	1.17	1.27	0.65	1.32	0.20	0.16	0.11	0.31
MnO	0.03	0.04	0.06	0.04	0.07	0.02	0.02	0.02	0.02	0.03
MgO	1.21	1.20	3.31	2.36	2.95	0.80	0.61	0.66	0.90	0.74
CaO	1.00	1.04	2.36	1.62	2.06	1.34	1.00	0.91	1.03	1.09
Na ₂ O	2.90	2.93	3.22	3.27	3.20	3.72	3.96	3.86	4.18	4.06
K ₂ O	5.01	4.47	3.74	4.68	3.50	5.29	5.20	4.90	5.06	4.51
P ₂ O ₅	0.13	0.12	0.41	0.31	0.42	0.12	0.05	0.06	0.07	0.06
S	b.d.	b.d.	-	-	b.d.	-	b.d.	0.01	b.d.	b.d.
LOI	0.61	0.63	1.32	1.73	0.59	1.32	0.69	0.63	0.86	0.65
Total	100.45	98.70	100.31	99.41	99.98	99.16	98.48	98.68	97.75	99.00
Q	193	199	169	156	181	140	143	156	136	154
P	-6	-19	-67	-36	-66	-32	-36	-37	-46	-54
A	50	50	3	13	29	12	20	33	-2	35
B	56	55	130	96	126	42	29	33	38	40
F	306	301	256	303	248	373	383	366	381	361
(Na+K)	200	190	183	205	177	232	238	229	242	227
K/(Na+K)	0.53	0.50	0.43	0.48	0.42	0.48	0.46	0.45	0.44	0.42
Mg/Fe+Mg	0.58	0.59	0.66	0.64	0.62	0.49	0.56	0.53	0.61	0.49
quartz	34.77	35.86	30.45	28.11	32.61	25.23	25.77	28.11	24.50	27.75
dark m.	10.09	9.91	23.42	17.30	22.70	7.57	5.23	5.95	6.85	7.21
feldsp.	55.14	54.23	46.13	54.59	44.68	67.21	69.01	65.95	68.65	65.05
R ₁	2625	2700	2466	2252	2541	2062	2089	2214	2003	2200
R ₂	447	444	686	560	641	467	426	422	427	449
A	73.73	73.61	52.36	62.88	51.92	79.61	86.50	84.20	82.80	80.55
F	14.99	14.45	22.74	18.45	25.22	13.32	7.74	9.46	9.13	12.49
M	11.28	11.94	24.90	18.67	22.86	7.07	5.76	6.34	8.07	6.96
A	58.03	59.20	37.97	42.48	42.65	56.72	58.00	60.54	39.08	58.85
F	31.94	30.28	47.82	44.64	46.08	23.16	24.80	25.81	41.26	26.60
C	10.03	10.52	14.21	12.88	11.26	20.11	17.19	13.64	19.66	14.55
Q'	35.99	37.86	30.58	29.10	33.46	26.18	26.42	29.07	24.54	28.44
ANOR	12.19	14.21	29.00	17.85	26.55	15.79	13.10	12.46	13.40	15.84
FeO*	1.61	1.45	3.02	2.33	3.25	1.51	0.82	0.98	1.02	1.33
Fe/Fe+Mg	0.57	0.55	0.48	0.50	0.52	0.65	0.57	0.60	0.53	0.64
A/NK	1.43	1.47	1.47	1.35	1.58	1.26	1.24	1.29	1.14	1.32
A/CNK	1.21	1.23	1.01	1.05	1.11	1.04	1.08	1.13	0.99	1.13
A	88.86	89.05	76.61	82.45	77.16	91.19	94.41	93.53	92.39	92.02
F	6.36	6.00	11.17	8.73	11.98	5.76	3.20	3.87	4.04	5.13
M	4.78	4.95	12.23	8.83	10.86	3.05	2.38	2.60	3.57	2.86
A	85.48	85.39	70.47	77.73	71.72	86.75	90.86	90.30	88.76	88.30
F	10.72	10.50	21.52	16.55	21.23	8.38	5.38	6.25	7.31	7.66
C	3.80	4.12	8.02	5.71	7.05	4.87	3.76	3.46	3.93	4.04

Appendix III. Major element data and normative values (cont.)

Country rocks (Teplá-Barrandian and Moldanubian Units)

Sample Locality	CR-1 Dobruša shale	CR-2 Ktiš kinzi- gite	CR-4 Rajov ortho- gneiss	CR-5 Chynov mica- schist	CR-7 Miličín para- gneiss	CR-9 Vrané shale	CR-10 Davle tuff	CR-11 Hněvkovice para- gneiss	CR-12 Hněvkovice para- gneiss	CR-13 Hněvkovice para- gneiss
SiO ₂	63.26	59.43	62.12	58.03	58.25	61.64	63.16	65.06	71.21	71.21
TiO ₂	0.68	0.81	0.64	0.72	0.84	0.64	0.57	0.76	0.55	0.55
Al ₂ O ₃	16.56	16.82	16.63	22.42	19.00	15.25	12.90	17.35	13.81	13.81
FeO	5.01	-	3.55	3.87	4.90	4.82	4.65	5.17	4.01	-
Fe ₂ O ₃	1.04	13.01	1.18	2.95	1.44	1.01	0.78	0.85	0.24	4.69
MnO	0.12	0.07	0.09	0.21	0.12	0.11	0.15	0.09	0.08	0.06
MgO	3.28	4.75	4.18	1.75	3.77	3.08	2.21	2.75	1.77	1.77
CaO	0.60	0.88	5.00	0.42	3.58	2.39	4.89	1.21	1.74	1.73
Na ₂ O	3.64	2.00	4.72	0.58	2.81	3.21	2.93	2.48	3.22	3.22
K ₂ O	2.97	4.01	1.95	5.34	3.21	2.91	0.96	3.14	2.57	2.57
P ₂ O ₅	0.14	0.08	0.28	0.14	0.16	0.28	0.11	0.18	0.14	0.13
S	-	-	-	-	-	-	-	-	-	-
LOI	-	-	-	-	-	-	-	-	-	-
Total	97.30	101.86	100.35	96.43	98.08	95.34	93.31	99.04	99.33	99.74
Q	164	169	92	185	121	147	177	199	215	215
P	-65	4	-200	87	-87	-85	-162	-35	-80	-80
A	123	148	-45	294	86	47	-36	149	50	50
B	173	291	176	143	191	164	137	161	110	110
F	218	95	287	227	243	244	241	195	230	230
(Na+K)	180	150	193	132	159	166	115	147	159	159
K/(Na+K)	0.35	0.57	0.21	0.86	0.43	0.37	0.17	0.46	0.35	0.35
Mg/Fe+Mg	0.49	0.42	0.62	0.32	0.52	0.49	0.42	0.45	0.43	0.43
quartz	29.55	30.45	16.58	33.33	21.80	26.49	31.89	35.86	38.74	38.74
dark m.	31.17	52.43	31.71	25.77	34.41	29.55	24.68	29.01	19.82	19.82
feldsp.	39.28	17.12	51.71	40.90	43.78	43.96	43.42	35.14	41.44	41.44
R ₁	2048	1973	1867	2223	1946	2122	2790	2542	2885	2885
R ₂	546	653	1066	567	936	703	883	602	542	536
A	41.74	26.75	43.14	41.71	37.66	40.99	33.97	39.29	49.13	49.15
F	37.55	52.11	29.83	45.96	38.76	38.37	46.73	41.49	35.86	35.82
M	20.71	21.14	27.03	12.33	23.58	20.63	19.30	19.22	15.02	15.03
A	47.65	57.78	35.98	75.19	49.08	42.68	40.35	55.13	46.86	61.04
F	49.89	37.78	41.58	23.77	37.12	45.79	34.93	39.92	41.57	23.85
C	2.46	4.43	22.44	1.03	13.80	11.52	24.73	4.95	11.58	15.11
Q'	29.95	34.78	12.42	43.81	18.78	26.54	34.89	39.46	40.23	42.22
ANOR	10.51	13.95	61.53	3.57	46.84	36.83	77.20	20.64	33.69	33.74
FeO*	5.95	11.71	4.61	6.52	6.20	5.73	5.35	5.93	4.23	4.22
Fe/Fe+Mg	0.64	0.71	0.52	0.79	0.62	0.65	0.71	0.68	0.70	0.70
A/NK	1.80	2.20	1.68	3.33	2.35	1.81	2.20	2.32	1.71	1.71
A/CNK	1.61	1.82	0.88	2.99	1.30	1.19	0.87	1.79	1.23	1.23
A	71.52	58.11	72.60	77.40	71.51	70.81	68.95	72.56	76.57	76.59
F	18.35	29.80	14.37	17.82	17.71	18.98	21.98	18.75	16.51	16.49
M	10.12	12.09	13.03	4.78	10.78	10.21	9.08	8.69	6.92	6.92
A	70.22	56.84	62.82	76.52	64.88	65.61	57.42	69.89	71.70	71.74
F	27.96	40.97	23.70	22.34	25.84	27.05	25.86	26.43	21.93	21.93
C	1.82	2.19	13.48	1.13	9.28	7.34	16.72	3.68	6.37	6.33

Appendix IV. Trace element geochemistry concentrations (ppm) [XRF]

Sázava suite

Sample	Sa-1	Sa-2	Sa-4	Sa-7	Sa-10	Sa-11	Sa-12	Sa-13	SaD-1	SaD-2	SaD-3	Gbs-1	Gbs-2	Gbs-3	Gbs-4	Gbs-5
Ba	1037	582	388	722	1036	1476	1004	998	1017	646	654	583	245	860	430	1165
Rb	76	53	56	57	62	64	87	45	43	50	34	21	31	43	17	101
Sr	539	540	472	537	382	378	530	541	430	436	415	352	278	325	216	182
Zr	76	55	56	57	79	74	95	146	88	78	76	76	27	72	43	185
Nb	6	10	5	10	8	5	6	7	10	9	11	4	8	4	5	12
Ga	17	19	19	20	15	16	17	19	18	20	22	16	14	21	14	17
La	25	15	22	20	21	30	29	22	24	13	11	5	b.d.	6	5	18
Ce	45	30	62	33	28	42	58	48	44	38	30	8	b.d.	34	b.d.	62
Y	25	30	38	24	19	17	19	19	36	25	29	20	10	42	14	45
U	b.d.	b.d.	b.d.	b.d.	b.d.	b.d.	9	b.d.	b.d.	b.d.	b.d.	b.d.	b.d.	b.d.	b.d.	9
Th	b.d.	b.d.	12	b.d.	b.d.	b.d.	21	12	b.d.	b.d.	b.d.	b.d.	b.d.	b.d.	b.d.	14
Ni	10	10	b.d.	b.d.	b.d.	b.d.	6	5	b.d.	b.d.	8	22	13	6	36	b.d.
Co	17	23	30	13	11	13	20	14	18	21	18	40	23	16	35	32
Pb	22	15	15	13	13	15	21	17	b.d.	12	b.d.	12	13	24	b.d.	16
Zn	71	76	104	50	53	73	75	70	85	80	93	75	51	124	49	137
Cu	27	39	41	15	b.d.	b.d.	7	14	9	7	b.d.	24	b.d.	b.d.	51	b.d.
Cr	29	60	53	33	38	50	40	43	43	46	93	217	159	30	172	61
Rb/Sr	0.14	0.10	0.12	0.11	0.16	0.17	0.16	0.08	0.10	0.11	0.08	0.06	0.11	0.13	0.08	0.55

Sázava suite (cont.)

Blatná suite

Sample	Po-1	Po-3	Po-4	Po-5	Ne-1	Ne-2	Mre-1	Mre-2	Koz-1	Koz-2	Koz-4	Koz-5	Koz-6	Koz-8	Koz-9	Koz-10
Ba	1024	1338	1284	1519	1029	1234	893	786	1490	1492	1135	1286	1289	1380	1681	1583
Rb	51	65	58	64	74	76	206	167	145	143	160	174	136	152	176	183
Sr	599	406	430	408	197	196	195	207	475	500	430	418	409	470	519	480
Zr	128	159	180	162	115	101	211	200	161	216	201	201	218	221	251	148
Nb	5	4	6	8	5	8	9	13	8	-	-	14	13	13	16	12
Ga	18	15	14	16	15	10	22	20	19	18	18	17	20	17	17	18
La	13	29	38	36	24	19	38	33	48	36	26	42	42	40	48	36
Ce	10	45	53	43	33	24	79	73	80	67	61	67	80	70	93	68
Y	11	8	7	5	15	13	18	23	33	24	20	22	30	20	23	22
U	b.d.	b.d.	b.d.	b.d.	b.d.	b.d.	b.d.	b.d.	b.d.	b.d.	b.d.	b.d.	b.d.	b.d.	b.d.	10
Th	b.d.	13	b.d.	b.d.	b.d.	12	24	15	19	24	21	20	17	21	19	28
Ni	b.d.	6	b.d.	b.d.	b.d.	b.d.	22	6	29	18	20	19	18	18	28	29
Co	b.d.	b.d.	4	4	b.d.	5	9	6	17	9	10	13	12	11	13	11
Pb	21	22	29	22	22	27	31	32	35	34	37	46	29	32	31	37
Zn	23	26	22	26	34	47	80	59	69	52	50	49	60	50	69	50
Cu	b.d.	b.d.	b.d.	b.d.	b.d.	b.d.	b.d.	b.d.	14	7	7	8	18	b.d.	6	8
Cr	15	32	16	121	88	b.d.	45	32	142	84	99	113	76	95	147	84
Rb/Sr	0.08	0.16	0.13	0.16	0.38	0.39	1.06	0.81	0.30	0.29	0.37	0.42	0.33	0.32	0.34	0.38

Appendix IV. Trace element geochemistry concentrations (ppm) (cont.) [XRF]

Blatná suite (cont.)

Sample	Koz-11	Koz-12	Koz-13	KozD1	Zal-1	Gbl-1	Gbl-2	Bl-1	Bl-2	Bl-3	Bl-4	Bl-5	Bl-6	Bl-7	Bl-8	BlD-1
Ba	1527	1154	1221	1175	2224	2329	1351	963	1204	1088	900	1136	956	928	1080	2016
Rb	182	173	214	187	221	154	171	199	185	167	190	190	184	175	147	169
Sr	458	385	349	379	510	540	218	333	413	443	348	387	389	338	361	486
Zr	156	211	139	146	251	62	77	177	188	188	171	209	163	149	169	159
Nb	14	11	13	9	16	11	7	12	12	9	13	12	16	18	14	9
Ga	19	16	20	20	19	18	14	21	23	21	19	21	23	20	b.d.	15
La	35	39	37	25	48	25	26	35	57	45	44	39	37	34	33	38
Ce	77	77	69	67	98	54	39	62	103	85	96	81	68	60	68	80
Y	24	17	17	27	26	20	25	14	12	24	19	33	21	25	34	32
U	10	b.d.	b.d.	b.d.	b.d.	b.d.	b.d.	b.d.	b.d.	b.d.	b.d.	b.d.	11	b.d.	b.d.	b.d.
Th	26	20	29	12	22	b.d.	b.d.	b.d.	14	b.d.	15	19	24	16	15	19
Ni	29	17	16	66	17	71	233	18	25	18	15	20	24	16	31	172
Co	18	12	10	20	25	37	57	8	11	12	10	9	8	7	12	36
Pb	42	36	46	42	31	19	12	40	24	34	41	27	44	43	24	25
Zn	58	52	50	85	85	85	59	63	79	72	58	72	62	54	51	85
Cu	15	b.d.	b.d.	37	b.d.	36	53	10	13	19	9	18	b.d.	4	11	4
Cr	170	57	52	171	198	496	1283	61	111	91	50	78	43	54	114	823
Rb/Sr	0.40	0.45	0.61	0.49	0.43	0.29	0.78	0.60	0.45	0.38	0.54	0.49	0.47	0.52	0.41	0.35

Blatná suite (cont.)

Čertovo břemeno suite

Sample	Cv-1	Cv-2	Cv-3	CvE-1	Kl-1	Kl-2	Mg-1	Mg-2	Se-1	Se-3	Se-4	Se-5	Se-6	Se-7	Se-8	Se-9
Ba	1149	1244	1181	728	1025	771	2288	1203	1079	1175	1204	1126	1115	1189	1058	1076
Rb	132	177	170	181	123	174	113	160	290	309	301	311	304	308	314	311
Sr	412	350	368	400	369	195	419	260	318	365	334	354	358	363	311	312
Zr	226	157	146	295	171	128	115	152	237	260	269	283	269	283	259	256
Nb	9	14	14	14	14	6	5	9	14	21	18	16	17	15	12	20
Ga	23	23	22	b.d.	22	18	13	18	20	22	20	20	20	20	18	19
La	54	36	35	21	37	35	42	87	35	41	47	42	40	43	42	44
Ce	115	82	69	52	66	58	49	76	75	85	105	103	84	95	102	97
Y	48	17	17	51	31	24	15	21	12	14	16	21	18	19	19	18
U	b.d.	b.d.	9	b.d.	b.d.	9	10	b.d.	b.d.	b.d.	b.d.	18	23	18	19	19
Th	14	12	b.d.	b.d.	16	29	23	23	24	23	25	23	22	22	25	25
Ni	24	24	38	80	19	16	b.d.	14	33	32	30	24	26	27	28	30
Co	15	16	16	25	15	7	5	7	10	11	14	12	12	14	11	8
Pb	17	27	34	17	35	55	27	38	53	59	54	70	68	68	65	68
Zn	74	79	84	111	71	52	46	58	55	59	56	58	50	58	57	53
Cu	5	7	8	42	11	b.d.	b.d.	b.d.	b.d.	12	18	16	14	13	11	9
Cr	75	147	131	182	60	66	16	76	168	149	152	160	132	146	185	166
Rb/Sr	0.32	0.50	0.46	0.45	0.33	0.89	0.27	0.62	0.91	0.85	0.90	0.88	0.85	0.85	1.01	1.00

Appendix IV. Trace element geochemistry concentrations (ppm) (cont.) [XRF]

Čertovo břemeno suite (cont.)

Sample	Se-10	Se-11	Se-12	Se-13	Se-14	Se-15	Se-16	SeE-1	Cb-1	Cb-2	Cb-3	Cb-4	Cb-5	Ta-1	Ta-2	Ta-3
Ba	1135	1020	1002	1044	1008	1084	1130	1072	1425	1232	2109	1363	1486	1797	2293	1747
Rb	280	297	293	286	372	354	273	322	431	367	360	375	213	355	321	354
Sr	335	328	312	300	250	302	319	311	401	330	495	343	366	418	500	423
Zr	266	274	259	240	315	229	249	258	291	294	405	282	299	390	305	405
Nb	14	19	16	11	11	19	19	19	19	18	23	18	23	13	11	19
Ga	18	19	18	19	20	19	22	18	19	20	20	18	23	19	20	20
La	33	34	37	39	38	41	31	39	45	37	49	46	35	54	50	44
Ce	77	85	74	97	98	104	78	93	121	88	123	95	87	121	107	100
Y	18	17	14	24	20	17	26	15	13	15	14	25	24	14	17	20
U	14	14	b.d.	19	b.d.	14	b.d.	9	9	10	9	21	12	b.d.	b.d.	b.d.
Th	20	18	15	24	29	35	28	29	29	33	39	48	25	27	18	27
Ni	27	28	27	27	46	45	43	30	66	63	135	115	66	59	61	68
Co	8	12	5	11	18	12	13	10	16	14	28	19	19	22	23	21
Pb	67	69	63	66	68	60	57	53	42	44	34	45	34	46	47	48
Zn	54	51	52	51	70	62	62	53	65	60	85	58	79	76	80	74
Cu	12	10	10	6	8	6	b.d.	7	12	17	25	10	4	23	24	10
Cr	134	146	122	171	256	157	126	202	335	302	498	364	271	425	473	396
Rb/Sr	0.84	0.91	0.94	0.95	1.49	1.17	0.86	1.03	1.08	1.11	0.73	1.09	0.58	0.85	0.64	0.84

Říčany suite

Sample	Mi-1	Mi-2	Ri-1	Ri-2	Ri-3	Ri-4	Ri-5	Ri-6	Ri-7	Ri-8	Ri-9	Ri-10	Ri-11	Ri-12	Ri-13	Ri-14
Ba	1578	2084	901	1015	816	1033	1038	1007	1231	910	936	812	792	803	805	811
Rb	409	350	320	346	334	336	331	333	329	303	285	346	349	336	331	332
Sr	355	350	378	372	365	373	398	381	433	367	372	314	312	312	311	313
Zr	372	544	240	246	239	246	219	238	268	224	224	214	193	196	215	217
Nb	20	-	21	12	15	15	15	15	15	17	15	15	16	18	17	15
Ga	18	18	24	24	26	23	24	25	23	22	22	24	25	23	23	23
La	60	50	29	27	29	28	21	23	35	32	26	22	30	25	22	27
Ce	139	153	57	65	173	b.d.	46	46	63	55	56	40	50	53	50	51
Y	19	26	b.d.	8	8	12	9	5	6	9	13	6	b.d.	2	b.d.	b.d.
U	15	24	b.d.	26	26	15	9	24	16	9	b.d.	24	b.d.	b.d.	b.d.	b.d.
Th	33	67	23	35	36	36	33	32	35	22	22	28	22	18	21	23
Ni	235	127	11	30	30	27	27	27	28	14	17	29	14	15	12	12
Co	28	30	b.d.	4	6	b.d.	12	6	5	b.d.	b.d.	b.d.	b.d.	b.d.	4	4
Pb	53	69	66	77	75	79	83	78	71	61	66	78	69	61	69	62
Zn	79	70	34	37	35	64	33	35	44	35	38	31	37	38	41	41
Cu	21	23	b.d.	b.d.	b.d.	b.d.	b.d.	b.d.	b.d.	6	b.d.	b.d.	b.d.	8	b.d.	b.d.
Cr	504	486	43	47	41	50	55	136	88	78	41	32	42	109	30	30
Rb/Sr	1.15	1.00	0.85	0.93	0.91	0.90	0.83	0.87	0.76	0.82	0.77	1.10	1.12	1.08	1.06	1.06

Appendix IV. Trace element geochemistry concentrations (ppm) (cont.) [XRF]

Říčany suite (cont.)

Sample	Ri-15	Ri-16	Ri-17	Ri-18	Ri-19	Ri-20	Ri-21	Ri-22	RiE-1	RiE-2	RiE-3	Je-1	Je-2	Je-3	Je-4	Je-5
Ba	941	856	864	634	665	634	470	427	864	800	514	920	832	968	839	952
Rb	358	305	321	332	328	440	386	374	352	338	280	255	225	263	227	187
Sr	296	331	327	294	293	212	209	193	299	312	299	577	510	508	521	734
Zr	237	213	225	187	187	163	159	166	389	263	314	149	137	164	139	94
Nb	17	20	13	15	14	14	17	15	26	18	20	20	20	14	18	13
Ga	23	25	23	25	23	25	24	24	23	21	26	24	23	24	23	23
La	25	31	28	25	33	113	22	19	40	32	42	26	25	23	27	17
Ce	49	62	59	47	35	38	42	35	b.d.	64	85	35	50	44	49	30
Y	b.d.	4	b.d.	7	8	9	b.d.	b.d.	11	8	17	8	12	7	8	4
U	b.d.	b.d.	b.d.	b.d.	b.d.	b.d.	b.d.	b.d.	12	b.d.	b.d.	20	b.d.	20	b.d.	b.d.
Th	27	26	25	22	17	25	23	19	77	42	38	36	31	42	30	19
Ni	15	14	18	15	15	36	8	11	78	60	39	16	b.d.	11	6	b.d.
Co	b.d.	5	3	3	3	5	3	b.d.	16	9	10	4	b.d.	3	b.d.	b.d.
Pb	59	66	65	64	60	92	62	59	51	55	45	88	76	94	75	66
Zn	49	40	38	45	43	50	41	46	57	51	88	33	18	26	22	26
Cu	5	4	7	b.d.	b.d.	b.d.	5	b.d.	b.d.	b.d.	b.d.	b.d.	b.d.	b.d.	b.d.	5
Cr	50	51	54	32	35	36	44	41	345	176	155	29	53	16	31	14
Rb/Sr	1.21	0.92	0.98	1.13	1.12	2.07	1.85	1.94	1.18	1.08	0.94	0.44	0.44	0.52	0.44	0.25

Country rocks (Teplá-Barrandian and Moldanubian units)

Sample	CR-1	CR-2	CR-3	CR-4	CR-5	CR-7	CR-8	CR-9	CR-10	CR-11	CR-12	CR-13
Ba	531	1268	285	947	619	581	899	658	459	548	527	848
Rb	110	128	53	44	160	118	217	100	32	125	98	182
Sr	121	161	209	726	86	275	610	149	212	163	136	158
Zr	161	195	307	179	121	195	105	154	104	190	193	182
Nb	14	16	14	10	14	16	7	15	4	16	16	16
Ga	19	31	11	18	27	25	20	16	12	19	15	28
La	19	21	12	37	33	23	12	19	8	19	17	21
Ce	56	66	39	104	84	66	34	56	32	56	41	64
Y	24	33	19	15	41	33	8	25	24	23	18	28
U	b.d.	11	b.d.	b.d.	9	b.d.	15	b.d.	b.d.	b.d.	b.d.	b.d.
Th	17	14	17	18	22	24	36	14	b.d.	16	14	17
Ni	39	52	8	47	44	39	b.d.	29	5	71	129	78
Co	19	17	5	18	22	22	b.d.	15	18	18	13	21
Pb	22	b.d.	25	15	26	29	61	14	14	26	25	34
Zn	95	14	22	55	98	132	28	82	68	89	56	123
Cu	42	b.d.	21	b.d.	77	32	b.d.	36	34	5	6	64
Cr	84	151	80	85	119	114	62	75	42	226	450	258
Rb/Sr	0.91	0.80	0.25	0.06	1.86	0.43	0.36	0.67	0.15	0.77	0.72	1.15

Appendix V. REE and other trace element concentrations (ppm)

[ICP-MS]

*Sázava suite**Blatná suite*

Sample	Sa-4	Sa-7	SaD-1	Po-1	Po-4	Mrc-1	Koz-2	Koz-6	Koz-12	KozD1	Zal-1	Gbl-1	Gbl-2
<i>REE (ppm)</i>													
<i>La</i>	21.7	20.8	20.0	11.6	26.2	28.5	35.0	34.8	32.7	25.9	43.9	27.7	26.0
<i>Ce</i>	71.8	42.0	46.8	18.0	39.0	64.4	64.4	68.3	58.4	58.3	94.3	60.3	54.1
<i>Pr</i>	6.9	5.0	6.1	1.8	3.9	8.2	7.9	8.2	7.3	7.8	11.7	7.7	7.1
<i>Nd</i>	29.7	17.4	23.5	5.4	11.5	28.8	27.5	29.4	24.9	28.6	45.5	29.2	26.0
<i>Sm</i>	6.2	3.8	5.9	1.4	1.8	5.7	5.7	6.0	4.9	5.9	10.0	7.0	6.4
<i>Eu</i>	1.5	1.8	2.0	1.3	1.0	1.1	1.5	1.6	1.3	1.5	2.5	2.2	1.6
<i>Gd</i>	6.1	3.8	6.2	1.1	1.4	4.8	4.7	5.3	4.3	4.9	8.4	7.0	5.8
<i>Tb</i>	0.9	0.6	1.0	0.1	0.2	0.6	0.7	0.8	0.6	0.7	1.0	0.7	0.8
<i>Dy</i>	5.8	2.7	5.1	0.6	0.8	2.6	3.5	4.1	3.1	3.4	5.6	3.7	4.2
<i>Ho</i>	1.0	0.6	1.1	0.1	0.1	0.4	0.6	0.7	0.6	0.6	1.0	0.7	0.8
<i>Er</i>	2.8	1.6	2.8	0.4	0.5	1.1	1.8	2.1	1.7	1.8	2.8	1.8	2.2
<i>Tm</i>	0.4	0.2	0.5	0.1	0.1	0.2	0.3	0.3	0.2	0.3	0.4	0.2	0.3
<i>Yb</i>	2.9	1.5	2.7	0.5	0.6	1.0	1.7	2.0	1.6	1.8	2.5	1.6	2.0
<i>Lu</i>	0.4	0.2	0.5	0.1	0.1	0.2	0.3	0.3	0.3	0.3	0.4	0.2	0.3
ΣREE	158.2	101.9	124.3	42.4	87.1	147.7	155.6	164.0	141.8	141.8	230.0	150.3	137.5
<i>Normalised to chondrite (Boynton, 1984)</i>													
<i>La_N</i>	69.9	67.0	64.6	37.3	84.5	92.0	113.0	112.2	105.5	83.7	141.6	89.4	83.8
<i>Ce_N</i>	88.8	52.0	57.9	22.3	48.2	79.7	79.7	84.5	72.3	72.1	116.7	74.7	67.0
<i>Pr_N</i>	56.9	40.6	50.3	14.4	32.2	67.5	64.9	67.6	59.5	63.7	96.2	63.4	58.0
<i>Nd_N</i>	49.5	29.1	39.2	9.0	19.1	48.0	45.8	49.0	41.5	47.7	75.8	48.6	43.3
<i>Sm_N</i>	32.0	19.3	30.2	7.2	9.1	29.3	29.1	31.0	25.4	30.2	51.1	36.1	32.7
<i>Eu_N</i>	20.4	24.1	26.9	17.5	14.3	14.9	21.0	21.2	17.0	20.2	33.7	30.3	22.2
<i>Gd_N</i>	23.5	14.5	24.0	4.3	5.2	18.6	18.2	20.6	16.4	19.0	32.3	27.2	22.5
<i>Tb_N</i>	19.3	11.8	21.3	2.7	3.4	12.7	13.7	15.8	12.3	14.8	22.1	15.7	17.0
<i>Dy_N</i>	18.0	8.4	15.7	2.0	2.5	8.0	10.7	12.6	9.6	10.6	17.4	11.6	12.9
<i>Ho_N</i>	14.3	7.8	15.2	1.5	2.0	5.9	8.9	10.3	7.8	8.8	13.9	9.1	10.9
<i>Er_N</i>	13.3	7.8	13.6	1.7	2.4	5.5	8.6	10.2	7.9	8.5	13.4	8.6	10.3
<i>Tm_N</i>	13.1	7.3	16.6	1.9	2.7	5.2	9.1	10.1	7.6	8.7	12.6	7.4	9.7
<i>Yb_N</i>	13.8	7.3	12.9	2.4	2.9	4.7	8.3	9.5	7.7	8.8	12.2	7.5	9.5
<i>Lu_N</i>	13.3	7.7	15.3	2.6	3.2	5.1	9.3	9.9	7.8	8.8	12.3	7.6	10.1
<i>Eu/Eu*</i>	0.7	1.4	1.0	3.2	2.1	0.6	0.9	0.8	0.8	0.8	0.8	1.0	0.8
<i>Ce_N/Yb_N</i>	6.4	7.2	4.5	9.2	16.6	17.0	9.6	8.9	9.4	8.2	9.6	9.9	7.1
<i>Other trace elements (ppm)</i>													
<i>Ga</i>	22.0	22.0	38.6	19.6	16.9	25.5	21.2	21.8	20.7	13.6	22.3	18.6	13.8
<i>Y</i>	33.5	20.6	5.8	5.9	6.7	16.3	24.0	29.6	23.2	14.9	34.5	24.0	27.0
<i>Nb</i>	8.1	9.1	3.2	3.6	6.4	10.1	15.2	15.8	14.7	8.3	20.3	12.1	10.4
<i>Cs</i>	5.7	6.6	2.3	3.0	3.0	14.5	9.9	6.8	13.0	21.3	17.7	7.8	13.1
<i>Ta</i>	0.5	0.6	1.1	0.3	0.2	1.0	1.2	0.7	1.1	1.5	1.1	0.7	0.8
<i>Hf</i>	2.5	3.6	1.8	4.2	5.4	5.4	5.8	6.1	7.2	4.7	13.3	4.3	5.0

Appendix V. REE and other trace element concentrations (ppm)
[ICP-MS]

Blatná suite (cont.)

Čertovo břemeno suite

Sample	Bl-2	Bl-4	Bl-7	Bl-8	Cv-1	Se-1	Se-5	Se-9	Se-15	Cb-3	Ta-1	Mi-1
<i>REE (ppm)</i>												
La	55.2	39.8	33.1	42.9	45.6	109.3	43.9	44.2	44.5	44.8	54.0	52.6
Ce	111.1	80.9	66.2	94.6	99.6	741.2	91.8	92.3	96.8	110.2	125.3	119.1
Pr	12.7	9.6	8.0	11.9	12.4	20.6	11.5	11.7	11.5	15.5	17.0	15.8
Nd	42.5	31.6	26.7	43.3	44.9	63.0	40.8	42.1	39.9	61.7	62.8	58.8
Sm	7.2	5.6	5.5	9.4	9.8	10.4	8.4	8.8	8.3	14.6	13.7	13.8
Eu	1.7	1.2	1.2	1.9	1.7	2.1	1.7	1.8	1.7	3.5	2.9	3.4
Gd	5.9	4.7	4.7	8.2	9.2	12.4	6.2	6.4	6.6	10.7	10.7	10.0
Tb	0.7	0.6	0.7	1.2	1.2	1.1	0.8	0.9	0.8	1.2	1.2	1.1
Dy	3.4	3.1	3.4	5.8	6.6	4.5	3.9	4.1	4.0	5.8	5.9	5.1
Ho	0.5	0.5	0.6	1.1	1.2	0.7	0.7	0.7	0.6	0.9	1.0	0.8
Er	1.4	1.6	1.8	2.9	3.2	2.0	1.9	2.0	1.7	2.5	2.6	2.3
Tm	0.2	0.3	0.3	0.5	0.4	0.3	0.3	0.3	0.2	0.3	0.3	0.3
Yb	1.2	1.8	1.8	2.7	2.6	1.9	1.7	1.9	1.6	2.1	2.1	1.9
Lu	0.2	0.3	0.3	0.4	0.3	0.3	0.3	0.3	0.2	0.3	0.3	0.3
ΣREE	244.0	181.7	154.0	226.7	238.5	969.9	213.9	217.4	218.6	274.2	299.9	285.3
<i>Normalised to chondrite (Boynton, 1984)</i>												
La _N	178.2	128.4	106.7	138.5	147.1	352.7	141.6	142.4	143.5	144.5	174.2	169.7
Ce _N	137.6	100.2	81.9	117.1	123.2	917.4	113.6	114.3	119.8	136.4	155.1	147.4
Pr _N	104.3	78.7	65.8	97.2	101.3	169.2	94.4	95.9	94.6	127.1	139.5	129.9
Nd _N	70.9	52.7	44.5	72.2	74.8	105.0	68.1	70.2	66.6	102.9	104.7	97.9
Pm _N	53.8	40.7	36.3	60.2	62.5	79.1	55.6	57.8	54.7	89.0	87.6	84.4
Sm _N	36.8	28.7	28.1	48.2	50.2	53.2	43.2	45.3	42.8	75.0	70.5	70.8
Eu _N	22.7	16.8	15.7	26.2	22.9	29.2	23.2	24.6	23.2	47.0	39.8	46.2
Gd _N	22.7	18.1	18.1	31.8	35.5	47.8	24.0	24.7	25.5	41.5	41.3	38.5
Tb _N	14.9	12.4	13.8	24.6	25.6	22.2	17.0	18.2	16.4	25.0	25.9	23.2
Dy _N	10.4	9.6	10.5	18.0	20.4	14.0	12.2	12.6	12.3	18.0	18.4	15.9
Ho _N	7.5	7.2	8.6	14.7	16.3	9.9	9.2	9.8	8.7	12.9	13.3	11.0
Er _N	6.9	7.8	8.4	13.7	15.1	9.7	9.0	9.7	8.2	12.1	12.2	10.8
Tm _N	6.7	7.9	8.0	14.3	13.3	9.0	8.5	8.7	7.7	10.2	10.5	9.5
Yb _N	5.9	8.7	8.4	12.8	12.2	9.1	8.3	9.0	7.6	10.0	10.0	9.2
Lu _N	5.3	8.8	8.8	12.6	10.3	8.6	8.0	9.0	7.6	8.9	9.5	8.6
Eu/Eu*	0.8	0.7	0.7	0.7	0.5	0.6	0.7	0.7	0.7	0.8	0.7	0.9
Ce _N /Yb _N	23.2	11.5	9.8	9.2	10.1	100.7	13.7	12.7	15.7	13.6	15.5	16.0
<i>Other trace elements (ppm)</i>												
Ga	26.6	23.8	23.3	24.8	24.2	25.3	24.2	22.4	22.0	23.9	23.2	22.2
Y	21.2	22.4	25.8	33.4	46.3	26.7	26.9	26.9	26.6	32.7	33.3	29.0
Nb	17.2	14.8	16.7	17.0	16.0	25.0	27.9	24.7	26.2	33.6	20.4	31.3
Ce	12.2	18.8	17.4	8.5	6.4	30.0	51.6	31.7	48.9	27.0	23.7	55.5
Ta	1.4	1.4	1.7	1.5	1.0	2.4	2.9	2.4	4.4	1.8	1.7	2.2
Hf	3.8	6.3	9.9	4.5	3.3	6.7	8.5	9.1	6.7	12.8	4.3	10.8

Appendix V. REE and other trace element concentrations (ppm)
[ICP-MS]

Říčany suite

Sample	Ri-1	Ri-2	Ri-6	Je-3
REE (ppm)				
La	18.2	34.1	18.1	11.3
Ce	35.4	68.3	40.1	24.3
Pr	4.2	8.6	4.9	3.0
Nd	15.2	27.2	16.4	9.5
Sm	2.9	5.3	3.4	2.0
Eu	0.7	1.1	0.9	0.7
Gd	2.1	3.5	2.5	1.4
Tb	0.3	0.4	0.3	-
Dy	1.3	2.0	1.4	0.8
Ho	0.2	0.3	0.2	0.1
Er	0.6	0.9	0.7	0.4
Tm	0.1	0.1	0.1	0.1
Yb	0.6	0.9	0.6	0.4
Lu	0.1	0.1	0.1	0.1
ΣREE	81.9	152.9	89.7	54.7
Normalised to chondrite				
La _N	58.8	109.9	58.3	36.3
Ce _N	43.8	84.5	49.6	30.1
Pr _N	34.6	70.4	40.2	24.3
Nd _N	25.4	45.4	27.3	15.9
Pm _N	20.2	36.3	22.4	13.1
Sm _N	15.0	27.2	17.6	10.4
Eu _N	10.2	14.4	12.3	9.1
Gd _N	8.0	13.5	9.8	5.4
Tb _N	5.4	9.1	6.0	-
Dy _N	3.9	6.2	4.3	2.5
Ho _N	3.0	4.5	3.2	1.9
Er _N	2.8	4.1	3.1	1.9
Tm _N	2.6	4.1	3.1	2.1
Yb _N	2.9	4.2	3.0	1.8
Lu _N	2.8	3.9	2.8	2.3
Eu/Eu*	0.9	0.8	0.9	1.2
Ce _N /Yb _N	15.0	20.0	16.4	16.5
Other trace elements (ppm)				
Ga	25.2	26.6	27.8	24.4
Y	11.2	13.8	12.2	7.7
Nb	21.8	22.4	21.5	20.3
Cs	66.0	55.3	56.7	13.7
Ta	2.3	2.5	2.8	1.4
Hf	8.8	8.4	6.9	6.8

<p>Appendices VI.-VIII. Mineral chemistry, the Central Bohemian Pluton</p>

Appendix VI. Feldspars

Appendix VII. Biotites

Appendix VIII. Amphiboles

In Appendices VI.-VIII. are presented raw microprobe data (wt %), together with recalculated values corresponding to mineral formulae; for details about these calculations see Chapter III. In the brief descriptions of the analysed grains, arrows were used to indicate a succession of analyses towards the core of the grain. Some abbreviations were also used, both for the mineral phases (plag, plg = plagioclase, bi, biot = biotite, amph = amphibole, px = pyroxene, carb = carbonate), as well as descriptive ones (C = core, R = rim, UZ = unzoned, phenoX = phenocryst).

Appendix VI. Composition of feldspars
(Structural formulae calculated on basis of 8 oxygens)

Sázava suite

Sa-3													
	plag 1	plag 3	plag 2	plag 4	plag 5	plag 6	plag 7	plag 8	plag 10	plag 9	plag 11	plag 12	
	large convolut. zoning		small unzoned		small unzoned		small unzoned		large zoned plagioclase		small in amph		
	large	convolut.	zoning	small	unzoned	small	unzoned	large	zoned	plagioclase	small	in amph	
SiO ₂	53.92	54.65	53.41	54.57	56.83	56.00	54.65	53.79	53.74	53.00	55.82	54.84	
TiO ₂	0.09	0.00	0.00	0.07	0.01	0.00	0.02	0.00	0.03	0.04	0.00	0.02	
Al ₂ O ₃	29.29	29.06	29.48	28.95	27.30	28.22	28.75	29.47	29.29	29.50	28.11	28.53	
FeO	0.10	0.09	0.09	0.13	0.18	0.06	0.10	0.09	0.09	0.12	0.11	0.10	
CaO	10.59	10.22	11.27	10.22	8.34	9.24	10.12	10.99	10.56	11.30	9.42	9.93	
Na ₂ O	5.51	5.73	5.05	5.76	6.70	6.23	5.63	5.28	5.28	5.00	6.16	5.80	
K ₂ O	0.11	0.16	0.12	0.16	0.17	0.12	0.13	0.17	0.13	0.15	0.16	0.13	
Σ	99.60	99.91	99.43	99.86	99.52	99.87	99.41	99.78	99.13	99.10	99.78	99.34	
Si	2.443	2.465	2.426	2.464	2.559	2.517	2.475	2.434	2.444	2.418	2.514	2.485	
Ti	0.003	0.000	0.000	0.002	0.000	0.000	0.001	0.000	0.001	0.001	0.000	0.001	
Al	1.564	1.545	1.579	1.541	1.449	1.496	1.535	1.573	1.570	1.586	1.493	1.524	
Fe	0.004	0.003	0.004	0.005	0.007	0.002	0.004	0.003	0.003	0.005	0.004	0.004	
Ca	0.514	0.494	0.549	0.495	0.403	0.445	0.491	0.533	0.515	0.552	0.455	0.482	
Na	0.484	0.501	0.445	0.504	0.585	0.543	0.494	0.464	0.466	0.442	0.538	0.509	
K	0.006	0.009	0.007	0.009	0.010	0.007	0.007	0.010	0.007	0.009	0.009	0.007	
Σ	5.018	5.017	5.010	5.020	5.013	5.010	5.007	5.017	5.006	5.013	5.013	5.012	
An	50.27	48.36	54.27	48.23	39.80	44.10	48.90	52.14	51.40	54.32	44.84	47.68	
Ab	47.33	49.05	43.99	49.11	57.78	53.81	49.20	45.39	46.51	43.50	53.02	50.35	
Or	0.59	0.88	0.69	0.88	0.99	0.69	0.70	0.98	0.70	0.89	0.89	0.69	

Appendix VI. Composition of feldspars (cont.)
(Structural formulae calculated on basis of 8 oxygens)
Sázava suite (cont.)

	Sa-10											Sa-7			
	plag17*	plag 1	plag 2	plag 3	plag 4	plag 6	plag 7	plag 8	KF3	KF4	KF5	plag8*	plag9*	plag16*	
	core, large	mantled (CL)			mantled (CL)			unznd core	unznd core	interstitial			large, core	small, core	large, core
SiO2	57.89	56.68	54.65	52.12	57.34	44.88	56.69	57.00	61.30	62.03	61.46	55.41	55.84	55.37	
TiO2	0.06	0.00	0.00	0.00	0.00	0.00	0.00	0.01	0.01	0.00	0.00	0.00	0.01	0.00	
Al2O3	27.82	27.53	28.06	29.91	26.72	35.23	27.62	27.84	19.65	19.76	19.39	27.90	26.90	27.36	
FeO	0.71	0.25	0.12	0.18	0.10	0.20	0.12	0.14	0.10	0.04	0.03	0.16	0.26	0.25	
CaO	9.18	7.55	8.63	10.63	6.89	16.17	7.69	8.04	0.00	0.05	0.00	10.11	9.50	9.92	
Na2O	6.48	7.19	6.53	5.50	7.74	2.26	7.07	7.18	1.21	1.32	0.75	5.49	5.80	5.67	
K2O	0.22	0.23	0.20	0.13	0.10	0.02	0.21	0.14	14.88	14.91	15.78	0.21	0.21	0.24	
Σ	102.35	99.43	98.19	98.47	98.89	98.76	99.40	100.35	97.15	98.11	97.41	99.27	98.53	98.80	
Si	2.543	2.555	2.502	2.395	2.592	2.090	2.554	2.547	2.917	2.921	2.926	2.510	2.545	2.519	
Ti	0.002	0.000	0.000	0.000	0.000	0.000	0.000	0.000	0.000	0.000	0.000	0.000	0.000	0.000	
Al	1.441	1.463	1.515	1.620	1.424	1.934	1.467	1.467	1.102	1.097	1.088	1.490	1.445	1.467	
Fe	0.026	0.009	0.005	0.007	0.004	0.008	0.005	0.005	0.004	0.002	0.001	0.006	0.010	0.010	
Ca	0.432	0.365	0.423	0.523	0.334	0.807	0.371	0.385	0.000	0.003	0.000	0.491	0.464	0.484	
Na	0.552	0.628	0.580	0.490	0.678	0.204	0.618	0.622	0.112	0.121	0.069	0.482	0.513	0.500	
K	0.012	0.013	0.012	0.008	0.006	0.001	0.012	0.008	0.903	0.896	0.958	0.012	0.012	0.014	
Σ	5.008	5.033	5.037	5.043	5.038	5.044	5.027	5.034	5.038	5.040	5.042	4.991	4.989	4.994	
An	42.98	35.15	40.36	49.31	31.83	75.67	36.00	36.86	0.00	0.29	0.00	49.10	46.15	47.91	
Ab	54.92	60.48	55.35	46.20	64.61	19.13	59.97	59.56	10.73	11.56	6.55	48.20	51.02	49.49	
Or	1.19	1.25	1.15	0.75	0.57	0.09	1.16	0.77	86.50	85.61	90.98	1.20	1.19	1.39	

Appendix VI. Composition of feldspars (cont.)
(Structural formulae calculated on basis of 8 oxygens)
Sázava suite (cont.)

	Sa-7										SaD-1					
	plag 17	plag 18	plag 19	plag 20	plag 21	plag 22	plag 23	plag 24								
	small, core	large, core	large, core	large, core	large, core	small, core	small unzoned		plag 1	plag 3	plag 2	plag 4	plag 5	plag 6		
SiO ₂	55.24	55.68	54.50	55.54	52.08	55.78	55.33	55.12	44.53	49.61	55.28	56.64	55.17	46.69		
TiO ₂	0.06	0.02	0.04	0.04	0.00	0.00	0.00	0.06	0.00	0.00	0.00	0.02	0.03	0.00		
Al ₂ O ₃	27.33	27.12	27.87	27.30	29.41	27.60	27.33	27.11	34.99	31.85	27.41	27.33	27.91	33.07		
FeO	0.20	0.12	0.19	0.18	0.19	0.17	0.15	0.12	0.13	0.26	0.12	0.05	0.04	0.17		
CaO	9.70	9.43	10.36	9.71	12.26	9.45	9.64	9.72	17.98	14.52	9.63	9.18	9.96	16.25		
Na ₂ O	5.80	5.85	5.48	5.73	4.48	5.87	5.68	5.98	1.21	3.34	6.03	6.25	5.73	2.15		
K ₂ O	0.25	0.18	0.17	0.17	0.12	0.17	0.22	0.19	0.02	0.06	0.15	0.15	0.17	0.02		
Σ	98.56	98.38	98.61	98.68	98.53	99.04	98.35	98.29	98.86	99.64	98.62	99.62	99.01	98.35		
Si	2.521	2.535	2.484	2.527	2.396	2.526	2.526	2.522	2.077	2.273	2.521	2.550	2.506	2.178		
Ti	0.002	0.001	0.001	0.001	0.000	0.000	0.000	0.002	0.000	0.000	0.000	0.001	0.001	0.000		
Al	1.470	1.455	1.498	1.464	1.595	1.474	1.471	1.462	1.924	1.720	1.474	1.450	1.495	1.819		
Fe	0.008	0.005	0.007	0.007	0.007	0.006	0.006	0.005	0.005	0.010	0.005	0.002	0.002	0.007		
Ca	0.474	0.460	0.506	0.473	0.604	0.458	0.472	0.476	0.899	0.713	0.471	0.443	0.485	0.812		
Na	0.513	0.516	0.484	0.506	0.399	0.515	0.503	0.530	0.109	0.297	0.533	0.546	0.505	0.194		
K	0.014	0.010	0.010	0.010	0.007	0.010	0.013	0.011	0.001	0.004	0.009	0.009	0.010	0.001		
Σ	5.002	4.982	4.990	4.988	5.008	4.989	4.991	5.008	5.015	5.017	5.013	5.001	5.004	5.011		
An	47.24	46.00	50.33	47.30	59.65	45.80	47.20	46.61	87.75	69.59	46.24	44.28	48.33	80.06		
Ab	51.13	51.60	48.14	50.60	39.41	51.50	50.30	51.90	10.64	28.99	52.32	54.58	50.32	19.13		
Or	1.40	1.00	1.00	1.00	0.69	1.00	1.30	1.08	0.10	0.39	0.88	0.90	1.00	0.10		

Appendix VI. Composition of feldspars (cont.)
(Structural formulae calculated on basis of 8 oxygens)
Sázava suite (cont.)

	SaD-1														
	plag 7	plag 8	plag 9	plag 10	plag 11	plag 12	plag 13	plag 14	plag 15	plag 16	plag 17	plag 18	plag 19	plag 20	
 →			→			mantled (CL)			mantled (CL), plag 16 dull 17+18 brighter			→		
	(contd.)												small unzoned		
SiO ₂	44.26	44.49	55.11	55.18	45.71	44.62	44.79	54.99	47.48	54.40	51.32	45.21	55.98	55.97	
TiO ₂	0.01	0.00	0.04	0.04	0.00	0.06	0.00	0.04	0.05	0.01	0.00	0.01	0.00	0.00	
Al ₂ O ₃	35.06	34.78	28.16	27.76	34.42	35.17	35.00	28.17	33.43	28.12	30.80	34.08	27.71	27.94	
FeO	0.12	0.20	0.20	0.12	0.09	0.21	0.17	0.11	0.12	0.14	0.07	0.07	0.14	0.14	
CaO	18.07	17.74	10.01	9.73	17.42	18.09	18.06	9.98	16.20	9.97	12.84	17.63	9.80	9.89	
Na ₂ O	1.20	1.49	5.92	5.88	1.73	1.36	1.33	5.66	2.40	5.83	4.36	1.38	5.99	5.84	
K ₂ O	0.03	0.03	0.10	0.22	0.03	0.03	0.03	0.14	0.04	0.08	0.04	0.02	0.14	0.12	
Σ	98.75	98.73	99.54	98.93	99.40	99.54	99.38	99.09	99.72	98.55	99.43	98.40	99.76	99.90	
Si	2.068	2.080	2.494	2.509	2.117	2.070	2.080	2.496	2.183	2.486	2.344	2.115	2.523	2.518	
Ti	0.000	0.000	0.001	0.001	0.000	0.002	0.000	0.001	0.002	0.000	0.000	0.000	0.000	0.000	
Al	1.931	1.917	1.502	1.488	1.879	1.924	1.916	1.508	1.812	1.515	1.658	1.880	1.472	1.482	
Fe	0.005	0.008	0.008	0.005	0.003	0.008	0.007	0.004	0.005	0.005	0.003	0.003	0.005	0.005	
Ca	0.905	0.889	0.485	0.474	0.865	0.899	0.899	0.485	0.798	0.488	0.628	0.884	0.473	0.477	
Na	0.109	0.135	0.519	0.518	0.155	0.122	0.120	0.498	0.214	0.517	0.386	0.125	0.524	0.509	
K	0.002	0.002	0.006	0.013	0.002	0.002	0.002	0.008	0.002	0.005	0.002	0.001	0.008	0.007	
Σ	5.020	5.031	5.015	5.008	5.021	5.027	5.024	5.000	5.016	5.016	5.021	5.008	5.005	4.998	
An	87.33	84.47	47.53	46.80	83.20	85.76	86.41	48.50	77.63	47.73	60.83	87.12	46.95	47.70	
Ab	10.52	12.83	50.86	51.15	14.91	11.64	11.53	49.80	20.82	50.56	37.39	12.32	52.01	50.90	
Or	0.19	0.19	0.59	1.28	0.19	0.19	0.19	0.80	0.20	0.49	0.19	0.10	0.79	0.70	

Appendix VI. Composition of feldspars (cont.)
(Structural formulae calculated on basis of 8 oxygens)
Sázava suite (cont.)

	P0-1										P0-3					
	plag 1	plag 2	plag 3	plag 4	plag 5	plag 6	plag 7	plag 9	plag 8		plag 1	plag 2	plag 3	plag 4	plag 5	
	mantled plagioclase			small unzoned, 4-5 cores, 6 rim			small oscillatory zoned				mantled (CL)					unzoned core
SiO2	57.09	54.98	53.29	57.16	53.57	55.53	59.06	56.01	53.76		60.57	58.48	54.84	55.31	59.65	
TiO2	0.00	0.02	0.00	0.04	0.00	0.10	0.05	0.00	0.06		0.03	0.00	0.00	0.01	0.00	
Al2O3	26.95	28.33	29.79	27.01	29.49	28.78	26.10	28.23	29.39		25.92	25.57	28.87	29.00	26.50	
FeO	0.13	0.10	0.20	0.17	0.11	0.25	0.12	0.09	0.15		0.05	0.10	0.07	0.06	0.19	
CaO	8.04	10.00	11.29	8.10	11.08	9.71	6.64	9.32	10.68		5.90	6.84	9.89	9.78	6.83	
Na2O	6.82	5.75	5.06	6.68	5.20	5.87	7.34	5.90	5.30		8.30	7.63	5.92	6.00	7.65	
K2O	0.15	0.20	0.16	0.26	0.12	0.18	0.24	0.21	0.20		0.13	0.40	0.24	0.16	0.41	
Σ	99.18	99.37	99.79	99.41	99.56	100.41	99.55	99.77	99.53		100.90	99.02	99.83	100.32	101.23	
Si	2.577	2.491	2.415	2.575	2.430	2.488	2.642	2.519	2.438		2.670	2.640	2.480	2.480	2.630	
Ti	0.000	0.001	0.000	0.001	0.000	0.003	0.002	0.000	0.002		0.000	0.000	0.000	0.000	0.000	
Al	1.434	1.513	1.592	1.434	1.577	1.521	1.376	1.497	1.572		1.350	1.360	1.540	1.530	1.380	
Fe	0.005	0.004	0.008	0.006	0.004	0.009	0.005	0.003	0.006		0.000	0.000	0.000	0.000	0.010	
Ca	0.389	0.486	0.548	0.391	0.538	0.466	0.318	0.449	0.519		0.280	0.330	0.480	0.470	0.320	
Na	0.597	0.505	0.445	0.583	0.457	0.510	0.637	0.515	0.466		0.710	0.670	0.520	0.520	0.650	
K	0.009	0.012	0.009	0.015	0.007	0.010	0.014	0.012	0.011		0.010	0.020	0.010	0.010	0.020	
Σ	5.011	5.012	5.017	5.005	5.013	5.007	4.994	4.995	5.014		5.020	5.020	5.030	5.010	5.010	
An	38.62	47.98	53.84	39.09	52.97	46.53	31.80	44.90	51.25		27.53	31.94	46.36	46.02	31.76	
Ab	59.26	49.86	43.72	58.28	45.00	50.92	63.70	51.50	46.02		69.96	64.46	50.24	51.11	64.30	
Or	0.89	1.19	0.88	1.50	0.69	1.00	1.40	1.20	1.09		0.69	2.22	1.36	0.88	2.26	

Appendix VI. Composition of feldspars (cont.)
(Structural formulae calculated on basis of 8 oxygens)
Sázava suite (cont.)

Po-3															
	plag 6	plag 7	plag 8	plag 9	plag 10	plag 11	plag 12	plag 15	plag 16	plag 17	plag 20	KF1	KF2 interstitial	KF3	
	mantled (CL)			large unzoned			zoned			zoned			interstitial		
	→	→	→	→	→	→	→	→	→	→	→	→	→	→	→
SiO ₂	57.95	57.37	53.32	61.06	57.76	57.48	57.68	59.05	55.07	57.46	50.28	64.21	63.61	63.33	
TiO ₂	0.00	0.07	0.07	0.05	0.02	0.07	0.02	0.00	0.00	0.02	0.10	0.00	0.02	0.03	
Al ₂ O ₃	26.69	27.30	30.08	23.64	26.28	26.24	26.01	25.27	28.12	26.14	30.38	19.64	19.47	18.78	
FeO	0.16	0.11	0.11	0.06	0.13	0.13	0.13	0.07	0.18	0.03	0.06	0.05	0.05	0.07	
CaO	6.95	7.54	10.77	3.38	7.46	7.66	7.23	6.46	9.70	7.78	13.11	0.04	0.00	0.04	
Na ₂ O	7.56	7.17	4.48	8.70	7.10	6.96	7.13	7.73	6.13	6.84	3.95	1.24	0.91	1.13	
K ₂ O	0.31	0.29	0.14	0.31	0.21	0.29	0.23	0.25	0.27	0.66	0.08	15.70	16.15	15.05	
Σ	99.62	99.85	98.97	97.20	98.96	98.83	98.43	98.83	99.47	98.93	97.96	100.88	100.21	98.43	
Si	2.600	2.570	2.420	2.771	2.609	2.602	2.617	2.663	2.496	2.603	2.333	2.950	2.940	2.970	
Ti	0.000	0.000	0.000	0.002	0.001	0.002	0.001	0.000	0.000	0.001	0.003	0.000	0.000	0.000	
Al	1.410	1.440	1.610	1.265	1.399	1.400	1.391	1.343	1.502	1.396	1.662	1.060	1.060	1.040	
Fe	0.010	0.000	0.000	0.002	0.005	0.005	0.005	0.003	0.007	0.001	0.002	0.000	0.000	0.000	
Ca	0.330	0.360	0.530	0.164	0.361	0.372	0.352	0.312	0.471	0.378	0.652	0.000	0.000	0.000	
Na	0.660	0.620	0.400	0.765	0.622	0.611	0.627	0.676	0.539	0.601	0.355	0.110	0.080	0.100	
K	0.020	0.020	0.010	0.018	0.012	0.017	0.013	0.014	0.016	0.038	0.005	0.920	0.950	0.900	
Σ	5.030	5.010	4.970	4.987	5.009	5.009	5.006	5.011	5.031	5.018	5.012	5.040	5.030	5.010	
An	32.22	35.21	52.50	16.40	35.89	36.83	35.11	30.84	45.10	36.81	63.81	0.19	0.00	0.20	
Ab	63.48	60.60	39.50	76.50	61.84	60.50	62.53	66.82	51.61	58.53	34.74	10.48	7.77	10.15	
Or	1.74	1.65	0.80	1.80	1.19	1.68	1.30	1.38	1.53	3.70	0.49	87.56	90.33	88.66	

Appendix VI. Composition of feldspars (cont.)
(Structural formulae calculated on basis of 8 oxygens)

Blatná suite

Koz-2														
	plag 1	plag 2	plag 3	plag 4	plag 5	plag 6	plag 7	plag 8	plag 9	plag 10	plag 11	plag 12	plag 13	KF1
	discontinuously zoned			oscillatory zoned			unzoned			unzoned			unzoned core	interstitial
	→	→	→	←	←	←	→	→	→	→	→	→	→	→
SiO ₂	61.22	58.13	57.41	58.08	56.41	57.23	60.35	64.85	56.32	54.13	57.33	58.14	58.24	63.39
TiO ₂	0.02	0.01	0.04	0.00	0.02	0.00	0.00	0.00	0.00	0.04	0.02	0.05	0.00	0.00
Al ₂ O ₃	25.05	27.27	27.74	27.34	28.74	27.91	25.55	22.92	28.66	29.96	27.78	27.22	27.38	19.28
FeO	0.04	0.16	0.18	0.23	0.09	0.05	0.10	0.15	0.08	0.06	0.18	0.01	0.06	0.02
CaO	5.26	7.68	8.25	7.77	9.18	8.29	5.86	3.31	9.26	10.49	8.35	7.72	7.74	0.00
Na ₂ O	8.55	7.11	6.65	6.95	6.17	6.84	8.28	9.52	6.36	5.53	6.71	6.98	7.09	0.63
K ₂ O	0.20	0.28	0.27	0.22	0.19	0.21	0.24	0.13	0.16	0.11	0.21	0.23	0.16	15.72
Σ	100.34	100.64	100.54	100.59	100.80	100.53	100.38	100.88	100.84	100.32	100.58	100.35	100.67	99.04
Si	2.708	2.585	2.558	2.583	2.511	2.551	2.676	2.832	2.509	2.432	2.554	2.589	2.585	2.956
Ti	0.001	0.000	0.001	0.000	0.001	0.000	0.000	0.000	0.000	0.001	0.001	0.002	0.000	0.000
Al	1.306	1.429	1.457	1.433	1.508	1.466	1.336	1.180	1.505	1.587	1.459	1.429	1.433	1.060
Fe	0.001	0.006	0.007	0.009	0.003	0.002	0.004	0.005	0.003	0.002	0.007	0.000	0.002	0.001
Ca	0.249	0.366	0.394	0.370	0.438	0.396	0.278	0.155	0.442	0.505	0.399	0.368	0.368	0.000
Na	0.733	0.613	0.575	0.599	0.533	0.591	0.712	0.806	0.549	0.482	0.580	0.603	0.610	0.057
K	0.011	0.016	0.015	0.012	0.011	0.012	0.014	0.007	0.009	0.006	0.012	0.013	0.009	0.935
Σ	5.009	5.015	5.007	5.006	5.005	5.018	5.020	4.985	5.017	5.015	5.012	5.004	5.007	5.009
An	24.70	36.13	39.40	37.00	43.80	38.84	27.21	15.50	43.35	49.64	39.59	36.80	36.69	0.00
Ab	72.71	60.50	57.50	59.90	53.30	57.96	69.69	80.60	53.85	47.38	57.55	60.30	60.81	5.66
Or	1.09	1.58	1.50	1.20	1.10	1.18	1.37	0.70	0.88	0.59	1.19	1.30	0.90	92.87

Appendix VI. Composition of feldspars (cont.)
(Structural formulae calculated on basis of 8 oxygens)
Blatná suite (cont.)

Koz-2		Koz-4													
	KF2 pheno- crist	KF3 pheno- crist	plag 1	plag 2	plag 4	plag 5	plag 6	plag 7	plag 8	plag 9	plag 10	KF1 phenoX core	KF2 phenoX rim	Kf3 small core	
			unzoned					zoned				unzoned			
SiO2	62.56	63.37	58.84	54.01	60.69	60.24	57.02	56.65	57.97	60.80	57.12	63.01	63.24	64.15	
TiO2	0.00	0.08	0.00	0.07	0.00	0.09	0.00	0.02	0.03	0.00	0.03	0.00	0.00	0.00	
Al2O3	19.71	19.51	26.03	29.48	24.87	25.09	27.40	27.38	26.44	24.66	27.44	19.35	18.87	19.51	
FeO	0.09	0.05	0.03	0.22	0.11	0.20	0.08	0.11	0.13	0.12	0.15	0.09	0.15	0.10	
CaO	0.07	0.03	7.08	10.94	5.99	6.04	8.65	8.60	8.03	5.88	8.70	0.04	0.00	0.25	
Na2O	1.80	1.27	7.76	5.29	8.28	7.90	6.39	6.30	7.04	8.21	6.57	1.05	0.50	2.12	
K2O	13.67	14.75	0.08	0.18	0.12	0.32	0.20	0.26	0.12	0.30	0.22	14.93	16.02	13.14	
Σ	97.90	99.06	99.82	100.19	100.06	99.88	99.74	99.32	99.76	99.97	100.23	98.47	98.78	99.27	
Si	2.934	2.946	2.631	2.436	2.698	2.685	2.561	2.556	2.600	2.706	2.556	2.950	2.964	2.956	
Ti	0.000	0.003	0.000	0.002	0.000	0.003	0.000	0.001	0.001	0.000	0.001	0.000	0.000	0.000	
Al	1.090	1.069	1.372	1.567	1.303	1.318	1.451	1.456	1.398	1.294	1.448	1.068	1.043	1.060	
Fe	0.004	0.002	0.001	0.008	0.004	0.007	0.003	0.004	0.005	0.004	0.006	0.004	0.006	0.004	
Ca	0.004	0.001	0.339	0.529	0.285	0.288	0.416	0.416	0.386	0.280	0.417	0.002	0.000	0.012	
Na	0.164	0.114	0.673	0.463	0.714	0.683	0.556	0.551	0.612	0.708	0.570	0.095	0.045	0.189	
K	0.818	0.875	0.005	0.010	0.007	0.018	0.011	0.015	0.007	0.017	0.013	0.892	0.958	0.773	
Σ	5.014	5.010	5.021	5.015	5.011	5.002	4.998	4.999	5.009	5.009	5.011	5.011	5.016	4.994	
An	0.40	0.10	32.89	52.02	28.14	28.80	41.60	41.60	38.17	27.70	41.26	0.20	0.00	1.20	
Ab	16.29	11.31	65.29	45.53	70.49	68.30	55.60	55.10	60.53	70.05	56.40	9.45	4.43	18.90	
Or	81.25	86.82	0.49	0.98	0.69	1.80	1.10	1.50	0.69	1.68	1.29	88.75	94.37	77.30	

Appendix VI. Composition of feldspars (cont.)
(Structural formulae calculated on basis of 8 oxygens)
Blatná suite (cont.)

	Koz-6							KozD-1						
	plag 1	plag 2	plag 3	plag 4	plag 5	plag 6	KF1	plag 1	plag 2	plag 3	plag 4	plag 5	plag 6	plag 7
	zoned			unzoned			phenoX core	mantled (CL)			mantled (CL)			
SiO2	56.17	54.68	55.94	56.24	56.14	56.16	62.83	60.62	50.71	55.94	58.46	57.66	53.30	50.51
TiO2	0.00	0.00	0.08	0.00	0.00	0.00	0.00	0.00	0.00	0.00	0.00	0.00	0.00	0.01
Al2O3	28.64	29.87	28.81	28.15	28.04	28.10	19.28	24.51	31.16	27.80	26.36	26.50	29.63	31.65
FeO	0.17	0.16	0.14	0.27	0.22	0.17	0.10	0.08	0.08	0.08	0.08	0.05	0.19	0.14
CaO	9.52	10.92	9.44	8.92	8.81	9.05	0.06	5.76	13.63	9.34	7.57	8.25	11.35	13.78
Na2O	6.19	5.49	6.24	6.41	6.27	6.35	1.00	8.19	3.91	6.12	7.16	6.88	5.00	3.75
K2O	0.27	0.14	0.24	0.27	0.37	0.29	15.77	0.32	0.10	0.18	0.16	0.15	0.12	0.05
Σ	100.97	101.25	100.88	100.27	99.83	100.11	99.04	99.48	99.59	99.46	99.79	99.49	99.59	99.89
Si	2.503	2.438	2.495	2.522	2.526	2.521	2.940	2.710	2.318	2.526	2.616	2.594	2.419	2.302
Ti	0.000	0.000	0.003	0.000	0.000	0.000	0.000	0.000	0.000	0.000	0.000	0.000	0.000	0.000
Al	1.505	1.570	1.515	1.488	1.487	1.487	1.064	1.292	1.679	1.480	1.391	1.405	1.586	1.700
Fe	0.006	0.006	0.005	0.010	0.008	0.006	0.004	0.003	0.003	0.003	0.003	0.002	0.007	0.005
Ca	0.455	0.521	0.451	0.429	0.425	0.435	0.003	0.276	0.667	0.452	0.363	0.398	0.552	0.673
Na	0.535	0.474	0.540	0.557	0.547	0.552	0.091	0.710	0.346	0.536	0.621	0.600	0.440	0.331
K	0.016	0.008	0.014	0.016	0.021	0.017	0.942	0.018	0.006	0.010	0.009	0.009	0.007	0.003
Σ	5.020	5.017	5.023	5.022	5.014	5.018	5.044	5.009	5.019	5.007	5.003	5.008	5.011	5.014
An	44.44	51.05	43.89	41.98	42.03	42.56	0.28	27.34	64.69	44.92	36.30	39.36	54.61	65.98
Ab	52.25	46.45	52.55	54.51	54.10	54.00	8.62	70.33	33.56	53.26	62.10	59.34	43.53	32.45
Or	1.56	0.78	1.36	1.57	2.08	1.66	89.19	1.78	0.58	0.99	0.90	0.89	0.69	0.29

Appendix VI. Composition of feldspars (cont.)
(Structural formulae calculated on basis of 8 oxygens)
Blatná suite (cont.)

KozD-1														
	plag 8 unzoned core	plag 9	plag 10	plag 11	plag 12	plag 13	plag 14	plg15	plg16	plg17	plg18	plg19	plg20	plg21
		mantled (CL)	→	unzoned rim	mantled (CL)	→	small UZ rim	small unzoned	→	←	small unzoned	→	mantled plag	→
SiO ₂	58.81	60.21	51.23	60.36	60.28	55.66	57.75	60.73	59.97	60.75	60.97	61.02	58.11	49.99
TiO ₂	0.02	0.01	0.02	0.00	0.00	0.02	0.04	0.05	0.06	0	0.07	0	0	0.1
Al ₂ O ₃	25.35	24.54	30.84	25.35	24.70	28.23	26.73	25.4	25.56	25.08	25.08	24.77	26.75	32.11
FeO	0.12	0.22	0.09	0.13	0.07	0.03	0.12	0.08	0.03	0.11	0.04	0.04	0.08	0.07
CaO	6.75	5.93	13.11	6.36	5.66	9.79	8.07	6.04	6.38	5.64	5.59	5.27	7.73	13.87
Na ₂ O	7.70	8.13	4.18	7.80	8.19	5.94	6.76	7.58	7.42	7.99	7.78	7.93	6.93	3.56
K ₂ O	0.25	0.25	0.07	0.12	0.27	0.17	0.16	0.23	0.16	0.19	0.28	0.29	0.26	0.12
Σ	99.00	99.29	99.54	100.12	99.17	99.84	99.63	100.11	99.58	99.76	99.81	99.32	99.86	99.82
Si	2.652	2.699	2.338	2.681	2.702	2.506	2.592	2.692	2.674	2.702	2.708	2.721	2.601	2.281
Ti	0.001	0.000	0.001	0.000	0.000	0.001	0.001	0.002	0.002	0	0.002	0	0	0.003
Al	1.347	1.297	1.660	1.327	1.305	1.499	1.414	1.327	1.344	1.315	1.313	1.302	1.411	1.727
Fe	0.005	0.008	0.003	0.005	0.003	0.001	0.004	0.003	0.001	0.004	0.002	0.001	0.003	0.003
Ca	0.326	0.285	0.641	0.303	0.272	0.472	0.388	0.287	0.305	0.269	0.266	0.252	0.371	0.678
Na	0.673	0.707	0.370	0.672	0.712	0.519	0.588	0.652	0.641	0.689	0.67	0.686	0.601	0.315
K	0.014	0.014	0.004	0.007	0.015	0.010	0.009	0.013	0.009	0.011	0.016	0.017	0.015	0.007
Σ	5.018	5.010	5.017	4.995	5.009	5.008	4.998	4.975	4.977	4.99	4.976	4.979	5.002	5.013
An	31.87	28.15	62.34	30.30	26.97	46.73	38.8	28.7	30.5	26.9	26.6	25.2	37.1	66.6
Ab	65.79	69.82	35.98	67.20	70.60	51.39	58.8	65.2	64.1	68.9	67	68.6	60.1	30.94
Or	1.37	1.38	0.39	0.70	1.49	0.99	0.9	1.3	0.9	1.1	1.6	1.7	1.5	0.69

Appendix VI. Composition of feldspars (cont.)
(Structural formulae calculated on basis of 8 oxygens)

Blatná suite (cont.)

		KozD-1					Bl-2							
	plg22→ cont.	plag23 bi-hb clot C	KF1	KF2 interstitial	KF3	plag 1 unzoned core	plag 2 unzoned in KF	plag 3 unzoned	plag 4 unzoned	plag 5 unzoned	plag 6 unzoned	KF1 interstic rim	KF2 phenoX rim	KF3 pheno- cryst
SiO ₂	57.7	61.16	64.03	64.11	63.34	58.13	57.78	58.25	58.13	58.65	58.18	62.72	62.84	62.76
TiO ₂	0.02	0.00	0.00	0.00	0.00	0.05	0.02	0.01	0.00	0.00	0.01	0.00	0.00	0.03
Al ₂ O ₃	26.73	24.61	19.31	18.70	18.82	25.88	26.05	25.88	25.59	25.55	25.96	18.63	18.76	18.63
FeO	0.07	0.17	0.08	0.08	0.11	0.01	0.09	0.09	0.06	0.01	0.05	0.19	0.00	0.02
CaO	7.66	5.69	0.16	0.00	0.02	6.89	7.48	7.29	7.35	7.12	7.49	0.00	0.04	0.06
Na ₂ O	6.85	8.25	3.19	0.99	1.25	7.25	7.16	7.41	7.20	7.50	7.46	1.01	1.43	1.26
K ₂ O	0.31	0.17	11.98	15.45	14.81	0.34	0.31	0.22	0.28	0.24	0.21	15.10	14.39	14.75
Σ	99.34	100.05	98.75	99.33	98.35	98.55	98.89	99.15	98.61	99.07	99.36	97.65	97.46	97.51
Si	2.596	2.715	2.958	2.978	2.968	2.631	2.613	2.625	2.633	2.643	2.618	2.966	2.966	2.967
Ti	0.001	0.000	0.000	0.000	0.000	0.002	0.001	0.000	0.000	0.000	0.000	0.000	0.000	0.001
Al	1.418	1.288	1.052	1.024	1.040	1.381	1.389	1.375	1.367	1.357	1.377	1.039	1.044	1.038
Fe	0.002	0.006	0.003	0.003	0.004	0.000	0.003	0.003	0.002	0.000	0.002	0.008	0.000	0.001
Ca	0.369	0.271	0.008	0.000	0.001	0.334	0.362	0.352	0.357	0.344	0.361	0.000	0.002	0.003
Na	0.598	0.71	0.286	0.089	0.114	0.636	0.628	0.648	0.632	0.655	0.651	0.093	0.131	0.115
K	0.018	0.01	0.706	0.916	0.885	0.020	0.018	0.013	0.016	0.014	0.012	0.911	0.867	0.890
Σ	5.002	5	5.013	5.010	5.012	5.004	5.014	5.016	5.007	5.013	5.021	5.017	5.010	5.015
An	36.9	27.1	0.79	0.00	0.10	33.34	35.53	34.39	35.36	33.74	34.86	0.00	0.20	0.30
Ab	59.8	71.0	28.28	8.79	11.28	63.48	61.64	63.31	62.61	64.24	62.87	9.16	12.96	11.29
Or	1.8	1.0	69.80	90.48	87.59	2.00	1.77	1.27	1.59	1.37	1.16	89.71	85.78	87.41

Appendix VI. Composition of feldspars (cont.)
(Structural formulae calculated on basis of 8 oxygens)
Blatná suite (cont.)

BI-3														
	plag 1 unznd in KF	plag 2	plag 3	plag 4	plag 5	plag 6	plag 7	plag 8	plag 9	plag 10	KF1	KF2	KF3	
				zoned	→	←	unzoned	→	←	zoned	←	phenocryst	phenocryst core	
SiO ₂	58.36	59.64	59.00	56.22	56.12	57.39	58.66	57.30	58.37	59.22	61.96	62.07	62.27	
TiO ₂	0.00	0.00	0.02	0.01	0.04	0.03	0.01	0.00	0.00	0.00	0.00	0.00	0.00	
Al ₂ O ₃	27.05	25.71	26.03	27.91	27.94	26.96	26.10	27.63	26.79	26.65	19.92	19.59	19.94	
FeO	0.00	0.01	0.06	0.04	0.02	0.08	0.04	0.06	0.04	0.05	0.04	0.04	0.04	
CaO	7.38	5.62	5.94	8.11	8.10	6.96	6.16	8.07	7.00	6.56	0.05	0.06	0.07	
Na ₂ O	7.38	8.36	7.94	6.72	6.97	7.53	8.15	6.90	7.40	7.80	2.00	1.53	1.43	
K ₂ O	0.21	0.30	0.27	0.23	0.24	0.36	0.21	0.27	0.27	0.19	13.96	14.61	14.67	
Σ	100.39	99.65	99.25	99.23	99.43	99.31	99.33	100.22	99.88	100.47	97.94	97.91	98.41	
Si	2.597	2.664	2.647	2.538	2.532	2.585	2.634	2.561	2.609	2.627	2.914	2.926	2.919	
Ti	0.000	0.000	0.001	0.000	0.001	0.001	0.000	0.000	0.000	0.000	0.000	0.000	0.000	
Al	1.419	1.354	1.376	1.485	1.486	1.432	1.381	1.456	1.412	1.394	1.105	1.089	1.102	
Fe	0.000	0.001	0.002	0.001	0.001	0.003	0.001	0.002	0.001	0.002	0.001	0.002	0.001	
Ca	0.352	0.269	0.285	0.392	0.392	0.336	0.296	0.387	0.335	0.312	0.003	0.003	0.003	
Na	0.637	0.724	0.690	0.588	0.610	0.657	0.709	0.597	0.641	0.671	0.183	0.140	0.130	
K	0.012	0.017	0.016	0.013	0.014	0.021	0.012	0.015	0.016	0.011	0.837	0.879	0.877	
Σ	5.017	5.029	5.017	5.017	5.036	5.035	5.033	5.018	5.014	5.017	5.043	5.039	5.032	
An	34.48	25.96	28.07	38.46	37.37	32.10	28.30	37.97	33.09	30.70	0.29	0.29	0.29	
Ab	62.40	69.86	67.95	57.69	58.15	62.76	67.79	58.58	63.32	66.02	17.39	13.37	12.54	
Or	1.18	1.64	1.58	1.28	1.34	2.01	1.15	1.47	1.58	1.08	79.55	83.97	84.57	

Appendix VI. Composition of feldspars (cont.)
(Structural formulae calculated on basis of 8 oxygens)
Blatná suite (cont.)

	B1-5													
	plag 1	plag 2	plag 3	plag 4	plag 5	plag 6	plag 7	plag 8	plag 9	KF1 phenoX core	KF2 phenoX core	plag 1 unzoned core	plag 2	plag 4
	zoned			→	as plag 3	unzoned		←	unzoned in KF				zoned	
SiO2	58.80	58.53	57.79	59.75	57.63	59.58	58.81	59.65	58.98	62.63	62.98	57.41	60.98	62.57
TiO2	0.00	0.02	0.03	0.00	0.00	0.00	0.02	0.03	0.02	0.11	0.00	0.00	0.00	0.00
Al2O3	25.70	26.29	26.67	25.51	27.10	25.80	26.01	25.29	26.17	19.24	19.31	26.60	23.93	23.03
FeO	6.49	7.04	7.74	5.98	7.79	6.36	6.69	5.94	6.70	0.03	0.02	0.03	0.05	0.07
CaO	0.18	0.03	0.09	0.13	0.06	0.10	0.11	0.13	0.08	0.16	0.10	8.20	5.00	4.01
Na2O	7.56	7.28	7.13	8.01	6.89	7.77	7.38	7.99	7.60	0.73	1.67	6.95	8.59	9.43
K2O	0.28	0.22	0.18	0.18	0.22	0.27	0.37	0.34	0.19	15.86	14.48	0.22	0.41	0.18
Σ	99.00	99.40	99.64	99.56	99.69	99.88	99.38	99.36	99.75	98.76	98.55	99.41	98.96	99.29
Si	2.648	2.625	2.594	2.670	2.584	2.657	2.639	2.673	2.636	2.940	2.945	2.586	2.736	2.788
Ti	0.000	0.001	0.001	0.000	0.000	0.000	0.001	0.001	0.001	0.004	0.000	0.000	0.000	0.000
Al	1.364	1.391	1.412	1.344	1.433	1.356	1.376	1.336	1.379	1.064	1.064	1.413	1.266	1.210
Fe	0.313	0.338	0.372	0.287	0.374	0.304	0.322	0.285	0.321	0.002	0.001	0.001	0.002	0.003
Ca	0.007	0.001	0.004	0.005	0.002	0.004	0.004	0.005	0.003	0.006	0.004	0.396	0.240	0.191
Na	0.660	0.633	0.621	0.694	0.599	0.672	0.642	0.694	0.658	0.067	0.152	0.607	0.747	0.815
K	0.016	0.012	0.010	0.010	0.013	0.015	0.021	0.019	0.011	0.950	0.864	0.013	0.023	0.010
Σ	5.008	5.001	5.014	5.010	5.005	5.008	5.005	5.013	5.009	5.033	5.030	5.016	5.014	5.017
An	31.23	33.80	36.59	28.53	37.40	30.26	32.20	28.12	31.94	0.19	0.10	38.61	23.54	18.64
Ab	65.85	63.30	61.09	68.99	59.90	66.90	64.20	68.48	65.48	6.45	14.68	59.19	73.25	79.53
Or	1.60	1.20	0.98	0.99	1.30	1.49	2.10	1.88	1.10	91.42	83.43	1.27	2.26	0.98

Appendix VI. Composition of feldspars (cont.)
(Structural formulae calculated on basis of 8 oxygens)
Blatná suite (cont.)

	BI-7						BI-8							
	plag 3	plag 5	plag 6	plag 7	KF1 phenoX rim	KF2 phenoX core	plag 1	plag 2	plag 3	plag 4	plag 5	plag 6	plag 7	plag 8
...→ cont.	← unzoned	← unzoned	← unznd in KF	← unznd in KF	← unzoned	← unzoned	← unzoned	← unzoned	← unzoned	← unzoned	← un-zoned rim	← un-zoned rim	← un-zoned rim	← un-zoned rim
SiO ₂	57.49	58.51	58.72	59.22	63.01	62.99	54.95	58.99	58.28	57.23	56.76	58.21	57.90	55.18
TiO ₂	0.01	0.03	0.00	0.00	0.00	0.00	0.00	0.00	0.00	0.00	0.00	0.02	0.00	0.03
Al ₂ O ₃	26.69	25.54	25.57	25.36	18.80	18.83	28.76	26.23	26.27	27.35	27.99	26.14	26.78	28.66
FeO	0.02	0.01	0.03	0.02	0.02	0.01	0.10	0.17	0.18	0.14	0.06	6.89	7.54	9.90
CaO	8.04	6.84	6.80	6.82	0.08	0.05	10.09	6.95	7.03	8.23	8.54	0.06	0.12	0.13
Na ₂ O	7.01	7.65	7.65	7.58	1.28	0.98	5.67	7.35	7.19	6.72	6.40	7.30	7.02	5.80
K ₂ O	0.16	0.20	0.22	0.30	14.93	15.10	0.14	0.21	0.31	0.18	0.17	0.22	0.14	0.13
Σ	99.42	98.78	98.99	99.30	98.12	97.96	99.71	99.90	99.26	99.85	99.92	98.84	99.50	99.83
Si	2.588	2.642	2.646	2.659	2.963	2.965	2.480	2.633	2.621	2.566	2.543	2.626	2.599	2.487
Ti	0.000	0.001	0.000	0.000	0.000	0.000	0.000	0.000	0.000	0.000	0.000	0.001	0.000	0.001
Al	1.416	1.360	1.358	1.342	1.042	1.045	1.530	1.380	1.393	1.446	1.479	1.390	1.417	1.523
Fe	0.001	0.000	0.001	0.001	0.001	0.000	0.004	0.006	0.007	0.005	0.002	0.000	0.000	0.000
Ca	0.388	0.331	0.328	0.328	0.004	0.003	0.488	0.332	0.339	0.395	0.410	0.002	0.005	0.005
Na	0.612	0.670	0.668	0.660	0.117	0.089	0.496	0.636	0.627	0.584	0.556	0.639	0.611	0.507
K	0.009	0.012	0.013	0.017	0.896	0.907	0.008	0.012	0.018	0.010	0.010	0.013	0.008	0.007
Σ	5.014	5.016	5.014	5.007	5.023	5.009	5.006	4.999	5.005	5.006	5.000	4.671	4.640	4.530
An	38.05	32.29	32.16	32.46	0.39	0.30	48.64	33.20	33.90	39.41	41.00	33.30	36.30	47.59
Ab	60.02	65.37	65.49	65.31	11.38	8.81	49.44	63.60	62.70	58.26	55.60	63.90	61.10	50.48
Or	0.88	1.17	1.27	1.68	87.13	89.82	0.80	1.20	1.80	1.00	1.00	1.30	0.80	0.70

Appendix VI. Composition of feldspars (cont.)
(Structural formulae calculated on basis of 8 oxygens)
Blatná suite (cont.)

	B1-8				
	plag 9	plag10	KF 1	KF 2	
	unzoned →		phenocryst →		
SiO2	57.27	56.93	62.97	62.08	
TiO2	0.00	0.05	0.00	0.02	
Al2O3	27.04	27.41	19.12	19.63	
FeO	7.80	8.26	0.02	0.08	
CaO	0.13	0.13	0.00	0.12	
Na2O	6.95	6.64	0.81	1.24	
K2O	0.21	0.14	15.81	14.86	
Σ	99.41	99.56	98.73	98.03	
Si	2.578	2.560	2.952	2.925	
Ti	0.000	0.002	0.000	0.001	
Al	1.435	1.453	1.057	1.090	
Fe	0.000	0.000	0.001	0.003	
Ca	0.005	0.005	0.000	0.006	
Na	0.607	0.579	0.074	0.113	
K	0.012	0.008	0.946	0.893	
Σ	4.637	4.607	5.030	5.031	
An	37.15	39.80	0.00	0.58	
Ab	59.98	57.90	7.14	10.91	
Or	1.19	0.80	91.26	86.21	

Appendix VI. Composition of feldspars (cont.)
(Structural formulae calculated on basis of 8 oxygens)

Čertovo břemeno suite

	Se-4												Se-5					
	plag 6* large, core	plag 9*	plag 10*	plag 11* large, core	KF 1* phenoX core	KF 2* phenocryst		KF 7* small phenoX	KF 8*	phenoX rim	KF 12*	pheno- cryst	KF 13*	pheno- cryst	KF 14*	pheno- cryst	plag 2	plag 3
						←	phenocryst	→									←	zoned
SiO ₂	59.56	58.78	57.92	58.10	64.33	63.54	63.68	63.30	62.45	64.39	63.96	64.17	63.96	64.17	64.17	64.17	58.92	56.61
TiO ₂	0.00	0.00	0.00	0.03	0.16	0.35	0.42	0.27	0.54	0.00	0.04	0.00	0.04	0.00	0.00	0.00	0.00	0.02
Al ₂ O ₃	25.09	25.86	25.80	25.63	20.35	18.53	18.49	18.74	18.53	18.38	18.29	18.32	18.29	18.32	18.32	18.32	25.25	26.82
FeO	0.00	0.02	0.02	0.08	0.01	0.15	0.06	0.00	0.11	0.11	0.05	0.02	0.05	0.02	0.02	0.02	0.00	0.08
CaO	6.73	7.64	7.93	7.86	1.67	0.12	0.08	0.00	0.20	0.11	0.10	0.06	0.10	0.06	0.06	0.06	6.74	8.63
Na ₂ O	7.33	6.87	6.87	7.01	5.92	1.14	0.93	0.43	1.28	1.19	0.87	0.95	0.87	0.95	0.95	0.95	7.65	6.51
K ₂ O	0.21	0.27	0.30	0.22	5.61	14.42	15.01	16.00	14.24	15.07	15.58	15.35	15.58	15.35	15.35	15.35	0.18	0.22
Σ	98.92	99.43	98.83	98.92	98.04	98.24	98.66	98.73	97.34	99.24	98.88	98.86	98.88	98.86	98.86	98.86	98.74	98.89
Si	2.673	2.633	2.617	2.623	2.917	2.967	2.972	2.957	2.948	2.988	2.982	2.988	2.982	2.988	2.988	2.988	2.658	2.566
Ti	0.000	0.000	0.000	0.001	0.005	0.012	0.015	0.010	0.019	0.000	0.001	0.000	0.001	0.000	0.000	0.000	0.000	0.001
Al	1.327	1.365	1.374	1.364	1.088	1.020	1.017	1.032	1.031	1.005	1.005	1.006	1.005	1.006	1.006	1.006	1.343	1.433
Fe	0.000	0.001	0.001	0.003	0.000	0.006	0.002	0.000	0.004	0.004	0.002	0.001	0.002	0.001	0.001	0.001	0.000	0.003
Ca	0.324	0.366	0.384	0.380	0.081	0.006	0.004	0.000	0.010	0.005	0.005	0.003	0.005	0.003	0.003	0.003	0.326	0.419
Na	0.638	0.597	0.602	0.613	0.520	0.103	0.084	0.039	0.117	0.107	0.079	0.085	0.079	0.085	0.085	0.085	0.669	0.572
K	0.012	0.015	0.017	0.013	0.324	0.859	0.894	0.953	0.858	0.892	0.926	0.912	0.926	0.912	0.912	0.912	0.010	0.013
Σ	4.974	4.977	4.995	4.997	4.935	4.973	4.988	4.991	4.987	5.001	5.000	4.995	5.000	4.995	4.995	4.995	5.006	5.007
An	32.40	36.60	38.04	37.40	8.10	0.60	0.40	0.00	1.00	0.50	0.49	0.30	0.49	0.30	0.30	0.30	32.22	41.46
Ab	63.80	59.70	59.64	60.33	52.00	10.30	8.40	3.88	11.70	10.63	7.79	8.47	7.79	8.47	8.47	8.47	66.13	56.60
Or	1.20	1.50	1.68	1.28	32.40	85.90	89.40	94.69	85.80	88.64	91.28	90.93	91.28	90.93	90.93	90.93	0.99	1.29

Appendix VI. Composition of feldspars (cont.)
(Structural formulae calculated on basis of 8 oxygens)
Čertovo břemeno suite (cont.)

	Se-5					Se-6									
	plag 1 resorb in KF	plag 4 unzoned core	KF1	KF2	Kf3 matrix (small)	plag 3	plag 4	plag 5	plag 6	plag 7	plag 8	plag 9	plag 10	plag 11	
			phenocryst			oscillatory zoned									zoned
SiO ₂	58.59	58.23	62.99	62.78	63.26	60.55	57.34	57.52	57.26	57.61	57.55	60.23	59.29	57.94	
TiO ₂	0.02	0.02	0.02	0.00	0.01	0.00	0.00	0.00	0.03	0.02	0.00	0.02	0.02	0.00	
Al ₂ O ₃	25.76	25.60	18.69	18.53	18.62	24.61	26.84	26.73	26.77	26.62	26.88	25.24	25.41	26.43	
FeO	0.09	0.02	0.07	0.02	0.04	5.01	7.70	7.48	7.64	7.54	7.88	5.85	6.11	7.33	
CaO	7.01	7.08	0.01	0.05	0.07	0.04	0.02	0.09	0.07	0.00	0.09	0.05	0.06	0.02	
Na ₂ O	7.53	7.30	0.89	1.09	0.97	8.51	7.14	6.94	7.02	7.15	6.86	8.01	7.98	7.10	
K ₂ O	0.16	0.18	15.35	14.86	15.57	0.25	0.18	0.33	0.26	0.33	0.24	0.17	0.24	0.25	
Σ	99.16	98.43	98.02	97.33	98.54	98.97	99.21	99.09	99.05	99.26	99.50	99.57	99.11	99.07	
Si	2.637	2.638	2.968	2.973	2.969	2.715	2.585	2.595	2.586	2.596	2.587	2.687	2.664	2.611	
Ti	0.001	0.001	0.001	0.000	0.000	0.000	0.000	0.000	0.001	0.001	0.000	0.001	0.001	0.000	
Al	1.367	1.367	1.038	1.034	1.030	1.301	1.426	1.422	1.426	1.414	1.424	1.328	1.346	1.404	
Fe	0.003	0.001	0.003	0.001	0.002	0.241	0.372	0.362	0.370	0.364	0.379	0.280	0.294	0.354	
Ca	0.338	0.344	0.001	0.003	0.004	0.001	0.001	0.003	0.003	0.000	0.003	0.002	0.002	0.001	
Na	0.657	0.641	0.081	0.100	0.088	0.739	0.624	0.607	0.615	0.625	0.598	0.693	0.695	0.620	
K	0.009	0.010	0.923	0.898	0.932	0.014	0.010	0.019	0.015	0.019	0.014	0.010	0.014	0.014	
Σ	5.012	5.002	5.015	5.009	5.025	5.011	5.018	5.008	5.016	5.019	5.005	5.001	5.016	5.004	
An	33.33	34.36	0.10	0.30	0.39	23.87	36.34	36.10	36.38	35.52	37.80	28.00	28.85	35.40	
Ab	64.79	64.03	7.98	9.91	8.52	73.20	60.96	60.54	60.47	61.00	59.64	69.30	68.19	62.00	
Or	0.89	1.00	90.89	88.99	90.19	1.39	0.98	1.90	1.48	1.85	1.40	1.00	1.37	1.40	

Appendix VI. Composition of feldspars (cont.)
(Structural formulae calculated on basis of 8 oxygens)
Čertovo břemeno suite (cont.)

	Se-6												Se-7		
	plag 12 core of previous	plag 13	plag 14	plag 15	plag 16	plag 17	plag 18	plag 19	plag 20	KF1	KF2	KF4	phenoX core	plag 1	plag 2
				oscillatory zoned				zoned in KF		phenocryst				zoned (CL)	
SiO ₂	57.63	59.83	55.28	57.79	56.51	55.46	55.85	55.35	66.84	63.62	62.67	62.56		62.16	58.02
TiO ₂	0.00	0.05	0.04	0.03	0.03	0.11	0.00	0.06	0.00	0.07	0.09	0.00		0.00	0.00
Al ₂ O ₃	26.74	24.86	28.15	26.54	27.39	28.17	27.47	27.76	20.70	19.24	19.09	19.16		22.91	26.34
FeO	7.50	5.38	9.52	7.50	8.44	9.27	8.78	9.03	0.36	0.02	0.04	0.02		0.04	0.05
CaO	0.09	0.05	0.04	0.06	0.16	0.08	0.06	0.04	0.00	0.03	0.02	0.04		4.03	7.48
Na ₂ O	6.76	7.99	6.01	6.86	6.31	5.95	6.16	6.42	10.90	1.16	0.70	1.04		9.12	7.12
K ₂ O	0.48	0.23	0.32	0.44	0.55	0.47	0.47	0.15	0.21	15.66	16.03	15.38		0.18	0.25
Σ	99.20	98.39	99.36	99.22	99.39	99.51	98.78	98.79	99.01	99.81	98.63	98.20		98.44	99.26
Si	2.597	2.698	2.503	2.603	2.552	2.507	2.538	2.517	2.948	2.950	2.946	2.946		2.791	2.611
Ti	0.000	0.002	0.001	0.001	0.001	0.004	0.000	0.002	0.000	0.003	0.003	0.000		0.000	0.000
Al	1.421	1.322	1.503	1.410	1.458	1.501	1.472	1.488	1.076	1.052	1.058	1.064		1.213	1.398
Fe	0.362	0.260	0.462	0.362	0.409	0.449	0.428	0.440	0.017	0.001	0.002	0.001		0.002	0.002
Ca	0.004	0.002	0.002	0.002	0.006	0.003	0.002	0.001	0.000	0.001	0.001	0.002		0.194	0.361
Na	0.591	0.699	0.528	0.600	0.553	0.521	0.543	0.566	0.932	0.105	0.064	0.095		0.794	0.621
K	0.028	0.013	0.018	0.025	0.032	0.027	0.027	0.009	0.012	0.926	0.961	0.924		0.010	0.014
Σ	5.003	4.996	5.017	5.003	5.011	5.012	5.010	5.023	4.985	5.038	5.035	5.032		5.004	5.007
An	36.20	26.00	45.14	36.20	40.57	44.28	42.33	42.51	1.70	0.10	0.19	0.10		19.34	35.88
Ab	59.10	69.90	51.58	60.00	54.85	51.38	53.71	54.69	93.20	10.01	6.12	9.15		79.15	61.72
Or	2.80	1.30	1.76	2.50	3.17	2.66	2.67	0.87	1.20	88.26	91.95	88.99		1.00	1.39

Appendix VI. Composition of feldspars (cont.)
(Structural formulae calculated on basis of 8 oxygens)
Čertovo břemeno suite (cont.)

	Se-7										Se-9			
	plag 3	plag 4	plag 5	plag 6	plag 7	plag 8	KF1	KF2	KF3	plag 1	plag 2	plag 3	plag 4	plag 5
	oscillatory zoned	oscill. zoned R	encl. in plg6	oscil. zoned R	encl. in plg6	oscil. zoned R	inter-stit.	phenocryst		←	zoned (CL); plag 3 is an inclusion			
SiO ₂	58.08	57.77	57.26	60.80	58.03	57.57	62.96	63.60	62.72	58.15	57.25	57.81	58.48	58.52
TiO ₂	0.00	0.00	0.02	0.00	0.04	0.00	0.00	0.01	0.00	0.05	0.02	0.03	0.01	0.03
Al ₂ O ₃	25.85	26.31	26.47	24.08	25.98	26.23	18.74	18.52	18.87	27.24	27.26	27.12	27.19	27.03
FeO	0.05	0.03	0.10	0.00	0.04	0.04	0.00	0.05	0.00	0.16	0.03	0.03	0.17	0.00
CaO	7.40	7.65	7.90	5.12	7.18	7.66	0.05	0.04	0.08	7.57	7.88	7.70	7.21	7.51
Na ₂ O	7.33	7.09	6.89	8.56	7.26	7.13	0.93	0.97	1.66	6.19	7.17	7.30	6.47	7.35
K ₂ O	0.20	0.39	0.38	0.34	0.32	0.40	15.54	15.59	13.80	0.19	0.14	0.16	0.21	0.13
Σ	98.91	99.24	99.02	98.90	98.85	99.03	98.22	98.78	97.13	99.55	99.75	100.15	99.74	100.57
Si	2.624	2.605	2.591	2.730	2.622	2.602	2.964	2.977	2.964	2.600	2.569	2.583	2.609	2.599
Ti	0.000	0.000	0.001	0.000	0.001	0.000	0.000	0.000	0.000	0.002	0.001	0.001	0.000	0.001
Al	1.377	1.399	1.412	1.275	1.384	1.398	1.040	1.022	1.051	1.436	1.442	1.428	1.430	1.415
Fe	0.002	0.001	0.004	0.000	0.002	0.002	0.000	0.002	0.000	0.006	0.001	0.001	0.006	0.000
Ca	0.358	0.370	0.383	0.246	0.348	0.371	0.003	0.002	0.004	0.363	0.379	0.369	0.345	0.357
Na	0.642	0.620	0.604	0.745	0.636	0.625	0.085	0.088	0.152	0.537	0.624	0.632	0.560	0.633
K	0.012	0.022	0.022	0.019	0.018	0.023	0.933	0.931	0.832	0.011	0.008	0.009	0.012	0.007
Σ	5.015	5.017	5.017	5.015	5.011	5.021	5.025	5.022	5.003	4.955	5.024	5.023	4.962	5.012
An	35.08	36.15	37.53	24.12	34.33	35.94	0.29	0.20	0.40	36.30	36.69	35.82	34.50	35.23
Ab	62.91	60.58	59.19	73.06	62.74	60.55	8.23	8.56	15.20	53.70	60.40	61.35	56.00	62.46
Or	1.18	2.15	2.16	1.86	1.78	2.23	90.37	90.55	83.20	1.10	0.77	0.87	1.20	0.69

Appendix VI. Composition of feldspars (cont.)
(Structural formulae calculated on basis of 8 oxygens)
Čertovo břemeno suite (cont.)

	Se-9									
	plag 6	plag 7	plag 8	plag 9	plag 10	KF1	KF2			
	oscil. zoned → unzoned core	plag 7 → unzoned core	plag 8 unzoned core	plag 9 filling cracks in plags	plag 10 filling cracks in plags	KF1	KF2	phenoX core		
SiO ₂	57.59	57.42	57.76	60.72	63.76	64.26	63.36			
TiO ₂	0.03	0.05	0.00	0.00	0.03	0.00	0.00			
Al ₂ O ₃	27.02	27.21	27.37	25.92	24.22	19.90	19.73			
FeO	0.06	0.06	0.00	0.00	0.01	0.04	0.01			
CaO	7.69	7.80	7.61	5.94	4.03	0.04	0.07			
Na ₂ O	7.21	6.93	7.32	8.19	9.29	3.36	1.31			
K ₂ O	0.21	0.40	0.15	0.16	0.21	12.37	14.94			
Σ	99.81	99.87	100.20	100.93	101.54	99.97	99.42			
Si	2.582	2.575	2.577	2.674	2.774	2.939	2.938			
Ti	0.001	0.002	0.000	0.000	0.001	0.000	0.000			
Al	1.428	1.438	1.440	1.345	1.242	1.073	1.079			
Fe	0.002	0.002	0.000	0.000	0.000	0.002	0.000			
Ca	0.369	0.375	0.364	0.280	0.188	0.002	0.003			
Na	0.627	0.603	0.633	0.699	0.783	0.298	0.118			
K	0.012	0.023	0.008	0.009	0.011	0.722	0.884			
Σ	5.021	5.018	5.022	5.007	4.999	5.036	5.022			
An	35.89	36.74	35.38	27.90	18.80	0.19	0.29			
Ab	60.98	59.08	61.53	69.64	78.30	28.58	11.51			
Or	1.17	2.25	0.78	0.90	1.10	69.26	86.23			

Appendix VI. Composition of feldspars (cont.)
(Structural formulae calculated on basis of 8 oxygens)

Říčany suite

	Ri-1													
	plag 2*	plag 5*	plag 6*	plag 17*	plag 18*	plag 21*	plag 22*	plag 26*	plag 1	plag 2	plag 3	plag 4	plag 6	plag 7
	large rim	large core	large core	small core	small core	small core	small core	small core	zoned in Kf		zoned in Kf		zoned	
SiO ₂	64.38	63.20	63.19	65.67	66.46	64.23	63.63	63.17	67.20	63.34	66.28	59.68	61.50	61.80
TiO ₂	0.01	0.06	0.01	0.05	0.02	0.00	0.00	0.00	0.00	0.00	0.00	0.00	0.00	0.00
Al ₂ O ₃	21.56	21.68	21.71	20.46	19.78	21.23	22.08	21.54	20.38	23.42	20.78	25.13	24.62	24.48
FeO	0.05	0.05	0.02	0.07	0.00	0.06	0.09	0.05	0.00	0.03	0.01	0.01	0.03	0.03
CaO	2.70	3.06	3.14	1.19	0.57	2.53	3.16	3.16	0.19	3.16	0.56	5.50	4.48	4.31
Na ₂ O	9.79	9.21	9.17	10.80	10.79	9.45	9.00	9.19	11.49	9.65	11.31	8.27	8.77	8.89
K ₂ O	0.25	0.23	0.16	0.13	0.18	0.21	0.18	0.23	0.14	0.11	0.17	0.14	0.28	0.35
Σ	98.74	97.48	97.39	98.38	97.80	97.70	98.14	97.33	99.40	99.71	99.11	98.73	99.68	99.86
Si	2.868	2.848	2.847	2.921	2.965	2.884	2.847	2.854	2.956	2.801	2.930	2.685	2.733	2.741
Ti	0.000	0.002	0.000	0.002	0.001	0.000	0.000	0.000	0.000	0.000	0.000	0.000	0.000	0.000
Al	1.132	1.152	1.153	1.073	1.040	1.124	1.165	1.147	1.057	1.221	1.083	1.333	1.290	1.280
Fe	0.002	0.002	0.001	0.003	0.000	0.002	0.003	0.002	0.000	0.001	0.000	0.000	0.001	0.001
Ca	0.129	0.148	0.152	0.057	0.027	0.122	0.151	0.153	0.009	0.150	0.027	0.265	0.213	0.205
Na	0.846	0.805	0.801	0.932	0.933	0.823	0.781	0.805	0.980	0.827	0.969	0.721	0.756	0.765
K	0.014	0.013	0.009	0.008	0.010	0.012	0.010	0.013	0.008	0.006	0.010	0.008	0.016	0.020
Σ	4.991	4.970	4.963	4.996	4.976	4.967	4.957	4.974	5.010	5.006	5.019	5.012	5.009	5.012
An	12.90	14.80	15.20	5.68	2.70	12.20	15.10	15.30	0.89	15.00	2.65	26.19	21.23	20.32
Ab	84.60	80.50	80.10	92.79	93.30	82.30	78.10	80.50	97.15	82.70	94.92	71.25	75.35	75.84
Or	1.40	1.30	0.90	0.80	1.00	1.20	1.00	1.30	0.79	0.60	0.98	0.79	1.60	1.98

Appendix VI. Composition of feldspars (cont.)
(Structural formulae calculated on basis of 8 oxygens)

Říčany suite (cont.)

Ri-1														
	plag 5 unzoned in KFC	plag 8 zoned	plag 9 unzoned core	plag 10 unzoned core	plag 11 large crystal	plag 12	plag 13 unznd in KF	KF 1*	KF 3* phenoX rim	KF 4* phenoX core	KF 7* phenocryst	KF 9* phenocryst	KF 19* phenoX rim	KF 20*
SiO ₂	67.77	62.42	62.23	63.17	62.54	63.62	64.73	63.88	64.44	63.46	63.00	63.18	63.62	63.20
TiO ₂	0.04	0.00	0.00	0.03	0.02	0.03	0.02	0.02	0.12	0.16	0.11	0.04	0.06	0.06
Al ₂ O ₃	20.83	24.16	24.21	23.72	23.81	23.22	22.60	17.97	18.26	18.27	18.15	18.01	18.31	18.18
FeO	0.02	0.08	0.03	0.03	0.04	0.00	0.08	0.00	0.02	0.02	0.01	0.04	0.00	0.08
CaO	0.24	4.07	3.99	3.44	3.91	3.23	2.47	0.00	0.01	0.04	0.11	0.47	0.03	0.07
Na ₂ O	11.42	9.23	8.89	9.63	9.25	9.72	10.09	0.81	1.00	1.16	1.20	0.95	1.07	1.09
K ₂ O	0.14	0.36	0.66	0.16	0.20	0.17	0.17	15.29	15.03	14.83	14.92	15.18	14.91	14.86
Σ	100.46	100.32	100.01	100.18	99.77	99.99	100.16	97.97	98.89	97.94	97.49	97.86	97.99	97.54
Si	2.949	2.756	2.756	2.785	2.771	2.807	2.844	3.003	2.990	2.981	2.980	2.980	2.986	2.984
Ti	0.001	0.000	0.000	0.001	0.001	0.001	0.001	0.001	0.004	0.006	0.004	0.001	0.002	0.002
Al	1.068	1.258	1.264	1.233	1.244	1.208	1.171	0.996	0.999	1.012	1.012	1.001	1.013	1.012
Fe	0.001	0.003	0.001	0.001	0.001	0.000	0.003	0.000	0.001	0.001	0.000	0.001	0.000	0.003
Ca	0.011	0.193	0.189	0.162	0.186	0.153	0.116	0.000	0.001	0.002	0.006	0.024	0.001	0.004
Na	0.963	0.790	0.764	0.823	0.795	0.831	0.860	0.074	0.090	0.105	0.110	0.087	0.097	0.100
K	0.008	0.020	0.037	0.009	0.011	0.010	0.010	0.917	0.890	0.889	0.900	0.913	0.893	0.895
Σ	5.001	5.020	5.011	5.014	5.009	5.010	5.005	4.991	4.975	4.996	5.012	5.007	4.992	5.000
An	1.10	18.89	18.73	16.00	18.47	15.18	11.60	0.00	0.10	0.20	0.59	2.29	0.10	0.40
Ab	96.30	77.32	75.71	81.28	78.96	82.45	86.00	7.40	9.00	10.48	10.78	8.31	9.70	9.97
Or	0.80	1.96	3.67	0.89	1.09	0.99	1.00	91.70	89.00	88.75	88.17	87.21	89.30	89.23

Appendix VI. Composition of feldspars (cont.)
(Structural formulae calculated on basis of 8 oxygens)

Říčany suite (cont.)

	Ri-1					
	KF 25*	KF1	KF2	KF3	KF4	KF5
	KF2 mantled by KF1, phenocrysts			phenocryst, KF4 bright CL		
SiO ₂	63.35	63.20	63.41	63.56	63.08	62.65
TiO ₂	0.14	0.00	0.07	0.00	0.02	0.00
Al ₂ O ₃	18.38	19.31	19.58	19.39	19.75	19.58
FeO	0.00	0.03	0.08	0.00	0.00	0.01
MnO	-	-	-	-	-	-
CaO	0.04	0.00	0.08	0.00	0.01	0.11
Na ₂ O	1.08	1.01	1.18	1.07	0.79	1.11
K ₂ O	14.94	14.74	14.44	14.62	15.09	14.46
Σ	97.93	98.29	98.84	98.64	98.74	97.92
Si	2.980	2.958	2.948	2.960	2.942	2.942
Ti	0.005	0.000	0.002	0.000	0.001	0.000
Al	1.019	1.065	1.073	1.065	1.086	1.084
Fe	0.000	0.001	0.003	0.000	0.000	0.000
Ca	0.002	0.000	0.004	0.000	0.000	0.006
Na	0.099	0.092	0.106	0.097	0.071	0.101
K	0.896	0.880	0.857	0.869	0.898	0.866
Σ	5.001	4.996	4.993	4.991	4.998	4.999
An	0.20	0.00	0.40	0.00	0.00	0.60
Ab	9.87	9.20	10.60	9.70	7.10	10.10
Or	89.33	88.00	85.70	86.90	89.80	86.60

Composition of
carbonates
(Structural formulae
on basis of 6 oxygens)

Sázava suite

	Po-3	Sa-10
	carb10*	carb5* carb19*
SiO ₂	0.25	0.32 0.20
TiO ₂	0.13	0.09 0.07
Al ₂ O ₃	0.02	0.10 0.01
FeO	0.95	0.16 0.79
MnO	1.63	1.65 1.12
MgO	0.16	0.47 0.35
CaO	52.23	52.92 55.17
Na ₂ O	0.04	0.28 0.02
Σ	52.67	53.87 57.71
Si	0.025	0.032 0.019
Ti	0.010	0.007 0.005
Al	0.003	0.011 0.001
Fe	0.080	0.095 0.064
Mn	0.014	0.138 0.092
Mg	0.025	0.069 0.051
Ca	5.675	5.575 5.724
Σ	5.832	5.927 5.956
Sid	1.35	1.62 1.08
Mst	0.42	1.17 0.86
Rho	2.37	2.35 1.55
Cte	95.86	94.86 96.51

Appendix VII. Composition of biotites

(Structural formulae are based on 22 oxygens)

Sázava suite

	Sa-3				Sa-10					
	bi1	bi2	bi3	bi4	biot2*	biot3*	biot6*	biot8*	biot 1	biot 4
	← large bi		← large bi		small core	large core	large core	small core	small centre	small core
SiO ₂	34.63	35.30	35.32	35.92	35.56	35.64	35.69	36.02	33.69	34.15
TiO ₂	2.43	1.98	2.11	2.00	3.47	3.50	3.75	3.46	2.70	3.02
Al ₂ O ₃	15.40	15.92	15.31	15.86	14.70	15.02	14.63	15.27	15.98	15.31
Fe ₂ O ₃	3.61	3.68	3.93	3.60	3.95	3.86	4.05	3.95	3.91	3.87
FeO	18.43	18.76	20.02	18.34	20.15	19.66	20.65	20.14	19.95	19.74
MnO	0.35	0.36	0.32	0.36	0.47	0.52	0.44	0.40	0.44	0.47
MgO	9.59	9.57	9.05	9.56	9.21	8.99	8.98	9.21	8.13	9.02
CaO	0.03	0.03	0.01	0.04	0.04	0.02	0.03	0.11	0.00	0.02
Na ₂ O	0.08	0.08	0.10	0.07	0.39	0.05	0.27	0.00	0.07	0.06
K ₂ O	9.56	9.62	9.81	9.82	9.07	9.20	9.13	9.13	9.22	9.50
Σ	94.10	95.29	95.97	95.57	96.99	96.46	97.61	97.68	94.09	95.16
Si	5.425	5.454	5.465	5.517	5.427	5.457	5.426	5.442	5.323	5.337
Al ^{IV}	2.575	2.546	2.535	2.483	2.573	2.543	2.574	2.558	2.677	2.663
Σ Z	8.000	8.000	8.000	8.000	8.000	8.000	8.000	8.000	8.000	8.000
Al ^{VI}	0.269	0.354	0.257	0.388	0.072	0.169	0.049	0.162	0.300	0.158
Ti	0.286	0.230	0.245	0.231	0.398	0.403	0.429	0.393	0.321	0.355
Fe ³⁺	0.426	0.428	0.457	0.416	0.454	0.444	0.463	0.449	0.465	0.455
Fe ²⁺	2.415	2.425	2.591	2.356	2.572	2.518	2.626	2.545	2.636	2.580
Mn	0.046	0.048	0.041	0.047	0.061	0.067	0.057	0.051	0.059	0.062
Mg	2.239	2.204	2.087	2.189	2.094	2.051	2.034	2.074	1.914	2.101
Σ Y	5.681	5.689	5.678	5.627	5.651	5.652	5.658	5.674	5.695	5.711
Ca	0.005	0.004	0.002	0.007	0.007	0.004	0.004	0.018	0.000	0.003
Na	0.025	0.022	0.030	0.021	0.115	0.014	0.079	0.000	0.021	0.018
K	1.910	1.896	1.937	1.924	1.766	1.796	1.771	1.760	1.859	1.894
Σ X	1.940	1.922	1.969	1.952	1.888	1.814	1.854	1.778	1.880	1.915
Σ cat	15.621	15.611	15.647	15.579	15.539	15.466	15.512	15.452	15.575	15.626
$\frac{\text{Fe}^*}{\text{Fe}^*+\text{Mg}}$	0.56	0.56	0.59	0.56	0.59	0.59	0.60	0.59	0.62	0.59

Appendix VII. Composition of biotites (cont.)

(Structural formulae are based on 22 oxygens)

Sázava suite (cont.)

Sa-10		Sa-7					SaD-1			
	biot 5 large core	biot1* large rim	biot2* small, core	biot3* small, core	biot4* small core	biot14* large core	biot 1 large biotites cores	biot 2	biot 6	biot 7 large biot
SiO ₂	32.53	35.18	35.52	35.43	35.62	35.43	34.95	35.64	35.53	35.25
TiO ₂	3.09	3.51	4.03	3.78	3.12	4.45	4.23	4.03	3.42	3.30
Al ₂ O ₃	15.21	15.59	15.12	15.42	15.94	14.96	15.24	14.95	15.67	15.72
Fe ₂ O ₃	3.96	3.71	3.72	3.81	3.66	3.73	3.34	3.52	3.78	3.77
FeO	20.21	18.94	18.99	19.42	18.68	19.04	17.03	17.94	19.28	19.23
MnO	0.38	0.24	0.21	0.29	0.24	0.20	0.19	0.14	0.17	0.16
MgO	8.78	8.82	8.97	9.06	9.44	9.12	9.42	9.72	8.89	9.27
CaO	0.04	0.07	0.00	0.10	0.12	0.00	0.00	0.00	0.04	0.02
Na ₂ O	0.11	0.18	0.15	0.22	0.12	0.00	0.31	0.19	0.10	0.12
K ₂ O	9.22	9.18	9.46	9.19	9.24	9.12	9.41	9.13	9.72	9.29
S	93.54	95.42	96.17	96.71	96.19	96.05	93.79	95.25	96.60	96.13
Si	5.208	5.405	5.436	5.384	5.431	5.418	5.425	5.469	5.426	5.4
Al ^{IV}	2.792	2.595	2.564	2.616	2.569	2.582	2.575	2.531	2.574	2.600
SZ	8.000	8.000	8.000	8.000	8.000	8.000	8.000	8.000	8.000	8.000
Al ^{VI}	0.079	0.228	0.163	0.146	0.297	0.114	0.214	0.174	0.248	0.239
Ti	0.372	0.406	0.463	0.432	0.357	0.511	0.494	0.465	0.393	0.38
Fe ³⁺	0.478	0.429	0.429	0.436	0.420	0.430	0.390	0.406	0.435	0.435
Fe ²⁺	2.706	2.433	2.430	2.468	2.382	2.435	2.211	2.302	2.463	2.464
Mn	0.052	0.031	0.027	0.037	0.031	0.026	0.025	0.018	0.021	0.02
Mg	2.095	2.020	2.046	2.051	2.145	2.079	2.179	2.223	2.024	2.117
SY	5.782	5.547	5.558	5.570	5.632	5.595	5.513	5.588	5.584	5.655
Ca	0.007	0.011	0.000	0.016	0.020	0.000	0.000	0.000	0.007	0.003
Na	0.034	0.054	0.045	0.063	0.036	0.000	0.093	0.057	0.029	0.034
K	1.883	1.799	1.846	1.782	1.798	1.780	1.863	1.787	1.893	1.816
SX	1.924	1.864	1.891	1.861	1.854	1.780	1.956	1.844	1.929	1.853
S cat	15.706	15.411	15.449	15.431	15.486	15.375	15.469	15.432	15.514	15.508
Fe* Fe*+Mg	0.60	0.59	0.58	0.59	0.57	0.58	0.54	0.55	0.59	0.58

Appendix VII. Composition of biotites (cont.)

(Structural formulae are based on 22 oxygens)

Sázava suite (cont.)

	SaD-1						Po-1			
	biot8	biot9	biot10	biot11	biot12	biot13	biot 1	biot 2	biot 3	biot 4
	← large bi		←		←		← large bi		← large bi	
SiO ₂	34.89	35.00	35.11	34.95	34.94	35.40	35.54	35.24	34.47	34.64
TiO ₂	3.55	3.94	3.40	3.32	3.62	3.65	2.93	2.79	2.79	2.72
Al ₂ O ₃	15.69	15.46	15.91	16.18	15.84	15.88	17.00	16.80	15.11	15.85
Fe ₂ O ₃	3.67	3.70	3.72	3.74	3.88	3.84	3.45	3.40	3.83	4.10
FeO	18.70	18.86	18.98	19.05	19.78	19.60	17.57	17.33	19.53	20.92
MnO	0.17	0.20	0.20	0.08	0.16	0.13	0.40	0.45	0.40	0.42
MgO	9.32	9.32	9.44	9.28	9.11	9.17	8.60	8.76	8.09	8.09
CaO	0.02	0.00	0.07	0.08	0.00	0.06	0.03	0.03	0.00	0.04
Na ₂ O	0.08	0.10	0.10	0.07	0.19	0.11	0.07	0.07	0.06	0.06
K ₂ O	9.12	9.39	9.23	9.33	9.33	9.38	9.41	9.56	9.40	8.91
Σ	95.20	95.96	96.14	96.06	96.84	97.23	94.99	94.41	93.68	95.74
Si	5.384	5.372	5.37	5.353	5.335	5.369	5.453	5.447	5.458	5.378
Al ^{IV}	2.616	2.628	2.630	2.647	2.665	2.631	2.547	2.553	2.542	2.622
Σ Z	8.000	8.000	8.000	8.000	8.000	8.000	8.000	8.000	8.000	8.000
Al ^{VI}	0.237	0.168	0.239	0.275	0.185	0.209	0.529	0.509	0.278	0.279
Ti	0.411	0.455	0.391	0.382	0.415	0.417	0.338	0.324	0.332	0.317
Fe ³⁺	0.426	0.427	0.428	0.431	0.446	0.439	0.398	0.395	0.456	0.479
Fe ²⁺	2.413	2.421	2.428	2.44	2.525	2.487	2.255	2.240	2.586	2.716
Mn	0.023	0.025	0.025	0.01	0.02	0.016	0.052	0.058	0.053	0.056
Mg	2.143	2.132	2.151	2.118	2.072	2.072	1.967	2.017	1.909	1.872
Σ Y	5.653	5.628	5.662	5.656	5.663	5.640	5.539	5.543	5.614	5.719
Ca	0.003	0	0.011	0.013	0	0.01	0.004	0.005	0.000	0.006
Na	0.024	0.029	0.028	0.02	0.057	0.034	0.019	0.020	0.018	0.018
K	1.796	1.838	1.801	1.822	1.816	1.815	1.842	1.884	1.899	1.765
Σ X	1.823	1.867	1.840	1.855	1.873	1.859	1.865	1.909	1.917	1.789
Σ cat	15.475	15.495	15.504	15.511	15.539	15.499	15.403	15.453	15.531	15.507
$\frac{\text{Fe}^*}{\text{Fe}^*+\text{Mg}}$	0.57	0.57	0.57	0.58	0.59	0.59	0.57	0.57	0.61	0.63

Appendix VII. Composition of biotites (cont.)

(Structural formulae are based on 22 oxygens)

Sázava suite (cont.)

	Po-1					Po-3				
	biot 5	biot 6	biot 7	biot 8	biot 9	biot 1	biot 2	biot 3	biot 4	biot 5
	large bi		large bi		large core	large core	small core	small core	large core	large core
SiO ₂	34.32	34.85	34.51	35.02	34.63	32.96	32.07	32.83	33.04	33.60
TiO ₂	2.95	2.75	3.14	2.35	3.10	3.12	3.20	3.04	3.34	3.77
Al ₂ O ₃	15.76	15.16	15.30	16.57	15.96	15.76	16.64	16.62	15.71	15.92
Fe ₂ O ₃	4.13	4.04	4.05	3.59	3.62	4.28	4.21	4.37	4.47	4.38
FeO	21.05	20.63	20.66	18.31	18.48	21.82	21.45	22.26	22.79	22.33
MnO	0.45	0.45	0.35	0.43	0.40	0.34	0.45	0.31	0.29	0.35
MgO	7.41	7.89	7.99	8.47	8.53	6.40	5.78	5.81	6.04	5.76
CaO	0.03	0.00	0.00	0.00	0.00	0.00	0.01	0.00	0.01	0.00
Na ₂ O	0.08	0.06	0.08	0.06	0.11	0.08	0.07	0.05	0.12	0.09
K ₂ O	9.29	9.49	9.23	9.66	9.46	9.31	9.42	9.41	8.68	8.89
Σ	95.47	95.31	95.30	94.48	94.29	94.07	93.30	94.70	94.49	95.09
Si	5.367	5.449	5.391	5.446	5.408	5.280	5.180	5.230	5.270	5.310
Al ^{IV}	2.633	2.551	2.609	2.554	2.592	2.720	2.820	2.770	2.730	2.690
Σ Z	8.000	8.000	8.000	8.000	8.000	8.000	8.000	8.000	8.000	8.000
Al ^{VI}	0.273	0.243	0.210	0.484	0.345	0.260	0.350	0.350	0.230	0.280
Ti	0.347	0.324	0.369	0.275	0.364	0.380	0.390	0.360	0.400	0.450
Fe ³⁺	0.486	0.476	0.476	0.420	0.426	0.520	0.510	0.520	0.540	0.520
Fe ²⁺	2.754	2.697	2.699	2.382	2.413	2.920	2.900	2.970	3.040	2.950
Mn	0.059	0.059	0.047	0.057	0.053	0.050	0.060	0.040	0.040	0.050
Mg	1.728	1.837	1.860	1.964	1.986	1.530	1.390	1.380	1.440	1.360
Σ Y	5.647	5.636	5.661	5.582	5.587	5.660	5.600	5.620	5.690	5.610
Ca	0.005	0.000	0.000	0.000	0.000	0.000	0.000	0.000	0.000	0.000
Na	0.025	0.019	0.025	0.019	0.032	0.030	0.020	0.020	0.040	0.030
K	1.853	1.894	1.839	1.917	1.885	1.900	1.940	1.910	1.770	1.790
Σ X	1.883	1.913	1.864	1.936	1.917	1.930	1.960	1.930	1.810	1.820
Σ cat	15.530	15.549	15.524	15.518	15.505	15.570	15.570	15.550	15.490	15.410
$\frac{\text{Fe}^*}{\text{Fe}^*+\text{Mg}}$	0.65	0.63	0.63	0.59	0.59	0.69	0.71	0.72	0.71	0.72

Appendix VII. Composition of biotites (cont.)

(Structural formulae are based on 22 oxygens)

Blatná suite

	Koz-2				Koz-4					
	biot 1	biot 2	biot clot2	biot clot3	biot 1	biot 2	biot 3	biot 4	biot clot1	biot clot2
	← small biotite		core of the clot	rim of the clot	enclosed by amphiboles	small bi core	large, core		rim of clot	core of clot
SiO ₂	35.38	35.63	35.73	34.73	35.92	35.76	35.97	35.6	35.85	35.71
TiO ₂	4.06	4.05	4.20	3.73	3.93	3.66	3.28	3.8	3.28	2.81
Al ₂ O ₃	14.60	14.82	14.88	14.87	14.65	14.65	14.61	14.66	14.18	14.52
Fe ₂ O ₃	3.31	3.36	3.35	3.46	3.44	3.41	3.32	3.25	3.39	3.39
FeO	16.89	17.13	17.06	17.64	17.54	17.37	16.94	16.55	17.26	17.27
MnO	0.32	0.29	0.30	0.29	0.33	0.33	0.36	0.27	0.26	0.41
MgO	10.95	10.52	10.57	9.93	10.3	10.56	10.34	10.02	10.7	10.54
CaO	0.01	0.01	0.02	0.32	0	0	0	0.03	0	0.02
Na ₂ O	0.08	0.09	0.08	0.08	0.08	0.07	0.07	0.12	0.1	0.12
K ₂ O	9.48	9.40	9.68	8.83	9.59	9.51	9.69	9.39	9.8	9.34
Σ	95.08	95.30	95.87	93.88	95.78	95.32	94.58	93.69	94.82	94.13
Si	5.433	5.455	5.443	5.414	5.486	5.484	5.550	5.529	5.535	5.543
Al ^{IV}	2.567	2.545	2.557	2.586	2.514	2.516	2.450	2.471	2.465	2.457
Σ Z	8.000	8.000	8.000	8.000	8.000	8.000	8.000	8.000	8.000	8.000
Al ^{VI}	0.076	0.130	0.115	0.147	0.124	0.133	0.207	0.213	0.116	0.200
Ti	0.469	0.466	0.481	0.437	0.451	0.422	0.381	0.444	0.381	0.328
Fe ³⁺	0.383	0.387	0.384	0.406	0.395	0.393	0.386	0.379	0.393	0.396
Fe ²⁺	2.169	2.193	2.173	2.300	2.241	2.228	2.186	2.150	2.229	2.242
Mn	0.042	0.038	0.039	0.038	0.043	0.043	0.047	0.036	0.034	0.054
Mg	2.506	2.400	2.400	2.307	2.345	2.413	2.378	2.319	2.462	2.438
Σ Y	5.645	5.614	5.592	5.635	5.599	5.632	5.585	5.541	5.615	5.658
Ca	0.002	0.002	0.003	0.053	0.000	0.000	0.000	0.005	0.000	0.003
Na	0.024	0.027	0.024	0.024	0.024	0.021	0.021	0.036	0.030	0.036
K	1.857	1.836	1.881	1.756	1.869	1.861	1.907	1.861	1.930	1.849
Σ X	1.883	1.865	1.908	1.833	1.893	1.882	1.928	1.902	1.960	1.888
Σ cat	15.528	15.479	15.500	15.468	15.492	15.514	15.513	15.443	15.575	15.546
Fe* Fe*+Mg	0.50	0.52	0.52	0.54	0.53	0.52	0.52	0.52	0.52	0.52

Appendix VII. Composition of biotites (cont.)

(Structural formulae are based on 22 oxygens)

Blatná suite (cont.)

	Koz-6			KozD-1						
	biot clot1 clot after px	biot 1 large, core	biot 2 C large, euhedral	biot 1 small core	biot 2 small bi core	biot 3 small bi core	biot 4 small biotites enlosed by amph	biot 5	biot clot1 rim of the clot	biot clot2 core of the clot
SiO ₂	36.01	34.23	34.45	35.81	35.54	36.95	35.89	37.69	35.56	36.45
TiO ₂	3.32	3.67	3.51	4.13	3.45	3.90	3.47	3.39	3.78	3.86
Al ₂ O ₃	14.48	14.38	14.86	14.52	14.23	14.26	14.40	13.12	14.62	14.29
Fe ₂ O ₃	3.61	3.60	3.41	3.14	3.02	2.98	3.07	3.04	2.99	3.04
FeO	18.43	18.35	17.37	15.99	15.40	15.17	15.64	15.52	15.23	15.49
MnO	0.27	0.26	0.29	0.24	0.27	0.29	0.23	0.25	0.26	0.08
MgO	10.83	10.19	10.54	11.71	12.26	11.87	11.96	12.35	11.46	11.99
CaO	0.03	0	0	0.00	0.00	0.00	0.05	1.16	0.02	0.02
Na ₂ O	0.08	0.12	0.11	0.10	0.08	0.08	0.09	0.14	0.14	0.09
K ₂ O	9.90	9.38	9.46	9.72	9.77	9.66	9.64	8.64	9.35	9.67
Σ	96.95	94.17	94.01	95.35	94.02	95.16	94.44	95.30	93.41	94.97
Si	5.467	5.367	5.378	5.457	5.486	5.598	5.509	5.695	5.502	5.547
Al ^{IV}	2.533	2.633	2.622	2.543	2.514	2.402	2.491	2.305	2.498	2.453
Σ Z	8.000	8.000	8.000	8.000	8.000	8.000	8.000	8.000	8.000	8.000
Al ^{VI}	0.059	0.024	0.113	0.066	0.075	0.145	0.115	0.032	0.169	0.111
Ti	0.379	0.432	0.412	0.473	0.400	0.444	0.401	0.385	0.440	0.442
Fe ³⁺	0.413	0.425	0.400	0.360	0.351	0.339	0.354	0.346	0.348	0.348
Fe ²⁺	2.340	2.406	2.268	2.038	1.988	1.923	2.008	1.961	1.971	1.971
Mn	0.035	0.034	0.039	0.031	0.035	0.037	0.030	0.032	0.034	0.010
Mg	2.450	2.381	2.452	2.659	2.820	2.680	2.736	2.781	2.643	2.719
Σ Y	5.676	5.702	5.684	5.627	5.669	5.568	5.644	5.537	5.605	5.601
Ca	0.005	0.000	0.000	0.000	0.000	0.000	0.008	0.188	0.003	0.003
Na	0.023	0.038	0.034	0.030	0.024	0.024	0.027	0.041	0.042	0.027
K	1.917	1.876	1.884	1.890	1.924	1.867	1.888	1.665	1.846	1.877
Σ X	1.945	1.914	1.918	1.920	1.948	1.891	1.923	1.894	1.891	1.907
Σ cat	15.621	15.616	15.602	15.547	15.617	15.459	15.567	15.431	15.496	15.508
$\frac{\text{Fe}^*}{\text{Fe}^*+\text{Mg}}$	0.53	0.54	0.52	0.47	0.45	0.46	0.46	0.45	0.47	0.46

Appendix VII. Composition of biotites (cont.)

(Structural formulae are based on 22 oxygens)

Blatná suite (cont.)

	B1-2						B1-3			
	biot 1 large bi core	biot 2 tiny bi core	biot 3 large bi core	biot 4 small bi in KF	biot 5 large bi	biot 6 large bi core	biot 1 tiny bi in KF	biot 2 small core	biot 3 small core	biot 4 large bi core
SiO ₂	36.06	36.33	36.22	36.05	36.60	35.23	35.79	35.58	35.21	35.74
TiO ₂	3.05	3.35	3.42	3.33	3.08	3.19	3.24	3.37	3.02	3.57
Al ₂ O ₃	14.51	14.53	14.28	15.01	14.69	14.39	15.16	14.85	15.05	14.96
Fe ₂ O ₃	2.99	3.01	3.07	3.06	3.07	2.91	3.19	3.15	3.32	3.36
FeO	15.22	15.37	15.66	15.61	15.67	14.84	16.29	16.06	16.93	17.11
MnO	0.27	0.33	0.31	0.30	0.33	0.30	0.33	0.24	0.36	0.29
MgO	11.53	11.89	12.00	11.29	11.52	11.91	11.41	11.79	11.40	11.70
CaO	0.00	0.00	0.01	0.00	0.00	0.01	0.00	0.00	0.00	0.00
Na ₂ O	0.19	0.10	0.05	0.13	0.09	0.06	0.12	0.08	0.07	0.09
K ₂ O	9.53	9.83	9.76	9.65	9.88	9.64	9.60	9.78	9.71	9.79
Σ	93.35	94.74	94.78	94.43	94.93	92.48	95.13	94.90	95.06	96.61
Si	5.581	5.550	5.540	5.526	5.583	5.512	5.467	5.452	5.416	5.407
Al ^{IV}	2.419	2.450	2.460	2.474	2.417	2.488	2.533	2.548	2.584	2.593
Σ Z	8.000	8.000	8.000	8.000	8.000	8.000	8.000	8.000	8.000	8.000
Al ^{VI}	0.229	0.167	0.115	0.239	0.225	0.166	0.198	0.135	0.144	0.075
Ti	0.355	0.385	0.393	0.384	0.353	0.375	0.373	0.389	0.349	0.407
Fe ³⁺	0.348	0.346	0.353	0.353	0.353	0.343	0.367	0.363	0.384	0.382
Fe ²⁺	1.971	1.963	2.003	2.001	1.999	1.942	2.081	2.058	2.178	2.165
Mn	0.035	0.043	0.040	0.039	0.043	0.040	0.043	0.031	0.047	0.037
Mg	2.660	2.707	2.736	2.579	2.619	2.777	2.598	2.692	2.614	2.638
Σ Y	5.598	5.611	5.640	5.595	5.592	5.643	5.660	5.668	5.716	5.704
Ca	0.000	0.000	0.002	0.000	0.000	0.002	0.000	0.000	0.000	0.000
Na	0.057	0.030	0.015	0.039	0.027	0.018	0.035	0.025	0.020	0.025
K	1.882	1.916	1.905	1.887	1.923	1.924	1.871	1.911	1.905	1.890
Σ X	1.939	1.946	1.922	1.926	1.950	1.944	1.906	1.936	1.925	1.915
Σ cat	15.537	15.557	15.562	15.521	15.542	15.587	15.566	15.604	15.641	15.619
∑(Fe*, Fe*+Mg)	0.47	0.46	0.46	0.48	0.47	0.45	0.49	0.47	0.49	0.49

Appendix VII. Composition of biotites (cont.)

(Structural formulae are based on 22 oxygens)

Blatná suite (cont.)

	B1-3	B1-5						B1-7		
	biot 5 small bi in KF	biot 1	biot 2	biot 3	biot 4	biot 5	biot 6	biot 1	biot 2	biot 3
		← large biotite		small core	bi in KF core	large, core	small in KF	large bi rim	small biotites enclosed by plag	
SiO ₂	35.63	35.50	35.92	36.25	35.79	36.52	35.76	36.04	35.95	36.11
TiO ₂	3.39	2.61	1.76	2.78	3.77	2.09	3.25	3.36	3.26	3.13
Al ₂ O ₃	15.09	14.97	15.09	14.98	14.66	15.36	14.95	14.59	14.19	14.15
Fe ₂ O ₃	3.31	11.32	11.54	11.29	10.92	11.68	11.12	3.15	3.19	3.11
FeO	16.90	0.00	0.00	0.00	0.00	0.03	0.00	16.07	16.24	15.85
MnO	0.29	0.31	0.31	0.25	0.32	0.35	0.34	0.34	0.26	0.29
MgO	11.74	3.52	3.42	3.28	3.41	3.37	3.39	11.28	11.43	11.50
CaO	0.00	17.93	17.43	16.75	17.38	17.17	17.30	0.03	0.00	0.00
Na ₂ O	0.08	0.08	0.07	0.15	0.09	0.16	0.10	0.11	0.10	0.06
K ₂ O	9.27	9.60	9.56	9.88	9.73	9.62	9.85	9.60	9.80	9.79
Σ	95.70	95.83	95.09	95.60	96.07	96.33	96.05	94.57	94.42	93.99
Si	5.419	5.435	5.517	5.525	5.453	5.521	5.450	5.533	5.543	5.579
Al ^{IV}	2.581	2.565	2.483	2.475	2.547	2.479	2.550	2.467	2.457	2.421
Σ Z	8.000	8.000	8.000	8.000	8.000	8.000	8.000	8.000	8.000	8.000
Al ^{VI}	0.125	0.137	0.249	0.216	0.086	0.259	0.135	0.174	0.122	0.156
Ti	0.388	0.300	0.204	0.318	0.432	0.237	0.372	0.388	0.378	0.364
Fe ³⁺	0.379	0.405	0.395	0.377	0.391	0.383	0.389	0.364	0.370	0.361
Fe ²⁺	2.149	2.295	2.239	2.135	2.215	2.171	2.205	2.064	2.095	2.048
Mn	0.037	0.040	0.040	0.032	0.041	0.045	0.044	0.044	0.034	0.038
Mg	2.662	2.584	2.642	2.563	2.480	2.631	2.524	2.581	2.627	2.648
Σ Y	5.740	5.761	5.769	5.641	5.645	5.726	5.669	5.615	5.626	5.615
Ca	0.000	0.000	0.000	0.000	0.000	0.004	0.000	0.005	0.000	0.000
Na	0.024	0.023	0.020	0.043	0.028	0.047	0.030	0.033	0.030	0.018
K	1.799	1.875	1.874	1.921	1.891	1.855	1.914	1.880	1.928	1.930
Σ X	1.823	1.898	1.894	1.964	1.919	1.906	1.944	1.918	1.958	1.948
Σ cat	15.563	15.659	15.663	15.605	15.564	15.632	15.613	15.533	15.584	15.563
Fe* Fe*+Mg	0.49	0.51	0.50	0.49	0.51	0.49	0.51	0.48	0.48	0.48

Appendix VII. Composition of biotites (cont.)

(Structural formulae are based on 22 oxygens)

Blatná suite (cont.)

	Bl-8					
	biot 1	biot 2	biot clot1 rim of the clot	biot clot3 core of the clot	biot clot4 rim of the clot	
	→ large biotite					
SiO ₂	35.94	35.89	35.30	37.34	35.87	
TiO ₂	1.17	3.81	3.16	1.39	3.27	
Al ₂ O ₃	15.96	14.67	14.66	14.90	14.86	
Fe ₂ O ₃	3.24	3.40	3.39	3.10	3.50	
FeO	16.50	17.32	17.31	15.78	17.86	
MnO	0.22	0.19	0.26	0.29	0.28	
MgO	12.28	10.79	10.92	12.87	11.09	
CaO	0.04	0.00	0.00	0.09	0.00	
Na ₂ O	0.08	0.08	0.06	0.11	0.08	
K ₂ O	9.19	9.91	9.43	9.65	9.43	
Σ	94.61	96.05	94.48	95.52	96.23	
Si	5.500	5.468	5.464	5.642	5.455	
Al ^{IV}	2.500	2.532	2.536	2.358	2.545	
Σ Z	8.000	8.000	8.000	8.000	8.000	
Al ^{VI}	0.378	0.102	0.139	0.295	0.119	
Ti	0.135	0.437	0.367	0.158	0.374	
Fe ³⁺	0.373	0.389	0.395	0.352	0.401	
Fe ²⁺	2.111	2.207	2.240	1.995	2.271	
Mn	0.028	0.025	0.034	0.037	0.036	
Mg	2.800	2.450	2.518	2.898	2.513	
Σ Y	5.825	5.610	5.693	5.735	5.714	
Ca	0.007	0.000	0.000	0.015	0.000	
Na	0.023	0.024	0.018	0.031	0.024	
K	1.793	1.926	1.862	1.861	1.828	
Σ X	1.823	1.950	1.880	1.907	1.852	
Σ cat	15.648	15.560	15.573	15.642	15.566	
$\frac{\text{Fe}^*}{\text{Fe}^*+\text{Mg}}$	0.47	0.51	0.51	0.45	0.52	

Appendix VII. Composition of biotites (cont.)

(Structural formulae are based on 22 oxygens)

Čertovo břemeno suite

	Se-4			Se-5				Se-6		
	biot 15* large, core	biot 17* large, core	biot 21* large, core	biot 1 large, core	biot 2 small in KF	biot 3 small core	biot clot1 core of the clot	biot 1 large euhedral bi	biot 2	biot clot1 rim of the clot
SiO ₂	37.09	37.02	37.50	36.61	36.43	36.35	36.67	36.85	36.69	36.47
TiO ₂	3.88	3.82	3.43	3.32	3.26	3.18	3.07	2.95	2.98	2.69
Al ₂ O ₃	13.76	14.09	13.56	13.76	14.23	13.99	13.92	14.15	14.41	14.02
Fe ₂ O ₃	2.68	2.84	2.74	2.62	2.67	2.68	2.69	2.71	2.73	2.74
FeO	13.67	14.48	13.96	13.34	13.63	13.69	13.72	13.84	13.94	13.95
MnO	0.25	0.33	0.34	0.27	0.28	0.24	0.35	0.36	0.29	0.36
MgO	13.59	13.46	13.81	13.51	13.41	13.40	13.62	13.82	13.78	13.77
CaO	0.00	0.02	0.00	0.04	0.00	0.03	0.00	0.00	0.00	0.00
Na ₂ O	0.19	0.30	0.28	0.10	0.05	0.06	0.08	0.08	0.06	0.09
K ₂ O	9.65	9.64	9.67	9.74	9.61	9.70	9.88	10.03	9.75	9.86
Σ	94.76	96.00	95.27	93.30	93.57	93.32	94.00	94.79	94.64	93.94
Si	5.588	5.532	5.637	5.618	5.576	5.586	5.600	5.585	5.561	5.582
Al ^{IV}	2.412	2.468	2.363	2.382	2.424	2.414	2.400	2.415	2.439	2.418
Σ Z	8.000	8.000	8.000	8.000	8.000	8.000	8.000	8.000	8.000	8.000
Al ^{VI}	0.032	0.015	0.039	0.107	0.144	0.121	0.106	0.113	0.136	0.111
Ti	0.440	0.429	0.387	0.383	0.375	0.368	0.353	0.336	0.340	0.310
Fe ³⁺	0.304	0.319	0.310	0.302	0.308	0.310	0.309	0.310	0.312	0.315
Fe ²⁺	1.722	1.810	1.755	1.712	1.744	1.759	1.752	1.754	1.768	1.786
Mn	0.031	0.042	0.043	0.035	0.036	0.031	0.045	0.046	0.037	0.047
Mg	3.052	2.997	3.093	3.090	3.059	3.069	3.100	3.120	3.113	3.141
Σ Y	5.581	5.612	5.627	5.629	5.666	5.658	5.665	5.679	5.706	5.710
Ca	0.000	0.003	0.000	0.006	0.000	0.005	0.000	0.000	0.000	0.000
Na	0.057	0.085	0.081	0.029	0.015	0.018	0.024	0.022	0.017	0.025
K	1.855	1.838	1.853	1.907	1.876	1.902	1.925	1.939	1.885	1.924
Σ X	1.912	1.926	1.934	1.942	1.891	1.925	1.949	1.961	1.902	1.949
Σ cat	15.525	15.586	15.579	15.571	15.557	15.583	15.614	15.641	15.607	15.661
Fe*										
Fe*+Mg	0.40	0.42	0.40	0.39	0.40	0.40	0.40	0.40	0.40	0.40

Appendix VII. Composition of biotites (cont.)

(Structural formulae are based on 22 oxygens)

Čertovo břemeno suite (cont.)

	Se-6						Se-7			
	biot clot2 core of the clot	biot 3	biot 4	biot 5	biot clot3 rim of the clot	biot clot4 core of the clot	biot 1	biot 2	biot 3	biot 4
		← large		small bi core			small bi core	small bi core	→ large biotite	
SiO ₂	36.78	36.51	36.51	36.40	36.74	37.15	36.52	36.36	37.04	37.44
TiO ₂	2.86	3.16	3.05	3.23	2.72	2.63	3.23	3.18	3.34	2.71
Al ₂ O ₃	14.23	14.40	14.43	14.72	14.38	14.59	14.29	14.46	13.54	13.32
Fe ₂ O ₃	2.76	2.90	2.75	2.79	2.67	2.65	2.74	2.71	2.64	2.49
FeO	14.05	14.77	14.00	14.21	13.63	13.53	13.98	13.80	13.47	12.68
MnO	0.33	0.36	0.30	0.35	0.24	0.43	0.28	0.27	0.23	0.23
MgO	13.67	13.44	13.13	13.28	13.53	14.05	12.86	13.46	13.80	14.16
CaO	0.00	0.01	0.04	0.00	0.02	0.02	0.00	0.00	0.00	0.00
Na ₂ O	0.06	0.07	0.09	0.07	0.08	0.10	0.03	0.12	0.10	0.14
K ₂ O	9.95	9.83	9.86	9.98	9.96	10.05	9.99	9.69	9.52	9.53
Σ	94.68	95.45	94.16	95.03	93.96	95.20	93.92	94.04	93.68	92.70
Si	5.583	5.518	5.572	5.514	5.604	5.590	5.589	5.545	5.650	5.742
Al ^{IV}	2.417	2.482	2.428	2.486	2.396	2.410	2.411	2.455	2.350	2.258
Σ Z	8.000	8.000	8.000	8.000	8.000	8.000	8.000	8.000	8.000	8.000
Al ^{VI}	0.129	0.085	0.168	0.143	0.190	0.179	0.167	0.145	0.085	0.151
Ti	0.327	0.360	0.350	0.368	0.311	0.297	0.372	0.365	0.383	0.313
Fe ³⁺	0.315	0.330	0.315	0.318	0.307	0.300	0.316	0.311	0.303	0.287
Fe ²⁺	1.784	1.868	1.787	1.801	1.738	1.703	1.790	1.760	1.719	1.627
Mn	0.042	0.046	0.039	0.045	0.031	0.054	0.036	0.035	0.030	0.030
Mg	3.092	3.027	2.985	2.997	3.077	3.152	2.933	3.059	3.137	3.237
Σ Y	5.689	5.716	5.644	5.672	5.654	5.685	5.614	5.675	5.657	5.645
Ca	0.000	0.002	0.007	0.000	0.003	0.003	0.000	0.000	0.000	0.000
Na	0.019	0.020	0.027	0.020	0.024	0.028	0.009	0.035	0.030	0.042
K	1.926	1.896	1.920	1.928	1.939	1.930	1.950	1.885	1.853	1.865
Σ X	1.945	1.918	1.954	1.948	1.966	1.961	1.959	1.920	1.883	1.907
Σ cat	15.633	15.632	15.597	15.619	15.619	15.647	15.572	15.595	15.539	15.550
Fe* Fe*+Mg	0.40	0.42	0.41	0.41	0.40	0.39	0.42	0.40	0.39	0.37

Appendix VII. Composition of biotites (cont.)

(Structural formulae are based on 22 oxygens)

Čertovo břemeno suite (cont.)

	Se-7		Se-9				
	biot clot1	biot 5 small in plag	biot 1 small in plag	biot clot1 core of the clot	biot 2 small core	biot 3 small core	
SiO ₂	36.13	36.80	37.32	37.34	37.17	36.14	
TiO ₂	3.35	3.31	2.75	2.38	2.82	2.68	
Al ₂ O ₃	14.16	13.77	14.52	14.88	14.81	14.69	
Fe ₂ O ₃	2.77	2.52	2.71	2.59	2.75	2.72	
FeO	14.14	12.86	13.80	13.20	14.03	13.87	
MnO	0.29	0.26	0.30	0.22	0.30	0.28	
MgO	13.50	14.12	13.89	14.43	13.59	13.57	
CaO	0.01	0.03	0.00	0.00	0.01	0.00	
Na ₂ O	0.09	0.10	0.08	0.06	0.12	0.05	
K ₂ O	9.75	9.77	9.85	9.77	9.71	10.00	
Σ	94.20	93.54	95.21	94.87	95.30	94.00	
Si	5.521	5.616	5.610	5.607	5.585	5.527	
Al ^{IV}	2.479	2.384	2.390	2.393	2.415	2.473	
Σ Z	8.000	8.000	8.000	8.000	8.000	8.000	
Al ^{VI}	0.072	0.093	0.183	0.241	0.208	0.176	
Ti	0.385	0.380	0.311	0.269	0.319	0.308	
Fe ³⁺	0.319	0.290	0.306	0.292	0.311	0.313	
Fe ²⁺	1.807	1.641	1.734	1.657	1.763	1.774	
Mn	0.038	0.034	0.038	0.027	0.039	0.036	
Mg	3.074	3.211	3.112	3.229	3.043	3.094	
Σ Y	5.695	5.649	5.684	5.715	5.683	5.701	
Ca	0.002	0.005	0.000	0.000	0.001	0.000	
Na	0.027	0.030	0.023	0.017	0.034	0.014	
K	1.901	1.902	1.889	1.872	1.861	1.951	
Σ X	1.930	1.937	1.912	1.889	1.896	1.965	
Σ cat	15.623	15.586	15.596	15.605	15.577	15.666	
Fe*							
Fe*+Mg	0.41	0.38	0.40	0.38	0.41	0.40	

Appendix VII. Composition of biotites (cont.)

(Structural formulae are based on 22 oxygens)

Říčany suite

	R1-1									
	biot 12* small, rim	biot 13* large, core	biot 15* C large euhed.	biot 29* small, core	biot 30*	biot 1	biot 2	biot 3	biot 4	biot 5
						← large elongate bi		← large euhedral bi		small bi clot
SiO ₂	37.15	37.43	37.62	37.91	37.51	37.51	37.32	36.75	36.99	36.88
TiO ₂	3.40	3.61	3.47	2.86	3.28	3.40	2.86	3.51	3.28	3.26
Al ₂ O ₃	14.55	13.95	13.92	14.64	14.05	14.89	15.45	15.36	15.62	15.43
Fe ₂ O ₃	2.75	2.69	2.73	2.63	2.74	2.69	2.74	2.83	2.67	2.81
FeO	14.02	13.72	13.94	13.39	13.97	13.70	13.95	14.41	13.60	14.32
MnO	0.36	0.25	0.29	0.26	0.28	0.23	0.20	0.25	0.28	0.21
MgO	12.57	12.77	12.85	12.74	12.75	12.66	12.45	12.13	12.25	12.10
CaO	0.00	0.08	0.05	0.00	0.00	0.00	0.00	0.00	0.03	0.01
Na ₂ O	0.15	0.15	0.43	0.05	0.15	0.08	0.04	0.09	0.08	0.09
K ₂ O	9.76	9.56	9.73	9.69	9.71	9.50	9.67	9.54	9.74	9.55
Σ	94.71	94.20	95.03	94.16	94.44	94.66	94.67	94.86	94.54	94.66
Si	5.618	5.672	5.669	5.728	5.670	5.646	5.626	5.551	5.584	5.576
Al ^{IV}	2.382	2.328	2.331	2.272	2.330	2.354	2.374	2.449	2.416	2.424
Σ Z	8.000	8.000	8.000	8.000	8.000	8.000	8.000	8.000	8.000	8.000
Al ^{VI}	0.211	0.164	0.142	0.336	0.174	0.288	0.372	0.286	0.364	0.327
Ti	0.386	0.411	0.393	0.325	0.373	0.385	0.324	0.399	0.372	0.371
Fe ³⁺	0.313	0.307	0.310	0.299	0.312	0.304	0.310	0.321	0.303	0.320
Fe ²⁺	1.773	1.739	1.756	1.692	1.766	1.725	1.758	1.820	1.717	1.811
Mn	0.046	0.032	0.037	0.034	0.036	0.029	0.026	0.032	0.036	0.027
Mg	2.833	2.885	2.884	2.869	2.872	2.840	2.797	2.731	2.756	2.727
Σ Y	5.562	5.538	5.522	5.555	5.533	5.571	5.587	5.589	5.548	5.583
Ca	0.001	0.012	0.008	0.000	0.001	0.000	0.000	0.000	0.005	0.002
Na	0.044	0.043	0.127	0.014	0.044	0.023	0.012	0.026	0.023	0.026
K	1.883	1.848	1.870	1.868	1.873	1.824	1.860	1.838	1.876	1.842
Σ X	1.928	1.903	2.005	1.882	1.918	1.847	1.872	1.864	1.904	1.870
Σ cat	15.490	15.441	15.527	15.437	15.451	15.418	15.459	15.453	15.452	15.453
Fe* Fe*+Mg	0.42	0.41	0.42	0.41	0.42	0.42	0.43	0.44	0.42	0.44

Appendix VIII. Composition of amphiboles
(Structural formulae are based on 23 oxygens)

Sázava suite

	Sa-3									
	amph 1	amph 2	amph 3	amph 4	amph 5	amph 6	amph 7	amph 8	amph 9	amph 10
	← large euhedral amph			→ large		→ large		→ large euhedral		large rim
SiO ₂	44.70	44.82	42.66	43.38	42.49	43.67	43.35	44.48	43.64	43.29
TiO ₂	1.16	0.95	1.09	0.72	0.62	1.23	1.39	0.97	1.17	0.94
Al ₂ O ₃	8.35	8.15	9.92	9.85	10.20	9.22	9.47	9.03	9.05	9.59
FeO	17.75	18.29	19.18	18.91	20.23	17.66	18.57	17.18	17.81	18.66
MnO	0.45	0.49	0.45	0.39	0.54	0.39	0.49	0.40	0.52	0.43
MgO	10.77	10.79	9.23	9.26	9.30	10.15	9.82	11.41	10.07	9.40
CaO	11.81	11.93	12.06	12.08	11.92	11.98	11.92	11.98	11.88	11.95
Na ₂ O	0.89	0.91	1.07	0.95	1.05	1.03	1.08	0.93	1.05	1.00
K ₂ O	0.84	0.87	1.01	1.04	1.17	1.04	1.02	0.91	1.03	1.13
Σ	96.71	97.20	96.66	96.58	97.52	96.36	97.10	97.30	96.22	96.38
Si	6.726	6.722	6.505	6.604	6.422	6.637	6.559	6.624	6.648	6.610
Al ^{IV}	1.274	1.278	1.495	1.396	1.578	1.363	1.441	1.376	1.352	1.390
Σ(T)	8.000	8.000	8.000	8.000	8.000	8.000	8.000	8.000	8.000	8.000
Al ^{VI}	0.207	0.162	0.288	0.371	0.241	0.288	0.247	0.209	0.273	0.336
Ti	0.132	0.107	0.125	0.083	0.071	0.140	0.158	0.108	0.134	0.108
Fe ³⁺	0.487	0.557	0.477	0.408	0.736	0.343	0.437	0.603	0.367	0.371
Mg	2.416	2.412	2.097	2.102	2.094	2.299	2.214	2.533	2.286	2.140
Fe ²⁺	1.746	1.737	1.969	2.000	1.821	1.902	1.913	1.537	1.902	2.011
Mn	0.013	0.024	0.045	0.037	0.037	0.028	0.031	0.010	0.039	0.035
Σ(C)	5.000	5.000	5.000	5.000	5.000	5.000	5.000	5.000	5.000	5.000
Fe ²⁺	0.000	0.000	0.000	0.000	0.000	0.000	0.000	0.000	0.000	0.000
Mn	0.045	0.039	0.014	0.014	0.032	0.023	0.032	0.041	0.028	0.021
Mg	0.000	0.000	0.000	0.000	0.000	0.000	0.000	0.000	0.000	0.000
Ca	1.904	1.917	1.970	1.970	1.931	1.951	1.932	1.911	1.939	1.955
Na(M4)	0.052	0.044	0.017	0.016	0.037	0.027	0.037	0.048	0.033	0.024
Σ(B)	2.000	2.000	2.000	2.000	2.000	2.000	2.000	2.000	2.000	2.000
Na(A)	0.207	0.222	0.301	0.265	0.272	0.277	0.280	0.222	0.278	0.271
K	0.161	0.167	0.196	0.203	0.225	0.201	0.198	0.173	0.200	0.221
Σ(A)	0.368	0.388	0.497	0.468	0.497	0.478	0.478	0.395	0.478	0.492
Σ cat	15.368	15.388	15.497	15.468	15.497	15.478	15.478	15.395	15.478	15.492
Mg Fe ²⁺ +Mg	0.574	0.576	0.514	0.511	0.530	0.544	0.532	0.616	0.542	0.513
Al ^T	1.480	1.440	1.783	1.768	1.818	1.561	1.689	1.586	1.625	1.726

Appendix VIII. Composition of amphiboles (cont.)

(Structural formulae are based on 23 oxygens)

Sázava suite (cont.)

	Sa-10						Sa-7			
	amph1*	amph4*	amph 1	amph 2	amph 3	amph 4	amph 5	amph7a	amph10	amph11
	small, core	large, core	large rim	large rim	large core	small core	large rim	small core	large rim	large rim
SiO ₂	44.04	45.73	43.98	43.15	42.93	43.96	46.81	47.36	45.26	45.42
TiO ₂	1.07	1.20	0.87	1.05	0.81	0.71	0.79	0.13	0.97	0.94
Al ₂ O ₃	8.79	7.70	8.17	7.89	8.14	7.30	7.55	6.43	8.32	8.47
FeO	20.75	20.48	20.66	20.25	20.03	19.74	19.22	19.72	20.62	20.20
MnO	0.81	1.04	0.90	0.88	0.82	0.98	0.46	0.36	0.74	0.47
MgO	9.26	9.92	9.45	9.56	9.76	9.99	10.60	10.00	10.01	9.46
CaO	11.18	11.37	11.11	10.97	10.91	10.99	11.67	12.28	10.55	11.38
Na ₂ O	1.32	1.35	1.17	0.97	1.18	0.99	0.80	0.53	1.04	1.12
K ₂ O	0.76	0.59	0.69	0.67	0.63	0.57	0.50	0.29	0.45	0.53
Σ	97.98	99.39	97.00	95.39	95.21	95.23	98.42	97.09	97.96	97.99
Si	6.623	6.764	6.664	6.632	6.603	6.744	6.909	7.105	6.729	6.791
Al ^{IV}	1.377	1.236	1.336	1.368	1.397	1.256	1.092	0.895	1.271	1.210
Σ(T)	8.000	8.000	8.000	8.000	8.000	8.000	8.000	8.000	8.000	8.000
Al ^{VI}	0.182	0.107	0.124	0.061	0.079	0.064	0.223	0.242	0.187	0.284
Ti	0.121	0.134	0.099	0.121	0.094	0.082	0.088	0.014	0.109	0.106
Fe ³⁺	0.638	0.575	0.746	0.851	0.871	0.830	0.535	0.443	0.783	0.478
Mg	2.076	2.187	2.134	2.190	2.237	2.284	2.331	2.235	2.218	2.109
Fe ²⁺	1.972	1.959	1.872	1.752	1.706	1.703	1.824	2.032	1.704	2.024
Mn	0.011	0.038	0.025	0.025	0.013	0.038	0.000	0.034	0.000	0.000
Σ(C)	5.000	5.000	5.000	5.000	5.000	5.000	5.000	5.000	5.000	5.000
Fe ²⁺	0.000	0.000	0.000	0.000	0.000	0.000	0.014	0.000	0.077	0.024
Mn	0.093	0.092	0.091	0.090	0.094	0.090	0.058	0.012	0.093	0.059
Mg	0.000	0.000	0.000	0.000	0.000	0.000	0.000	0.000	0.000	0.000
Ca	1.801	1.801	1.804	1.807	1.798	1.807	1.846	1.974	1.681	1.823
Na(M4)	0.107	0.106	0.105	0.104	0.108	0.104	0.083	0.014	0.150	0.095
Σ(B)	2.000	2.000	2.000	2.000	2.000	2.000	2.000	2.000	2.000	2.000
Na(A)	0.277	0.282	0.239	0.185	0.244	0.191	0.147	0.139	0.150	0.231
K	0.145	0.111	0.133	0.131	0.124	0.112	0.094	0.056	0.084	0.101
Σ(A)	0.422	0.393	0.372	0.317	0.367	0.302	0.241	0.195	0.234	0.332
Σ cat	15.422	15.393	15.372	15.317	15.367	15.302	15.241	15.195	15.234	15.332
$\frac{Mg}{Fe^{2+}+Mg}$	0.513	0.527	0.533	0.556	0.567	0.573	0.559	0.524	0.555	0.507
Al ^T	1.559	1.343	1.460	1.430	1.476	1.320	1.314	1.137	1.458	1.493

Appendix VIII. Composition of amphiboles (cont.)
(Structural formulae are based on 23 oxygens)

Sázava suite (cont.)

	Sa-7			SaD-1						
	amph12	amph1 3	amph1 5	amph 1	amph 2	amph 3	amph 4	amph 5	amph 6	amph 7
				small core	small core	large rim	large		small	
SiO ₂	46.22	47.56	45.20	45.78	44.26	44.95	44.69	41.99	40.67	46.09
TiO ₂	1.03	0.59	1.04	0.98	1.46	1.26	1.42	2.46	2.27	0.93
Al ₂ O ₃	7.59	6.15	8.08	7.65	9.01	7.92	8.72	12.88	12.83	7.18
FeO	21.03	19.90	19.54	17.81	19.67	19.51	17.93	13.52	18.35	20.47
MnO	0.80	0.77	0.56	0.39	0.48	0.58	0.39	0.27	0.34	0.62
MgO	10.00	10.73	9.62	9.82	9.50	10.19	10.05	11.46	8.43	10.65
CaO	10.35	10.89	11.20	11.52	10.76	10.16	11.02	11.45	11.86	9.28
Na ₂ O	1.15	0.88	1.17	0.77	2.90	0.88	1.13	1.46	1.14	0.79
K ₂ O	0.46	0.31	0.52	0.38	3.80	4.40	4.10	0.58	0.50	0.35
Σ	98.62	97.79	96.92	95.10	101.84	99.85	99.45	96.07	96.40	96.36
Si	6.843	7.058	6.827	6.997	6.676	6.813	6.779	6.266	6.185	6.950
Al ^{IV}	1.157	0.942	1.173	1.003	1.324	1.187	1.221	1.734	1.816	1.050
Σ(T)	8.000	8.000	8.000	8.000	8.000	8.000	8.000	8.000	8.000	8.000
Al ^{VI}	0.169	0.135	0.266	0.376	0.278	0.228	0.338	0.532	0.485	0.226
Ti	0.115	0.065	0.118	0.113	0.166	0.144	0.162	0.276	0.259	0.105
Fe ³⁺	0.671	0.618	0.431	0.221	0.527	0.599	0.363	0.298	0.450	0.546
Mg	2.206	2.374	2.164	2.237	2.135	2.302	2.272	2.549	1.910	2.393
Fe ²⁺	1.839	1.808	2.022	2.054	1.895	1.728	1.865	1.345	1.883	1.730
Mn	0.000	0.000	0.000	0.000	0.000	0.000	0.000	0.000	0.013	0.000
Σ(C)	5.000	5.000	5.000	5.000	5.000	5.000	5.000	5.000	5.000	5.000
Fe ²⁺	0.094	0.044	0.016	0.002	0.060	0.146	0.047	0.044	0.000	0.305
Mn	0.100	0.097	0.072	0.051	0.061	0.075	0.050	0.034	0.031	0.079
Mg	0.000	0.000	0.000	0.000	0.000	0.000	0.000	0.000	0.000	0.000
Ca	1.641	1.732	1.812	1.887	1.739	1.650	1.791	1.831	1.932	1.499
Na(M4)	0.165	0.127	0.101	0.061	0.140	0.129	0.112	0.091	0.036	0.116
Σ(B)	2.000	2.000	2.000	2.000	2.000	2.000	2.000	2.000	2.000	2.000
Na(A)	0.165	0.127	0.241	0.168	0.223	0.129	0.221	0.332	0.301	0.116
K	0.087	0.058	0.100	0.074	0.106	0.074	0.087	0.110	0.097	0.068
Σ(A)	0.252	0.185	0.342	0.242	0.329	0.203	0.308	0.442	0.398	0.184
Σ cat	15.252	15.185	15.342	15.242	15.329	15.203	15.308	15.442	15.397	15.184
Mg Fe ²⁺ Mg	0.533	0.562	0.515	0.521	0.522	0.551	0.543	0.647	0.504	0.540
Al ^T	1.325	1.077	1.438	1.379	1.602	1.415	1.559	2.266	2.301	1.276

Appendix VIII. Composition of amphiboles (cont.)

(Structural formulae are based on 23 oxygens)

Sázava suite (cont.)

	amph 8 large core	SaD-1								
		1	2	3	4	5	6	7	8	9
		scan across zoned amphibole								
SiO ₂	41.65	44.89	45.16	45.10	46.72	46.66	45.48	41.43	40.61	41.71
TiO ₂	2.00	0.91	0.91	1.28	0.86	0.80	1.12	1.50	2.68	2.99
Al ₂ O ₃	11.10	8.03	8.14	8.41	8.76	8.22	8.13	11.33	13.16	14.23
FeO	19.91	10.15	10.09	10.26	10.47	11.62	10.55	9.19	9.60	10.69
MnO	0.53	10.90	11.02	10.93	11.45	11.41	11.54	11.63	11.48	11.46
MgO	8.29	0.64	0.49	0.55	0.44	0.44	0.44	0.39	0.37	0.27
CaO	11.23	18.78	19.12	19.05	17.78	17.09	17.83	18.55	16.17	13.05
Na ₂ O	1.41	1.03	1.02	1.10	0.87	0.77	0.83	1.25	1.59	1.90
K ₂ O	0.57	0.36	0.40	0.39	0.50	0.46	0.42	0.72	0.60	0.54
Σ	96.70	95.71	96.34	97.07	97.84	97.45	96.34	95.97	96.27	96.84
Si	6.355	6.807	6.811	6.747	6.904	6.869	6.837	6.326	6.149	6.190
Al ^{IV}	1.645	1.193	1.189	1.253	1.096	1.131	1.163	1.674	1.851	1.810
Σ(T)	8.000	8.000	8.000	8.000	8.000	8.000	8.000	8.000	8.000	8.000
Al ^{VI}	0.352	0.243	0.259	0.230	0.431	0.296	0.278	0.364	0.497	0.679
Ti	0.230	0.104	0.103	0.144	0.095	0.089	0.127	0.172	0.305	0.333
Fe ³⁺	0.481	0.612	0.583	0.607	0.333	0.566	0.460	0.561	0.308	0.108
Mg	1.885	2.294	2.267	2.288	2.307	2.549	2.364	2.090	2.166	2.365
Fe ²⁺	2.052	1.747	1.788	1.731	1.834	1.500	1.771	1.807	1.724	1.511
Mn	0.000	0.000	0.000	0.000	0.000	0.000	0.000	0.005	0.000	0.003
Σ(C)	5.000	5.000	5.000	5.000	5.000	5.000	5.000	5.000	5.000	5.000
Fe ²⁺	0.008	0.023	0.040	0.045	0.031	0.039	0.010	0.000	0.016	0.000
Mn	0.069	0.083	0.062	0.070	0.056	0.054	0.055	0.045	0.047	0.031
Mg	0.000	0.000	0.000	0.000	0.000	0.000	0.000	0.000	0.000	0.000
Ca	1.835	1.772	1.780	1.753	1.813	1.800	1.859	1.902	1.863	1.822
Na(M4)	0.088	0.122	0.118	0.133	0.100	0.107	0.075	0.052	0.074	0.148
Σ(B)	2.000	2.000	2.000	2.000	2.000	2.000	2.000	2.000	2.000	2.000
Na(A)	0.329	0.182	0.182	0.186	0.148	0.112	0.167	0.318	0.394	0.400
K	0.111	0.070	0.077	0.074	0.094	0.086	0.080	0.140	0.116	0.103
Σ(A)	0.440	0.252	0.259	0.260	0.241	0.198	0.247	0.458	0.510	0.503
Σ cat	15.440	15.252	15.259	15.260	15.241	15.198	15.247	15.458	15.510	15.503
$\frac{Mg}{Fe^{2+}Mg}$	0.478	0.564	0.554	0.563	0.553	0.624	0.570	0.536	0.555	0.610
Al ^T	1.997	1.436	1.448	1.483	1.527	1.427	1.441	2.039	2.348	2.489

Appendix VIII. Composition of amphiboles (cont.)

(Structural formulae are based on 23 oxygens)

Sázava suite (cont.)

	SaD-1									
	10	12	13	14	16	17	18	20	21	22
	scan across zoned amphibole									
SiO ₂	40.76	40.38	40.63	40.22	41.12	41.09	41.43	41.28	43.19	45.69
TiO ₂	2.96	3.87	2.24	3.15	2.75	2.85	2.40	2.82	0.58	1.21
Al ₂ O ₃	13.61	13.16	13.66	13.73	14.14	13.58	12.52	13.81	8.82	8.78
FeO	11.94	13.03	11.80	12.06	12.36	12.68	10.63	12.37	11.35	12.31
MnO	11.79	11.53	11.90	11.57	11.85	11.65	11.89	11.94	9.98	11.77
MgO	0.21	0.19	0.24	0.35	0.12	0.14	0.29	0.17	0.35	0.41
CaO	12.56	11.60	12.97	12.76	11.67	11.61	14.87	11.61	18.31	14.21
Na ₂ O	1.73	1.84	1.56	1.71	1.81	1.68	1.15	1.78	0.61	0.95
K ₂ O	0.51	0.47	0.53	0.50	0.55	0.49	0.55	0.47	0.23	0.34
Σ	96.07	96.06	95.54	96.05	96.37	95.76	95.73	96.25	93.43	95.67
Si	6.081	5.995	6.087	5.993	6.091	6.105	6.243	6.123	6.621	6.815
Al ^{IV}	1.919	2.005	1.913	2.007	1.909	1.896	1.757	1.878	1.379	1.185
Σ(T)	8.000	8.000	8.000	8.000	8.000	8.000	8.000	8.000	8.000	8.000
Al ^{VI}	0.474	0.299	0.500	0.406	0.560	0.483	0.467	0.537	0.216	0.358
Ti	0.332	0.432	0.252	0.353	0.306	0.319	0.271	0.315	0.067	0.135
Fe ³⁺	0.305	0.403	0.449	0.470	0.242	0.355	0.390	0.220	0.985	0.345
Mg	2.654	2.882	2.634	2.678	2.729	2.807	2.388	2.734	2.594	2.737
Fe ²⁺	1.235	0.984	1.165	1.094	1.163	1.037	1.483	1.195	1.138	1.425
Mn	0.000	0.000	0.000	0.000	0.000	0.000	0.000	0.000	0.000	0.000
Σ(C)	5.000	5.000	5.000	5.000	5.000	5.000	5.000	5.000	5.000	5.000
Fe ²⁺	0.027	0.053	0.011	0.027	0.041	0.050	0.000	0.027	0.224	0.003
Mn	0.026	0.024	0.031	0.044	0.015	0.017	0.037	0.021	0.046	0.052
Mg	0.000	0.000	0.000	0.000	0.000	0.000	0.000	0.000	0.000	0.000
Ca	1.885	1.834	1.911	1.847	1.880	1.854	1.919	1.898	1.640	1.881
Na(M4)	0.062	0.089	0.048	0.082	0.064	0.078	0.043	0.055	0.091	0.064
Σ(B)	2.000	2.000	2.000	2.000	2.000	2.000	2.000	2.000	2.000	2.000
Na(A)	0.439	0.439	0.405	0.412	0.456	0.406	0.294	0.458	0.091	0.211
K	0.098	0.089	0.102	0.095	0.104	0.092	0.107	0.089	0.044	0.065
Σ(A)	0.537	0.529	0.507	0.507	0.559	0.499	0.400	0.546	0.135	0.276
Σ cat	15.537	15.529	15.507	15.507	15.559	15.499	15.400	15.547	15.136	15.276
$\frac{\text{Mg}}{\text{Fe}^{2+}+\text{Mg}}$	0.678	0.735	0.691	0.705	0.694	0.721	0.617	0.691	0.656	0.657
Al ^T	2.393	2.304	2.413	2.412	2.469	2.378	2.224	2.415	1.595	1.544

Appendix VIII. Composition of amphiboles (cont.)

(Structural formulae are based on 23 oxygens)

Sázava suite (cont.)

	SaD-1			
	23	24	25	

	zoned amphibole scan			
SiO ₂	45.65	45.02	45.19	
TiO ₂	0.74	1.67	1.52	
Al ₂ O ₃	8.07	8.57	8.70	
FeO	10.96	11.00	10.25	
MnO	11.80	10.99	10.66	
MgO	0.36	0.51	0.61	
CaO	17.38	16.99	18.57	
Na ₂ O	0.86	0.77	0.89	
K ₂ O	0.30	0.43	0.36	
Σ	96.14	95.95	96.73	
Si	6.854	6.757	6.765	
Al ^{IV}	1.146	1.243	1.235	
Σ(T)	8.000	8.000	8.000	
Al ^{VI}	0.283	0.273	0.302	
Ti	0.084	0.189	0.171	
Fe ³⁺	0.497	0.511	0.524	
Mg	2.453	2.460	2.287	
Fe ²⁺	1.684	1.568	1.718	
Mn	0.000	0.000	0.000	
Σ(C)	5.000	5.000	5.000	
Fe ²⁺	0.002	0.055	0.084	
Mn	0.046	0.065	0.077	
Mg	0.000	0.000	0.000	
Ca	1.898	1.768	1.710	
Na(M4)	0.055	0.113	0.129	
Σ(B)	2.000	2.000	2.000	
Na(A)	0.196	0.113	0.129	
K	0.058	0.082	0.068	
Σ(A)	0.254	0.194	0.197	
Σ cat	15.254	15.194	15.197	
$\frac{\text{Mg}}{\text{Fe}^{2+}+\text{Mg}}$	0.593	0.603	0.559	
Al ^T	1.429	1.517	1.536	

Appendix VIII. Composition of amphiboles (cont.)

(Structural formulae are based on 23 oxygens)

Blatná suite

	Koz-2									
	amph 1	amph 2	amph 3	amph 4	amph 5	amph 6	amph 7	amph 8	amph 9	amph 10
	→		→		→		→		→	
	large euhedral		small euhedral		large euhedral		large euhedral		large	
SiO ₂	44.95	46.25	45.75	46.64	44.95	44.97	47.18	46.71	46.88	46.97
TiO ₂	1.03	1.17	0.94	1.01	1.44	1.17	0.82	0.90	0.81	0.98
Al ₂ O ₃	7.54	7.47	7.57	7.36	7.88	7.73	5.93	6.89	6.37	6.62
FeO	16.95	16.41	16.28	14.91	16.79	17.15	16.17	15.71	16.45	15.55
MnO	0.51	0.53	0.41	0.47	0.48	0.46	0.49	0.50	0.58	0.60
MgO	11.20	11.58	11.54	12.41	11.00	11.38	11.96	12.41	11.77	12.36
CaO	11.54	11.30	11.53	11.38	11.73	11.52	11.92	11.16	11.42	11.40
Na ₂ O	1.36	1.31	1.26	1.30	1.24	1.36	0.90	1.21	1.09	1.11
K ₂ O	0.79	0.79	0.77	0.66	0.88	0.86	0.55	0.63	0.58	0.61
Σ	95.87	96.81	96.05	96.14	96.39	96.60	95.92	96.12	95.95	96.20
Si	6.831	6.922	6.906	6.971	6.805	6.780	7.106	6.987	7.061	7.026
Al ^{IV}	1.169	1.078	1.095	1.029	1.195	1.220	0.894	1.013	0.939	0.974
Σ(T)	8.000	8.000	8.000	8.000	8.000	8.000	8.000	8.000	8.000	8.000
Al ^{VI}	0.182	0.240	0.253	0.268	0.212	0.154	0.159	0.202	0.193	0.193
Ti	0.118	0.132	0.107	0.114	0.164	0.133	0.093	0.101	0.092	0.110
Fe ³⁺	0.327	0.268	0.256	0.246	0.225	0.387	0.263	0.364	0.301	0.307
Mg	2.537	2.583	2.596	2.765	2.482	2.557	2.685	2.766	2.642	2.755
Fe ²⁺	1.827	1.778	1.789	1.608	1.901	1.770	1.774	1.566	1.772	1.634
Mn	0.010	0.000	0.000	0.000	0.016	0.000	0.027	0.000	0.001	0.000
Σ(C)	5.000	5.000	5.000	5.000	5.000	5.000	5.000	5.000	5.000	5.000
Fe ²⁺	0.000	0.009	0.010	0.010	0.000	0.006	0.000	0.035	0.000	0.004
Mn	0.056	0.067	0.052	0.060	0.045	0.059	0.035	0.063	0.073	0.076
Mg	0.000	0.000	0.000	0.000	0.000	0.000	0.000	0.000	0.000	0.000
Ca	1.879	1.812	1.865	1.823	1.903	1.861	1.924	1.789	1.843	1.827
Na(M4)	0.065	0.112	0.073	0.108	0.052	0.075	0.041	0.113	0.084	0.093
Σ(B)	2.000	2.000	2.000	2.000	2.000	2.000	2.000	2.000	2.000	2.000
Na(A)	0.336	0.268	0.296	0.269	0.312	0.323	0.222	0.238	0.234	0.229
K	0.153	0.151	0.148	0.126	0.170	0.165	0.106	0.120	0.112	0.116
Σ(A)	0.489	0.419	0.445	0.395	0.482	0.489	0.328	0.358	0.346	0.346
Σ cat	15.489	15.419	15.445	15.395	15.482	15.489	15.328	15.358	15.346	15.346
$\frac{\text{Mg}}{\text{Fe}^{2+}+\text{Mg}}$	0.581	0.591	0.591	0.631	0.566	0.590	0.602	0.633	0.599	0.627
Al ^T	1.351	1.318	1.347	1.297	1.407	1.374	1.053	1.215	1.131	1.167

Appendix VIII. Composition of amphiboles (cont.)

(Structural formulae are based on 23 oxygens)

Blatná suite (cont.)

	Koz-2					Koz-4				
	amph clot 1 rim of the clot	amph clot 2 core of clot	amph clot 3 C of clot light	amph clot 4 rim of clot light	amph clot 5 rim of the clot	amph 2*	amph 3*	amph clot1*	amph 1	amph 2
									← small amph	
SiO ₂	49.13	48.11	50.79	45.34	45.92	45.94	48.43	46.87	46.53	46.05
TiO ₂	0.77	0.64	0.32	0.95	1.09	0.86	0.28	0.80	0.90	0.89
Al ₂ O ₃	4.62	5.45	3.14	7.44	7.13	6.82	5.29	6.61	6.65	6.79
FeO	14.72	16.14	14.80	17.12	16.94	16.24	15.09	15.82	16.16	15.91
MnO	0.40	0.50	0.52	0.59	0.61	0.46	0.44	0.49	0.43	0.61
MgO	13.22	12.50	14.41	11.06	11.38	11.60	12.82	12.20	11.53	11.64
CaO	12.33	12.00	11.99	11.79	11.55	11.82	11.91	11.86	11.86	11.67
Na ₂ O	0.62	0.76	0.54	1.13	1.14	1.05	0.76	1.05	1.01	1.12
K ₂ O	0.38	0.41	0.22	0.71	0.71	0.77	0.42	0.66	0.71	0.68
Σ	96.19	96.51	96.01	96.13	96.47	95.56	95.44	96.36	95.78	95.36
Si	7.308	7.164	7.495	6.865	6.912	6.973	7.261	7.020	7.044	6.995
Al ^{IV}	0.692	0.836	0.505	1.135	1.088	1.027	0.739	0.980	0.956	1.005
Σ(T)	8.000	8.000	8.000	8.000	8.000	8.000	8.000	8.000	8.000	8.000
Al ^{VI}	0.118	0.121	0.041	0.193	0.177	0.193	0.196	0.188	0.231	0.211
Ti	0.086	0.072	0.036	0.108	0.123	0.098	0.032	0.090	0.103	0.102
Fe ³⁺	0.188	0.366	0.309	0.350	0.342	0.263	0.271	0.284	0.169	0.238
Mg	2.931	2.774	3.169	2.496	2.553	2.624	2.865	2.723	2.601	2.635
Fe ²⁺	1.643	1.644	1.429	1.818	1.791	1.799	1.621	1.697	1.877	1.783
Mn	0.034	0.024	0.017	0.035	0.014	0.023	0.016	0.017	0.020	0.032
Σ(C)	5.000	5.000	5.000	5.000	5.000	5.000	5.000	5.000	5.000	5.000
Fe ²⁺	0.000	0.000	0.000	0.000	0.000	0.000	0.000	0.000	0.000	0.000
Mn	0.016	0.040	0.049	0.041	0.064	0.036	0.040	0.045	0.035	0.047
Mg	0.000	0.000	0.000	0.000	0.000	0.000	0.000	0.000	0.000	0.000
Ca	1.965	1.915	1.896	1.913	1.863	1.922	1.913	1.903	1.924	1.899
Na(M4)	0.019	0.046	0.056	0.047	0.074	0.042	0.046	0.052	0.041	0.054
Σ(B)	2.000	2.000	2.000	2.000	2.000	2.000	2.000	2.000	2.000	2.000
Na(A)	0.160	0.174	0.099	0.285	0.259	0.267	0.175	0.253	0.256	0.276
K	0.072	0.078	0.041	0.137	0.136	0.149	0.080	0.126	0.137	0.132
Σ(A)	0.232	0.252	0.140	0.422	0.396	0.417	0.255	0.379	0.393	0.408
Σ cat	15.232	15.252	15.140	15.422	15.396	15.417	15.255	15.379	15.393	15.408
$\frac{Mg}{Fe^{2+}+Mg}$	0.641	0.628	0.689	0.579	0.588	0.593	0.639	0.616	0.581	0.596
Al ^T	0.810	0.957	0.546	1.328	1.265	1.220	0.935	1.167	1.187	1.216

Appendix VIII. Composition of amphiboles (cont.)

(Structural formulae are based on 23 oxygens)

Blatná suite (cont.)

	Koz-4							Koz-6		
	amph 3	amph 4	amph 5	amph 6	amph clot1	amph clot3	amph clot4	amph 1	amph 2	amph 3
	small, rim	large, rim	small, core	small, core	rim of the clot	core of clot	core clot darker	pseudo morph px R	pseudo morph px R	pseudo morph px C
SiO ₂	46.86	46.50	45.95	47.11	46.79	45.41	49.24	45.43	45.81	44.34
TiO ₂	0.89	1.14	1.04	0.95	0.88	1.01	0.06	0.98	0.94	1.02
Al ₂ O ₃	6.49	6.59	7.55	6.14	6.24	7.62	4.86	8.18	7.64	8.10
FeO	15.85	15.80	16.10	16.12	16.03	16.85	15.21	17.82	17.28	18.23
MnO	0.46	0.44	0.56	0.52	0.53	0.56	0.42	0.48	0.56	0.54
MgO	11.60	12.03	11.29	11.81	11.87	10.71	12.44	10.81	11.50	10.96
CaO	11.84	11.86	11.79	11.83	11.70	11.91	12.57	11.30	11.52	11.46
Na ₂ O	1.05	1.15	1.29	0.90	1.04	1.08	0.53	1.38	1.31	1.40
K ₂ O	0.58	0.67	0.86	0.58	0.61	0.79	0.24	0.82	0.79	0.85
Σ	95.62	96.18	96.43	95.96	95.69	95.94	95.57	97.20	97.34	96.88
Si	7.093	6.999	6.933	7.096	7.071	6.905	7.406	6.815	6.838	6.685
Al ^{IV}	0.907	1.001	1.067	0.904	0.930	1.096	0.594	1.185	1.162	1.315
Σ(T)	8.000	8.000	8.000	8.000	8.000	8.000	8.000	8.000	8.000	8.000
Al ^{VI}	0.251	0.168	0.276	0.186	0.182	0.270	0.268	0.262	0.182	0.125
Ti	0.101	0.129	0.118	0.108	0.100	0.116	0.007	0.110	0.105	0.115
Fe ³⁺	0.123	0.204	0.128	0.225	0.238	0.186	0.000	0.343	0.410	0.548
Mg	2.617	2.699	2.539	2.651	2.673	2.427	2.789	2.417	2.558	2.462
Fe ²⁺	1.884	1.785	1.904	1.805	1.788	1.957	1.913	1.869	1.745	1.750
Mn	0.024	0.016	0.036	0.024	0.019	0.045	0.024	0.000	0.000	0.000
Σ(C)	5.000	5.000	5.000	5.000	5.000	5.000	5.000	5.000	5.000	5.000
Fe ²⁺	0.000	0.000	0.000	0.000	0.000	0.000	0.000	0.025	0.002	0.001
Mn	0.035	0.041	0.036	0.042	0.049	0.028	0.030	0.061	0.071	0.068
Mg	0.000	0.000	0.000	0.000	0.000	0.000	0.000	0.000	0.000	0.000
Ca	1.920	1.913	1.906	1.909	1.894	1.940	1.970	1.816	1.843	1.851
Na(M4)	0.045	0.047	0.058	0.049	0.057	0.032	0.000	0.098	0.084	0.080
Σ(B)	2.000	2.000	2.000	2.000	2.000	2.000	2.000	2.000	2.000	2.000
Na(A)	0.263	0.289	0.320	0.214	0.248	0.287	0.155	0.302	0.293	0.328
K	0.112	0.129	0.166	0.112	0.118	0.153	0.046	0.156	0.150	0.164
Σ(A)	0.375	0.418	0.485	0.326	0.366	0.440	0.201	0.459	0.443	0.492
Σ cat	15.375	15.418	15.485	15.326	15.366	15.440	15.201	15.459	15.443	15.492
$\frac{\text{Mg}}{\text{Fe}^{2+}+\text{Mg}}$	0.581	0.602	0.571	0.595	0.599	0.554	0.593	0.561	0.594	0.584
Al ^T	1.158	1.169	1.343	1.090	1.112	1.366	0.862	1.447	1.344	1.439

Appendix VIII. Composition of amphiboles (cont.)

(Structural formulae are based on 23 oxygens)

Blatná suite (cont.)

	Koz-6					KozD-1				
	amph 4 with relic px C	amph 5	amph 6	amph clot1 pseudo morph px L	amph clot2 pseudo morph px D	amph 1 large, rim	amph 2 large, core	amph 3 small core	amph 5 large rim	amph 6 small core
SiO ₂	45.07	45.26	45.04	52.39	46.67	49.94	49.14	48.22	48.87	47.00
TiO ₂	1.06	0.92	0.74	0.12	0.74	0.54	0.51	0.56	0.73	0.64
Al ₂ O ₃	7.90	7.90	7.51	1.79	6.59	4.77	5.15	5.57	5.56	6.58
FeO	18.33	18.11	17.83	14.04	17.55	13.62	13.89	14.28	14.5	16.04
MnO	0.55	0.56	0.54	0.58	0.46	0.45	0.36	0.51	0.4	0.48
MgO	10.64	11.11	10.98	15.14	11.33	13.87	13.75	13.21	13.35	12.58
CaO	11.60	10.98	11.82	12.11	11.81	12.26	11.73	12.16	11.97	12.01
Na ₂ O	1.27	1.37	1.05	0.35	1.04	0.63	0.82	0.8	0.86	0.99
K ₂ O	0.83	0.88	0.74	0.12	0.65	0.37	0.41	0.48	0.51	0.54
Σ	97.24	97.10	96.24	96.61	96.83	96.45	95.76	95.79	96.75	96.86
Si	6.779	6.785	6.815	7.710	7.003	7.360	7.294	7.197	7.219	6.980
Al ^{IV}	1.221	1.215	1.185	0.290	0.997	0.640	0.707	0.803	0.781	1.020
Σ(T)	8.000	8.000	8.000	8.000	8.000	8.000	8.000	8.000	8.000	8.000
Al ^{VI}	0.179	0.181	0.154	0.020	0.169	0.189	0.195	0.177	0.187	0.133
Ti	0.120	0.104	0.084	0.013	0.083	0.060	0.057	0.063	0.081	0.072
Fe ³⁺	0.413	0.514	0.502	0.000	0.346	0.151	0.229	0.236	0.202	0.450
Mg	2.385	2.483	2.475	3.320	2.534	3.046	3.042	2.939	2.939	2.784
Fe ²⁺	1.894	1.719	1.754	1.648	1.857	1.528	1.479	1.547	1.590	1.543
Mn	0.009	0.000	0.030	0.000	0.012	0.026	0.000	0.039	0.001	0.019
Σ(C)	5.000	5.000	5.000	5.000	5.000	5.000	5.000	5.000	5.000	5.000
Fe ²⁺	0.000	0.039	0.000	0.080	0.000	0.000	0.017	0.000	0.000	0.000
Mn	0.060	0.071	0.039	0.072	0.047	0.030	0.045	0.026	0.049	0.041
Mg	0.000	0.000	0.000	0.000	0.000	0.000	0.000	0.000	0.000	0.000
Ca	1.870	1.763	1.916	1.848	1.899	1.936	1.866	1.945	1.895	1.911
Na(M4)	0.070	0.127	0.045	0.000	0.054	0.034	0.072	0.030	0.056	0.048
Σ(B)	2.000	2.000	2.000	2.000	2.000	2.000	2.000	2.000	2.000	2.000
Na(A)	0.300	0.272	0.263	0.099	0.247	0.146	0.164	0.202	0.190	0.239
K	0.159	0.167	0.143	0.022	0.124	0.070	0.078	0.091	0.096	0.103
Σ(A)	0.458	0.439	0.406	0.121	0.371	0.216	0.242	0.293	0.286	0.341
Σ cat	15.458	15.439	15.406	15.121	15.371	15.216	15.242	15.293	15.286	15.341
Mg Fe ²⁺ +Mg	0.557	0.586	0.585	0.658	0.577	0.67	0.67	0.66	0.65	0.643
Al ^T	1.400	1.396	1.340	0.310	1.166	0.829	0.901	0.980	0.968	1.153

Appendix VIII. Composition of amphiboles (cont.)

(Structural formulae are based on 23 oxygens)

Blatná suite (cont.)

	KozD-1							BI-3		
	amph 7	amph 8	amph 9	amph10	amph11	amph clot1 rim of clot	amph clot2 core of the clot	amph 1	amph 2	
	→ small euhedral		← large		C big needle			small, core	small, core	
SiO ₂	49.19	49.58	48.99	49.32	48.05	48.59	47.69	45.30	45.74	
TiO ₂	0.63	0.48	0.44	0.34	0.51	0.67	0.98	0.85	0.85	
Al ₂ O ₃	5.51	5.09	5.63	5.61	6.05	5.46	6.33	7.53	7.03	
FeO	15.10	14.97	15.54	15.33	15.59	14.13	14.73	16.33	16.42	
MnO	0.38	0.36	0.44	0.45	0.40	0.45	0.38	0.48	0.49	
MgO	13.29	13.56	13.15	13.58	12.89	13.32	12.72	11.92	12.22	
CaO	11.94	12.22	11.91	12.09	11.92	11.85	12.1	11.65	11.64	
Na ₂ O	0.74	0.73	0.76	0.92	0.93	0.91	0.94	1.20	1.14	
K ₂ O	0.52	0.45	0.48	0.44	0.55	0.47	0.54	0.76	0.73	
Σ	97.30	97.45	97.33	98.07	96.89	95.85	96.41	96.02	96.25	
Si	7.222	7.265	7.194	7.183	7.114	7.240	7.104	6.826	6.864	
Al ^{IV}	0.778	0.735	0.806	0.817	0.886	0.760	0.896	1.174	1.136	
Σ(T)	8.000	8.000	8.000	8.000	8.000	8.000	8.000	8.000	8.000	
Al ^{VI}	0.176	0.145	0.169	0.146	0.170	0.199	0.215	0.163	0.107	
Ti	0.069	0.052	0.049	0.037	0.056	0.075	0.110	0.096	0.096	
Fe ³⁺	0.286	0.281	0.369	0.377	0.351	0.176	0.161	0.449	0.503	
Mg	2.908	2.962	2.878	2.947	2.844	2.958	2.824	2.676	2.733	
Fe ²⁺	1.560	1.554	1.535	1.490	1.578	1.585	1.674	1.610	1.558	
Mn	0.000	0.007	0.000	0.003	0.000	0.007	0.016	0.006	0.003	
Σ(C)	5.000	5.000	5.000	5.000	5.000	5.000	5.000	5.000	5.000	
Fe ²⁺	0.009	0.000	0.004	0.000	0.001	0.000	0.000	0.000	0.000	
Mn	0.048	0.038	0.054	0.052	0.050	0.050	0.032	0.055	0.059	
Mg	0.000	0.000	0.000	0.000	0.000	0.000	0.000	0.000	0.000	
Ca	1.878	1.919	1.874	1.887	1.890	1.892	1.931	1.881	1.872	
Na(M4)	0.065	0.044	0.068	0.060	0.059	0.059	0.037	0.064	0.068	
Σ(B)	2.000	2.000	2.000	2.000	2.000	2.000	2.000	2.000	2.000	
Na(A)	0.145	0.164	0.149	0.199	0.208	0.204	0.235	0.287	0.262	
K	0.097	0.084	0.089	0.082	0.104	0.089	0.103	0.146	0.140	
Σ(A)	0.242	0.248	0.238	0.281	0.312	0.294	0.337	0.433	0.402	
Σ cat	15.242	15.248	15.238	15.281	15.312	15.294	15.337	15.433	15.402	
Mg Fe ²⁺ +Mg	0.650	0.656	0.652	0.664	0.643	0.65	0.628	0.624	0.637	
Al ^T		1.400	1.396	1.340	0.310	0.959	1.1116	1.337	1.243	

Appendix VIII. Composition of amphiboles (cont.)

(Structural formulae are based on 23 oxygens)

Blatná suite (cont.)

	B1-5								B1-8	
	amph 1	amph 2	amph 3	amph 4	amph 5	amph 6	amph 7	amph 8	amph 1	amph 2
	← large amph		← large amph		small core	small core	large rim	small core	← small	
SiO ₂	44.30	45.15	45.27	45.90	45.75	43.66	44.03	46.42	45.80	46.42
TiO ₂	1.24	0.64	1.13	0.48	1.15	1.36	0.90	0.63	1.03	0.74
Al ₂ O ₃	8.19	7.55	7.21	6.86	7.02	8.55	8.23	6.43	7.30	6.51
FeO	17.36	16.82	16.41	17.11	16.41	17.86	17.80	16.62	16.12	15.81
MnO	0.38	0.50	0.42	0.45	0.50	0.46	0.48	0.45	0.30	0.45
MgO	11.15	11.65	11.67	11.68	11.74	10.72	10.56	11.60	12.03	12.56
CaO	11.84	11.92	11.73	11.76	11.89	11.75	11.76	11.92	11.37	11.81
Na ₂ O	1.30	1.07	1.17	0.96	1.16	1.27	1.24	1.01	1.35	1.07
K ₂ O	0.90	0.77	0.75	0.63	0.78	1.04	0.99	0.65	0.74	0.66
Σ	96.66	96.06	95.75	95.82	96.40	96.66	95.98	95.73	96.01	96.04
Si	6.690	6.813	6.859	6.928	6.892	6.616	6.718	7.029	6.898	6.964
Al ^{IV}	1.310	1.187	1.141	1.072	1.108	1.384	1.282	0.971	1.102	1.036
Σ(T)	8.000	8.000	8.000	8.000	8.000	8.000	8.000	8.000	8.000	8.000
Al ^{VI}	0.147	0.156	0.147	0.149	0.139	0.143	0.199	0.178	0.193	0.115
Ti	0.141	0.073	0.128	0.054	0.130	0.154	0.103	0.071	0.116	0.084
Fe ³⁺	0.417	0.504	0.353	0.518	0.307	0.457	0.402	0.298	0.319	0.425
Mg	2.510	2.619	2.636	2.626	2.636	2.422	2.401	2.618	2.700	2.809
Fe ²⁺	1.775	1.619	1.727	1.642	1.761	1.807	1.870	1.808	1.671	1.558
Mn	0.009	0.030	0.010	0.012	0.027	0.017	0.026	0.027	0.000	0.010
Σ(C)	5.000	5.000	5.000	5.000	5.000	5.000	5.000	5.000	5.000	5.000
Fe ²⁺	0.000	0.000	0.000	0.000	0.000	0.000	0.000	0.000	0.039	0.000
Mn	0.039	0.034	0.044	0.045	0.038	0.043	0.036	0.031	0.038	0.047
Mg	0.000	0.000	0.000	0.000	0.000	0.000	0.000	0.000	0.000	0.000
Ca	1.916	1.928	1.904	1.902	1.919	1.908	1.922	1.934	1.835	1.899
Na(M4)	0.045	0.039	0.051	0.052	0.043	0.050	0.042	0.035	0.089	0.054
Σ(B)	2.000	2.000	2.000	2.000	2.000	2.000	2.000	2.000	2.000	2.000
Na(A)	0.336	0.274	0.291	0.228	0.294	0.324	0.325	0.261	0.304	0.257
K	0.174	0.147	0.145	0.122	0.150	0.200	0.193	0.126	0.142	0.126
Σ(A)	0.510	0.421	0.437	0.350	0.444	0.524	0.518	0.388	0.447	0.383
Σ cat	15.510	15.421	15.437	15.350	15.444	15.524	15.518	15.388	15.447	15.383
Mg Fe ²⁺ Mg	0.586	0.618	0.604	0.615	0.599	0.573	0.562	0.592	0.612	0.643
Al ^T	1.457	1.343	1.288	1.221	1.247	1.527	1.481	1.148	1.295	1.151

Appendix VIII. Composition of amphiboles (cont.)

(Structural formulae are based on 23 oxygens)

Blatná suite (cont.)

	BI-8				
	amph 3	amph 4	amph clot 1	amph clot 2	amph clot 3
	→ large		rim of the clot	core of clot	core of clot
SiO ₂	47.16	46.30	48.29	53.66	49.55
TiO ₂	0.70	1.10	0.67	0.01	0.46
Al ₂ O ₃	5.80	6.79	5.39	1.06	5.08
FeO	16.17	16.50	14.60	10.71	11.16
MnO	0.41	0.45	0.40	0.49	0.53
MgO	12.50	12.13	13.82	17.42	16.05
CaO	11.77	11.40	11.40	12.29	11.73
Na ₂ O	1.07	1.35	0.95	0.26	0.93
K ₂ O	0.61	0.67	0.50	0.07	0.46
Σ	96.18	96.70	96.02	95.98	95.94
Si	7.072	6.929	7.159	7.810	7.232
Al ^{IV}	0.928	1.071	0.841	0.182	0.768
Σ(T)	8.000	8.000	8.000	7.993	8.000
Al ^{VI}	0.098	0.127	0.100	0.000	0.106
Ti	0.079	0.124	0.074	0.000	0.050
Fe ³⁺	0.360	0.360	0.426	0.000	0.392
Mg	2.794	2.706	3.053	3.779	3.492
Fe ²⁺	1.667	1.683	1.347	1.221	0.960
Mn	0.001	0.000	0.000	0.000	0.000
Σ(C)	5.000	5.000	5.000	5.000	5.000
Fe ²⁺	0.000	0.023	0.038	0.083	0.011
Mn	0.051	0.057	0.050	0.061	0.066
Mg	0.000	0.000	0.000	0.000	0.000
Ca	1.891	1.829	1.811	1.856	1.834
Na(M4)	0.059	0.092	0.102	0.000	0.089
Σ(B)	2.000	2.000	2.000	2.000	2.000
Na(A)	0.253	0.299	0.173	0.074	0.173
K	0.116	0.129	0.095	0.013	0.085
Σ(A)	0.369	0.428	0.267	0.087	0.258
Σ cat	15.369	15.428	15.267	15.080	15.258
$\frac{\text{Mg}}{\text{Fe}^{2+}+\text{Mg}}$	0.626	0.613	0.688	0.744	0.782
Al ^T	1.026	1.198	0.941	0.182	0.874

Appendix VIII. Composition of amphiboles (cont.)

(Structural formulae are based on 23 oxygens)

Čertovo břemeno suite

	Se-6			Se-7			Se-9			
	amph 2	amph	amph	amph 1	amph 3	amph	amph 1	amph 2	amph 3	amph 4
	rim of	clot1	clot2	small	small	clot1	→		→	
	small	rim of	core of	amph	amph	rim of	large amph		large amph	
	amph	the clot	the clot	core	core	the clot				
SiO ₂	50.98	54.09	54.82	50.38	50.42	53.62	50.31	51.82	51.25	50.82
TiO ₂	0.51	0.00	0.12	0.53	0.45	0.11	0.46	0.44	0.40	0.36
Al ₂ O ₃	4.42	1.18	0.80	3.97	4.26	1.25	4.24	2.55	3.98	4.15
FeO	13.05	10.05	8.37	12.48	12.07	11.49	12.58	11.96	13.04	13.86
MnO	0.52	0.44	0.58	0.46	0.49	0.57	0.43	0.55	0.52	0.51
MgO	14.90	18.09	19.67	14.79	15.02	17.20	15.01	15.58	15.10	14.71
CaO	11.34	11.86	12.00	11.40	11.62	10.89	11.44	11.83	11.80	11.22
Na ₂ O	0.89	0.38	0.33	0.81	0.80	0.37	0.81	0.51	0.84	0.89
K ₂ O	0.41	0.12	0.09	0.39	0.38	0.11	0.39	0.22	0.36	0.37
Σ	97.01	96.21	96.76	95.21	95.51	95.61	95.67	95.46	97.28	96.89
Si	7.402	7.803	7.819	7.453	7.427	7.810	7.402	7.616	7.436	7.408
Al ^{IV}	0.599	0.197	0.134	0.548	0.573	0.190	0.598	0.384	0.564	0.592
Σ(T)	8.000	8.000	7.953	8.000	8.000	8.000	8.000	8.000	8.000	8.000
Al ^{VI}	0.158	0.004	0.000	0.145	0.166	0.025	0.137	0.058	0.116	0.121
Ti	0.055	0.000	0.000	0.059	0.050	0.012	0.051	0.049	0.044	0.040
Fe ³⁺	0.305	0.079	0.000	0.233	0.217	0.136	0.286	0.202	0.250	0.348
Mg	3.224	3.889	4.181	3.261	3.297	3.734	3.291	3.413	3.264	3.195
Fe ²⁺	1.257	1.027	0.819	1.302	1.270	1.093	1.235	1.268	1.326	1.297
Mn	0.000	0.000	0.000	0.000	0.000	0.000	0.000	0.011	0.000	0.000
Σ(C)	5.000	5.000	5.000	5.000	5.000	5.000	5.000	5.000	5.000	5.000
Fe ²⁺	0.022	0.106	0.179	0.008	0.000	0.170	0.027	0.000	0.006	0.046
Mn	0.064	0.054	0.070	0.058	0.061	0.070	0.054	0.057	0.064	0.063
Mg	0.000	0.000	0.000	0.000	0.000	0.000	0.000	0.000	0.000	0.000
Ca	1.764	1.833	1.752	1.807	1.834	1.700	1.804	1.863	1.834	1.752
Na(M4)	0.151	0.008	0.000	0.127	0.105	0.060	0.116	0.080	0.096	0.139
Σ(B)	2.000	2.000	2.000	2.000	2.000	2.000	2.000	2.000	2.000	2.000
Na(A)	0.100	0.099	0.090	0.105	0.124	0.044	0.116	0.066	0.140	0.113
K	0.076	0.022	0.016	0.074	0.071	0.020	0.073	0.041	0.067	0.069
Σ(A)	0.175	0.121	0.106	0.179	0.195	0.065	0.189	0.107	0.207	0.182
Σ cat	15.175	15.121	15.059	15.179	15.195	15.065	15.189	15.107	15.207	15.182
$\frac{\text{Mg}}{\text{Fe}^{2+}+\text{Mg}}$	0.716	0.774	0.807	0.713	0.722	0.747	0.723	0.729	0.710	0.704
Al ^T	0.757	0.201	0.134	0.692	0.740	0.215	0.735	0.442	0.680	0.713

Appendix VIII. Composition of amphiboles (cont.)

(Structural formulae are based on 23 oxygens)

Čertovo břemeno suite (cont.)

	Se-9								
	amph 5	amph 6	amph 7	amph 8	amph 9	amph1 0	amph1 1	amph12	
	← small amph		← large amph		large rim	← small amph		small core	
SiO ₂	52.41	52.53	50.92	50.87	50.91	50.28	53.28	53.89	
TiO ₂	0.25	0.23	0.39	0.45	0.30	0.45	0.15	0.06	
Al ₂ O ₃	2.58	2.35	4.14	4.19	4.40	4.46	2.14	1.46	
FeO	13.06	12.98	13.09	12.77	12.63	13.07	12.20	11.80	
MnO	0.56	0.43	0.49	0.48	0.47	0.52	0.65	0.48	
MgO	15.51	15.45	15.03	15.01	14.86	15.15	16.10	16.21	
CaO	12.02	11.85	11.29	11.54	11.83	11.92	12.41	12.44	
Na ₂ O	0.48	0.48	0.84	0.72	0.74	0.80	0.39	0.23	
K ₂ O	0.21	0.20	0.35	0.38	0.39	0.40	0.19	0.10	
Σ	97.07	96.49	96.53	96.40	96.51	97.07	97.52	96.66	
Si	7.596	7.658	7.425	7.427	7.434	7.313	7.663	7.801	
Al ^{IV}	0.404	0.342	0.575	0.573	0.566	0.687	0.337	0.199	
Σ(T)	8.000	8.000	8.000	8.000	8.000	8.000	8.000	8.000	
Al ^{VI}	0.036	0.061	0.137	0.148	0.192	0.078	0.026	0.050	
Ti	0.027	0.025	0.043	0.049	0.033	0.050	0.017	0.007	
Fe ³⁺	0.274	0.199	0.316	0.279	0.208	0.361	0.229	0.118	
Mg	3.351	3.357	3.266	3.266	3.234	3.284	3.451	3.496	
Fe ²⁺	1.309	1.357	1.238	1.258	1.333	1.227	1.239	1.310	
Mn	0.003	0.000	0.000	0.000	0.000	0.000	0.038	0.020	
Σ(C)	5.000	5.000	5.000	5.000	5.000	5.000	5.000	5.000	
Fe ²⁺	0.000	0.026	0.043	0.022	0.001	0.002	0.000	0.000	
Mn	0.066	0.053	0.060	0.059	0.058	0.064	0.041	0.038	
Mg	0.000	0.000	0.000	0.000	0.000	0.000	0.000	0.000	
Ca	1.867	1.851	1.764	1.806	1.851	1.858	1.912	1.930	
Na(M4)	0.067	0.070	0.133	0.113	0.091	0.076	0.047	0.033	
Σ(B)	2.000	2.000	2.000	2.000	2.000	2.000	2.000	2.000	
Na(A)	0.067	0.065	0.103	0.091	0.119	0.151	0.062	0.032	
K	0.039	0.037	0.066	0.070	0.072	0.074	0.034	0.019	
Σ(A)	0.106	0.102	0.169	0.161	0.191	0.225	0.096	0.051	
Σ cat	15.106	15.102	15.169	15.161	15.191	15.225	15.096	15.051	
$\frac{\text{Mg}}{\text{Fe}^{2+}+\text{Mg}}$	0.719	0.708	0.718	0.718	0.708	0.728	0.736	0.727	
Al ^T	0.757	0.201	0.134	0.692	0.740	0.215	0.735	0.442	

Appendix IX. Geochronology in the CBP [see Chapter I.4.]

Most published granitoid geochronology in the CBP is based on K-Ar data (Šmejkal 1960, 1964; Pudilová 1968; Steinocher, 1969; Pudilová and Dubanský, 1969; Afanasjev *et al.*, 1977) and is of very variable quality. In the early studies, only the volumetric measurement of the released gas was made, without mass spectrometric control on the content of atmospheric argon (Šmejkal, 1960; majority of data in Šmejkal, 1964). In addition, the analysed material was variable (whole-rocks, 'mica concentrates', muscovite, biotite, amphibole and feldspars) and interpretations were made before there was much information about blocking temperatures or the sensitivity of the isotopic system to late disturbances, such as Ar loss due to weathering, hydrothermal alteration or resetting by adjacent intrusions.

Accordingly, the geological significance of the ages given is of doubtful value, although many probably represent cooling ages, i.e. they record the particular time of closing the isotope system of a given mineral (Faure, 1986; Burchart nad Král', 1987; Geyh and Schleicher, 1990). These blocking temperatures are linked to the mineral species, the cooling rate, and the grain size (Dodson, 1973, 1976, 1986; Ehlers and Powell, 1994). Clearly, compilations, or even averages of unconstrained data, lack any real meaning (cf. for instance Bernard and Klomínský, 1975; Klomínský and Dudek, 1978).

The amount of Rb-Sr data is very limited (Afanasjev *et al.*, 1977; van Bremen *et al.*, 1982; Bendl, 1988; Bendl and Vokurka, 1989; Janoušek, 1991).

With the Blatná intrusion, the problem of insufficient spread in the $^{87}\text{Rb}/^{86}\text{Sr}$ ratios was bypassed by introduction of samples of younger aplites (van Bremen *et al.*, 1982) or even aplite-granodiorite mixtures (Bendl, 1988; Bendl and Vokurka, 1989). The resulting age of 331 ± 4 Ma (van Bremen *et al.*, 1982) should be therefore viewed as a lower age-constraint, although the real Rb-Sr whole-rock age of the granodiorite is not likely to differ considerably.

As for the work of Bendl (1988) and Bendl and Vokurka (1989), the recorded age of 331 ± 9 Ma was not calculated by the weighted linear regression (York, 1969). The re-calculation after York (1969) yields a regression line, characterised by a high MSWD (Mean Squared Weighted Deviation) of 3.84. This parameter, expressing the scatter of the points around the regression line, could potentially discriminate between isochrons and 'errorchrons', provided accurate error estimates were made. There are two approaches to calculate the cut-off value, above which the scatter around the isochron could not be accounted for by statistical reasons only ('excess scatter'; Brooks *et al.*, 1972; Wendt and Carl, 1991). If the F-test based approach of Brooks *et al.* (1972) is applied, the observed MSWD (for $n = 6$, 2σ confidence level) would correspond to an excessive scatter if more than 8 measurements of the standard were performed to find out the uncertainties. After Wendt and Carl (1991), the expected value of MSWD (at 2σ confidence level) is $1 \pm 2\sqrt{2/f}$, where f stands for degrees of freedom. Here ($f = 4$), the cut-off value equals 2.41. The high MSWD, which exceeds a statistically justifiable range, implies that error magnification procedure should apply (e.g. Kalsbeek and Hansen, 1989; Kullerud, 1991) and the re-calculated age is lower and the error higher (322 ± 15 Ma) than those reported by Bendl (1988) and Bendl and Vokurka (1989).

The Rb-Sr age determinations made on muscovite in leucogranite from Písek (336 ± 11 Ma), muscovite from the pegmatite dyke cross-cutting this intrusion (336 ± 9 Ma) and muscovite from aplopegmatite dyke penetrating the Tábor syenite (425 ± 9 Ma) were recorded by Afanasjev *et al.* (1977). It is not stated which decay constant has been used for the age calculation, as the new set of

constants was introduced shortly prior the publication of the data (*Steiger and Jäger, 1977*). However, even if the older constant was used, correction is not possible as only the ages were presented without the corresponding data.

A preliminary Ar - Ar plateau age of 336 Ma for biotite of the Čertovo břemeno intrusion has been published by *Matte et al., (1990)*. The error and additional data from the CBP is expected in a separate paper (*H. Maluski, pers.com., 1993*).

VIII. References

- Afanasjev GD, Arakeljanc MM, Bogatikov OA, Borsuk AM, Palivcová M, 1977. The problem of the age and genesis of granitoids of the Central Bohemian Pluton. In: Afanasjev GD (ed) An attempt on correlation of magmatic and metamorphic rocks of Czechoslovakia and some regions of the USSR (in Russian). Nauka, Moscow, 131-144.
- Allègre CJ, Ben Othman D, 1980. Nd-Sr isotopic relationship in granitoid rocks and continental crust development: a chemical approach to orogenesis. *Nature* 286, 335-342.
- Andrusov D, 1932. Geological map of the Vltava valley between Zvíkov and Orlík (in Czech). *Věstník Státního geologického ústavu Československé republiky* 8, 35-38.
- Arakawa Y, 1990. Two types of granitic intrusions in the Hida belt, Japan: Sr isotopic and chemical characteristics of the Mesozoic Funatsu granitic rocks. *Chemical Geology* 85, 101-117.
- Arndt NT, Goldstein SL, 1987. Use and abuse of crust-formation ages. *Geology* 15, 893-895.
- Arth JG, 1976. Behaviour of trace elements during magmatic processes- A summary of theoretical models and their application. *Journal of Research of the US Geological Survey* 4, 41-47.
- Arth JG, Barker F, Peterman ZE, Friedman I, 1978. Geochemistry of the gabbro - diorite - tonalite - trondhjemite suite of southwest Finland and its implications for the origin of tonalitic and trondhjemitic magmas. *Journal of Petrology* 19, 289-316.
- Barbarin B, 1990a. Granitoids: main petrogenetic classifications in relation to origin and tectonic setting. *Geological Journal* 25, 227-238.
- Barbarin B, 1990b. Plagioclase xenocrysts and mafic magmatic enclaves in some granitoids of the Sierra Nevada Batholith, California. *Journal of Geophysical Research* 95, 17747-17756.
- Barbarin B, Didier J, 1991. Macroscopic features of mafic microgranular enclaves. In: Didier J, Barbarin B, (eds) *Enclaves and Granite Petrology*. Elsevier, Amsterdam, 253-262.
- Bard JP, 1987. Microtextures of igneous and metamorphic rocks. D.Reidel Publishing Co., Dordrecht, 1-264.
- Batchelor RA, Bowden P, 1985. Petrogenetic interpretation of granitoid rock series using multicationic parameters. *Chemical Geology* 48, 43-55.
- Bateman R, 1993a. Geology of restite. In: Bateman R, Castro A, (eds) *Heterogeneities in felsic igneous rocks, at scales from crystals to plutons*. Workshop notes, Universidad de Sevilla, 21-23.
- Bateman R, 1993b. Mineral disequilibria under the microscope. In: Bateman R, Castro A, (eds) *Heterogeneities in felsic igneous rocks at scales from crystals to plutons*. Workshop notes, Universidad de Sevilla, 4-7.
- Bates RL, Jackson JA, 1987. Glossary of geology. American Geological Institute, Alexandria, 1-788.
- Beard BL, Medaris Jr. LG, Johnson CM, Brueckner HK, Mísař Z, 1992. Petrogenesis of Variscan high-temperature group A eclogites from the Moldanubian zone of the Bohemian Massif, Czechoslovakia. *Contributions to Mineralogy and Petrology* 111, 468-483.
- Bendl J, 1988. Age and origin of the Blatná granodiorite by the Rb-Sr method (in Czech). PhD. thesis (unpublished), Geological Survey, Prague, 1-104.
- Bendl J, Vokurka K, 1989. Strontium isotope model of formation of Blatná granodiorite. *Geologický Zborník Geologica Carpathica* 40, 655-664.
- Beneš K, 1970. Flow and structure fabrics and their relationship in some granitic bodies of the Bohemian Massif. *Krystalinikum* 8, 149-166.

- Ben Othman D, Fourcade S, Allégre CJ, 1984. Recycling processes in granite-granodiorite complex genesis: the Querigut case studied by Nd-Sr isotope systematics. *Earth and Planetary Science Letters* 69, 290-300.
- Bernard JH, Klomínský J, 1975. Geochronology of the Variscan plutonism in the Bohemian Massif. *Věstník Ústředního Ústavu geologického* 50, 71-81.
- Bernard-Griffiths J, Peucat JJ, Sheppard S, Vidal P, 1985. Petrogenesis of Hercynian leucogranites from the southern Armorican Massif: contribution of REE and isotopic (Sr,Nd,Pb and O) geochemical data to the study of source rocks characteristics and ages. *Earth and Planetary Science Letters* 74, 235-250.
- Blake S, Koyaguchi T, 1991. Insights on the magma mixing model from volcanic rocks. In: Didier J, Barbarin B, (eds) *Enclaves and Granite Petrology*. Elsevier, Amsterdam, 403-414.
- Blízkovský M, Mašín J, Máilová E, Mitrenga P, Novotný A, Pokorný L, Rejl L, Šatlanský K, 1988. Linear structures of the Czechoslovak part of the Bohemian Massif based on geophysical data. In: Kukal Z, (ed) *Proceedings of the 1st International Conference on the Bohemian Massif*. Czech Geological Survey, Prague, 29-32.
- Blundy JD, Holland TJB, 1990. Calcic amphibole equilibria and a new amphibole-plagioclase geothermometer. *Contributions to Mineralogy and Petrology* 104, 208-224.
- Blundy JD, Holland TJB, 1992a. "Calcic amphibole equilibria and a new amphibole-plagioclase geothermometer": reply to the comments of Hammastrom and Zen, and Rutherford and Johnson. *Contributions to Mineralogy and Petrology* 111, 269-272.
- Blundy JD, Holland TJB, 1992b. "Calcic amphibole equilibria and a new amphibole-plagioclase geothermometer" - reply to the comment of Poli and Schmidt. *Contributions to Mineralogy and Petrology* 111, 278-282.
- Bonin B, 1990. From orogenic to anorogenic settings: evolution of granitoid suites after a major orogenesis. *Geological Journal* 25, 261-270.
- Bourne J, Danis D, 1987. A proposed model for the formation of reversely zoned plutons based on study of the Lacorne Complex, Superior Province, Quebec. *Canadian Journal of Earth Sciences* 24, 2506-2520.
- Bouška V, Jelínek E, Pačesová M, Řanda Z, Ulrych J, 1984. Rare Earth elements and other trace elements in the rocks of the Central Bohemian Pluton. *Geologický Zborník Geologica Carpathica* 35, 355-376.
- Bowden P, Batchelor RA, Chappell BW, Didier J, Lameyre J, 1984. Petrological, geochemical and source criteria for the classification of granitic rocks: a discussion. *Physics of the Earth and Planetary Interiors* 35, 1-11.
- Bowes DR, Košler J, 1993. Geochemical comparison of the subvolcanic appinite suite of the British Caledonides and the durbachite suite of the Central European Hercynides: evidence for associated shoshonitic and granitic magmatism. *Mineralogy and Petrology* 48, 47-63.
- Bowes DR, Hopgood AM, Tonika J, 1994. Discrimination by structural criteria of the southern Fichtelgebirge tectonic domain from the Bohemian Forest and Mariánské Lázně domains in the Bohemian Massif, northwestern Czech Republic. *Zentralblatt für Geologie und Paläontologie, Teil I*, 1992, 773-783.
- Boynton WV, 1984. Cosmochemistry of the rare earth elements: meteorite studies. In: Henderson P, (ed) *Rare Earth Element Geochemistry*. Elsevier, Amsterdam, 63-114.
- Brooks C, Hart SR, Wendt I, 1972. Realistic use of two-error regression treatments as applied to rubidium-strontium data. *Reviews of Geophysics and Space Physics* 10, 551-577.
- Brueckner HK, Medaris Jr. LG, Bakun-Czubarow N, 1991. Nd and Sr age and isotope patterns from Variscan eclogites of the eastern Bohemian Massif. *Neues Jahrbuch für Mineralogie, Abhandlungen* 163, 169-196.

- Bryan WB, Finger LW, Chayes F, 1969. Estimating proportions in petrographic mixing equations by least-squares approximation. *Science* **163**, 926-927.
- Burchart J, Král' J, 1987. K-Ar radiation system in geological conditions (in Slovak). *Mineralia Slovaca* **19**, 363-374.
- Castro A, 1993. Biotite-hornblende relationships in calc-alkaline granitoids and enclaves. In: Bateman R, Castro A, (eds) *Heterogeneities in felsic igneous rocks at scales from crystals to plutons. Workshop notes*, Univesidad de Sevilla, 3.
- Castro A, Stephens WE, 1992. Amphibole-rich polycrystalline clots in calc-alkaline granitic rocks and their enclaves. *Canadian Mineralogist* **30**, 1093-1112.
- Castro A, de la Rosa JD, Stephens WE, 1990a. Magma mixing in the subvolcanic environment: petrology of the Gerena interaction zone near Seville, Spain. *Contributions to Mineralogy and Petrology* **105**, 9-26.
- Castro A, Moreno-Ventas I, de la Rosa JD, 1990b. Microgranular enclaves as indicators of hybridisation processes in granitoid rocks, Hercynian belt, Spain. *Geological Journal* **25**, 391-404.
- Castro A, Moreno-Ventas I, de la Rosa JD, 1991a. Multistage crystallization of tonalitic enclaves in granitoid rocks (Hercynian belt, Spain) - implications for magma mixing. *Geologische Rundschau* **80**, 109-120.
- Castro A, Moreno-Ventas I, de la Rosa JD, 1991b. H (Hybrid)- type granitoids: a proposed revision of the granite- type classification and nomenclature. *Earth Science Reviews*, **31**, 237-253
- Chaloupský J, 1989. Major stratigraphic units of the Bohemian Massif. In: Dallmeyer RD, (ed) *Terranes in Circum-Atlantic Paleozoic orogens*. Geological Society of America Special Paper **230**, 101-114.
- Chappell BW, Stephens WE, 1988. Origin of infracrustal (I-type) granite magmas. *Transactions of the Royal Society of Edinburgh, Earth Sciences* **79**, 71-86.
- Chappell BW, White AJR, 1992. I- and S-type granites in the Lachlan Fold Belt. *Transactions of the Royal Society of Edinburgh, Earth Sciences* **83**, 1-26.
- Chappell BW, White AJR, Wyborn D, 1987. The importance of residual source material (restite) in granite petrogenesis. *Journal of Petrology* **28**, 571-604.
- Chayes F, 1960. On correlation between variables of constant sum. *Journal of Geophysical Research* **65**, 4185-4193.
- Chlupáč I, 1988. The metamorphic Palaeozoic of the "Islet Zone" as a possible link between the Barrandian and the Moldanubicum. In: Kukal Z (ed) *Proceedings of the 1st International Conference on the Bohemian Massif*. Czech Geological Survey, Prague, 49-52.
- Cimbáľníková A, Palivcová M, Hejl V, Arakeljanc MM, 1977. Biotite from the Říčany granite and its biotite-rich xenoliths (ČSSR, Central Bohemian Pluton). In: Afanasjev GD (ed) *An attempt on correlation of magmatic and metamorphic rocks of Czechoslovakia and some regions of the USSR (in Russian)*. Nauka, Moscow, 178-187.
- Cimbáľníková A, Palivcová M, Hejl V, Maštálka A, 1976. Biotite in tonalites and their basic xenoliths (Teletín quarry, Central Bohemian Pluton). *Acta Universitatis Carolinae, Geologica*, 1-20.
- Clarke DB, 1992. *Granitoid rocks*. Chapman & Hall, London, 1-283.
- Collins WJ, Beams SD, White AJR, Chappell BW, 1982. Nature and origin of A- type granites with particular reference to southeastern Australia. *Contributions to Mineralogy and Petrology* **80**, 189-200.
- Condie K, 1981. *Archaean greenstone belts*. Elsevier, Amstredam, 1-434.

- Cox KG, Bell JD, Pankhurst RJ, 1979. The Interpretation of Igneous Rocks. George Allen & Unwin, London, 1-450.
- Cox RA, 1994. Controls on the development and distribution of the K-feldspar megacrysts: evidence from the Shap granite. MSc. thesis (unpublished), University of Glasgow, 1-140.
- Cullers RL, Graf JL, 1984. Rare Earth Elements in igneous rocks of the continental crust: intermediate and silicic rocks - ore petrogenesis. In: Henderson P, (ed) Rare Earth Element Geochemistry. Elsevier, Amsterdam, 275-308.
- Čech V, 1964. An contribution to the geology and petrography of the Tábor syenite Massif (in Czech). *Časopis pro mineralogii a geologii* 9, 291-299.
- Čepek L, Koutek J, 1941. Quarries in Horních Požárech and Mrači in the Sázava valley (in Czech). *Knihovna Geologického ústavu pro Čechy a Moravu* 21 b, 1-62.
- De la Roche H, Leterrier J, Grand Claude P, Marchal M, 1980. A classification of volcanic and plutonic rocks using R1-R2 diagrams and major element analyses - its relationships with current nomenclature. *Chemical Geology* 29, 183-210.
- De Jongh WK, 1973. X-ray fluorescence analysis applying theoretical matrix corrections. *X-ray Spectrometry* 2, 151-158.
- Debon F, Le Fort P, 1983. A chemical-mineralogical classification of common plutonic rocks and associations. *Transactions of the Royal Society of Edinburgh, Earth Sciences* 73, 135-149.
- Debon F, Le Fort P, 1988. A cationic classification of common plutonic rocks and their magmatic associations: principles, method, applications. *Bulletin de Mineralogie* 111, 493-510.
- Deer WA, Howie RA, Zussman J, 1982. Rock forming minerals - 1A Orthosilicates. Longman, London, 1-919.
- Deer WA, Howie RA, Zussman J, 1992. An introduction to the rock-forming minerals. Longman, London, 1-696.
- DePaolo DJ, 1981. Trace element and isotopic effects of combined wall-rock assimilation and fractional crystallization. *Earth and Planetary Science Letters* 53, 189-202.
- DePaolo DJ, 1988. Neodymium isotope geochemistry. Springer, Berlin, 1-187.
- Diaconis P, Efron B, 1983. Computer-intensive methods in statistics. *Scientific American* 248, 96-108.
- Didier J, 1987. Contribution of enclave studies to the understanding of origin and evolution of granitic magmas. *Geologische Rundschau* 76, 41-50.
- Didier J, Barbarin B, 1991. The different types of enclaves in granites- Nomenclature. In: Didier J, Barbarin B, (eds) *Enclaves and Granite Petrology*. Elsevier, Amsterdam, 19-24.
- Dobeš M, Pokorný L, 1988. Usage of gravimetry to solve morphology of the Čertovo břemeno durbachite body in the Central Bohemian Pluton (in Czech). *Věstník Ústředního Ústavu geologického* 63, 129-135.
- Dodge FCW, Kistler RW, 1990. Some additional observations on inclusions in the granitic rocks of the Sierra Nevada. *Journal of Geophysical Research* 95, 17841-17848.
- Dodson MH, 1973. Closure temperature in cooling geochronological and petrological systems. *Contributions to Mineralogy and Petrology* 40, 259-274.
- Dodson MH, 1976. Kinetic processes and thermal history of slowly cooling liquids. *Nature* 259, 551-553.
- Dodson MH, 1986. Closure profiles in cooling systems. *Material Science Forum* 7, 145-154.

- Dubanský A, 1984. Determination of the radiogenic age by the potassium-argon method (geochronological data from the Bohemian Massif in the region of ČSR) (in Czech). *Sborník vědeckých prací Vysoké školy báňské v Ostravě, Řada hornicko-geologická* 30, 137-170.
- Dudek A, Fediuk F, 1953. A preliminary report on geological investigations in environs of Blatná (in Czech). *Zprávy o geologických výzkumech v roce 1953*, 11-13.
- Dudek A, Fediuk F, 1956. Geology and petrography of the Hudčice quarrying district (in Czech). *Sborník Ústředního Ústavu geologického, oddíl geologický*, 23, 159-213.
- Dudek A, Fediuk F, 1958. Mafic enclaves and fluid dynamic phenomena in a granodiorite at the margin of the Central Bohemian Pluton at Teletín (in Czech). *Sborník Ústředního Ústavu geologického, oddíl geologický, Slavík's Volume*, 97-112.
- Dudek A, Fediuk F, 1960. Granodiorite quarries in the environs of Blatná (in Czech). *Geotechnica* 30, 1-63.
- Dudek A, Záruba Q, 1967. The contact zone of the Central Bohemian Pluton exposed at quarry for aggregate, Slapy dam (Czechoslovakia). *Engineering Geology* 2, 267-275.
- Dudek A, Jelínek E, Nekovařík Č, 1988. Geochronological data for the units of the Bohemian Massif (in Czech). (unpublished report), Charles University, Prague, 1-16.
- Eby GN, 1990. The A-type granitoids: a review of their occurrence and chemical characteristics and speculations on their petrogenesis. *Lithos* 26, 115-134.
- Ehlers K, Powell R, 1994. An empirical modification of Dodson's equation for closure temperature in binary systems. *Geochimica et Cosmochimica Acta* 58, 241-248.
- Ellam RM, Hawkesworth CJ, 1988. Is average continental crust generated at subduction zones ? *Geology* 16, 314-317.
- Evans OC, Hanson GN, 1993. Accessory-mineral fractionation of rare-earth element (REE) abundances in granitoid rocks. *Chemical Geology* 110, 69-93.
- Fairbairn HW, 1949. Structural petrology of deformed rocks. Addison-Wesley Publishing Co., Reading, Mass., 1-344
- Faure G, 1986. Principles of Isotope Geology. J.Wiley & Sons, Chichester, 1-589.
- Fediuk F, 1992a. Metaboninite in the Proterozoic Jílové Belt of Central Bohemia. *Věstník Ústředního Ústavu geologického* 67, 297-310.
- Fediuk F, 1992b. Metavolcanic rocks of the boninite type in the Islet Zone of the Central Bohemian Pluton (in Czech). *Časopis pro mineralogii a geologii* 37, 329-332.
- Fernandez AN, Barbarin B, 1991. Relative rheology of coeval mafic and felsic magmas: nature of resulting interaction processes. Shape and mineral fabric of mafic microgranular enclaves. In: Didier J, Barbarin B, (eds) *Enclaves and Granite Petrology*. Elsevier, Amsterdam, 263-276.
- Fiala F, Vejnar Z, Kučerová D, 1976. Composition of the biotites and coexisting biotite-hornblende pairs in the granitic rocks of the Central Bohemian Pluton. *Krystalinikum* 12, 79-110.
- Flood RH, Vernon RH, 1988. Microstructural evidence of orders of crystallization in granitoid rocks. *Lithos* 21, 237-245.
- Foley SF, Wheller GE, 1990. Parallels in the origin of the geochemical signatures of island arc volcanics and continental potassic igneous rocks: the role of residual titanates. *Chemical Geology* 85, 1-18.
- Fourcade S, Allègre CJ, 1981. Trace elements behavior in granite genesis: a case study the calc-alkaline plutonic association from the Querigut Complex (Pyrénées, France). *Contributions to Mineralogy and Petrology* 76, 177-195.

- Fowler MB, 1988. Ach'uaine hybrid appinite pipes: evidence for mantle-derived shoshonitic parent magmas in Caledonian granite genesis. *Geology* 16, 1026-1030.
- Franke W, 1989. Tectonostratigraphic units in the Variscan belt of central Europe. In: Dallmeyer RD, (ed) *Terranes in Circum-Atlantic Paleozoic orogens*. Geological Society of America Special Paper 230, 67-90.
- Frejvald M, Jakeš P, 1964. Report on the structural relation between the Tábor syenite and the Moldanubian Unit (in Czech). *Časopis pro mineralogii a geologii* 9, 93-94.
- Fridrich CJ, Mahood GA, 1984. Reverse zoning in the resurgent intrusions of the Grizzly Peak cauldron, Sawatch Range, Colorado. *Geological Society of America Bulletin* 95, 779-787.
- Gastil G, Nozawa T, Tainosho Y, 1991. The tectonic implications of asymmetrically zoned plutons. *Earth and Planetary Science Letters* 102, 302-309.
- Gebauer D, Friedl G, 1994. A 1.38 Ga protolith age for the Dobra orthogneiss (Moldanubian zone of the southern Bohemian Massif, NE-Austria): evidence from ion-microprobe (SHRIMP) dating of zircon. *Journal of the Czech Geological Society* 39, 34-35.
- Gebauer D, Williams IS, Compston W, Grünenfelder M, 1989. The development of the Central European continental crust since the Early Archaean based on conventional and ion-microprobe dating of up to 3.84 b.y. old detrital zircons. *Tectonophysics* 157, 91-96.
- Geist D, McBirney A, 1992. A program package for storing analytical data and performing petrochemical calculations (Version 2 for Macintosh). 1-40.
- Geyh MA, Schleicher H, 1990. Absolute age determination. Springer-Verlag, Berlin, 1-503.
- Gilbert MC, Helz RT, Popp RK, Spear FS, 1982. Experimental studies of amphibole stability. In: Veblen DR, Ribbe PH, (eds) *Amphiboles: Petrology and experimental phase relations*. Mineralogical Society of America Reviews in Mineralogy 9B, 229-267.
- Giret A, Bonin B, Leger JM, 1980. Amphibole compositional trends in oversaturated and undersaturated alkaline plutonic ring-complexes. *Canadian Mineralogist* 18, 481-495.
- Gorokhov IM, Losert I, Varshavskaya ES, Kutyavin EP, Mel'nikov NN, Czekupayev VP, 1977. Rb - Sr geochronology of the metamorphic rocks of the eastern part of the Bohemian Massif (region of the Železné Hory Mts. and adjacent Czech - Moravian Uplands). In: Afanasjev GD (ed) *An attempt on correlation of magmatic and metamorphic rocks of Czechoslovakia and some regions of the USSR* (in Russian). Nauka, Moscow, 81-92.
- Govindaraju K, 1989. 1989 Compilation of working values and sample description for 170 international reference samples of mainly silicate rocks and minerals. *Geostandards Newsletter* 13, 1-113.
- Gromet LP, Silver LT, 1983. Rare earth element distribution among minerals in a granodiorite and their petrogenetic implications. *Geochimica et Cosmochimica Acta* 47, 925-939.
- Gruntorád J, Křištiak J, Mištarka J, Vácha J, Zális Z, 1988. Detailed geoelectrical measurements on the territory of the Bohemian Massif. In: Kukal Z, (ed) *Proceedings of the 1st International Conference on the Bohemian Massif*. Czech Geological Survey, Prague, 94-100.
- Hammarstrom JM, Zen E-an, 1986. Aluminium in hornblende: an empirical igneous geobarometer. *American Mineralogist* 71, 1297-1313.
- Hammarstrom JM, Zen E-an, 1992. Discussion of Blundy and Holland's (1990) "Calcic amphibole equilibria and a new amphibole-plagioclase geothermometer". *Contributions to Mineralogy and Petrology* 111, 264-268.
- Hanson GN, 1978. The application of trace elements to the petrogenesis of igneous rocks of granitic composition. *Earth and Planetary Science Letters* 38, 26-43.
- Hanson GN, 1980. Rare earth elements in petrogenetic studies of igneous systems. *Annual Reviews of Earth and Planetary Science* 8, 371-406.

- Hanuš V, Palivcová M, 1970. Relic variolitic texture in basic plutonites. *Neues Jahrbuch für Mineralogie, Monatshefte* 10, 435-455.
- Hanuš V, Palivcová M, 1971a. Presence and significance of amygdales in hornblende gabbros. *Krystalinikum* 8, 27-43.
- Hanuš V, Palivcová M, 1971b. Ocellar texture of Pecerady gabbro in Central Bohemian Pluton. *Acta Universitatis Carolinae, Geologica*, 175-187.
- Harland WB, Armstrong RL, Cox AV, Craig LE, Smith AG, Smith DG, 1990. A geologic time scale 1989. Cambridge University Press, Cambridge, 1-263.
- Harmon RS, Halliday AN, Clayburn JAP, Stephens WE, 1984. Chemical and isotopic systematics of the Caledonian intrusions of Scotland and Northern England: a guide to magma source region and magma-crust interaction. *Philosophical Transactions of the Royal Society of London A* 310, 709-742.
- Harris NBW, Pearce JA, Tindle AG, 1986. Geochemical characteristics of collision- zone magmatism. In: Coward MP, Ries AC, (eds) *Collision tectonics*. Geological Society Special Publication No. 19, 67-81.
- Harrison TM, Watson EB, 1984. The behavior of apatite during crustal anatexis: equilibrium and kinetic considerations. *Geochimica et Cosmochimica Acta* 48, 1467-1477.
- Harvey PK, Atkin BP, 1982. The estimation of mass absorption coefficients by Compton scattering: extension of the use of RhK_{α} Compton radiation and intensity ratios. *American Mineralogist* 67, 534-537.
- Harvey PK, Taylor DM, Hendry RD, Bancroft F, 1973. An accurate fusion method for the analysis of rocks and chemically related materials by X-ray fluorescence spectrometry. *X-ray Spectrometry* 2, 33-34.
- Haskin LA, 1984. Petrogenetic modelling-use of Rare Earth Elements. In: Henderson P, (ed) *Rare Earth Element Geochemistry*. Elsevier, Amsterdam, 115-152.
- Hawkesworth CJ, Vollmer R, 1979. Crustal contamination versus enriched mantle: $^{143}Nd/^{144}Nd$ and $^{87}Sr/^{86}Sr$ evidence from the Italian Volcanics. *Contributions to Mineralogy and Petrology* 69, 151-165.
- Hawthorne FC, 1985 Crystal chemistry of amphiboles. In: Veblen DR, (ed) *Amphiboles and other hydrous pyriboles - mineralogy*. Mineralogical Society of America Reviews in Mineralogy 9A, 1-102.
- Hejtman B, 1941. An outline of progression of the differentiation in the Požáry quarry (in Czech). *Rozpravy České akademie věd a umění, Třída II.* 51, 1-14.
- Hejtman B, 1948. Granite quarries of the Kozárovce-Zalužany district (in Czech). *Geotechnica* 6, 1-50.
- Hejtman B, 1955. Enclaves within the granodiorite in Kozárovce in the Mirovice area (in Czech). *Rozpravy ČSAV* 59: 1-25.
- Henderson P, 1982. *Inorganic geochemistry*. Pergamon Press, London, 1-353.
- Hibbard MJ, 1981. The magma mixing origin of mantled feldspars. *Contributions to Mineralogy and Petrology* 76, 158-170.
- Hibbard MJ, 1991. Textural anatomy of twelve magma-mixed granitoid systems. In: Didier J, Barbarin B, (eds) *Enclaves and Granite Petrology*. Elsevier, Amsterdam, 431-444.
- Hill RI, 1988. San Jacinto Intrusive Complex: 1. Geology and mineral chemistry, and a model for intermittent recharge of tonalitic magma chambers. *Journal of Geophysical Research* 93, 10325-10348.

- Hogan J, 1993. Monomineralic glomerocrysts: textural evidence for mineral resorption during crystallization of igneous rocks. *Journal of Geology* 101, 531-540.
- Hollister LS, Grissom GC, Peters EK, Stowell HH, Sisson VB, 1987. Confirmation of the empirical correlation of Al in hornblende with pressure of solidification of calc-alkaline plutons. *American Mineralogist* 72, 231-239.
- Holub FV, 1973. Enclaves in durbachites and some problems concerning the genesis of the durbachitic rocks (in Czech). Unpublished thesis, Charles University, Prague, 1-116.
- Holub FV, 1974. Enclaves in durbachitic rocks in the ČSR (in Czech). Unpublished thesis, Charles University, Prague, 1-113.
- Holub FV, 1977. Petrology of inclusions as a key to petrogenesis of the durbachitic rocks from Czechoslovakia. *Tschermaks Mineralogische und Petrographische Mitteilungen* 24, 133-150.
- Holub FV, 1978. Contribution to the geochemistry of the durbachitic rocks (in Czech). *Acta Universitatis Carolinae, Geologica*, 351-364.
- Holub FV, 1980. Xenoliths with Al-minerals from lamproid plutonic rocks of the Bohemian Massif (in Czech). In: *Petrogenetic problems of rock-forming minerals* (unpublished report), Charles University, Prague, 1-107.
- Holub FV, 1985. Some of the results of the geochemical-petrological investigation of potassic lamproids of the Bohemian Massif (in Czech). *Zprávy o geologických výzkumech v roce 1985*, 61-63.
- Holub FV, 1988. Deep processes involved in the origin of potassic lamproid magmas of the Bohemian Massif (in Czech). *Acta Universitatis Carolinae, Geologica*, 481-512.
- Holub FV, 1989a. Granitoids of the Central Bohemian Pluton: Petrochemical groups and some problems of their origin (in Czech). In: *Prognózy scheelitu (Au)*. Sborník prací Geoindustria Praha a PřF UK. Prague, 86-89.
- Holub FV, 1989b. Preliminary results of an enclave study in the central part of the Central Bohemian Massif (in Czech). In: *Prognózy scheelitu (Au)*. Sborník prací Geoindustria Praha a PřF UK, Prague, 78-81.
- Holub FV, 1990. Petrogenetic interpretation of potassic lamproids of the European Hercynides (in Czech). PhD. thesis (unpublished), Charles University, Prague, 1-265.
- Holub FV, 1992. Contribution to the petrochemistry of the Central Bohemian Pluton (in Czech). In: Souček J, (ed) *Horniny ve vědách o Zemi*. Charles University, Prague, 117-140.
- Holub FV, Vácha J, 1989. Petrographic and petrochemical character of the rocks of the SE-margin of the Central Bohemian Pluton east of Milevsko (in Czech). In: *Prognózy scheelitu (Au)*- Sborník prací Geoindustria Praha a PřF UK. Prague, 95-99.
- Holub FV, Žezulková V, 1978. Relative age of intrusive rocks of the Central Bohemian Pluton in the environs of Zvíkov (in Czech). *Věstník Ústředního Ústavu geologického* 53, 289-297.
- Humphris SE, 1984. The mobility of the Rare Earth Elements in the crust. In: Henderson P, (ed) *Rare Earth Element Geochemistry*. Elsevier, Amsterdam, 317-342.
- Huppert E, Sparks RSJ, 1988. The fluid dynamics of crustal melting by injection of basaltic sills. *Transactions of the Royal Society of Edinburgh, Earth Sciences* 79, 237-243.
- Hutchison CS, 1974. *Laboratory handbook of petrographic techniques*. John Wiley & Sons, New York, 1-527.
- Hutchison CS, 1975. The norm, its variations, their calculation and relationships. *Schweizerische Mineralogische Petrographische Mitteilungen* 55, 243-256.

- Hutton DHW, Dempster TJ, Brown PE, Becker SD, 1990. A new mechanism of granite emplacement: intrusion in active shear zones. *Nature* 343, 452-455.
- Irvine TN, Baragar WRA, 1971. A guide to the chemical classification of the common volcanic rocks. *Canadian Journal of Earth Sciences* 8, 523-548.
- Jacobsen SB, Wasserburg GJ, 1980. Sm-Nd evolution of chondrites. *Earth and Planetary Science Letters* 50, 139-155.
- Jakeš P, 1968. Variation in the chemical and modal composition of the Tábor Massif (in Czech). *Časopis pro mineralogii a geologii* 13, 63-73.
- Jakeš P, 1977. Geochemical characteristics of the rock types within the Central Bohemian Pluton (in Czech). P 117/1977 (unpublished report), Geological Survey, Prague 1-16.
- Janoušek V, 1991. Isotopes of strontium in the Říčany granite (in Czech). MSc. thesis (unpublished), Charles University, Prague, 1-87.
- Johnson MC, Rutherford M, 1989. Experimental calibration of the aluminium-in-hornblende geobarometer with application to Long Valley caldera (California) volcanic rocks. *Geology* 17, 837-841.
- Kalsbeek F, Hansen M, 1989. Statistical analysis of Rb-Sr isotope data by the "bootstrap" method. *Chemical Geology (Isotope Geoscience Section)* 73, 289-297.
- Kašpar JV, 1936. Concise outline of the mineralogy and geochemistry of the Říčany granite (in Czech). *Věda přírodní* 17, 168-171.
- Katzer F, 1888. Geologische Beschreibung der Umgebung von Říčan. *Jahrbuch der Geologischen Reichsanstalt* 38, 355-417.
- Kettner R, 1926. About the granite region in the environs of Mnichovice, Velké Popovice and Pyšely (in Czech). *Věstník Ústředního Ústavu geologického* 2, 135-141.
- Kettner R, 1930. Geology of the Central Bohemian Granite Massif (in Czech). *Příroda* 23, 431-437.
- Klomínský J, Dudek A, 1978. The plutonic geology of the Bohemian Massif and its problems. *Sborník geologických věd, Geologie* 31, 47-69.
- Knotek M, Lang M, 1985. Granitoids of the broader surroundings of Nahošín (Central Bohemian Pluton) (in Czech). *Acta Montana ČSAV* 70, 39-58.
- Kodym O, 1925. A remark about the geology of the Říčany granite (in Czech). 1, 77-83.
- Kodym O, 1951. Geological and petrographical setting of the area south-west of Nepomuk (in Czech). *Sborník Ústředního Ústavu geologického, oddíl geologický* 18, 1-48.
- Kodym O, 1955. Report about geological mapping in the environs of Blatná and Strakonice (in Czech). *Zprávy geologických výzkumech v roce 1955*, 88-89.
- Kodym O, 1963. Explanations to the geological map of ČSSR 1:200 000 M-33-XXI Tábor (in Czech). Geological Survey, Prague, 1-232.
- Kodym O, 1966 Moldanubicum. In: Svoboda J, (ed) Regional geology of Czechoslovakia I. Geological Survey, Prague, 40-98.
- Kodym O, Suk M, 1958. Overview of the geological and petrographical setting of the Blatná and Strakonice area (in Czech). *Geologické práce, Zošity* 50, 50-115.
- Kodym O, Suk M, 1960. Overview of the geology of the western part of the Central Bohemian Pluton (in Czech). *Věstník Ústředního Ústavu geologického* 35, 269-276.

- Kodymová A, Vejnar Z, 1974. Accessory heavy minerals in deep rocks of the Central Bohemian Pluton (in Czech). *Sborník geologických věd, Ložisková geologie - mineralogie* 16, 89-123.
- Köhler A, Raaz F, 1951. Über eine neue Berechnung und graphische Darstellung von Gesteinsanalysen. *Neues Jahrbuch für Mineralogie, Monatshefte* 247-263.
- Köhler H, Müller-Sohnius D, 1980. Rb-Sr systematics on paragneiss series from the Bavarian Moldanubikum. *Contributions to Mineralogy and Petrology* 71, 387-392.
- Košler J, 1993. Age and geochemistry of the Staré Sedlo and Mirovice complexes, Bohemian Massif, Czech Republic. PhD. thesis, Glasgow University, Glasgow, 1-266.
- Košler J, Aftalion M, Bowes DR, 1993. Mid-late Devonian plutonic activity in the Bohemian Massif: U-Pb zircon isotopic evidence from the Staré Sedlo and Mirovice gneiss complexes, Czech Republic. *Neues Jahrbuch für Mineralogie, Monatshefte* 1993, 417-431.
- Kotek J, Zikmund J, 1965. Report about 1:10000 geological mapping in the Central Bohemian Pluton between Kostelec nad Vltavou and Varvažov in 1964 (in Czech). (unpublished report). Geofond, Prague.
- Kouchi A, Sunagawa I, 1985. A model for mixing basaltic and dacitic magmas as deduced from experimental data. *Contributions to Mineralogy and Petrology* 89, 17-23.
- Koyaguchi T, Blake S, 1991. Origin of mafic enclaves: constraints on the magma mixing model from fluid dynamic experiments. In: Didier J, Barbarin B, (eds) *Enclaves and Granite Petrology*. Elsevier, Amsterdam, 415-430.
- Kukal Z, 1994. Siliciclastic termination of the carbonate sequence- signal of Variscan orogeny. *Journal of the Czech Geological Society* 39, 63.
- Kullerød L, 1991. On the calculation of isochrons. *Chemical Geology (Isotope Geoscience Section)* 87, 115-124.
- Lang M, Cimbálníková A, Kašpar P, Palivcová M, Pivec E, Ulrych J, 1978. The rocks of the Teletín quarries. Petrology of the intrusive contact of the tonalite at Teletín (in Czech). *Studie ČSAV* 3, 1-110.
- Le Maitre RW, 1989. A classification of igneous rocks and glossary of terms. Recommendations of the IUGS Commission on the Systematics of Igneous Rocks. Blackwell, Oxford, 1-193.
- Leake BE, 1968. A catalog of analysed calciferous and subcalciferous amphiboles together with their nomenclature and associated minerals. *Geological Society of America Special Paper* 98, 1-210.
- Leake BE, 1971. On aluminous and edenitic hornblendes. *Mineralogical Magazine* 38, 389-407.
- Leake BE, 1978. Nomenclature of amphiboles. *Canadian Mineralogist* 16, 501-520.
- Leake BE, Hendry GL, Kemp A, Plant AG, Harvey PK, Wilson JR, Coats JS, Aucott JW, Lünell T, Howarth RJ, 1969. The chemical analysis of rock powders by automatic X-ray fluorescence. *Chemical Geology* 5, 7-86.
- Ledvinková V, 1985. Gabbroids in the Mirovice Metamorphic Islet (in Czech). *Sborník geologických věd, Geologie* 40, 35-61.
- Liew TC, Hofmann AW, 1988. Precambrian crustal components, plutonic associations, plate environment of the Hercynian Fold Belt of central Europe: indications from a Nd and Sr isotopic study. *Contributions to Mineralogy and Petrology* 98, 129-138.
- Liew TC, Finger F, Höck V, 1989. The Moldanubian granitoid plutons in Austria: chemical and isotopic studies bearing on their environmental setting. *Chemical Geology* 76, 41-55.
- Lobkovic M, 1987. Shear deformation of the rocks of the Varied Group and Central Bohemian Pluton around Votice (in Czech). MSc. thesis (unpublished), Charles University, Prague, 1-108.

- Lorenc MV, 1990. Magmatic mafic enclaves in granitoids of northern Sierra de Paiman, Argentina. *Geological Journal* 25, 405-412.
- Ludwig KR, 1993. Isoplot, a plotting and regression program for radiogenic-isotope data, version 2.60. US Geological Survey Open-File Report 91-445, 1-40.
- Lugmair GW, Marti K, 1978. Lunar initial $^{143}\text{Nd}/^{144}\text{Nd}$: differential evolution of the lunar crust and mantle. *Earth and Planetary Science Letters*, 39, 349-357.
- Machart J, 1989. Petrochemistry of granitoids in the southern part of the Central Bohemian Pluton (in Czech). In: Prognózy scheelitu (Au). Sborník prací Geoindustria Praha a PrF UK. Prague, 90-94.
- Machart J, 1992. Petrochemical granitoid types in the southern part of the Central Bohemian Pluton (in Czech). In: Souček J, (ed) Horniny ve vědách o Zemi. Charles University, Prague, 107-116.
- Mahood G, Hildreth W, 1983. Large partition coefficients for trace elements in high-silica rhyolites. *Geochimica et Cosmochimica Acta* 47, 11-30.
- Malecha A, Suk M, Vachtl J, 1960. Geology and petrography of the crystalline basement between Sušice and Horažďovice (in Czech). Sborník Ústředního Ústavu geologického, oddíl geologický 26, 531-583.
- Maniar PD, Piccoli PM, 1989. Tectonic discriminations of granitoids. *Geological Society of America Bulletin* 101, 635-643.
- Marek F, Palivcová M, 1968. Deep structure of the Central Bohemian Pluton based on density analysis (in Czech). *Časopis pro mineralogii a geologii* 13, 333-345.
- Marshall DJ, 1988. Cathodoluminescence of geological materials. Unwin Hyman, Boston, 1-145.
- Martin H, 1987. Petrogenesis of Archaean trondhjemites, tonalites, and granodiorites from eastern Finland: major and trace element geochemistry. *Journal of Petrology* 28, 921-953.
- Máška M, Zoubek V, 1960. Variscan structural territorial units of the Czech Massif and their development. In: Buday T, (ed) Tectonic development of Czechoslovakia. Czech Geological Survey, Prague, 25-94.
- Matte Ph, Maluski H, Rajlich P, Franke W, 1990. Terrane boundaries in the Bohemian Massif: result of large-scale Variscian shearing. *Tectonophysics* 177, 151-170.
- Maury RC, Didier J, 1991. Xenoliths and the role of assimilation. In: Didier J, Barbarin B, (eds) Enclaves and Granite Petrology. Elsevier, Amsterdam, 529-544.
- McCarthy TS, Groves DI, 1979. The Blue Tier Batholith, northeastern Tasmania: a cumulate-like product of fractional crystallization. *Contributions to Mineralogy and Petrology* 71, 193-209.
- McCulloch MT, Chappell BW, 1982. Nd isotopic characteristics of S- and I-type granites. *Earth and Planetary Science Letters* 58, 51-64.
- Michael P, 1991. Intrusion of basaltic magma into a crystallizing granitic magma chamber: the Cordillera del Paine pluton in southern Chile. *Contributions to Mineralogy and Petrology* 108, 396-418.
- Mielke P, Winkler HGF, 1979. Eine bessere Berechnung der Mesonorm für granitische Gesteine. *Neues Jahrbuch für Mineralogie, Monatshefte* 471-480.
- Miller CF, 1985. Are strongly peraluminous magmas derived from pelitic sources? *Journal of Geology* 93, 673-689.
- Minařík L, 1972. Geochemistry of potassium feldspars from durbachitic rocks (in Czech). PhD. thesis (unpublished), GÚ ČSAV, Prague, 1-137.

- Minařík L, Pivec E, 1977. Thermal and crystallization history of the perthites from "Marginal" type of granitoids of the Central Bohemian Pluton (Czechoslovakia). *Acta Universitatis Carolinae, Geologica*, Slavík's Volume, 319-333.
- Minařík L, Povondra P, 1976. Geochemistry of potassium feldspars from Čertovo břemeno (in Czech). *Studie ČSAV* 9, 1-63.
- Minařík L, Cimbáľníková A, Ulrych J, 1988. Coexisting amphibole-biotite pairs in durbachitic rocks of the Central Bohemian Pluton. *Acta Universitatis Carolinae, Geologica*, 259-287.
- Minařík L, Lang M, Absolon K, 1978. Geochemistry of plagioclases from the Pecerady gabbro and associated tonalites (Central Bohemian Pluton). *Časopis pro mineralogii a geologii* 23, 129-148.
- Minařík L, Palivcová M, Hejl V, Cimbáľníková A, 1979. Trace elements - indicators in the Central Bohemian Pluton (in Czech). In: Cambel B, (ed) *Sympózium o petrogenéze a geochemii geologických procesov*. Veda, Bratislava, 73-83.
- Montel JM, Didier J, Pichavant M, 1991. Origin of surmicaceous enclaves in intrusive granites. In: Didier J, Barbarin B, (eds) *Enclaves and Granite Petrology*. Elsevier, Amsterdam, 509-528.
- Moreno-Ventas I 1991. *Petrología de los granitoides y rocas básicas asociadas de la Sierra de Gredos, Sistema Central, Español*. PhD. thesis (unpublished), University of Sevilla, 1-433.
- Müller D, Rock NMS, Groves DI, 1992. Geochemical discrimination between shoshonitic and potassic volcanic rocks in different tectonic settings: a pilot study. *Mineralogy and Petrology* 46, 259-289.
- Nagasawa H, 1970. Rare earth concentrations in zircons and apatites and their host dacites and granites. *Earth and Planetary Science Letters* 9, 359-364.
- Nelson DR, McCulloch MT, Sun SS, 1986. The origins of ultrapotassic rocks as inferred from Sr, Nd and Pb isotopes. *Geochimica et Cosmochimica Acta* 50, 231-245.
- Němec D, 1974. Petrochemistry of the dyke rocks of the Central Bohemian Pluton. *Neues Jahrbuch für Mineralogie, Monatshefte* 115, 193-209.
- Neužilová M, 1973. Study of alkali-feldspar phenocrysts of the Těchnice granodiorite in the Central Bohemian Pluton (in Czech). *Sborník geologických věd, Geologie* 25, 145-175.
- Neužilová M, 1978. Alkali-feldspar phenocrysts of the rocks of the Čertovo břemeno type and the Sedlčany granodiorite (in Czech). *Sborník geologických věd, Geologie* 32, 129-150.
- Němec D, 1978. Genesis of aplite in the Říčany massif, central Bohemia. *Neues Jahrbuch für Mineralogie, Abhandlungen* 132, 322-339.
- Němec D, 1988. Origin of syenite porphyries in the Central Bohemian Pluton by magma mixing. *Neues Jahrbuch für Mineralogie, Abhandlungen* 159, 59-71.
- Orel P, 1975. Metallogenetic and prognostic consequences of establishing the Říčany-Kutná Hora Batholith (in Czech). *Sborník Nerostné surovinové zdroje, vědecká konference-sekce 2-geologie*, VŠB Ostrava 1-118.
- Orlov A, 1928. Contribution to the chemical-petrographical characterization of the Central Bohemian Granite (in Czech). *Věstník Státního geologického ústavu Československé republiky* 4, 66-70.
- Orlov A, 1932. Contribution to the petrography of the Central Bohemian Massif (in the Blatná-Horažďovice - Nepomuk area) (in Czech). *Věstník Státního geologického ústavu Československé republiky* 8, 45-51.

- Orlov A, 1933. Contribution to the petrography of the Central Bohemian Massif (in the Říčany-Benešov-Milevsko-Písek area) (in Czech). *Věstník Státního geologického ústavu Československé republiky* 9, 135-144.
- Orlov A, 1934. Today's situation in a chemical study of the Central Bohemian Pluton and thoughts about its petrographic nature (in Czech). *Věstník Státního geologického ústavu Československé republiky* 10, 226-227.
- Orlov A, 1935. Zur Kenntnis der Petrochemie des Mittelböhmisches Plutons. *Tschermaks Mineralogische und Petrographische Mitteilungen* 46, 416-446.
- Orlov A, 1938. Overview of the geology of the Central Bohemian Pluton (in Czech). *Časopis Národního muzea, oddíl přírodovědný* 112, 49-60.
- Orlov A, 1940. Granitization and migmatitization in the area of the Central Bohemian Pluton (in Czech). *Věstník Státního geologického ústavu Československé republiky* 16, 119-144.
- Palivcová M, 1965. The Central Bohemian Pluton- a petrographic review and an attempt at a new genetic interpretation. *Krystalinikum* 3, 99-131.
- Palivcová M, 1966. Dioritisation of metabasites of the spilite-keratophyre association at the contact of the Central Bohemian Pluton, the "Islets" zone and the Moldanubicum. In: *Paleovolcanites of the Bohemian Massif*. Prague, 61-74.
- Palivcová M, 1972. Modal variation of the rocks of tonalitic association ("Slapy granite") of the Central Bohemian Pluton. *Časopis pro mineralogii a geologii* 17, 121-146.
- Palivcová M, 1978. Ocellar quartz leucogabbro (Central Bohemian Pluton) and the genetic problems of ocellar rocks. *Geologický Zborník Geologica Carpathica* 29, 19-41.
- Palivcová M, 1984. Basic series of an 'Andinotype' batholithic association in the Variscian Central Bohemian Pluton. *Geologický Zborník Geologica Carpathica* 35, 39-60.
- Palivcová M, Hejl V, 1976. Dioritic rocks with actinolite, sphene and epidote, originating by alteration of biotite granitoids (Central Bohemian Pluton). *Časopis pro mineralogii a geologii* 21, 147-166.
- Palivcová M, Cimbáliková A, Hejl V, 1977. Decomposition of biotite in hydrothermally altered (leucodioritic) rocks of the Central Bohemian Pluton. *Acta Universitatis Carolinae, Geologica Slavík's Volume.*, 129-144.
- Palivcová M, Ledvinková V, Waldhausrová J, Žezulková V, 1988. Cambrian conglomerates as a substrate of the Kozlovice granodiorite and adjacent Moldanubicum (NW of Kasejovice) (in Czech). *Časopis pro mineralogii a geologii* 2: 171-186.
- Palivcová M, Waldhausrová J, Ledvinková V, 1989a. Granitisation problem - once again. *Geologický Zborník Geologica Carpathica* 40, 521-546.
- Palivcová M, Waldhausrová J, Ledvinková V, 1989b. Precursors lithology and the origin of the Central Bohemian Pluton (Bohemian Massif). *Geologický Zborník Geologica Carpathica* 40, 521-546.
- Palivcová M, Waldhausrová J, Ledvinková V, Fatková J, 1992. Říčany granite (Central Bohemian Pluton) and its ocelli- and ovoids- bearing mafic enclaves. *Krystalinikum* 21, 33-66.
- Paterson BA, Rogers G, Stephens WE, 1992a. Evidence for inherited Sm-Nd isotopes in granitoid zircons. *Contributions to Mineralogy and Petrology* 111, 378-390.
- Paterson BA, Stephens WE, Rogers G, Williams IS, Hinton RW, Herd DA, 1992b. The nature of zircon inheritance in two granite plutons. *Transactions of the Royal Society of Edinburgh, Earth Sciences* 83, 459-471.
- Paterson SR, Tobisch OT, 1988. Using pluton ages to date regional deformations: problems with commonly used criteria. *Geology* 16, 1108-1111.

- Paterson SR, Vernon RH, Tobisch OT, 1989. A review of criteria for the identification of magmatic and tectonic foliations in granitoids. *Journal of Structural Geology* 11, 349-363.
- Pearce JA, Harris NW, Tindle AG, 1984. Trace element discrimination diagrams for the tectonic interpretation of granitic rocks. *Journal of Petrology* 25, 956-983.
- Peccerillo A, 1992. Potassic and ultrapotassic rocks: compositional characteristics, petrogenesis, and geologic significance. *Episodes* 15, 243-251.
- Peccerillo R, Taylor SR, 1976. Geochemistry of Eocene calc-alkaline volcanic rocks from the Katamonu area, Northern Turkey. *Contributions to Mineralogy and Petrology* 58, 63-81.
- Peucat JJ, Jegouzo P, Vidal P, Bernard-Griffiths J, 1988. Continental crust formation seen through the Sr and Nd isotope systematics of S-type granites in the Hercynian belt of western France. *Earth and Planetary Science Letters* 88, 60-68.
- Philpotts AR, 1990. *Principles of igneous and metamorphic petrology*. Prentice Hall, New Jersey, 1-498.
- Pidgeon RT, Aftalion M, 1978. Cogenetic and inherited zircon U-Pb systems in granites: Palaeozoic granites of Scotland and England. In: Bowes DR, Leake BE, (eds) *Crustal evolution in northwestern Britain and adjacent regions*. *Geological Journal* 10, 183-220.
- Pimentel MM, Charnley N, 1991. Intracrustal REE fractionation and implications for Sm-Nd model age calculations in late-stage granitic rocks: an example from central Brazil. *Chemical Geology (Isotope Geoscience Section)* 86, 123-138.
- Pin C, Duthou JL, 1990. Sources of Hercynian granitoids from the French Massif Central: inferences from Nd isotopes and consequences for crustal evolution. *Chemical Geology* 83, 281-296.
- Pitcher WS, 1979. The nature, ascent and emplacement of granite magmas. *Journal of the Geological Society, London* 136, 627-662.
- Pitcher WS, 1991. Synplutonic dykes and mafic enclaves. In: Didier J, Barbarin B, (eds) *Enclaves and Granite Petrology*. Elsevier, Amsterdam, 383-392.
- Pitcher WS, 1993. *The nature and origin of granite*. Chapman & Hall, London, 1-321.
- Pivec E, 1969. Potassium feldspars with hourglass structure in biotite adamellite and their genetic interpretation. *Acta Universitatis Carolinae, Geologica*, 20-30.
- Pivec E, 1970. On the origin of phenocrysts of potassium feldspars in some granitic rocks of the Central Bohemian Pluton. *Acta Universitatis Carolinae, Geologica*, 11-25.
- Pivec E jr, 1992. Zoned phlogopites rimmed by biotite in minettes from Krhanice village, Czechoslovakia. *Neues Jahrbuch für Mineralogie, Monatshefte* 1992, 169-176.
- Poli S, Schmidt MW, 1992. A comment on "Calcic amphibole equilibria and a new amphibole-plagioclase geothermometer" by J.D. Blundy and J.B. Holland (*Contrib Mineral Petrol* (1990) 104, 208-224). *Contributions to Mineralogy and Petrology* 111, 273-282.
- Poubová M, 1971. Optical and chemical characteristics of some hornblendes from the Central Bohemian Pluton. *Krystalinikum* 7, 119-133.
- Poubová M, 1974. Composition of amphiboles and rock type subdivision in the Central Bohemian Pluton. *Krystalinikum* 10, 149-169.
- Poubová M, Jurek K, 1976. Recrystallisation of hornblende into actinolite in the dioritic rocks, Central Bohemian Pluton. *Věstník Ústředního Ústavu geologického* 51, 331-337.
- Pratt JP, 1894. On the determination of ferrous iron in silicates. *American Journal of Science* 48, 149-151.
- Provost A, 1990. An improved diagram for isochron data. *Chemical Geology (Isotope Geoscience Section)* 80, 85-99.

- Pudilová M, 1968. Determination of the D/H isotopic ratio in hydroalumosilicate minerals of the rocks from the Central Bohemian Pluton (in Czech). PhD. thesis (unpublished), GÚ ČSAV, Prague, 1-96.
- Pudilová M, Dubanský A, 1969. Deuterium content in micas and amphiboles of the rocks from the Central Bohemian Pluton (in Czech). *Chemické listy* 63, 1020-1036.
- Rajlich P, 1990. Variscian shearing tectonics in the Bohemian Massif. *Mineralia Slovaca* 22, 33-40.
- Rajlich P, Vlašimský P, 1983. Regional chemical trends in the Central Bohemian Pluton (in Czech). *Acta Universitatis Carolinae, Geologica*, 193-213.
- Rapp RP, Watson EB, Miller CF, 1991. Partial melting of amphibolite / eclogite and the origin of Archean trondhjemites and tonalites. *Precambrian Research* 51, 1-25.
- Reid JBJr, Murray DP, Hermes OD, Steig EJ, 1993. Fractional crystallization in granites of the Sierra Nevada: how important is it ? *Geology* 21, 578-590.
- Ribbe PH, 1982. Titanite (sphene). In: Ribbe PH, (ed) *Orthosilicates*. Mineralogical Society of America *Reviews on Mineralogy* 5, 137-154.
- Rock NMS, 1991. *Lamprophyres*. Blackie, Glasgow and London, 1-285.
- Rock NMS, Hunter RH, 1987. Late Caledonian dyke-swarms of northern Britain: spatial and temporal intimacy between lamprophyric and granitic magmatism around the Ross of Mull pluton, Inner Hebrides. *Geologische Rundschau* 76, 805-826.
- Roden MF, Murthy VR, 1985. Mantle metasomatism. *Annual Reviews of Earth and Planetary Science* 13, 269-296.
- Rogers G, Hawkesworth C, 1989. A geochemical traverse across the North Chilean Andes: evidence for crust generation from the mantle wedge. *Earth and Planetary Science Letters*, 91, 271-285
- Röhlichová M, 1964a. Petrographie und Genese der Durbachitischen Gesteine (typus "Čertovo břemeno") in der Umgebung von Písek. *Acta Universitatis Carolinae, Geologica*, 209-221.
- Röhlichová M, 1964b. On the genesis of the granitoids at the southern margin of the Central Bohemian Pluton (Červená type) (in Czech). *Časopis pro mineralogii a geologii* 9, 1-8.
- Rollinson HR, 1992. Another look at the constant sum problem in geochemistry. *Mineralogical Magazine* 56, 469-475.
- Rollinson HR, 1993. *Using geochemical data: Evaluation, presentation, interpretation*. Longman, London, 1-352.
- Rub MG, Pavlov VA, Palivcová M, Cimbáľníková A, 1977. Accessory magnetites of some rock types in the Central Bohemian Pluton. In: Afanasjev GD (ed) *An attempt on correlation of magmatic and metamorphic rocks of Czechoslovakia and some regions of the USSR* (in Russian). Nauka, Moscow, 162-177.
- Rutherford MJ, 1973. The phase relations of aluminous iron biotites in the system $KAlSi_3O_8 - Al_2O_3 - Fe - O - H$. *Journal of Petrology* 14, 159-180.
- Rutherford MJ, Johnson MC, 1992. Comment on Blundy and Holland's (1990) "Calcic amphibole equilibria and a new amphibole-plagioclase geothermometer". *Contributions to Mineralogy and Petrology* 111, 266-268.
- Rutter MJ, van der Laan SR, Wyllie PJ, 1989. Experimental data for a proposed empirical igneous geobarometer: aluminium in hornblende at 10 kbar pressure. *Geology* 17, 897-900.
- Saunders AD, Norry MJ, Tarney J, 1991. Fluid influence on the trace element compositions of subduction zone magmas. In: Tarney J, Pickering KT, Knipe RJ, Dewey JF, (eds) *The behaviour and influence of fluids in subduction zones*. The Royal Society, London, 151-166.

- Sawka WN, 1988. REE and trace element variations in accessory minerals and hornblende from the strongly zoned McMurtry Meadows Pluton, California. *Transactions of the Royal Society of Edinburgh, Earth Sciences* 79, 157-168.
- Scharbert S, Veselá M, 1990. Rb-Sr systematics of intrusive rocks from the Moldanubicum around Jihlava. In: Minaříková D, Lobitzer H, (eds) *Thirty years of geological cooperation between Austria and Czechoslovakia*. Geological Survey, Prague, 262-271.
- Schumacher JC, 1991. Empirical ferric iron corrections: necessity, assumptions and effects on selected geothermometers. *Mineralogical Magazine* 55, 3-18.
- Shaw A, Downes H, Thirlwall MF, 1993. The quartz-diorites of Limousin: elemental and isotopic evidence for Devonian-Carboniferous subduction in the Hercynian belt of the French Massif Central. *Chemical Geology* 107, 1-18.
- Shelley D, 1993. *Igneous and metamorphic rocks under the microscope: classification, textures, microstructures and mineral preferred orientations*. Chapman and Hall, London, 1-445.
- Sobotková O, 1977. Prognostic evaluation of the ČSSR for uranium, II. stage, region no. 7- Central Bohemian Pluton (in Czech). Unpublished report, ČSÚP, Příbram, 1-230.
- Souček J, 1965. Petrography of rocks in the northern surroundings of Písek (in Czech). Unpublished thesis, Charles University, Prague, 1-106.
- Souček J, 1969. Minerals of the Červená granodiorite and pearl gneisses from the north-western surroundings of Písek (in Czech). *Věstník Ústředního Ústavu geologického* 44, 231-238.
- Souček J, 1971. Basic inclusions in the Červená Granodiorite in the area of Písek. *Acta Universitatis Carolinae, Geologica*, 153-166.
- Souček J, 1972. The Červená granodiorite and its relationship to the adjacent Moldanubian rocks in the area between Vltava and Sušice (in Czech). Unpublished thesis, Charles University, Prague, 1-85.
- Souček J, 1974. The contact between the Červená granodiorite and the Moldanubicum (in Czech). *Časopis pro mineralogii a geologii* 19, 47-60.
- Spear KS, Kimball KL, 1984. Recamp: a FORTRAN IV program for estimating Fe³⁺ contents in amphiboles. *Computers and Geosciences* 10, 317-325.
- Steiger RH, Jäger E, 1977. Subcommittee on Geochronology; convention on the use of decay constants in geo- and cosmochemistry. *Earth and Planetary Science Letters* 36, 359-362.
- Steinöcher V, 1969. The geochemistry, subdivision and petrogenesis of the Central Bohemian Pluton (in Czech). *Rozpravy ČSAV* 79, 1-98.
- Streckeisen A, 1976. To each plutonic rock its proper name. *Earth Science Reviews* 13, 1-33.
- Streckeisen A, Le Maitre RW, 1979. A chemical approximation to the modal QAPF classification of the igneous rocks. *Neues Jahrbuch für Mineralogie, Abhandlungen* 136, 169-206.
- Suk M, 1973. Reconstruction of the mantle of the Central Bohemian Pluton. *Časopis pro mineralogii a geologii* 18, 345-364.
- Svoboda J, 1932. A contribution to research on the Central Bohemian Massif (in Czech). *Věstník Státního geologického ústavu Československé republiky* 8, 302-308.
- Svoboda J, 1966. Algonkian - Lower Carboniferous. In: Svoboda J, (ed) *Regional geology of Czechoslovakia I*. Czech Geological Survey, Prague, 281-366.
- Svojtka M, 1993. Migmatitized rocks of the Suchdol Metamorphic Islet (in Czech). MSc. thesis (unpublished), Charles University, Prague, 1-144.

- Sylvester PJ, 1989. Post-collisional alkaline granites. *Journal of Geology* 97, 261-280.
- Šmejkal V, 1960. The absolute age of some granitoids and metamorphic rocks of the Bohemian Massif determined by the potassium-argon method (in Czech). *Věstník Ústředního Ústavu geologického* 35, 441-449.
- Šmejkal V, 1964. The absolute age of some granitoids and metamorphic rocks of the Bohemian Massif determined by the potassium-argon method (in Czech). *Sborník geologických věd, Geologie* 4, 121-136.
- Šmejkalová H, 1960. Petrochemistry of the Jevany granite (in Czech). *Sborník Vysoké školy chemicko-technologické v Praze, oddělení fakult anorganické a organické technologie* 4, 383-388.
- Šmejkalová M, 1965. Chemistry and petrography of the Tábor syenite (in Czech). *Sborník Vysoké školy chemicko-technologické v Praze, G-mineralogie* 7, 479-507.
- Šponar P, Komínek E, 1985. Revision of the panning anomalies, region I- Říčany, Sn, W, Au (in Czech). (unpublished report), Geoindustria, Jihlava.
- Štěpánek J, 1930. Petrochemistry of the Central Bohemian Granitic Massif (in Czech). *Příroda* 23, 395-396.
- Tauson LV, Kozlov VD, Palivcová M, Cimbálníková A, 1977. Geochemical peculiarities of the Central Bohemian granitoids and some problems of their genesis. In: Afanasjev GD (ed) *An attempt on correlation of magmatic and metamorphic rocks of Czechoslovakia and some regions of the USSR* (in Russian). Nauka, Moscow, 145-161.
- Thomas WM, Ernst WG, 1990. The aluminium content of hornblende in calc-alkaline granitic rocks: a mineralogic barometer calibrated experimentally to 12 kbars. In: Spencer RJ, Chou I-Ming, (eds) *Fluid- mineral interactions: A tribute to H.P. Eugster*. Geochemical Society, Special publication No.2, 59-63.
- Turpin L, Cuney M, Friedrich M, Bouchez J-L, Aubertin M, 1990. Meta-igneous origin of Hercynian granites in N.W. French Massif Central: implications for crustal history reconstructions. *Contributions to Mineralogy and Petrology* 104, 163-172.
- Turpin L, Velde D, Pinte G, 1988. Geochemical comparison between minettes and kersantites from the Western European Hercynian orogen: trace element and Pb-Sr-Nd isotope constraints on their origin. *Earth and Planetary Science Letters* 87, 73-86.
- Ulrych J, 1972. Leucocratic granitoids from the contact between the Central Bohemian Pluton and the Moldanubicum (in Czech). *Časopis pro mineralogii a geologii* 17, 71-84.
- Ulrych J, 1974. Amphiboles of the Pecerady basic body and surrounding rocks (in Czech). PhD. thesis (unpublished), GÚ ČSAV, Prague, 1-122.
- Ulrych J, 1985. Evolution of chemistry of zoned amphiboles from mafic rocks in the Central Bohemian Pluton (in Czech). *Acta Universitatis Carolinae, Geologica* 25-48.
- Ulrych J, Cimbálníková A, Fiala J, Kašpar P, Lang M, Minařík L, Palivcová M, Pivec E, 1976. Petrology of the Petrovice melagabbro. *Rozpravy Československé akademie věd, Řada matematických a přírodních věd* 86, 1-57.
- Urban K, 1930. Geological setting of the area at the confluence of the Vltava and Otava rivers (in Czech). *Sborník Státního geologického ústavu Československé republiky* 9, 109-187.
- Vácha J, 1987. Petrology of the contact zone of the Central Bohemian Pluton east of Milevsko (in Czech). MSc. thesis (unpublished), Charles University, Prague, 1-104.
- Vachtl J, 1933. Porphyritic augite-bearing diorite and assimilation mixing in the Central Bohemian Granitic Massif at Hudčice SW of Březnice (in Czech). *Věda přírodní* 16, 131-133.

- Valbracht PJ, Vrána S, Beetsma JJ, Fiala J, Matějka D, 1994. Sr and Nd isotopic determinations in three Moldanubian granulite massifs in southern Bohemia. *Journal of the Czech Geological Society* 39, 114.
- van Breemen O, Aftalion M, Bowes DR, Dudek A, Mísař Z, Povondra P, Vrána S, 1982. Geochronological studies of the Bohemian Massif, Czechoslovakia, and their significance in the evolution of Central Europe. *Transactions of the Royal Society of Edinburgh, Earth Sciences* 73, 89-108.
- van der Laan SR, Wyllie PJ, 1993. Experimental interaction of granitic and basaltic magmas and implications for mafic enclaves. *Journal of Petrology* 34, 491-517.
- van der Mollen I, Paterson MS, 1979. Experimental deformation of partially-melted granite. *Contributions to Mineralogy and Petrology* 70, 299-318.
- van Kooten GK, 1981. Pb and Sr systematics of ultrapotassic and basaltic rocks from the Central Sierra Nevada, California. *Contributions to Mineralogy and Petrology* 76, 378-385.
- Vance JA, 1965. Zoning in igneous plagioclase: patchy zoning. *Journal of Geology* 73, 636-651.
- Vejnar Z, 1954. Geological-petrographical setting of the Kolinec apophysis of the Central Bohemian Pluton and metamorphic rocks in its vicinity (in Czech). *Sborník Ústředního Ústavu geologického, oddíl geologický* 21, 1-50.
- Vejnar Z, 1972. Petrology of the Tužinka gabbro, Central Bohemian Pluton. *Acta Universitatis Carolinae, Geologica*, 253-262.
- Vejnar Z, 1973. Petrochemistry of the Central Bohemian Pluton. *Geochemical methods and data* 2, 1-115.
- Vejnar Z, 1974a. Application of cluster analysis in multivariate chemical classification of the rocks from the Central Bohemian Pluton (in Czech). *Věstník Ústředního Ústavu geologického* 49, 29-34.
- Vejnar Z, 1974b. Trace elements in rocks of the Central Bohemian Pluton. *Věstník Ústředního Ústavu geologického* 49, 159-165.
- Vejnar Z, Žežulková V, Tomas J, 1975. Granitoids of the Central Bohemian Pluton from the water-supply gallery "Želivka" (in Czech). *Sborník geologických věd, Geologie* 27, 31-50.
- Venturelli G, Thorpe RS, Dal Piaz GV, Del Moro A, Potts PJ, 1984. Petrogenesis of calc-alkaline, shoshonitic and associated ultrapotassic Oligocene volcanic rocks from the northwestern Alps, Italy. *Contributions to Mineralogy and Petrology* 86, 209-220.
- Veress C, 1992. Isotopische Entwicklung des oberen Erdmantels im Bereich der NW-Böhmischen Masse (ČSFR - Deutschland). PhD. thesis (unpublished), Ludwig-Maximilian Universität, Munich, 1-110.
- Vernon RH, 1984. Microgranitoid enclaves in granites- globules of hybrid magma quenched in a plutonic environment. *Nature* 309, 438-439.
- Vernon RH, 1986. K-feldspar megacrysts in granites- Phenocrysts, not porphyroblasts. *Earth Science Reviews* 23, 1-63.
- Vernon RH, 1990. Crystallization and hybridism in microgranitoid enclave magmas: microstructural evidence. *Journal of Geophysical Research* 95, 17849-17859.
- Vernon RH, 1991. Interpretation of microstructures of microgranitoid enclaves. In: Didier J, Barbarin B, (eds) *Enclaves and Granite Petrology*. Elsevier, Amsterdam, 277-291.
- Vernon RH, Etherige MA, Wall VJ, 1988. Shape and microstructure of microgranitoid enclaves- Indicators of magma mingling and flow. *Lithos* 22, 1-11.

- Vlašimský P, 1973. Stocks of basic and tonalitic rocks in the external contact zone of the Central Bohemian Pluton in the Příbram area (in Czech). *Acta Universitatis Carolinae, Geologica*, 179-195.
- Vlašimský P, Ledvinková V, Palivcová M, Waldhausrová J, 1992. Ghost stratigraphy and origin of the Central Bohemian Pluton (in Czech). *Časopis pro mineralogii a geologii* 37, 31-44.
- Voshage H, Hunziker JC, Hofmann AW, Zingg A, 1987. A Nd and Sr isotopic study of the Ivrea Zone, southern Alps, N-Italy. *Contributions to Mineralogy and Petrology* 97, 31-42.
- Vrána S, 1994. Structure of the Bohemian Massif. *Journal of the Czech Geological Society* 39, 117-118.
- Vugrinovich RG, 1981. A distribution-free alternative to least-squares regression and its application to Rb/Sr isochron calculations. *Mathematical Geology* 13, 443-454.
- Waldhausrová J, 1984. Proterozoic volcanites and intrusive rocks of the Jílové zone in Central Bohemia. *Krystalinikum* 17, 77-97.
- Wall VJ, Clemens JD, Clarke DB, 1987. Models for granitoid evolution and source compositions. *Journal of Geology* 95, 731-749.
- Watson EB, Capobianco CJ, 1981. Phosphorus and the rare earth elements in felsic magmas: an assessment of the role of apatite. *Geochimica et Cosmochimica Acta* 45, 2349-2358.
- Watson EB, Harrison M, 1983. Zircon saturation revisited: temperature and composition effects in a variety of crustal magma types. *Earth and Planetary Science Letters* 64, 295-304.
- Watson EB, Harrison TM, 1984. Accessory minerals and the geochemical evolution of crustal magmatic systems: a summary and prospectus of experimental approaches. *Physics of the Earth and Planetary Interiors* 35, 19-30.
- Watson EB, Vicenzi EP, Rapp RP, 1989. Inclusion / host relations involving accessory minerals in high-grade metamorphic and anatectic rocks. *Contributions to Mineralogy and Petrology* 101, 220-231.
- Wendt I, 1993. Isochron or mixing line? *Chemical Geology (Isotope Geoscience Section)* 104, 301-305.
- Wendt I, Carl C, 1991. The statistical distribution of the mean square weighted deviation. *Chemical Geology (Isotope Geoscience Section)* 86, 275-285.
- Wendt JI, Kröner A, Fiala J, Todt W, 1993. Evidence from zircon dating for existence of approximately 2.1 Ga old crystalline basement in southern Bohemia, Czech Republic. *Geologische Rundschau* 82, 42-50.
- Wendt JI, Kröner A, Fiala J, Todt W, 1994. U-Pb zircon and Sm-Nd dating of Moldanubian HP/HT granulites from south Bohemia, Czech Republic. *Journal of the Geological Society, London* 151, 83-90.
- Wenzel T, Ramseyer K, 1992. Mineralogical and mineral-chemical changes in a fractionation-dominated diorite-monzodiorite-monzonite sequence - evidence from cathodoluminescence. *European Journal of Mineralogy* 4, 1391-1399.
- Whalen JB, Currie KL, Chappell BW, 1987. A-type granites: geochemical characteristics, discrimination and petrogenesis. *Contributions to Mineralogy and Petrology* 95, 407-419.
- White AJR, 1990. Crustal protoliths of granites. Workshop notes (unpublished), University of St. Andrews, St. Andrews, 1-80.
- White AJR, Chappell BW, 1988. Some supracrustal (S-type) granites of the Lachlan Fold Belt. *Transactions of the Royal Society of Edinburgh, Earth Sciences* 79, 169-181.
- Whitney JA, 1988. The origin of granite: the role and source of water in the evolution of granitic magmas. *Geological Society of America Bulletin* 100, 1886-1897.

- Wickham SM, 1987. The segregation and emplacement of granitic magmas. *Journal of the Geological Society*, London 144, 281-297.
- Wiebe RA, 1968. Plagioclase stratigraphy: a record of magmatic conditions and events in a granite stock. *American Journal of Science* 266, 690-703.
- Wiebe RA, 1991. Comingling of contrasted magmas and generation of mafic enclaves in granitic rocks. In: Didier J, Barbarin B, (eds) *Enclaves and Granite Petrology*. Elsevier, Amsterdam, 393-402.
- Wilson M, 1989. *Igneous Petrogenesis*. Unwin Hyman, London, 1-466.
- Wilson M, 1993. Magmatic differentiation. *Journal of the Geological Society*, London 150, 611-624.
- Wones DR, Eugster HP, 1965. Stability of biotite: experiment, theory, and application. *American Mineralogist* 50, 1228-1272.
- Working Group for Regional Geological Classification , 1994. Regional geological subdivision of the Bohemian Massif on the territory of the Czech Republic. *Journal of the Czech Geological Society* 39, 127-144.
- Wyllie PJ, 1984. Sources of granitoid magmas at convergent plate boundaries. *Physics of the Earth and Planetary Interiors* 35, 12-18.
- Wyllie PJ, Cox KG, Biggar GM, 1962. The habit of apatite in synthetic systems and igneous rocks. *Journal of Petrology* 3, 238-243.
- York D, 1966. Least-squares fitting of a straight line. *Canadian Journal of Physics* 44, 1079-1086.
- York D, 1967. The best isochron. *Earth and Planetary Science Letters* 2, 479-482.
- York D, 1969. Least-squares fitting of a straight line with correlated errors. *Earth and Planetary Science Letters* 5, 320-324.
- Zárubová M, 1934. Sedimentary xenoliths in the Central Bohemian Pluton in the environs of Sedlčany (in Czech). *Věstník Ústředního Ústavu geologického* 10, 182-191.
- Zeithamová M, 1990. Xenoliths in granitoids of the Central Bohemian Pluton in the Sedlčany area (in Czech). MSc. thesis (unpublished), Charles University, Prague, 10-79.
- Zeithamová M, Holub FV, 1989. Xenoliths in granitoids of the Central Bohemian Pluton in the Sedlčany area (in Czech). In: *Prognózy scheelitu (Au)*. Sborník prací Geoindustria Praha a PřF UK, Prague, 82-85.
- Zeman J, 1978. Deep-seated fault structures in the Bohemian Massif. *Sborník geologických věd, Geologie* 31, 155-182.
- Zen E-an, Hammastrom JM, 1984. Magmatic epidote and its petrologic significance. *Geology* 12, 515-518.
- Zikmund J, 1974. Uranium-mineralization in the central part of the Central Bohemian Pluton (in Czech). PhD. thesis (unpublished), Prague, 1-73.
- Žežulková V, 1982a. Dyke rocks in the southern part of the Central Bohemian Pluton (in Czech). *Sborník geologických věd, Geologie* 37, 71-102.
- Žežulková V, 1982b. Granitoids of the so-called Dehetník type in the Central Bohemian Pluton (in Czech). *Věstník Ústředního Ústavu geologického* 57, 205-212.

